PARAMETER VARIATION EFFECTS IN SENSORLESS VECTOR CONTROLLED INDUCTION MACHINES

MINGYU WANG

A thesis submitted in partial fulfilment of the
requirements of Liverpool John Moores University
for the degree of Doctor of Philosophy

July 1999

ABSTRACT

Vector control of induction machines has established itself during the last two decades as the most suitable way of achieving high performance in induction motor drives. In its basic form, vector control relies on the existence of the speed sensor. This is at present considered to be the major drawback and enormous efforts have been put in development of so-called sensorless vector controlled drives during the last decade.

Vector control principles require utilisation of the mathematical model of an induction machine within the controller. Furthermore, most of the schemes, used for speed estimation in sensorless drives, are based on the model of the machine as well. The standard model regards all the machine parameters as constant and ignores the existence of the iron loss. Hence any variation of the actual machine parameters leads to detuned operation and deterioration of the performance takes place. The objectives of this project are to investigate detuning in the sensorless indirect feed-forward rotor flux orientated induction motor drive, to develop improved sensorless vector control schemes with compensation of iron loss and main flux saturation, and to perform experimental investigation with the aim of confirming some of the theoretical studies.

A detailed investigation to quantitatively assess detuning effects in the sensorless vector-controlled drive, that utilises MRAC based speed estimator of rotor flux type, is undertaken. Detuning due to parameter variations (stator and rotor resistance, stator and rotor leakage inductance), iron loss and main flux saturation is evaluated for steady-state and transient operation. Simulation studies show that parameter variations, iron loss and main flux saturation lead to deterioration in performance of the sensorless induction motor drive. It is therefore necessary to compensate the detuning effects on-line.

Based on advanced induction machine models, several improved sensorless vector control schemes are developed. The first scheme provides compensation of iron loss. The second scheme provides compensation of main flux saturation. The third one, obtained by combining the previous two schemes, provides simultaneous compensation of both the iron loss and main flux saturation. By employing the novel sensorless schemes, detuning effects are reduced significantly. The improved performance of the novel sensorless vector controlled induction motor drives is confirmed by simulation studies.

Experimental investigation is performed to confirm the theoretical findings. Speed estimator is operated at all times in parallel with an existing sensored vector controlled drive. Detuning due to parameter variations is at first investigated. Next, improved performance of one of the developed modified MRAC speed estimators, that compensates for the main flux saturation, is confirmed experimentally.

ACKNOWLEDGEMENTS

I would like to sincerely thank my Director of studies, Dr. Emil Levi, for brilliant guidance and lot of patience throughout my studies. Many thanks also go to the second supervisor, Prof. David Williams.

I would like to acknowledge the assistance provided by all the members of the staff and research colleagues in the School of Engineering.

I am also indebted to my family. I couldn't have managed to finish my studies without the support from my wife Hong Li.

CONTENTS

LIST OF FIGURERS

NOMENCLATURE

General remarks:

underlined variables denote matrices

overlined variables denote space vectors

Subscripts:

a,b,c	- phases of the original three-phase system, stator phase variables,
A,B,C	- phases of the original three-phase system, rotor phase variables,
d,q	- axes of the two-phase system in the rotating reference frame,
α,β	- axes of the two-phase system in the stationary reference frame,
s	- stator,
r	- rotor,
m	- parameters and variables associated with magnetising (air-gap) flux,
σ	- leakage,
Fe	- iron,
L	- load,
sl	- slip (angular speed),
sh	- slot harmonics,
e	- synchronous (frequency, speed),
n	- rated values,
LPF	- low pass filter,
FB	- feedback,
cmp	- compensation,

Superscripts:

est	- estimated value,
t	- matrix transposition,
*	- commanded value, parameter value in the control system; complex conjugate,

Symbols:

f	- frequency,
i	- current,

j	- imaginary unit,
J	- inertia,
L	- inductance,
n	- speed in rpm,
P	- number of pole pairs,
R	- electrical resistance,
p	- Laplace's operator,
t	- time,
T_e, T_L	- electromagnetic and load torque, respectively,
T	- time constant,
v	- voltage,
ψ	- flux linkage,
θ	- angle,
ω	- angular speed, angular frequency,
s	- slip (per unit value),
Z	- number of rotor slots,

Abbreviations:

DC	- direct current,
AC	- alternating current,
EKF	- extended Kalman filter,
FFT	- fast Fourier transform,
MRAC	- model reference adaptive control,
PWM	- pulse width modulation,
RFO	- rotor flux oriented,
DTC	- direct torque control,
PI	- proportional plus integral (controller),

1 INTRODUCTION

1.1Origins of vector control of induction machines

Variable speed electric drives are used in a variety of industrial applications. With the rapid development of automation, more and more applications demand high performance, low cost variable speed drives. The continuing trend is towards cheaper, more cost effective drives, characterised with better quality of the speed control [Novotny and Lipo, 1996]. The majority of electric machines employed in industry are squirrel cage induction machines as they are characterised with low cost and low maintenance requirements. Therefore, high performance induction motor drives have been under extensive development in the recent years. The aim of the research described in this thesis is to make a contribution in this field. The investigation is devoted to one specific sub-class of high performance drives, so-called sensorless vector controlled induction motor drives.

There are two basic types of machines that are used in industry, i.e. alternating current (AC) machines and direct current (DC) machines. Squirrel cage induction (AC) machines are predominant due to their robustness and low operational cost. In the past, it was very difficult to control their speed. Nevertheless, induction machines were still widely used in the most of the industrial applications that required running at constant speed. In contrast to an induction machine, the flux and torque of a DC machine can be easily controlled by the field and armature current. Therefore, a DC machine has fast response and four quadrant operation with high performance is easily achievable. For the applications where the variable speed is essential, DC machines and wound rotor induction machines had to be used in the past because their speed could be controlled. In particular, the separately excited DC machine has been used in applications where there was a requirement of fast response and four-quadrant operation with high performance near zero speed. However, DC machines have certain disadvantages, which are due to the existence of the commutator and the brushes. That is, they require periodic maintenance; they can not be used in explosive or corrosive environments; they have limited maximum speed of operation due to commutator and they have limited current/torque capability due to commutator [Vas, 1990]. Similar considerations

apply to wound rotor induction machine as well. To overcome these problems, the solution was found in development of high performance brushless AC drives.

The advent of thyristors, the first semi-controllable semiconductor power switches, and the development of variable frequency converters based on these switches, made possible control of squirrel-cage induction machines over a wide speed range. The most popular, so-called scalar control method, consists of simultaneous adjustments of the frequency and magnitude of the voltage supplied to the machine. This allows making steady state operating characteristics of an induction machine similar to those of a DC machine. Adjustable speed AC drive systems, employing scalar control principles, have been replacing DC drives in numerous industrial applications [Leonhard, 1985; Trzynadlowski, 1994]. Open loop volts/Hz speed control was developed in the beginning. Gradually, closed-loop scalar control techniques were introduced to improve the performance. Unfortunately, induction machines are non-linear, parameter-varying, multi-variable control objects with coupling effect, and have complex dynamics of high order. Although scalar control methods enable good speed holding in steady-state operation, they cannot provide a controllable speed transition from one operating speed to another. This is so because scalar control methods are developed from steady-state models of AC machines. If dynamic behaviour of an AC machine is to be controlled, it becomes a pre-requisite that dynamic models are used for the control system development and that control is performed in closed loop manner [Bose, 1997].

The field orientation (vector) control principle was introduced in the early seventies [Hasse, 1969; Blaschke, 1971]. The basic idea of vector (field oriented) control of an induction motor drive is to decouple the control of flux and torque of an induction machine not only in steady-state but in transient as well. As in DC machines, independent flux and torque control in AC machines is achieved by controlling the machine currents in a suitable manner. However, in contrast to a DC machine where only current magnitude has to be controlled, in an AC machine it is necessary to simultaneously control frequency, amplitude and phase of the current. Theoretically, it is possible to realise perfectly decoupled control of flux and torque in induction machines, just like in a separately excited DC machine. In the past, it was very difficult to implement the idea because only analogue means were available to solve the complex control problem. However, in the early eighties, the technology in power

electronics, micro-electronics, and processors advanced rapidly. Various schemes of field oriented control were developed by many researchers in the last twenty years. It should be mentioned that the field orientation principle can be used in control of not only induction (asynchronous) machines, but in control of all kinds of synchronous machines as well [Trzynadlowski, 1994]. Actually, field orientation in synchronous machines is simpler than in induction machines, since the position of the flux generated by the rotor winding or permanent magnets is easy to monitor.

Regardless of whether vector control is applied in conjunction with an induction machine or a synchronous machine, there are two common features that will be shared: vector control schemes are derived from an appropriate dynamic (transient) model of the machine under consideration, and a co-ordinate transformation has to be used in order to correlate the control system with the real physical world. The co-ordinate transformation requires information on the instantaneous spatial position of the appropriate flux space vector.

Vector control techniques can be classified as indirect or feed-forward control methods, and direct or feedback control methods, depending on the method of unit vector generation for vector rotation (i.e. co-ordinate transformation) [Boldea and Nasar, 1992]. The direct vector control methods rely on the generation of unit vector signals, that describe co-ordinate transformation, from the measured stator quantities or air-gap flux signals. The air-gap flux can be measured directly, while any flux can be estimated from the stator voltage and current signals. The stator, air-gap or rotor flux components can be directly computed from stator quantities. In the indirect vector control method, the rotor flux angle information and thus the unit vector are directly obtained by integration of the sum of the rotor speed and reference value of the slip frequency, that is created using reference rather than measured electromagnetic variables.

Field orientation control of induction machine can be realised by controlling the magnitude of the stator current space vector and its position with respect to the chosen flux space vector. There are different field orientation schemes depending on the chosen flux space vector [Vas, 1990]. If the rotor flux vector is chosen as the vector with respect to which stator current space vector is orientated, so-called rotor flux oriented control of induction machine is obtained. This scheme is the most popular one in practical drive realisations, because of its relative simplicity. The stator current space

vector can also be orientated with respect to stator flux space vector to form stator flux oriented control of an induction machine. Another alternative is air-gap flux oriented control and the stator current space vector is then orientated with respect to the air-gap flux. Although there are three types of vector control, the one used in commercially available drives is the rotor flux oriented control, and this is the vector controlled method dealt with in this research.

1.2 The idea and methods of sensorless vector control

With advances in power electronics, microelectronics and control technology, variable speed AC drives are becoming the most important industrial drives in all areas of manufacturing, factory automation and transportation. The availability of digital signal processors operating at high clock frequencies has made it possible to implement a high performance vector controlled drive. As already noted, a vector controlled drive is a drive with closed-loop speed control, so that the information on actual speed of rotation is required. In many industrial applications, it is neither possible nor desirable to install additional speed sensors for speed control of induction machines. If high performance is not required, then open-loop scalar control methods can be used. However these open-loop control schemes have shortcomings, such as slow and uncontrolled dynamic response, low-speed regulation accuracy and limited speed control range [Tzou et al, 1996].

For high precision control system, closed-loop control is essential to control the speed with good performance in both dynamic and steady-state operation. Closed-loop control requires a feed-back signal from the machine shaft. The speed signal is obtained by a speed or position sensor mounted on the machine shaft.

In spite of many advantages of the vector controlled drives, the shaft-mounted speed sensor, required for precise speed control, is a significant drawback of the control system. Most of the sensors and the associated electronics are temperature sensitive and are also sensitive to the electromagnetic noises, limiting the machine's applicability. Additionally, these sensors increase the size, weight and cost of the drive. Moreover, there are some special applications where the sensor either can not be mounted directly on the machine shaft or could reduce the reliability of the drive when used. With this in

mind, it is an advantage to dispense with the speed sensor and obtain the speed feedback only from the easily measurable voltages and currents of the machine. In other words, it is advantageous to estimate the speed of the rotation, so that a speed sensor is not required any more. Speed estimate then takes the role of the measured speed signal. It is for these reasons that sensorless vector control of induction machines is receiving wide attention recently [Rajashekara et al, 1996; Schauder, 1992; Ohtani et al, 1992; Peng and Fukao, 1994]. The development of sensorless induction machine drives has become an important research topic. The research has concentrated on the elimination of the speed sensor at the machine shaft without deteriorating the dynamic performance of the drive system. Considering the present trend, it can be predicted that sensorless vector controlled AC drives will emerge as the industry standard in the next century, and oust the DC drive completely [Bose, 1997].

The advantages of speed sensorless induction machine drives are, as already noted, lower cost, reduced size of the drive, elimination of the sensor cable, and increased reliability. As speed is not measured any more, it has now to be estimated from measurable electromagnetic quantities, such as stator currents and stator voltages. Various approaches to speed estimation have been developed in recent years. They are reviewed by Holtz [1995], Rajashekara et al, [1996] and Vas [1998]. The speed estimation methods can be broadly classified into two principal categories:

1. those which analyse the current (or voltage) harmonic spectrum and estimate the rotor speed on the basis of certain harmonic properties of the spectrum [Hurst and Habetler, 1997]. The spectrum based methods have an advantage of yielding an accurate measure of rotor speed, which remains totally independent of parameter variations.

2. those which use the induction machine model to identify the speed.

Apart from spectrum based and model based speed estimation techniques, it is possible to define the third category. Machine speed can be estimated by means of artificial-intelligence-based techniques, which do not require a mathematical model of the machine and the drive system. At present, artificial-intelligence-based estimation methods include:

- Neural network based speed estimation [Ben-Brahim and Kurosawa, 1993; Ben-Brahim, 1995; Mehrotra et al, 1996; Kulkarni and El-Sharkawi, 1997]
- Fuzzy-neural based speed estimation [Vas, 1998]

The neural network technique is based on a learning process. Neural networks have the advantage of extremely fast parallel computation due to distributed network intelligence. Many neurons or processing elements are interconnected to form a parallel neurocomputing network. The most commonly used neural networks are of feed-forward multilayer type. Feedback signals are used only during training of the neural network. Generally, the back propagation method is used for adjusting the neural network weights during training. This is a slow and very time-consuming process, as the algorithm takes a long time to converge.

It is also possible to estimate the rotor speed by using a fuzzy-neural network estimator. The fuzzy-neural estimator is basically a neural network with fuzzy features. A conventional neural network uses a fixed topology and back-propagation learning. However, it is difficult to relate the structure of the network to the physical processes and there are no guidelines for the selection of the number of hidden layers and nodes. A fuzzy-neural system combines the advantages of fuzzy-logic and neural networks. In a fuzzy-neural system the structure of the network is based on a fuzzy-logic system. It is another advantage of a fuzzy-neural network that the number of layers and also the number of nodes is known [Vas, 1998].

Neural network and fuzzy-neural based speed estimations are at present emerging techniques and are beyond the scope of interest in this thesis.

The model based techniques can generally be divided into two groups [Blaabjerg et al, 1996; Holtz, 1995; Rajashekara et al, 1996]:

1. open-loop estimators; and
2. closed-loop estimators

It should be noted that, in this context, notion of open-loop and closed-loop speed estimation is correlated purely with the speed estimation process itself and that a drive with closed-loop speed control is under consideration at all times. The distinction between the two groups is made on the basis whether or not a correction term,

involving the estimation error, is used to adjust the response of the estimator [Vas, 1998]. In an open-loop speed estimator, rotor speed is calculated on the basis of the machine model equations only and there is no correlation between the estimated output and speed calculation procedure within it. For a closed-loop speed estimator, rotor speed is estimated based on the machine model and the estimated speed is used as a feedback signal to control the estimation procedure within the estimator. Open-loop estimators and closed-loop estimators differ with respect to accuracy, robustness and limits of applicability. The slip frequency calculation method was the first one to be used in an attempt to operate an induction machine with closed-loop speed control without speed sensor [Rajashekara et al, 1996]. The slip frequency is the difference between the stator frequency and the electrical frequency corresponding to the rotor speed of rotation. By calculating the slip frequency from measured stator currents and stator voltages, the rotor speed can be determined. Slip compensation methods are usually simpler but can guarantee good dynamic performances only when the slip is estimated from machine dynamic equations [Holtz, 1993]. In general, open-loop speed estimators rely on knowledge of various parameters of the induction machine, as rotor speed and slip frequency estimators are based on the voltage equations of the induction machine model. When estimator parameters are mismatched with the actual values in the machine, the accuracy of the open-loop estimators deteriorates. Parameter variations have great influence on both the steady-state and transient performance of the drive. However, it is possible to obtain a rather good and accurate estimate by suitably identifying machine parameters on-line. Speed calculation based purely on machine model equations has been discussed by many authors [Kim and Kawamura, 1996; Baader et al, 1992; Ohtani, et al, 1992; Bonanno et al, 1995]. For high performance induction motor drives, closed-loop speed estimators can provide good behaviour of speed estimation, which is in general better that the one obtainable with open-loop speed estimators.

According to the way of implementation, the closed-loop speed estimation methods based on the induction machine model are further classified into the following sub-groups:

- Observer-based speed estimation [Kubota and Matsuse, 1994a; Yang and Chin, 1993]

- Model reference adaptive control based speed estimation [Schauder, 1992; Tajima and Hori, 1993; Kim and Hung, 1995]
- Extended Kalman filter based speed estimation [Kim et al, 1994]

A state observer is a model-based state estimator which can be used for the state (and/or parameter) estimation of a non-linear dynamic system in real time. In the calculations, the states are predicted by using a mathematical model. Predicted states are continuously corrected using a feedback correction scheme. This scheme makes use of actual measured states by adding a correction term to the predicted states. This correction term contains the weighted difference of some of the measured and estimated outputs signals (the difference is multiplied by the observer feedback gain). Based on the deviation from the estimated value, the state observer provides an optimum estimated output value at the next sampling instant. In an induction machine drive, the rotor speed of the machine can be estimated by a state observer. This is possible since a mathematical dynamic model of the induction machine is sufficiently well known. For this purpose, the stator currents and stator voltages are monitored on-line and the rotor speed of the machine can be obtained by the observer quickly and precisely. The accuracy of the state observer also depends on the model parameters used [Vas, 1998].

In the model reference adaptive control based speed estimation method, a comparison is made between the outputs of the two estimators. These outputs can take different form, as discussed later on. The estimator that does not involve the quantity to be estimated (i.e. rotor speed) is considered as the reference model. The other estimator, which involves the estimated quantity, is called the adjustable model. The error between two estimates, obtained from the reference and adjustable model, is used to drive a suitable adaptation mechanism that generates the estimated rotor speed for adjustable model. When the estimated rotor speed in the adjustable model attains such a value that the difference between the output of the reference model and the output of the adjustable model is zero, the estimated rotor speed is equal to the actual rotor speed under ideal conditions (i.e., when there is perfect match between actual motor parameters and the values used in the speed estimator.).

The extended Kalman filter can be employed to identify the rotor speed of an induction machine based on the complete machine model. The machine is modelled as a fifth

order system, with the unknown rotor speed being a state variable. Since the model is non-linear, the extended Kalman filter algorithm must be applied. It linearises the non-linear model in the actual operating point. The extended Kalman filter is a viable but computationally very intensive candidate for on-line estimation of the rotor speed. The rotor speed is estimated using the state equations and Kalman filter, on the basis of measured quantities [Rajashekara et al, 1996].

The specific type of the sensorless vector control, investigated in this research, is the indirect feed-forward rotor flux oriented control, with the speed estimator based on the induction machine model. The estimator is of MRAC type.

1.3 Problems experienced in sensorless vector control

As described in the previous section, sensorless vector controlled induction motor drive is a desirable solution for many applications. Various concepts for sensorless vector control of induction machines have been developed in the last ten years. Each scheme of speed estimation has some advantages and some disadvantages. In a speed sensorless vector controlled system, it is not only the rotor speed but also the field angle which needs to be estimated.

Speed estimation using stator current harmonic spectrum has the advantage of being independent of machine parameters. However, as harmonics are extracted from stator current spectrum on-line, the procedure has limited accuracy in transient states due to the time required for current acquisition and FFT calculations. Furthermore, the techniques using current harmonic analysis are dependent on specific machine structural parameters. For example, the machine slot harmonic magnitude and frequencies depend on unknown parameters, such as the number of rotor slots. Therefore, the algorithm requires user-defined input data and the data vary from machine to machine [Wong and Lefley, 1996].

Most estimation methods rely directly or indirectly on the induction machine model. Therefore, accurate induction machine parameters are essential for proper speed estimation. The machine parameters are affected by temperature, saturation level in the machine and frequency of operation. In any of these methods, the estimation error

increases as the speed reduces [Holtz et al, 1997]. Parameter variations therefore always cause detuned operation of the system.

The correct information regarding parameters and measured electrical quantities determines the accuracy of the speed estimation. Nowadays, the accurate measurement of stator currents and stator voltages is not a problem. Therefore, machine parameters play an important role in the machine model-based speed estimation schemes. If there are any discrepancies between the actual machine parameters and the values used in the speed estimator, estimation of the speed is erroneous. This affects the performance of the drive and controller operates with error, so that so-called detuned operation results.

As already noted, there is a huge variety of speed estimation schemes that are based on the machine model. Different techniques perform different calculations, for which different parameters are used. Therefore, the overall sensitivity to parameter variations is heavily dependent on the applied technique. Generally, open-loop speed estimation methods are more sensitive to parameter variations than closed-loop speed estimation methods. Whatever the scheme, it is absolutely crucial to have as accurate knowledge as possible about the parameters involved in the particular speed estimation scheme. It has to be stressed that initial correct determination of the required parameters is not a guarantee for accurate speed estimation at all times. Each of the parameters is determined for a specific operating point and their values might change when the operating conditions are altered. There are many phenomena that cause parameter variations in an induction machine. Magnetic saturation affects the values of all the inductances in the machine. Variations in temperature and skin effect change the values of the resistances in the machine. All of the above mentioned effects alter the value of the rotor time constant, which is used for speed estimation in many schemes. Iron loss, normally neglected in the machine model, takes part in power balance of the machine and thus reduces the accuracy of speed estimation.

Variations of inductances due to magnetic saturation are dependent on machine operating conditions. Magnetic saturation in an induction machine can be separated into main flux saturation, rotor leakage flux saturation and stator leakage flux saturation. They cause variations of the magnetising inductance, rotor leakage inductance and stator leakage inductance, respectively. When a vector controlled induction machine is designed for speed operation above rated speed, the flux of the machine has to be

reduced for speeds higher than rated, in order to provide operation with constant power. When the flux in the machine is reduced, the value of the magnetising inductance increases. The effects of main flux saturation have been considered in the past in detail for a vector control scheme with speed sensor [Levi and Vuckovic, 1989].

Rotor resistance is influenced by the skin effect which depends on the geometrical shape of the rotor bars and the amplitude and frequency of the rotor current. The variations of the rotor resistance and stator resistance due to thermal effect are correlated to operating conditions. An induction machine is heated by various losses in it. Copper losses occur in both stator and rotor windings and are determined by stator and rotor currents. Meanwhile, iron loss is determined by flux level and the operating frequency. Both types of losses depend also on the spectra of the voltage and current waveforms supplied by the inverter. Cooling conditions are of the same importance and are as complex as heating phenomenon. Different cooling systems provide different conditions. If the cooling is provided by the cooling fan affixed to the machine shaft, the cooling is affected by the operating speed of the machine. It is quite different when cooling is provided by a separate air cooling system. Both of the cases are also affected by the ambient temperature. All of the heating sources inside the machine combine to determine the temperature of the machine and the resulting variations of the resistances.

The problem of satisfactory operation at all speeds can be alleviated by on-line adaptation of the machine model parameters, such as stator resistance, rotor resistance, and rotor time constant [Blasco-Gimenez et al, 1996a]. Due to thermal effects stator and rotor resistance change during operation, and it is essential to obtain correct parameter information by on-line identification. As thermally caused changes in resistances are slow in nature, it is appropriate to compensate for these variations by on-line resistance identification. Many proposals have been made to remedy this situation. These have, in the main, taken the form of parameter adaptation schemes that run alongside the main vector control algorithm and the speed estimation scheme. The main feature of such schemes is their ability to track the variation of machine parameters. On-line identification of rotor resistance and stator resistance is discussed in [Blasco-Gimenez et al, 1996b; Lee et al, 1996; Zhen and Xu, 1995]. On-line identification of rotor time constant in sensorless drives is reported as well [Jansen and Lorenz, 1993]. A

possible way of improving the speed estimation at low speeds by on-line identification of stator resistance is reported in [Yang and Chin, 1993].

Main flux saturation and iron loss are another sources of speed estimation errors, as standard induction machine model neglects both of these phenomena. Williamson and Healey [1996] proposed a transient induction machine model that accounts for skin effect in rotor and saturation in both the main and rotor leakage flux path. Models that allow for main flux path saturation have been also developed in a form that is suitable for use in vector control schemes [Levi and Vuckovic, 1993]. Induction machine model with iron loss representation has been proposed by [Levi, 1995]. Detuning due to iron loss and main flux saturation in vector control system with speed sensor has been studied in detail by [Sokola, 1998]. The results show that iron loss and main flux saturation may deteriorate the performance of the system. In contrast to thermally induced variations in resistances, that are slow, variations in saturation level and iron loss are of electromagnetic nature and are therefore inherently fast. Any attempt to compensate for these phenomena by on-line identification would therefore be applicable to steady-state operation only. A different approach towards compensation, so-called model based approach, is favourable in this case. The basic idea behind this method is to develop the vector control system (and the speed estimator) from modified induction machine models, that account for one or more phenomena that are usually neglected. Compensation in both steady-state and transient operation then becomes possible. Model based approach has been used extensively in the past in conjunction with vector controlled drives that do possess the speed sensor [Novotny and Lipo, 1996; Levi, 1995; Levi and Vuckovic, 1989; Williamson and Healey, 1996]. However, there is no evidence that such an approach has been applied in conjunction with sensorless vector controlled drives and it is believed that this thesis for the first time proposes use of model based approach in sensorless drives.

1.4 Aims of the research

1.4.1 Research objectives

Sensorless vector control of induction machines has become one important area of research in recent times. Numerous authors have introduced speed estimators that are

based on induction machine models. Since there are inevitable parameter variations during normal operation of the drive, speed estimation error takes place in a sensorless vector controlled induction machine drive with machine model based speed estimator. Although some schemes are equipped with on-line parameter identification of stator and/or rotor resistance, iron loss and main flux saturation as possible detuning sources have not received attention so far. Most of the existing schemes are based on the standard induction machine model in which iron loss and main flux saturation are neglected. As an ideal induction machine does not exist in reality, evaluation of detuning due to parameter variations (stator and rotor resistance, stator and rotor leakage inductance), iron loss and main flux saturation is one of the main aims of this study. Furthermore, in order to compensate detuning effects caused by iron loss and main flux saturation, improved vector controller and speed estimator schemes, based on improved induction machine models, are to be developed.

Since MRAC-based speed estimator is a relatively simple scheme to implement, it has attracted a lot of attention in recent years. One specific type of MRAC-based speed estimator is used throughout this research. The vector control system utilised here consists of indirect feed-forward rotor flux oriented controller and a rotor flux based MRAC type of speed estimator. At first, impact of iron loss on operation of the drive is investigated based on standard vector controller and constant parameter speed estimator. Induction machine model which includes iron loss representation is utilised. Next, detuning due to parameter variations (magnetising inductance, stator resistance and rotor resistance, stator and rotor leakage inductance) is investigated by using induction machine model with main flux saturation accounted for. Detailed studies are performed for both steady-state and transient operation of the drive. In order to compensate a given phenomenon, the improved induction models are used further on to design modified vector controllers and speed estimators. The improved schemes of sensorless vector control are finally verified. The main objectives of the study can be summarised as follows:

1. To qualitatively and quantitatively investigate detuning effects due to iron loss, main flux saturation and parameter variations in a sensorless vector control system, based on standard indirect vector controller and standard rotor flux based MRAC speed estimator, in steady-state operation.

2. To investigate detuning effects due to iron loss, main flux saturation and parameter variations in transient operation of the same system.

3. To develop a novel vector controller and speed estimator scheme, based on an improved induction machine model, that accounts for iron loss and therefore compensates its detuning effects.

4. To develop a novel sensorless vector control scheme that compensates for main flux saturation effects and therefore enables satisfactory operation of the drive in the field-weakening region.

5. To develop a novel sensorless vector control scheme with simultaneous compensation of both the iron loss and main flux saturation.

6. To confirm the effectiveness of modified vector controllers and novel speed estimators, developed in 3-5, by extensive simulations of transient operation.

7. To experimentally investigate operation of the rotor flux based MRAC type of speed estimator in the base speed region and in the field-weakening region and to experimentally evaluate detuning effects in steady-state and transient operation.

8. To implement in the experimental rig newly developed speed estimator with compensation of main flux saturation (objective 4) and to verify it by performing experiments in the field-weakening region.

1.4.2 Investigation approaches

In order to realise the research objectives listed above, appropriate approaches have been applied.

a) Qualitative investigations of detuning effects due to parameter variations in sensorless vector controlled induction machines are performed by deriving appropriate detuning expressions for steady-state operation. Quantitative analysis of detuning effects in steady-state operation of the drive is then done for a specific drive. For different detuning cases, several different machine models for steady-state representation are utilised. In order to solve the

equations, the iterative calculation method is utilised. Several programs are developed in Matlab environment to obtain results.

b) For transient analysis of detuning effects, the whole sensorless vector controlled induction machine drive transient model is utilised. Simulation models, which include an appropriate dynamic induction machine model and a full sensorless vector control system, are built using Simulink/Matlab.

c) Compensation of given phenomenon by modified vector controller and speed estimator is confirmed for each case based on transient simulations using Simulink/Matlab.

d) Experimental verification of the theoretical results is conducted by means of an existing computer controlled experimental rig. The rig comprises an indirect rotor flux oriented machine that is equipped with position sensor. Data acquisition system is constructed and experimental investigation (objectives 7 and 8) is performed by operating the speed estimator in parallel with the rig.

1.4.3 Originality of the research

Parameter variations cause detuned operation of a vector controlled induction machine without a speed sensor. Existing research regarding parameter variations in sensorless vector controlled induction machines has mostly been restricted to stator and rotor resistance variations. The originality of this thesis lies in the following:

1. Evaluation of detuning in a sensorless vector controlled induction machine drive due to iron loss in both steady-state and transient operation is performed for the first time.
2. Evaluation of detuning in a sensorless vector controlled induction machine drive due to main flux saturation in both steady-state and transient operation is investigated for the first time.
3. Comparative evaluation of detuning in a sensorless vector controlled induction machine drive due to parameter variations (magnetising

inductance, stator and rotor leakage inductance rotor resistance and stator resistance), in both steady-state and transient operation is conducted.

4. A novel sensorless vector control scheme with iron loss compensation is developed.
5. A novel sensorless vector control scheme with main flux saturation compensation is developed.
6. A novel sensorless vector control scheme with compensation of both main flux saturation and iron loss is proposed.
7. Compensating effects are verified by dynamic simulations and experiments.

Original research results are the complete chapters 6, 7, 8 and 9.

1.5 Thesis outline

Principles of vector control of induction machines are reviewed in chapter 2. In order to explain the principles, constant parameter induction model is at first derived in section 2.2. Principles of rotor flux oriented control and stator flux oriented control are elaborated in section 2.3 and 2.4, respectively, and reasons for discussion of stator flux oriented control at this stage are given. The control system of a standard rotor flux oriented induction machine with speed sensor is discussed in section 2.5, in which indirect feed-forward rotor flux oriented control and direct feedback rotor flux oriented control of a current-fed induction machine are described.

A review of methods of sensorless rotor flux oriented control is presented in chapter 3. Several speed estimation schemes are discussed. Speed estimation by using stator current spectrum is at first reviewed in section 3.2. Speed estimation using induction machine model only (open-loop speed estimators) is elaborated in section 3.3. The most popular closed-loop speed estimation schemes, based on the induction machine model, are presented in section 3.4. The schemes encompassed are model reference adaptive control (MRAC) based speed estimation, observer based speed estimation and extended Kalman filter (EKF) based speed estimation.

Chapter 4 focuses on MRAC based speed estimation methods. As MRAC can be applied in a number of different ways, section 4.2 introduces at first the most popular

speed estimation method, based on rotor flux. Back emf based MRAC scheme of speed estimation is discussed in section 4.3. Reactive power based MRAC scheme and air-gap power based MRAC scheme are elaborated in sections 4.4 and 4.5, respectively.

In order to investigate the detuning effects due to iron loss and main flux saturation, knowledge of improved induction machine models which include iron loss and main flux saturation representation is essential. In chapter 5, improved induction machine models are introduced. Dynamic and steady-state models with iron loss accounted for are presented in section 5.2. Dynamic and steady-state models with main flux saturation accounted for are reviewed in section 5.3. Induction machine models which include both iron loss and main flux saturation representation are given in section 5.4. All the induction models presented in chapter 5 are utilised further on, in chapters 6 and 7 for investigation of detuning due to the given phenomena, and in chapter 8 for development of novel, improved sensorless vector control schemes.

Detailed analysis of detuning effects in steady-state operation due to iron loss, main flux saturation and parameter variations in a rotor flux based MRAC type of sensorless vector control system is given in chapter 6. In order to investigate the detuning effects, constant parameter MRAC based speed estimator is used in this chapter. Iron loss induced detuning is analysed in section 6.2. Detuning due to magnetising inductance variation is elaborated in section 6.3. Detuning due to leakage inductance variation is presented in section 6.4. Detuning due to rotor resistance and stator resistance variations are covered in sections 6.5 and 6.6, respectively. Simultaneous impact of iron loss and incorrect setting of the magnetising inductance is discussed in section 6.7. Contributions of the chapter are summarised in section 6.8.

Detuning effects in transient operation of the MRAC rotor flux based sensorless vector control system are analysed in chapter 7. In order to quantify detuning due to iron loss, main flux saturation and parameter variations, improved dynamic induction machine models are utilised. Problems of integration of the stator flux in the reference model of the MRAC speed estimator are discussed in section 7.2. Operation of the induction machine under tuned conditions is elaborated in section 7.3. Detuning due to incorrect setting of the magnetising inductance is discussed in section 7.4. Detuning due to rotor resistance and stator resistance variations are investigated in sections 7.5 and 7.6, respectively. Detuning due to iron loss only is presented in section 7.7. Combined

detuning due to iron loss and incorrect setting of the magnetising inductance is covered in section 7.8. Section 7.9 summaries the contributions of the chapter.

Schemes with iron loss and/or main flux saturation compensation are discussed in chapter 8. Their effectiveness is confirmed by dynamic simulations. Scheme with compensation of iron loss for a sensorless indirect rotor flux oriented induction machine is proposed and analysed in section 8.2. A scheme with compensation of main flux saturation by means of modified rotor flux based MRAC speed estimator is developed in section 8.3. A scheme with compensation of both iron loss and main flux saturation is suggested in section 8.4. Contributions of the chapter are summarised in section 8.5.

Chapter 9 deals with experimental investigation. Detailed description of the experimental rig is given in section 9.2. Tuning of the speed estimator is described in section 9.3. Results of the study of the speed estimator operation in the based speed region, under tuned and detuned conditions are given in sections 9.4 and 9.5 respectively. Operation of the speed estimator in the field-weakening is elaborated in section 9.6, while section 9.7 investigates the novel speed estimator with compensation of main flux saturation. Section 9.8 summaries the chapter.

The conclusions of the research are summarised and further work is discussed in chapter 10.

Referenced literature is listed in chapter 11.

Machine data are given in Appendix A. Analysis of detuning due to iron loss with reactive power based MRAC speed estimator is presented in Appendix B. Simulink models of the sensorless vector controlled induction machine are given in Appendix C. Appendix D contains material relevant for the experimental investigation. Finally, all the published and accepted papers which contain the results of the research are attached in Appendix E.

2 PRINCIPLES OF VECTOR CONTROL OF INDUCTION MACHINES

2.1 Introduction

The basic idea of vector control is to control an induction machine in the same way as a DC machine is controlled. A DC machine has two separate windings, excitation and armature, that are used for independent flux and torque control. However, in an induction machine torque producing current and flux producing current are parts of the same phase currents. In other words, the stator current is the source of both the "excitation" and "armature" currents. In the most frequently used squirrel-cage type machines, only the stator currents can be directly controlled, since the rotor winding is not accessible. Hence, the key point for vector control of an induction machine is to resolve the current into separate torque producing current and flux producing current. This turns out to be possible only if the induction machine model is at first transformed from the physical phase domain into a fictitious domain that does not exist in reality. This chapter therefore at first reviews induction machine modelling and delivers a mathematical model of an induction machine in an arbitrary reference frame. This is followed by a summary of the rotor flux oriented and stator flux oriented control principles.

2.2 Constant parameter dynamic model of an induction machine in an arbitrary reference frame

In this section constant parameter dynamic model of an induction machine in an arbitrary reference frame will be given. The three-phase induction machine model in phase domain serves as the starting point. This model is then transformed into arbitrary reference frame and notion of space vector is introduced.

A perfectly smooth-air-gap induction machine is considered. It is assumed that induction machine phase windings are displaced in space by 120 degrees from each other, at both stator and rotor (i.e. squirrel cage is represented with a three-phase winding). The winding resistance and leakage inductance are assumed to be constant

parameters. The eddy currents and iron losses are neglected. A symmetrical three phase smooth-air-gap induction machine with sinusoidal distribution of windings is considered and the effects of mmf space harmonics are neglected [Vas, 1992; Boldea and Nasar, 1992]. The schematic of the machine is shown in Figure 2.1.

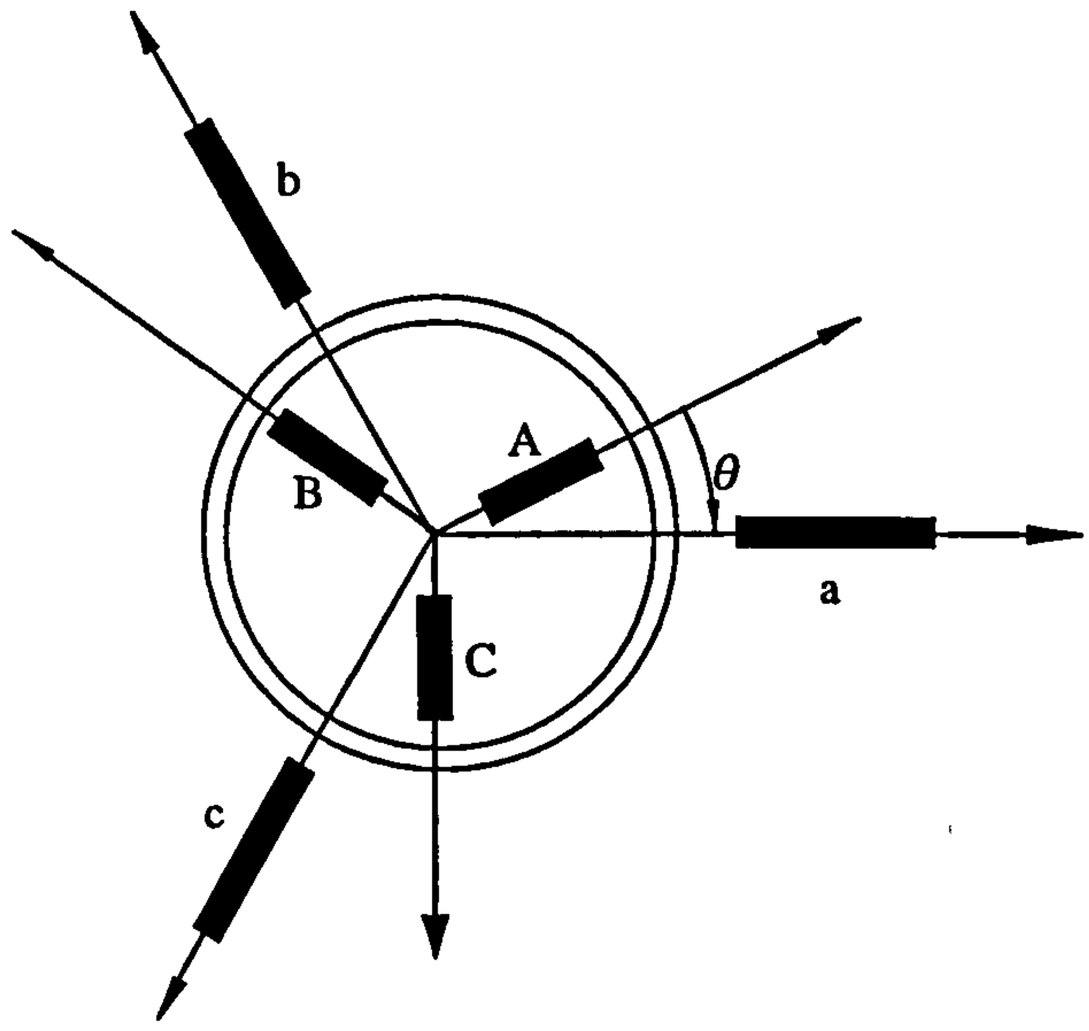

Figure 2.1: Schematic representation of a three-phase induction machine.

Stator voltage equations can be expressed in terms of time domain instantaneous phase variables as:

$$v_a = R_s i_a + \frac{d\psi_a}{dt}$$
$$v_b = R_s i_b + \frac{d\psi_b}{dt} \qquad (2.1)$$
$$v_c = R_s i_c + \frac{d\psi_c}{dt}$$

where v_a, v_a, and v_c, i_a, i_b, and i_c are the instantaneous values of the stator phase voltages and currents, respectively, R_s is the resistance of the stator winding, and ψ_a, ψ_b, and ψ_c are the instantaneous values of the stator flux linkages.

Similar expressions hold true for the rotor voltage equations expressed in the reference frame fixed to the rotor:

$$v_A = R_r i_A + \frac{d\psi_A}{dt}$$
$$v_B = R_r i_B + \frac{d\psi_B}{dt} \qquad (2.2)$$
$$v_C = R_r i_C + \frac{d\psi_C}{dt}$$

where v_A, v_B, and v_C, i_A, i_B, and i_C are the instantaneous values of the rotor voltages and currents, respectively, R_r is the resistance of the rotor winding, and ψ_A, ψ_B, and ψ_C are the instantaneous values of the rotor flux linkages.

Stator flux linkages and rotor flux linkages are defined in terms of the instantaneous current values and inductances as [Vas, 1992]:

$$\psi_a = L_{aa} i_a + L_{ab} i_b + L_{ac} i_c + L_{aA} i_A \cos\theta + L_{aB} i_B \cos(\theta + 2\pi/3) + L_{aC} i_C \cos(\theta + 4\pi/3)$$
$$\psi_b = L_{ba} i_a + L_{bb} i_b + L_{bc} i_c + L_{bA} i_A \cos(\theta + 4\pi/3) + L_{bB} i_B \cos\theta + L_{bC} i_C \cos(\theta + 2\pi/3)$$
$$\psi_c = L_{ca} i_a + L_{cb} i_b + L_{cc} i_c + L_{cA} i_A \cos(\theta + 2\pi/3) + L_{cB} i_B \cos(\theta + 4\pi/3) + L_{cC} i_C \cos\theta$$

(2.3)

$$\psi_A = L_{AA} i_A + L_{AB} i_B + L_{AC} i_C + L_{Aa} i_a \cos\theta + L_{Ab} i_b \cos(\theta + 4\pi/3) + L_{Ac} i_c \cos(\theta + 2\pi/3)$$
$$\psi_B = L_{BA} i_A + L_{BB} i_B + L_{BC} i_C + L_{Ba} i_a \cos(\theta + 2\pi/3) + L_{Bb} i_b \cos\theta + L_{Bc} i_c \cos(\theta + 4\pi/3)$$
$$\psi_C = L_{CA} i_a + L_{CB} i_B + L_{CC} i_C + L_{Ca} i_a \cos(\theta + 4\pi/3) + L_{Cb} i_b \cos(\theta + 2\pi/3) + L_{Cc} i_c \cos\theta$$

(2.4)

The angle θ is the angle shown in Figure 2.1. It describes instantaneous position of the rotor winding A magnetic axis with respect to the stationary stator phase a magnetic axis. The equation of mechanical motion is given as:

$$T_e - T_L = \frac{J}{P}\frac{d\omega}{dt} \qquad (2.5)$$

where T_e is the developed electromagnetic torque of the machine, T_L is the load torque, P is the number of pairs of poles, and J is the inertia constant, while ω is the electrical speed of rotor rotation (rad/s), that is correlated with angle θ through

$$\theta = \int \omega dt \qquad (2.6)$$

The electromagnetic torque of the machine can be expressed in terms of instantaneous phase currents as:

$$T_e = -L_{aA}[\sin\theta(i_a i_A + i_b i_B + i_c i_C) + \sin(\theta + 4\pi/3)(i_a i_C + i_b i_A + i_c i_B) + \sin(\theta + 2\pi/3)(i_a i_B + i_b i_C + i_c i_A)] \quad (2.7)$$

It is obvious that these equations are much more complicated than equations of a DC machine. They constitute a seventh order system of differential equations with time varying coefficients.

For convenience, the stator and rotor voltage equations and stator and rotor flux linkage equations can be combined into matrix equations [Vas,1990]:

$$\underline{v}_{abc} = R_s \underline{i}_{abc} + \frac{d\underline{\psi}_{abc}}{dt}$$
$$\underline{v}_{ABC} = R_r \underline{i}_{ABC} + \frac{d\underline{\psi}_{ABC}}{dt} \quad (2.8)$$

$$\underline{\psi}_{abc} = \underline{L}_s \underline{i}_{abc} + \underline{L}_{sr} \underline{i}_{ABC}$$
$$\underline{\psi}_{ABC} = \underline{L}_r \underline{i}_{ABC} + \underline{L}'_{sr} \underline{i}_{abc} \quad (2.9)$$

where

$$\underline{v}_{abc} = \begin{bmatrix} v_a \\ v_b \\ v_c \end{bmatrix} \quad \underline{i}_{abc} = \begin{bmatrix} i_a \\ i_b \\ i_c \end{bmatrix} \quad \underline{v}_{ABC} = \begin{bmatrix} v_A \\ v_B \\ v_C \end{bmatrix} \quad \underline{i}_{ABC} = \begin{bmatrix} i_A \\ i_B \\ i_C \end{bmatrix} \quad (2.10)$$

$$\underline{L}_{sr} = L_{aA} \begin{bmatrix} \cos\theta & \cos(\theta + 2\pi/3) & \cos(\theta + 4\pi/3) \\ \cos(\theta + 4\pi/3) & \cos\theta & \cos(\theta + 2\pi/3) \\ \cos(\theta + 2\pi/3) & \cos(\theta + 4\pi/3) & \cos\theta \end{bmatrix} \quad (2.11)$$

$$\underline{L}_s = \begin{bmatrix} L_{aa} & L_{ab} & L_{ac} \\ L_{ba} & L_{bb} & L_{bc} \\ L_{ca} & L_{cb} & L_{cc} \end{bmatrix} \quad \underline{L}_r = \begin{bmatrix} L_{AA} & L_{AB} & L_{AC} \\ L_{BA} & L_{BB} & L_{BC} \\ L_{CA} & L_{CB} & L_{CC} \end{bmatrix} \quad (2.12)$$

Equations (2.1)-(2.4) (or (2.8)-2.12)) are rarely used even for induction machine simulation and are useless from the control point of view. Both stator and rotor equations are therefore transformed into a common system of perpendicular axes, that rotate at an arbitrary angular speed ω_a. The transformation is accomplished by applying two different transformation matrices for stator and rotor equations and quantities. These matrices are given with [Vas,1990]:

$$\underline{A}_s = \frac{2}{3}\begin{bmatrix} \cos\theta_s & \cos(\theta_s - 2\pi/3) & \cos(\theta_s + 2\pi/3) \\ -\sin\theta_s & -\sin(\theta_s - 2\pi/3) & -\sin(\theta_s + 2\pi/3) \\ 1/2 & 1/2 & 1/2 \end{bmatrix} \tag{2.13}$$

$$\underline{A}_r = \frac{2}{3}\begin{bmatrix} \cos\theta_r & \cos(\theta_r - 2\pi/3) & \cos(\theta_r + 2\pi/3) \\ -\sin\theta_r & -\sin(\theta_r - 2\pi/3) & -\sin(\theta_r + 2\pi/3) \\ 1/2 & 1/2 & 1/2 \end{bmatrix} \tag{2.14}$$

where the angles θ_s and θ_r are indicated in Figure 2.2 and $\theta_r=\theta_s-\theta$. The relationship between the new stator voltage and stator current components and the corresponding three phase components is established in the following way:

$$\begin{aligned} \underline{v}_s &= \underline{A}_s \underline{v}_{abc} & \underline{v}_r &= \underline{A}_r \underline{v}_{ABC} & \underline{\psi}_s &= \underline{A}_s \underline{\psi}_{abc} \\ \underline{i}_s &= \underline{A}_s \underline{i}_{abc} & \underline{i}_r &= \underline{A}_r \underline{i}_{ABC} & \underline{\psi}_r &= \underline{A}_r \underline{\psi}_{ABC} \end{aligned} \tag{2.15}$$

where

$$\underline{v}_s = \begin{bmatrix} v_{ds} \\ v_{qs} \\ v_{os} \end{bmatrix} \qquad \underline{i}_s = \begin{bmatrix} i_{ds} \\ i_{qs} \\ i_{os} \end{bmatrix} \qquad \underline{v}_r = \begin{bmatrix} v_{dr} \\ v_{qr} \\ v_{or} \end{bmatrix} \qquad \underline{i}_r = \begin{bmatrix} i_{dr} \\ i_{qr} \\ i_{or} \end{bmatrix} \tag{2.16}$$

Indices 's' and 'r' denote stator and rotor variables and parameters, respectively. The schematic illustration of the relationship between the two reference frames is shown in Figure 2.2.

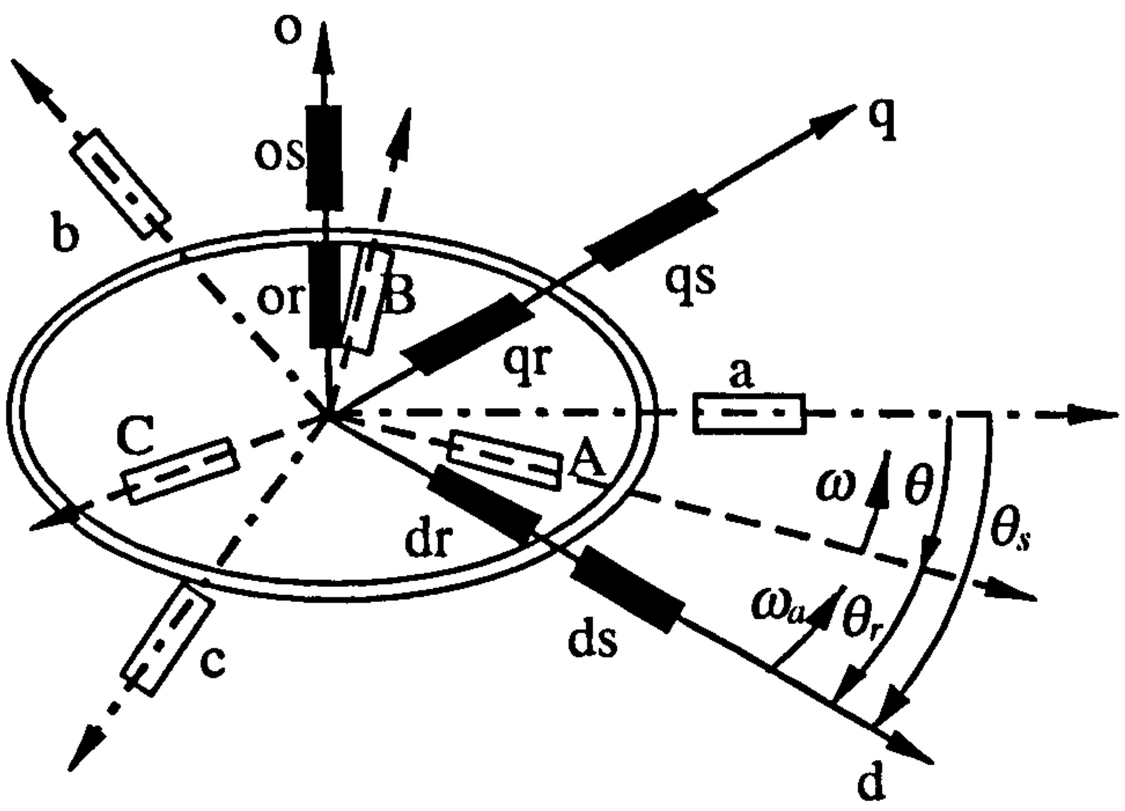

Figure 2.2: Illustration of winding transformation from three-phase domain to an arbitrary reference frame.

As induction machine stator winding is assumed to be star connected with isolated neutral and rotor winding is short circuited, there are no zero-sequence voltages and currents in the stator and rotor. Hence it follows that

$$v_{os}=v_{or}=0 \tag{2.17}$$

$$i_{os}=i_{or}=0 \tag{2.18}$$

$$\psi_{os}=\psi_{or}=0 \tag{2.19}$$

Upon completion of the transformation, the two-axis equations of an induction machine in an arbitrary reference frame are obtained in the following form:

$$\begin{aligned} v_{ds} &= R_s i_{ds} + \frac{d\psi_{ds}}{dt} - \omega_a \psi_{qs} \\ v_{qs} &= R_s i_{qs} + \frac{d\psi_{qs}}{dt} + \omega_a \psi_{ds} \end{aligned} \tag{2.20}$$

$$\begin{aligned} v_{dr} &= R_r i_{dr} + \frac{d\psi_{dr}}{dt} - (\omega_a - \omega)\psi_{qr} \\ v_{qr} &= R_r i_{qr} + \frac{d\psi_{qr}}{dt} + (\omega_a - \omega)\psi_{dr} \end{aligned} \tag{2.21}$$

where d-q axis flux linkages are given with:

$$\begin{aligned} \psi_{ds} &= L_s i_{ds} + L_m i_{dr} \\ \psi_{qs} &= L_s i_{qs} + L_m i_{qr} \end{aligned} \tag{2.22}$$

$$\begin{aligned} \psi_{dr} &= L_r i_{dr} + L_m i_{ds} \\ \psi_{qr} &= L_r i_{qr} + L_m i_{qs} \end{aligned} \tag{2.23}$$

Here L_s and L_r represent stator and rotor self-inductances and L_m stands for magnetising inductance. Speed ω_a is the angular speed of the reference frame. The relationship between stator inductance, rotor inductance and magnetising inductance and three-phase domain inductances is:

$$L_s=L_{aa} - L_{ab}=L_{\sigma s}+L_m \tag{2.24}$$

$$L_r=L_{AA} - L_{AB}= L_{\sigma r}+L_m \tag{2.25}$$

$$L_m=(3/2)L_{aA} \tag{2.26}$$

where $L_{\sigma s}$ and $L_{\sigma r}$ represent stator and rotor leakage inductances, respectively.

The equation of mechanical equilibrium remains the same,

$$T_e - T_L = \frac{J}{P}\frac{d\omega}{dt} \tag{2.5}$$

while electromagnetic torque may be expressed in terms of *d-q* axis variables as:

$$T_e = \frac{3}{2}P\left(\psi_{ds} i_{qs} - \psi_{qs} i_{ds}\right) \tag{2.27}$$

Correlation between stator quantities in an arbitrary reference frame and in phase domain is from (2.13) and (2.15)

$$\begin{aligned} f_{ds} &= \frac{2}{3}\left[f_a \cos\theta_s + f_b \cos\left(\theta_s - 2\pi/3\right) + f_c \cos\left(\theta_s + 2\pi/3\right)\right] \\ f_{qs} &= -\frac{2}{3}\left[f_a \sin\theta_s + f_b \sin\left(\theta_s - 2\pi/3\right) + f_c \sin\left(\theta_s + 2\pi/3\right)\right] \end{aligned} \tag{2.15a}$$

where *f* stands for voltage, current or flux linkage. The inverse correlation is

$$\begin{aligned} f_a &= f_{ds}\cos\theta_s - f_{qs}\sin\theta_s \\ f_b &= f_{ds}\cos\left(\theta_s - 2\pi/3\right) - f_{qs}\sin\left(\theta_s - 2\pi/3\right) \\ f_c &= f_{ds}\cos\left(\theta_s + 2\pi/3\right) - f_{qs}\sin\left(\theta_s + 2\pi/3\right) \end{aligned} \tag{2.15b}$$

The new induction machine model in *d-q* axis reference frame is significantly simplified, compared with equations (2.1) - (2.7). In particular, the model is now of the fifth order and even more importantly, all the coefficients in the differential equations are constants. On the other hand, all the *d-q* axis voltages and currents are fictitious and correlation with physically existing variables has to be established by means of (2.15). Based on the model in an arbitrary reference frame, induction machine models for any specified common reference frame can be obtained by appropriate setting of the reference frame angular speed value.

If reference frame angular speed equals zero (ω_d=0), induction machine model in stationary α-β reference frame results:

$$\begin{aligned} v_{\alpha s} &= R_s i_{\alpha s} + \frac{d\psi_{\alpha s}}{dt} \\ v_{\beta s} &= R_s i_{\beta s} + \frac{d\psi_{\beta s}}{dt} \end{aligned} \tag{2.28}$$

$$v_{\alpha r} = R_r i_{\alpha r} + \frac{d\psi_{\alpha r}}{dt} + \omega\psi_{\beta r}$$
$$v_{\beta r} = R_r i_{\beta r} + \frac{d\psi_{\beta r}}{dt} - \omega\psi_{\alpha r} \qquad (2.29)$$

$$T_e = \frac{3}{2} P\left(\psi_{\alpha s} i_{\beta s} - \psi_{\beta s} i_{\alpha s}\right) \qquad (2.30)$$

Flux linkage equations (2.22) - (2.23) remain to be valid, with appropriate change of indices $d \rightarrow \alpha$, $q \rightarrow \beta$. As in a squirrel-cage induction machine rotor winding is short-circuited, then $v_{dr}=v_{qr}=0$ and $v_{\alpha r}=v_{\beta r}=0$. Transformation angles in (2.13)-(2.14) are now $\theta_s=0$ and $\theta_r=-\theta$. Correlation between phase domain and transformed quantities is still given with (2.15a), (2.15b), where now $\theta_s=0$.

As the transformed model is formed in the orthogonal system of axes, it is possible to view one axis as a real axis and the other axis as an imaginary axis of a complex plane. It is therefore possible to introduce complex variables that will substitute real variables in the model. Complex variables defined in this way are called space vectors.

If the stator voltage space vector and stator current space vector are defined in stationary reference frame as

$$\bar{v}_s^s = v_{\alpha s} + j v_{\beta s} = \mathrm{v}_s e^{j\beta_s}$$
$$\bar{i}_s^s = i_{\alpha s} + j i_{\beta s} = \mathrm{i}_s e^{j\varepsilon_s} \qquad (2.31)$$

where

$$\bar{v}_s = \frac{2}{3}\left(v_a + \bar{a} v_b + \bar{a}^2 v_c\right)$$
$$\bar{i}_s = \frac{2}{3}\left(i_a + \bar{a} i_b + \bar{a}^2 i_c\right) \qquad (2.32)$$

$$\bar{a} = e^{j2\pi/3} \qquad (2.33)$$

then it follows that in arbitrary reference frame stator voltage and current space vectors can be expressed as:

$$\bar{v}_s = \bar{v}_s^s e^{-j\theta_s} = \mathrm{v}_s e^{j(\beta_s - \theta_s)} = v_{ds} + j v_{qs}$$
$$\bar{i}_s = \bar{i}_s^s e^{-j\theta_s} = \mathrm{i}_s e^{j(\varepsilon_s - \theta_s)} = i_{ds} + j i_{qs} \qquad (2.34)$$

From equations (2.20)-(2.23) and (2.34), the complex time domain model of an induction machine in arbitrary reference frame is obtained:

$$\begin{aligned} \bar{v}_s &= R_s \bar{i}_s + \frac{d\bar{\psi}_s}{dt} + j\omega_a \bar{\psi}_s \\ 0 &= R_r \bar{i}_r + \frac{d\bar{\psi}_r}{dt} + j(\omega_a - \omega)\bar{\psi}_r \end{aligned} \tag{2.35}$$

$$\begin{aligned} \psi_s &= L_s i_s + L_m i_r \\ \bar{\psi}_r &= L_r \bar{i}_r + L_m \bar{i}_s \end{aligned} \tag{2.36}$$

where

$$\bar{\psi}_s = \psi_s e^{j(\varphi_s - \theta_s)} \qquad \bar{\psi}_r = \psi_r e^{j(\varphi_r - \theta_s)} \qquad \bar{i}_r = i_r e^{j(\varepsilon_r - \theta_s)} \tag{2.37}$$

Angles β_s, ε_s, φ_s, φ_r and ε_r in (2.34) and (2.37) define instantaneous position of stator voltage, stator current, stator flux, rotor flux and rotor current space vectors, respectively, with respect to the stationary phase *a* magnetic axis.

Electromagnetic torque can be expressed in terms of space vectors as:

$$T_e = \frac{3}{2} P \frac{L_m}{L_r} \mathrm{Im}\left(\bar{i}_s \bar{\psi}_r^{\,*}\right) \tag{2.38}$$

where * denotes complex conjugation. Equations (2.35)-(2.36) describe space vector equivalent circuit of an induction machine, shown in Figure 2.3.

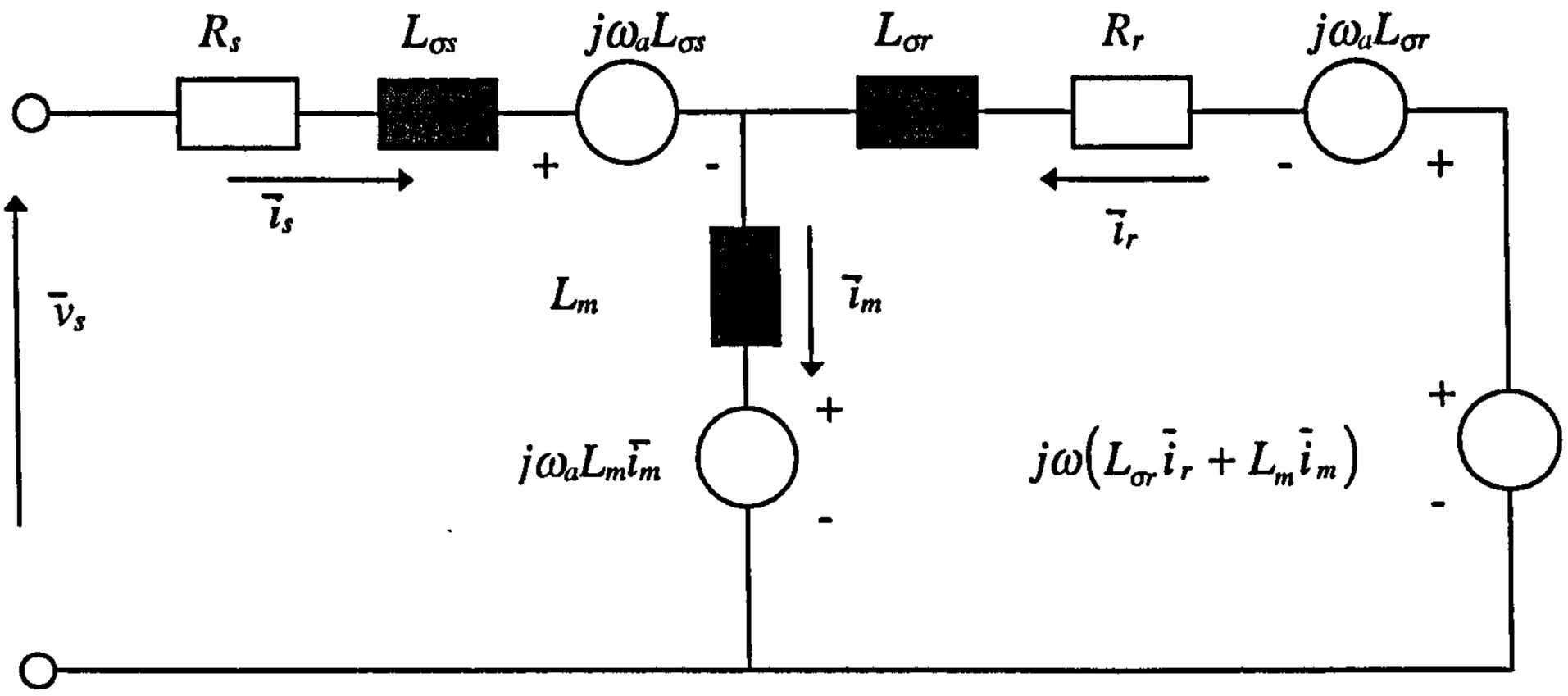

Figure 2.3: Equivalent circuit of an induction machine in terms of space vectors in an arbitrary reference frame.

2.3 Principles of rotor flux oriented control

The clue for successful decoupled flux and torque control in an induction machines is in the choice of the speed of the reference frame. If the angular speed of the reference frame is selected as equal at all times to the angular speed of rotation of the rotor flux space vector ω_r, d-axis of the reference frame will at all times coincide with the rotor flux space vector [Vas,1990]. This is illustrated in Figure 2.4.

It can be seen from Figure 2.4 that the stator transformation angle θ_s is equal to rotor flux space vector position angle φ_r, and that the d-axis of the reference frame is fixed to the rotor flux vector. The following relationships hold true:

$$\theta_s=\phi_r \qquad \theta_r=\phi_r-\theta \qquad \omega_a=\omega_r \qquad \omega_r=d\phi_r/dt \tag{2.39}$$

and

$$\overline{\psi}_r = \psi_{dr} + j\psi_{qr} = \psi_r \tag{2.40}$$

i.e.

$$\psi_{dr}=\psi_r,\ \psi_{qr}=0 \qquad d\psi_{qr}/dt = 0 \tag{2.41}$$

Figure 2.4 shows the positions of stator current and rotor flux space vectors in the rotor flux oriented reference frame.

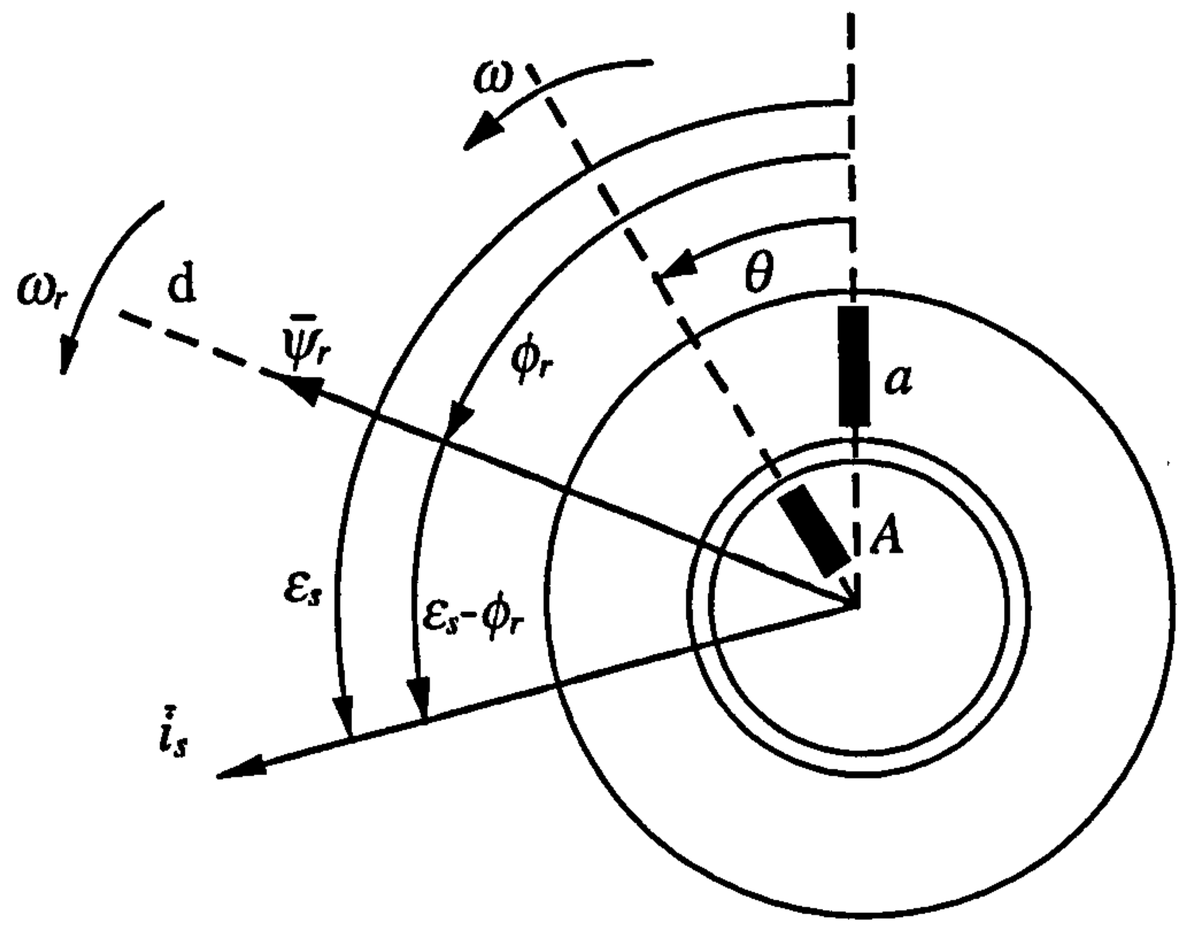

Figure 2.4: Illustration of space vectors in common reference frame fixed to the rotor flux space vector.

Combining equations (2.38) and (2.40), electromagnetic torque can be expressed as

$$T_e = \frac{3}{2} P \frac{L_m}{L_r} \psi_r i_{qs} \tag{2.42}$$

It is assumed further on that the induction machine is supplied from a current source. Therefore stator currents are impressed and stator voltage equation in (2.35) can be omitted from further consideration. This leads to the concept of the current-fed machine, that significantly simplifies the vector control system structure [Vas, 1990]. In practice, current-fed induction machine is obtained by controlling the voltage source inverter switching instants on the basis of motor phase current closed-loop control [Boldea and Nasar, 1992; Vas, 1990; Novotny and Lipo, 1996; Trzynadlowski, 1994]. Hysteresis current control is the most frequently utilised method of stator phase current closed-loop control.

Substituting equation (2.40) into the rotor voltage equation of (2.35), the rotor voltage equation can be rewritten as:

$$0 = \frac{1}{T_r} \psi_r + \frac{d\psi_r}{dt} + j(\omega_r - \omega)\psi_r - \frac{1}{T_r} L_m \bar{i}_s \tag{2.43}$$

where rotor time constant is introduced as

$$T_r = L_r / R_r \tag{2.44}$$

Separation of equation (2.43) into real part and imaginary part yields the following equations:

$$\begin{aligned} \psi_r + T_r \frac{d\psi_r}{dt} &= L_m i_{ds} \\ (\omega_r - \omega)\psi_r T_r &= L_m i_{qs} \end{aligned} \tag{2.45}$$

where $\omega_{sl} = \omega_r - \omega$ is the angular slip frequency. The equations (2.42) and (2.45) fully describe a current fed induction machine in rotor flux oriented reference frame. It follows that rotor flux can be controlled by stator d-axis current only. As electromagnetic torque is proportional to rotor flux then, if stator d-axis current is constant, electromagnetic torque depends on stator q-axis current only. Rotor flux is therefore controllable by stator d-axis current component and is constant if i_{ds} is constant. Torque is then controllable directly by stator q-axis current. Current i_{ds} plays the role of excitation current in a DC machine, while current i_{qs} corresponds to armature current in a DC machine. An induction machine has therefore been converted into its

DC equivalent in this specific reference frame. Block-diagram of a current-fed rotor flux oriented induction machine is shown in Figure 2.5.

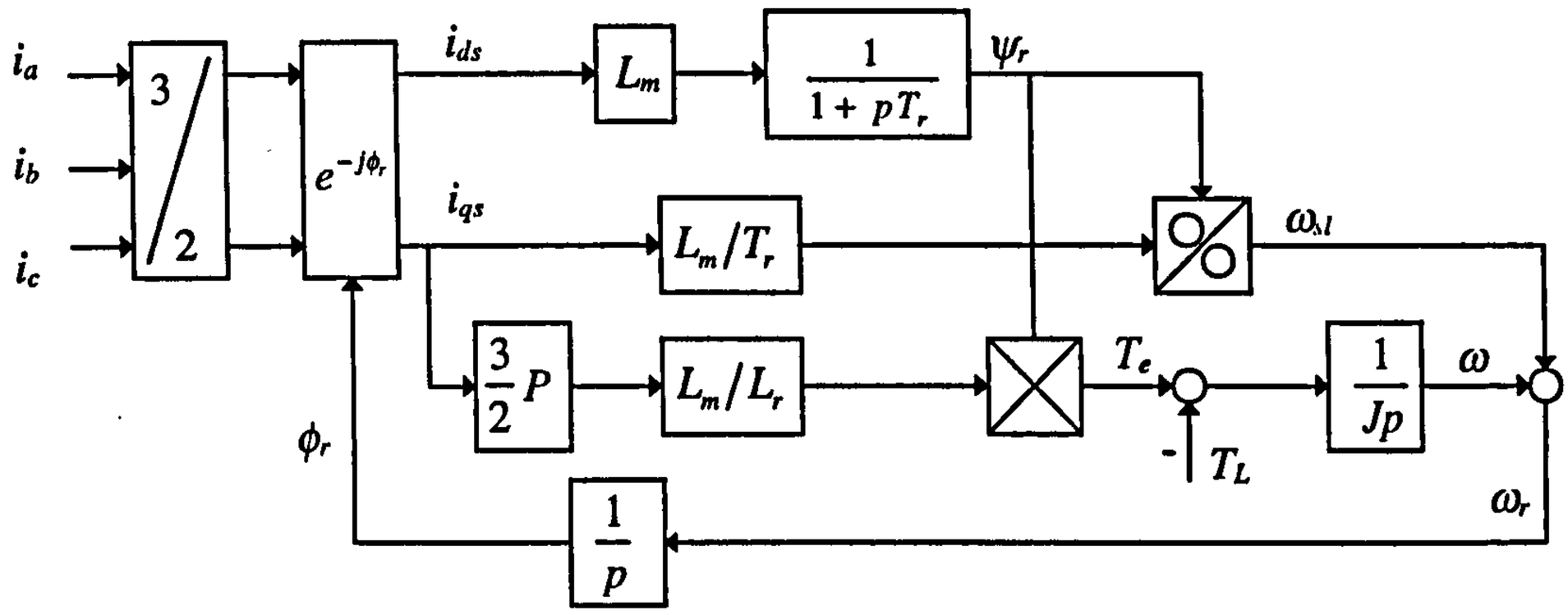

Figure 2.5: Block-diagram of a rotor flux oriented induction machine.

Blocks "3/2" and "exp($-j\phi_r$)" in Fig. 2.5 describe the co-ordinate transformation given with (2.15a) as a two-step transformation (phase domain to two-phase stationary system of axis to rotating two-phase system of axis).

It should be emphasised once more that decoupled rotor flux and torque control, described with (2.42) and (2.45), is obtained if the machine can be regarded as being fed from a current source, so that omission of stator voltage equation of (2.35) from further considerations is enabled. If the machine cannot be considered as being current-fed, it becomes necessary to take into account the stator voltage equation as well. Resulting control structure becomes significantly more involved as correlation between stator *d-q* axis voltages and currents is not decoupled. As practical realisations predominantly utilise current-controlled voltage source inverter (CRPWM) as a supply, and as current control can be done in such a way that current-fed concept holds true, the more complicated voltage-fed case is excluded from further consideration.

2.4 Principles of stator flux oriented control

As mentioned previously, induction machine can be operated with orientation along one of the three flux space vectors. When the reference frame is fixed to stator flux space vector, stator flux oriented control of an induction machine results [Vas, 1990; Novotny and Lipo, 1996].

The basic principle of stator flux oriented control of an induction machine can be again derived from the constant parameter induction machine model in an arbitrary reference frame given with (2.35)-(2.36). The procedure closely follows the one explained in the preceding section. Reference frame angular speed is now selected as equal to the speed of rotation of the stator flux space vector, that is $\omega_a=\omega_s$. Stator flux space vector therefore coincides at all times with *d*-axis of the common reference frame, so that

$$\omega_a=\omega_s \qquad \theta_s=\phi_s \qquad \theta_r=\phi_s-\theta \qquad \omega_s=d\phi_s/dt \tag{2.46}$$

Therefore

$$\overline{\psi}_s = \psi_{ds} + j\psi_{qs} = \psi_s \qquad \psi_{qs} = 0 \qquad d\psi_{qs}/dt = 0 \tag{2.47}$$

Rotor current and rotor flux space vector now become

$$\bar{i}_r = \frac{1}{L_m}\left(\psi_s - L_s\bar{i}_s\right) \tag{2.48}$$

$$\overline{\psi}_r = \frac{L_r}{L_m}\left(\psi_s - L_s\bar{i}_s\right) + L_m\bar{i}_s \tag{2.49}$$

Hence, rotor voltage equation of (2.35) can be expressed as:

$$0 = R_r\left(\frac{\psi_s}{L_m} - \frac{L_s}{L_m}\bar{i}_s\right) + \frac{L_r}{L_m}\frac{d\psi_s}{dt} - \frac{L_sL_r}{L_m}\frac{d\bar{i}_s}{dt} + L_m\frac{d\bar{i}_s}{dt} + j\omega_{sl}\left(\frac{L_r}{L_m}\psi_s - \frac{L_sL_r}{L_m}\bar{i}_s + L_m\bar{i}_s\right) \tag{2.50}$$

where $\omega_{sl}=\omega_s-\omega$ is the angular slip frequency. The position of space vectors is shown in Figure 2.6 for the stator flux oriented reference frame.

Torque equation becomes

$$T_e = \frac{3}{2}P\psi_s i_{qs} \tag{2.51}$$

It is again assumed that the machine can be treated as being current fed, so that stator voltage equation is omitted from consideration.

It follows that equation (2.50) is more complicated than the rotor voltage equation formulated in the rotor flux oriented reference frame. This has the consequence that when the induction machine is current fed, the implementation of stator flux oriented

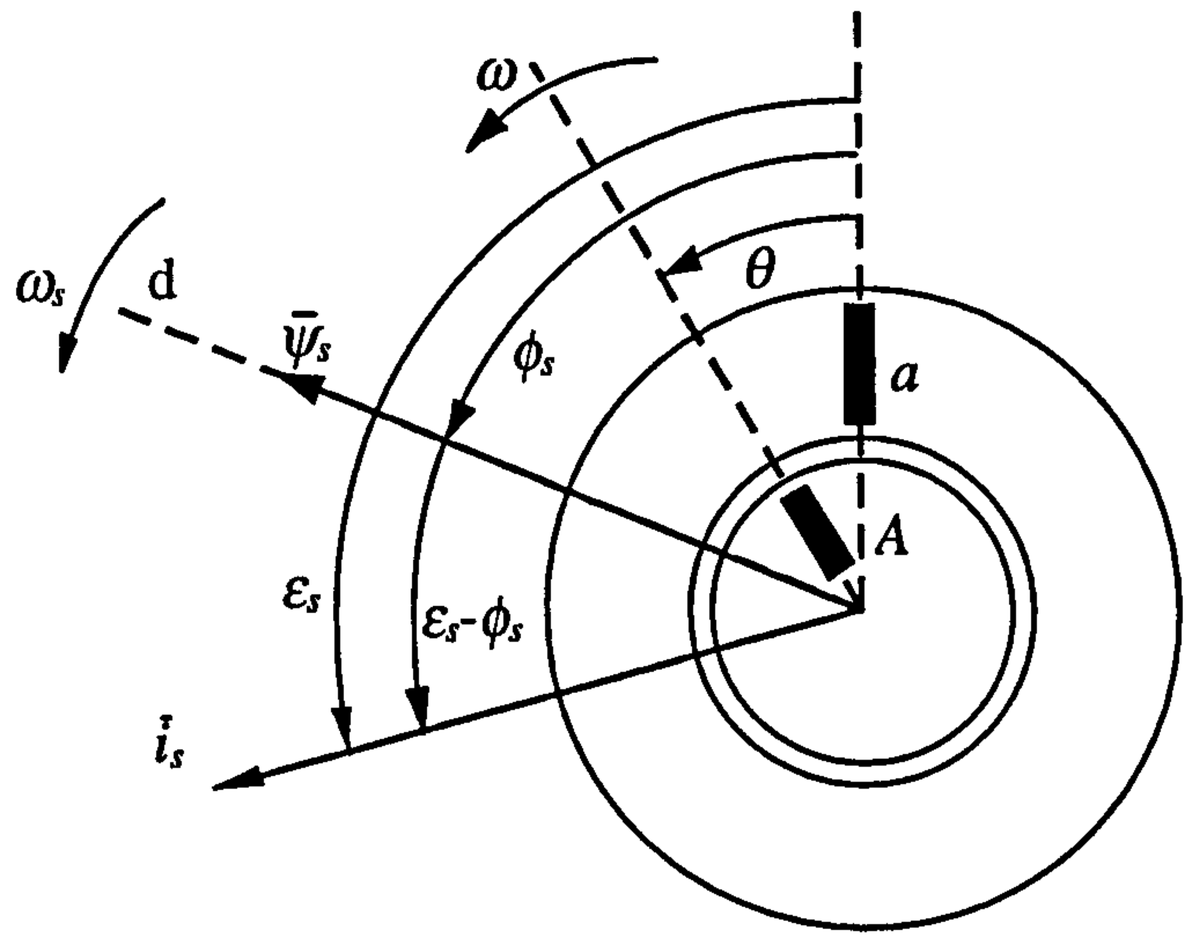

Figure 2.6: Illustration of space vectors in common reference frame fixed to the stator flux space vector.

control will be more complicated than the implementation of the rotor flux oriented control. This is also the reason why stator flux oriented control of induction machines is less frequently used in industrial applications.

Resolution of equation (2.50) into real and imaginary components yields

$$\begin{aligned} \psi_s + T_r \frac{d\psi_s}{dt} &= L_s i_{ds} + \left(L_s T_r - \frac{L_m^2}{R_r} \right) \left(\frac{di_{ds}}{dt} - \omega_{sl} i_{qs} \right) \\ L_s i_{qs} &= \omega_{sl} T_r \psi_s - \left(L_s T_r - \frac{L_m^2}{R_s} \right) \left(\frac{di_{qs}}{dt} - \omega_{sl} i_{ds} \right) \end{aligned} \tag{2.52}$$

Equations (2.52) have to be used for stator flux oriented control. However, it can be seen that there exists a coupling between the torque producing stator current component i_{qs} and the stator flux producing current component i_{ds}. In order to eliminate the cross-coupling between these two current components, a decoupling circuit has to be utilised. If the leakage coefficient is introduced as $\sigma = 1 - L_m^2/(L_s L_r)$, equations (2.52) can be expressed as follows

$$\begin{aligned} \psi_s + T_r \frac{d\psi_s}{dt} &= L_s \left(i_{ds} + \sigma T_r \frac{di_{ds}}{dt} \right) - \sigma L_s T_r \omega_{sl} i_{qs} \\ i_{qs} + \sigma T_r \frac{di_{qs}}{dt} &= \omega_{sl} \frac{T_r}{L_s} \left(\psi_s - \sigma L_s i_{qs} \right) \end{aligned} \tag{2.53}$$

Thus, it follows from equation (2.53) that the required stator d-axis current reference and slip frequency can be expressed as

$$i_{ds}^{*} = \frac{1}{1+p\sigma T_r^{*}}\left[\left(1+pT_r^{*}\right)\frac{\psi_s^{*}}{L_s^{*}} + \sigma T_r^{*}\omega_{sl}^{*} i_{qs}^{*}\right] \tag{2.54}$$

and

$$\omega_{sl}^{*} = \frac{\left(1+p\sigma T_r^{*}\right) i_{qs}^{*}}{\psi_s^{*} T_r^{*} / L_s - \sigma T_r^{*} i_{ds}^{*}} \tag{2.55}$$

where $p=d/dt$. Asterisk denotes reference quantities.

Equations (2.54), (2.55) define the required decoupling circuit. Thus, when the correct machine parameters are used in these equations, the correct value of i_{ds} is obtained for a given value of i_{qs} and stator flux ψ_s is not altered by any changes in the torque current reference. Equations (2.54) - (2.55) serve directly as a mean for creation of an indirect feed-forward stator flux oriented control scheme. Figure 2.7 shows schematic of such an indirect stator flux orientated induction machine, supplied by a current-regulated PWM inverter. Blocks "$\exp(j\phi_s)$" and "2/3" describe inverse co-ordinate transformation, given with (2.15b), as a two-step transformation.

As has already been noted, the research described in this thesis applies to rotor flux oriented control. The reason for inclusion of this section, that describes stator flux oriented control, is that a number of schemes of sensorless vector control, that are to be reviewed in chapter 3, have been developed for stator flux oriented control (or its simplified versions).

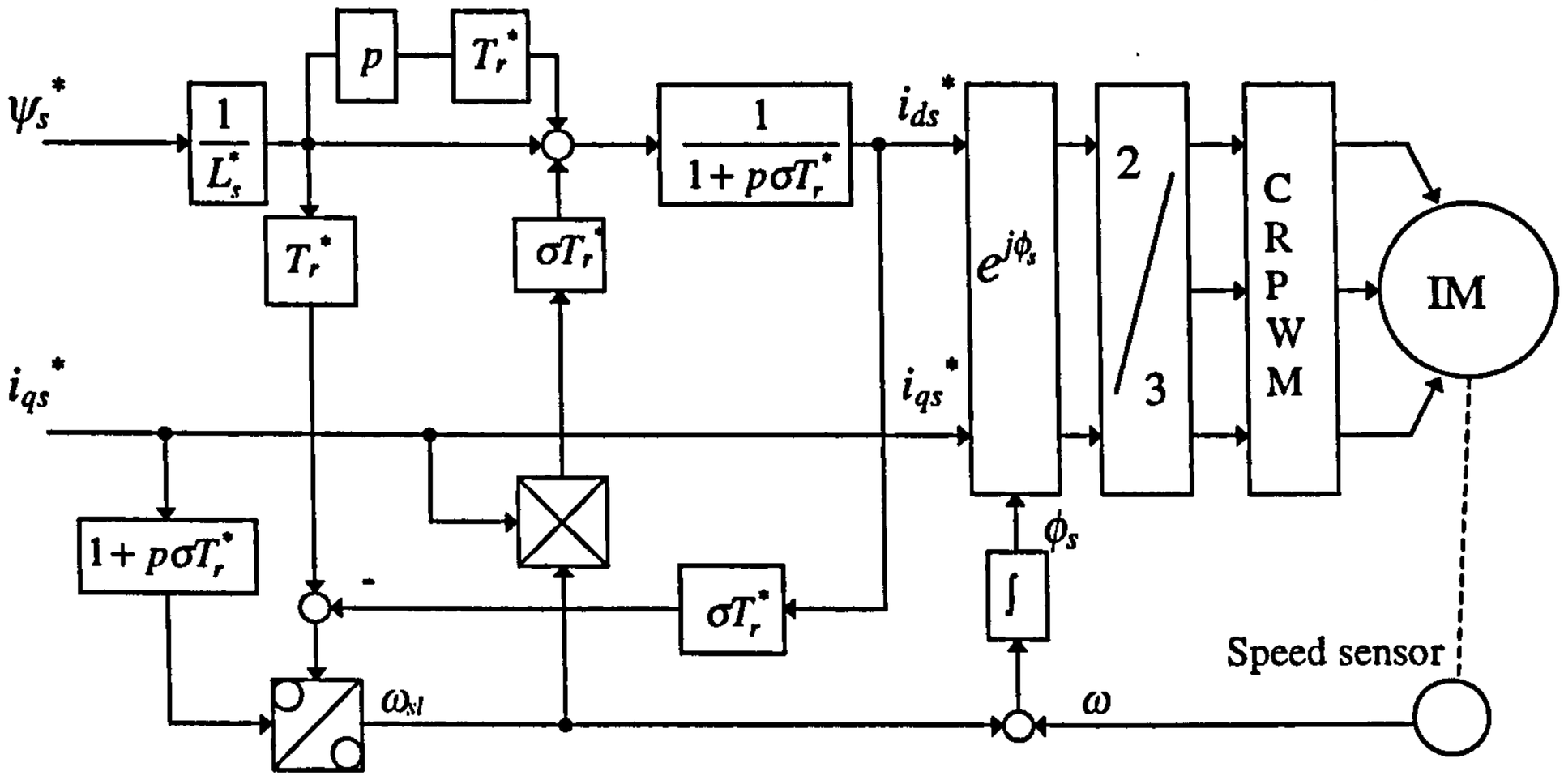

Figure 2.7: Indirect feed-forward stator flux oriented control of an induction machine.

2.5 Control schemes of a rotor flux oriented induction machine with speed sensor

There are basically two different types of rotor flux oriented control: direct and indirect control techniques. The direct scheme relies on the direct measurement or estimation of the rotor flux or stator flux vector amplitude and position. The indirect method uses a machine model in the feed-forward manner and performs calculations on the basis of references. In contrast to direct methods, the indirect methods are highly dependent on machine parameters. Traditional direct vector control schemes use search coils, tapped windings, or Hall effect sensors for flux sensing. This introduces limitations due to requirement to change the machine structure. Many applications use indirect schemes, since these require relatively simpler hardware and can have better overall performance.

2.5.1 Indirect feed-forward rotor flux oriented control

The basic structure of indirect feed-forward rotor flux oriented control is illustrated in Figure 2.8. The control system structure is directly derived from (2.42), (2.45) and it is assumed that the drive operates in the base speed region only, so that rotor flux reference is constant and equal to rated rotor flux value.

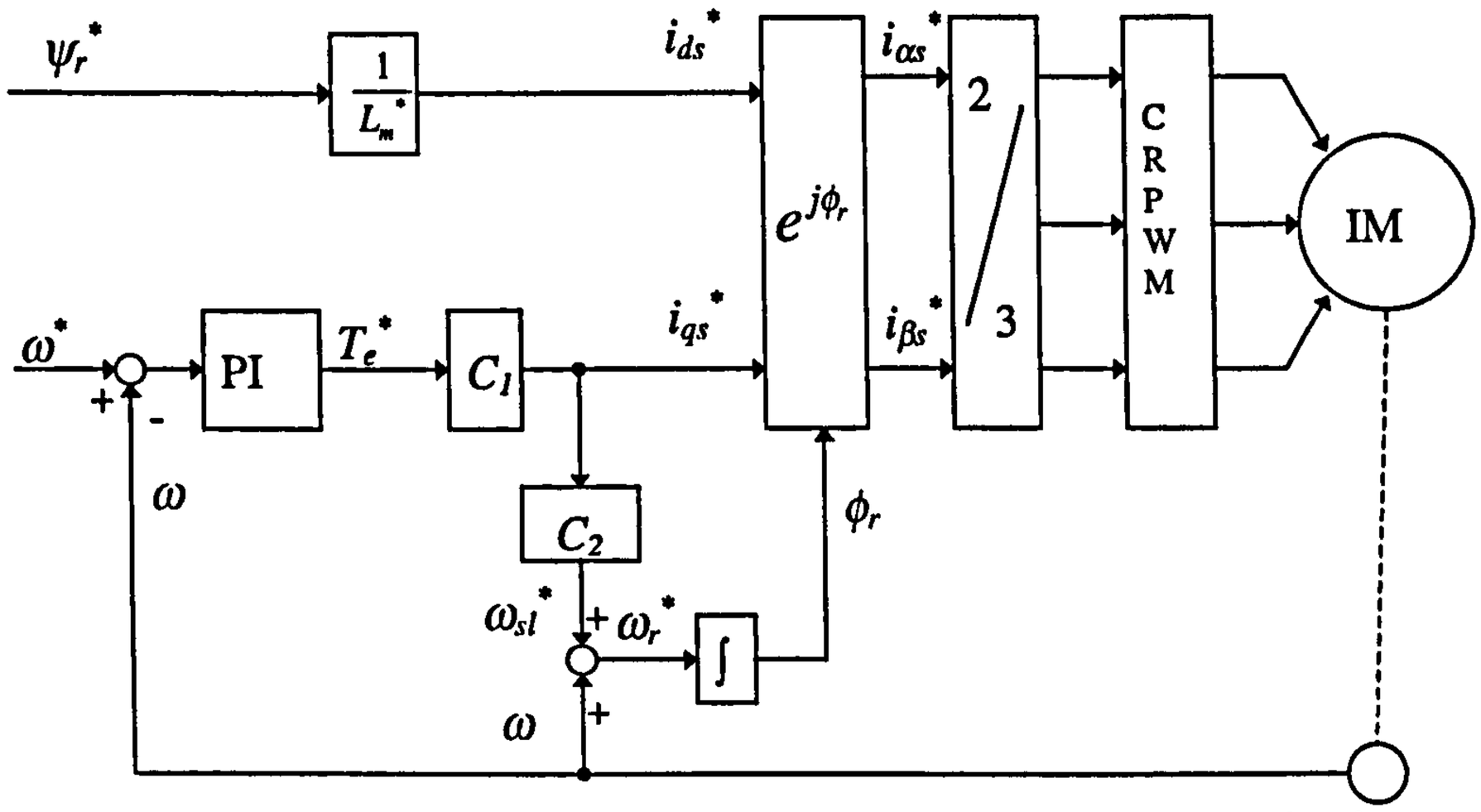

$$C_1 = \left(\frac{3}{2} P \frac{L_m^*}{L_r^*} \psi_r^*\right)^{-1} \qquad C_2 = \frac{L_m^*}{T_r^* \psi_r^*}$$

Figure 2.8: Indirect feed-forward rotor flux oriented control of an induction machine.

The induction machine is current-fed using a current regulated PWM inverter. In Figure 2.8, the torque producing current reference i_{qs}^* is obtained as the scaled output of the PI speed controller. Flux producing current reference i_{ds}^* is generated from flux reference by division with the magnetising inductance. These two currents are then transformed to stator currents in the stationary reference frame. The stator current components in stationary reference frame can be obtained by applying the following transformation:

$$\begin{aligned} i_{\alpha s}^* &= i_{ds}^* \cos\phi_r - i_{qs}^* \sin\phi_r \\ i_{\beta s}^* &= i_{ds}^* \sin\phi_r + i_{qs}^* \cos\phi_r \end{aligned} \tag{2.56}$$

Block "2/3" completes transition from *d-q* to phase variables, described with (2.15b). The angular slip frequency reference is calculated by using i_{qs}^*. Integration of the sum of the measured speed and angular speed reference yields transformation angle ϕ_r. The rotor speed is monitored by a speed sensor (or is derived from position sensor output) and is utilised as feedback signal for closed-loop speed control and for calculation of the orientation angle.

The expressions used for the calculations of i_{qs}^* and ω_{sl}^* in Figure 2.8 can be obtained from (2.42) and (2.45). If rotor flux reference is constant, then:

$$i_{ds}^* = \frac{\psi_r^*}{L_m^*} \tag{2.57}$$

and

$$i_{qs}^* = \frac{2}{3P}\frac{T_e^*}{\psi_r^*}\frac{L_r^*}{L_m^*} \tag{2.58}$$

$$\omega_{sl}^* = \frac{L_m^*}{T_r^*}\frac{i_{qs}^*}{\psi_r^*} = \frac{1}{T_r^*}\frac{i_{qs}^*}{i_{ds}^*} \tag{2.59}$$

$$\phi_r = \int (\omega_{sl}^* + \omega) dt \tag{2.60}$$

Hence C_1 of Figure 2.8 equals $C_1 = \frac{2}{3P}\frac{L_r^*}{L_m^*}\frac{1}{\psi_r^*}$ and C_2 of Figure 2.8 equals $C_2 = \frac{L_m^*}{T_r^*}\frac{1}{\psi_r^*}$.

2.5.2 Direct feedback rotor flux oriented control

Direct rotor flux oriented control means that rotor flux space vector is estimated directly from measured quantities. Figure 2.9 shows the schematic of the drive with a current-fed induction machine employing direct rotor flux oriented control. Drive operation in field-weakening region is now included.

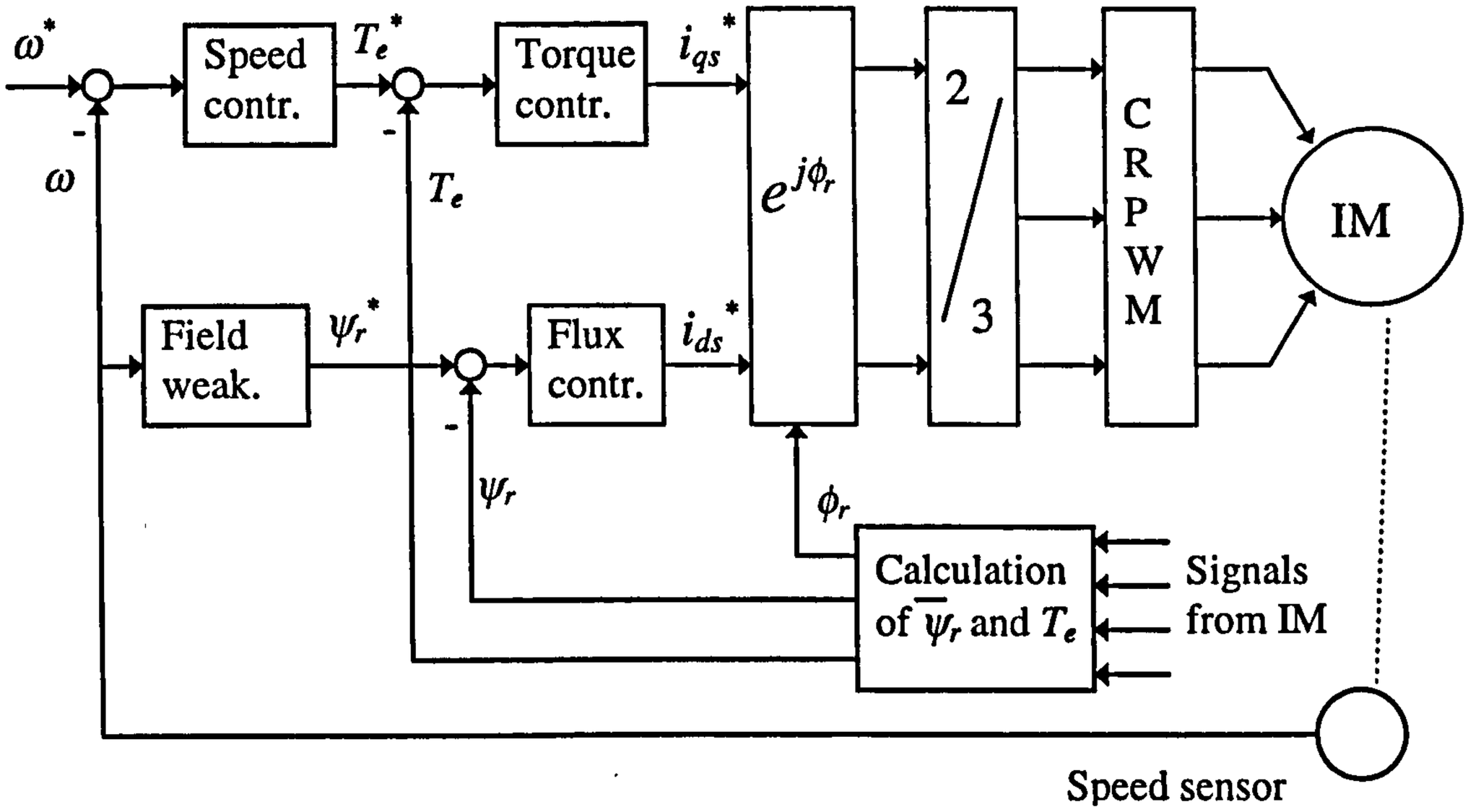

Figure 2.9: Direct feedback control of rotor flux oriented induction machine.

In the drive scheme of Figure 2.9, rotor flux space vector is estimated from, say, measured stator currents and voltages. Speed sensor is utilised to provide feedback signal for speed control. The flux producing stator current reference i_{ds}^* is obtained as the output of the flux controller, while the torque producing stator current reference i_{qs}^* is obtained as the output of the torque controller (torque controller is optional and may be omitted). The reference currents are then transformed into the stator phase currents. Reference torque, which is the input of the torque controller, is obtained from the speed controller. Reference rotor flux is obtained from the field-weakening block. When the conventional field-weakening technique is used, then below base speed rotor flux reference is constant, and above base speed it is reduced inversely proportionally to the rotor speed.

The rotor flux estimation method in Figure 2.9 can be based on measurement of stator currents and stator voltages. From induction machine model equations (2.22), (2.23),

(2.28), (2.29), the procedure of estimation can be realised by using the following equations:

$$\psi_{\alpha s} = \int \left(v_{\alpha s} - R_s i_{\alpha s}\right) dt$$
$$\psi_{\beta s} = \int \left(v_{\beta s} - R_s i_{\beta s}\right) dt \qquad (2.61)$$

$$\psi_{\alpha r} = \left(1+\sigma_r\right)\psi_{\alpha s} - \sigma \frac{L_s L_r}{L_m} i_{\alpha s}$$
$$\psi_{\beta r} = \left(1+\sigma_r\right)\psi_{\beta s} - \sigma \frac{L_s L_r}{L_m} i_{\beta s} \qquad (2.62)$$

$$\psi_r = \sqrt{\psi_{\alpha r}^2 + \psi_{\beta r}^2} \qquad \cos\varphi_r = \psi_{\alpha r} / \psi_r \qquad \sin\varphi_r = \psi_{\beta r} / \psi_r \qquad (2.63)$$

where $\sigma_r = L_{\sigma r}/L_m$.

Equation for torque calculation is

$$T_e = \frac{3}{2} P\left(\psi_{\alpha s} i_{\beta s} - \psi_{\beta s} i_{\alpha s}\right) \qquad (2.30)$$

The principle difference between direct and indirect field orientation is the way in which rotor flux spatial position is calculated. In the indirect scheme this calculation does not require measurement of electromagnetic quantities. Only speed (position) measurement is required for orientation purposes. In the direct schemes rotor flux angle estimation requires measurement of electromagnetic variables such as stator currents and voltages. Apart from the scheme based on stator voltage and current measurement, another frequently employed method of rotor flux position estimation relies on stator current and rotor speed (position) measurement.

The scheme of rotor flux oriented control dealt with further on in this thesis is the indirect feed-forward scheme of subsection 2.5.1.

2.6 Summary

The principles of vector control of induction machines are presented in this chapter. Constant parameter induction model is at first introduced. Starting from the basic model of an induction machine, the transformation of induction machine from three-phase to *d-q* reference frame is described. Induction machine model in terms of space

vectors is developed next. In order to control the torque producing and flux producing currents in an induction machine separately, induction machine model in rotor flux oriented reference frame is derived. It is shown that if suitable reference frame is selected, it is possible to control an induction machine in the similar way to a DC machine.

Schemes of stator flux oriented control and rotor flux oriented control of induction machine are discussed as well. Stator flux oriented control is more complicated than rotor flux oriented control as a decoupling circuit is needed for elimination of the cross-coupling between torque producing component and flux producing component of the stator current.

The basic structures of direct control and indirect control of rotor flux oriented induction machine are reviewed. They differ with respect to the ways of obtaining the rotor flux position angle. The scheme selected for further investigation is, as already pointed out, indirect feed-forward rotor flux oriented control.

3 REVIEW OF METHODS OF SENSORLESS VECTOR CONTROL

3.1 Introduction

Sensorless vector control of an induction machine, as discussed previously, has attracted wide attention in recent years. Many attempts have been made in the past to extract the speed signal of the induction machine from measured stator currents and voltages. The first attempts have been restricted to techniques which are only valid in the steady-state and can only be used in low cost drive applications, not requiring high dynamic performance [Abbondanti and Brennen, 1975]. Different, more sophisticated techniques are required for high performance applications in vector controlled drives. In a sensorless drive, speed information and control should be provided with an accuracy of 0.5% or better, from zero to the highest speed, for all operating conditions and independent of saturation levels and parameter variations [Vas, 1998]. In order to achieve good performance of sensorless vector control, different speed estimation methods have been proposed, so that a variety of schemes exist nowadays In this chapter, basic principles of different speed estimation schemes will be reviewed and discussed. Speed estimation by utilising various parasitic effects (rotor slot harmonics, saliency etc.) will be discussed in section 3.2. Majority of existing speed estimation schemes are based on the induction machine model. Hence detailed discussion of induction machine model based speed estimation occupies the remainder of the chapter. In section 3.3, speed estimation schemes based purely on an induction machine model are reviewed. All the schemes discussed in section 3.3 belong to open-loop speed estimation group of methods. Previous work on closed-loop speed estimation is reviewed in section 3.4. Model reference adaptive control (MRAC) based, observer based and extended Kalman filter based speed estimation schemes are elaborated in each of the three consecutive sub-sections, respectively. Finally, section 3.5 summaries the chapter.

3.2 Speed estimation from stator current spectrum

Stator current harmonics arising from rotor mechanical and magnetic saliencies, such as rotor slotting, rotor eccentricity and magnetic saturation, are speed dependent. They are

independent of time-varying machine parameters and exist at any non-zero speed. Digital signal processing and spectral estimation techniques have made it possible to extract these harmonics with minimal data collection and processing time. Therefore, the slip frequency and rotor speed of the machine can be estimated by utilising, for example the rotor slot harmonics, monitored from the stator currents.

Many schemes that employ saliency harmonics for slip frequency and rotor speed estimation have been reported. These methods can be divided into two major groups [Degner and Lorenz, 1997]:

1) those that use the fundamental excitation to estimate the rotor speed, and
2) those that use a separate excitation signal from the fundamental excitation to estimate the rotor speed.

The rotor slot harmonics can be detected by using monitored stator currents or stator voltages. As monitoring of stator currents is always required anyway, detection of rotor slot harmonics by using stator currents is preferred, so that voltage monitoring can be avoided. Rotor slot harmonic based speed estimation does not require separate excitation signal.

Ferrah at al [1992b] proposed a speed estimation scheme that uses FFT technique to extract rotor slot harmonics. In this technique it is assumed that these air-gap flux harmonics are a result of the interaction of air-gap permeance and harmonic magnetomotive force waves. Only harmonics due to slotting and saturation are considered. The rotor slots produce air-gap permeance waves with a spatial distribution dependent on the number of rotor slots. This interacts with the fundamental (magnetising) component of air-gap magnetomotive force (mmf) resulting from both stator and rotor fundamental mmf's. The modulation process produces two harmonic components of air-gap flux density with frequencies displaced from the rotor speed related frequency by the fundamental frequency of the stator current [Ferrah et al, 1992b]. Speed is estimated by decomposition of stator current signal into its harmonic components to determine the speed dependent slot harmonic frequency, f_{sh}, and the machine fundamental frequency f_e.

The basic principle of this scheme is as follows. For a given pole pitch and supply frequency f_e, the speed of the fundamental rotating field is constant and is the

synchronous speed $\omega_e=2\pi f_e$. Synchronous speed of the rotor in mechanical revolutions per minute (rpm) is given by the well-known equation:

$$n_e = \frac{60 f_e}{P} \tag{3.1}$$

where n_e is the synchronous speed and P is the number of pole pairs. The slip, s, is the difference between the synchronous speed n_e and the actual speed n. It is often expressed as a fraction of the synchronous speed as:

$$s = \frac{n_e - n}{n_e} \tag{3.2}$$

It follows that

$$n=(1-s)n_e \tag{3.3}$$

and

$$f=(1-s)f_e \tag{3.4}$$

Angular frequency of slot harmonics is given with [Ferrah, 1992a]:

$$\omega_{sh} = \frac{Z}{P}\omega \pm \omega_e \tag{3.5}$$

where Z is the number of rotor slots. Therefore, using (3.1) to (3.5), the rotor mechanical speed n in rpm is expressed and calculated by the following expression:

$$n = \frac{60}{Z}(f_{sh} \pm f_e) \tag{3.6}$$

The proposed scheme was operated quite satisfactorily in a wide speed range, down to 2 Hz. The error between the detected and reference speeds was within ± 15 rpm. Due to the limited processing power and sampling rate of the hardware, the dynamic performance was relatively poor. Beguenane et al [1995, 1996], reported on extraction of slip speed estimate rather than speed estimate on the basis of the slot harmonic frequency identification.

The rotor slot signal is regarded as insufficient in bandwidth for use as speed feedback signal in a high performance drive. However, it can be used for parameter tuning of a sensorless drive with speed estimation based on machine-model method [Jiang and Holtz, 1997; Hurst et al 1994]. The proposed algorithm [Hurst et al, 1994] employs

digital signal processing techniques including the FFT, to detect the speed-related harmonics induced by rotor slots and rotor eccentricity. The estimation result is then used to tune the parameters of a model of the machine and the load. A speed observer based on the mechanical model provides a speed signal to the field-oriented control algorithm. As current harmonic spectral estimation provides a parameter-independent speed signal, the sensorless field-oriented drive has a good performance at very low speed.

A similar scheme was proposed by Hurst et al [1997]. The estimated speed obtained from current harmonic spectrum was used to tune the parameters of a MRAC based speed estimator. The proposed scheme combined the best attributes of both model based speed estimation and harmonic detection method to obtain improved sensorless control of an induction machine. The harmonic detection scheme provides accurate rotor speed updates during steady-state operation down to 1 Hz source frequency.

The speed can also be detected through the machine terminal voltage spectrum. Zinger et al [1990] proposed speed estimation scheme through detecting the harmonics from measured voltages of the tapped stator windings.

It is also possible to estimate rotor speed in an induction machine by tracking of high frequency magnetic saliency created by magnetic saturation (main flux or leakage flux saturation) at zero or low speeds. For this purpose high frequency voltages are injected in the stator. The injected voltage can be produced by the PWM voltage source inverter used in the drive. Jansen and Lorenz [1996] proposed a sensorless control of an induction machine by utilising saturation induced saliencies. The tracking method incorporates a signal injection scheme utilising the same inverter that supplies the fundamental excitation, and a demodulation scheme.

Degner and Lorenz [1997] proposed a speed estimation scheme utilising rotor slot harmonics and carrier frequency signal injection. A carrier frequency voltage excitation is used to produce a carrier frequency current which contains the desired information. A closed-loop tracking observer is then used to estimate the rotor position. Due to its reliance on a spatial saliency and carrier frequency signal injection, the technique is very robust over a wide speed range, including low and zero speed. A method based on high frequency current injection into d-axis current was proposed by [Yong et al, 1994].

Speed estimation using multiple saliencies was proposed by Degner and Lorenz [1998], where an induction machine model with multiple spatial saliencies was developed.

Cilia et al [1998b] presented another method of speed estimation by using real-time adaptive filter. The recursive maximum likelihood technique is used to track the slot harmonics. The recursive maximum likelihood method tunes the centre frequency of the bandpass filter and ensures the final speed estimate with an error less than 0.1%. Ferrah et al [1996, 1998] proposed a speed estimator based on real-time adaptive filter, whose parameters are updated in time using a recursive algorithm, for rotor slot harmonic analysis. It was claimed that the accuracy is better than 0.1 %.

Rotor eccentricity in any induction machine is an unavoidable result of the manufacturing process. The compromise between cost and performance means that eccentricity will be present in all machines to varying degrees of severity. Speed estimator based on rotor eccentricity was proposed by Holliday et al [1995]. However, designed rotor asymmetries should yield position signals that are more robust than those due to dynamic eccentricity and not as subject to mechanical vibration. For the estimation of the rotor speed, it is possible to use saliency effects, which are intentionally created by using special rotor construction, where spatial modulation of the rotor leakage inductance is created. This can be achieved, for example, by periodically varying the rotor slot opening widths or by varying the depths of the rotor slot openings [Jansen and Lorenz, 1995a]. Speed estimation method, proposed by Jansen and Lorenz [1995b], made use of the spatial modulation of the rotor leakage inductance which was achieved via a periodic variation in the rotor slot opening widths. The approach incorporated two features deemed necessary for accurate and robust estimation independent of speed and load: 1) trackable magnetic saliency, and 2) high-frequency signal injection. The method was experimentally verified.

Another method of using rotor asymmetry was proposed by Cilia et al [1997]. The principle of the proposed scheme is to use a designed rotor resistance asymmetry which is conceived with the aim of making the rotor position harmonics independent of the machine flux and load conditions. A sensorless vector controlled induction motor drive using an asymmetrical outer-section cage was presented. The method imposes asymmetry in the outer cage of a double-cage machine, in the outer section of a standard deep bar cage machine or in a separate cage winding embedded in the rotor

surface. A theoretical study has shown that rotor position tracking through the use of circumferential variation in outer-section cage resistance is feasible.

Dixon and Rivarola [1996] proposed a speed estimator based on the addition of specific irregularities in the rotor, which will produce small air gap variations in the machine. The detection of irregularities is based on the introduction of a constant high frequency carrier signal (400 Hz) in the stator currents. Speed and position are estimated through the detection of irregularities in the rotor. These irregularities generate amplitude oscillations in the currents generated by the high frequency carrier, which are proportional to the rotor position. At the same time, the frequency of these amplitude modulations is proportional to machine speed. By detecting the side-band frequency, the machine speed can be estimated. It was reported that the speed estimator worked well at a speed as low as 11 rpm, which was proved by simulation and experiments.

In order to estimate the rotor speed on the basis of rotor asymmetries, a high frequency signal injection has to be used. Speed information is then obtained from asymmetries, caused by rotor resistance, rotor leakage inductance or rotor eccentricity. However, it has been found that iron saturation degrades the speed estimation [Staines et al, 1998]. This is due to the saturation establishing a degree of saliency in addition to that of the asymmetry used to derive the speed. In order to overcome saturation problems, speed estimation method which is not affected by saturation has been developed by Staines et al [1998]. The estimation algorithm uses a periodic high frequency voltage burst rather than continuous voltage injection. Experimental results show that the method is effective.

A good comparative study of different spectrum estimation methods is available in Hurst and Habetler [1997]. A significant limitation of this approach is the lack of robustness with respect to machine specific structural characteristics. Slot harmonic magnitudes and frequencies depend on typically unknown parameters, such as the number of rotor slots. Thus user-selectable aspects of the algorithm, such as filter cut-off frequencies, the particular PWM switching scheme, and the slot harmonic equation itself often must be redesigned for each particular machine. Furthermore, these methods are very computationally intensive. The procedures are designed for steady-state operation and have limited accuracy in transient state due to the time required for current acquisition and FFT calculation.

3.3 Speed estimation using induction machine model only

The first attempt to operate the induction machine in closed-loop without using a speed sensor was reported by Abbondanti and Brennen [1975]. The scheme was based on an analogue slip calculator that computed the slip frequency in the speed range of 1:10. The slip frequency is the difference between the stator frequency and the electrical frequency corresponding to rotor speed. By calculation of the slip frequency, the speed of the rotor can be determined. The slip information is obtained by measuring the electrical quantities applied to the machine. By performing simple signal processing operations on the measured quantities, an analogue signal proportional to the slip level is derived and used to control the machine. The proposed scheme is applicable only in steady-state, in a limited speed range.

During the last couple of years, several open-loop rotor speed estimation methods were developed for sensorless vector control of induction machine. In most open-loop speed estimation methods calculation of the rotor speed is essentially based on the induction machine dynamic model. In majority of techniques of open-loop speed estimation rotor speed is calculated as the difference between the machine synchronous electrical angular speed and the angular slip frequency.

One such scheme was proposed by Ben-Brahim and Kawamura [1992], Trzynadlowski [1994] and Orlowska-Kowalska and Wojsznis [1996]. In this scheme, the rotor speed is calculated as

$$\omega = \omega_r - \omega_{sl} \tag{3.7}$$

where ω is the rotor speed, ω_r is the speed of rotor flux and ω_{sl} is the angular slip frequency. In a rotor flux oriented induction machine, it is possible to obtain the angular slip frequency by using the rotor voltage equation of the machine in the rotor flux oriented reference frame. The angular slip frequency can be calculated from:

$$\omega_{sl} = \frac{L_m}{T_r}\frac{i_{qs}}{\psi_r} \tag{3.8}$$

where i_{qs} can be obtained from the torque equation as:

$$i_{qs} = \frac{2T_e}{3P}\frac{L_r}{L_m\psi_r} \tag{3.9}$$

Substitution of equation (3.9) into (3.8), considering that $\psi_r=\psi_{dr}$ in the rotor flux oriented reference frame and that

$$T_e = \frac{3}{2} P \frac{L_m}{L_r} (\psi_{\alpha r} i_{\beta s} - \psi_{\beta r} i_{\alpha s}) \tag{3.10}$$

in the stationary reference frame, yields

$$\omega_{sl} = \frac{L_m}{T_r} \frac{1}{\psi_r^2} \left(\psi_{\alpha r} i_{\beta s} - \psi_{\beta r} i_{\alpha s} \right) \tag{3.11}$$

The electrical angle ϕ_r of the rotor flux vector is defined as:

$$\phi_r = \tan^{-1} \left(\frac{\psi_{\beta r}}{\psi_{\alpha r}} \right) \tag{3.12}$$

The derivative of the angle equation (3.12) can be used to obtain the electrical angular speed of the rotor flux. Therefore,

$$\omega_r = \frac{d\phi_r}{dt} = \frac{\psi_{\alpha r} \dfrac{d\psi_{\beta r}}{dt} - \psi_{\beta r} \dfrac{d\psi_{\alpha r}}{dt}}{\psi_{\alpha r}^2 + \psi_{\beta r}^2} \tag{3.13}$$

If the rotor flux components are known, the electrical angular speed of rotor flux can be calculated by using equation (3.13). It is convenient to estimate the rotor flux components from the stator voltage equations. Substitution of equations (2.22) and (2.23) into (2.20) gives the following equations for derivatives of the rotor flux components:

$$\begin{aligned} \frac{d\psi_{\alpha r}}{dt} &= \frac{L_r}{L_m} \left(v_{\alpha s} - R_s i_{\alpha s} - \sigma L_s \frac{di_{\alpha s}}{dt} \right) \\ \frac{d\psi_{\beta r}}{dt} &= \frac{L_r}{L_m} \left(v_{\beta s} - R_s i_{\beta s} - \sigma L_s \frac{di_{\beta s}}{dt} \right) \end{aligned} \tag{3.14}$$

Hence

$$\begin{aligned} \psi_{\alpha r} &= \frac{L_r}{L_m} \left[\int \left(v_{\alpha s} - R_s i_{\alpha s} \right) dt - \sigma L_s i_{\alpha s} \right] \\ \psi_{\beta r} &= \frac{L_r}{L_m} \left[\int \left(v_{\beta s} - R_s i_{\beta s} \right) dt - \sigma L_s i_{\beta s} \right] \\ \psi_r &= \sqrt{\psi_{\alpha r}^2 + \psi_{\beta r}^2} \end{aligned} \tag{3.15}$$

Electrical angular speed of rotor flux, given with (3.13), and angular slip frequency (3.11), are thus calculated using (3.14) - (3.15) and measured stator voltages and currents. Finally, the rotor speed is estimated from:

$$\omega = \omega_r - \omega_{sl} = \frac{\psi_{\alpha r}\dfrac{d\psi_{\beta r}}{dt} - \psi_{\beta r}\dfrac{d\psi_{\alpha r}}{dt}}{\psi_{\alpha r}^2 + \psi_{\beta r}^2} - \frac{L_m}{T_r}\frac{1}{\psi_r^2}\left(\psi_{\alpha r} i_{\beta s} - \psi_{\beta r} i_{\alpha s}\right) \qquad (3.16)$$

Figure 3.1 shows the diagram of implementation of the speed estimation scheme based on the equations given above. The inputs are stator currents and stator voltages in stationary reference frame. Stator currents can be measured at the machine terminals. Stator voltages can be measured at the machine terminals or reconstructed from the inverter switching states and measured DC link voltage.

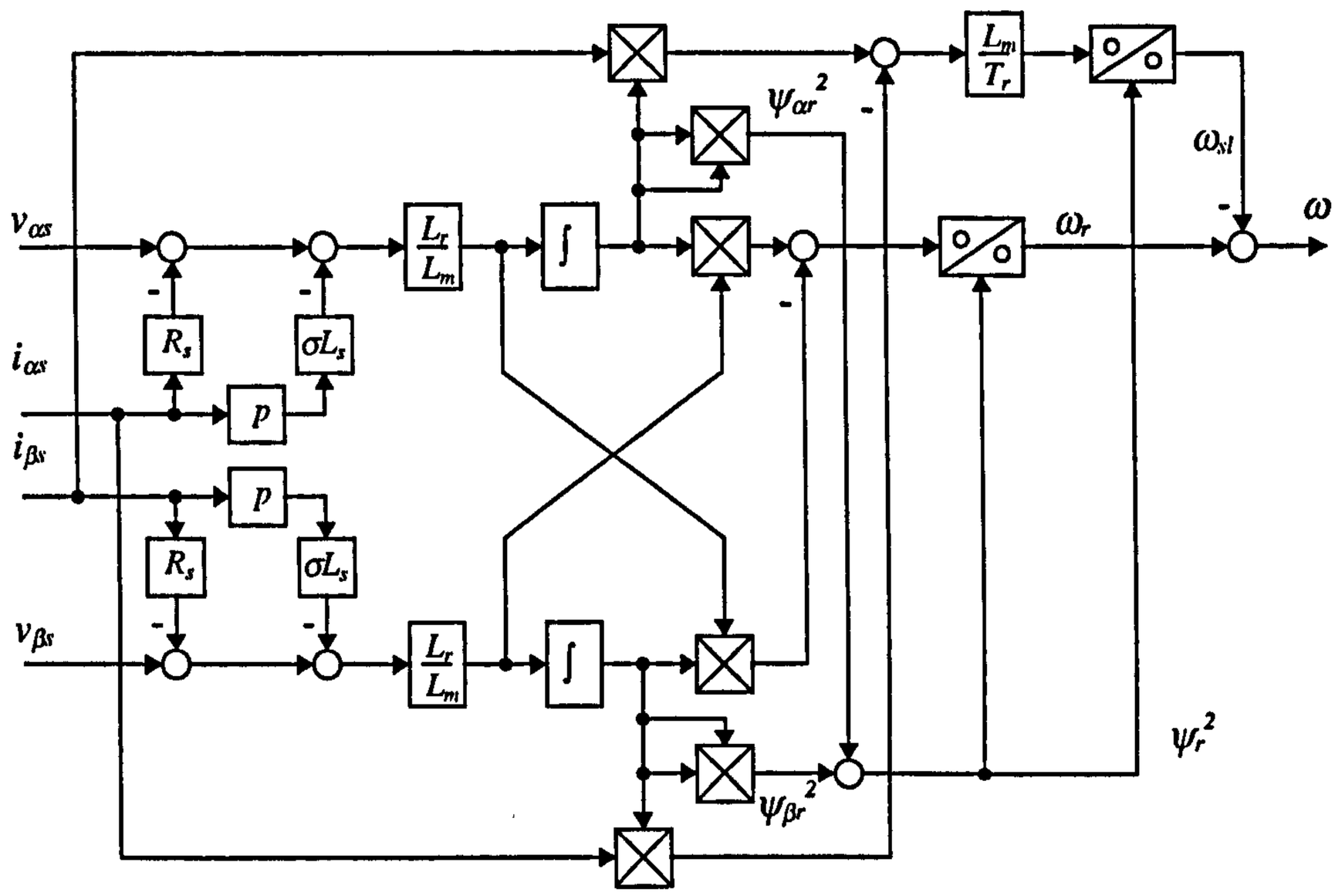

Figure 3.1: Diagram of an open-loop speed calculation method.

The same scheme, but improved for low speed estimation by addition of stator resistance identification, was presented by Ohmori et al [1997]. This method has problems at low speeds due to parameter variations and it is known that this kind of speed estimator works without failure above 10% of synchronous speed [Bose, 1988]. In order to reduce the parameter sensitivity, Ben-Brahim and Kawamura [1992] proposed a similar speed estimation scheme for a rotor flux oriented induction machine, but based on using the stator flux instead of rotor flux in the process of speed

estimation. Such a scheme estimates the rotor speed with less sensitivity to parameter variations than the one described here.

As slip frequency can be calculated in different ways, speed estimation in a rotor flux oriented reference frame was also proposed [Ohtani et al, 1992; Lai et al, 1997]. It is essentially the same principle as reviewed previously. The only difference is the calculation of angular slip frequency. In this method, the angular slip frequency is calculated in rotor flux oriented reference frame using

$$\omega_{sl} = \frac{L_m}{L_r}\frac{R_r}{\psi_r} i_{qs} \tag{3.17}$$

A similar scheme, that again uses stator current components in rotor flux oriented reference frame [Zhang, 1996; Lin and Chen, 1996], and additionally makes use of the correlation between rotor flux and stator *d*-axis current component, calculates angular slip frequency as:

$$\omega_{sl} = \frac{L_m}{T_r \psi_r} i_{qs} = \frac{1 + pT_r}{T_r}\frac{i_{qs}}{i_{ds}} \tag{3.18}$$

In both cases stator *d-q* axis current components in rotor flux oriented reference frame are used (commanded or measured values). It can be seen that if synchronous electrical speed and angular slip frequency are calculated, the rotor speed can always be obtained from equation (3.7). A similar speed estimation method was proposed by Bonanno et al [1995]. In this scheme, an improved rotor flux observer was developed so that the rotor flux components can be estimated at very low speed.

An alternative speed estimation method was discussed by [Ilas et al, 1994; Kanmachi and Takahashi, 1993]. It is again based on the induction machine voltage equations and the flux equations in stationary reference frame. The rotor speed can be calculated directly using these equations. From the machine flux equations (2.22), the rotor current components in stationary reference can be expressed as a function of the stator flux:

$$\begin{aligned} i_{\alpha r} &= \frac{1}{L_m}\left(\psi_{\alpha s} - L_s i_{\alpha s}\right) \\ i_{\beta r} &= \frac{1}{L_m}\left(\psi_{\beta s} - L_s i_{\beta s}\right) \end{aligned} \tag{3.19}$$

From rotor voltage equation (2.29), eliminating the rotor resistance R_r, it is possible to obtain the rotor speed as follows:

$$\omega = \frac{i_{\alpha r}\dfrac{d\psi_{\beta r}}{dt} - i_{\beta r}\dfrac{d\psi_{\alpha r}}{dt}}{i_{\alpha r}\psi_{\alpha r} + i_{\beta r}\psi_{\beta r}} \tag{3.20}$$

Substitution of equations (3.19) into rotor speed equation (3.20) enables rotor speed to be expressed as:

$$\omega = \frac{\left(\psi_{\alpha s} - L_s i_{\alpha s}\right) d\psi_{\beta r}/dt - \left(\psi_{\beta s} - L_s i_{\beta s}\right) d\psi_{\alpha r}/dt}{\left(\psi_{\alpha s} - L_s i_{\alpha s}\right)\psi_{\alpha r} + \left(\psi_{\beta s} - L_s i_{\beta s}\right)\psi_{\beta r}} \tag{3.21}$$

where stator flux components and rotor flux components can be estimated by means of the following equations:

$$\begin{aligned} \psi_{\alpha s} &= \int \left(v_{\alpha s} - R_s i_{\alpha s}\right) dt \\ \psi_{\beta s} &= \int \left(v_{\beta s} - R_s i_{\beta s}\right) dt \end{aligned} \tag{3.22}$$

$$\begin{aligned} \psi_{\alpha r} &= \frac{L_r}{L_m}\psi_{\alpha s} - \frac{\sigma L_s L_r}{L_m} i_{\alpha s} \\ \psi_{\beta r} &= \frac{L_r}{L_m}\psi_{\beta s} - \frac{\sigma L_s L_r}{L_m} i_{\beta s} \end{aligned} \tag{3.23}$$

Another speed estimation method for a stator flux oriented control was proposed by Jiang and Holtz [1995], Xu and Novotny [1991], Bose and Simoes [1995]. In this scheme, the stator flux speed and the slip frequency are calculated by means of the following equations:

$$\omega_{sl} = \frac{i_{qs} L_s (1 + \sigma T_r p)}{T_r (\psi_{ds} - \sigma L_s i_{ds})} \tag{3.24}$$

$$\omega_s = \frac{(v_{\beta s} - i_{\beta s} R_s)\psi_{\alpha s} - (v_{\alpha s} - i_{\alpha s} R_s)\psi_{\beta s}}{\psi_s^2} \tag{3.25}$$

Equation (3.24) directly follows from equation (2.53), while equation (3.25) essentially represents:

$$\frac{d\phi_s}{dt} = \frac{d}{dt}\left(\tan^{-1}\frac{\psi_{\beta s}}{\psi_{\alpha s}}\right) = \frac{(d\psi_{\beta s}/dt)\psi_{\alpha s} - (d\psi_{\alpha s}/dt)\psi_{\beta s}}{\psi_s^2} \tag{3.26}$$

where

$$d\psi_{\alpha s}/dt = v_{\alpha s} - R_s i_{\alpha s}$$
$$d\psi_{\beta s}/dt = v_{\beta s} - R_s i_{\beta s} \tag{3.27}$$

and therefore it fully corresponds to (3.13), valid for rotor flux oriented control.

In order to improve accuracy of speed estimation, a rotor resistance adaptation technique can be employed [Jiang and Holtz, 1995]. The rotor resistance can be updated by means of the second rotor speed estimate, obtained from rotor slot harmonics. It was confirmed by experiment that the speed estimation error is less than 0.2 %. In the scheme proposed by Bose and Simoes [1995], stator resistance compensation technique was applied.

Zeng et al [1997] proposed a speed calculation method based on the decoupled induction machine model in rotor flux reference frame. The method is verified by simulation. Yoo et al [1994] proposed a speed estimation method which does not involve any pure integration. The method is derived from an induction machine model in the polar coordinate reference frame. The proposed method was further improved with on-line parameter identification scheme for both stator and rotor resistances [Lee et al, 1996].

Some other speed estimation schemes, based on induction machine model, were also reported by Pana [1996, 1997], Kelmen et al [1996]. Rotor speed can also be calculated directly from the dynamic model of the machine given in different formats [Shirsavar and McCulloch, 1996; Nguyen et al, 1998].

The open-loop speed estimation methods, reviewed here, are simple to implement. However, it should be noted that the accuracy of open-loop speed estimators depends greatly on the accuracy of the machine parameters used. In general, at low speed the accuracy of open-loop speed estimators is reduced [Vas, 1998].

3.4 Speed estimation based on induction machine model

In section 3.3 various open-loop speed estimation methods have been reviewed. These have utilised the stator and rotor voltage equations of the induction machine. However, the accuracy of these open-loop schemes depends strongly on the machine parameters. In closed-loop speed estimators the accuracy of estimation can be improved. There are three types of closed-loop machine model based speed estimators that are discussed in this section. The first one is the model reference adaptive control (MRAC) based speed estimator. The second one is the speed estimator based on an observer. The third type of speed estimation relies on extended Kalman filter (EKF) technique.

3.4.1 Model reference adaptive control (MRAC) based speed estimation

Model reference adaptive control is increasingly being used to identity plant parameters and inaccessible variables. A successful MRAC design can yield the desired variables with less computational effort than other methods and is often simple to implement.

The measured signals that are used in MRAC based speed estimators (and in all other model based approaches) are stator phase voltages and currents. Alternatively, stator voltages are reconstructed from measured DC link voltage and inverter switching functions. The model reference approach makes use of two independent machine models of different structure to estimate the same state variable on the basis of different sets of inputs variables. The estimator that does not involve the quantity to be estimated (in this case, the rotor speed) is considered as a reference model of the induction machine. The other estimator, which involves the estimated quantity, is regarded as an adjustable model. The error between the outputs of the two estimators is used to drive a suitable adaptive mechanism that generates the estimated rotor speed for the adjustable model. When the estimated rotor speed in the adjustable model attains the correct value, the difference between the output of the reference model and the output of the adjustable model becomes zero. The estimated rotor speed is then equal to the actual rotor speed, under ideal conditions. The idea of a MRAC based speed estimator is illustrated in Figure 3.2.

The outputs of the reference and the adjustable model in Figure 3.2 are shown as reactive powers [Peng and Fukao, 1994]. The most frequently used scheme has rotor

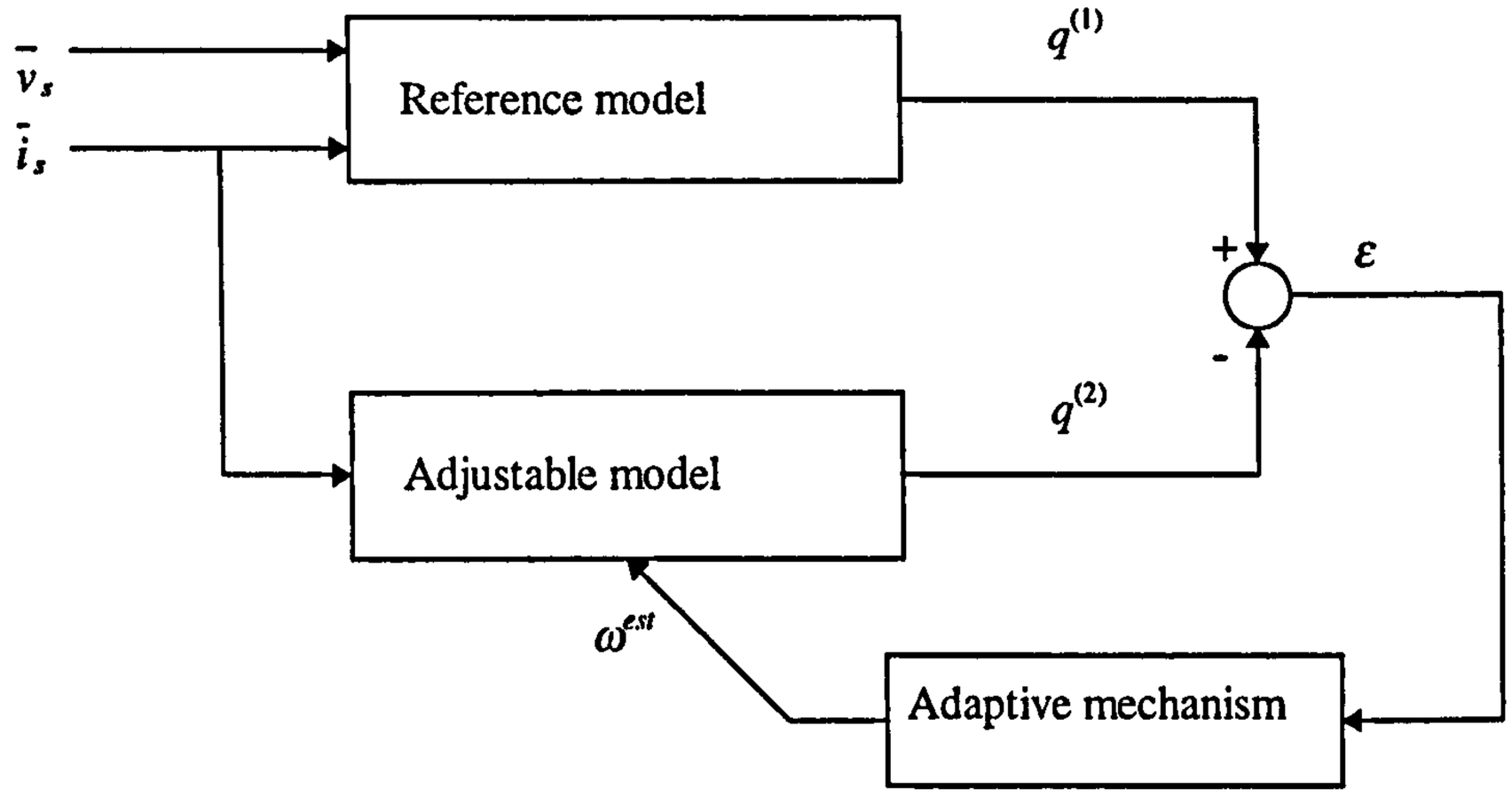

Figure 3.2: Conceptual block diagram of MRAC estimator.

flux space vectors at the output of the reference and the adjustable model [Schauder, 1992; Tajima and Hori, 1993]. However, other solutions are possible as well. The outputs of the two models may be back emf [Peng and Fukao, 1994] or air-gap power [Zhen and Xu, 1995].

Comparative studies of speed estimation based on MRAC and extended Kalman filter approaches have been done by Armstrong and Atkinson [1997] and Armstrong et al [1997]. The transient performance of MRAC schemes is similar to that of sensored indirect rotor flux oriented vector controller and is much simpler to understand and commission. It was suggested that rotor flux MRAC is the better choice for use in a sensorless rotor flux oriented vector controlled induction motor drive in situations where hardware economy is an important consideration.

All the most important different forms of MRAC based speed estimators will be discussed in detail in the next chapter.

3.4.2 Observer based speed estimation

For sensorless vector control of an induction machine it is required to estimate both the machine speed and the rotor flux spatial position. One of the possible solutions is to use a full order state observer and a suitable adaptation mechanism. Based on the measured quantities (stator currents and voltages) and on the previous speed estimate, the observer calculates the rotor fluxes and the stator currents. The difference between the

measured and the estimated stator currents is used by the adaptation mechanism to estimate the rotor speed.

A state observer is a model-based estimator which can be used for state (and/or parameter) estimation of a dynamic system in real time. In an induction machine drive a state observer can also be used for the real time estimation of the machine speed and some of the machine parameters, e.g. stator resistance. Many authors have developed sensorless vector control systems based on observers.

Speed estimation schemes based on an observer are presented by Kubota et al [1993] and Kubota and Matsuse [1994a]. The full-order state observer can be obtained by using the induction machine model. Based on the constant parameter induction machine model given in section 2.2, an induction machine can be described by the following state equations in the stationary reference frame:

$$\frac{d}{dt}\begin{bmatrix}\underline{i}_s\\ \underline{\psi}_r\end{bmatrix}=\begin{bmatrix}\underline{A}_{11} & \underline{A}_{12}\\ \underline{A}_{21} & \underline{A}_{22}\end{bmatrix}\begin{bmatrix}\underline{i}_s\\ \underline{\psi}_r\end{bmatrix}+\begin{bmatrix}\underline{B}_1\\ 0\end{bmatrix}\underline{v}_s=\underline{A}\underline{x}+\underline{B}\underline{v}_s \tag{3.28}$$

$$\underline{i}_s=\underline{C}\underline{x} \tag{3.29}$$

where

$$\underline{i}_s=\begin{bmatrix}i_{\alpha s}\\ i_{\beta s}\end{bmatrix}\qquad \underline{\psi}_r=\begin{bmatrix}\psi_{\alpha r}\\ \psi_{\beta r}\end{bmatrix}\qquad \underline{v}_s=\begin{bmatrix}v_{\alpha s}\\ v_{\beta s}\end{bmatrix} \tag{3.30}$$

$$\underline{A}_{11}=\begin{bmatrix}-\{R_s/(\sigma L_s)+(1-\sigma)/(\sigma T_r)\} & 0\\ 0 & -\{R_s/(\sigma L_s)+(1-\sigma)/(\sigma T_r)\}\end{bmatrix} \tag{3.31}$$

$$\underline{A}_{12}=\begin{bmatrix}L_m/(\sigma L_s L_r T_r) & L_m/(\sigma L_s L_r)\omega\\ -L_m/(\sigma L_s L_r)\omega & L_m/(\sigma L_s L_r T_r)\end{bmatrix} \tag{3.32}$$

$$\underline{A}_{21}=\begin{bmatrix}L_m/T_r & 0\\ 0 & L_m/T_r\end{bmatrix} \tag{3.33}$$

$$\underline{A}_{22}=\begin{bmatrix}-1/T_r & -\omega\\ \omega & -1/T_r\end{bmatrix} \tag{3.34}$$

$$\underline{B}_1=\begin{bmatrix}1/(\sigma L_s) & 0\\ 0 & 1/(\sigma L_s)\end{bmatrix} \tag{3.35}$$

The full order state observer which estimates the stator current and rotor flux components is written in the form:

$$\frac{d\underline{\hat{x}}}{dt} = \underline{\hat{A}}\underline{\hat{x}} + \underline{B}\underline{v}_s + \underline{G}(\underline{\hat{i}}_s - \underline{i}_s) \tag{3.36}$$

where ^ denotes the estimated values and G is the observer gain matrix which is selected so that the observer is stable. The machine speed is estimated by the following adaptive scheme which is derived by using the Lyapunov's stability theorem [Kubota et al, 1993]:

$$\omega^{est} = K_p(e_{i\alpha s}\hat{\psi}_{\beta r} - e_{i\beta s}\hat{\psi}_{\alpha r}) + K_i\int(e_{i\alpha s}\hat{\psi}_{\beta r} - e_{i\beta s}\hat{\psi}_{\alpha r})dt \tag{3.37}$$

where

$$e_{i\alpha s} = i_{\alpha s} - \hat{i}_{\alpha s} \qquad e_{i\beta s} = i_{\beta s} - \hat{i}_{\beta s} \tag{3.38}$$

From previous considerations if follows that motor speed is in observer-based speed estimation considered as a parameter rather than as a state. In other words, speed is assumed to be constant during one sampling interval and change in electro-magnetic states is observed. Speed estimate is obtained by observing the difference between monitored and estimated stator currents.

Figure 3.3 shows the block diagram of the state observer for induction machine speed estimation.

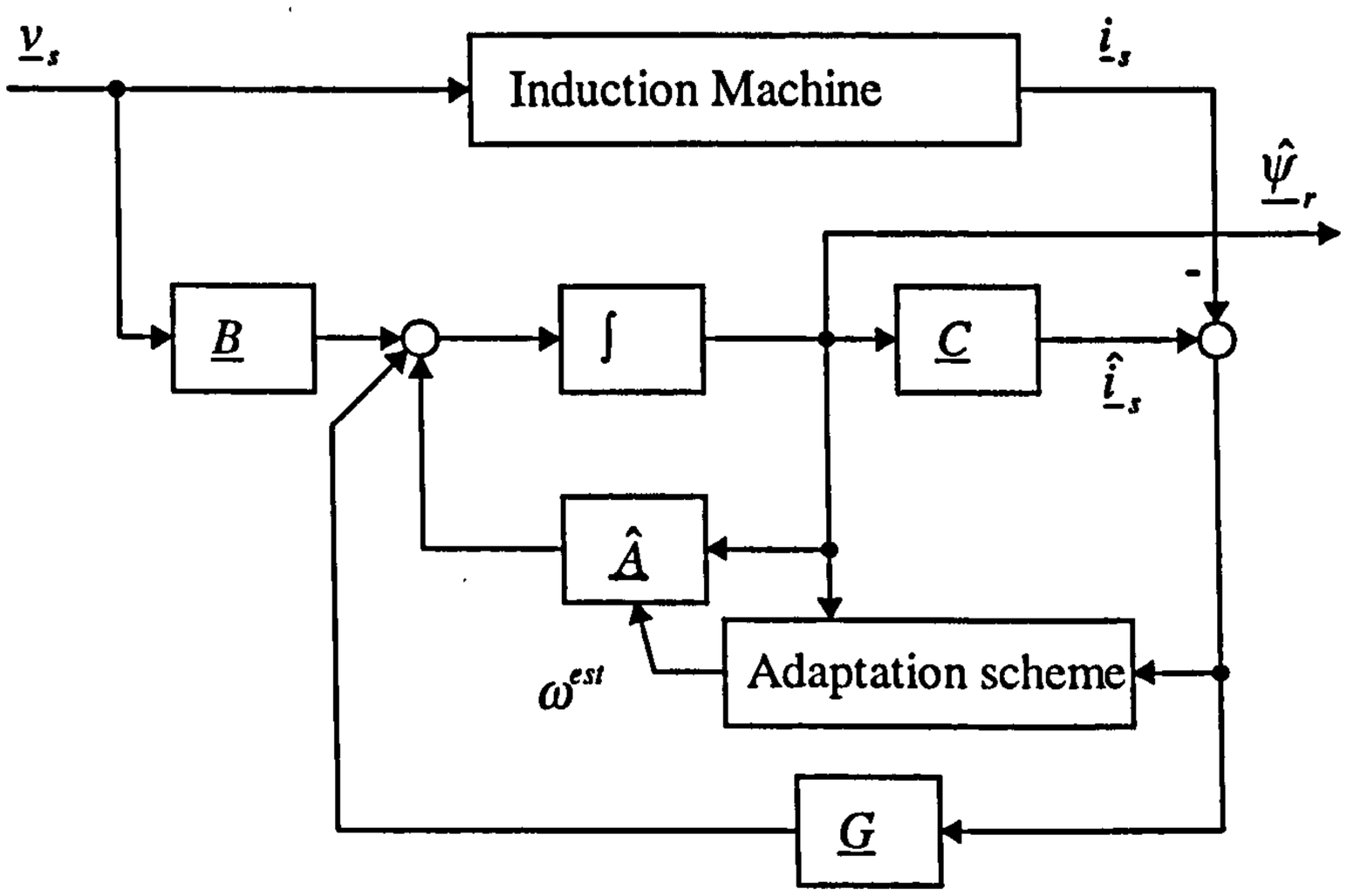

Figure 3.3: Structure of the full-order state observer.

The method proposed by Kubota and Matsuse [1994b] can identify simultaneously the machine speed and the rotor resistance using the adaptive flux observer. Another similar rotor speed estimation method based on a full-order adaptive observer with stator resistance identification was also reported by [Yang and Chin, 1993].

As the observer based speed estimation methods again identify the speed by measuring stator voltages and stator currents, the accuracy of speed estimation is again not only strongly dependent on the machine parameters, but also on measured quantities. Lower the speed is, lower the stator voltage becomes. It is very difficult to measure the stator voltage precisely at low speed. In order to estimate the rotor speed at low speed, Kubota and Matsuse [1996] proposed an improved speed estimation scheme based on adaptive observer with offset compensation of stator voltage. A sensorless vector controlled induction motor drive with stator voltage offset compensation was also reported by Kataoka et al [1997]. A successfully implemented sensorless direct field oriented control of induction motor drives based on adaptive observer was described by Ilas and Magureanu [1996].

In order to reduce the computational burden, it is possible to use a reduced order dynamic induction machine model to derive the state observer. Reduced order observer with real-time parameter identification scheme was proposed by Hur et al [1996]. This scheme utilises a reduced order induction machine model, which was obtained by substitution of equation (2.36) into the stator current equation (3.28). The reduced order induction machine model is obtained as follows:

$$\frac{d}{dt}\begin{bmatrix} i_{\alpha s} \\ i_{\beta s} \end{bmatrix} = \begin{bmatrix} i_{\alpha s} & -i_{\beta s} & \psi_{\alpha s} & \psi_{\beta s} & v_{\alpha s} \\ i_{\beta s} & i_{\alpha s} & \psi_{\beta s} & -\psi_{\alpha s} & v_{\beta s} \end{bmatrix} \begin{bmatrix} a - 1/T_r \\ \omega \\ 1/(\sigma L_s T_r) \\ \omega/(\sigma L_s) \\ 1/\sigma L_s \end{bmatrix} = \underline{\Phi}^T \underline{\Theta} \qquad (3.39)$$

where $a = -\{R_s / (\sigma L_s) + (1-\sigma) / (\sigma T_r)\}$

Based on the reduced order model (3.39), the state observer is obtained as:

$$\frac{d}{dt}\underline{\hat{i}}_s = \underline{\Phi}^T \underline{\hat{\Theta}} + \underline{G}(\underline{\hat{i}}_s - \underline{i}_s) \qquad (3.40)$$

The stator flux is estimated by equation (3.22). The proposed method worked well in the speed region above 5-10 % of the rated speed.

Many schemes, based on observer theory, have been proposed. Speed estimation with sliding observer was suggested by Doki et al [1992], Benchaib et al [1997], Nardocci et al [1997]. An observer with rotor resistance adaptation was introduced by Ilas et al [1994] and stator voltage error compensation was discussed by Tsuji et al [1996]. Sng et al [1998] proposed an improved speed observer functioning continuously at low or zero speed, where rapid change of speed does not occur and signal frequency can be zero. Based on the variable structure control theory, variable structure observer was applied in speed estimation of an induction machine. Kim et al [1997] and Arcker-Hissel et al [1998] presented speed estimation schemes using variable structure observer. Simultaneous on-line identification of rotor speed and parameters, based on a full-order observer, was proposed by Attaianese et al [1997]. In this scheme, the rotor resistance and magnetising inductance are identified simultaneously with the rotor speed estimation. Speed estimation with rotor time constant identification was also suggested by Attaianese et al [1995]. Speed observer for a stator flux oriented induction motor drive was developed by Marchesoni et al [1997].

When an appropriate observer is used in a sensorless vector controlled drive, stable operation can be obtained over a wide speed range. Due to higher computational burden, observer based methods are more computationally intensive then MRAC based methods.

3.4.3 Extended Kalman filter (EKF) based speed estimation

The extended Kalman filter is a recursive optimum stochastic state estimator which can be used for the joint state and parameter estimation of a non-linear dynamic system in real-time by using noisy monitored signals that are disturbed by random noise. This assumes that the measurement noise and disturbance noise are uncorrelated. The noise sources take account of measurement and modelling inaccuracies. The extended Kalman filter is a variant of the Kalman filter, but the extended version can deal with a non-linear system. It should be noted that in the full-order state observer the noise has not been considered. Furthermore, in the state observer the speed was considered as a

parameter, but in extended Kalman filter it is considered as a state. Similarly to the observer, where the state variables are adapted by the gain matrix, in the extended Kalman filter the state variables are adapted by the Kalman gain matrix.

The extended Kalman filter algorithm is based on a mathematical model for the determination of the system state. The estimation is constantly corrected by using a feedback correction scheme. This scheme makes use of actual measured states by adding a term to the predicted states. The additional term contains the weighted difference of the measured and estimated output signals. Based on the deviation from the estimated values the extended Kalman filter provides an optimum output value at the next input instant. In an induction motor drive the extended Kalman filter can be used for the real-time estimation of the rotor speed, but it can also be used for joint state and parameter estimation. For this purpose the stator voltages and stator currents are again measured.

Kim et al [1994] proposed a speed estimation method using extended Kalman filter. A dynamic model for an induction machine is formed in the stationary reference frame, by choosing the stator currents and rotor flux components as state variables. These are augmented with the estimated quantity, which in this case is the rotor angular speed. The equations of the induction machine are the following:

$$\begin{aligned} \frac{d\underline{x}(t)}{dt} &= \underline{A}\underline{x}(t) + \underline{B}\underline{v}(t) \\ \underline{y}(t) &= \underline{C}\underline{x}(t) \end{aligned} \tag{3.41}$$

where

$$\underline{x} = \begin{bmatrix} i_{\alpha s} & i_{\beta s} & \psi_{\alpha r} & \psi_{\beta r} & \omega \end{bmatrix}^t \tag{3.42}$$

$$\underline{y} = \begin{bmatrix} i_{\alpha s} & i_{\beta s} \end{bmatrix}^t \tag{3.43}$$

$$\underline{v} = \begin{bmatrix} v_{\alpha s} & v_{\beta s} \end{bmatrix}^t \tag{3.44}$$

$$\underline{A}=\begin{bmatrix} -\left(\frac{R_s}{\sigma L_s}+\frac{1-\sigma}{\sigma T_r}\right) & 0 & \frac{L_m}{\sigma L_s L_r}\frac{1}{T_r} & \omega\frac{L_m}{\sigma L_s L_r} & 0 \\ 0 & -\left(\frac{R_s}{\sigma L_s}+\frac{1-\sigma}{\sigma T_r}\right) & -\omega\frac{L_m}{\sigma L_s L_r} & \frac{L_m}{\sigma L_s L_r}\frac{1}{T_r} & 0 \\ \frac{L_m}{T_r} & 0 & -\frac{1}{T_r} & -\omega & 0 \\ 0 & \frac{L_m}{T_r} & \omega & -\frac{1}{T_r} & 0 \\ 0 & 0 & 0 & 0 & 0 \end{bmatrix} \tag{3.45}$$

$$\underline{B}=\begin{bmatrix} \frac{1}{\sigma L_s} & 0 \\ 0 & \frac{1}{\sigma L_s} \\ 0 & 0 \\ 0 & 0 \\ 0 & 0 \end{bmatrix} \tag{3.46}$$

$$\underline{C}=\begin{bmatrix} 1 & 0 & 0 & 0 & 0 \\ 0 & 1 & 0 & 0 & 0 \end{bmatrix} \tag{3.47}$$

It should be noted that in equation (3.45) it has been assumed that the rotor speed derivative is negligible, $d\omega/dt=0$. Although this corresponds to infinite inertia, the required correction is performed by the Kalman filter (by the system noise, which also takes account of the computational inaccuracies). The EKF algorithm contains basically two main stages, a prediction stage and a filtering stage. During the prediction stage, the next predicted values of the states and the predicted state covariance matrix are obtained. For this purpose, the state variable equations of the induction machine are used. During the filtering stage, the filtered states are obtained from the predicted estimates by adding a correction term to the predicted value. This correction term is an error term. This error is minimised in the EKF. The EKF equation is:

$$\frac{d\hat{\underline{x}}}{dt}=\underline{A}(\hat{x})\hat{\underline{x}}+\underline{Bv}+\underline{K}(\hat{\underline{i}}_s-\underline{i}_s) \tag{3.48}$$

By considering the system noise, $\underline{u}$, and measurement noise, $\underline{w}$, which are assumed to be zero-mean, white Gaussian, and independent of states $\underline{x}$, the structure of the extend Kalman filter for speed estimation, shown in Figure 3.4, results.

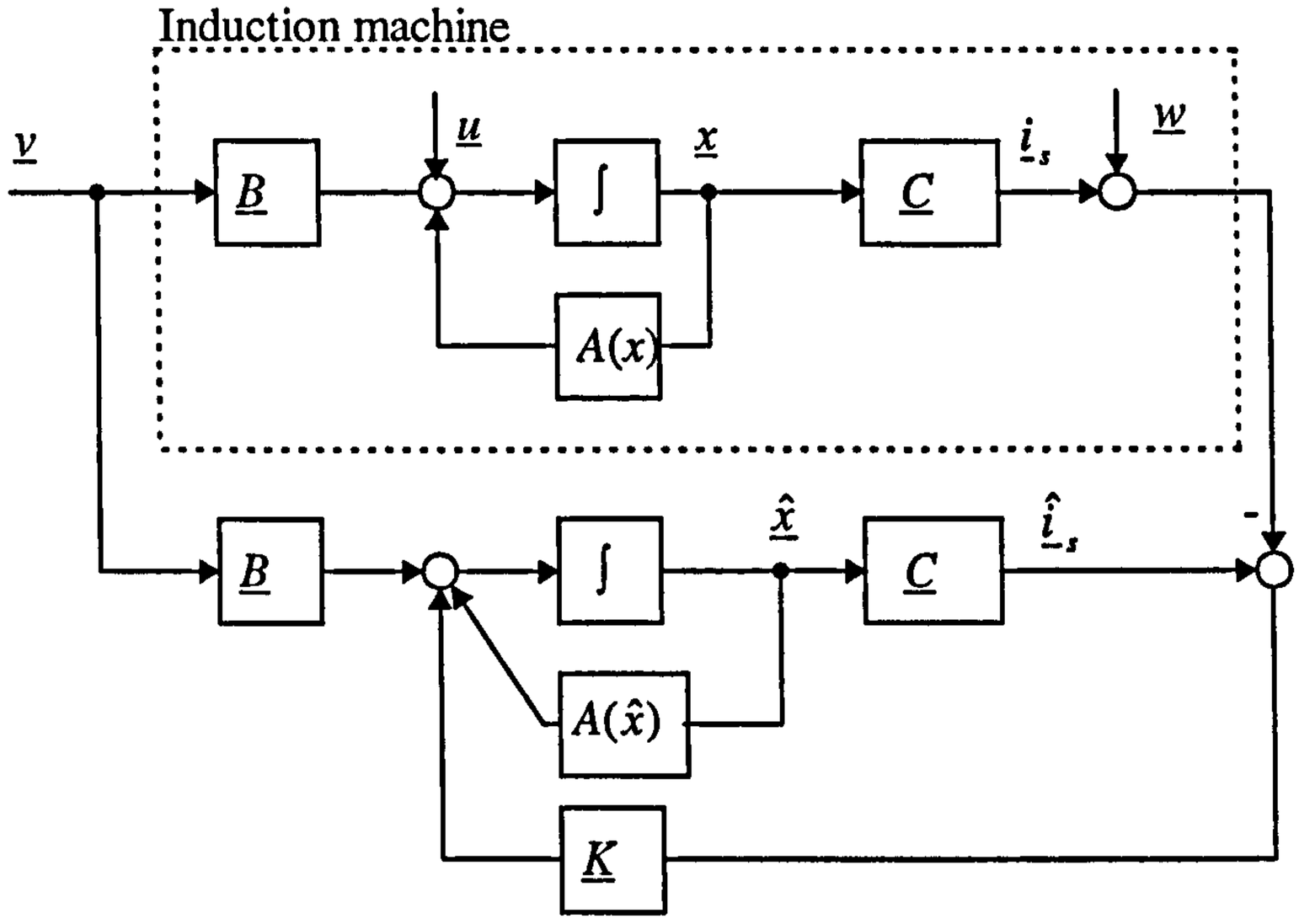

Figure 3.4: Structure of extended Kalman filter.

A number of different EKF based schemes have been proposed recently. Westerholt [1997] proposed one of them. Based on the non-linear induction machine model, a 6^{th} order extended Kalman filter was constructed and used to observe the machine state variables including the rotor speed and the load torque. A very satisfactory overall performance was obtained with standard inverters. Another implementation of DSP based sensorless induction motor drive which uses the extended Kalman filter was described by Salvatore et al [1998]. The proposed method has the ability of on-line updating of the mathematical model parameters, so that the high accuracy of speed estimation is obtained. As various mathematical models can be used, the overall sensitivity to parameter variations depends on the structure of the estimator. It is possible to employ alternative models of induction machines. Beierke et al [1997] proposed a scheme by using an induction machine model in which the number of machine parameters is reduced.

A study that compares directly parameterised observers and extended Kalman filters for sensorless induction motors has been performed by Harnefors [1998]. It was shown that although the noise content of the estimates of the EKF is lower than that of the directly parameterised observers, EKF tends to be less accurate in the presence of erroneous machine model parameters. Furthermore, the computational requirements of the EKF based methods are much higher than those of observers.

3.5 Summary

In this chapter, a review of existing speed estimation methods was presented. Speed estimation methods based on stator current harmonics were discussed first. As stator current harmonics contain rotor speed information, speed estimate can be obtained by analysis of current spectrum and is independent of machine parameters. However, it is computationally complex and time-consuming. Due to vast amount of computation required, speed estimation based on current harmonics is accurate in steady-state operation, while it has limited accuracy in fast transient operation.

The basics of model based speed estimation schemes were explained. Speed estimation methods based on induction machine model only (open-loop speed estimators) were discussed. These methods are the simplest and easy to implement. The drawback of the open-loop speed estimation is that it is very sensitive to parameter variations and has poor behaviour in low speed region. For better quality of speed estimation, speed estimation based on induction machine model in conjunction with modern control theory forms the closed-loop group. There are three types in this group. Speed estimation based on MRAC was briefly introduced and will be discussed in detail in the following chapter. Speed estimation schemes based on observer and extended Kalman filter were reviewed. In the observer based methods, the rotor flux is estimated through an observer and the rotor speed is derived using the stator current errors and the estimated rotor flux. The Kalman filter based methods have been employed by many researchers to identify rotor speed and flux of an induction machine. These methods also require high speed DSP which will lead to costly hardware and software. Among these methods, MRAC based speed estimation methods are the simplest to implement. The methods based on Kalman filters and observers are more computationally intensive than the MRAC based speed estimation methods and are therefore excluded from further considerations.

4 SENSORLESS ROTOR FLUX ORIENTED CONTROL USING MRAC BASED SPEED ESTIMATION

4.1 Introduction

Many different speed estimation algorithms have been developed in recent past. Among them, the model reference adaptive control (MRAC) based speed estimators are the most attractive approach due to their relatively simple implementation requirements [Marwali and Keyhani, 1997]. The basic idea of MRAC is that one quantity can be calculated in two different ways. Based on MRAC theory, it is possible to construct the MRAC based speed estimator in different forms. The estimation schemes primarily differ with respect to which quantity is selected for adaptation purposes. In this chapter, detailed analysis of different MRAC based speed estimation methods will be presented. Scheme based on rotor flux is the first one to be discussed in section 4.2. Back emf based speed estimation method is elaborated in section 4.3. This is followed by discussion of reactive power based MRAC speed estimation in section 4.4 and air-gap power based MRAC speed estimation scheme in section 4.5. Finally, section 4.6 gives the summary of this chapter.

4.2 Rotor flux based MRAC scheme for speed estimation

MRAC based speed estimation method makes use of two independent observers which are constructed to estimate the same quantity, using measured stator voltages and currents. The two observers can be obtained from the induction machine model equations. One of the observers does not involve the quantity that is to be estimated (in this case rotor speed). This observer is regarded as a reference model of the induction machine. The second observer does involve the quantity that is to be estimated, and it is regarded as an adjustable model. The error between the outputs of the reference model and the adjustable model is then used to drive a suitable adaptation mechanism, which generates the estimated rotor speed for the adjustable model. The appropriate adaptation mechanism can be derived by using Popov's criterion of hyperstability. This results in a stable and quick response system, where the differences between the outputs of the reference model and the adjustable model are manipulated into a speed tuning signal.

The speed tuning signal is the input to a PI controller. The estimated rotor speed is obtained at the output of the PI controller.

Rotor flux based MRAC method was proposed by Schauder [1992]. In this scheme the outputs of the two observers are two rotor flux space vectors. Based on the induction motor space vector model expressed in an arbitrary reference frame (2.35) and (2.36), the induction machine voltage equations in stationary reference frame can be obtained by letting ω_a=0.

$$\begin{aligned} \bar{v}_s &= R_s \bar{i}_s + \frac{d\bar{\psi}_s}{dt} \\ 0 &= R_r \bar{i}_r + \frac{d\bar{\psi}_r}{dt} - j\omega\bar{\psi}_r \end{aligned} \tag{4.1}$$

Considering (2.36) and (4.1) and eliminating stator flux vector and rotor current vector, enables derivative of the rotor flux vector to be expressed in the form of:

$$\frac{d\bar{\psi}_r}{dt} = \frac{L_r}{L_m}\left(\bar{v}_s - R_s \bar{i}_s - \sigma L_s \frac{d\bar{i}_s}{dt}\right) \tag{4.2}$$

$$\frac{d\bar{\psi}_r}{dt} = \left(-\frac{1}{T_r} + j\omega\right)\bar{\psi}_r + \frac{L_m}{L_r}\bar{i}_s \tag{4.3}$$

By resolving equations (4.2) and (4.3) into two-axis components, the rotor flux components in the stationary reference frame are obtained as:

$$p\begin{bmatrix}\psi_{\alpha r}\\ \psi_{\beta r}\end{bmatrix} = \frac{L_r}{L_m}\left[\begin{bmatrix}v_{\alpha s}\\ v_{\beta s}\end{bmatrix} - \begin{bmatrix}(R_s + \sigma L_s p) & 0\\ 0 & (R_s + \sigma L_s p)\end{bmatrix}\begin{bmatrix}i_{\alpha s}\\ i_{\beta s}\end{bmatrix}\right] \tag{4.4}$$

$$p\begin{bmatrix}\psi_{\alpha r}\\ \psi_{\beta r}\end{bmatrix} = \begin{bmatrix}-1/T_r & -\omega\\ \omega & -1/T_r\end{bmatrix}\begin{bmatrix}\psi_{\alpha r}\\ \psi_{\beta r}\end{bmatrix} + \frac{L_m}{T_r}\begin{bmatrix}i_{\alpha s}\\ i_{\beta s}\end{bmatrix} \tag{4.5}$$

where p is the differential operator. Equation (4.4) represents so-called voltage model, which does not contain the rotor speed and is therefore the reference model. Equation (4.5) is the current model, it contains the rotor speed, and therefore it represents the adjustable model. The reference model and the adjustable model are used to estimate the rotor fluxes. The angular difference between the two rotor flux space vector positions is used as the speed tuning signal (error signal). The speed tuning signal actuates the rotor speed estimation algorithm, which makes the error signal converge to

zero in steady-state. The adaptation mechanism of MRAC based speed estimation method was derived by Schauder [1992] and has the form of

$$\omega^{est} = K_p \varepsilon + K_i \int \varepsilon dt \tag{4.6}$$

where

$$\varepsilon = \psi_{\beta r}^{(1)} \psi_{\alpha r}^{(2)} - \psi_{\alpha r}^{(1)} \psi_{\beta r}^{(2)} \tag{4.7}$$

K_p and K_i are arbitrary positive constants (parameters of a PI controller) and superscripts (1) and (2) identify outputs of the reference and adjustable model, respectively.

Figure 4.1 shows the complete scheme of the MRAC based speed estimation using rotor flux for adaptation purposes.

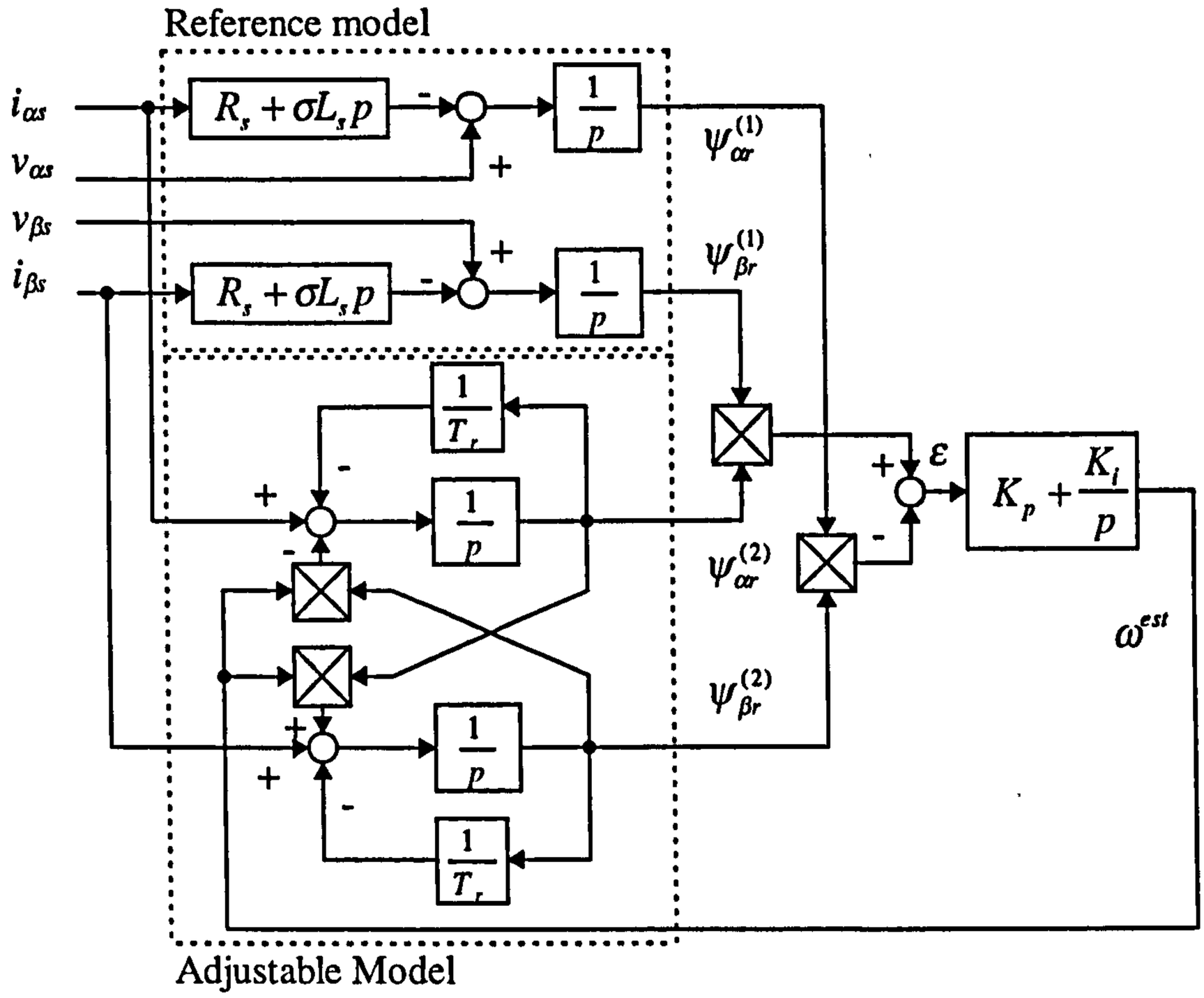

Figure 4.1: Block diagram of MRAC based speed estimator using rotor flux for the speed tuning signal creation.

It should be noted that the factors L_r/L_m in (4.4) and L_m/T_r in (4.5) have been incorporated into the adaptation mechanism gain constants K_p and K_i. The outputs of the two models thus only represent the rotor flux space vector in angle.

In practice, it is very difficult to implement the pure integrator in the reference model due to the problems of initial conditions and drift. In order to eliminate the pure integrator, Schauder [1992] suggested that it is possible to implement the reference model by using a low-pass filter, with the transfer function $1/(p+1/T)$, instead of the pure integrator. However, since $1/(p+1/T) = (1/p)[p/(p+1/T)]$, the pure integrator can be eliminated by inserting a high pass filter $[p/(p+1/T)]$ in the output side of the reference model (which contains $1/p$). Since the output of the reference model gives the modified rotor flux, the adjustable model needs to be modified as well. Therefore, the identical high pass filter $[p/(p+1/T)]$ can be placed on either the input of the adjustable model or the output of the adjustable model. Two types of modified rotor flux based MRAC speed estimation schemes using auxiliary variables are illustrated in Figure 4.2.

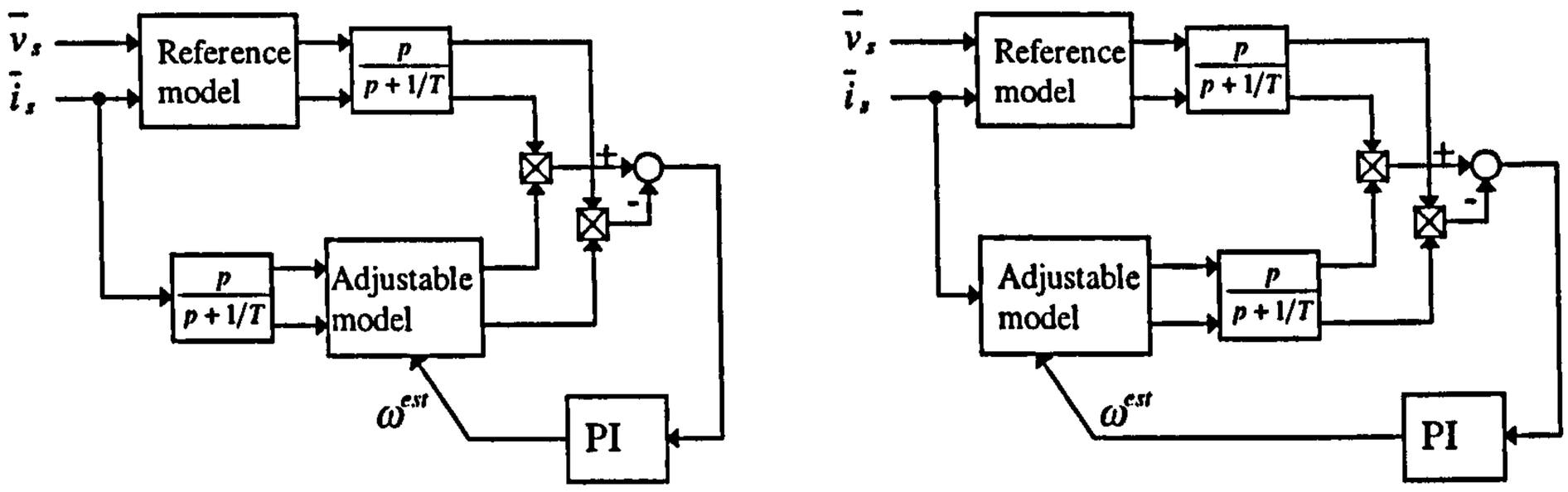

Figure 4.2: Modified rotor flux based MRAC speed estimator.

In order to overcome the pure integration problem in the voltage model of the MRAC speed estimator, Hu and Wu [1997] proposed a new integration algorithm for estimating the motor flux. It was claimed that the new algorithm can estimate the motor flux over a wide speed range. Akin et al [1998] also presented an alternative integration algorithm for the calculation of stator flux in the reference model.

Another successful application of the rotor flux based MRAC speed estimation was presented by Tajima and Hori [1993]. In this application, the modified rotor flux is obtained as in Figure 4.2a. It was also suggested by Kim and Hung [1995] that the rotor flux based MRAC speed estimator can be derived in the rotor flux oriented reference frame. In this MRAC based speed estimator, the pure integrators are replaced by the first order delay. The structure is very similar to the scheme of Figure 4.2b.

Rotor flux based speed estimation scheme for sensorless indirect field oriented control of induction motor drives with rotor resistance identification was presented by Jemli et al [1998]. The simulation results show that the performance of the proposed scheme is satisfactory in wide speed range and robust with respect to rotor resistance variations. Based on rotor flux based MRAC, Jansen and Lorenz [1993] proposed an improved topology that utilises an integrated closed-loop flux observer and a mechanical system model in the process of rotor speed estimation. Incorporation of the mechanical system model into the MRAC system has been shown to significantly improve the speed estimation dynamics.

Dynamic studies for MRAC based speed and flux observers in high performance sensorless induction motor drives have been performed by Cilia et al [1998a]. The authors argue that the MRAC estimator based on rotor flux error vector offers perhaps the best performance for sensorless drives. This conclusion is almost the same as that stated by Marwali and Keyhani [1997]. They did a comparative study of rotor flux based MRAC and back emf based MRAC speed estimators. For these reasons, the rotor flux based speed estimator has been selected for analysis in this thesis.

4.3 Back emf based MRAC scheme for speed estimation

To avoid the pure integrators in the reference model of rotor flux based MRAC speed estimator, an alternative MRAC speed estimation method was proposed by Peng and Fukao [1994]. The proposed back emf based speed estimation method does not require any pure integrators in its reference model and adjustable model, so that this method can achieve wider bandwidth speed control.

In this case, the outputs of the two observers are the back emf space vectors, instead of the rotor flux space vectors. When the back emf is used, problems of pure integration in the reference model do not exist.

From equation (4.2), the back emf components in stationary reference frame can be obtained. As these equations do not contain the quantity that is to be estimated, they may be regarded as the reference model of the speed estimator.

$$e_{m\alpha}^{(1)} = \frac{L_m}{L_r}\frac{d\psi_{\alpha r}}{dt} = v_{\alpha s} - R_s i_{\alpha s} - \sigma L_s \frac{di_{\alpha s}}{dt}$$
$$e_{m\beta}^{(1)} = \frac{L_m}{L_r}\frac{d\psi_{\beta r}}{dt} = v_{\beta s} - R_s i_{\beta s} - \sigma L_s \frac{di_{\beta s}}{dt} \qquad (4.8)$$

Equations for the adjustable model can be obtained from equation (4.3):

$$e_{m\alpha}^{(2)} = \frac{L_m}{L_r}\frac{d\psi_{\alpha r}}{dt} = \frac{L_m}{L_r}\left(\frac{L_m}{T_r} i_{\alpha s} - \frac{1}{T_r}\psi_{\alpha r} - \omega\psi_{\beta r}\right)$$
$$e_{m\beta}^{(2)} = \frac{L_m}{L_r}\frac{d\psi_{\beta r}}{dt} = \frac{L_m}{L_r}\left(\frac{L_m}{T_r} i_{\beta s} - \frac{1}{T_r}\psi_{\beta r} + \omega\psi_{\alpha r}\right) \qquad (4.9)$$

Back emf based MRAC speed estimator can be constructed using (4.8) and (4.9). By introducing the equivalent rotor magnetising current as:

$$i_{m\alpha} = \frac{\psi_{\alpha r}}{L_m} \qquad i_{m\beta} = \frac{\psi_{\beta r}}{L_m} \qquad (4.10)$$

equations (4.9) can be rewritten as:

$$e_{m\alpha}^{(2)} = \frac{L_m^2}{L_r}\frac{di_{m\alpha}}{dt} = \frac{L_m^2}{L_r}\left(-\omega i_{m\beta} - \frac{1}{T_r} i_{m\alpha} + \frac{1}{T_r} i_{\alpha s}\right)$$
$$e_{m\beta}^{(2)} = \frac{L_m^2}{L_r}\frac{di_{m\beta}}{dt} = \frac{L_m^2}{L_r}\left(\omega i_{m\alpha} - \frac{1}{T_r} i_{m\beta} + \frac{1}{T_r} i_{\beta s}\right) \qquad (4.11)$$

The block diagram of the speed estimation system is shown in Figure 4.3. It should be noted that the factor L_m^2/L_r has been incorporated into the adaptation mechanism gain constant. Although in the back emf based method pure integration is removed from the reference model, differential term appears in the reference model.

The adaptation mechanism for this MRAC system can be derived, using the hyperstability criterion in the following form [Peng and Fukao 1994]:

$$\omega^{est} = K_p(e_{m\beta}^{(1)} e_{m\alpha}^{(2)} - e_{m\alpha}^{(1)} e_{m\beta}^{(2)}) + \int K_i(e_{m\beta}^{(1)} e_{m\alpha}^{(2)} - e_{m\alpha}^{(1)} e_{m\beta}^{(2)})dt \qquad (4.6a)$$

Although the low speed performance of the back emf based MRAC speed estimator is better than the one of the rotor flux based MRAC speed estimator, the back emf based speed estimator is more difficult to design due to the non-linear effects of the adaptation gain constants [Marwali and Keyhani, 1997].

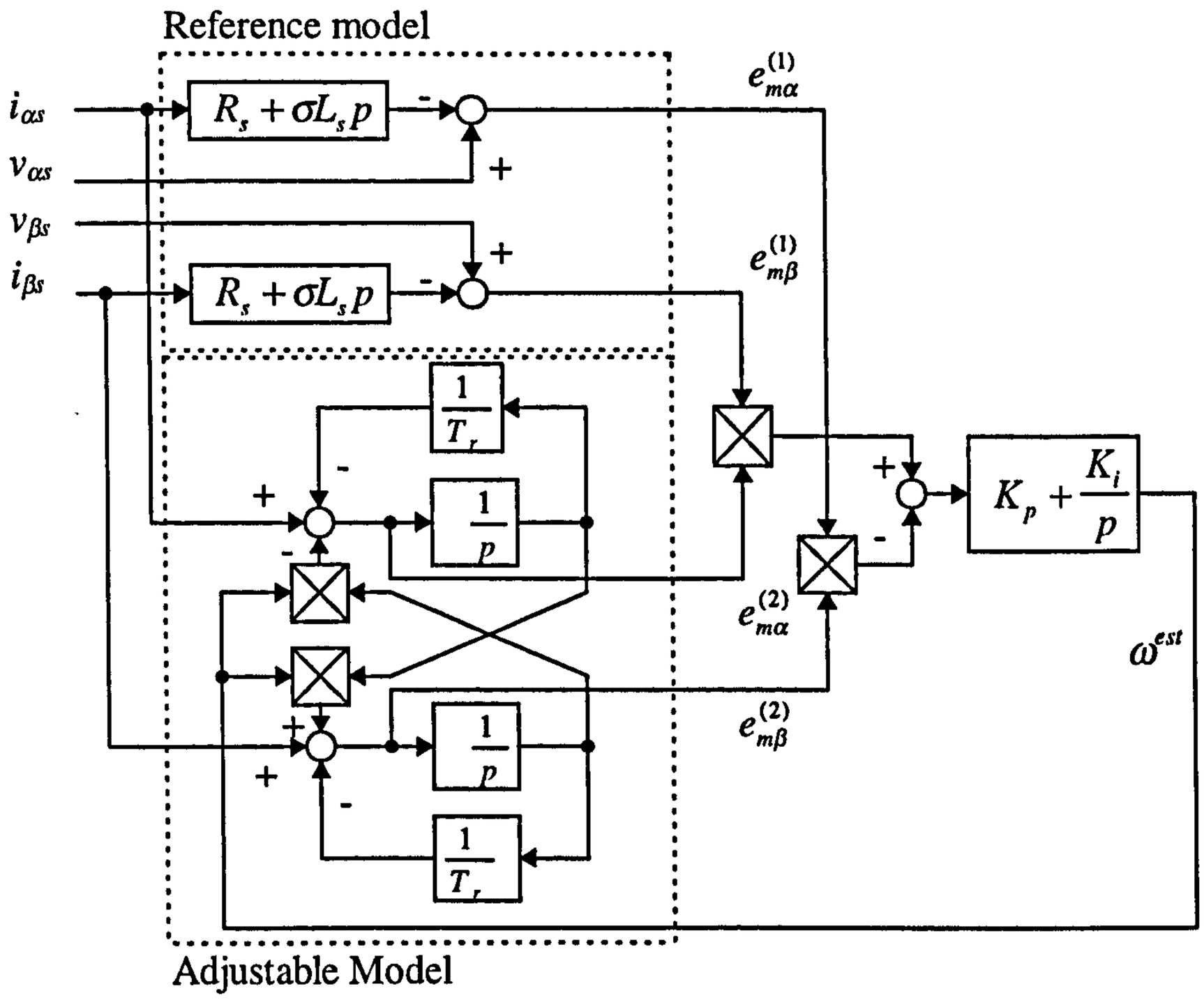

Figure 4.3: Back emf based MRAC speed estimator.

4.4 Reactive power based MRAC scheme for speed estimation

Back emf based speed estimation method has no pure integration in its reference model. However, stator resistance still remains in the reference model. In order to eliminate stator resistance from the MRAC based speed estimation, an alternative quantity for the output of the reference and adjustable models was introduced by Peng and Fukao [1994]. The new quantity is the cross product of the back emf vector and the stator current vector:

$$q = \bar{i}_s \otimes \bar{e}_m \tag{4.12}$$

It should be pointed out that the new quantity represents the instantaneous reactive power. By considering equation (4.2) and noting that $\bar{i}_s \otimes \bar{i}_s = 0$, the output of the reference model is obtained in the form of:

$$q^{(1)} = \bar{i}_s \otimes \left(\bar{v}_s - \sigma L_s \frac{d\bar{i}_s}{dt} \right) \tag{4.13}$$

It can be seen that stator resistance does not appear in the reference model. There is also no pure integration in the reference model. In the similar manner, by considering equation (4.3), the output of the adjustable model is obtained as:

$$q^{(2)} = \bar{i}_s \otimes \frac{L_m}{L_r}\left(-\frac{1}{T_r} + j\omega\right)\bar{\psi}_r \tag{4.14}$$

From equations (4.13) and (4.14) reactive powers of the reference model and the adjustable model are expressed as follows:

$$q^{(1)} = v_{\beta s} i_{\alpha s} - v_{\alpha s} i_{\beta s} - \sigma L_s\left(i_{\alpha s}\frac{di_{\beta s}}{dt} - i_{\beta s}\frac{di_{\alpha s}}{dt}\right) \tag{4.15}$$

$$q^{(2)} = \frac{L_m}{L_r}\left[\frac{1}{T_r}\left(\psi_{\alpha r} i_{\beta s} - \psi_{\beta r} i_{\alpha s}\right) + \omega\left(\psi_{\alpha r} i_{\alpha s} + \psi_{\beta r} i_{\beta s}\right)\right] \tag{4.16}$$

The rotor flux components are estimated by equation (4.5). The full block diagram of reactive power based MRAC speed estimator is given in Figure 4.4.

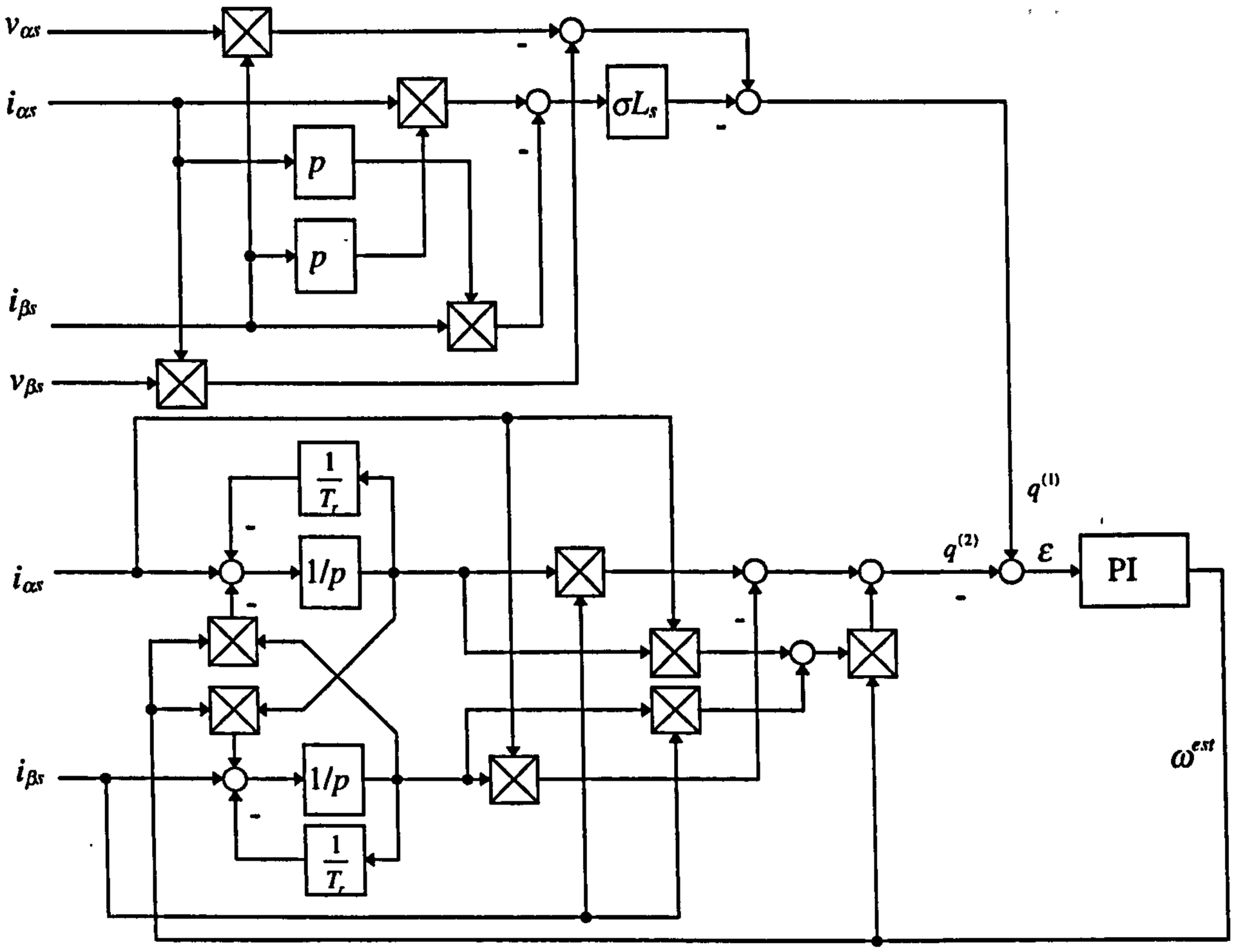

Figure 4.4: Reactive power based MRAC speed estimator.

Good features of reactive power based MRAC method are that it is independent of stator resistance variations and the calculations are relatively simple as no integration is involved. However, differentiation is required in the reference model.

Rotor time constant, which is sensitive to temperature variations, still remains in the adjustable model. In order to remove the rotor time constant from the adjustable model, Perng et al [1997] proposed the following MRAC based speed identification scheme for sensorless vector controlled induction motor drives. The reactive power equations for the reference model and adjustable model are derived from the machine model in the rotor flux oriented reference frame:

$$q^{(1)} = v_{qs} i_{ds} - v_{ds} i_{qs} \tag{4.17}$$

$$q^{(2)} = \omega_r (\sigma L_s i_{qs}^2 + L_s i_{ds}^2) + i_{ds} \sigma L_s p i_{qs} - i_{qs} L_s p i_{ds} \tag{4.18}$$

Reactive power in the adjustable model is function of rotor flux angular speed, so that this speed rather than rotor speed is initially estimated using MRAC. It is worth noting that equations (4.17) and (4.18) do not contain either rotor resistance or stator resistance. Moreover, there is no pure integration in both equations. Once the synchronous speed is estimated, the rotor speed can be calculated as:

$$\omega^{est} = \omega_r - \frac{i_{qs}^*}{T_r^* i_{ds}^*} \tag{4.19}$$

Choy et al [1996] proposed an alternative speed estimation approach with high performance over a wide speed range. The method introduces a new quantity as the output of the reference and adjustable model. The quantity is the weighted sum of reactive power and cross-product of stator current and rotor flux. The new quantity h_m has the form of:

$$h_m = \bar{i}_s \otimes (\alpha \bar{e}_m + k(1-\alpha)\bar{\psi}_r) \tag{4.20}$$

where the weighting factor α has the values of $0 \leq \alpha \leq 1$, and k is a normalising factor with $k \geq 0$.

The proposed method is robust with respect to variations in stator resistance at low speed and to variations in leakage inductance at high speed.

A comparative study of rotor flux based, back emf based and reactive power based MRAC speed estimation methods was performed by Conroy et al [1995]. The behaviour of these methods was evaluated in medium performance sensorless vector controlled drives. The results show that the rotor flux based method can provide good performance in all operating conditions except near zero and low speeds. Back emf based method has excellent performance over a wide speed range, however its accuracy at low speed is affected by inaccuracy in stator resistance. Reactive power based method has the advantage of eliminating stator resistance but it is difficult to get stable control in all operating conditions.

4.5 Air-gap power based MRAC scheme for speed estimation

In previous section, an instantaneous reactive power based speed estimation scheme is reviewed. In that scheme, the stator resistance is eliminated from the reference model. However, the stator transient inductance is still present in the reference model. The accuracy of speed estimation is affected by variations of stator transient inductance. In order to eliminate the impact of stator transient inductance on speed estimation and eliminate the pure integration in the reference model, Zhen and Xu [1995] proposed another way to improve the performance of the MRAC based speed estimation method. In the proposed method, stator transient inductance is eliminated from the reference model, but stator resistance is still present. However, an on-line stator resistance identification scheme is applied so that an accurate speed estimate can be obtained at all speeds.

The proposed speed estimation method is derived from the basic induction machine equations (4.5) and (4.8). In order to eliminate the stator transient inductance, the first equation of (4.8), multiplied by $pi_{\alpha s}$, is subtracted from the second equation of (4.8), multiplied by $pi_{\beta s}$. The difference is defined as $D_m^{(1)}$ and is given with:

$$D_m^{(1)} = (v_{\beta s} pi_{\alpha s} - v_{\alpha s} pi_{\beta s}) - R_s (i_{\beta s} pi_{\alpha s} - i_{\alpha s} pi_{\beta s}) \tag{4.21}$$

It should be noted that equation (4.21) represents the air-gap power of the induction machine.

Similarly, the first equation of (4.11) is multiplied by $pi_{\alpha s}$, the second equation of (4.11) is multiplied by $pi_{\beta s}$, and the difference is defined as $D_m^{(2)}$:

$$D_m^{(2)} = \frac{L_m^2}{L_r}\left(\omega(i_{\alpha m} pi_{\alpha s} + i_{\beta m} pi_{\beta s}) + \frac{1}{T_r}((i_{\alpha m} pi_{\beta s} - i_{\beta m} pi_{\alpha s}) + (i_{\beta s} pi_{\alpha s} - i_{\alpha s} pi_{\beta s}))\right) \tag{4.22}$$

Based on equations (4.21) and (4.22), the air-gap power based MRAC speed estimator is obtained. Equation (4.21), which does not involve the rotor speed, is used as the reference model and equation (4.22), which involves the rotor speed, as the adjustable model. Figure 4.5 illustrates the complete diagram of the air-gap power based speed estimation scheme.

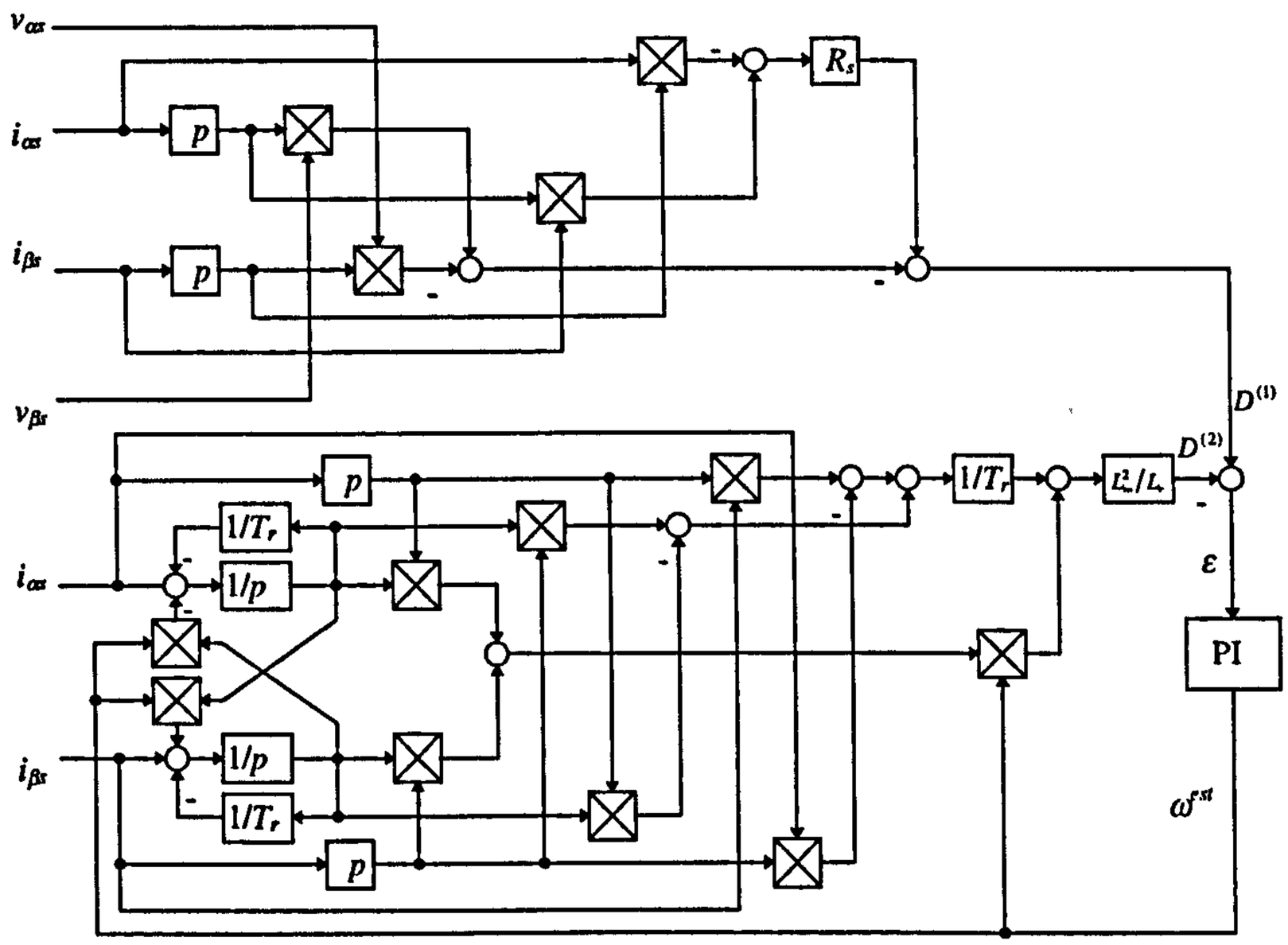

Figure 4.5: Air-gap power based MRAC speed estimator.

As there is no stator transient inductance in the reference model and the stator resistance is identified by an on-line identification scheme, the speed estimator has good performance over a wide speed range.

4.6 Summary

Different types of MRAC speed estimation schemes are reviewed. They mainly differ with respect to which quantity is selected as the output of the reference model and

adjustable model. Among these methods, rotor flux based MRAC speed estimation method is believed to be the most common choice due to its design simplicities. Although there are some problems due to the pure integration in the reference model, it is possible to modify the algorithm to solve these problems. Therefore, rotor flux based MRAC speed estimation scheme will be used in further study of the sensorless vector controlled induction motor drives.

Back emf based MRAC speed estimation method was developed to overcome the integration problem. It eliminates the pure integration from the reference model. However, existing literature suggests that it is difficult to properly design the gain constants of the adaptation mechanism.

Reactive power based MRAC speed estimation method has the advantage of being completely robust with respect to the stator resistance variations as the stator resistance is eliminated from the reference model.

Air-gap power based speed estimation method eliminates the transient stator inductance from the reference model, but the stator resistance still remains. However, the stator resistance can be identified on-line, so that the good performance of the speed estimation can be obtained over a wide speed range.

5 MODELS OF AN INDUCTION MACHINE USED FOR STEADY-STATE AND TRANSIENT ANALYSIS OF THE DRIVE

5.1 Introduction

Fundamental principles of vector control of an induction machine, described in Chapter 2, were developed using a constant parameter induction machine model, under the assumption of ideal magnetic conditions. Consequently, in a constant parameter induction machine model, the iron loss and main flux saturation are neglected. However, the iron loss and saturation do exist in any induction machine in reality. The omission of iron loss and main flux saturation representation in the control system of a vector controlled induction machine will result in deterioration of the drive performance with respect to idealised, theoretical behaviour. Therefore, for a high performance induction machine drive, improved induction machine models need to be used for development of the controller, if accurate control is to be achieved under varying operating conditions.

In order to analyse the detuning caused by iron loss and main flux saturation and to compensate these detuning sources in vector controlled induction machine drives, different improved induction machine models have to be used. In recent past, improved induction machine models that account for iron loss, main flux saturation or both iron loss and main flux saturation have been developed and proposed in literature. These models are reviewed in this chapter.

The improved induction machine models presented in this chapter will be subsequently used for representation of induction machine in quantitative analysis of detuning in sensorless vector controlled induction machine drives. Furthermore, the improved induction machine models will be utilised to develop improved vector controllers and speed estimators that compensate detuning in vector controlled induction motor drives. It should be noted that all the models of this chapter result by appropriate modification of the basic machine model, given in chapter 2 with equations (2.35) to (2.38).

Dynamic and steady-state induction machine models that account for iron loss are presented in section 5.2. Dynamic and steady-state induction machine models that include main flux saturation representation are elaborated in section 5.3. In section 5.4,

dynamic and steady-state induction machine models that simultaneously account for both iron loss and main flux saturation are given.

5.2 Dynamic and steady-state models with included iron loss

Investigation of iron loss impact on vector control of an induction machine has been reported in a number of recent publications [Kubota and Matsuse, 1992; Garcia et al, 1994; Levi, 1995; Sokola, 1998]. All these studies apply to the case when an induction machine is equipped with a speed or position sensor. In general, inclusion of iron loss representation in a dynamic model of an induction machine closely parallels the method used in steady-state analysis of induction machines supplied from a sinusoidal source [Vas, 1992]. A dynamic model, with all the winding currents selected as state-space variables, that includes iron loss representation, was proposed for the first time by Boldea and Nasar [1987]. This model can be regarded as the starting point in derivation of appropriate models, applicable to different types of vector control that include iron loss representation and that were developed by Levi [1994]. In this section, the improved induction machine model with included iron loss representation, developed by Levi [1994], is reviewed. The model is derived in an arbitrary system of orthogonal axis. Iron loss is represented with an equivalent resistance, which is placed in parallel to the magnetising branch in the space vector equivalent circuit of the induction machine. The iron loss equivalent resistance can be experimentally determined [Levi et al,1996]. Leakage flux saturation and main flux saturation effects are neglected.

The dynamic space vector equivalent circuit of an induction machine in an arbitrary frame of reference is shown in Figure 5.1. The equivalent circuit is more complicated than the standard circuit with neglected iron loss, since there is an additional branch with the equivalent iron loss resistance.

The equations that describe an induction machine with included iron loss representation, shown in Figure 5.1, can be expressed in terms of space vectors in an arbitrary reference frame as:

$$\begin{aligned} \bar{v}_s &= R_s \bar{i}_s + \frac{d\bar{\psi}_s}{dt} + j\omega_a \bar{\psi}_s \\ 0 &= R_r \bar{i}_r + \frac{d\bar{\psi}_r}{dt} + j(\omega_a - \omega)\bar{\psi}_r \end{aligned} \tag{5.1}$$

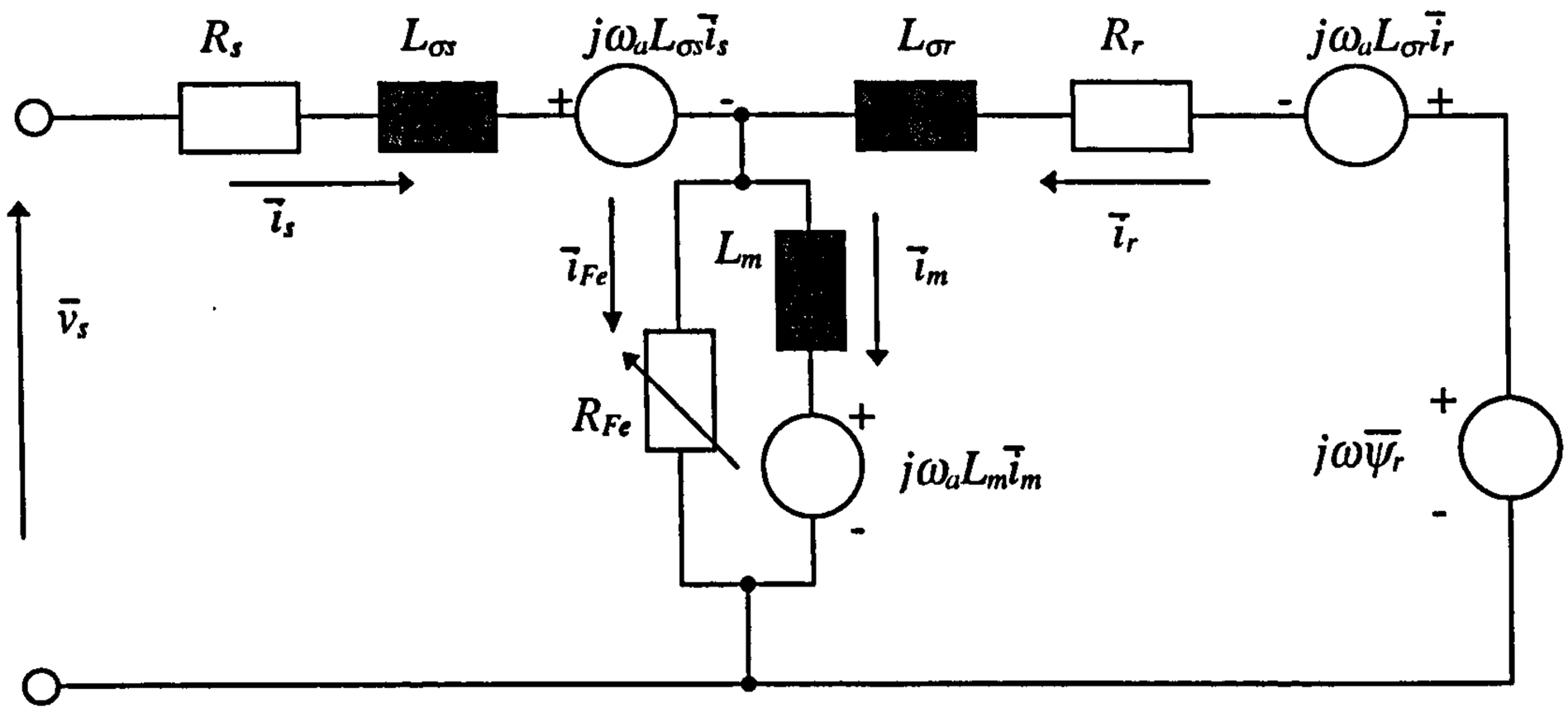

Figure 5.1: Space vector equivalent circuit of an induction machine, in an arbitrary reference frame, that includes iron loss representation.

$$\begin{aligned}\bar{\psi}_s &= L_{\sigma s}\bar{i}_s + L_m\bar{i}_m = L_{\sigma s}\bar{i}_s + \bar{\psi}_m \\ \bar{\psi}_r &= L_{\sigma r}\bar{i}_r + L_m\bar{i}_m = L_{\sigma r}\bar{i}_r + \bar{\psi}_m\end{aligned} \tag{5.2}$$

$$R_{Fe}\bar{i}_{Fe} = L_m\frac{d\bar{i}_m}{dt} + j\omega_a L_m\bar{i}_m \tag{5.3}$$

$$\bar{i}_m + \bar{i}_{Fe} = \bar{i}_s + \bar{i}_r \tag{5.4}$$

$$T_e = \frac{3}{2}P\frac{L_m}{L_{\sigma r}}(\psi_{dr}i_{qm} - \psi_{qr}i_{dm}) \tag{5.5}$$

and

$$T_e - T_L = \frac{J}{P}\frac{d\omega}{dt} \tag{5.6}$$

where $R_{Fe} = f(f_e)$, and ω_a is the angular speed of the reference frame. It is important to note that function $R_{Fe} = f(f_e)$ models only the fundamental component of the iron loss. Model (5.1) - (5.6) should therefore be used only under the assumption of ideal sinusoidal supply. The reason for this restriction is that, with a PWM supply, there are higher order voltage harmonics for which function $R_{Fe} = f(f_e)$ can be quite different when compared to the one valid for fundamental harmonic [Levi et al, 1996]. Another important note is that in general, equivalent iron loss resistance is a function of both the frequency and flux density. Identification procedure of [Levi et al, 1996] is performed

in such a way that dependence on flux density is automatically taken into account, so that the identified function $R_{Fe}=f(f_e)$ is directly applicable for vector controlled drives.

If ω_a=0, the two axis dynamic induction machine model in stationary reference frame is obtained in the following form:

$$v_{\alpha s} = R_s i_{\alpha s} + L_{\sigma s}\frac{di_{\alpha s}}{dt} + L_m\frac{di_{\alpha m}}{dt}$$
$$v_{\beta s} = R_s i_{\beta s} + L_{\sigma s}\frac{di_{\beta s}}{dt} + L_m\frac{di_{\beta m}}{dt} \qquad (5.7)$$

$$0 = R_r i_{\alpha r} + L_{\sigma r}\frac{di_{\alpha r}}{dt} + L_m\frac{di_{\alpha m}}{dt} + \omega\left(L_{\sigma r} i_{\beta r} + L_m i_{\beta m}\right)$$
$$0 = R_r i_{\beta r} + L_{\sigma r}\frac{di_{\beta r}}{dt} + L_m\frac{di_{\beta m}}{dt} - \omega\left(L_{\sigma r} i_{\alpha r} + L_m i_{\alpha m}\right) \qquad (5.8)$$

$$i_{\alpha m} + i_{\alpha Fe} = i_{\alpha s} + i_{\alpha r} \qquad i_{\beta m} + i_{\beta Fe} = i_{\beta s} + i_{\beta r} \qquad (5.9)$$

$$R_{Fe} i_{\alpha Fe} = L_m\frac{di_{\alpha m}}{dt} \qquad R_{Fe} i_{\beta Fe} = L_m\frac{di_{\beta m}}{dt} \qquad (5.10)$$

$$T_e = \frac{3}{2}P\frac{L_m}{L_{\sigma r}}(\psi_{\alpha r} i_{\beta m} - \psi_{\beta r} i_{\alpha m}) \qquad (5.5)$$

$$T_e - T_L = \frac{J}{P}\frac{d\omega}{dt} \qquad (5.6)$$

For steady-state analysis, an induction machine model valid under steady-state conditions has to be utilised. Such a model can be easily obtained from (5.1) - (5.6) if sinusoidal supply condition are assumed and speed of the reference frame ω_a is selected as equal to the fundamental frequency of the supply, $\omega_e=2\pi f_e$. Then, in steady-state, all the time-derivatives become zero and induction machine model for steady-state operation is obtained as:

$$\bar{v}_s = R_s\bar{i}_s + j\omega_e\bar{\psi}_s$$
$$0 = R_r\bar{i}_r + j(\omega_e - \omega)\bar{\psi}_r \qquad (5.12)$$
$$R_{Fe}\bar{i}_{Fe} = j\omega_e L_m\bar{i}_m$$

$$\bar{\psi}_s = L_{\sigma s}\bar{i}_s + L_m\bar{i}_m = L_{\sigma s}\bar{i}_s + \bar{\psi}_m$$
$$\bar{\psi}_r = L_{\sigma r}\bar{i}_r + L_m\bar{i}_m = L_{\sigma r}\bar{i}_r + \bar{\psi}_m \qquad (5.2)$$

$$\bar{i}_m + \bar{i}_{Fe} = \bar{i}_s + \bar{i}_r \tag{5.4}$$

$$T_e = \frac{3}{2} P \frac{L_m}{L_{\sigma r}} \mathrm{Im}\{\bar{i}_m \overline{\psi}_r^*\} \tag{5.5}$$

where the asterisk represents complex conjugation.

Dynamic model (5.5) - (5.10) and steady-state model (5.2), (5.4), (5.5), (5.12) will be used in both assessment of iron loss induced detuning and in development of compensations schemes. In particular, steady-state model (5.2), (5.4), (5.11), (5.12) is applied in section 6.2 in assessment of iron loss induced detuning in steady-state operation. State-space form of the model (5.6) - (5.11), in which stator voltage equations are omitted due to assumed ideal current feeding ($i_{\alpha s}=i_{\alpha s}^*$ and $i_{\beta s}=i_{\beta s}^*$), iron loss current components are eliminated, and state-space variables are selected as rotor speed and rotor current and magnetising current α-β components, is used in simulation of transients in section 7.7. State-space form of this model is

$$\begin{aligned}
\frac{di_{\alpha m}}{dt} &= \frac{1}{T_{Fe}}\left(i_{\alpha s}^* + i_{\alpha r} - i_{\alpha m}\right) \\
\frac{di_{\beta m}}{dt} &= \frac{1}{T_{Fe}}\left(i_{\beta s}^* + i_{\beta r} - i_{\beta m}\right) \\
\frac{di_{\alpha r}}{dt} &= -\frac{1}{T_{\sigma r}} i_{\alpha r} - \frac{L_m}{L_{\sigma r}} \frac{1}{T_{Fe}}\left(i_{\alpha s}^* + i_{\alpha r} - i_{\alpha m}\right) - \omega\left(i_{\beta r} + \frac{L_m}{L_{\sigma r}} i_{\beta m}\right) \\
\frac{di_{\beta r}}{dt} &= -\frac{1}{T_{\sigma r}} i_{\beta r} - \frac{L_m}{L_{\sigma r}} \frac{1}{T_{Fe}}\left(i_{\beta s}^* + i_{\beta r} - i_{\beta m}\right) + \omega\left(i_{\alpha r} + \frac{L_m}{L_{\sigma r}} i_{\alpha m}\right) \\
\frac{d\omega}{dt} &= \frac{P}{J}\left[\frac{3}{2} P L_m \left(i_{\alpha r} i_{\beta m} - i_{\beta r} i_{\alpha m}\right) - T_L\right]
\end{aligned} \tag{5.11}$$

where $T_{Fe}=L_m/R_{Fe}$, $T_{\sigma r}=L_{\sigma r}/R_r$.

Induction machine will be represented with (5.11) in simulations of section 7.7, while stator voltage equations (5.7) will be used to reconstruct the voltages (that are required as inputs of the speed estimator).

Finally, the use of the model (5.5) - (5.10) will be made in development of a modified speed estimation scheme that provides for compensation of the iron loss in section 8.2.

5.3 Dynamic and steady-state models with included main flux saturation

In a constant parameter induction machine model main flux saturation is neglected. However, many research results show that main flux saturation in induction machines plays an important role in a number of operating regimes. Therefore, main flux saturation has to be accounted for in the induction machine model.

A number of publications describe how main flux saturation can be included in an induction machine model [Boldea and Nasar, 1987; Vas, 1992; Levi and Krzeminski, 1996]. The induction machine model, based on all the winding currents as state-space variables [Vas, 1992] is given at first in this section. To start with, the model of an induction machine with included main flux saturation consists of the same equations as the constant parameter machine model. The voltage equations, in terms of space vectors in an arbitrary frame of reference, are written from (5.1) and (5.2) in the form:

$$\begin{aligned}\bar{v}_s &= R_s\bar{i}_s + L_{\sigma s}\frac{d\bar{i}_s}{dt} + j\omega_a L_{\sigma s}\bar{i}_s + \frac{d\bar{\psi}_m}{dt} + j\omega_a\bar{\psi}_m \\ 0 &= R_r\bar{i}_r + L_{\sigma r}\frac{d\bar{i}_r}{dt} + j\omega_a L_{\sigma r}\bar{i}_r + \frac{d\bar{\psi}_m}{dt} + j\omega_a\bar{\psi}_m - j\omega\left(L_{\sigma r}\bar{i}_r + \bar{\psi}_m\right)\end{aligned} \tag{5.13}$$

Thus it is assumed that leakage flux can be separated from main flux and these two flux components are further treated independently.

The dynamic equivalent circuit of the saturated induction machine, in an arbitrary reference frame can be constructed based on equations (5.13) and is shown in Figure 5.2. The only difference compared to the equivalent circuit of a constant parameter

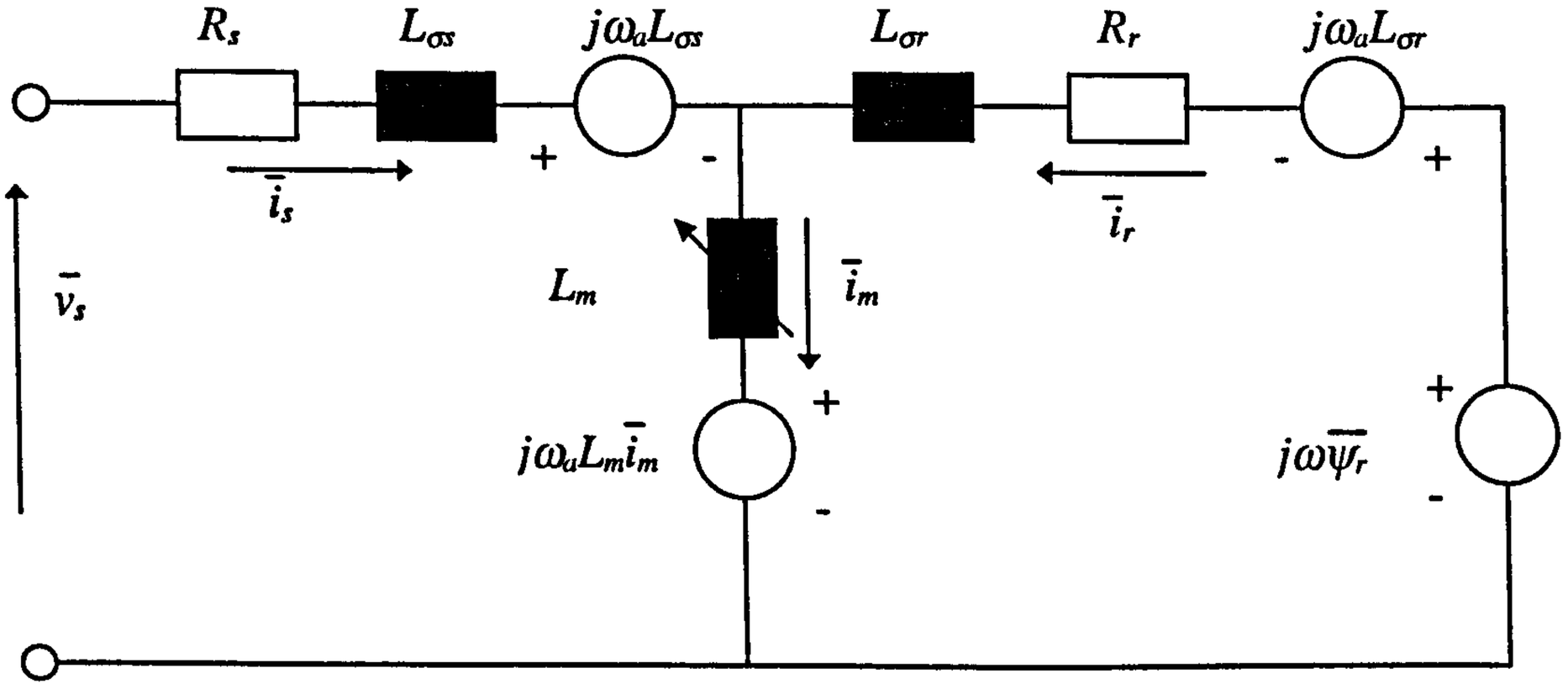

Figure 5.2: Dynamic equivalent circuit of a saturated induction machine in an arbitrary reference frame.

induction machine is that the magnetising inductance is now a variable parameter.

Derivation of the developed form of the model further proceeds along the lines detailed in [Vas,1992], using (5.13) as the starting point. All the winding currents are selected as state-space variables and main flux linkage space vector is eliminated from (5.13) using correlation

$$\bar{\psi}_m = L_m \bar{i}_m \tag{5.14}$$

As this elimination involves time derivative of $\bar{\psi}_m$ and as L_m is a variable parameter, then it is necessary to perform differentiation of L_m in (5.14) as well. In other words

$$d\bar{\psi}_m / dt = (dL_m / dt)\bar{i}_m + L_m d\bar{i}_m / dt \tag{5.15}$$

Detailed derivation procedure is available in [Vas, 1992]. Upon completion of the derivation, the model is obtained in matrix form as:

$$\underline{v} = \underline{L}\frac{d\underline{i}}{dt} + \underline{B}\underline{i} \tag{5.16}$$

where

$$\underline{v} = \begin{bmatrix} v_{ds} & v_{qs} & 0 & 0 \end{bmatrix}^t \qquad \underline{i} = \begin{bmatrix} i_{ds} & i_{qs} & i_{dr} & i_{qr} \end{bmatrix}^t \tag{5.17}$$

$$\underline{B} = \begin{bmatrix} R_s & -\omega_a(L_m + L_{\sigma s}) & 0 & -\omega_a L_m \\ \omega_a(L_m + L_{\sigma s}) & R_s & \omega_a L_m & 0 \\ 0 & -(\omega_a - \omega)L_m & R_r & -(\omega_a - \omega)(L_m + L_{\sigma r}) \\ (\omega_a - \omega)L_m & 0 & (\omega_a - \omega)(L_m + L_{\sigma r}) & R_r \end{bmatrix} \tag{5.18}$$

$$\underline{L} = \begin{bmatrix} L_{\sigma s} + L_{ddm} & L_{dq} & L_{ddm} & L_{dq} \\ L_{dq} & L_{\sigma s} + L_{qqm} & L_{dq} & L_{qqm} \\ L_{ddm} & L_{dq} & L_{\sigma r} + L_{ddm} & L_{dq} \\ L_{dq} & L_{qqm} & L_{dq} & L_{\sigma r} + L_{qqm} \end{bmatrix} \tag{5.19}$$

$$T_e = \frac{3}{2} P L_m (i_{dr} i_{qs} - i_{qr} i_{ds}) \tag{5.20}$$

Inductances in (5.19) L_{ddm} and L_{qqm} are the transient magnetising inductances along the direct and quadrature axes of the arbitrary reference frame, and L_{dq} is the cross-coupling

inductance between the two *d*-*q* axes windings, which are in space quadrature. These inductances are defined as follows:

$$L_{ddm}=L\cos^2\mu+L_m\sin^2\mu \tag{5.21}$$

$$L_{qqm}=L\sin^2\mu+L_m\cos^2\mu \tag{5.22}$$

$$L_{dq}=(L-L_m)\cos\mu\sin\mu \tag{5.23}$$

where L is the dynamic inductance defined as

$$L=d\psi_m/di_m, \quad L=f(i_m) \tag{5.24}$$

and L_m is the steady-state saturated magnetising inductance:

$$L_m=\psi_m/i_m, \quad L_m=f(i_m) \tag{5.25}$$

The angle μ is the angle between the *d*-axis of the arbitrary reference frame and the magnetising current (flux) space vector whose real and imaginary components are i_{dm} and i_{qm} (ψ_{dm} and ψ_{qm}), respectively. Due to the non-linearity of the magnetising curve of the machine, both the steady-state magnetising inductance and the dynamic inductance are variables and depend on the corresponding value of the magnetising flux (i.e. magnetising current):

$$\psi_m=\left(\psi_{dm}^2+\psi_{qm}^2\right)^{1/2} \qquad i_m=\left(i_{dm}^2+i_{qm}^2\right)^{1/2} \tag{5.26}$$

The magnetising current and magnetising flux *d*-*q* axis components are

$$i_{dm}=i_{ds}+i_{dr} \qquad i_{qm}=i_{qs}+i_{qr} \tag{5.27}$$

$$\psi_{dm}=L_m i_{dm} \qquad \psi_{qm}=L_m i_{qm} \tag{5.28}$$

The model given with equations (5.16) to (5.25) is the current state space model and it completely describes a single cage saturated induction machine.

When equation (5.16) is compared with equation (2.35), which describes the linear model, it follows that as a result of saturation, all the inductance terms are modified in the matrix $\underline{L}$ and there are 16 variable inductance terms in the inductance matrix. Furthermore, in the saturated model the transient inductances of both the stator windings and the rotor windings in the system matrix are unequal along *d*- and *q*-axis, and all the windings in space quadrature are coupled owing to cross-saturation.

In steady state operation, taking again $\omega_a=\omega_e$, all the time derivatives in the dynamic model are zero, and thus the model becomes:

$$\begin{aligned}\bar{v}_s &= R_s\bar{i}_s + j\omega_e[(L_{\sigma s}+L_m)\bar{i}_s + L_m\bar{i}_r]\\ 0 &= R_r\bar{i}_r + j(\omega_e-\omega)[(L_{\sigma r}+L_m)\bar{i}_r + L_m\bar{i}_s]\end{aligned} \tag{5.29}$$

$$\begin{aligned}\bar{i}_m &= \bar{i}_s+\bar{i}_r\\ L_m &= f(i_m)\end{aligned} \tag{5.30}$$

$$T_e=\frac{3}{2}PL_m\left(i_{dr}i_{qs}-i_{qr}i_{ds}\right) \tag{5.20}$$

Current state-space model is used further on for representation of a saturated induction machine in detuning studies. In particular, steady-state model (5.20), (5.29), (5.30) is used in detuning studies of sections 6.3 to 6.7. Dynamic model, given with (5.16) - (5.25) is accommodated to the assumption of ideal current feeding, so that stator voltage equations are omitted from consideration. Rotor currents and rotor speed are selected as state-space variables. The model for simulation purposes is formed in the stationary reference frame (ω_a=0) and $i_{\alpha s}=i_{\alpha s}^*$, $i_{\beta s}=i_{\beta s}^*$ is accounted for. The equations used to model the machine in sections 7.3 - 7.8 are thus in state-space form:

$$\begin{aligned}\frac{di_{\alpha r}}{dt} &= -\frac{1}{L_{\sigma r}+L_{\alpha\alpha m}-\dfrac{L_{\alpha\beta}^2}{L_{\sigma r}+L_{\beta\beta m}}}\left\{R_r i_{\alpha r}+\omega L_m i_{\beta s}^*+\omega\left(L_m+L_{\sigma r}\right)i_{\beta r}+L_{\alpha\alpha m}\frac{di_{\alpha s}^*}{dt}+L_{\alpha\beta}\frac{di_{\beta s}^*}{dt}\right.\\ &\left.-\frac{L_{\alpha\beta}}{L_{\sigma r}+L_{\beta\beta m}}\left[R_r i_{\beta r}-\omega L_m i_{\alpha s}^*-\omega\left(L_m+L_{\sigma r}\right)i_{\alpha r}+L_{\alpha\beta}\frac{di_{\alpha s}^*}{dt}+L_{\beta\beta m}\frac{di_{\beta s}^*}{dt}\right]\right\}\\ \frac{di_{\beta r}}{dt} &= -\frac{1}{L_{\sigma r}+L_{\beta\beta m}-\dfrac{L_{\alpha\beta}^2}{L_{\sigma r}+L_{\alpha\alpha m}}}\left\{R_r i_{\beta r}-\omega L_m i_{\alpha s}^*-\omega\left(L_m+L_{\sigma r}\right)i_{\alpha r}+L_{\alpha\beta}\frac{di_{\alpha s}^*}{dt}+L_{\beta\beta m}\frac{di_{\beta s}^*}{dt}\right.\\ &\left.-\frac{L_{\alpha\beta}}{L_{\sigma r}+L_{\alpha\alpha m}}\left[R_r i_{\alpha r}+\omega L_m i_{\beta s}^*+\omega\left(L_m+L_{\sigma r}\right)i_{\beta r}+L_{\alpha\alpha m}\frac{di_{\alpha s}^*}{dt}+L_{\alpha\beta}\frac{di_{\beta s}^*}{dt}\right]\right\}\\ \frac{d\omega}{dt} &= \frac{P}{J}\left[\frac{3}{2}PL_m\left(i_{\alpha r}i_{\beta s}^*-i_{\beta r}i_{\alpha s}^*\right)-T_L\right]\end{aligned} \tag{5.31}$$

where

$$L_{\alpha\alpha m}=L\cos^2\mu+L_m\sin^2\mu \tag{5.21}$$

$$L_{\beta\beta m}=L\sin^2\mu+L_m\cos^2\mu \tag{5.22}$$

$$L_{\alpha\beta}=(L-L_m)\cos\mu\sin\mu \tag{5.23}$$

Stator voltage components, required as inputs into the speed estimator, are obtained using stator voltage equations of (5.16) - (5.19) in the stationary reference frame.

Current state-space model is inconvenient for development of a modified control system and/or speed estimator, due to high complexity of the inductance matrix. Alternative models are therefore used for this purpose in chapter 8. These models are those in which state-space variables are stator current and rotor flux, and magnetising flux and stator current [Levi and Krzeminski, 1996], respectively.

In all the cases mathematical model of a saturated induction machine is given in the form

$$\underline{v}=\underline{A}\frac{d\underline{x}}{dt}+\underline{B}\underline{x} \tag{5.32}$$

The mixed stator current-rotor flux model is derived from the general model by elimination of the rotor current space vector and stator flux space vector. Vector of voltages is once more:

$$\underline{v}=[v_{ds}\quad v_{qs}\quad 0\quad 0]^t \tag{5.33}$$

while the state vector is now:

$$\underline{x}=[i_{ds}\quad i_{qs}\quad \psi_{dr}\quad \psi_{qr}]^t \tag{5.34}$$

The matrices $\underline{A}$ and $\underline{B}$ are [Levi and Krzeminski, 1996]

$$\underline{A}=\begin{bmatrix} L_{\sigma s}+L_{\sigma r}-\frac{L_{\sigma r}^2}{L_{dd}} & -\frac{L_{\sigma r}^2}{L_{dq}} & 1-\frac{L_{\sigma r}}{L_{dd}} & -\frac{L_{\sigma r}}{L_{dq}} \\ -\frac{L_{\sigma r}^2}{L_{dq}} & L_{\sigma s}+L_{\sigma r}-\frac{L_{\sigma r}^2}{L_{qq}} & -\frac{L_{\sigma r}}{L_{dq}} & 1-\frac{L_{\sigma r}}{L_{qq}} \\ 0 & 0 & 1 & 0 \\ 0 & 0 & 0 & 1 \end{bmatrix} \tag{5.35}$$

$$\underline{B}=\begin{bmatrix} R_s & -\omega_a\left(L_{\sigma s}+L_{\sigma r}-\frac{L_{\sigma r}^2}{L_r}\right) & 0 & -\omega_a\frac{L_m}{L_r} \\ -\omega_a\left(L_{\sigma s}+L_{\sigma r}-\frac{L_{\sigma r}^2}{L_r}\right) & R_s & -\omega_a\frac{L_m}{L_r} & 0 \\ -\frac{L_m}{T_r} & 0 & \frac{1}{T_r} & -(\omega_a-\omega) \\ 0 & -\frac{L_m}{T_r} & \omega_a-\omega & \frac{1}{T_r} \end{bmatrix} \tag{5.36}$$

The saturation dependent coefficients in (5.36) are:

$$\begin{aligned} \frac{1}{L_{dd}} &= \frac{1}{L_r^{\cdot}}\left(\frac{\Psi_d}{\Psi}\right)^2+\frac{1}{L_r}\left(\frac{\Psi_q}{\Psi}\right)^2 \\ \frac{1}{L_{qq}} &= \frac{1}{L_r^{\cdot}}\left(\frac{\Psi_q}{\Psi}\right)^2+\frac{1}{L_r}\left(\frac{\Psi_d}{\Psi}\right)^2 \\ \frac{1}{L_{dq}} &= \left(\frac{1}{L_r^{\cdot}}-\frac{1}{L_r}\right)\frac{\Psi_d}{\Psi}\frac{\Psi_q}{\Psi} \end{aligned} \tag{5.37}$$

where

$$\begin{aligned} \Psi_d &= \psi_{dr}+L_{\sigma r}i_{ds}\equiv(L_{\sigma r}+L_m)i_{dm} \\ \Psi_q &= \psi_{qr}+L_{\sigma r}i_{qs}\equiv(L_{\sigma r}+L_m)i_{qm} \\ \Psi &= \sqrt{\Psi_d^2+\Psi_q^2} \end{aligned} \tag{5.38}$$

is the so-called generalised flux vector amplitude and its *d-q* axis components [Levi and Krzeminski, 1996], and

$$L_r^{\cdot}=L_{\sigma r}+L=\frac{d\Psi}{di_m} \tag{5.39}$$

The mechanical equation of motion remains unchanged. The electromagnetic torque is expressed, in terms of *d-q* variables, as:

$$T_e=\frac{3}{2}P\frac{L_m}{L_r}\left(\psi_{dr}i_{qs}-\psi_{qr}i_{ds}\right) \tag{5.40}$$

The magnetising flux-stator current model, presented in [Levi and Krzeminski, 1996], is derived from the general model by selecting the *d-q* components of the magnetising

flux and the stator current as state variables. The vector of voltages is given with (5.33), while the state vector is now:

$$\underline{x} = [i_{ds} \quad i_{qs} \quad \psi_{dm} \quad \psi_{qm}]^t \tag{5.41}$$

Matrices $\underline{A}$ and $\underline{B}$ are now:

$$\underline{A} = \begin{bmatrix} L_{\sigma s} & 0 & 1 & 0 \\ 0 & L_{\sigma s} & 0 & 1 \\ -L_{\sigma r} & 0 & 1+\dfrac{L_{\sigma r}}{L_{dd}} & \dfrac{L_{\sigma r}}{L_{dq}} \\ 0 & -L_{\sigma r} & \dfrac{L_{\sigma r}}{L_{dq}} & 1+\dfrac{L_{\sigma r}}{L_{qq}} \end{bmatrix} \tag{5.42}$$

$$\underline{B} = \begin{bmatrix} R_s & -\omega_a L_{\sigma s} & 0 & -\omega_a \\ \omega_a L_{\sigma s} & R_s & \omega_a & 0 \\ -R_r & \omega_{sl} L_{\sigma r} & \dfrac{R_r}{L_m} & -\omega_{sl}\left(1+\dfrac{L_{\sigma r}}{L_m}\right) \\ -\omega_{sl} L_{\sigma r} & -R_r & \omega_{sl}\left(1+\dfrac{L_{\sigma r}}{L_m}\right) & \dfrac{R_r}{L_m} \end{bmatrix} \tag{5.43}$$

The saturation-dependent coefficients in (5.42) are

$$\begin{aligned} \frac{1}{L_{dd}} &= \frac{1}{L}\left(\frac{\psi_{dm}}{\psi_m}\right)^2 + \frac{1}{L_m}\left(\frac{\psi_{qm}}{\psi_m}\right)^2 \\ \frac{1}{L_{qq}} &= \frac{1}{L}\left(\frac{\psi_{qm}}{\psi_m}\right)^2 + \frac{1}{L_m}\left(\frac{\psi_{dm}}{\psi_m}\right)^2 \\ \frac{1}{L_{dq}} &= \left(\frac{1}{L} - \frac{1}{L_m}\right)\frac{\psi_{dm}}{\psi_m}\frac{\psi_{qm}}{\psi_m} \end{aligned} \tag{5.44}$$

where the dynamic inductance L is defined by (5.24). The mechanical equation of motion remains unchanged. The electromagnetic torque, expressed in terms of *d-q* variables, becomes:

$$T_e = \frac{3}{2} P\left(\psi_{dm} i_{qs} - \psi_{qm} i_{ds}\right) \tag{5.45}$$

The last two induction machine models will be used in design of an improved speed estimator in chapter 8 that enables compensation of main flux saturation. Accommodation of these models to the actual needs is elaborated in more detail in section 8.3.

5.4 Dynamic and steady-state models with included iron loss and main flux saturation

Induction machine models with either iron loss or with main flux saturation have been presented in the previous two sections, respectively. However, both iron loss and main flux saturation should be considered simultaneously, as these effects do exist in the induction machine at the same time. Detailed analysis of the detuning due to both iron loss and main flux saturation and means for simultaneous compensation in vector controlled induction motor drives have been elaborated in detail by [Sokola, 1998] for the case when speed (position) sensor exists.

The induction machine model with iron loss represented by an equivalent resistance placed in parallel with magnetising branch, and with main flux saturation accounted for, is expressed in terms of space vector as [Sokola, 1998]:

$$\bar{v}_s = R_s \bar{i}_s + L_{\sigma s} \frac{d\bar{i}_s}{dt} + \frac{d\bar{\psi}_m}{dt} + j\omega_a \bar{\psi}_s \tag{5.46}$$

$$0 = R_r \bar{i}_r + L_{\sigma r} \frac{d\bar{i}_r}{dt} + \frac{d\bar{\psi}_m}{dt} + j(\omega_a - \omega)\bar{\psi}_r \tag{5.47}$$

$$R_{Fe} \bar{i}_{Fe} = j\omega_a \bar{\psi}_m + \frac{d\bar{\psi}_m}{dt} \tag{5.48}$$

$$\bar{i}_{Fe} + \bar{i}_m = \bar{i}_s + \bar{i}_r \tag{5.49}$$

$$\begin{aligned} \bar{\psi}_s &= L_{\sigma s} \bar{i}_s + L_m \bar{i}_m \\ \bar{\psi}_r &= L_{\sigma r} \bar{i}_r + L_m \bar{i}_m \end{aligned} \tag{5.2}$$

$$\bar{\psi}_m = L_m \bar{i}_m \tag{5.50}$$

$$R_{Fe} = f(f_e) \qquad L_m = f(i_m) \text{ or } L_m = f(\psi_m) \tag{5.51}$$

The equivalent circuit of an induction machine with both iron loss and main flux saturation taken into consideration can be constructed from the above equations. The corresponding equivalent circuit is shown in Figure 5.3. Both equivalent iron loss resistance and magnetising inductance are variables.

Based on equations (5.46) - (5.51), model of an induction machine in stationary reference frame is obtained in the following form [Sokola,1998]:

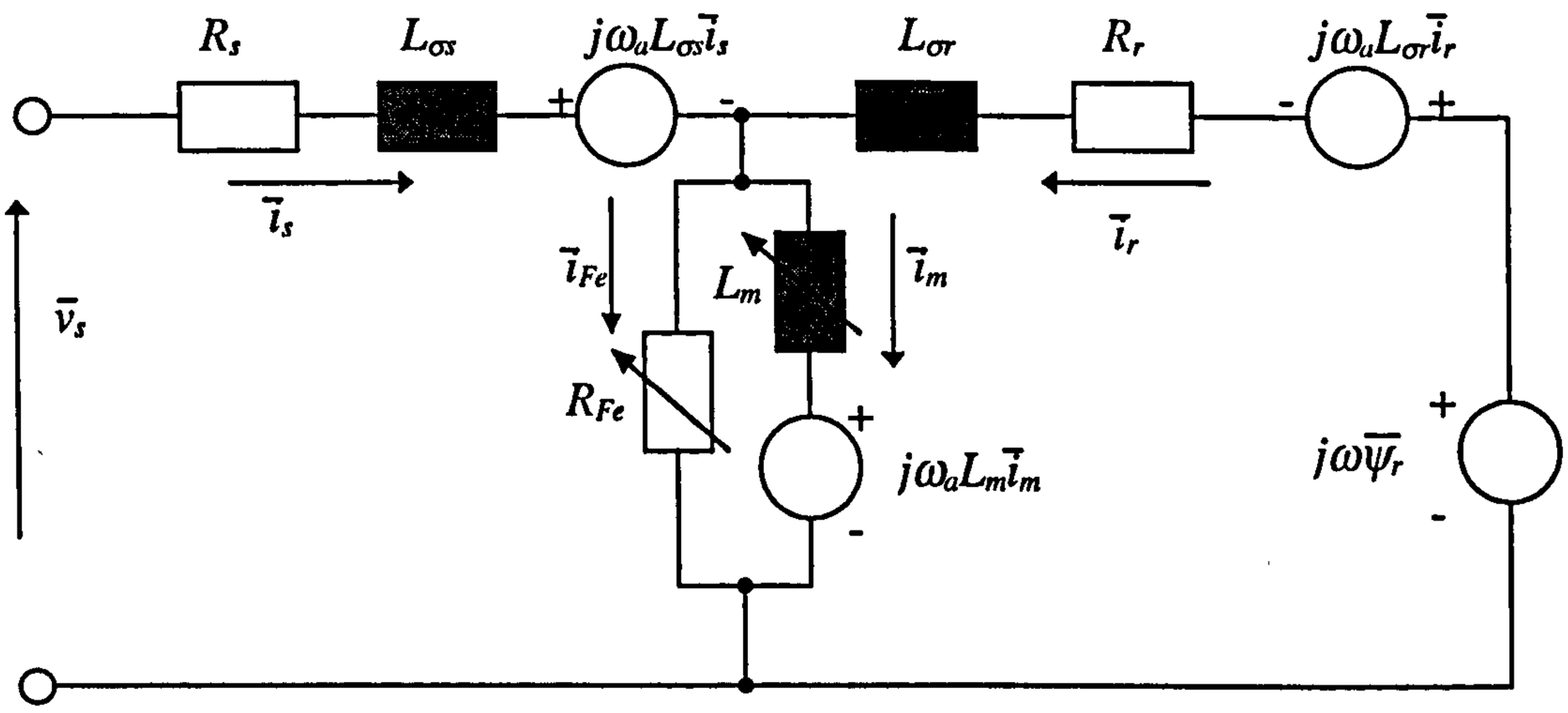

Figure 5.3: Induction machine dynamic equivalent circuit, with both iron loss and main flux saturation, in an arbitrary reference frame.

$$\frac{di_{\alpha s}}{dt} = \frac{v_{\alpha s}}{L_{\sigma s}} - \frac{1}{T_{\sigma s}} i_{\alpha s} - \frac{1}{T_{\sigma s Fe}}\left(i_{\alpha s} + i_{\alpha r} - \frac{\psi_{\alpha m}}{L_m}\right)$$
$$\frac{di_{\beta s}}{dt} = \frac{v_{\beta s}}{L_{\sigma s}} - \frac{1}{T_{\sigma s}} i_{\beta s} - \frac{1}{T_{\sigma s Fe}}\left(i_{\beta s} + i_{\beta r} - \frac{\psi_{\beta m}}{L_m}\right) \qquad (5.52)$$

$$\frac{di_{\alpha r}}{dt} = -\frac{1}{T_{\sigma r}} i_{\alpha r} - \frac{1}{T_{\sigma Fe}}\left(i_{\alpha s} + i_{\alpha r} - \frac{\psi_{\alpha m}}{L_m}\right) - \omega i_{\beta r} - \omega\frac{\psi_{\beta m}}{L_{\sigma r}}$$
$$\frac{di_{\beta r}}{dt} = -\frac{1}{T_{\sigma r}} i_{\beta r} - \frac{1}{T_{\sigma Fe}}\left(i_{\beta s} + i_{\beta r} - \frac{\psi_{\beta m}}{L_m}\right) + \omega i_{\alpha r} + \omega\frac{\psi_{\alpha m}}{L_{\sigma r}} \qquad (5.53)$$

$$\frac{d\psi_{\alpha m}}{dt} = R_{Fe}\left(i_{\alpha s} + i_{\alpha r} - \frac{\psi_{\alpha m}}{L_m}\right)$$
$$\frac{d\psi_{\beta m}}{dt} = R_{Fe}\left(i_{\beta s} + i_{\beta r} - \frac{\psi_{\beta m}}{L_m}\right) \qquad (5.54)$$

$$T_e = \frac{3}{2} P\left(i_{\alpha r}\psi_{\beta m} - i_{\beta r}\psi_{\alpha m}\right) \qquad (5.55)$$

$$T_e - T_L = \frac{J}{P}\frac{d\omega}{dt} \qquad (5.6)$$

$$R_{Fe} = f(f_e) \qquad L_m = f(i_m) \text{ or } L_m = f(\psi_m) \qquad (5.56)$$

Time constants $T_{\sigma s}$, $T_{\sigma r}$, $T_{\sigma s Fe}$ and $T_{\sigma Fe}$ are defined as $T_{\sigma s}=L_{\sigma s}/R_s$, $T_{\sigma r}=L_{\sigma r}/R_r$, $T_{\sigma s Fe}=L_{\sigma s}/R_{Fe}$ and $T_{\sigma Fe}=L_{\sigma r}/R_{Fe}$.

State-space variables are selected as stator current, rotor current and magnetising flux components. Assumption of current feeding will enable omission of (5.52) from the model in simulations of transients in section 7.8. In particular, as $i_{\alpha s}=i_{\alpha s}^*$ and $i_{\beta s}=i_{\beta s}^*$, equations (5.53) - (5.56) and (5.6) will be used to describe the machine, while equations (5.52) will be used to reconstruct stator voltage components that are inputs into the speed estimator.

For the purpose of steady-state analysis, the steady-state induction machine model can be obtained from equation (5.46) - (5.51) by setting $\omega_a=\omega_e$ and equating all the time derivatives to zero. Steady-state induction machine model is obtained as:

$$\begin{aligned} \bar{v}_s &= R_s\bar{i}_s + j\omega_e(L_{\sigma s}\bar{i}_s + \bar{\psi}_m) \\ R_{Fe}(\bar{i}_s + \bar{i}_r - \bar{i}_m) &= j\omega_e\bar{\psi}_m \\ 0 &= R_r\bar{i}_r + j(\omega_e-\omega)(L_{\sigma r}\bar{i}_r + \bar{\psi}_m) \end{aligned} \tag{5.64}$$

$$\bar{\psi}_m = L_m\bar{i}_m \tag{5.2}$$

$$L_m = f(\psi_m) \qquad R_{Fe} = f(f_e) \tag{5.65}$$

$$T_e = \frac{3}{2}P\frac{L_m}{L_r}\mathrm{Im}\{\bar{i}_s\bar{\psi}_m^*\} \tag{5.66}$$

This model is used for evaluation of steady-state detuning due to combined impact of iron loss and main flux saturation in section 6.7.

5.5 Summary

Three types of improved induction machine models were presented in this chapter. They are given for both dynamic and steady-state operation. In induction machine model with iron loss included, the iron loss is represented by an equivalent iron loss resistance placed in parallel with the magnetising branch. This model will be used for analysis of iron loss induced detuning and compensation of iron loss in a sensorless rotor flux oriented induction machine. Saturated induction machine models are discussed next. Three models reviewed in this section are the pure winding current state space model, mixed stator current-rotor flux state space model and mixed magnetising flux-stator current state space model. The first one will be used for induction machine

representation in all the relevant simulations, while the other two will play a role in designing the improved speed estimator that compensates for main flux saturation. Since there are cross-coupling inductances between two axes, the dynamic saturated induction model is more complicated than the constant parameter induction machine model. Finally, an improved induction machine model with included both iron loss and main flux saturation is given. Based on this induction machine model, it is possible to design a high performance sensorless induction motor drive with compensation for both iron loss and main flux saturation, as will be shown in Chapter 8.

6 DETUNING IN STEADY-STATE OPERATION OF A SENSORLESS ROTOR FLUX ORIENTED INDUCTION MACHINE WITH ROTOR FLUX BASED MRAC SPEED ESTIMATOR

6.1 Introduction

The aim of this chapter is to evaluate detuning effects due to iron loss, main flux saturation and parameter variations in steady-state operation of the sensorless vector controlled induction motor drive supplied from the current regulated PWM (CRPWM) voltage source inverter.

In a sensorless vector control of an induction machine, parameter variations will affect the accuracy of speed estimation. They will lead to deterioration of the drive performance. All the parameters involved in the sensorless vector control of an induction machine, such as stator resistance, rotor resistance, and magnetising inductance, are subject to change under certain conditions. Iron loss and main flux saturation, as possible sources of detuned operation in sensorless control of rotor flux oriented induction machine have received little attention so far. In order to quantify the amount of detuning caused by iron loss, main flux saturation and other parameter variations, steady-state operation in the speed mode (i.e. with closed loop speed control) is analysed in this chapter. The analyses and the results presented here are available in [Levi and Wang, 1997; Levi and Wang, 1998; Levi et al, 1999; Wang and Levi, 1999]. Detuning is evaluated for operation in the base speed region only, except in section 6.2 where field-weakening region is encompassed as well.

Section 6.2 discusses impact of iron loss on operation of the sensorless indirect rotor flux oriented induction machine. Detuning due to incorrect setting and/or variation in leakage inductances is elaborated in section 6.3, while section 6.4 evaluates detuning due to incorrect setting of the magnetising inductance. Sections 6.5 and 6.6 are devoted to detuning caused by incorrect setting and/or variation of stator resistance and rotor resistance, respectively. Combined impact of iron loss and incorrect setting of the magnetising inductance is investigated in section 6.7. On the basis of results of sections 6.2 - 6.7, relative importance of various parameter variation effects is discussed in section 6.8. Section 6.9 summaries the chapter.

6.2 Detuning due to iron loss

In this investigation, a 4-pole, 50 Hz, 4kW induction machine is used. All the parameters of the machine used here are taken from [Sokola, 1998], and are given in Appendix A. The iron loss is represented by an equivalent iron loss resistance, R_{Fe}, which is the function of frequency, as explained in chapter 5. Its analytical approximation is:

$$R_{Fe} = \begin{cases} 128.92 + 8.242 f_e + 0.07788 f_e^2 & f_e \le 50 \text{ Hz} \\ 1841 - 55275 / f_e & f_e > 50 \text{ Hz} \end{cases} \tag{6.1}$$

The magnetising curve is given in terms of RMS values with:

$$\Psi_m = \begin{cases} 0.1964285 I_m & I_m \le 2.2 \text{ A} \\ 0.8374 + 0.0067 I_m - 0.924 / I_m & I_m > 2.2 \text{ A} \end{cases} \tag{6.2}$$

Hence the magnetising inductance can be expressed as:

$$L_m = \begin{cases} 0.1964285 & \Psi_m \le 0.432 \text{ Wb} \\ 0.8032 - 0.6874 \Psi_m - 0.1338 / \Psi_m & \Psi_m > 0.432 \text{ Wb} \end{cases} \tag{6.3}$$

Main flux saturation is neglected in this section. Equations (6.2) and (6.3) will be used however in all the subsequent sections.

6.2.1 Analysis

Indirect rotor flux oriented current-fed induction machine is studied. The estimator used in this system is rotor flux based MRAC speed estimator discussed in section 4.2. Iron loss is represented in induction machine model with an equivalent iron loss resistance in parallel with magnetising inductance, as described in section 5.2. Structure of the sensorless rotor flux oriented induction machine is shown in Figure 6.1.

Rotor flux reference is constant and equal to the rated value in the base speed region. In the field-weakening region rotor flux reference is reduced in inverse proportion to rotor speed. Rate of change of the rotor flux reference in the field-weakening region is neglected in the control system of Figure 6.1. The current controlled PWM inverter is

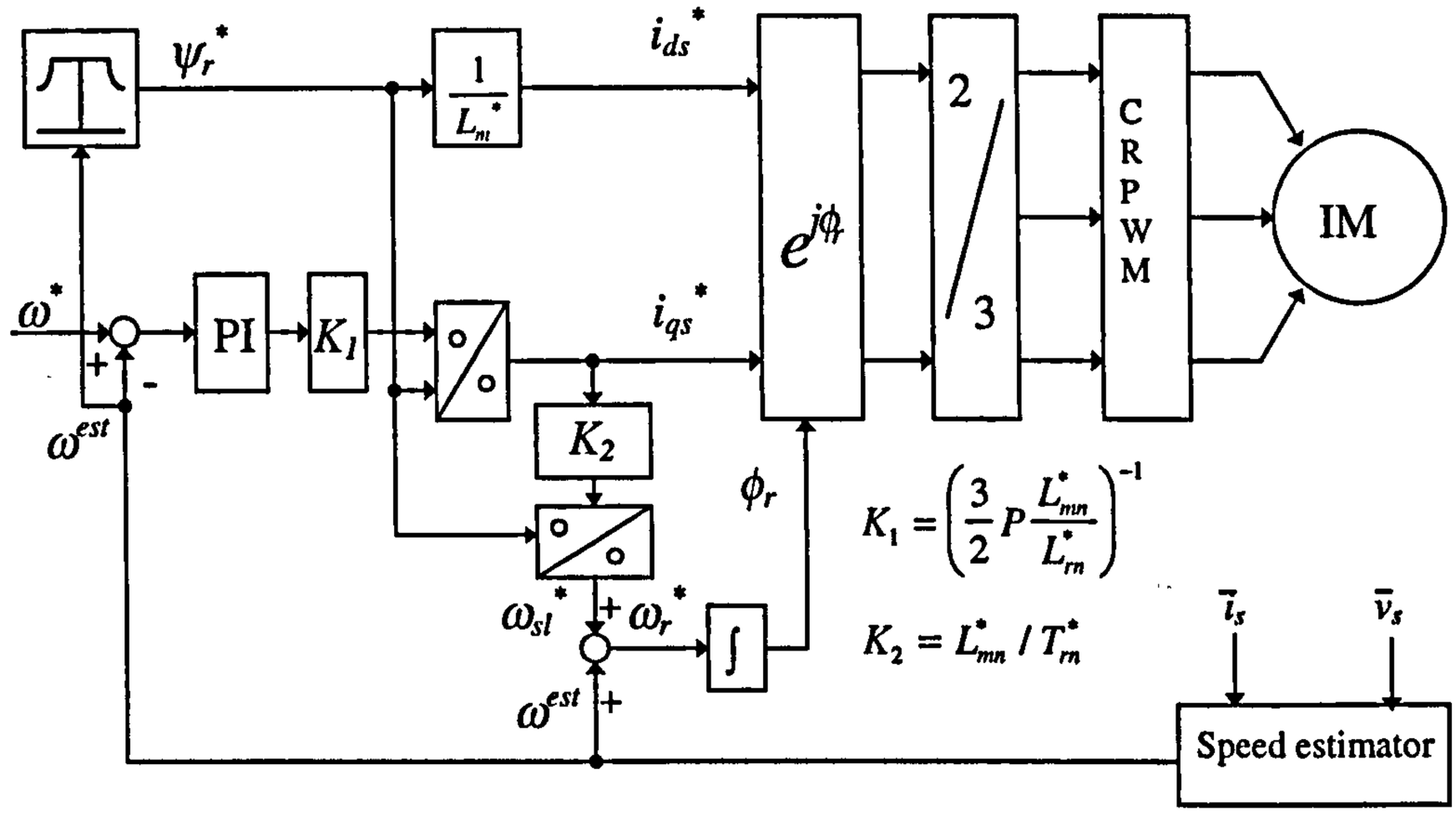

Figure 6.1: Sensorless rotor flux oriented induction machine.

assumed to be ideal and steady-state operation is discussed only. Mathematical modelling is performed in the reference frame firmly attached to the commanded rotor flux space vector. The speed estimator of Figure 6.1 is the one of section 4.2 (Figure 4.1) and is shown again in Figure 6.2. It relies on measurement of stator currents and voltages.

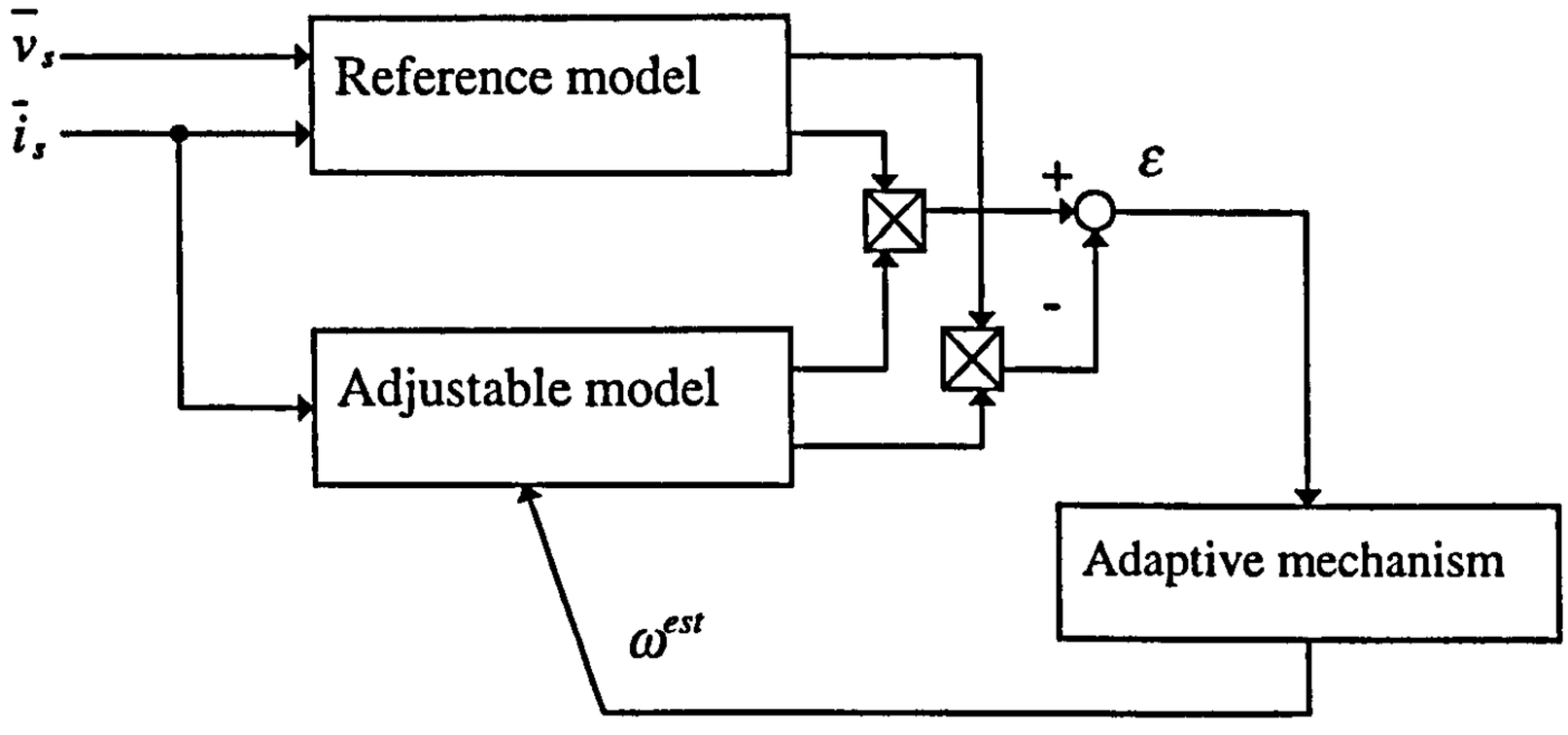

Figure 6.2: Basic configuration of MRAC speed estimator.

The outputs of the reference and adjustable part of the speed estimator are rotor flux space vectors. In steady-state operation it follows from (4.2) and (4.3) that, by letting $d/dt=j\omega_e^*$, the two rotor flux space vectors can be given as ($\omega_r^*=\omega_e^*$):

$$\overline{\psi}_r^{(1)} = -j\frac{L_r^*}{\omega_e^* L_m^*}[\overline{v}_s - (R_s^* + j\omega_e^* \sigma^* L_s^*)\overline{i}_s^*]$$

$$\overline{\psi}_r^{(2)} = \frac{L_m^*}{T_r^*}\overline{i}_s^* \frac{1}{\frac{1}{T_r^*} + j(\omega_e^* - \omega_r^*)} \tag{6.4}$$

where once more $\sigma^* = 1 - \frac{L_m^{*2}}{L_r^* L_s^*}$ is the total leakage coefficient. In any steady-state operation, the PI controller forces the estimated speed to be equal to the commanded speed ($\omega^* = \omega^{est}$), as the estimated speed is used as feedback signal to form the closed loop system. The independent inputs in the control system of Figure 6.1 are reference speed and reference rotor flux. The output of the PI speed controller is reference torque, whose value is in general unknown. However, for each value of the torque command there is a corresponding value of the actual torque. In any steady-state, actual torque must equal load torque. Therefore, it is possible to regard torque command as an independent input. From Figure 6.1 the relationship between the reference rotor flux and reference stator *d*-axis current is:

$$\psi_r^* = L_m^* i_{ds}^* \tag{6.5}$$

$$\psi_r^* = \begin{cases} \psi_{rn} & |\omega| \le \omega_n \\ \psi_{rn}\omega_n / \omega & |\omega| > \omega_n \end{cases} \tag{6.6}$$

$$i_{ds}^* = \psi_r^* / L_m^* \tag{6.7}$$

The commanded torque is equal to:

$$T_e^* = \frac{3}{2} P \frac{L_m^*}{L_r^*} \psi_r^* i_{qs}^* \tag{6.8}$$

The commanded slip angular speed and the commanded electrical angular frequency are:

$$\omega_{sl}^* = \frac{L_m^* i_{qs}^*}{T_r^* \psi_r^*} \tag{6.9}$$

$$\omega_e^* = \omega_{sl}^* + \omega^{est} \tag{6.10}$$

Commanded *q*-axis current can be expressed from equation (6.8) as:

$$i_{qs}^{*} = \frac{T_e^{*}}{\frac{3}{2} P \frac{L_m^{*}}{L_r^{*}} \psi_r^{*}} \tag{6.11}$$

The steady-state induction machine model, with iron loss accounted for, given in section 5.2, is utilised here. Equations (5.2), (5.4), (5.5) and (5.12) are re-written for convenience:

$$\begin{aligned}
\bar{v}_s &= R_s^{*} \bar{i}_s + j\omega_e^{*} \bar{\psi}_s \\
R_{Fe} \bar{i}_{Fe} &= j\omega_e^{*} L_m^{*} \bar{i}_m \\
0 &= R_r^{*} \bar{i}_r + j\omega_{sl} \bar{\psi}_r \\
\bar{i}_m + \bar{i}_{Fe} &= \bar{i}_s + \bar{i}_r \\
\bar{\psi}_s &= L_{\sigma s}^{*} \bar{i}_s + L_m^{*} \bar{i}_m \\
\bar{\psi}_r &= L_{\sigma r}^{*} \bar{i}_r + L_m^{*} \bar{i}_m \\
T_e &= \frac{3}{2} P \frac{L_m^{*}}{L_{\sigma r}^{*}} (\psi_{dr} i_{qm} - \psi_{qr} i_{dm})
\end{aligned} \tag{6.12}$$

All the parameters in the machine model, that are the same as those of the controller/estimator, are identified with an asterisk.

Elimination of iron loss current vector by means of (5.4), elimination of stator flux and rotor current space vectors using (5.2) and, finally, resolution of (6.12) into *d-q* axis components yields:

$$\begin{aligned}
v_{ds} &= R_s^{*} i_{ds}^{*} - \omega_e^{*} L_{\sigma s}^{*} i_{qs}^{*} - \omega_e^{*} L_m^{*} i_{qm} \\
v_{qs} &= R_s^{*} i_{qs}^{*} + \omega_e^{*} L_{\sigma s}^{*} i_{ds}^{*} + \omega_e^{*} L_m^{*} i_{dm}
\end{aligned} \tag{6.13}$$

$$\begin{aligned}
\psi_{dr} &= L_m^{*} i_{dm} + \omega_{sl} T_{\sigma r}^{*} \psi_{qr} \\
\psi_{qr} &= L_m^{*} i_{qm} - \omega_{sl} T_{\sigma r}^{*} \psi_{dr} \\
\psi_{dm} &= \frac{L_m^{*}}{L_r^{*}} (\psi_{dr} + L_{\sigma r}^{*} i_{ds}^{*} + \omega_e^{*} T_{\sigma Fe} \psi_{qm}) \\
\psi_{qm} &= \frac{L_m^{*}}{L_r^{*}} (\psi_{qr} + L_{\sigma r}^{*} i_{qs}^{*} - \omega_e^{*} T_{\sigma Fe} \psi_{dm})
\end{aligned} \tag{6.14}$$

The torque equation remains as in (6.12) and electrical angular frequency is determined with (6.10). Simultaneously, however:

$$\omega_e^{*} = \omega^{*} + \omega_{sl}^{*} = \omega + \omega_{sl} \tag{6.15}$$

Time constants in (6.13) and (6.14) are defined as $T_{\sigma Fe}=L_{\sigma r}^{*}/R_{Fe}$ and $T_{\sigma r}^{*}=L_{\sigma r}^{*}/R_{r}^{*}$.

Inspection of equations (6.13)-(6.14) shows that there are six equations that contain seven unknowns (stator voltage, magnetising current and rotor flux *d-q* axis components, plus angular slip frequency). Thus, it is not possible to solve this system of equations without determining which of the seven variables is only apparently unknown.

However, it is possible to solve these equations in conjunction with the speed estimator equations. Due to the presence of the PI controller in the speed estimator, the constraint that

$$\varepsilon=0 \tag{6.16}$$

is valid in any steady state. This means that instantaneous positions of the two rotor flux estimates with respect to the fixed stator axis are equal, i.e.

$$\phi_r^{(1)} = \phi_r^{(2)} = \phi_r \tag{6.17}$$

The rotor speed estimator does not require that magnitudes of the two rotor flux estimates are the same. Hence, in rotor flux oriented reference frame determined with the control system, rotor flux estimates are:

$$\begin{aligned} &\bar{\psi}_r^{(2)} = \psi_{dr}^{(2)} + j\psi_{qr}^{(2)} \qquad \psi_{dr}^{(2)} = \psi_r^{*} \quad \psi_{qr}^{(2)} = 0 \\ &\bar{\psi}_r^{(1)} = \psi_{dr}^{(1)} + j\psi_{qr}^{(1)} \qquad \psi_{qr}^{(1)} \neq \psi_r^{*} \quad \psi_{qr}^{(1)} = 0 \end{aligned} \tag{6.18}$$

As the consequence of (6.17), rotor flux *q*-axis component in the commanded reference frame equals zero for both flux estimates. However, *d*-axis component of the first estimate is not necessarily equal to the commanded rotor flux (the magnitude of the second flux estimate is by default equal to the rotor flux reference). If the *q*-axis component of the first rotor flux estimate is expressed from (6.4) and equated to zero (in the commanded rotor flux reference frame), *d*-axis component of the stator voltage is calculated from (2.35) as:

$$v_{ds} = R_s^{*} i_{ds}^{*} - \omega_e^{*}\sigma^{*} L_s^{*} i_{qs}^{*} \tag{6.19}$$

This is the well known stator voltage *d*-axis equation, valid under the correct rotor flux orientation conditions (with neglected iron loss). The speed estimator will force stator *d*-axis voltage to be equal to the one required for perfect rotor flux orientation.

However, as the estimator does not force equality of magnitudes of rotor flux estimates, stator q-axis voltage will deviate from the one required for perfect rotor flux orientation.

As v_{ds} is pre-determined by the speed estimator, the machine model (6.13)-(6.15) becomes solvable. In particular, magnetising current q-axis component can be obtained directly from the first of equations (6.13). Hence its value is known for specified operating conditions,

$$i_{qm} = \frac{1}{\omega_e^* L_m^*}(-v_{ds} + R_s^* i_{ds}^* - \omega_e^* L_{\sigma s}^* i_{qs}^*) \tag{6.20}$$

since v_{ds} is given with (6.19). Next, the magnetising current d-q axis components can be expressed as functions of angular slip frequency, with i_{ds}^* and i_{qs}^* as independent inputs. They may be derived from the machine model equations (6.13)-(6.15) in the form:

$$\begin{aligned} i_{dm} &= \frac{B i_{qs}^* - A i_{ds}^*}{A^2 + B^2} \\ i_{qm} &= \frac{-B i_{ds}^* - A i_{qs}^*}{A^2 + B^2} \end{aligned} \tag{6.21}$$

where

$$\begin{aligned} A &= \frac{L_m^*}{L_{\sigma r}^*}\frac{1}{1+(\omega_{sl} T_{\sigma r}^*)^2} - \frac{L_r^*}{L_{\sigma r}^*} \\ B &= \frac{L_m^*}{L_{\sigma r}^*}\frac{\omega_{sl} T_{\sigma r}^*}{1+(\omega_{sl} T_{\sigma r}^*)^2} + \omega_e^* T_{Fe} \end{aligned} \tag{6.22}$$

Hence, in any steady-state with given i_{ds}^* and i_{qs}^*, the two q-axis magnetising current components given in (6.20) and (6.21) must be equal, i.e.

$$i_{qm}^{(1)} = i_{qm}^{(2)} \tag{6.23}$$

The actual angular slip frequency can then be found numerically, by forcing $i_{qm}^{(1)}=i_{qm}^{(2)}$, using iterative calculation method. It therefore follows that the detuning effects due to iron loss in speed sensorless vector control of induction machine can be evaluated using the described procedure, originally developed in [Levi and Wang, 1997].

Detuning is characterised with the following quantities:

Speed estimation error (in mechanical rpm):

$$\Delta n = n - n^{est} \tag{6.24}$$

Torque ratio (in p.u.):

$$\frac{T_e}{T_e^*} \tag{6.25}$$

Rotor flux ratio (in p.u.):

$$\frac{\psi_r}{\psi_r^*} \tag{6.26}$$

Orientation angle error (in degrees):

$$\Delta\phi = (180/\pi)\arctan\frac{\psi_{qr}}{\psi_{dr}} \tag{6.27}$$

In contrast to an induction machine with rotor flux oriented control which includes speed sensor, here $\omega^*=\omega^{est}$ but $\omega^*\neq\omega$. Simultaneously, $\omega_{sl}{}^*\neq\omega_{sl}$. In other words, if the speed sensor exists, actual slip and rotor speed equal commanded values and impact of iron loss is mostly pronounced in the orientation angle error [Levi, 1995]. If speed sensor does not exist, $\omega_{sl}{}^*\neq\omega_{sl}$, $\omega^*\neq\omega$ (but $\omega_e{}^*=\omega+\omega_{sl}=\omega^{est}+\omega_{sl}{}^*=\omega^*+\omega_{sl}{}^*$), and iron loss leads to an error in speed estimation, as shown next. It should be noted once more that main flux saturation is completely neglected in the study whose results are to follow, although field-weakening region is encompassed by the study. The reason for doing so is that only in this way it is possible to visualise detuning effects purely due to iron loss.

6.2.2 Results of the study

Impact of iron loss on behaviour of the drive is studied first for constant speed command operation, with torque command as the independent input. Torque command is varied from zero up to twice the rated value and is given in all the figures in per unit. Figure 6.3a shows speed estimation error for three values of the reference speed, namely one fifth of the rated speed, rated speed and twice the rated speed.

Speed estimation error is from Figure 6.3a load dependent and it increases as load increases. Speed estimation error appears to be typically two to three rpm for operation

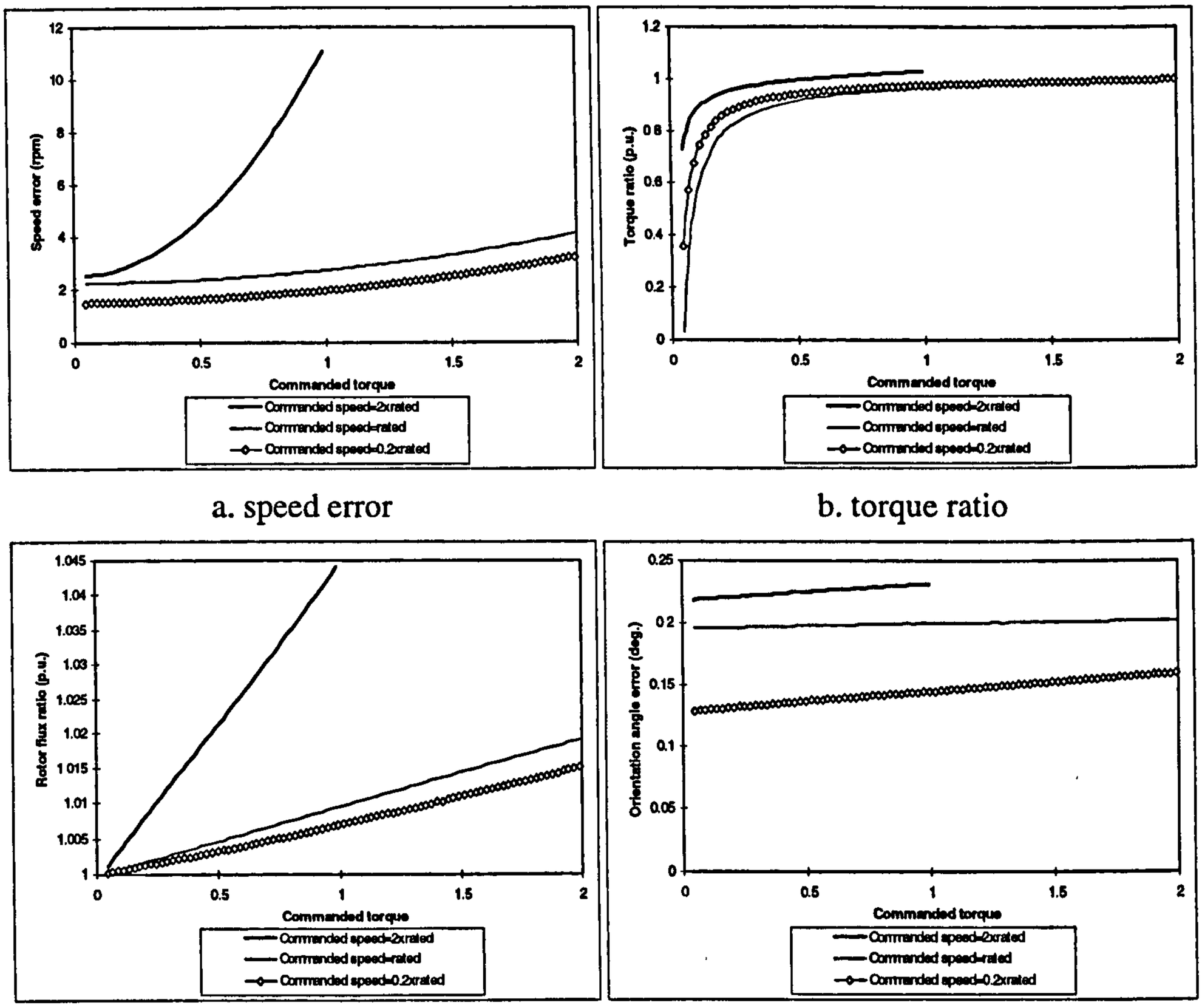

a. speed error b. torque ratio

c. rotor flux ratio d. orientation angle error

Figure 6.3: Detuning effects due to iron loss as function of commanded torque for operation with constant speed command.

at the rated speed, for commanded torque up to the rated. Speed estimation error is speed (frequency) dependent and is smaller at lower speeds, typically 1.5 to 2 rpm at one fifth of the rated speed for variation of the torque command from zero to the rated torque value. If the machine is operated in the field weakening region, speed estimation error may increase significantly, reaching 11 rpm for operation at twice the rated speed with the rated torque command. On the other hand, torque ratio (Figure 6.3b) has maximum error always at low torque commands. As the torque command increases error in the torque ratio decreases. This is explained by the fact that higher the load is, smaller the relative value of the iron loss with respect to output power is.

Figure 6.3c shows rotor flux ratio for constant speed operation. Error in rotor flux magnitude is extremely small. For operation in the base speed region actual rotor flux in the machine exceeds commanded rotor flux by less than 1% for all the operating points. Maximum error appears for operation with the rated speed and rated torque

command, when ratio of actual to commanded rotor flux equals 1.0092. The error of rotor flux increases in the field-weakening region. If the machine runs at twice the rated speed with rated torque, the error in rotor flux is 4.5%.

Orientation angle error is shown in Figure 6.3d. For machine operating in the base speed region, the orientation angle error is between 0.1 to 0.2 degree. Even when the machine operates in the field-weakening region, the error is still less than 0.25 degree. This result shows that in a sensorless drive the orientation angle error caused by iron loss is negligibly small.

The impact of iron loss on sensorless vector controlled induction machine is further studied with commanded speed taken as independent variable (normalised with respect to the rated speed) and the commanded torque set to a constant value in the base speed region. For operation in the field-weakening region, torque command is reduced inversely proportionally to the speed so that constant power operation is obtained. Figure 6.4a shows the speed estimation error as function of the speed command [Levi et al, 1999]. In base speed region, the error is 2 to 3 rpm with torque command between one fifth and rated torque value. It increases as speed is increased. If the machine is running at twice the rated speed with rated power, the speed estimation error is up to 4.5 rpm.

Torque error increases with decreasing load. Actual torque is up to 5% less than the commanded torque with rated torque/power command operation from zero to twice the rated speed command. When machine is operating with light load, say one fifth of the rated torque value, in base speed region, the error becomes up to 20%, Figure 6.4b.

The impact of iron loss on rotor flux ratio and orientation angle error is extremely small, Figures 6.4c and 6.4d. For base speed region with rated torque command, the rotor flux error is about 1% and the orientation angle error is only 0.2 degrees. When the machine runs in the field-weakening region, the maximum rotor flux error is just above 2% and the orientation angle error is still around 0.2 to 0.25 degrees, which is identical to the result shown in Figure 6.3d.

A study similar to this one, but for the reactive power based MRAC speed estimation scheme, has been performed as well. It is described in Appendix B and the results are reported in [Wang et al, 1997].

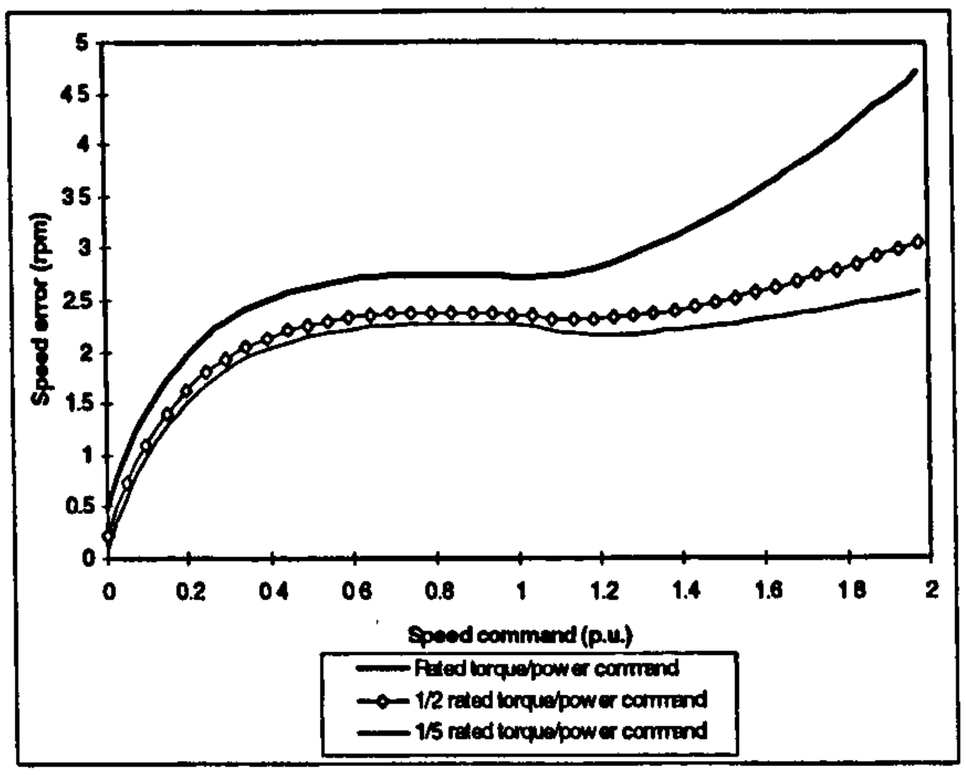

a. speed error

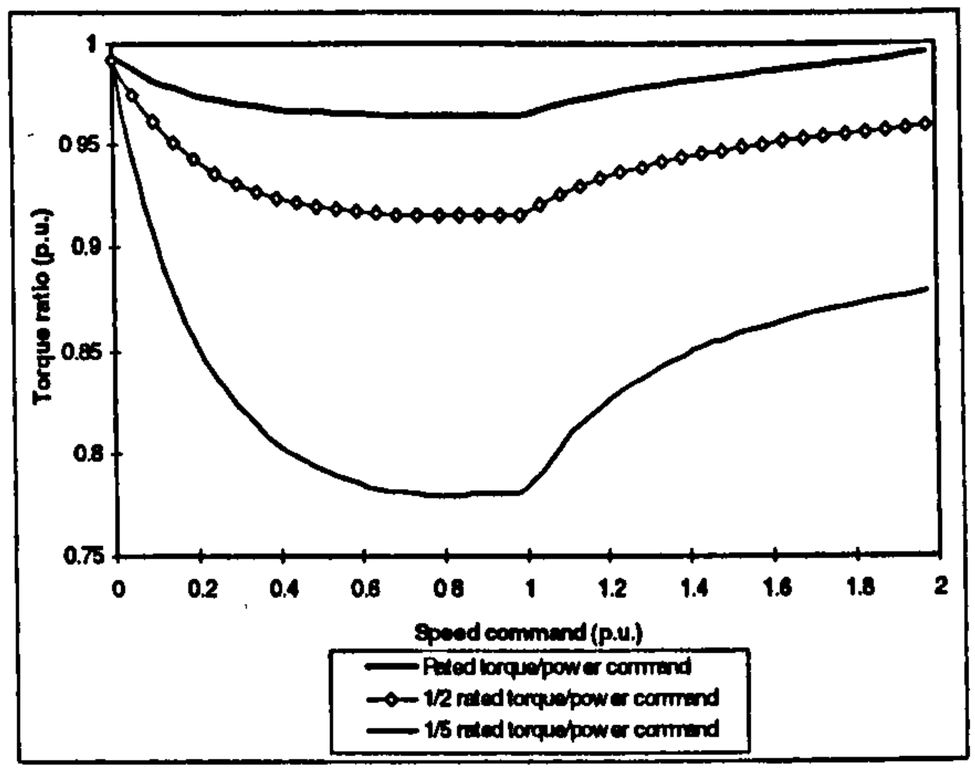

b. torque ratio

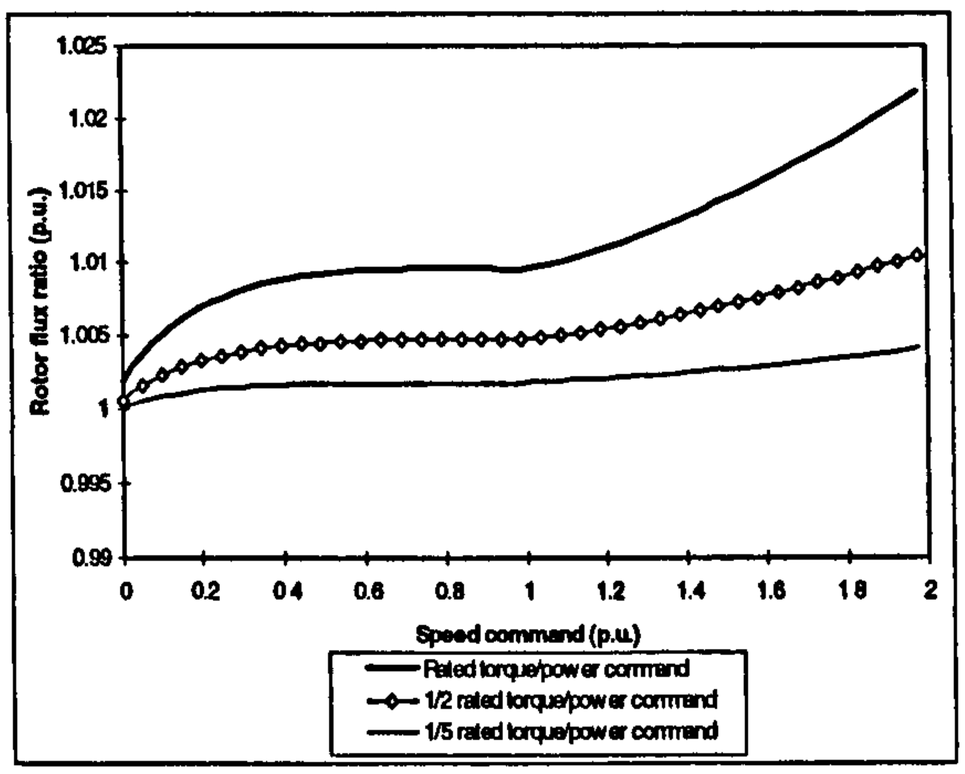

c. rotor flux ratio

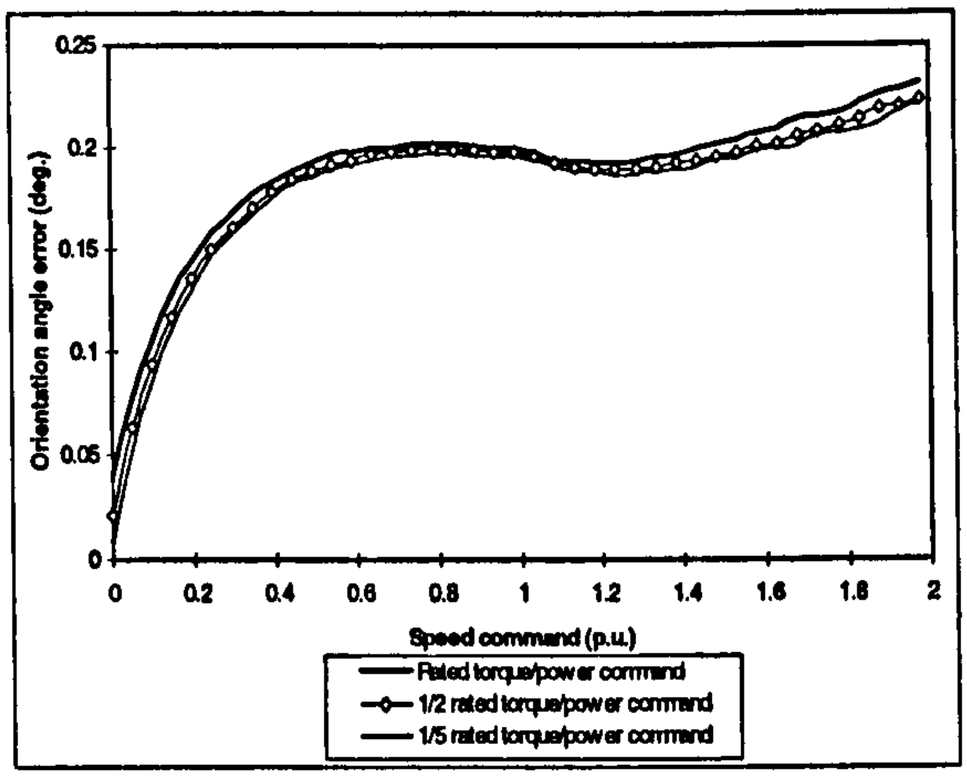

d. orientation angle error

Figure 6.4: Detuning effects due to iron loss as function of commanded speed for operation with constant torque/power command.

6.3 **Detuning due to incorrect setting and/or variation of leakage inductances**

Leakage inductance variation, as a possible source of detuning, is studied next. Leakage inductances may change due to saturation of the leakage flux paths. This can be caused by differing currents under different operating conditions. When the machine is running with heavy load, the current is high. Light load asks for low current. Hence, leakage inductances vary for different currents. Another possible problem with leakage inductances is that their values are not easy to obtain accurately, because they are normally calculated from measured quantities. There are always some assumptions when the calculations are performed and there are always some measurement errors. Therefore, the values of leakage inductances used in the controller and speed estimator

may differ from the actual values in the machine. In this section, the detuning effects due to variation of leakage inductance are elaborated.

6.3.1 Analysis

The induction machine model utilised here is given in section 5.3. In the machine model, the main flux saturation is accounted for while iron loss is neglected. All the operating conditions remain the same as before. In this study, rotor and stator resistance are assumed to be constant and equal to the rated values (i.e $R_r^*=R_r=R_{rn}$, $R_s^*=R_s=R_{sn}$). The study focuses only on the influence of leakage inductance.

Actual data regarding variation of leakage inductances with currents for the machine used in the study were not available. The following procedure is therefore adopted. Both stator and rotor leakage inductance in the controller and speed estimator are assumed to differ by the same amount from correct values in the motor (that are rated). Three sets of leakage inductance values are considered, namely $L_{\sigma s}^*=0.8\ L_{\sigma sn}$, $L_{\sigma r}^*=0.8\ L_{\sigma rn}$; $L_{\sigma s}^*=1.2\ L_{\sigma sn}$, $L_{\sigma r}^*=1.2\ L_{\sigma rn}$ and $L_{\sigma s}^*=L_{\sigma sn}$, $L_{\sigma r}^*=L_{\sigma rn}$. The three cases are studied in order to determine the detuning effects due to variation of leakage inductances, with main flux saturation included in the machine model. The definition of detuning quantities (speed estimation error, torque ratio, rotor flux ratio and orientation angle error) is the same as in section 6.2. Due to leakage inductance variation, the value of the magnetising inductance will be affected. Therefore, the error in magnetising inductance is additionally introduced. It is defined as ratio of actual magnetising inductance to magnetising inductance value used in the controller and speed estimator (that equals rated in the base speed region).

The procedure of evaluation is almost the same as the one described in section 6.2. Commanded stator *d-q* axis currents, commanded torque, commanded slip angular speed and commanded electrical angular speed are given with:

$$\psi_r^* = \begin{cases} \psi_{rn} & \omega \le \omega_n \\ \psi_{rn}\omega_n / \omega & \omega > \omega_n \end{cases} \tag{6.6}$$

$$i_{ds}^* = \psi_r^* / L_m^* \tag{6.7}$$

$$T_e^* = \frac{3}{2} P \frac{L_m^*}{L_r^*} \psi_r^* i_{qs}^* \tag{6.8}$$

$$\omega_{sl}^* = \frac{L_m^* i_{qs}^*}{T_r^* \psi_r^*} \tag{6.9}$$

$$\omega_e^* = \omega_{sl}^* + \omega^{est} \tag{6.10}$$

$$i_{qs}^* = \frac{T_e^*}{\frac{3}{2} P \frac{L_m^*}{L_r^*} \psi_r^*} \tag{6.11}$$

The induction machine model, with main flux saturation accounted for, can be written for steady-state operation from (5.29), (5.31) of section 5.3 in the following form:

$$\begin{aligned} \bar{v}_s &= R_s^* \bar{i}_s^* + j\omega_e^* \left(L_{\sigma s} \bar{i}_s + L_m \bar{i}_m \right) \\ 0 &= R_r^* \bar{i}_r^* + j\omega_{sl} \left(L_{\sigma r} \bar{i}_r + L_m \bar{i}_m \right) \\ T_e &= \frac{3}{2} P \frac{L_m}{L_{\sigma r}} (\psi_{dr} i_{qm} - \psi_{qr} i_{dm}) \end{aligned} \tag{6.28}$$

Parameters that are the same in the machine model and in the controller/estimator bear once more an asterisk.

Resolution of (6.28) into *d-q* axis components yields:

$$\begin{aligned} v_{ds} &= R_s^* i_{ds}^* - \omega_e^* L_{\sigma s} i_{qs}^* - \omega_e^* L_m i_{qm} \\ v_{qs} &= R_s^* i_{qs}^* + \omega_e^* L_{\sigma s} i_{ds}^* + \omega_e^* L_m i_{dm} \end{aligned} \tag{6.29}$$

$$\begin{aligned} \psi_{dr} &= L_m i_{ds}^* + \omega_{sl} T_r \psi_{qr} \\ \psi_{qr} &= L_m i_{qs}^* - \omega_{sl} T_r \psi_{qr} \end{aligned} \tag{6.30}$$

where from (5.2)

$$\begin{aligned} \psi_{dr} &= -L_{\sigma r} i_{ds}^* + \psi_{dm} \left(1 + \frac{L_{\sigma r}}{L_m} \right) = -L_{\sigma r} i_{ds}^* + i_{dm} \left(L_m + L_{\sigma r} \right) \\ \psi_{qr} &= -L_{\sigma r} i_{qs}^* + \psi_{qm} \left(1 + \frac{L_{\sigma r}}{L_m} \right) = -L_{\sigma r} i_{qs}^* + i_{qm} \left(L_m + L_{\sigma r} \right) \end{aligned} \tag{6.31}$$

The torque equation remains as in (6.28).

Main flux saturation is represented by the $L_m(\psi_m)$ non-linear function:

$$L_m = f(\psi_m) \tag{6.32}$$

$$\psi_m = \sqrt{\psi_{dm}{}^2 + \psi_{qm}{}^2} \tag{6.33}$$

Inspection of (6.29) to (6.31) shows that there are essentially four equations that contain five unknowns (stator voltage and magnetising flux *d-q* axis components, plus angular slip speed). It is again not possible to solve this system of equations without determining which of the five variables is only apparently unknown. As discussed in section 6.2, v_{ds} can be obtained from speed estimator equations as:

$$v_{ds} = R_s{}^* i_{ds}{}^* - \omega_e{}^* \sigma^* L_s{}^* i_{qs}{}^* \tag{6.19}$$

Thus, magnetising current *q*-axis component is from (6.29) known for specified operating conditions,

$$i_{qm} = \frac{1}{\omega_e{}^* L_m}(-v_{ds} + R_s{}^* i_{ds}{}^* - \omega_e{}^* L_{\sigma s} i_{qs}{}^*) \tag{6.34}$$

Insertion of (6.19) into (6.34) yields

$$i_{qm} = \frac{1}{L_m} i_{qs}^* \left(L_m^* \left(1 - \frac{L_m{}^*}{L_r{}^*} \right) + \left(L_{\sigma s}^* - L_{\sigma s} \right) \right) \tag{6.35}$$

Next, magnetising flux *d-q* axis components can be expressed as functions of angular slip frequency, with $i_{ds}{}^*$ and $i_{qs}{}^*$ as independent inputs. They can be derived from machine equations (6.30) - (6.31) in the form:

$$\begin{aligned} i_{dm} &= \frac{C i_{ds}{}^* + D i_{qs}{}^*}{E} \\ i_{qm} &= \frac{C i_{qs}{}^* - D i_{ds}{}^*}{E} \end{aligned} \tag{6.36}$$

where

$$\begin{aligned} C &= 1 + (\omega_{sl} T_{\sigma r})^2 \left(1 + \frac{L_m}{L_{\sigma r}} \right) \\ D &= \omega_{sl} T_{\sigma r} \frac{L_m}{L_{\sigma r}} \\ E &= 1 + (\omega_{sl} T_{\sigma r})^2 \left(1 + \frac{L_m}{L_{\sigma r}} \right)^2 \end{aligned} \tag{6.37}$$

The two magnetising q-axis current components, given with (6.35) and (6.36) must be equal, i.e.:

$$\frac{1}{L_m}\left(L_m^*\left(1-\frac{L_m^*}{L_r^*}\right)+\left(L_{\sigma s}^*-L_{\sigma s}\right)\right)i_{qs}^* = \left(\frac{Ci_{qs}^* - Di_{ds}^*}{E}\right) \tag{6.38}$$

or

$$\left(L_m^*\left(1-\frac{L_m^*}{L_r^*}\right)+\left(L_{\sigma s}^*-L_{\sigma s}\right)\right)i_{qs}^* = L_m\left(\frac{Ci_{qs}^* - Di_{ds}^*}{E}\right) \tag{6.39}$$

Thus, in any steady-state with given i_{ds}^* and i_{qs}^*, the two q-axis magnetising current components are equal, so that the actual angular slip frequency can be found numerically, by forcing $i_{qm}^{(1)} = i_{qm}^{(2)}$, using iterative calculation method. It follows that the detuning effects due to leakage inductance variations in speed sensorless vector controlled induction machine can be evaluated.

6.3.2 Results of the study

Induction machine is assumed to run at constant speed with rated speed command. It should be noted that detuning effects due to leakage inductance variations are speed (frequency) independent, in contrast to the iron loss induced detuning. The study, whose results follow, therefore applies to the complete base speed region. Figure 6.5a shows the speed estimation error against torque command. The absolute errors caused by leakage inductance variation are small. When the values of leakage inductance are less than rated values, say 0.8 rated values, the error is negative and is only up to -1 rpm. When the values of leakage inductance are changed to 1.2 rated values, the error is also up to 1 rpm with rated torque command.

Torque errors are load dependent. The maximum torque error appears with light load. When machine runs with light load with ± 20% variation of leakage inductance, the errors in torque are less than ± 1%, Figure 6.5b. For rotor flux ratio, Figure 6.5c, the errors behave similarly to the speed estimation errors. When the values of leakage inductance vary from 0.8 to 1.2 of the rated values, the rotor flux errors are less than ± 2%.

The orientation angle error due to variation of leakage inductances is shown in Figure 6.5d. The error increases with torque command. When machine runs with rated torque command at rated speed and leakage inductances vary by ± 20%, the orientation angle error is only ± 1.5 degrees, respectively.

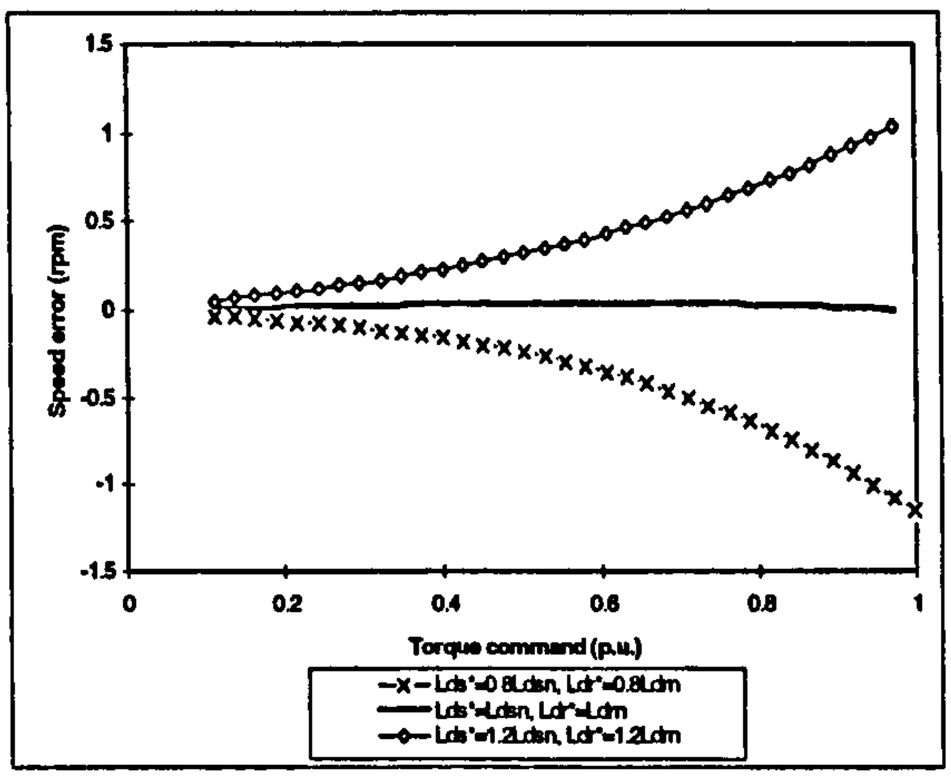

a. speed error

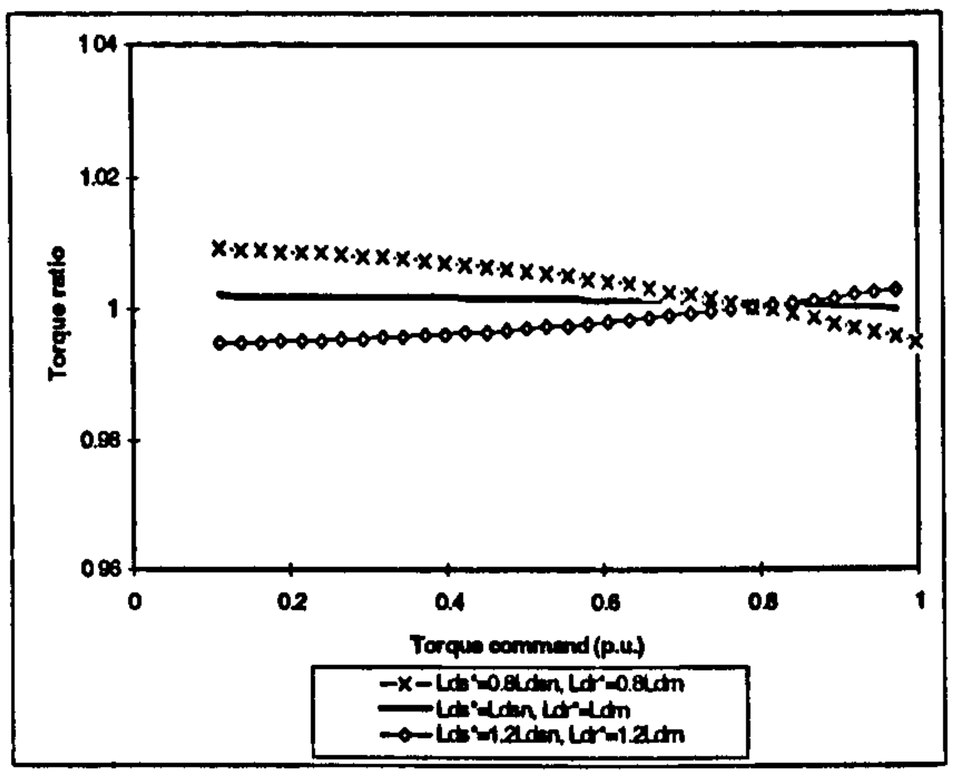

b. torque ratio

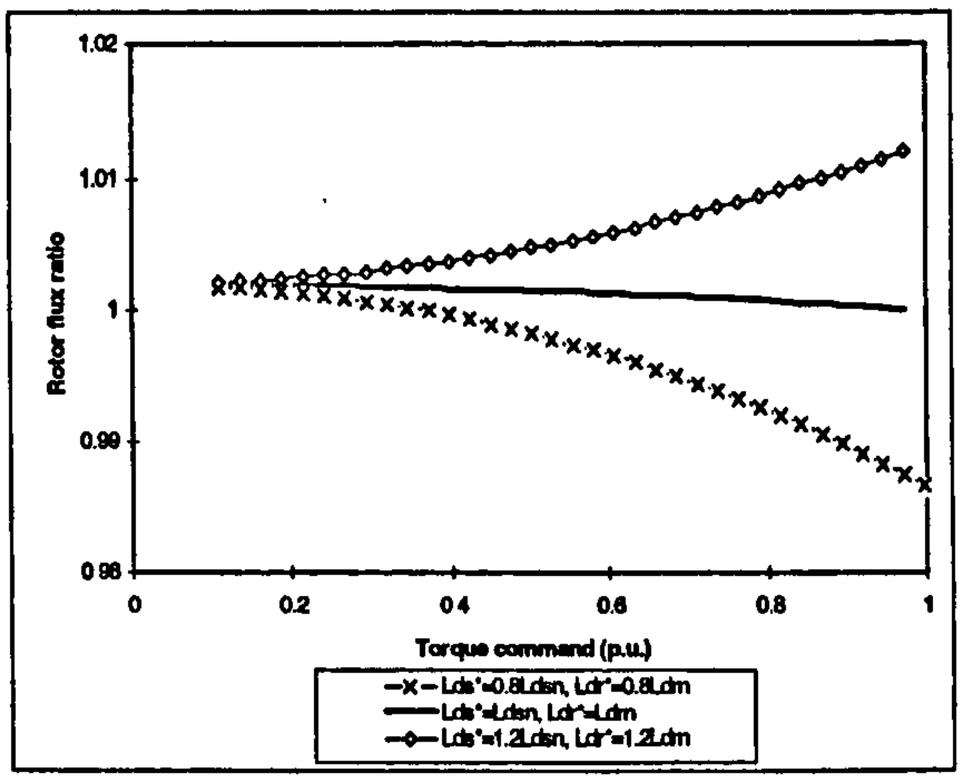

c. rotor flux ratio

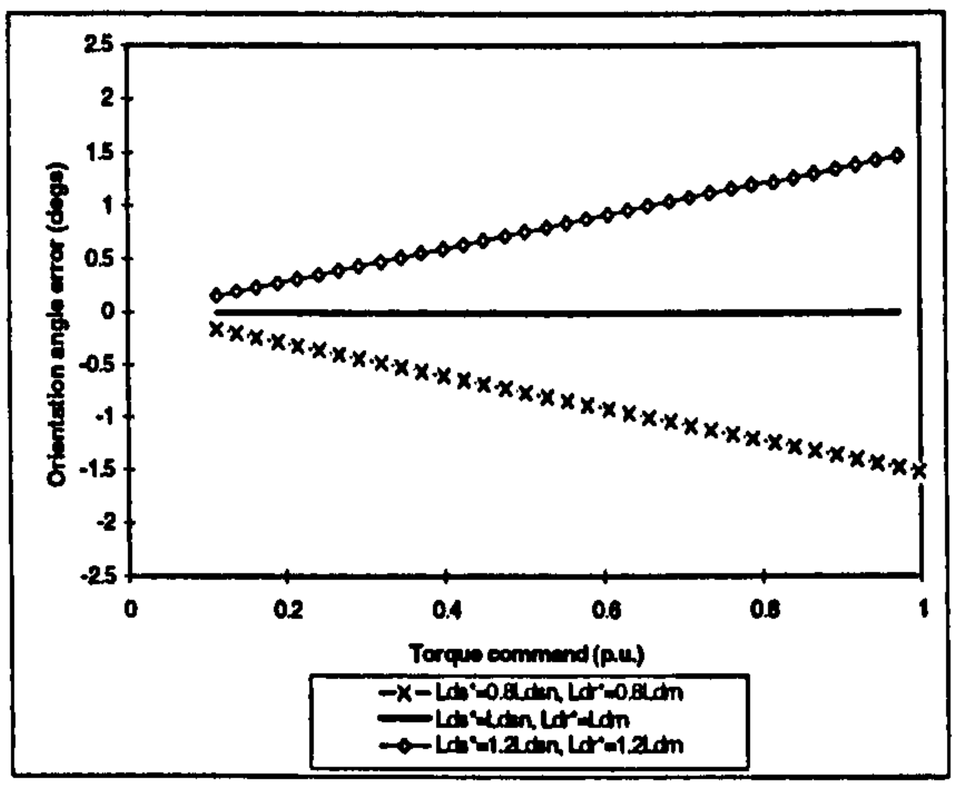

d. orientation angle error

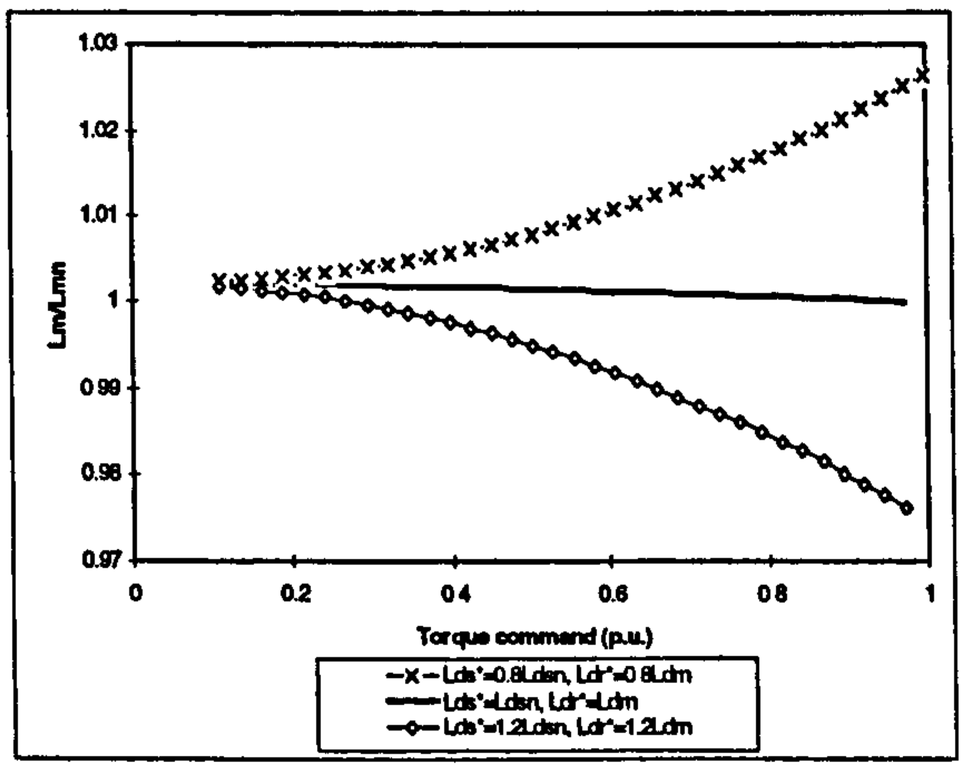

e. magnetising inductance ratio

Figure 6.5: Detuning effects due to incorrect setting of the leakage inductances against torque command.

Figure 6.5e shows the magnetising inductance ratio against torque command. When machine runs with light load, the errors are small. When machine runs with full load

with ± 20% variations of leakage inductance, the errors in magnetising inductance are about ± 3%, respectively.

6.4 Detuning due to incorrect setting of the magnetising inductance

Magnetising inductance in the controller/estimator may differ from the actual value in the machine due to an error in measurement. Additionally, when the machine runs in the field-weakening region, the actual value of the magnetising inductance will change due to change of the reference rotor flux.

6.4.1 Analysis

All the definitions of detuning effects remain the same as in previous sections. The magnetising inductance is set to different values in the controller and speed estimator in order to investigate its influence on operation of the drive. Stator and rotor resistance, as well as stator and rotor leakage inductance, are all assumed to be equal to rated values both in the controller/estimator and in the machine model. Therefore, the variation of the magnetising inductance is the only detuning source to be considered. Induction machine model that includes main flux saturation, given in section 5.3, is again utilised here for machine representation. Its form for steady-state operation is identical to (6.29) - (6.31) (leakage inductances are constant now):

$$\begin{aligned} v_{ds} &= R_s^* i_{ds}^* - \omega_e^* L_{\sigma s}^* i_{qs}^* - \omega_e^* L_m i_{qm} \\ v_{qs} &= R_s^* i_{qs}^* + \omega_e^* L_{\sigma s}^* i_{ds}^* + \omega_e^* L_m i_{dm} \end{aligned} \tag{6.29}$$

$$\begin{aligned} \psi_{dr} &= L_m i_{ds} + \omega_{sl} T_r \psi_{qr} \\ \psi_{qr} &= L_m i_{qs} - \omega_{sl} T_r \psi_{qr} \end{aligned} \tag{6.30}$$

$$\begin{aligned} \psi_{dr} &= -L_{\sigma r}^* i_{ds}^* + \psi_{dm}\left(1 + \frac{L_{\sigma r}^*}{L_m}\right) = -L_{\sigma r}^* i_{ds}^* + i_{dm}\left(L_m + L_{\sigma r}^*\right) \\ \psi_{qr} &= -L_{\sigma r}^* i_{qs}^* + \psi_{qm}\left(1 + \frac{L_{\sigma r}^*}{L_m}\right) = -L_{\sigma r}^* i_{qs}^* + i_{qm}\left(L_m + L_{\sigma r}^*\right) \end{aligned} \tag{6.31}$$

Once more, parameters that are the same in the machine model and in the controller/estimator have an asterisk.

The procedure for deriving the expressions for detuning due to the L_m variations is exactly the same as the procedure presented in the previous sub-section, so that an equation similar to (6.39) is used for iterative calculation to determine the actual angular slip frequency (in (6.39) now $L_{\sigma s}^{*} = L_{\sigma s}$):

$$\frac{L_m^{*}}{L_m}\left(1-\frac{L_m^{*}}{L_r^{*}}\right)i_{qs}^{*}=\left(\frac{Ci_{qs}^{*}-Di_{ds}^{*}}{E}\right) \tag{6.40}$$

Coefficients C, D and E are still given with (6.37), but now $T_{\sigma r}^{*} = T_{\sigma r}$ and $L_{\sigma r}^{*} = L_{\sigma r}$. The actual angular slip frequency is again found numerically, by forcing $i_{qm}^{(1)} = i_{qm}^{(2)}$, using iterative calculation method. It follows that the detuning effects due to magnetising inductance variations in speed sensorless vector controlled induction machine can be evaluated.

The value of the magnetising inductance in the controller and estimator is varied from 0.8 to 1.2 of the rated value. Detuning effects are again speed independent in the base speed region. Analysis is performed for rated speed command operation. However, the results apply to the complete base speed region.

6.4.2 Results of the study

Figure 6.6a shows the speed estimation error caused by incorrect value of the magnetising inductance. The error is linear and load dependent. With the deviation of the magnetising inductance increasing, the error increases as well. When magnetising inductance is varied by ± 10% from the rated value in the controller/estimator, speed estimation error is about ± 1.5 rpm. Maximum speed estimation error is up to ± 3 rpm at rated torque command when magnetising inductance value in the controller/estimator deviates by ± 20% from the rated value. When machine runs in light load condition, the error is quite small. It will reach zero when load torque equals zero.

Torque error is shown in Figure 6.6b. It can be seen that torque error is load independent. It varies only with change in magnetising inductance. When magnetising inductance deviates ± 10% from the rated value in the controller/estimator, torque error is about ± 4%. When magnetising inductance deviates ± 20% from the rated value, the maximum torque error is up to ± 8%.

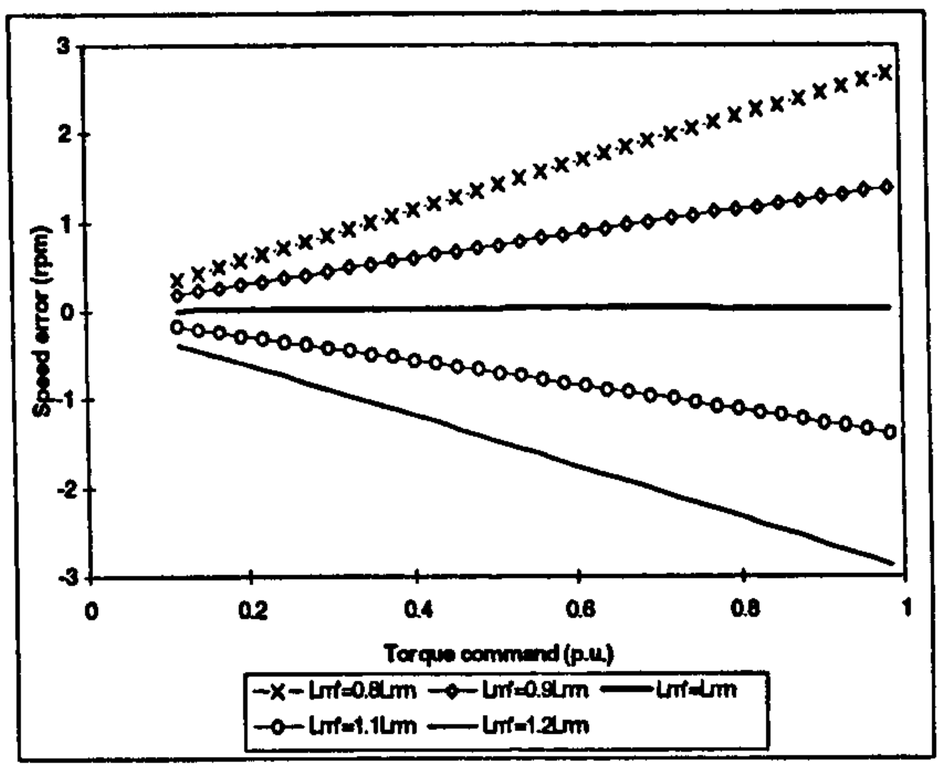

a. speed error

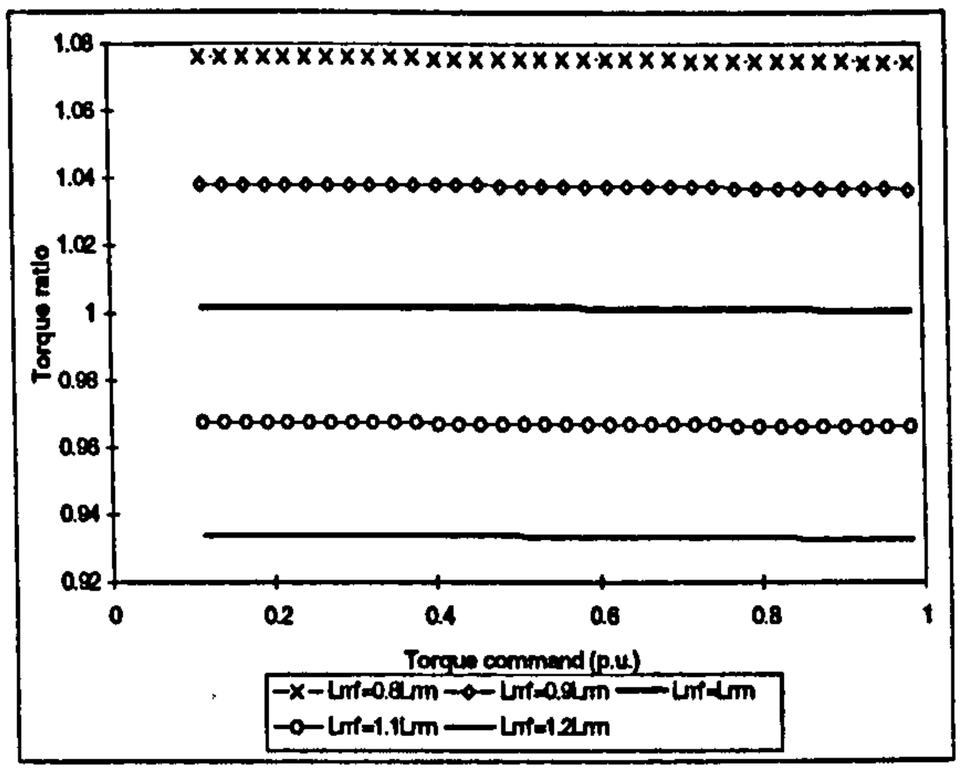

b. torque ratio

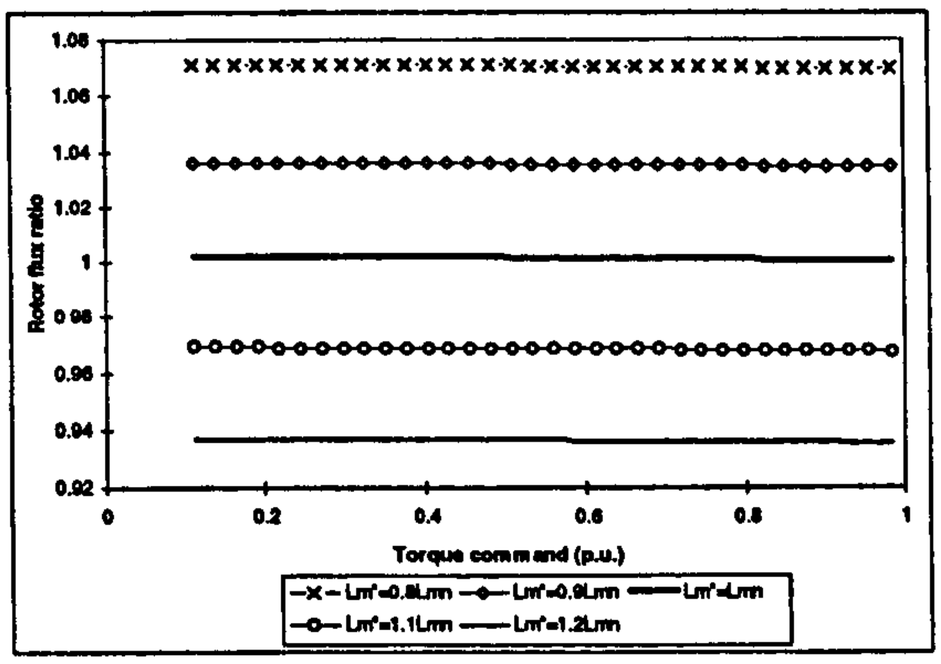

c. rotor flux ratio

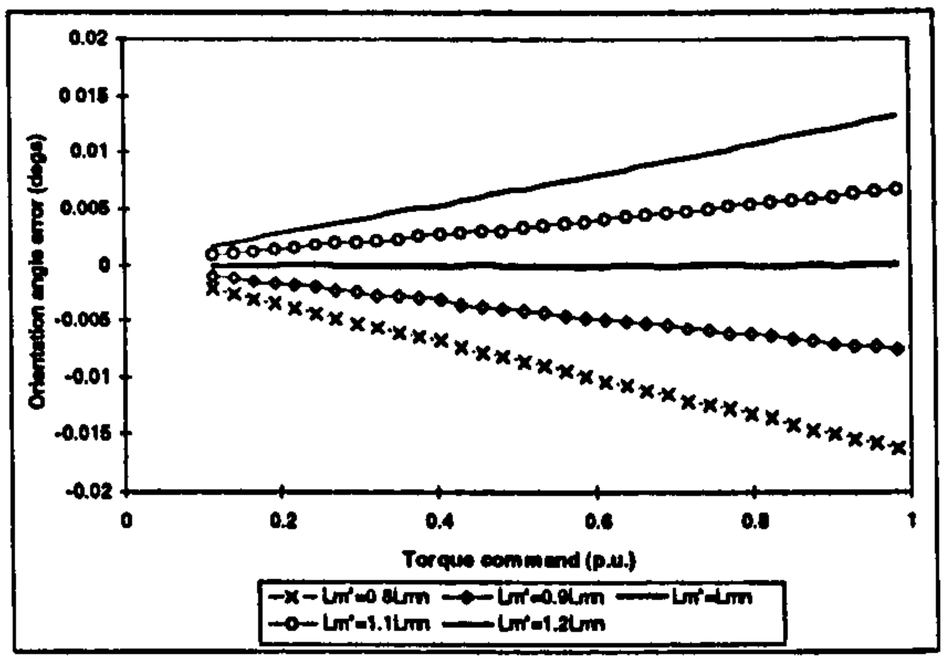

d. orientation angle error

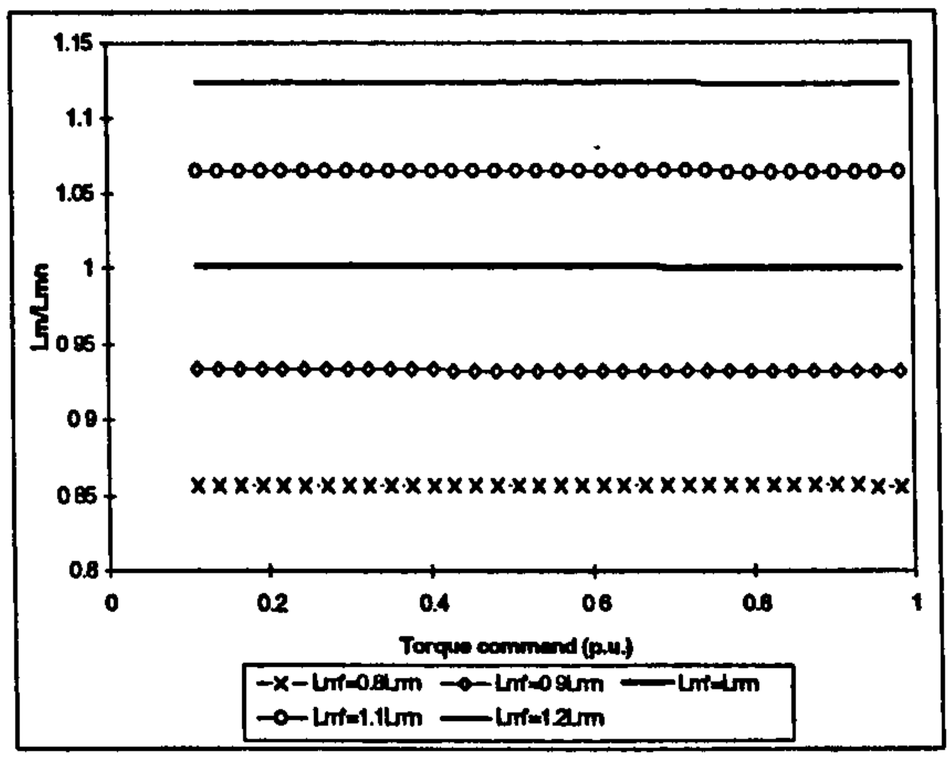

e. magnetising inductance ratio

Figure 6.6: Detuning effects due to incorrect setting of the magnetising inductance.

Rotor flux ratio has the same features as the torque ratio. This can be seen from Figure 6.6c. The only difference is that the rotor flux error is slightly smaller that torque error.

Orientation angle error caused by incorrect magnetising inductance setting is once more negligible small. Maximum orientation angle error is only about ± 0.02 degrees when magnetising inductance deviates ± 20% from the rated value. Figure 6.6d shows the orientation angle error against torque command.

Incorrect setting of the magnetising inductance in the controller/estimator affects the level of main flux saturation. Figure 6.6e shows the ratio of actual to rated magnetising inductance. It is linear and independent of load torque as well. The values of this ratio are quite close to the values of the ratio of controller/estimator to rated magnetising inductance.

6.5 Detuning due to incorrect setting and /or variation of the stator resistance

Stator and rotor resistance will vary in an induction machine due to temperature changes. The influence of variation of stator and rotor resistance on a sensorless vector controlled induction machine is investigated in this and next section.

6.5.1 Analysis

Main flux saturation is accounted for in the induction machine model. In order to investigate the detuning effects caused by stator resistance variation, it is assumed that stator leakage inductance, rotor leakage inductance and rotor resistance all have the rated values in both the controller/estimator and the machine. Magnetising inductance has the rated value in the controller/estimator. Magnetising inductance in the machine will be determined by the saturation level. All the operating conditions are the same as before.

Steady-state induction machine model, with main flux saturation accounted for, is again given with

$$\begin{aligned} v_{ds} &= R_s i_{ds}^{*} - \omega_e^{*} L_{\sigma s}^{*} i_{qs}^{*} - \omega_e^{*} L_m i_{qm} \\ v_{qs} &= R_s i_{qs}^{*} + \omega_e^{*} L_{\sigma s}^{*} i_{ds}^{*} + \omega_e^{*} L_m i_{dm} \end{aligned} \tag{6.29}$$

$$\begin{aligned} \psi_{dr} &= L_m i_{ds} + \omega_{sl} T_r \psi_{qr} \\ \psi_{qr} &= L_m i_{qs} - \omega_{sl} T_r \psi_{qr} \end{aligned} \tag{6.30}$$

$$\begin{aligned} \psi_{dr} &= -L_{\sigma r}^{*} i_{ds}^{*} + \psi_{dm}\left(1 + \frac{L_{\sigma r}^{*}}{L_m}\right) \\ \psi_{qr} &= -L_{\sigma r}^{*} i_{qs}^{*} + \psi_{qm}\left(1 + \frac{L_{\sigma r}^{*}}{L_m}\right) \end{aligned} \tag{6.31}$$

In order to solve these equations, as discussed in section 6.2, v_{ds} can be obtained from speed estimator as:

$$v_{ds} = R_s^* i_{ds}^* - \omega_e^* \sigma^* L_s^* i_{qs}^* \tag{6.19}$$

Thus, magnetising current q-axis component is known for specified operating conditions,

$$i_{qm} = \frac{1}{\omega_e^* L_m}(-v_{ds} + R_s i_{ds}^* - \omega_e^* L_{\sigma s}^* i_{qs}^*) \tag{6.41}$$

Substitution of (6.19) into (6.41) yields

$$i_{qm} = \frac{1}{\omega_e^* L_m}((R_s - R_s^*) i_{ds}^* + L_m^* \left(1 - \frac{L_m^*}{L_r^*}\right) \omega_e^* i_{qs}^*) \tag{6.42}$$

Next, magnetising flux d-q axis components can be expressed as functions of angular slip frequency, with i_{ds}^* and i_{qs}^* as independent inputs in the form:

$$\begin{aligned} i_{dm} &= \frac{C i_{ds}^* + D i_{qs}^*}{E} \\ i_{qm} &= \frac{C i_{qs}^* - D i_{ds}^*}{E} \end{aligned} \tag{6.36}$$

where C, D and E remain to be given with (6.37), where $T_{\sigma r} = T_{\sigma r}^*$ and $L_{\sigma r} = L_{\sigma r}^*$.

In any steady-state, the two q-axis components in (6.42) and (6.36) must be equal, i.e.

$$\frac{1}{\omega_e^* L_m}((R_s - R_s^*) i_{ds}^* + L_m^* \left(1 - \frac{L_m^*}{L_r^*}\right) \omega_e^* i_{qs}^*) = \frac{C i_{qs}^* - D i_{ds}^*}{E} \tag{6.43}$$

so that in any steady-state with given i_{ds}^* and i_{qs}^* the two q-axis magnetising current components must be equal. The actual angular slip frequency can then be found numerically, by forcing $i_{qm}^{(1)} = i_{qm}^{(2)}$, using once more iterative calculation method.

The value of stator resistance in the machine model is set to vary by up to ± 20% from the rated value. Detuning in base speed region is elaborated only. Detuning effects due to stator resistance variation are speed (frequency) dependent, as is obvious from (6.43). Two series of results for two speed references, 5% of the rated and the rated are therefore presented. These illustrate impact of stator resistance on low speed and high speed operation, respectively.

6.5.2 Results of the study

Figure 6.7 illustrates the impact of incorrect stator resistance value on low speed operation. The results are given for speed command equal to 5% of the rated. Speed estimation error is given as function of the torque command. The error is slightly dependent on load torque. When the value of stator resistance deviates by ± 10%, the

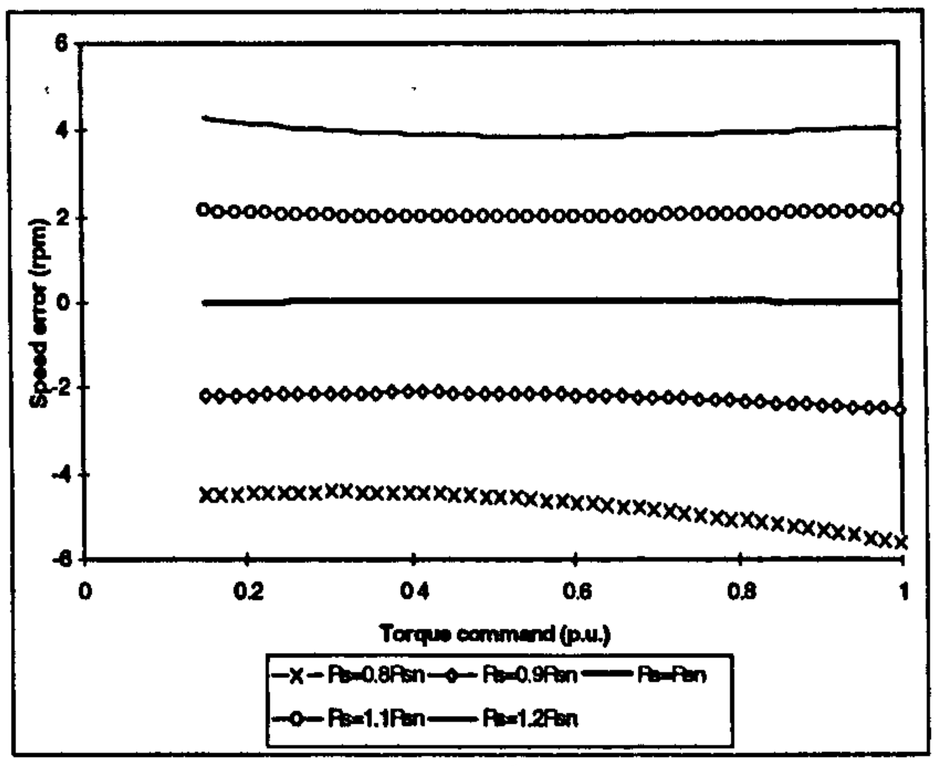

a. speed error

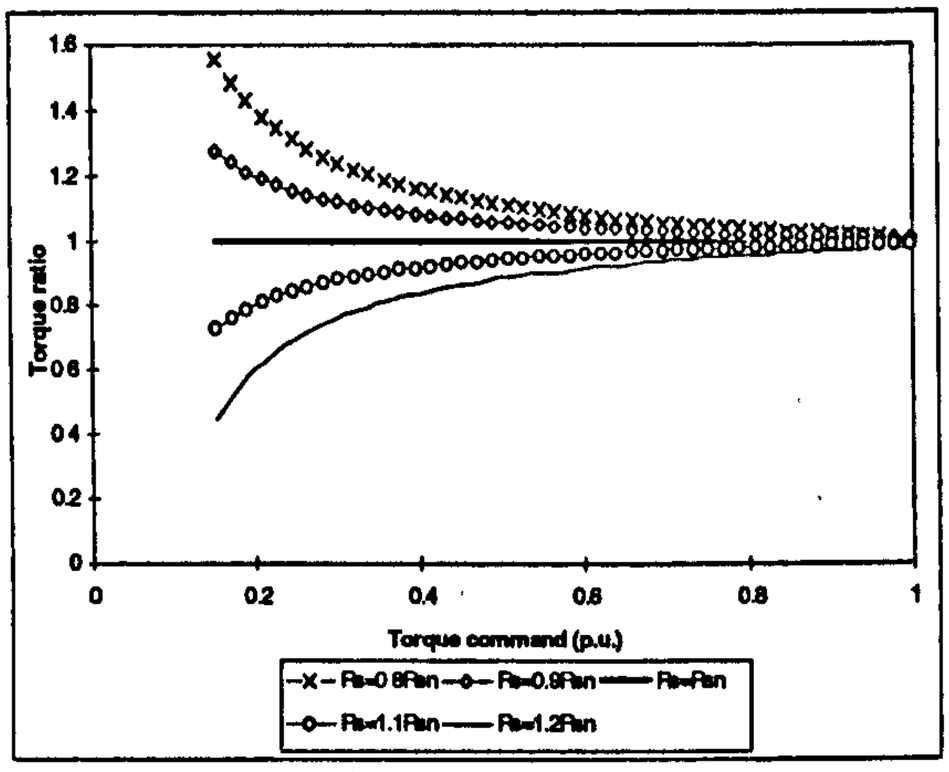

b. torque ratio

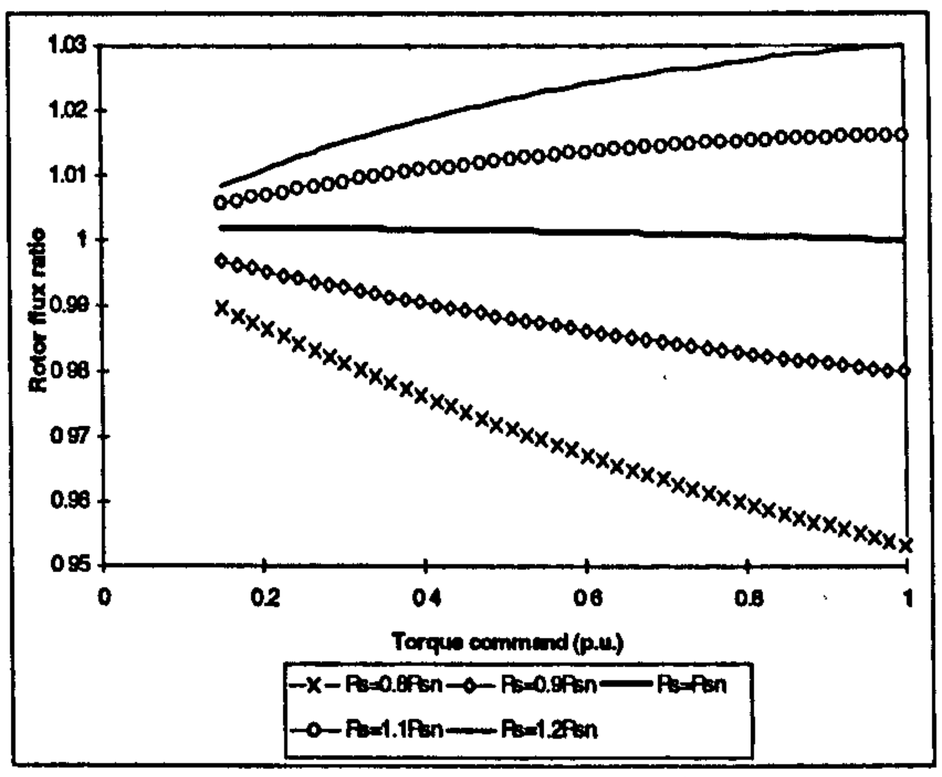

c. rotor flux ratio

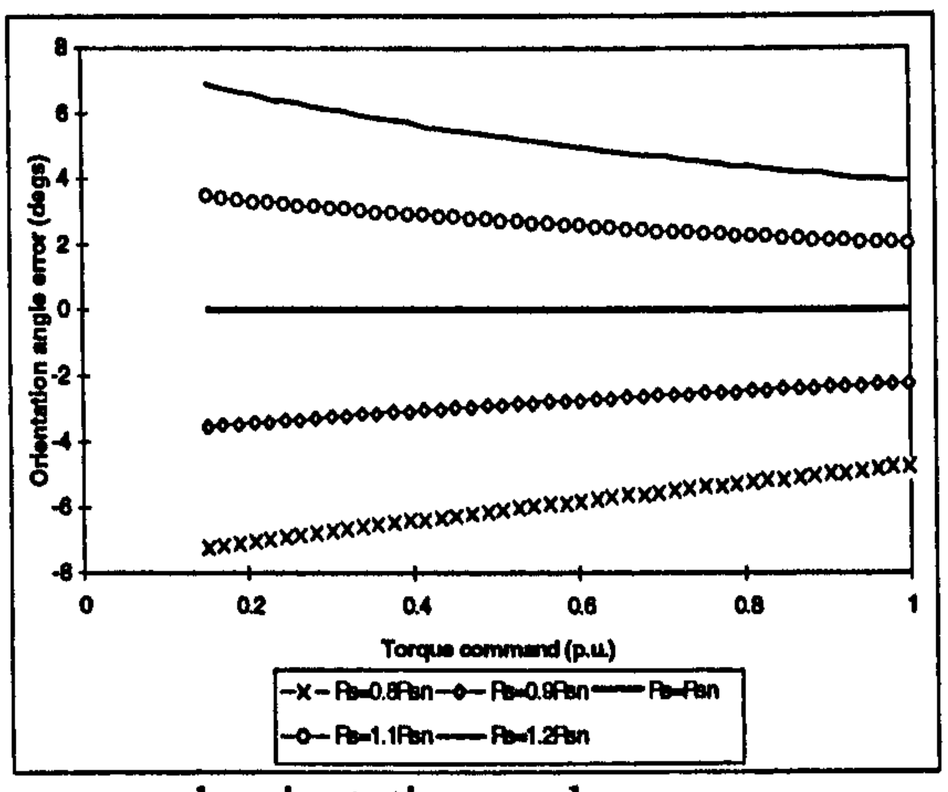

d. orientation angle error

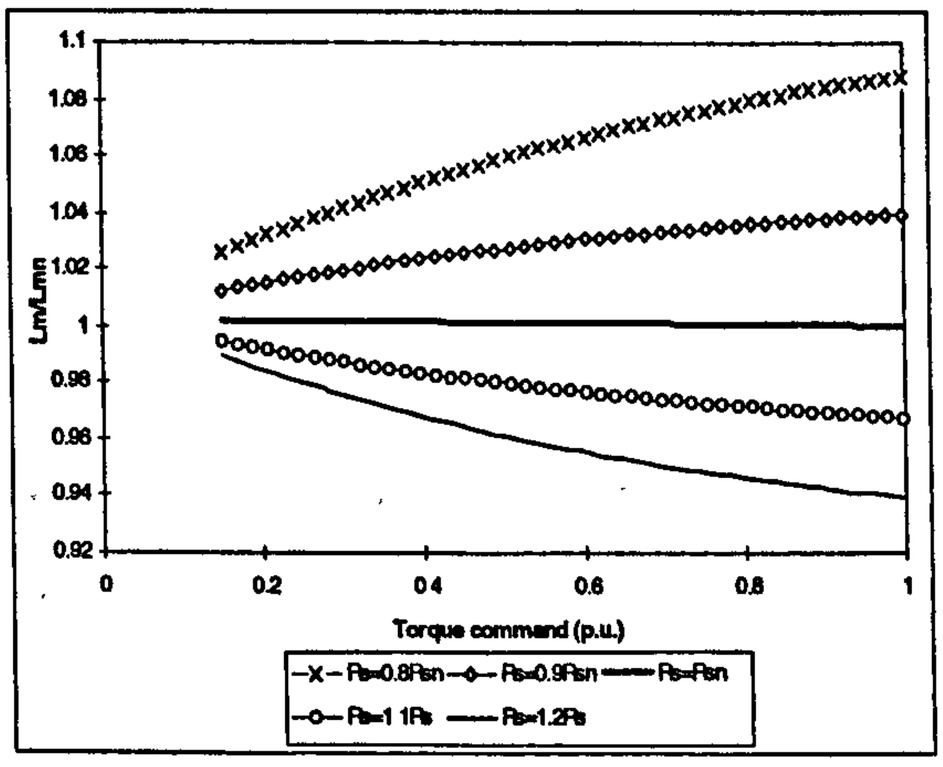

e. magnetising inductance ratio

Figure 6.7: Detuning due to incorrect stator resistance value - speed reference equal to 5% of the rated speed.

speed estimation error is about ± 2 rpm. When the value of stator resistance deviates by ± 20%, maximum speed estimation error is up to ± 6 rpm with rated torque command. It follows from Figure 6.7b that torque error is excessively high at low torque command values. As the load torque increases, torque error decreases. When machine runs with rated torque command, torque error becomes zero. Rotor flux ratio is shown in Figure 6.7c. Rotor flux error is increasing when torque command increases. Maximum rotor flux error is up to ± 5% at rated torque command when stator resistance value in the machine deviates by ± 20% from the rated value. Orientation angle error (Figure 6.7d) is significant and is up to 8 degrees. Main flux saturation level in the machine is affected as well, as witnessed by the ratio of actual to rated magnetising inductance, Figure 6.7e. It increases with an increase in torque command. When machine runs with the rated torque command, error in magnetising inductance is up to ± 10%.

Figure 6.8 displays detuning effects due to incorrect stator resistance value for rated speed command operation. It shows that detuning effects diminish as the speed is increased. Speed estimation error is only up to 0.4 rpm at rated torque, when stator resistance varies by ± 20%. All the other detuning effects are very small as well. These results show that stator resistance variation affects significantly the system behaviour only at low speed.

6.6 Detuning due to incorrect setting and/or variation of the rotor resistance

Rotor resistance value changes due to temperature variation. Correct setting of the rotor resistance is crucial for successful operation of the drive with speed sensor [Vas, 1990]. As shown shortly, detuning in rotor resistance causes the largest speed estimation error in a sensorless drive without speed sensor.

6.6.1 Analysis

Induction machine model that includes main flux saturation is utilised once more. In order to investigate the detuning effects due to rotor resistance variation, stator resistance and leakage inductances have the rated values both in the controller/estimator and in the induction machine model. Magnetising inductance in the controller/estimator

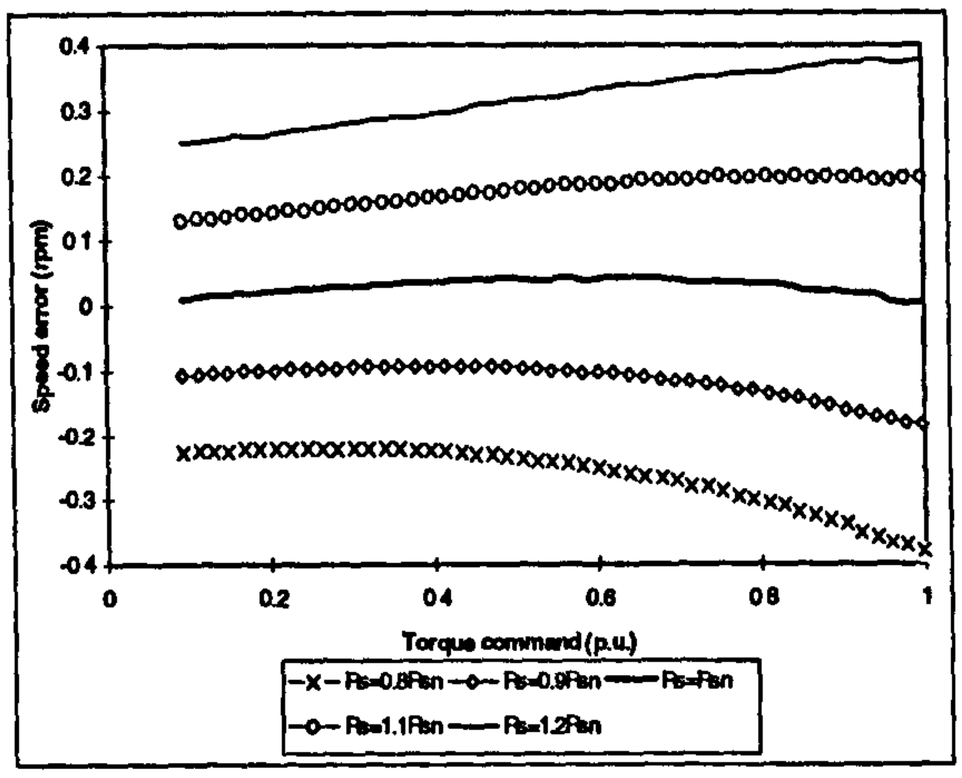

a. speed error

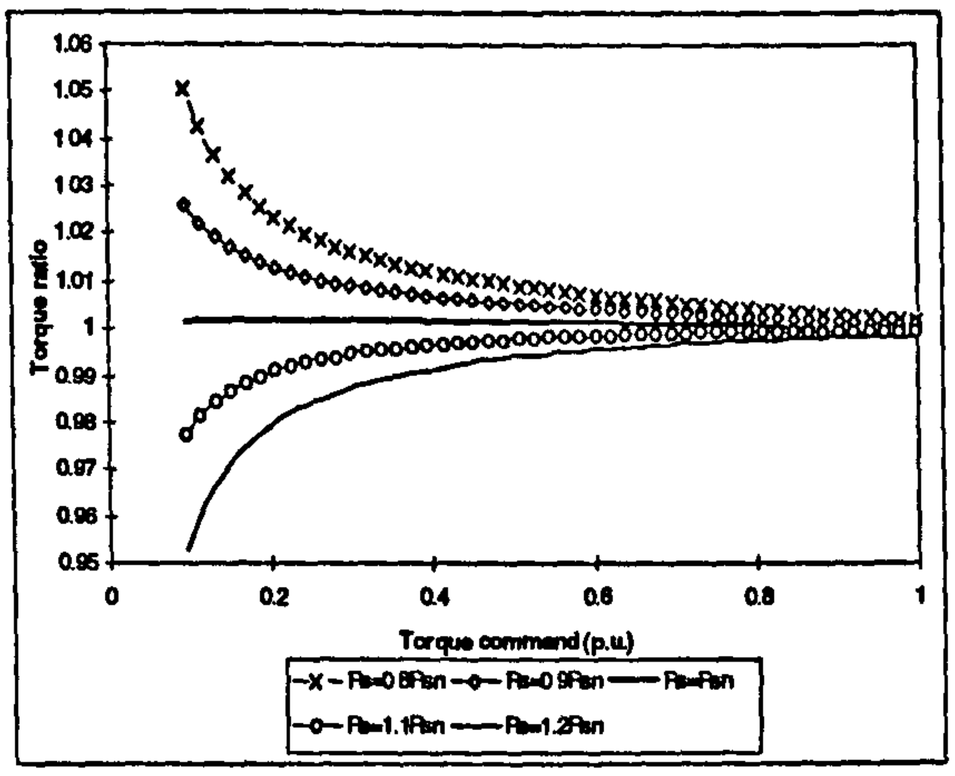

b. torque ratio

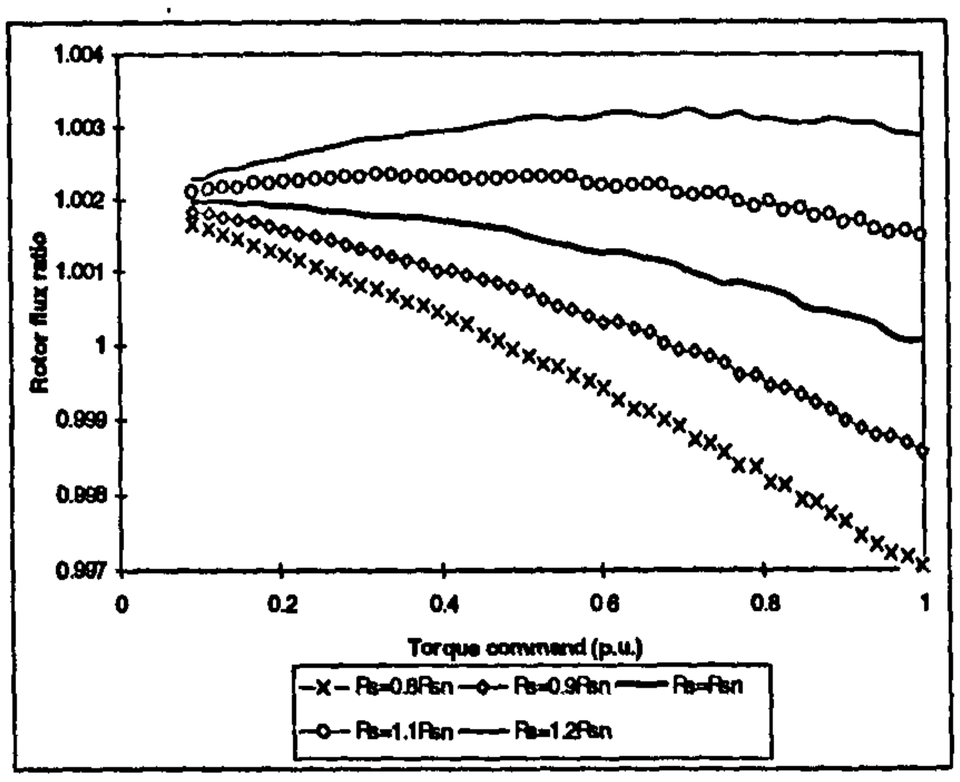

c. rotor flux ratio

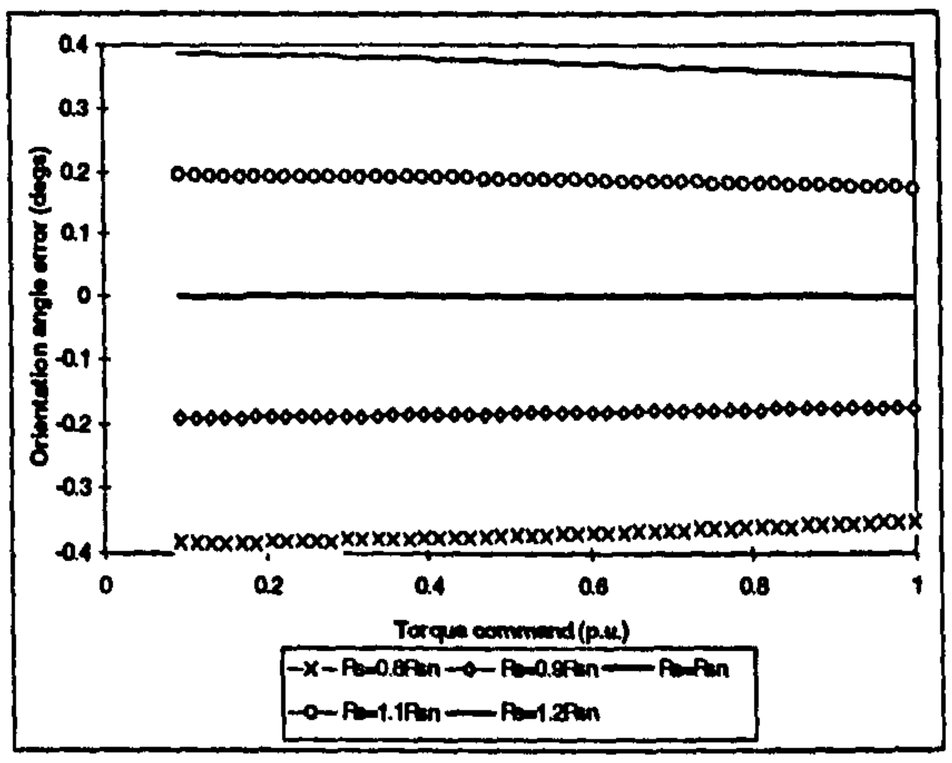

d. orientation angle error

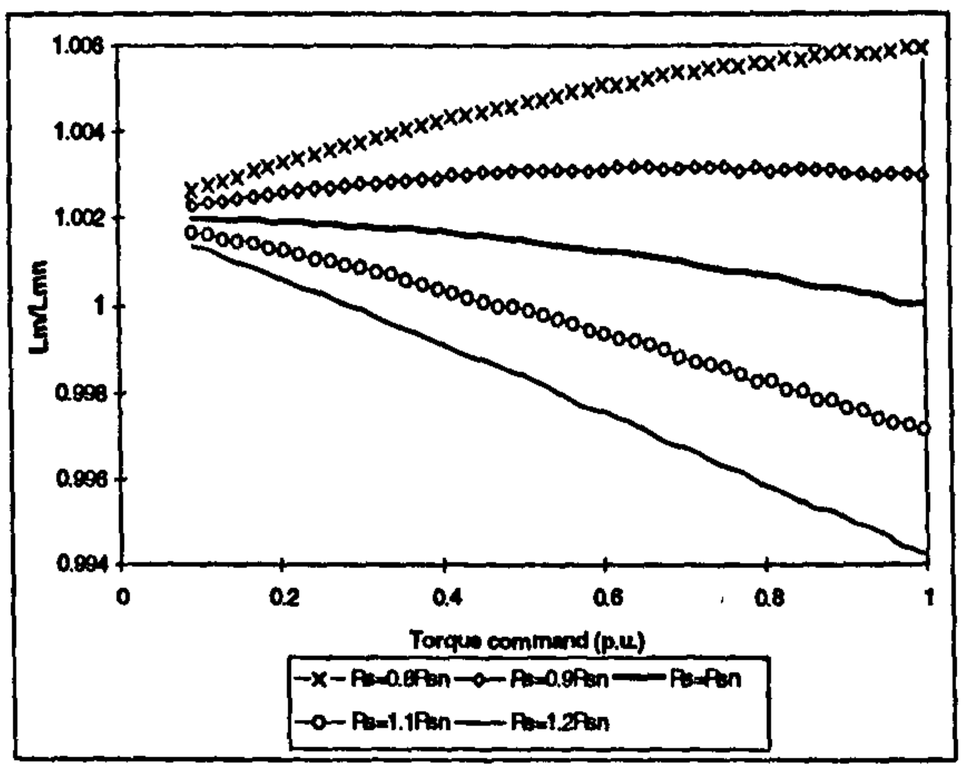

e. magnetising inductance ratio

Figure 6.8: Detuning due to incorrect stator resistance value - speed reference equal to the rated speed.

has the rated value. Magnetising inductance in induction machine will change with variation in saturation level.

Induction machine model in *d-q* axis reference frame is once more the same as in previous sections and is given with (6.29) - (6.31):

$$v_{ds} = R_s^* i_{ds}^* - \omega_e^* L_{\sigma s}^* i_{qs}^* - \omega_e^* L_m i_{qm}$$
$$v_{qs} = R_s^* i_{qs}^* + \omega_e^* L_{\sigma s}^* i_{ds}^* + \omega_e^* L_m i_{dm} \quad (6.29)$$

$$\psi_{dr} = L_m i_{ds} + \omega_{sl} T_r \psi_{qr}$$
$$\psi_{qr} = L_m i_{qs} - \omega_{sl} T_r \psi_{qr} \quad (6.30)$$

$$\psi_{dr} = -L_{\sigma r}^* i_{ds}^* + \psi_{dm}\left(1 + \frac{L_{\sigma r}^*}{L_m}\right)$$
$$\psi_{qr} = -L_{\sigma r}^* i_{qs}^* + \psi_{qm}\left(1 + \frac{L_{\sigma r}^*}{L_m}\right) \quad (6.31)$$

The procedure of mathematical analysis is also exactly the same as described in section 6.4.1, except for the difference between rotor resistances in motor and controller/ estimator. The actual angular slip frequency can be again found numerically. Then, the detuning effects due to rotor resistance variation can be evaluated. It should be noted that detuning due to rotor resistance variation is speed (frequency) independent.

It is assumed that induction machine is running at rated speed. The value of rotor resistance is set to vary from 0.8 to 1.2 of the rated value. Operation in the base speed region is discussed once more.

6.6.2 **Results of the study**

Figure 6.9 displays the calculation results of detuning due to rotor resistance variation. Speed estimation error depends on load torque. It increases with increase in torque command, Figure 6.9a. The error is symmetrical with respect to x-axis. When rotor resistance varies by ± 20%, the speed estimation error is up to ± 10 rpm with rated torque command. Speed estimation error is ± 5 rpm when rotor resistance varies by ± 10%. Figure 6.9 also shows the torque error, rotor flux error, orientation angle error and magnetising inductance error. They are all very small. Maximum errors occur at light load and are only about 0.2%. Orientation angle error is negligible small, Figure 6.9d. It is within 0.0002 degrees for torque commands up to rated value. Saturation level in the machine is hardly affected, Figure 6.9e.

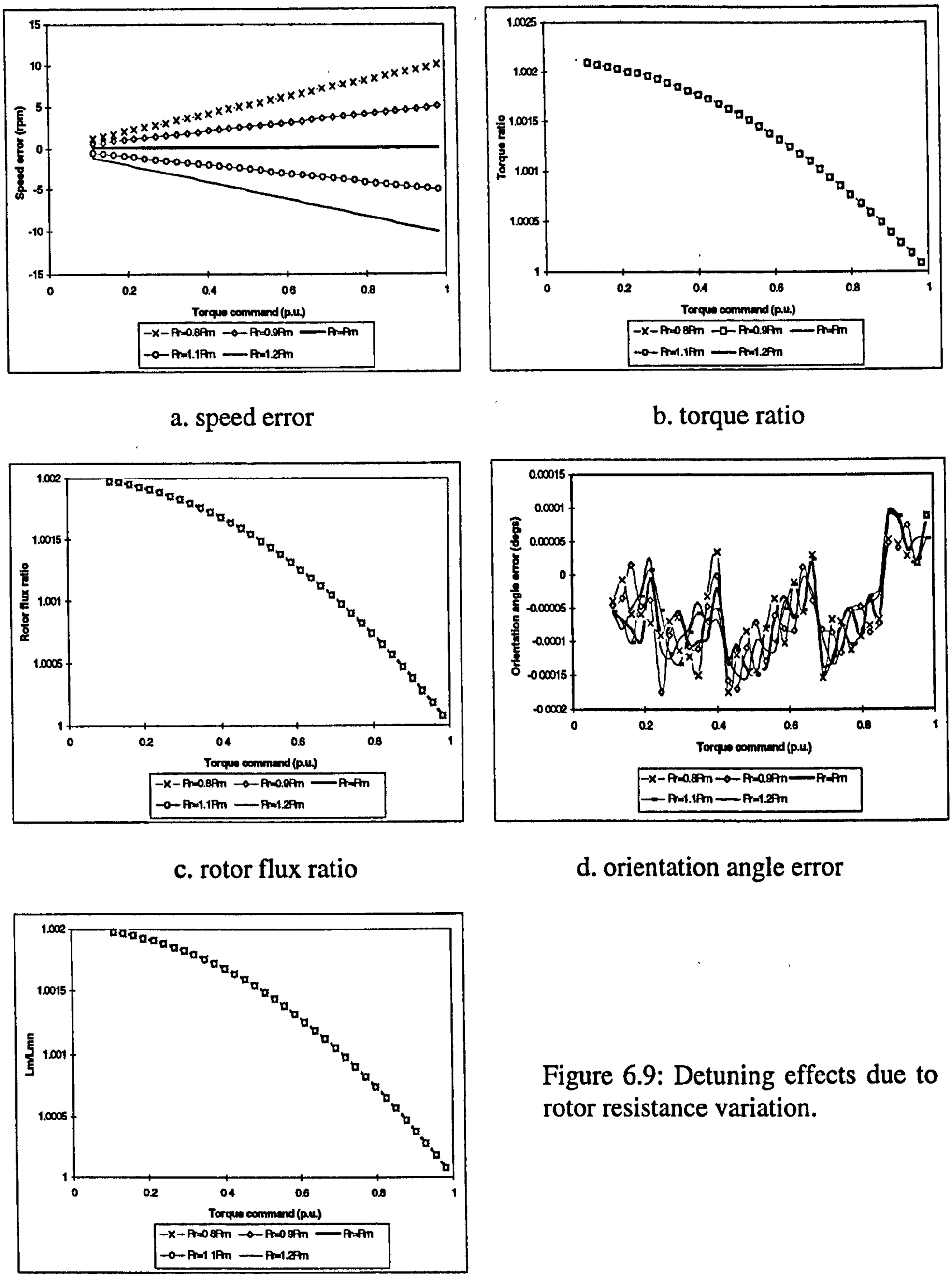

a. speed error

b. torque ratio

c. rotor flux ratio

d. orientation angle error

e. magnetising inductance ratio

Figure 6.9: Detuning effects due to rotor resistance variation.

6.7 Combined impact of iron loss and incorrect setting of the magnetising inductance

Until now, the detuning effects due to iron loss and main flux saturation have been investigated separately. However, the phenomena of iron loss and main flux saturation

appear simultaneously in practical case. Therefore, it is necessary to investigate the combined detuning effects due to both iron loss and main flux saturation.

6.7.1 Analysis

In this study, induction machine model that includes iron loss and main flux saturation, given in section 5.4, is utilised. In order to investigate the detuning effects due to both iron loss and main flux saturation, stator resistance, rotor resistance and leakage inductances have the rated values both in the controller/estimator and in the machine model. Magnetising inductance in the controller/estimator is set to different values between 0.8 and 1.2 of the rated value.

In steady-state operation, induction machine model, with iron loss and main flux saturation accounted for, can be written from (5.64) - (5.66) as:

$$\begin{aligned}
\bar{v}_s &= R_s^* \bar{i}_s + j\omega_e^* \bar{\psi}_s \\
R_{Fe}\bar{i}_{Fe} &= j\omega_e^* L_m \bar{i}_m \\
0 &= R_r^* \bar{i}_r + j\omega_{sl} \bar{\psi}_r \\
T_e &= \frac{3}{2} P \frac{L_m}{L_{\sigma r}^*} (\psi_{dr} i_{qm} - \psi_{qr} i_{dm})
\end{aligned} \tag{6.44}$$

Elimination of $\bar{i}_{Fe}, \bar{i}_r$ and $\bar{\psi}_s$, and resolution of (6.44) into *d-q* axis components yields:

$$\begin{aligned}
v_{ds} &= R_s^* i_{ds}^* - \omega_e^* L_{\sigma s}^* i_{qs}^* - \omega_e^* L_m i_{qm} \\
v_{qs} &= R_s^* i_{qs}^* + \omega_e^* L_{\sigma s}^* i_{ds}^* + \omega_e^* L_m i_{dm}
\end{aligned} \tag{6.45}$$

$$\begin{aligned}
\psi_{dr} &= L_m i_{dm} + \omega_{sl} T_{\sigma r}^* \psi_{qr} \\
\psi_{qr} &= L_m i_{qm} - \omega_{sl} T_{\sigma r}^* \psi_{dr}
\end{aligned} \tag{6.46}$$

$$\begin{aligned}
\psi_{dm} &= \frac{L_m}{L_r} (\psi_{dr} + L_{\sigma r}^* i_{ds}^* + \omega_e^* T_{\sigma Fe} \psi_{qm}) \\
\psi_{qm} &= \frac{L_m}{L_r} (\psi_{qr} + L_{\sigma r}^* i_{qs}^* - \omega_e^* T_{\sigma Fe} \psi_{dm})
\end{aligned} \tag{6.47}$$

Main flux saturation is represented by the non-linear function:

$$L_m = f(\psi_m) \tag{6.32}$$

$$\psi_m = \sqrt{\psi_{dm}{}^2 + \psi_{qm}{}^2} \tag{6.33}$$

and $T_{\sigma Fe}=L_{\sigma r}{}^*/R_{Fe}$, where R_{Fe} is given with (6.1).

The torque equation remains as given by (6.44) and electrical angular frequency is determined with (6.10). Simultaneously, however:

$$\omega_e{}^* = \omega + \omega_{sl} \tag{6.16}$$

Voltage v_{ds} is again pre-determined by the speed estimator,

$$v_{ds} = R_s{}^* i_{ds}{}^* - \omega_e{}^* \sigma^* L_s{}^* i_{qs}{}^* \tag{6.19}$$

From the first equation of (6.45) magnetising q-axis component can be obtained directly:

$$i_{qm} = \frac{1}{\omega_e{}^* L_m}(-v_{ds} + R_s{}^* i_{ds}{}^* - \omega_e{}^* L_{\sigma s}{}^* i_{qs}{}^*) \tag{6.41}$$

Next, the magnetising current d-q axis components can be expressed as functions of angular slip frequency, with $i_{ds}{}^*$ and $i_{qs}{}^*$ as independent inputs. They may be derived from (6.45)-(6.47) in the form:

$$\begin{aligned} i_{dm} &= \frac{B_1 i_{qs}{}^* - A_1 i_{ds}{}^*}{A_1{}^2 + B_1{}^2} \\ i_{qm} &= \frac{-B_1 i_{ds}{}^* - A_1 i_{qs}{}^*}{A_1{}^2 + B_1{}^2} \end{aligned} \tag{6.48}$$

where

$$\begin{aligned} A_1 &= \frac{L_m}{L_{\sigma r}{}^*}\frac{1}{1+(\omega_{sl}T_{\sigma r}{}^*)^2} - \frac{L_r}{L_{\sigma r}{}^*} \\ B_1 &= \frac{L_m}{L_{\sigma r}{}^*}\frac{\omega_{sl}T_{\sigma r}{}^*}{1+(\omega_{sl}T_{\sigma r}{}^*)^2} + \omega_e{}^* T_{Fe} \end{aligned} \tag{6.49}$$

Hence, in any steady-state with given $i_{ds}{}^*$ and $i_{qs}{}^*$, the two q-axis magnetising current components must be equal, i.e.

$$\frac{1}{\omega_e{}^* L_m}(-v_{ds} + R_s{}^* i_{ds}{}^* - \omega_e{}^* L_{\sigma s}{}^* i_{qs}{}^*) = \frac{-B_1 i_{ds}{}^* - A_1 i_{qs}{}^*}{A_1{}^2 + B_1{}^2} \tag{6.50}$$

The actual angular slip frequency can be found once more numerically by means of (6.50), using iterative calculation method. Then, the detuning effects due to magnetising inductance variation and iron loss can be found. Detuning effects are now, due to inclusion of iron loss, again speed (frequency) dependent. Study is performed for operation with rated speed command only.

6.7.2 Results of the study

Figure 6.10 displays the calculation results. Speed estimation error is function of torque command, Figure 6.10a. When magnetising inductance is set to rated value, the speed estimation error is about 2.2 rpm in the whole torque range. When magnetising inductance is set to 0.8 of the rated value, speed estimation error is up to 2.5 rpm with light load and 6 rpm with the rated torque. When magnetising inductance is bigger than the rated value, speed estimation error is decreasing with increase in torque. For operation at rated speed with rated torque, speed estimation error is up to -1 rpm, when magnetising inductance is set to 1.2 of the rated value. It is worth noting that speed estimation error here is about 2 rpm shifted with respect to speed estimation error shown in Figure 6.6a (detuning due to main flux saturation only). This amount corresponds to the speed estimation error introduced by iron loss only, Figure 6.4a.

Torque ratio is shown in Figure 6.10b. It can be seen that torque error increases in light load region. Torque error is within 20% in the torque range from half to the rated torque.

Rotor flux ratio is shown in Figure 6.10c. It is independent of load torque and up to 8% when magnetising inductance is varied from 0.8 to 1.2 of the rated. Orientation angle error is torque dependent and is very small. It is only 0.5 degree when magnetising inductance is 80% of the rated value with rated torque. It is about 0.2 degrees for magnetising inductance variation from 0.8 to 1.2 of the rated with light load torque. The ratio of magnetising inductance shown in Figure 6.10e has the same behaviour as the one shown in Figure 6.6e.

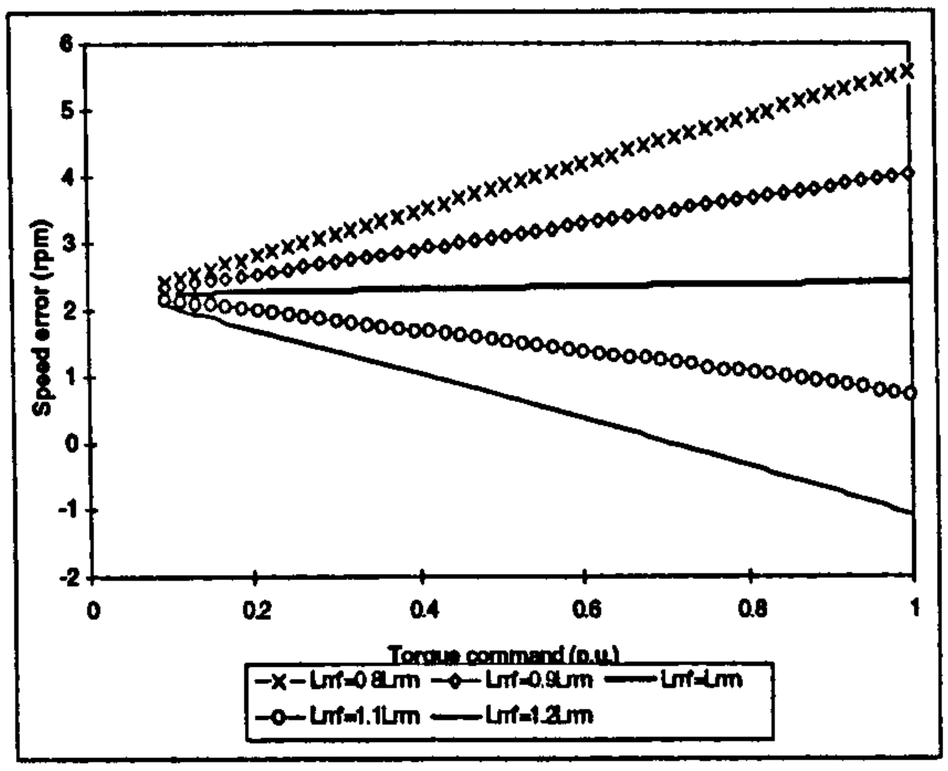

a. speed error

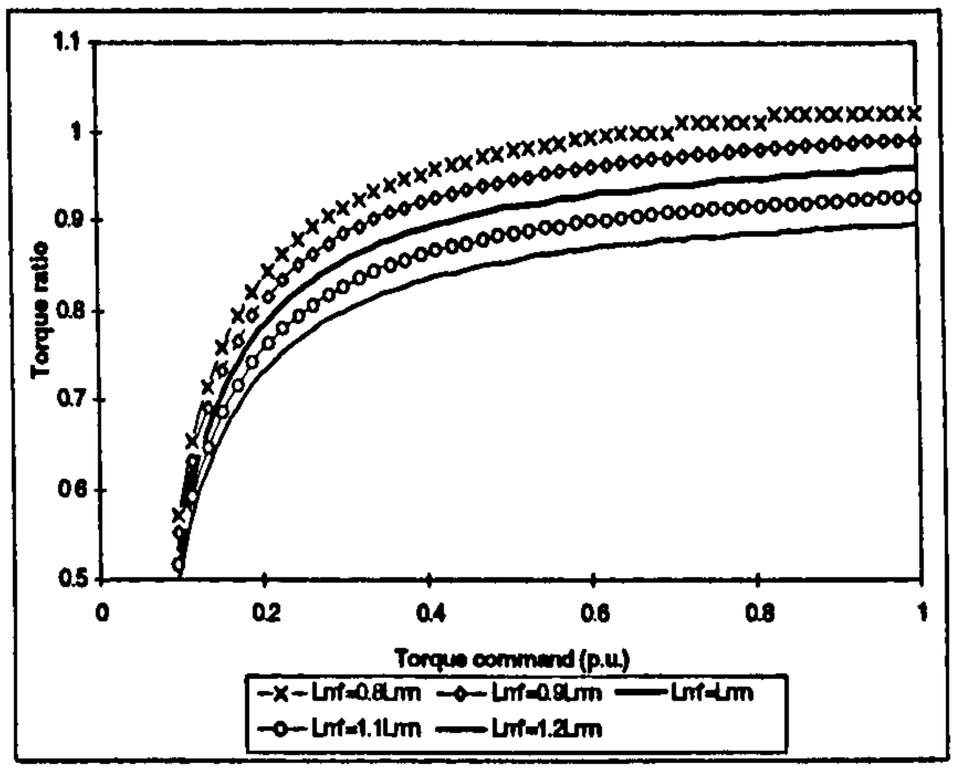

b. torque ratio

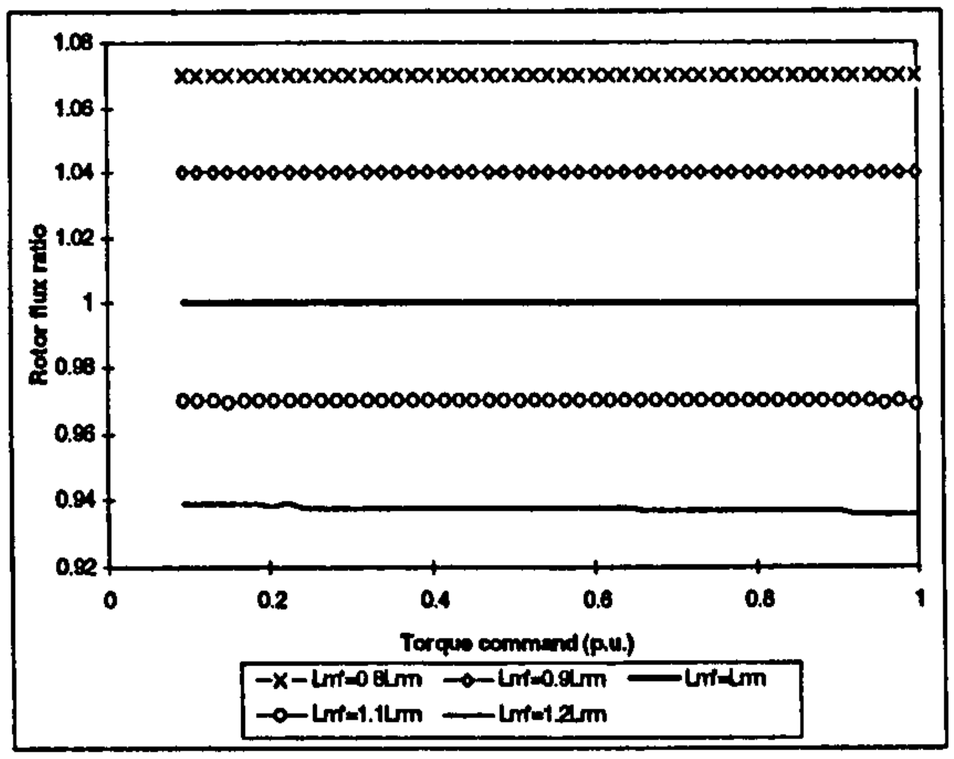

c. rotor flux ratio

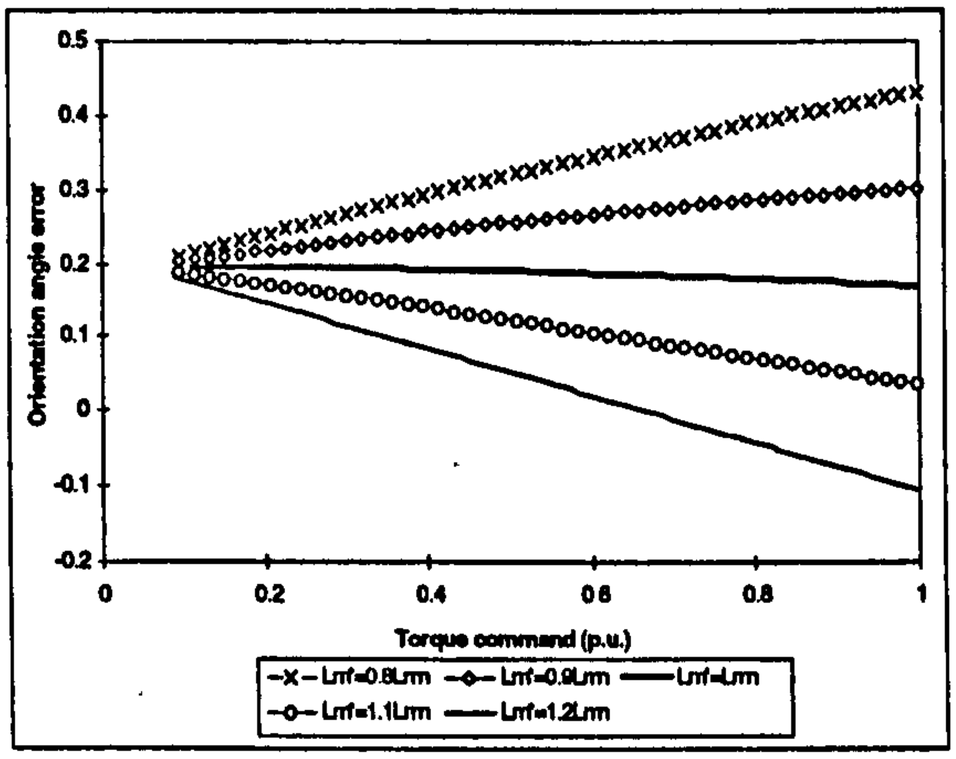

d. orientation angle error

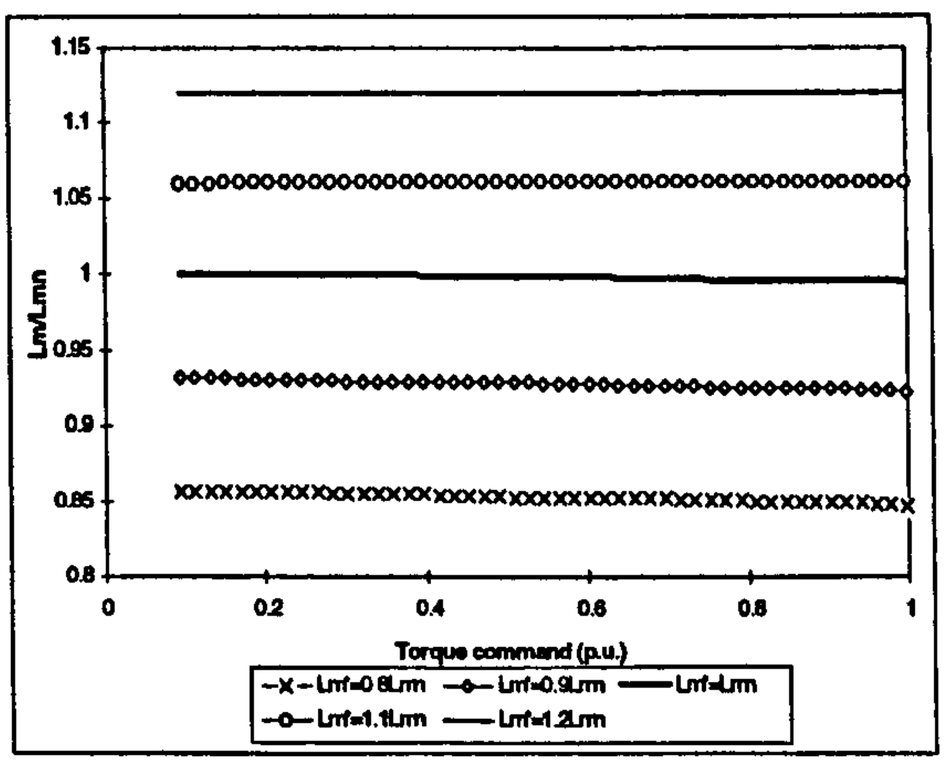

e. magnetising inductance ratio

Figure 6.10: Detuning effects due to magnetising inductance variation for machine model that includes iron loss and main flux saturation (rated speed operation).

6.8 **Relative importance of various parameter variation effects**

On the basis of the results of steady-state analysis, presented in sections 6.2 to 6.7, it is possible to draw a number of important conclusions regarding relative importance of

various sources of detuning. These are summarised in Table 6.1, taken from [Wang and Levi, 1999]. Comparison is based on the speed estimation error, torque ratio error, orientation angle error and main flux saturation level in the machine, and applies to operation in the base speed region.

It follows from Table 6.1 that the critical parameter from the point of view of orientation (and therefore associated dynamics of the drive) is stator resistance at very low speeds of operation. All the other source of detuning hardly affect the orientation angle, so that one can expect dynamic performance in detuned operation to be of the same quality as in tuned operation. Indeed, this expectation will be confirmed by the study of dynamics in the following chapter.

Table 6.1 Summary of relative importance of various parameter variation effects.

	Speed estimation error	Torque ratio error	Orientation angle error	Main flux saturation level
Rotor resistance variation	speed independent, load dependent, large (10 rpm)	negligible	negligible	not affected
Incorrect magnetising inductance setting	speed independent, load dependent, moderate	moderate	negligible	affected
Incorrect value of leakage inductances	speed independent, load dependent, small	small	small	slightly affected
Stator resistance variation	speed dependent, almost load independent; moderate at low speed, very small at high speed	large at low speeds and light load, moderate to small as speed increases	large at low speeds (up to 8°), small at high speeds	affected at low speed only
Iron loss	speed dependent, lightly load dependent, moderate	moderate to large as load decreases	negligible	not affected

As far as the speed estimation error is concerned, variation of rotor resistance leads to the highest values. Stator resistance variation at low speed of operation, iron loss and incorrect magnetising inductance setting all lead to a moderate speed estimation error.

Torque ratio error can be large due to stator resistance variation at low speed and light load, and due to iron loss at light load, while it is moderate for incorrect setting of the magnetising inductance. Main flux saturation level is in general not affected significantly for any of the detuning sources. One interesting observation is that the rotor resistance variation does not affect the saturation level, this being in huge contrast with the situation in a vector controlled drive with speed sensor.

Actual data regarding variation of leakage inductances with currents for the machine under consideration were not available. However, from Table 6.1 it appears that the least important detuning effect is the incorrect setting and/or variation in leakage inductances. This source of detuning is therefore excluded from the transient study, that follows in the next chapter.

6.9 Summary

A number of quantitative studies were performed for a 4 kW induction machine in order to investigate the impact of iron loss, main flux saturation and parameter variations in MRAC based sensorless rotor flux oriented induction machine on steady-state operation. Comprehensive analysis is performed for various steady-states and results are presented. Speed estimation error due to leakage inductance variation is much smaller than the one caused by other parameter variations. It is shown that speed estimation error due to iron loss is of the same order as are the errors due to other parameter variation effects. It may be therefore concluded that iron loss should be compensated in a sensorless rotor flux oriented induction machine. It is also shown that variation of stator and rotor resistance will affect the behaviour of system. The highest speed estimation error results from rotor resistance deviation, while stator resistance variation is critical at low speed. Combined impact of iron loss and main flux saturation was examined. Most of the results presented in this chapter will be confirmed by dynamic simulations in the next chapter.

7 DETUNING IN TRANSIENT OPERATION OF A SENSORLESS ROTOR FLUX ORIENTED INDUCTION MACHINE WITH ROTOR FLUX BASED MRAC SPEED ESTIMATOR

7.1 Introduction

Detuning during transient operation of a sensorless indirect rotor flux oriented induction machine due to iron loss, main flux saturation and parameter variations is evaluated in this chapter on the basis of programmes developed using Simulink and Matlab. The machine under consideration is the same 4 kW induction motor analysed in chapter 6. At first problems of integration of the stator flux equation are discussed in section 7.2. A couple of existing integration methods are analysed. On the basis of the results of this section the most suitable integration method is selected for further investigations and is then utilised in all the subsequent sections. Section 7.3 presents simulation results regarding transient operation of the drive under tuned conditions. Detuning due to incorrect magnetising inductance is studied in section 7.4. Detuning effects caused by rotor resistance and stator resistance variation are elaborated in sections 7.5 and 7.6, respectively. Impact of iron loss is investigated in section 7.7. The combined impact of both iron loss and main flux saturation is finally addressed in section 7.8. Contributions of the chapter are summarised in section 7.9.

7.2 Problem of integration in the process of speed estimation

The basic structure of the MRAC based speed estimator is shown again in Figure 7.1. The outputs of the reference and the adjustable models are two estimates of rotor flux components in stationary reference frame, as already discussed in section 4.2.

The estimator shown in Figure 7.1 involves pure integration within the reference model. This leads to problems with initial conditions and drift. To solve this problem, two improved schemes that use auxiliary variables have been suggested by Schauder [1992]. Two identical linear transfer functions are inserted into both the reference model and the adjustable model. In the first case, the transfer function is placed at the output side of the reference model and at the input side of the adjustable model. In the

second case, the transfer functions appear at the output side of both the reference and the

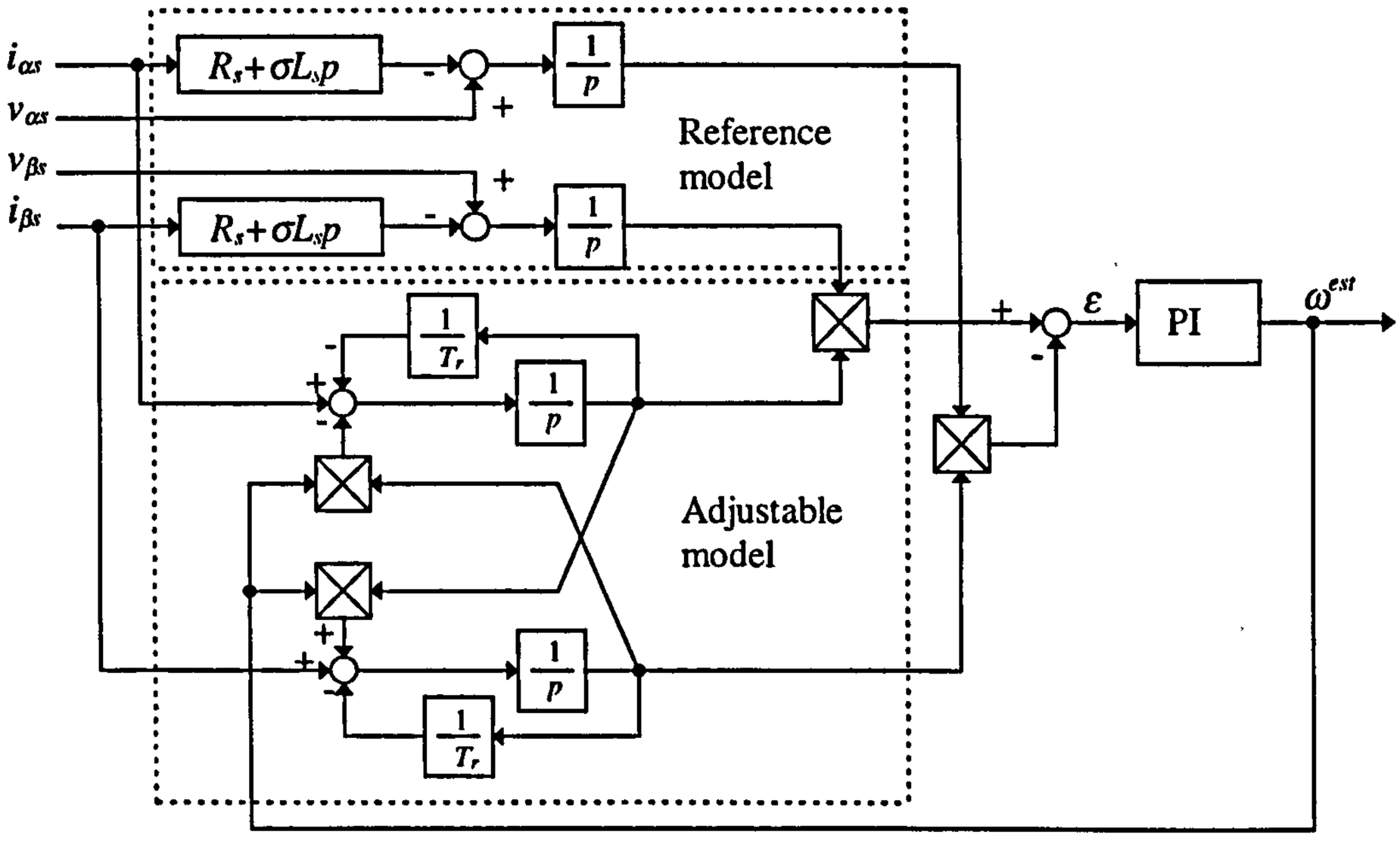

Figure 7.1: Basic structure of a MRAC based speed estimator.

adjustable models. These two modified MRAC estimators are shown in Figure 7.2 and Figure 7.3, respectively. The transfer function is of the form $\frac{p}{p+1/T}$.

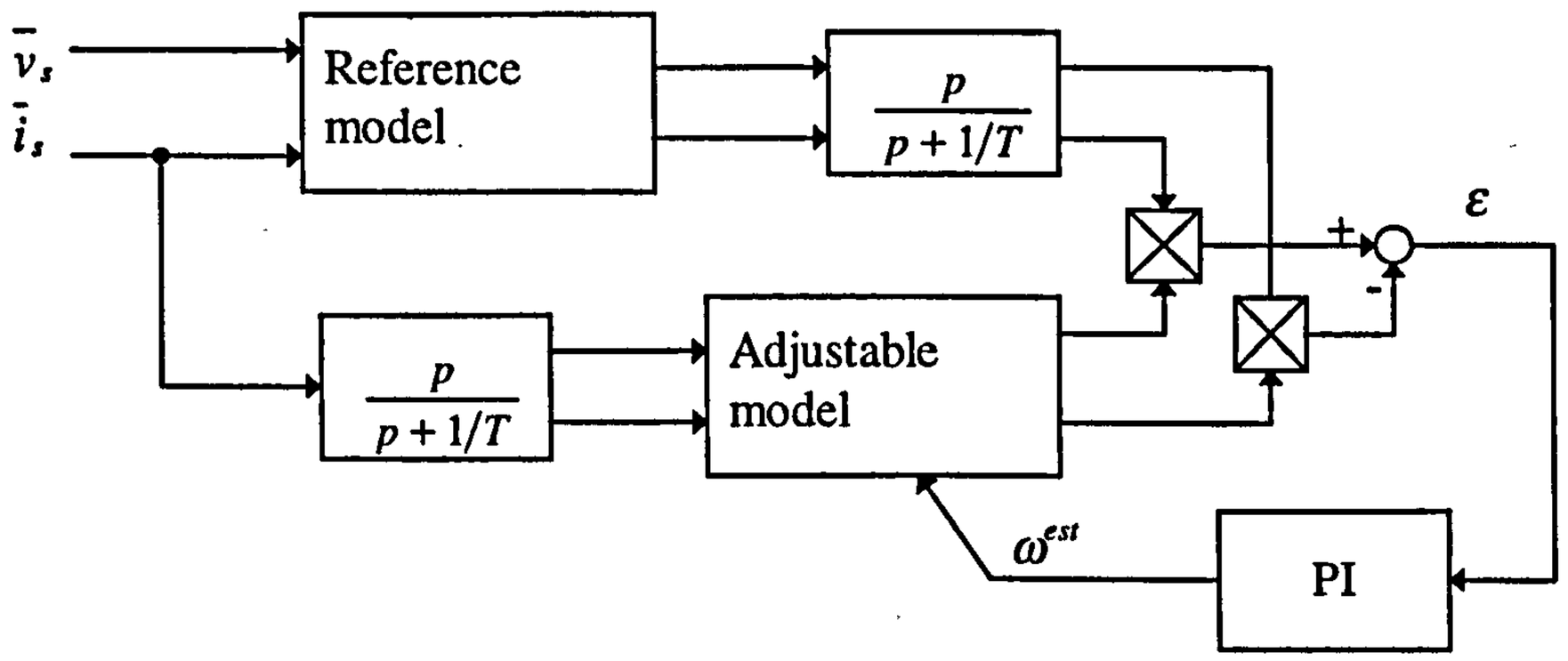

Figure 7.2: MRAC based speed estimator with auxiliary variables - Scheme 1.

As shown in [Schauder, 1992] addition of these elements has no adverse impact on the operation of the estimator, since attenuation and phase shift introduced are the same for both the output of the reference model and the output of the adjustable model, and the error quantity ε is the difference between the two instantaneous positions of the two rotor flux vector estimates.

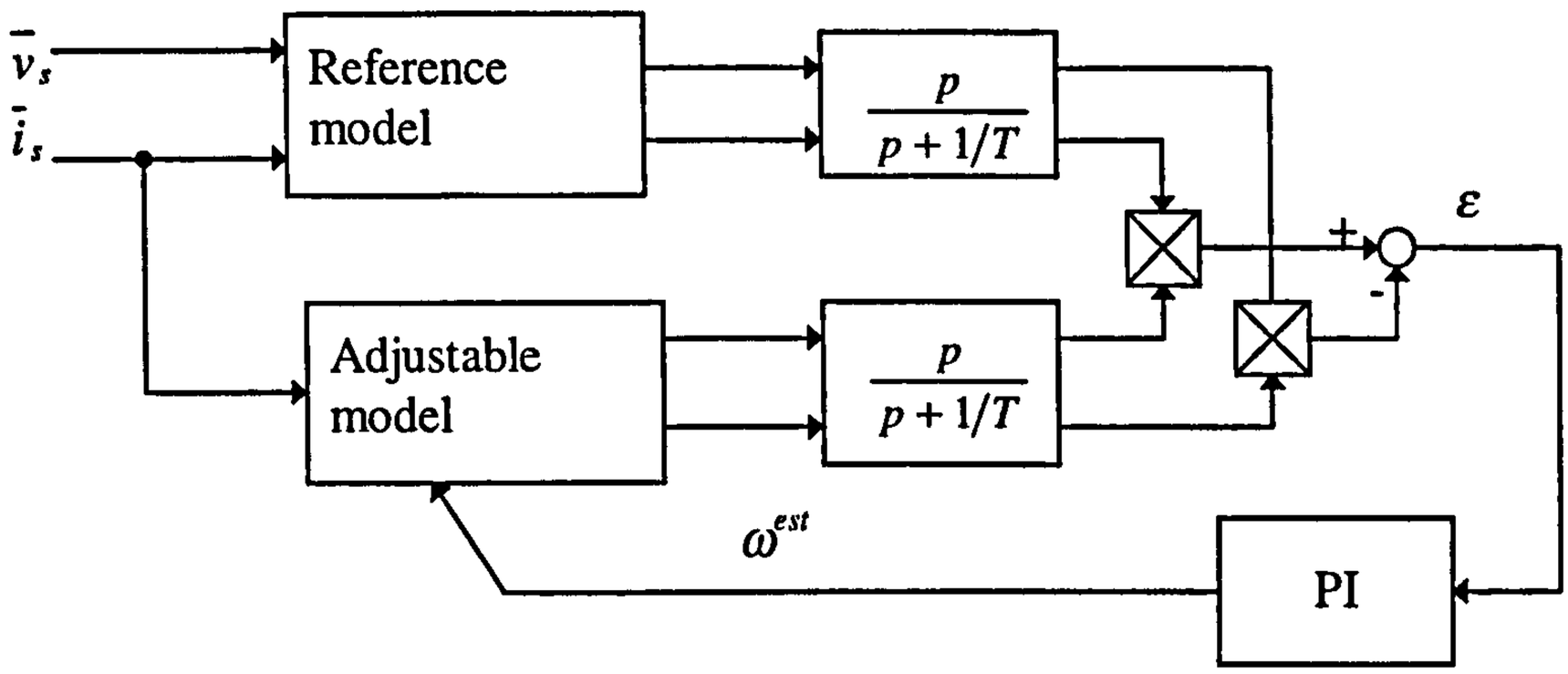

Figure 7.3: MRAC based speed estimator with auxiliary variables - Scheme 2.

The behaviour of these two estimators has been investigated by simulation, using Simulink/Matlab. The induction machine model is the constant parameter one, in which all the parameter variation effects, as well as main flux saturation and iron loss are neglected. The induction machine is assumed to be fed from an ideal current source (i.e. current controlled PWM inverter is taken as ideal). As input stator currents are known, stator voltage components are created by means of stator voltage equations in stationary reference frame. The control scheme for simulation is illustrated in Figure 7.4. Actual

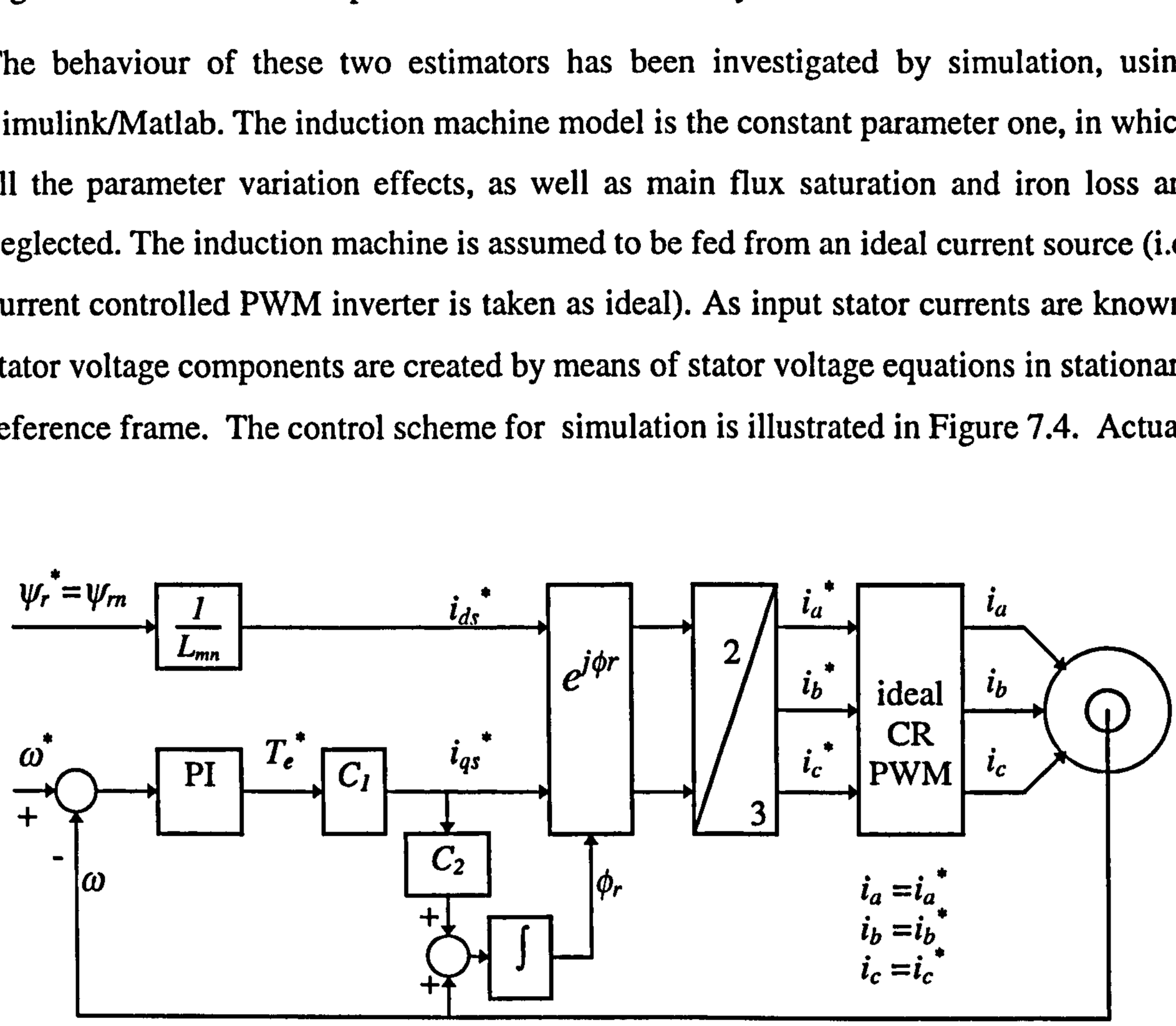

Figure 7.4: Control scheme of indirect rotor flux oriented induction machine with speed estimator placed in parallel.

speed is used for control purposes in indirect rotor flux oriented induction machine and the speed estimator is operated in parallel. Note that estimated speed is not used either for speed control or for rotor flux space vector spatial position calculation.

In each case, three values of $1/T$ are selected in order to investigate impact of T on estimated speed. The conditions of simulation are the following:

1. Initial excitation is started at zero speed under no-load conditions at $t = 0$ s with $\psi_r^* = \text{constant} = \psi_m$.
2. The rated speed command is applied at $t = 0.1$ s in a ramp-wise manner. The reference speed becomes rated at $t = 0.32$ s.
3. Rated load torque is applied at $t = 0.5$ s.

Simulation results obtained with Scheme 1 of Figure 7.2 are given in Figures 7.5 -7. 7.

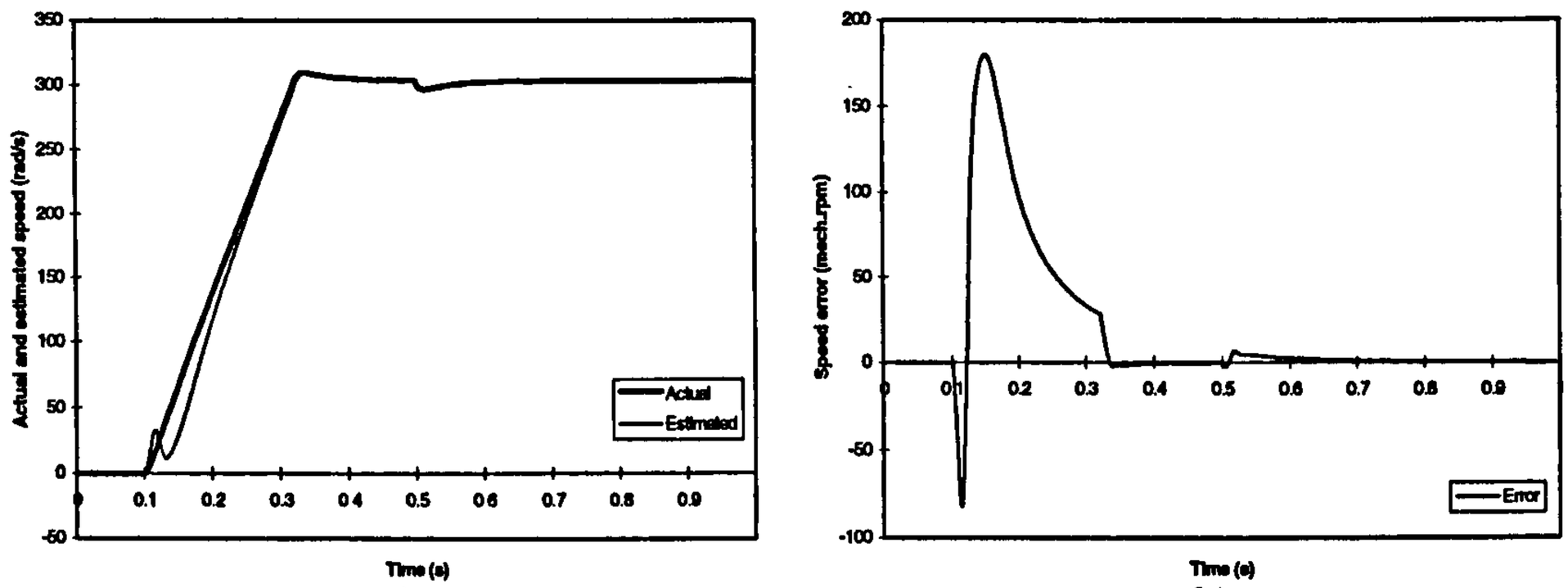

a) b)

Figure 7.5: a) Actual speed and estimated speed (electrical angular) and b) rotor speed error (mechanical, rpm) with speed estimator of Scheme 1 and $1/T = 100$.

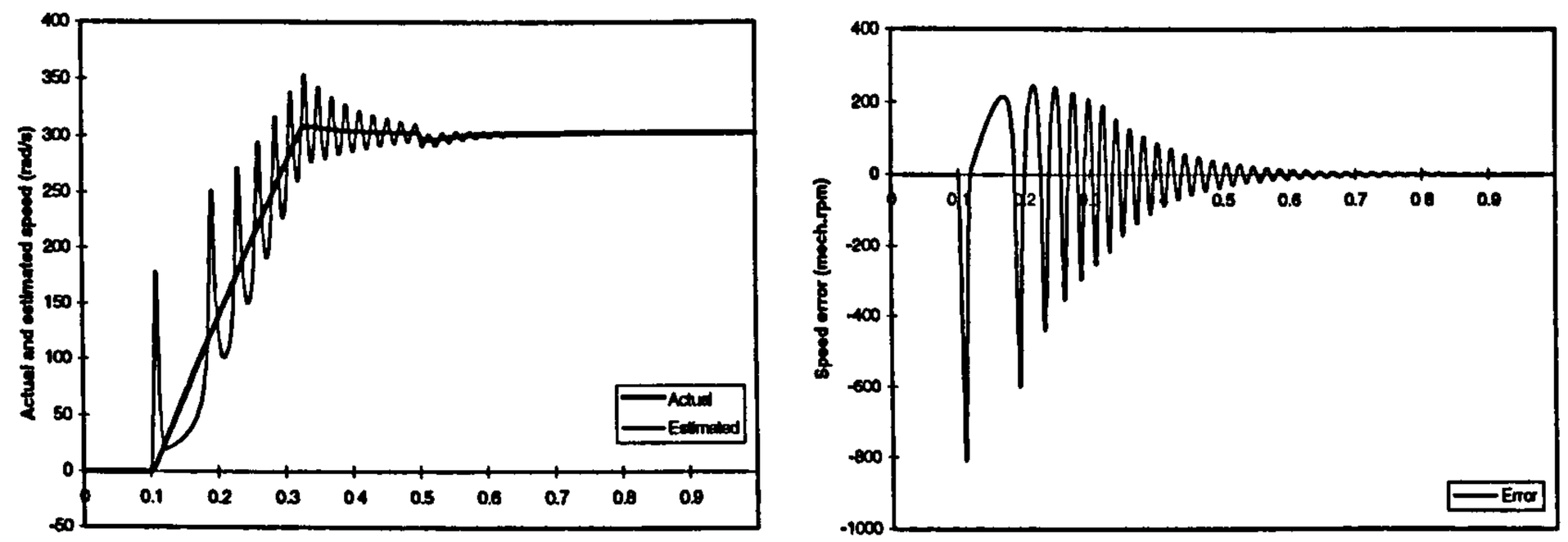

a) b)

Figure 7.6: a) Actual speed and estimated speed (electrical angular) and b) rotor speed error (mechanical, rpm) with speed estimator of Scheme 1 and $1/T = 10$.

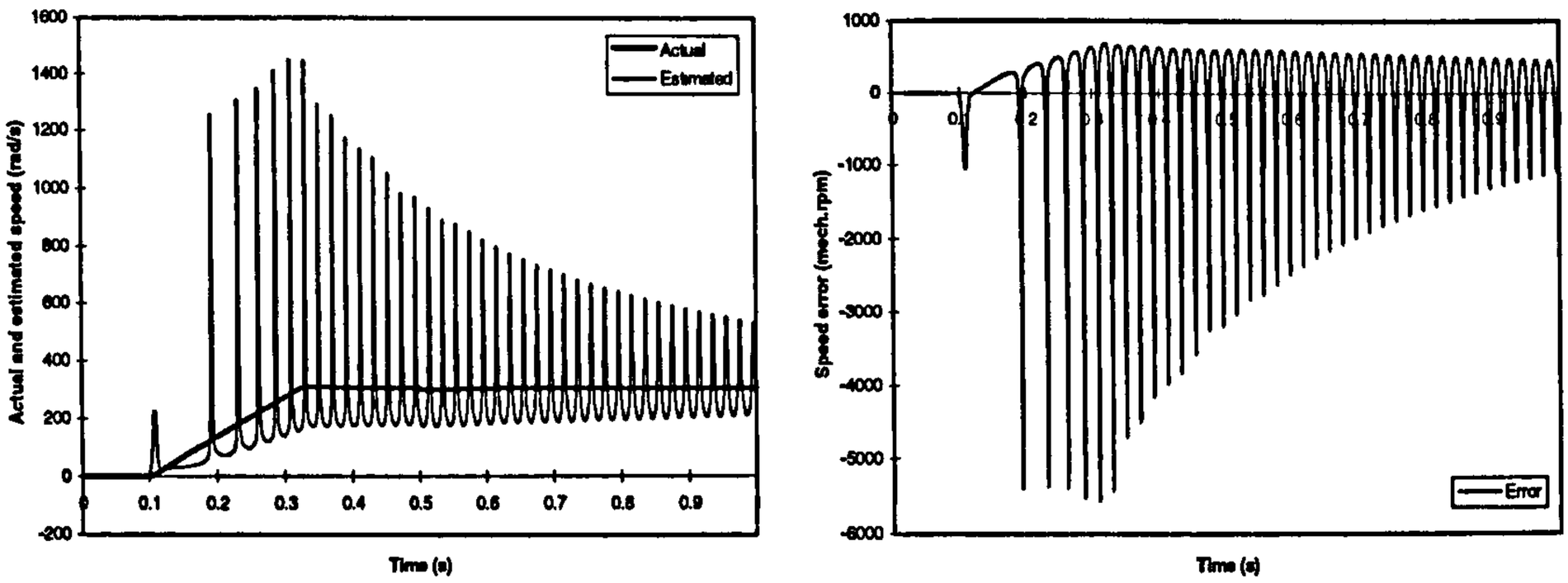

a) b)

Figure 7.7: a) Actual speed and estimated speed (electrical angular) and b) rotor speed error (mechanical, rpm) with speed estimator of Scheme 1 and $1/T = 1$.

Simulation results that apply to the Scheme 2 of Figure 7.3 are given in Figures 7.8 - 7.10.

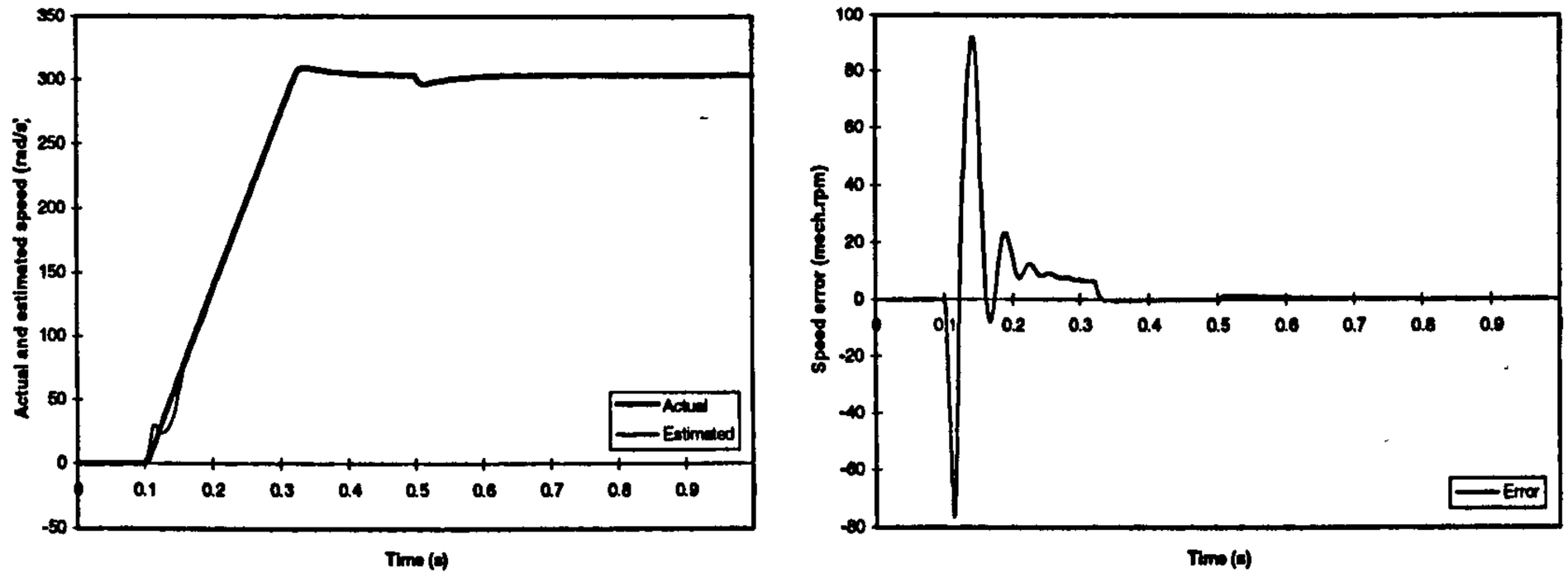

a) b)

Figure 7.8: a) Actual speed and estimated speed (electrical angular) and b) rotor speed error (mechanical, rpm) with speed estimator of Scheme 2 and $1/T = 100$.

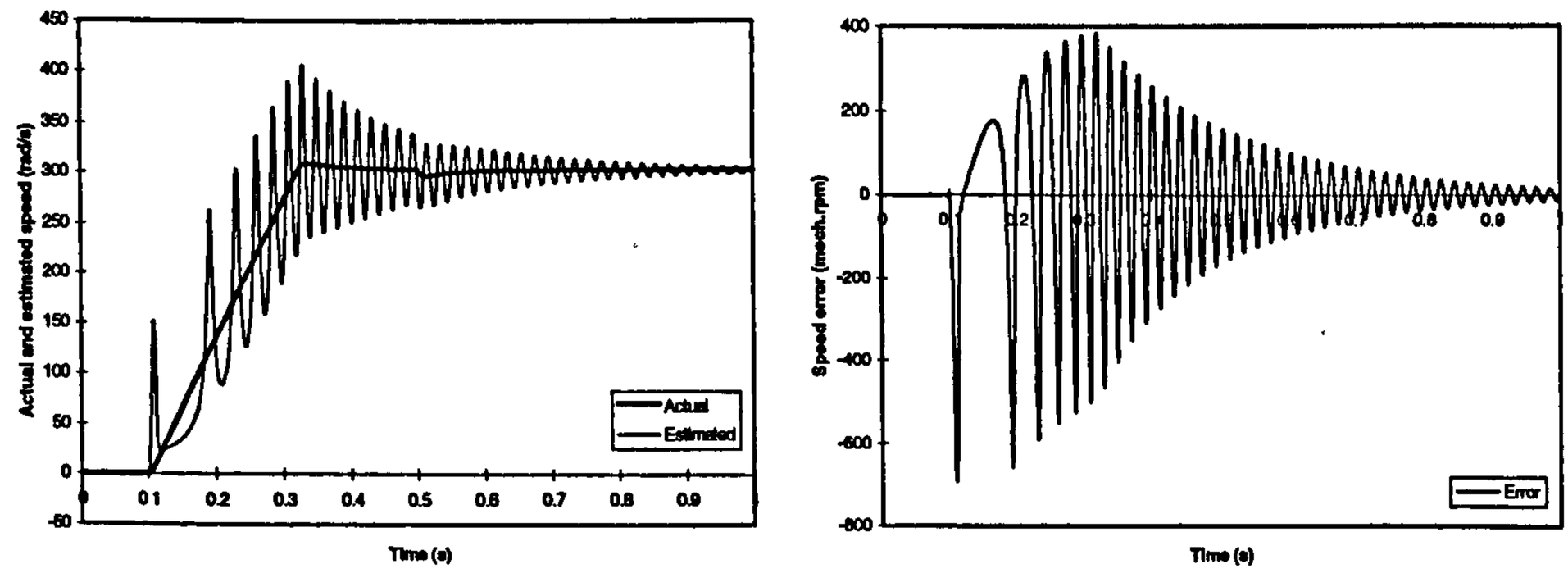

a) b)

Figure 7.9: a) Actual speed and estimated speed (electrical angular) and b) rotor speed error (mechanical, rpm) with speed estimator of Scheme 2 and $1/T = 10$.

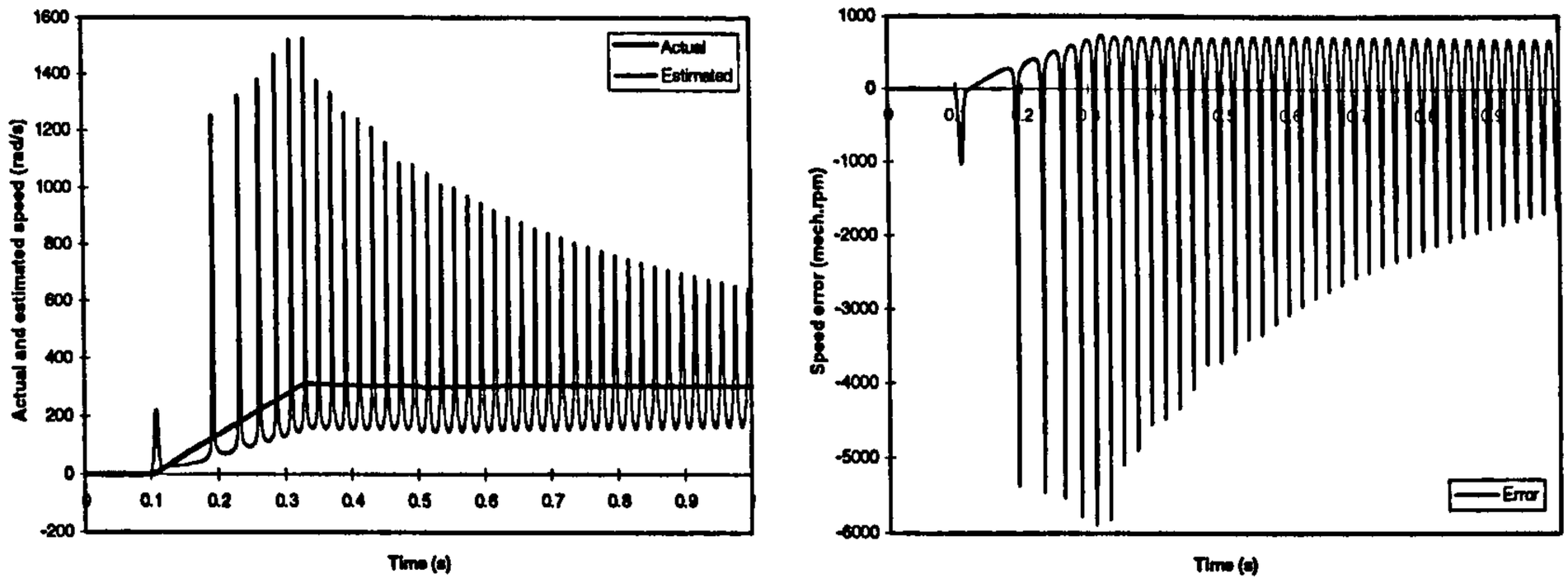

a) b)

Figure 7.10: a) Actual speed and estimated speed (electrical angular) and b) rotor speed error (mechanical, rpm) with speed estimator of Scheme 2 and $1/T = 1$.

From the results shown above one can conclude that the MRAC speed estimator is very sensitive to the value of $1/T$. Figure 7.5a shows actual speed and estimated speed with $1/T = 100$, while Figure 7.5b shows the speed error $\Delta n = n - n^{est}$ for Scheme 1 when $1/T$ is equal to 100. One can see that the estimated speed in Figure 7.5a is stable. The speed error is very close to zero in steady state. It becomes significant only during initial run-up time. As a comparison, the actual speed and estimated speed and speed error are also shown in Figure 7.6 and Figure 7.7 when 1/T is set to 10 and 1, respectively. From these two Figures one can see that the estimated speed becomes unstable with $1/T$ decreasing. In Figure 7.6 the oscillations of the estimated speed appear in the period from 0.1 s to 0.7 s. After that, the estimated speed stabilises and the speed error becomes zero. For $1/T = 1$ the magnitudes of oscillations become very high, up to 1400 rad/s, as shown in Figure 7.7a. Oscillatory behaviour lasts much longer than in Figure 7.6a.

For Scheme 2 of Figure 7.3 the simulation results for $1/T = 100$, $1/T = 10$ and $1/T = 1$ are shown in Figures 7.8 - 7.10. One can see that this set of results is similar to the set discussed previously. It is worth noting that the maximum speed error when $1/T = 100$ (Figure 7.8b) is smaller than in Figure 7.5b. Therefore the better choice for speed estimation appears to be $1/T = 100$ with Scheme 2.

The initial condition and drift problems in a MRAC based speed estimator can also be solved based on a modified integration algorithm with an adaptive magnitude compensation, which is suggested in [Hu and Wu, 1997]. The block can be used to replace the pure integrators in MRAC's reference model. The scheme is shown in Figure 7.11.

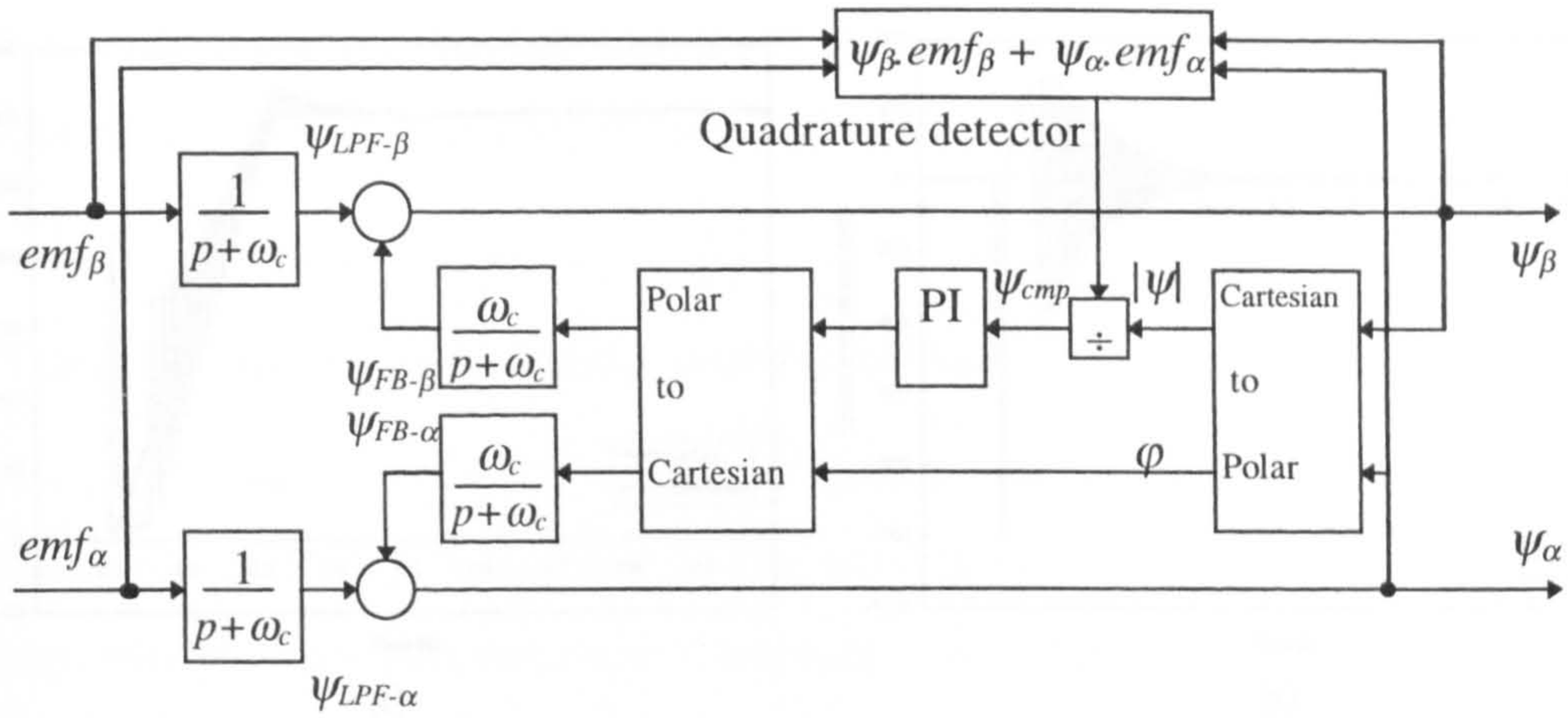

Figure 7.11: Modified integration algorithm with an adaptive magnitude compensation (*LPF* = low pass filter, *FB* = feedback, *cmp* = compensation).

The principle of this scheme is based on the fact that the motor flux is orthogonal to the back emf. A quadrature detector is proposed to detect the orthogonality between the estimated flux and the emf. A PI regulator is used to generate an appropriate compensation level so that the motor flux is orthogonal to the back emf. The inputs of this algorithm are back emf and the outputs are motor flux components in stationary reference frame. This estimator with modified integration algorithm is called Scheme 3.

In this algorithm the cut-off frequency ω_c must be selected carefully. Simulations have been done for different values of ω_c. For ω_c = 20, 50 and 100 rad/s the simulation results are shown in Figures 7.12, 7.13, and 7.14, respectively.

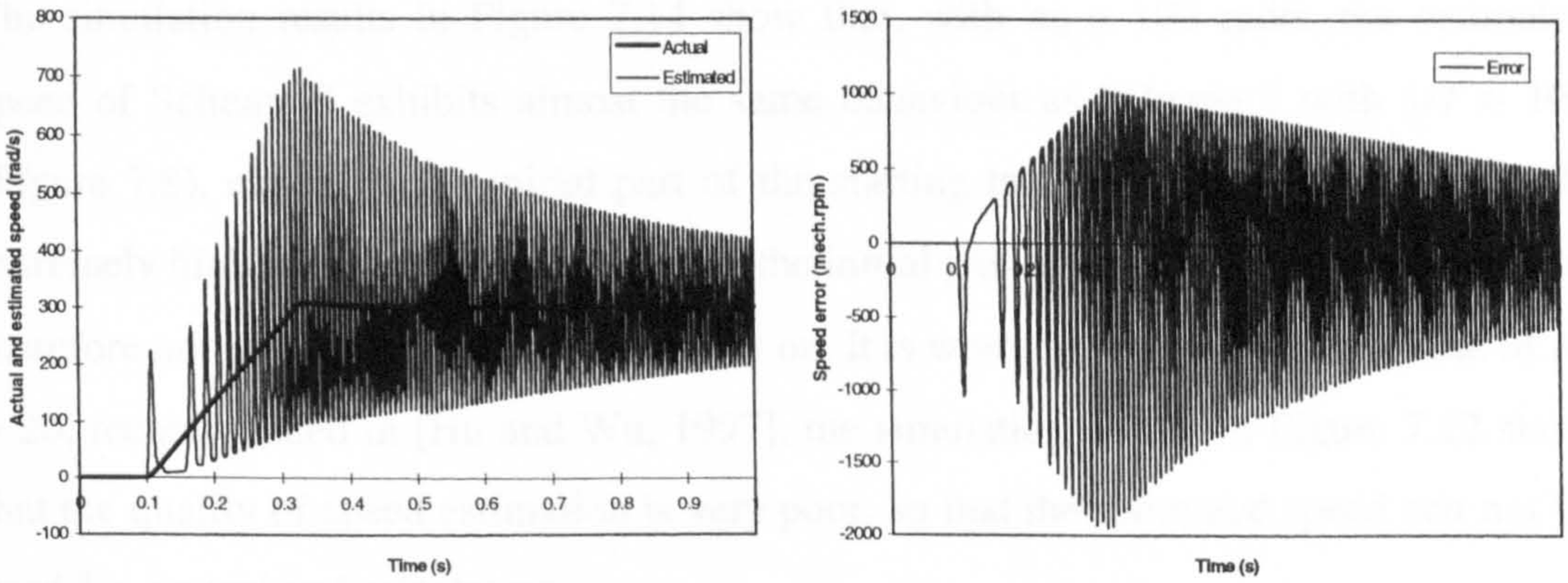

a) b)

Figure 7.12: a) Actual speed and estimated speed (electrical angular) and b) rotor speed error (mechanical, rpm) with speed estimator of Scheme 3 (ω_c = 20).

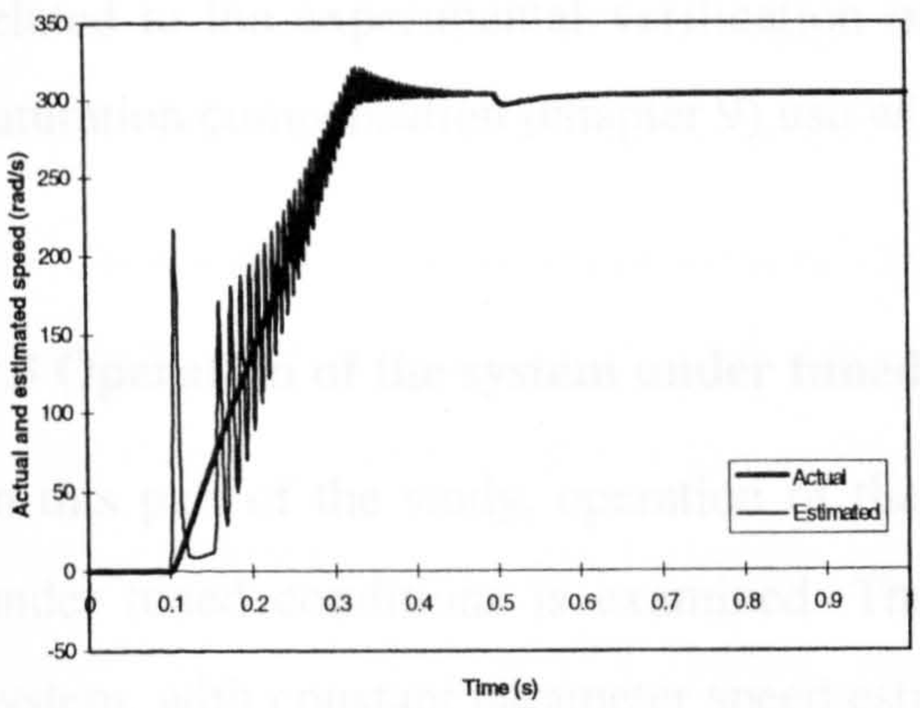

a)

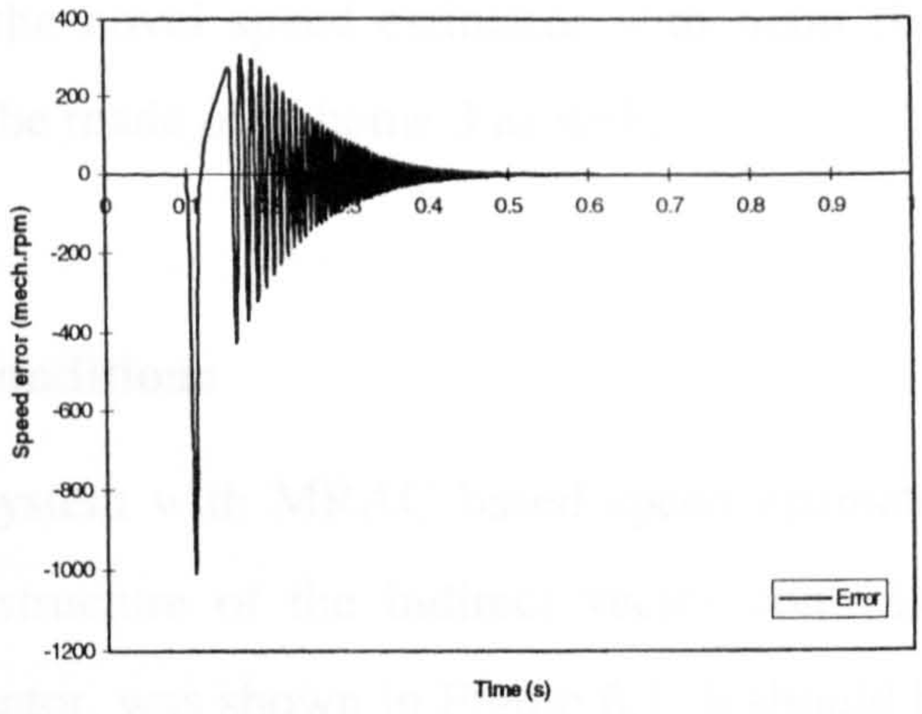

b)

Figure 7.13: a) Actual speed and estimated speed (electrical angular) and b) rotor speed error (mechanical, rpm) with speed estimator of Scheme 3 ($\omega_c = 50$).

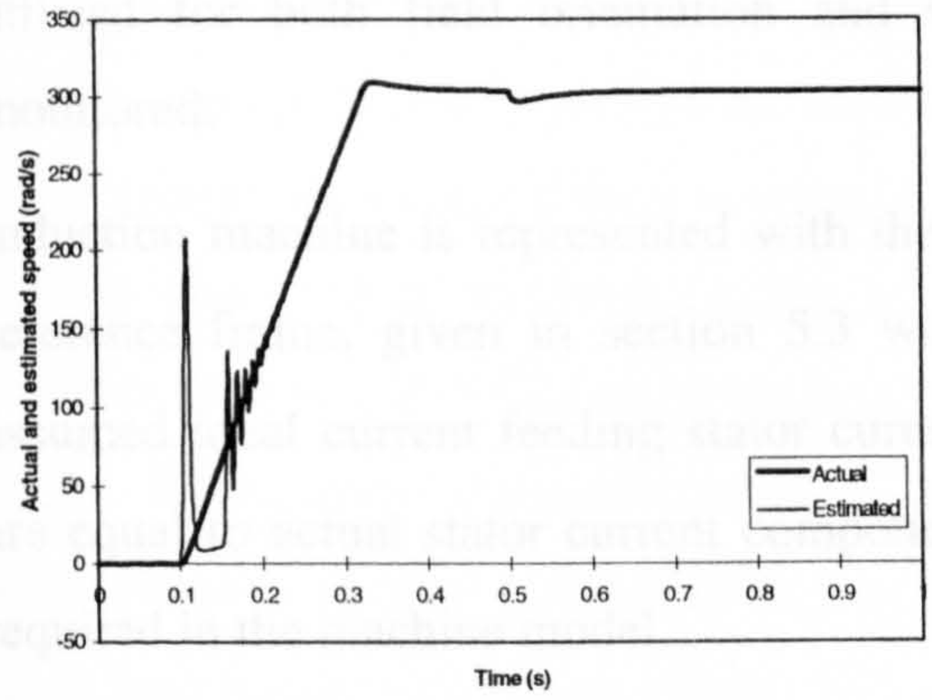

a)

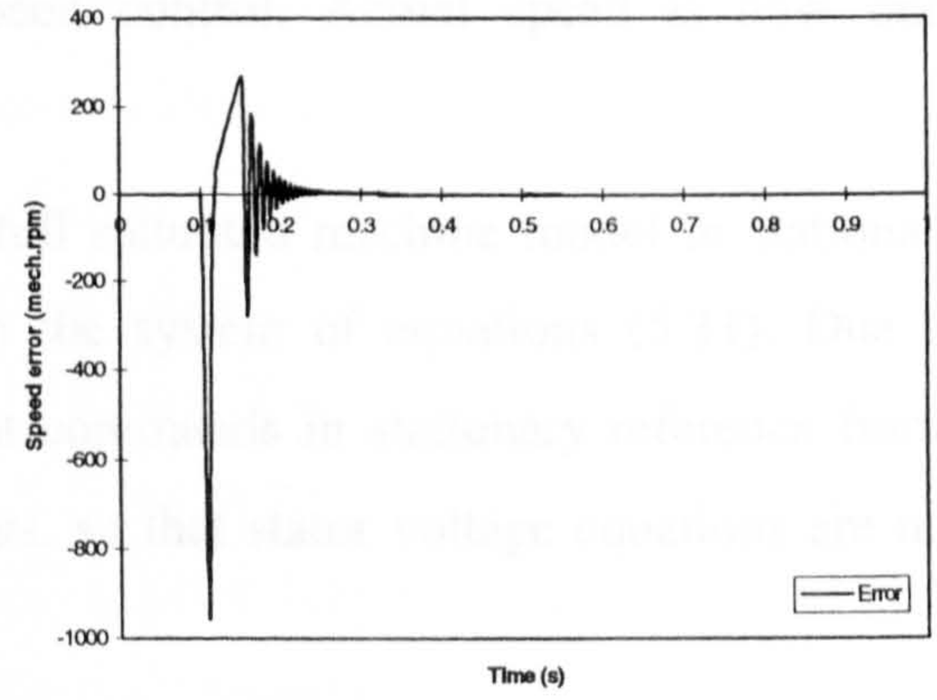

b)

Figure 7.14: a) Actual speed and estimated speed (electrical angular) and b) rotor speed error (mechanical, rpm) with speed estimator of Scheme 3 ($\omega_c = 100$).

The simulation results in Figure 7.14 show that, with $\omega_c = 100$ rad/s, the estimated speed of Scheme 3 exhibits almost the same behaviour as Scheme 2 with $1/T = 100$ (Figure 7.8), except in the initial part of the starting transient. There is unfortunately extremely high value of the speed error in the initial part of the transient. The scheme is therefore not utilised in simulations further on. It is worth noting that for the value of $\omega_c = 20$, recommended in [Hu and Wu, 1997], the simulation results in Figure 7.12 show that the quality of speed estimation is very poor, so that the estimated speed can not be used for control and orientation.

On the basis of the simulation results given in Figures 7.5 to 7.10 and 7.12 to 7.14, Scheme 2 with $1/T = 100$ is selected for all the subsequent simulations. Scheme 2 will be used additionally in experimental work, described in chapter 9. In one specific case,

related to the experimental verification of the novel speed estimator with main flux saturation compensation (chapter 9) use will be made of Scheme 3 as well.

7.3 Operation of the system under tuned conditions

In this part of the study, operation of the system with MRAC based speed estimator under tuned conditions is examined. The structure of the indirect vector controller system, with constant parameter speed estimator, was shown in Figure 6.1. It should be noted that, in contrast to section 7.2 where actual speed was used for speed control and field orientation, in this section and in all the subsequent sections estimated speed is utilised for both field orientation and speed control. Actual speed is now only monitored.

Induction machine is represented with the full saturated machine model in stationary reference frame, given in section 5.3 with the system of equations (5.31). Due to assumed ideal current feeding stator current commands in stationary reference frame are equal to actual stator current components, so that stator voltage equations are not required in the machine model.

Inputs of speed estimator are stator voltage components and stator currents components in stationary reference frame. Stator voltage components can be reconstructed by using stator current components and their derivatives, as well as various required saturated inductance values and rotor current components in stationary reference frame from the machine model. On the basis of complete induction machine model given in section 5.3 with (5.16) - (5.20), stator voltage components are found in the stationary reference frame as:

$$\begin{aligned} v_{\alpha s} &= \left(L_{\sigma s} + L_{\alpha\alpha m}\right)\frac{di_{\alpha s}^{*}}{dt} + L_{\alpha\beta}\frac{di_{\beta s}^{*}}{dt} + L_{\alpha\alpha m}\frac{di_{\alpha r}}{dt} + L_{\alpha\beta}\frac{di_{\beta r}}{dt} + R_s i_{\alpha s}^{*} \\ v_{\beta s} &= L_{\alpha\beta}\frac{di_{\alpha s}^{*}}{dt} + \left(L_{\sigma s} + L_{\beta\beta m}\right)\frac{di_{\beta s}^{*}}{dt} + L_{\alpha\beta}\frac{di_{\alpha r}}{dt} + L_{\beta\beta m}\frac{di_{\beta r}}{dt} + R_s i_{\beta s}^{*} \end{aligned} \tag{7.1}$$

where all the inductance terms are defined in (5.21) - (5.23).

The Simulink model for simulation of the drive system is included in Appendix C. All the parameters in both the controller/estimator and in the machine model have the rated

values (given in Appendix A). Representation of the machine and therefore the Simulink model as well are the same for subsequent sections 7.4 to 7.6.

The machine is excited under no-load conditions at zero speed with rated rotor flux reference. Speed command of rated value is applied at $t = 0.1$ s in a ramp-wise manner. Rated torque is applied at $t = 0.6$ s. Figure 7.15 shows the simulation results of the sensorless system. The results shown are actual and estimated speed response, speed estimation error ($\Delta n = n - n^{est}$), actual and commanded torque, magnetising current components, reference and actual rotor flux, rotor flux components, and actual and controller/estimator magnetising inductance.

As is evident from Figures 7.15a, b, c, the estimated speed tracks the actual one very well, except in the initial part of the acceleration. Commanded and actual torque are in good agreement, except during acceleration, Figure 7.15d. Field orientation is initially lost, as witnessed by oscillatory torque behaviour. In steady-state operation, orientation angle error is negligibly small again, as rotor flux q-axis component is essentially zero, Figure 7.15h. Speed estimation error, initially large, is zero for both full load and no-load operation at rated speed and has negligibly small values during transient caused by rated load torque application, Figure 7.15 b and c. Commanded and actual rotor flux are in good agreement and magnetising inductances in the controller/estimator and in the machine are equal, except during acceleration, Figures 7.15 f and g. It should be noted that rather unsatisfactory performance during acceleration transient can be improved by reducing the gains of the speed PI controller of Figure 6.1.

7.4 Detuning due to incorrect magnetising inductance setting

In this part of study detuning due to incorrect magnetising inductance setting during transient operation is elaborated. Detuning due to magnetising inductance variation is independent of speed, but load independent as discussed in section 6.4. It is at maximum when load torque is rated, Figure 6.6. The same simulation study as in section 7.3 is performed again, with the magnetising inductance set to constant values from 0.8 to $1.2L_{mn}$ in the controller and estimator. All the other parameters in the controller/estimator and in the machine remain the same and equal to rated values.

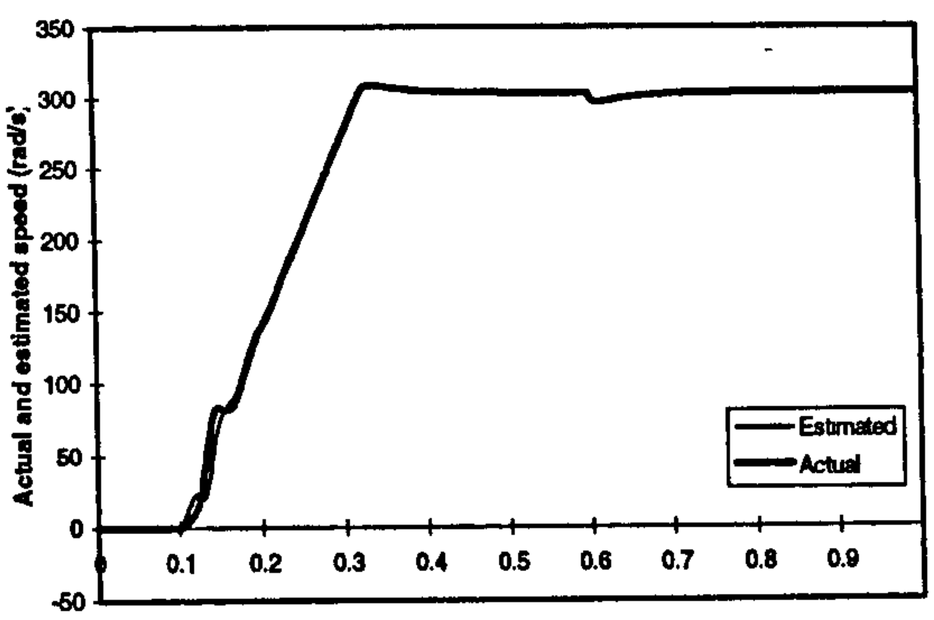

a)

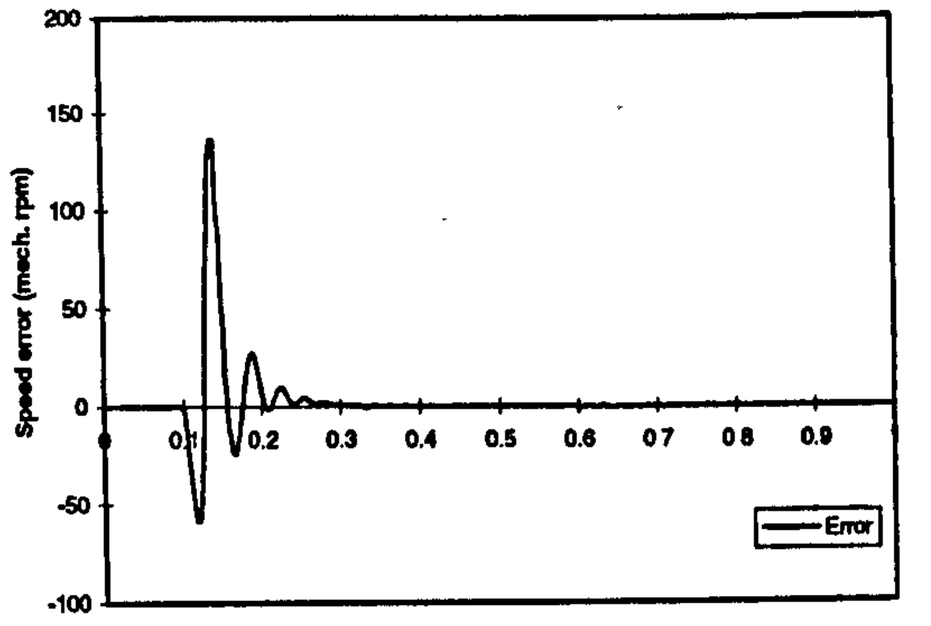

b)

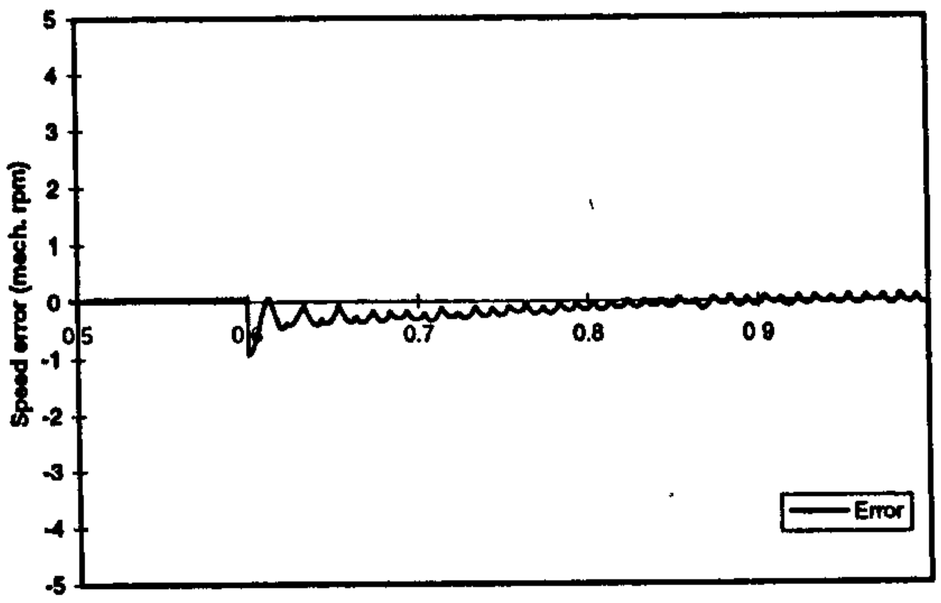

c)

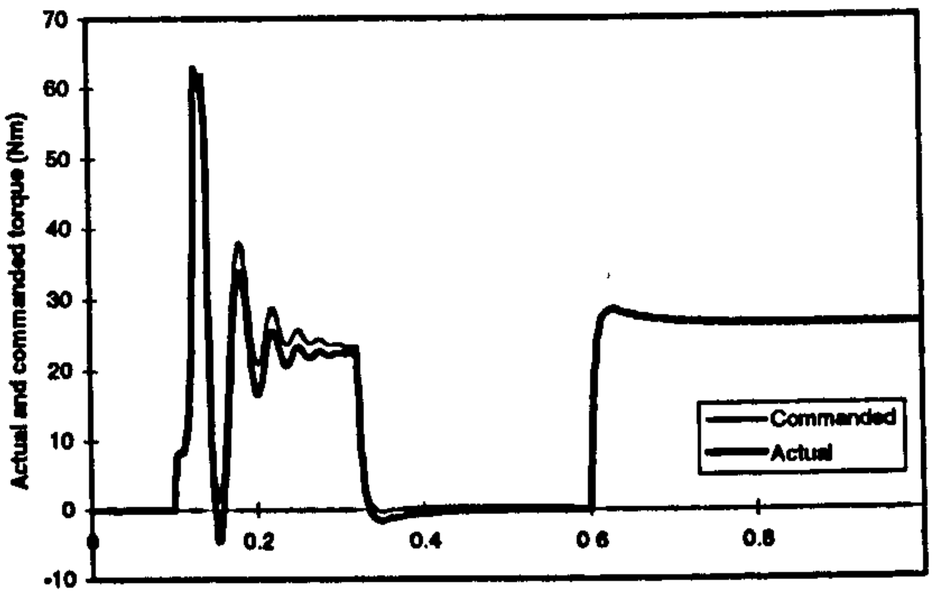

d)

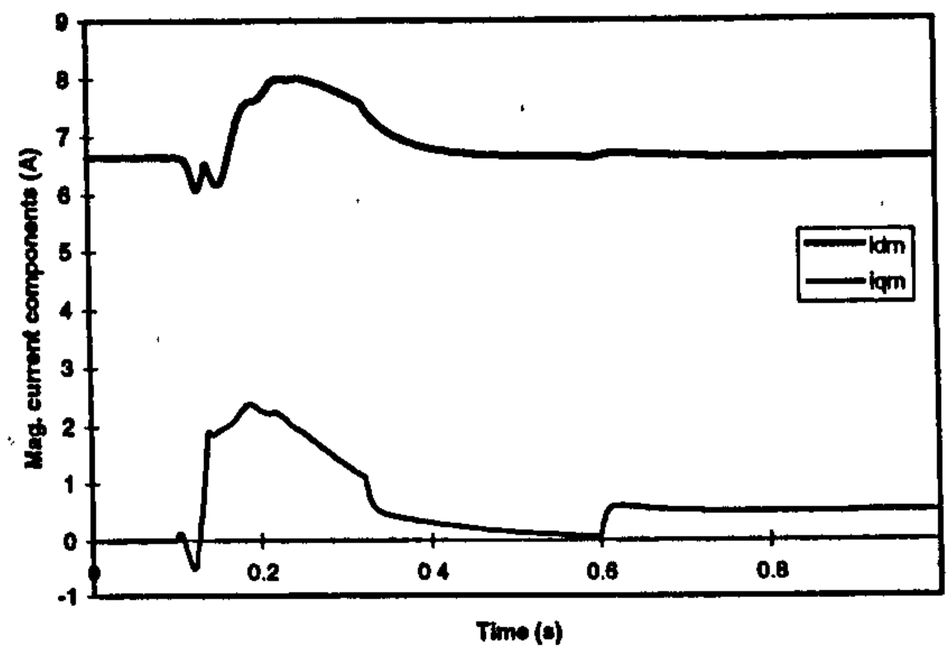

e)

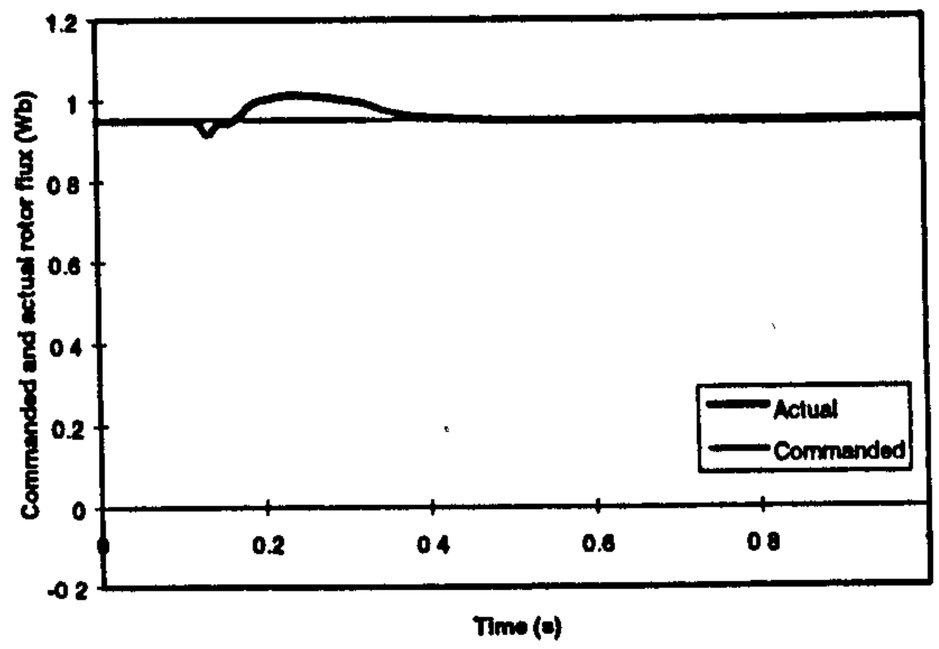

f)

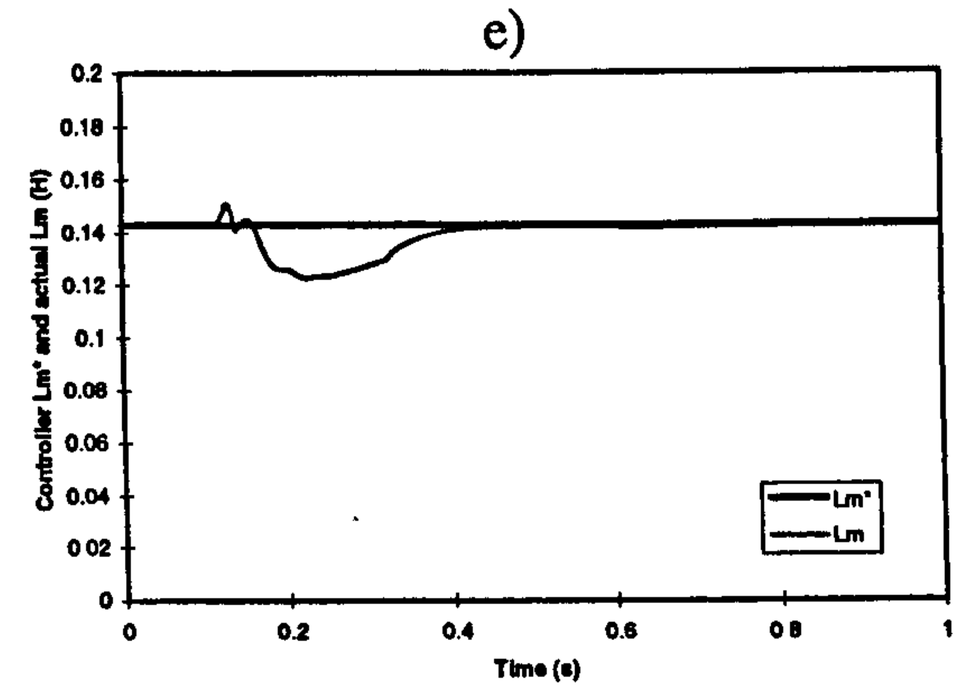

g)

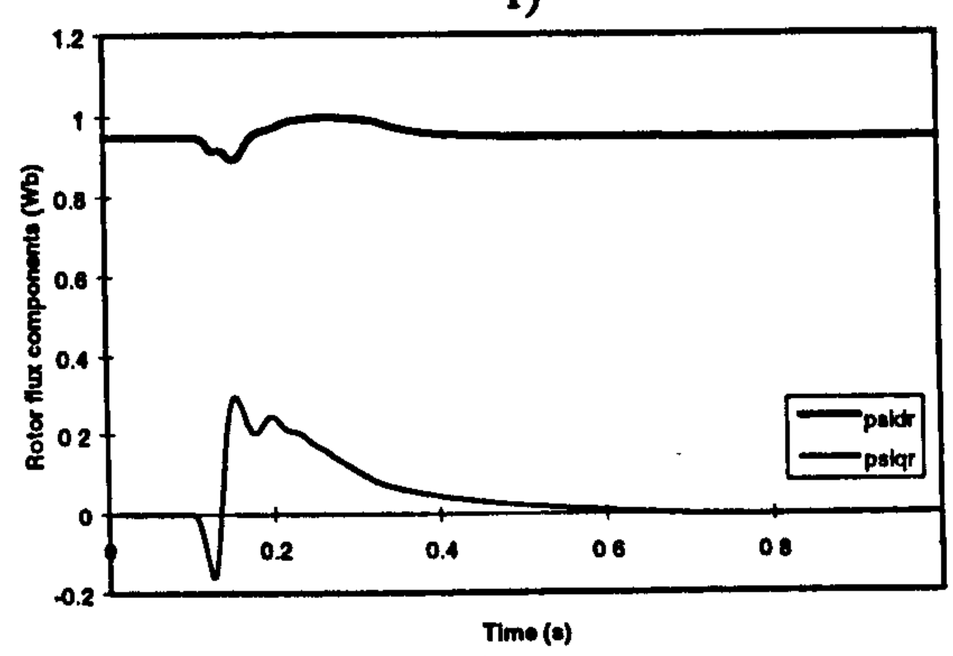

h)

Figure 7.15: Dynamic response of sensorless indirect rotor flux oriented induction machine under tuned condition: a) actual and estimated speed b) speed estimation error c) speed estimation error in time interval 0.5 - 1 second d) actual and commanded torque e) magnetising current components f) commanded and actual rotor flux g) actual magnetising inductance and controller/estimator magnetising inductance h) rotor flux components

Figure 7.16 displays a sample of simulation results. Speed estimation error, and commanded and actual torque are shown for $L_m^* = 0.8, 0.9, 1.1$ and $1.2L_{mn}$, respectively

Speed estimation error during acceleration remains the same as in Figure 7.15. Therefore, the results, given in Figure 7.16, contain speed estimation error for time interval $t \in (0.5s, 1s)$. One can observe that speed estimation error in steady-state operation with rated speed and rated load torque is around +3 rpm, +1.8 rpm, -1.7 rpm and -4 rpm for $L_m^* = 0.8$ to $1.2L_{mn}$ respectively ([Wang and Levi, 1998]), which closely agrees with results of steady-state analysis (section 6.4). Torque response to load torque application is again instantaneous, indicating absence of orientation angle error. However, it also can be seen from Figure 7.16 that there are some discrepancies in steady-state operation between commanded and actual torque, caused by magnetising inductance variations. When magnetising inductance is smaller than rated, actual torque is greater than commanded torque. When magnetising inductance is greater than rated, actual torque is less than commanded torque, which is in agreement with results of steady-state analysis of section 6.4. Orientation angle errors are in all the cases negligibly small. Rotor flux components have similar response characteristics as in Figure 7.15, and are therefore not shown in Figure 7.16.

If magnetising inductance value in the controller and speed estimator is set to correct, rated value (that is $L_m^* = L_{mn}$), main flux saturation will cause detuned operation mainly in field-weakening region due to non-linear nature of the magnetising curve. Therefore, induction machine operation in field-weakening region is further examined.

If an evaluation of detuning purely due to omission of the main flux saturation representation in the speed estimator is to be obtained, it is necessary to at first modify the structure of the indirect vector controller of Figure 6.1. In particular, compensation of main flux saturation effects in the indirect vector controller is necessary. A convenient way of achieving this is the method developed in [Levi et al, 1990].

As shown in [Levi et al, 1990], an indirect feed-forward rotor flux oriented controller with partial compensation of main flux saturation is described with the following equations:

$$\psi_m = \psi_r^* + T_{\sigma r} d\psi_r^* / dt \qquad (7.2)$$

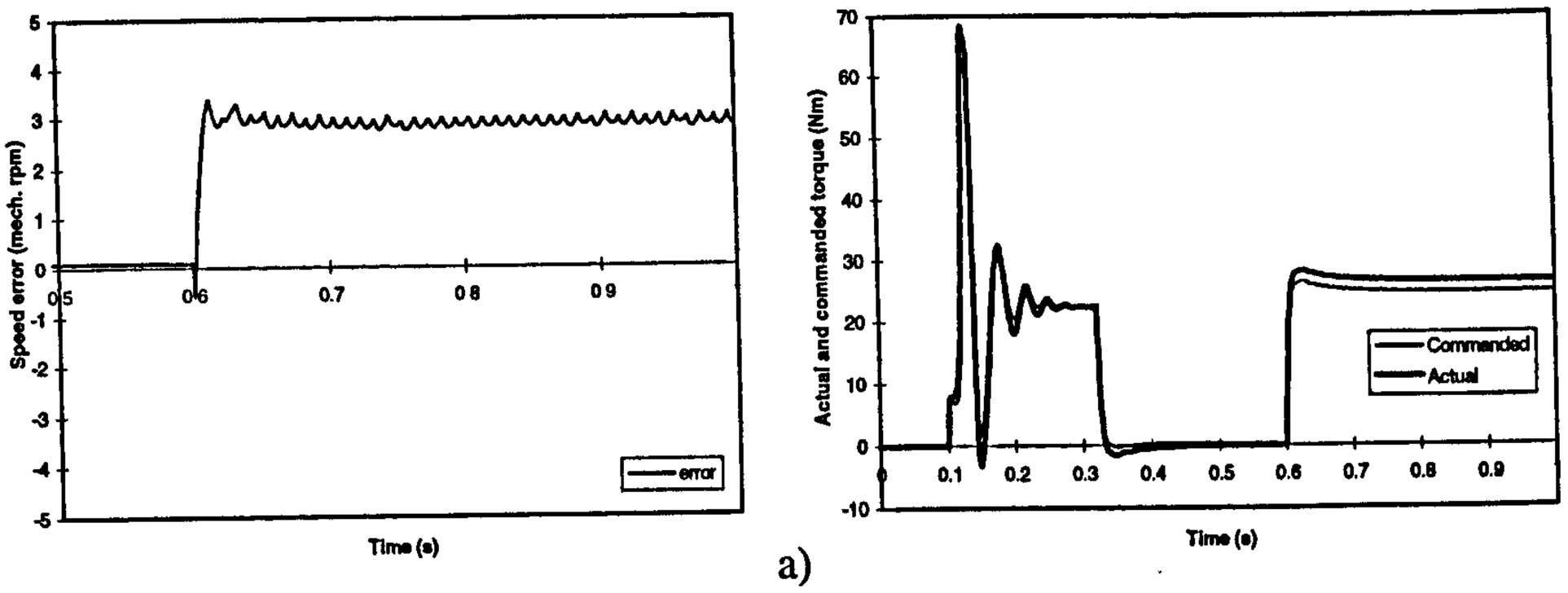

Figure 7.16: Speed error and torque response of the drive for operation with incorrect setting of the magnetising inductance: a) $L_m^* = 0.8L_{mn}$, b) $L_m^* = 0.9L_{mn}$, c) $L_m^* = 1.1L_{mn}$ and d) $L_m^* = 1.2L_{mn}$, respectively.

$$i_{ds}^{*} = i_m(\psi_m) + (1/L_{\sigma r})T_{\sigma r}\, d\psi_r^{*}/dt \tag{7.3}$$

$$\omega_{sl}^{*} = K_1 i_{qs}^{*}/\psi_r^{*} \tag{7.4}$$

$$i_{qs}^{*} = (1/K_2)T_e^{*}/\psi_r^{*} \tag{7.5}$$

where $K_1 = L_{mn}^{*}/T_{rn}^{*}$ and $K_2 = (3/2)P\,L_{mn}^{*}/L_{rn}^{*}$ are constants. An indirect vector controller, described by (7.2)-(7.5), ignores the cross-saturation effect and neglects the change in the ratio of magnetising inductance to rotor inductance in (7.4)-(7.5) [Levi et al, 1990].

If the rotor speed is assumed to vary much more slowly than the electromagnetic transients, then the rate of change of the rotor flux reference in (7.2)-(7.3) is slow. It is therefore possible to further simplify (7.2)-(7.3), by neglecting the rate of change of rotor flux reference. Hence:

$$\psi_m = \psi_r^{*} \qquad i_{ds}^{*} = i_m(\psi_m) \tag{7.6}$$

The indirect vector controller based on (7.4)-(7.6) is illustrated in Figure 7.17. It is now used in simulation instead of the one of Figure 6.1, that was sufficient for operation in

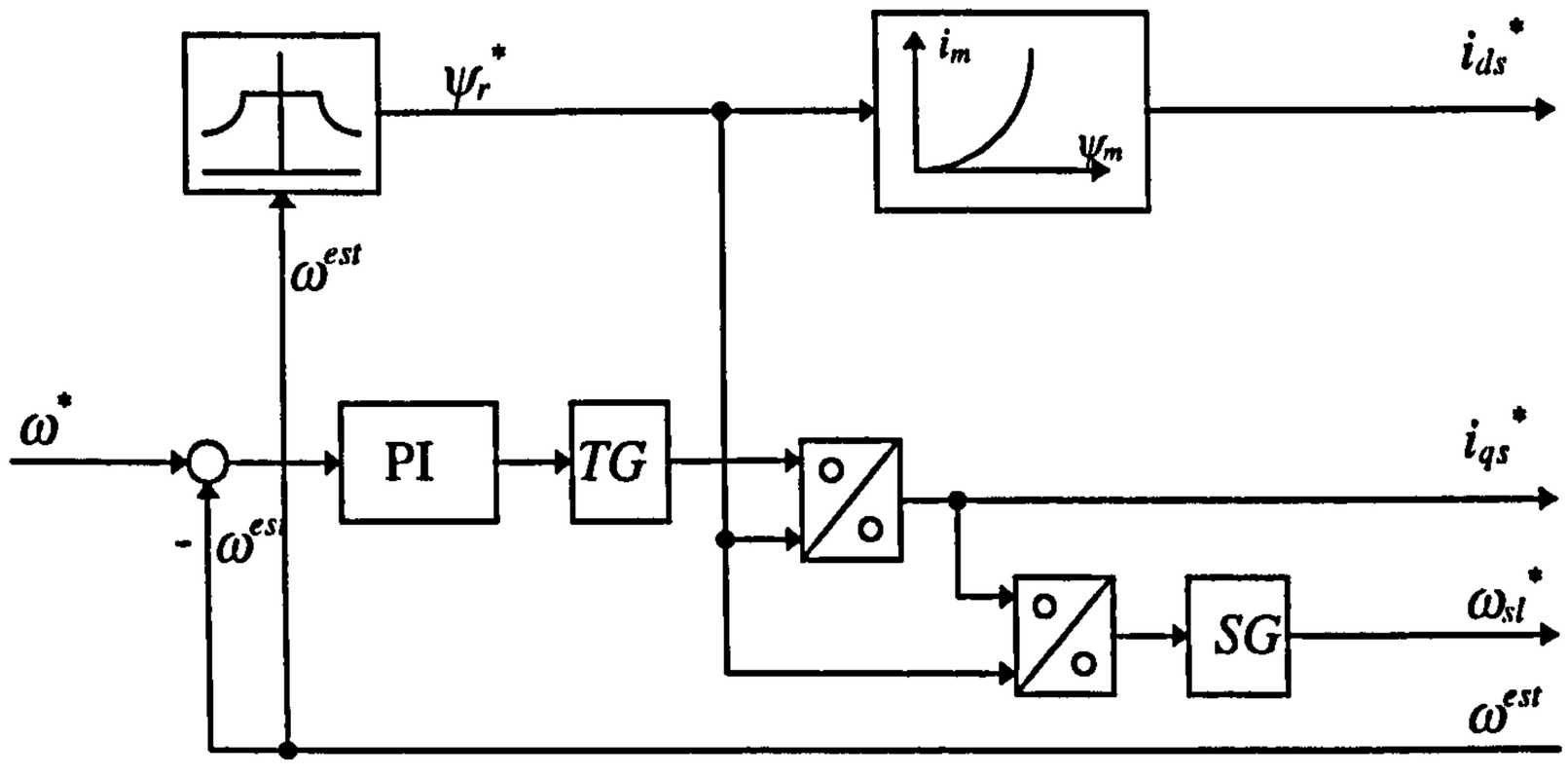

Figure 7.17: Indirect rotor flux oriented controller with compensation of main flux saturation.

the base speed region. Symbols TG and SG in Figure 7.17 stand for $SG = L_{mn}^{*}/T_{rn}^{*} = K_1$ and $TG = 2/(3P)\,L_{rn}^{*}/L_{mn}^{*} = 1/K_2$.

The same type of simulation is done again with rated values of all the parameters (including magnetising inductance in the speed estimator) in the machine and

controller/estimator. The machine is initially excited at zero speed under no load conditions. Speed command is then applied so that rated speed operation under no load condition is achieved. During operation at rated speed a load of 1 p.u. is applied in a step-wise manner at $t = 0.5$ s. At $t = 1$ s load torque is stepped down to one half of the rated and this value is not changed any more. Final operating steady-state is therefore with 0.5 p.u. load torque. Transients for four different final speeds are simulated, namely speed commands of 1.25 p.u., 1.5 p.u., 1.75 p.u. and 2 p.u. Results are displayed in Figures 7.18 to 7.21. Actual and estimated speed, speed error, actual and commanded torque, and rotor flux components are shown in all the four Figures.

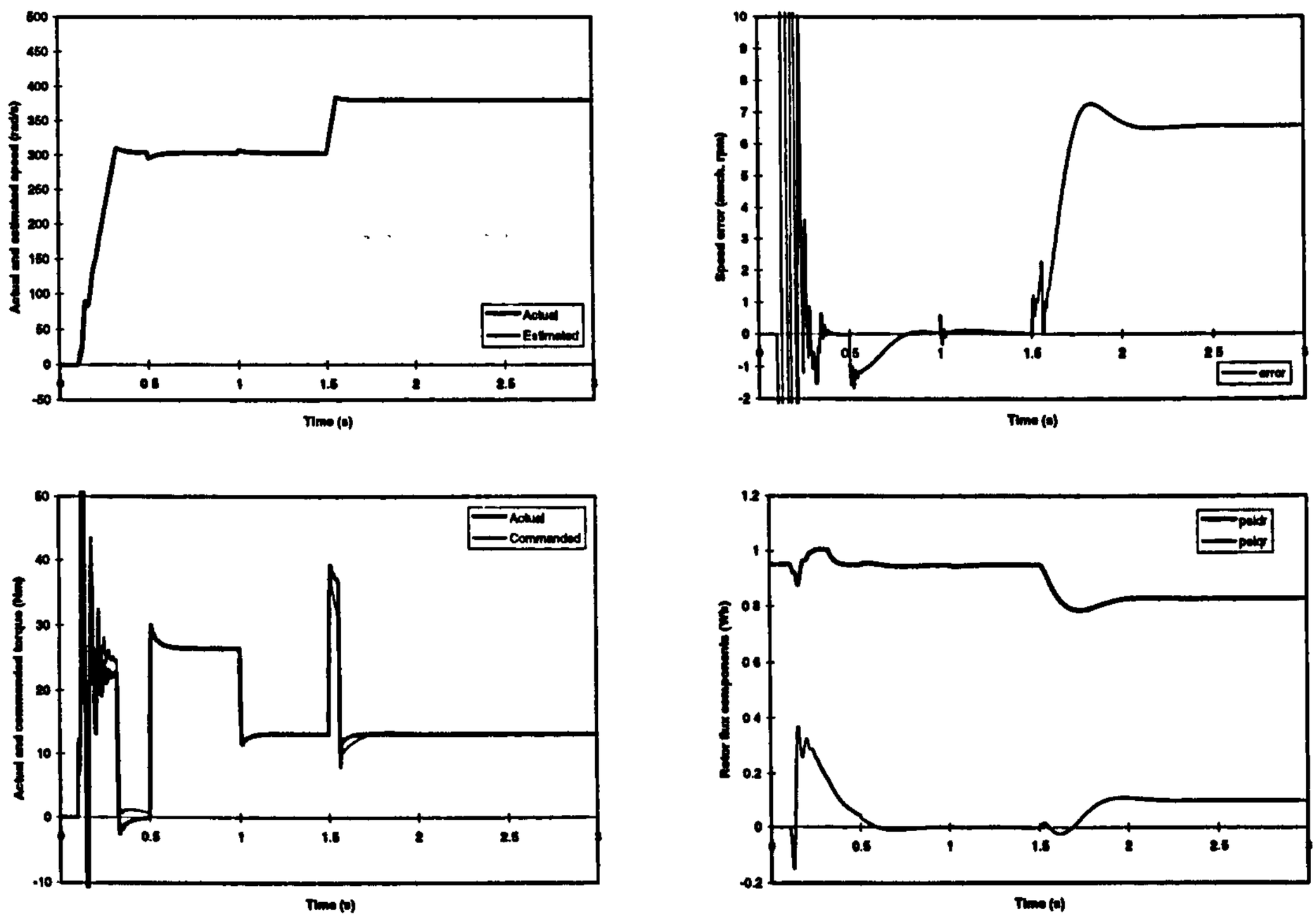

Figure 7.18: Dynamic response of the machine (final operating speed is $1.25\omega_{n.}$)

Transient behaviour of the machine while it runs in base speed region remains the same as discussed for tuned conditions, section 7.3. Undoubtedly, constant parameter speed estimator enables satisfactory quality of rotor flux oriented control in the base speed region if all the parameters are tuned. The problems however begin once when the field-weakening operation is initiated at $t = 1.5$ s. Speed estimation error quickly increases. For machine running in field-weakening region, one can see that detuning effects are speed dependent. Speed estimation error in final steady-state operation is 6.75 rpm, 11.6 rpm, 16.56 rpm and 21.5 rpm for machine running at 1.25, 1.5, 1.75 and

2 p.u. speed, respectively. Rotor flux orientation is lost due to main flux saturation effect in field-weakening region, as final steady-state is characterised with substantial

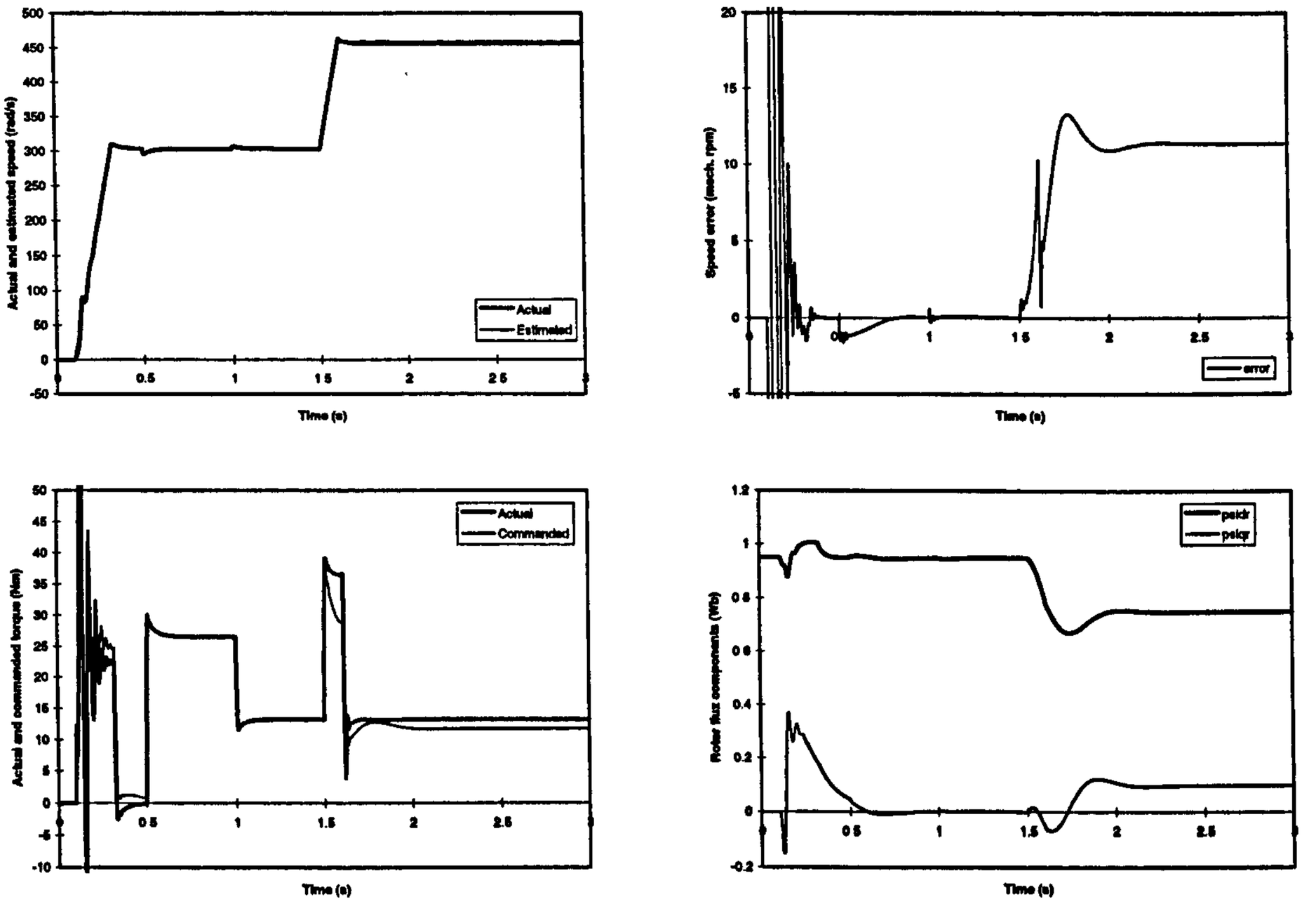

Figure 7.19: Dynamic response of the machine (final operating speed is $1.5\omega_n$.)

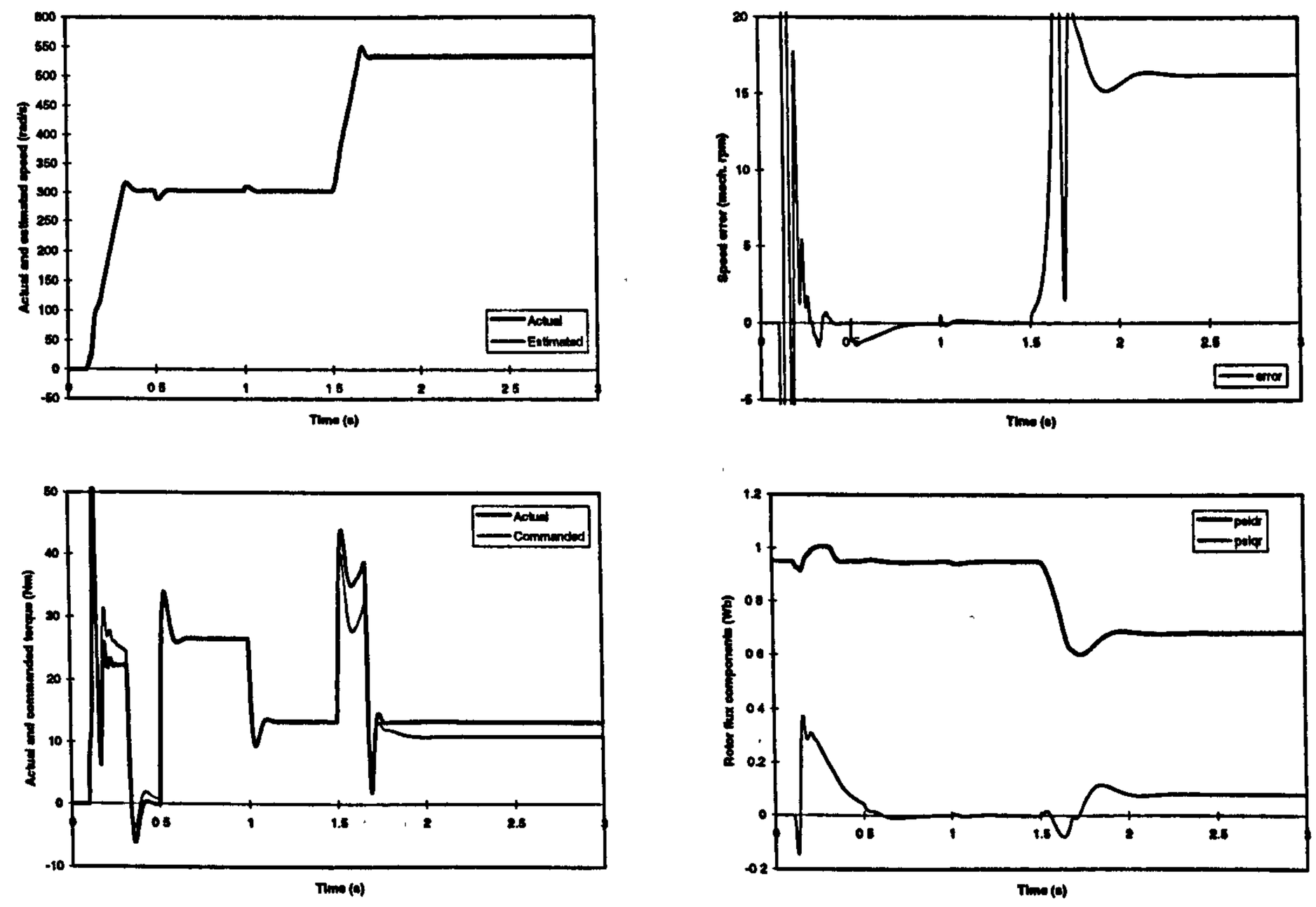

Figure 7.20: Dynamic response of the machine (final operating speed is $1.75\omega_n$.)

value of rotor flux q-axis component in all the cases. Torque error in steady-state operation increases with increase in final speed. The highest torque error appears at final speed reference speed of 2 p.u. These results show that main flux saturation in induction machine may cause serious problems when machine runs in field-weakening region. Results shown here clearly demonstrate the need for incorporation of the main flux saturation in the speed estimator, if satisfactory performance is to be achieved in the field-weakening region. This issue will be addressed in section 8.3.

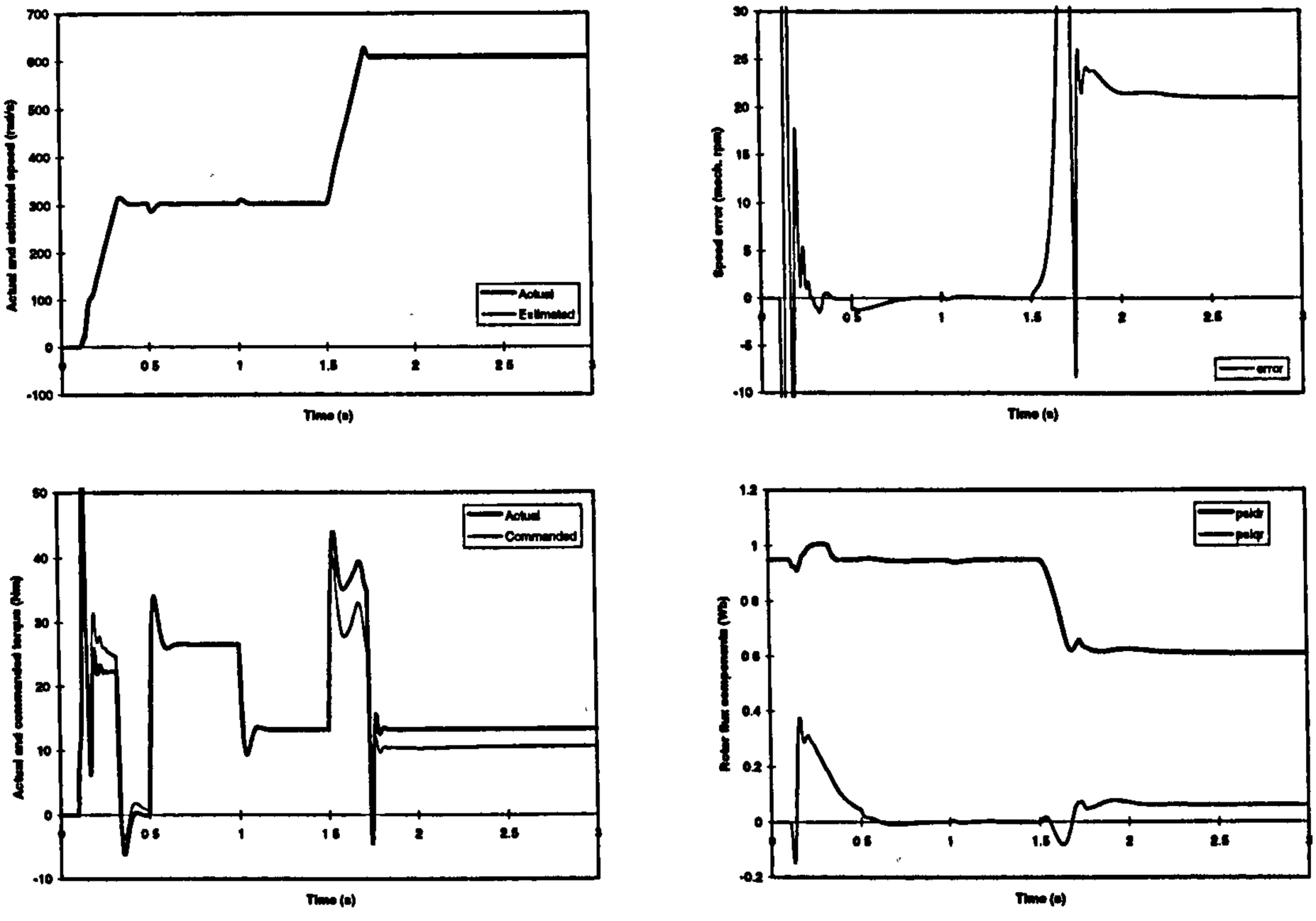

Figure 7.21: Dynamic response of the machine (final operating speed is $2\omega_n$.)

7.5 Detuning due to rotor resistance variation

Thermal variation of rotor resistance causes detuned operation. As discussed in section 6.6, detuning effects due to rotor resistance variation are independent of speed, but load dependent. Maximum detuning occurs when machine runs with rated torque command. In order to evaluate detuning effects due to rotor resistance variation, the same simulation procedure is repeated again. Rotor resistance is fixed to values between 0.8 and $1.2R_m$ in the machine while the one in the controller/estimator is rated. All the other parameters in the machine and in the estimator/controller remain the same and

equal to rated values (magnetising inductance in the controller/estimator is equal to rated). Sequence of transients is the same as in section 7.3.

Figure 7.22 displays a sample of simulation results. Speed estimation error, and actual and commanded torque are given for $R_r = 0.8$, 0.9, 1.1 and 1.2 R_{rn}, respectively.

Transient behaviour during acceleration remains essentially the same as in Figure 7.15. Therefore, Figure 7.22 shows speed estimation errors for the four cases for time interval $t \in$ (0.5s; 1s). Torque response is included as well. It is interesting to note that the orientation angle error is negligibly small when rotor resistance varies, so that transient-free torque response is maintained irrespective of the speed estimation error. This is in close agreement with results of steady-state analysis given in section 6.6. Furthermore, speed estimation errors in steady-state operation at rated speed with rated load torque are +10 rpm, +5 rpm, -5 rpm and -10 rpm, [Wang and Levi, 1998], which equals the values predicted by steady-state analysis in section 6.6. Torque error in steady-state is negligibly small, this again being in full agreement with results of the steady-state analysis presented in section 6.6.

7.6 Detuning due to stator resistance variation

Detuning due to stator resistance variation is speed (frequency) dependent and is most pronounced at low speeds as discussed in section 6.5. On the other hand, impact of loading is smaller than in the previous two cases. The simulation model is the same as the previous one. The simulation is done for reference speed of 0.05 p.u.. Load of 0.2 p.u. is applied at t = 0.6 s, while rated load torque is applied at t = 0.8 s. Stator resistance in the machine is taken as $R_s = 0.8R_{sn}$ and $R_s = 1.2R_{sn}$, respectively, while the one in the estimator equals rated value. All the other parameters are the same in both machine model and controller/estimator (i.e. all have rated values). Results obtained for the value of 1.2 p.u. of the stator resistance in the machine are shown in Figure 7.23a. Actual and estimated speed, speed error, and actual and commanded torque are given. However, for stator resistance of 0.8 p.u., it was not possible to get the results for the same speed command. It is worth noting that a similar problem at low speeds was observed in experimental study of detuning reported by [Armstrong and Atkinson, 1997]. Therefore, speed command for this stator resistance is increased to 0.1 p.u. and

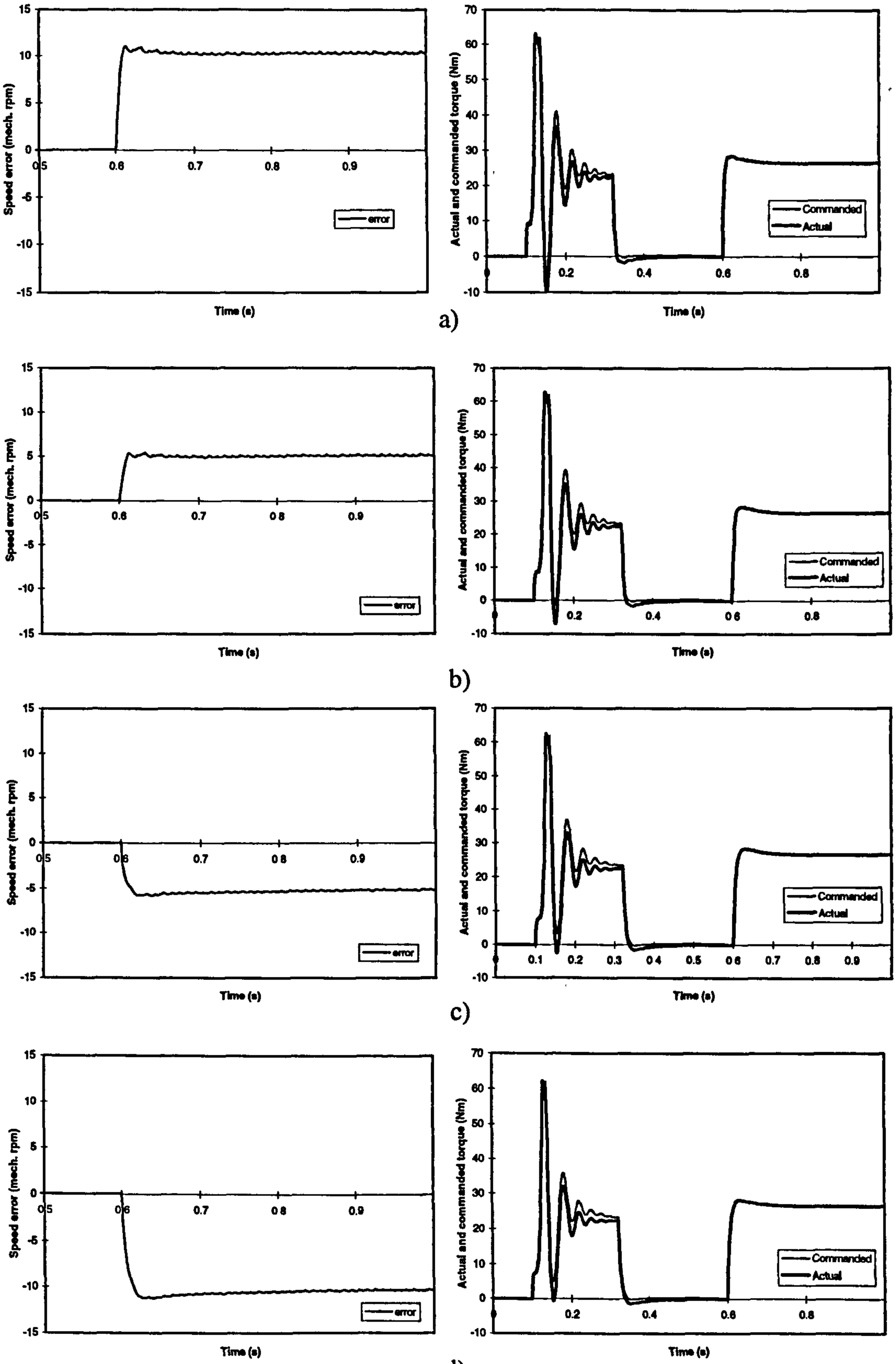

Figure 7.22: Dynamic response of the drive with detuned rotor resistance $R_r^*=R_{rn}$: a) $R_r=0.8R_{rn}$, b) $R_r=0.9R_{rn}$, c) $R_r=1.1R_{rn}$, d) $R_r=1.2R_{rn}$.

results are shown in Figure 7.23b.

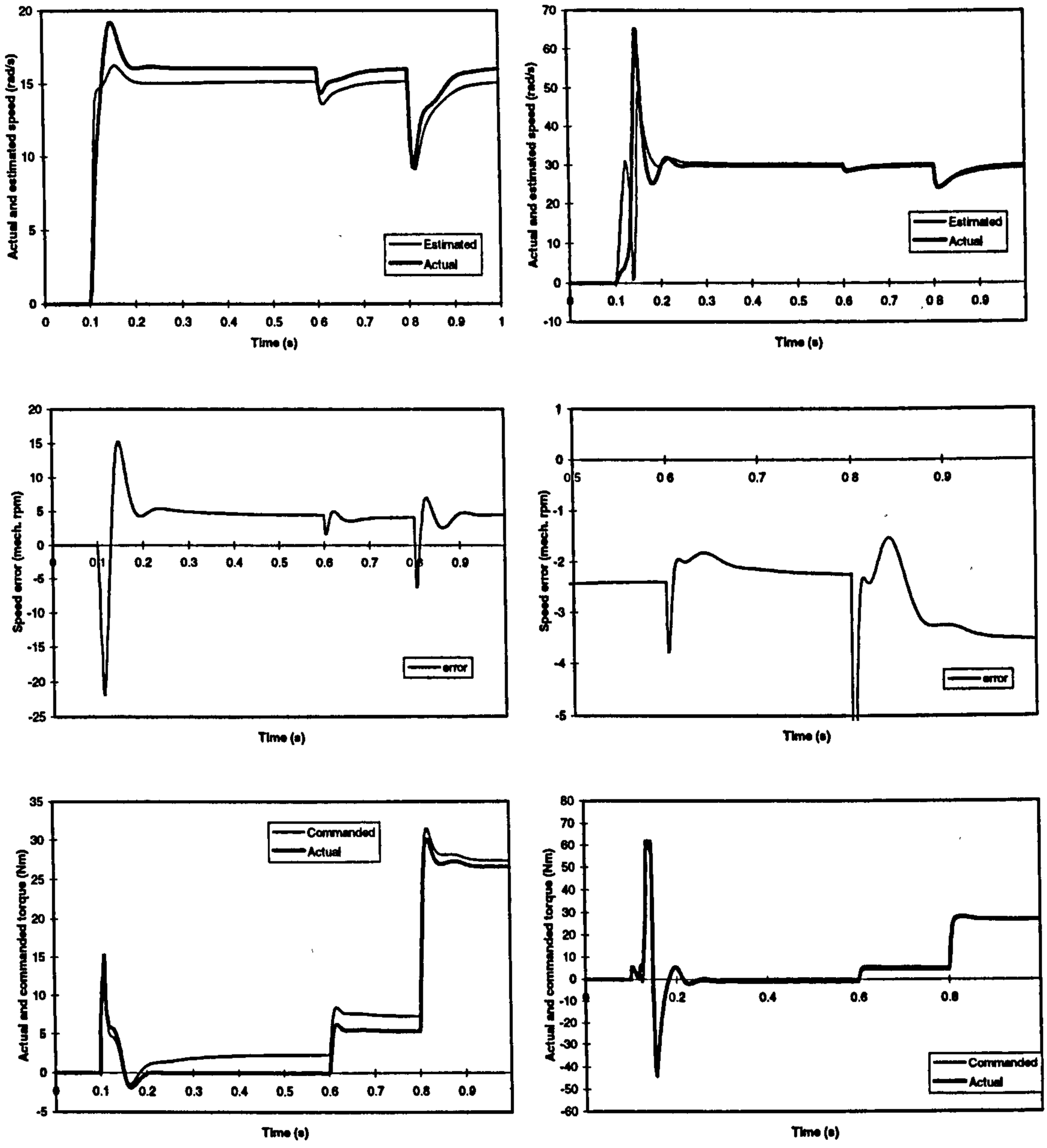

a) b)

Figure 7.23: Dynamic response for operation with incorrect setting of the stator resistance, $R_s^*=R_{sn}$: a) $R_s = 1.2R_{sn}$, $\omega^*=0.05$ p.u. b) $R_s = 0.8R_{sn}$, $\omega^*=0.1$ p.u..

It can be seen that speed estimation error is speed dependent, with weak load dependence, and is the highest at low speed.

Speed estimation error is around 4 rpm for speed command of 0.05 p.u. with $R_s = 1.2R_{sn}$ in Figure 7.23a. It is close to -4 rpm for speed command of 0.1 p.u. with $R_s = 0.8R_{sn}$, [Wang and Levi, 1998]. Stator resistance variation also causes significant discrepancy between actual and commanded torque at low speeds. Moreover, orientation angle error

is of rather significant value at low speeds as well. These results are in good agreement with results of the steady-state analysis, section 6.4. As complete failure of the speed estimator may result, accurate adjustment of stator resistance appears to be of crucial importance.

7.7 Detuning due to iron loss

As discussed in section 6.2, detuning effects due to iron loss are speed dependent and load dependent. In order to evaluate detuning effects due to iron loss in transient operation, main flux saturation is neglected in the machine model. Although omission of main flux saturation representation in the field-weakening region is unrealistic, this approach enables examination of detuning purely due to iron loss. Structure of the sensorless vector controlled induction machine drive remains the same as shown in Figure 6.1, with estimated speed used for speed control and orientation purposes. All the parameters have the rated values both in the machine model and in the controller/estimator. However, induction machine model with iron loss accounted for (given in section 5.2) is utilised here. Due to assumed current feeding, the machine model does not include stator voltage equations and is given with system of equations (5.11). The stator equations are however utilised for calculation of stator voltage components, required by the estimator. From section 5.2, equations (5.7), one has

$$v_{\alpha s} = R_s i_{\alpha s}^{*} + L_{\sigma s}\frac{di_{\alpha s}^{*}}{dt} + L_m\frac{di_{\alpha m}}{dt}$$
$$v_{\beta s} = R_s i_{\beta s}^{*} + L_{\sigma s}\frac{di_{\beta s}^{*}}{dt} + L_m\frac{di_{\beta m}}{dt} \qquad (7.7)$$

In order to investigate the influence of iron loss at different speeds and with different load torques, four cases are simulated. The first simulation is done with reference speed of 0.5 p.u. with rated load application at $t = 1$ s. Load torque is then reduced to 0.5 p.u. at $t = 1.5$ s. The second simulation is done for rated speed command. Rated load torque is applied at $t = 1$ s and is subsequently reduced to 0.5 p.u. at $t = 1.5$ s. Next, simulations for speed commands equal to 1.5 p.u. and 2 p.u. are done.

Figure 7.24 presents simulation results for speed command of 0.5 p.u.. It can be seen that speed estimation error is load dependent. In steady-state operation, speed

estimation error is 2 rpm for zero load torque. For rated load torque and 0.5 p.u. load torque, speed estimation error is 2.6 rpm and 2.25 rpm, respectively. Torque response to load torque application is instantaneous. In steady-state operation, torque error is evident. It increases when load torque decreases, the actual torque being smaller than commanded torque. Orientation angle error is negligibly small, except during acceleration, as indicated by rotor flux q-axis component trace shown in Figure 7.24.

Simulation results shown in Figure 7.25 apply to the rated speed reference. Speed estimation error in steady-state operation is 2.2 rpm for zero load torque. It is 2.8 rpm and 2.4 rpm for rated load torque and 0.5 p.u. load torque, respectively. Torque error

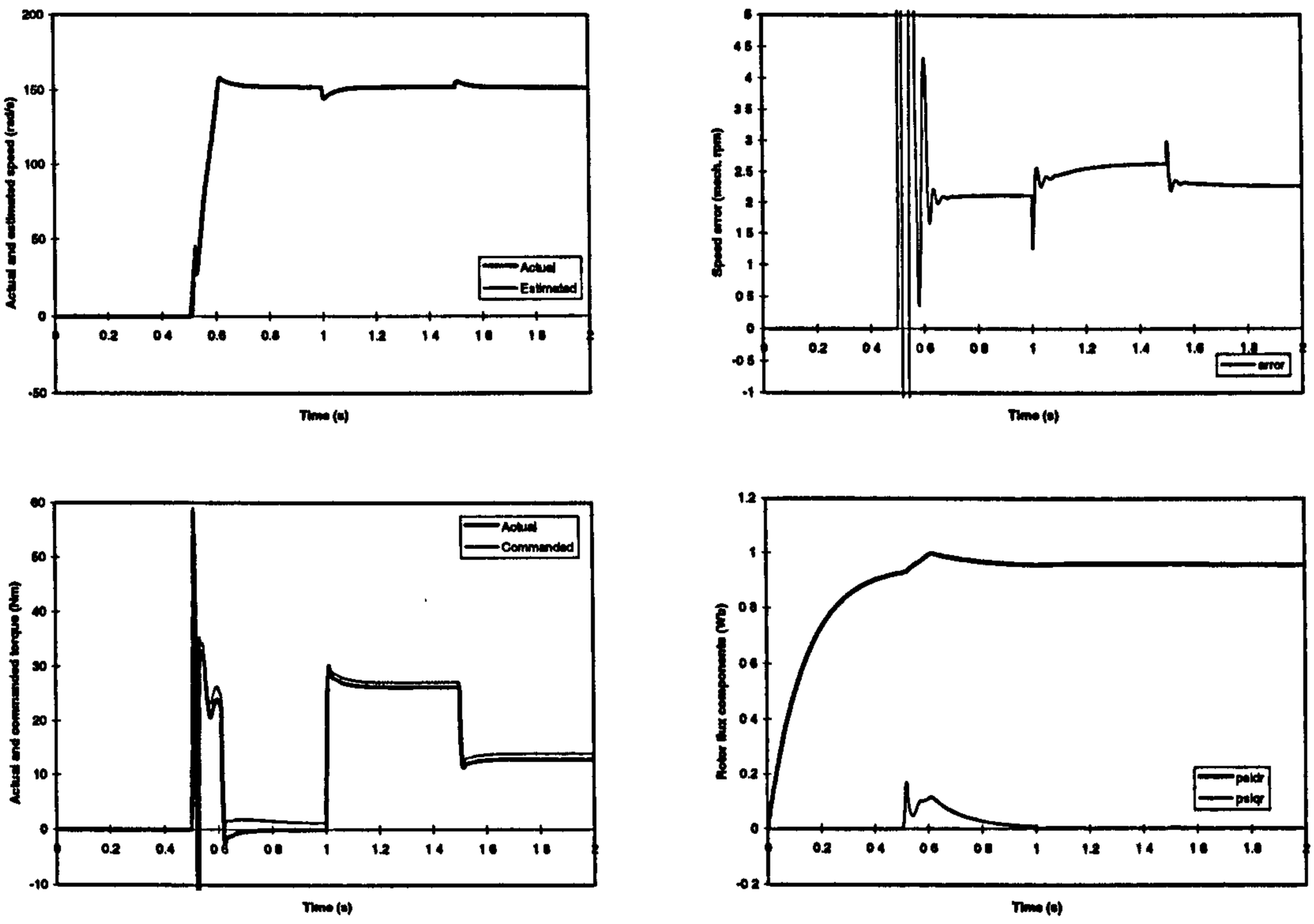

Figure 7.24: Detuning in transient operation due to iron loss (speed command of 0.5 p.u.).

has the same features as discussed above. Field orientation angle error is again negligibly small as rotor flux q-axis component is essentially zero, except during acceleration.

Simulations are done next when the machine runs in field-weakening region. For speed command of 1.5 p.u., rated load torque is applied at $t = 1$ s and is then reduced to 0.5 p.u. at $t = 1.5$ s. For speed command of twice the rated speed, rated torque is applied at $t = 1.5$ s and is then reduced to 0.5 p.u. at $t = 2.5$ s. Figure 7.26 displays simulation

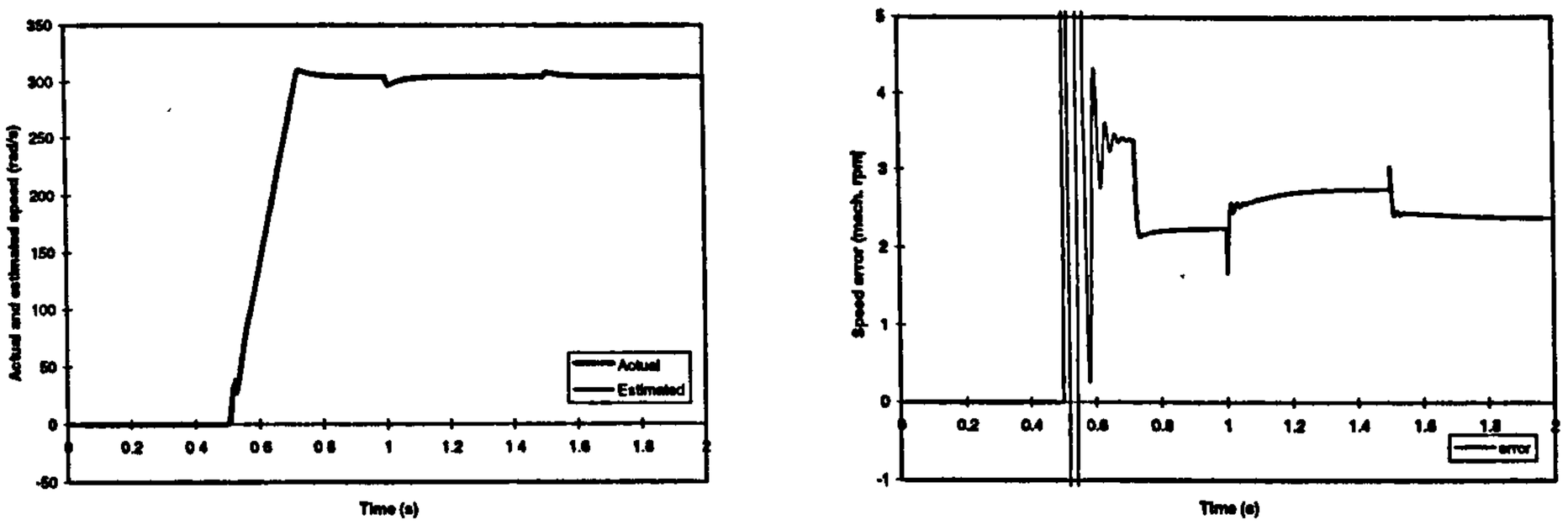

Figure 7.25: Detuning in transient operation due to iron loss (speed command equal to rated).

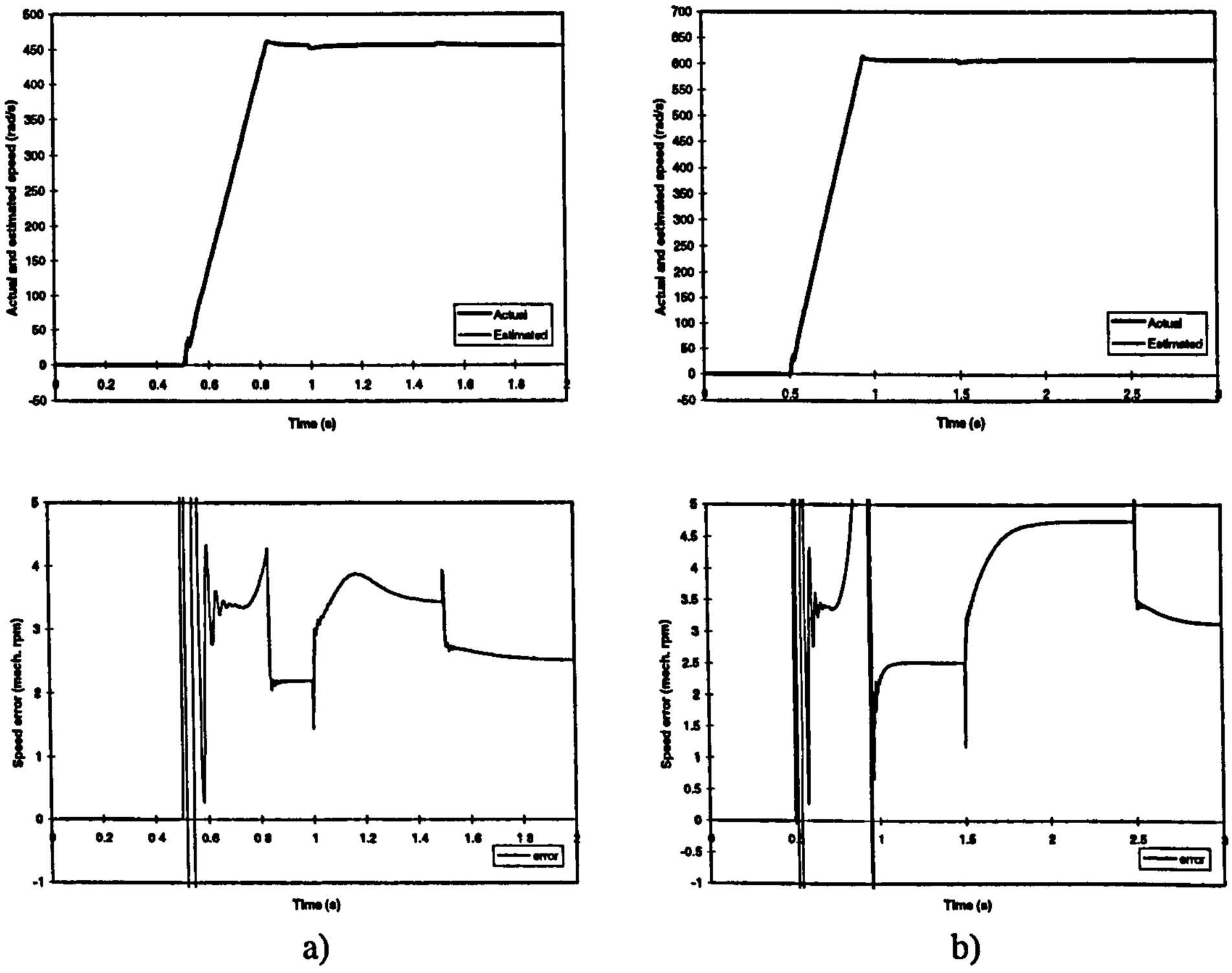

a) b)

Figure 7.26: Speed response and speed estimation error due to iron loss for speed command of: a) 1.5 p.u. and b) 2 p.u..

results for 1.5 and 2 p.u. reference speed. Torque and rotor flux component behaviour is similar as before and is therefore not shown in this Figure. In steady-state operation at 1.5 p.u. speed estimation error is 3.5 rpm with rated load torque and 2.5 rpm with 0.5 p.u. load torque, Figure 7.26a. Speed estimation error at 2 p.u. speed is 4.7 rpm with rated load torque and 3.1 rpm with 0.5 p.u. load torque, 7.26b.

Comparing the speed estimation errors shown in Figures 7.24-26, one can conclude that speed estimation error is speed dependent and load dependent. It increases with speed increase. The results presented in this section are in good agreement with results of steady-state analysis given in section 6.2.

7.8 Detuning due to iron loss and incorrect setting of the magnetising inductance

Investigation of detuning effect due to iron loss and incorrect setting of the magnetising is performed in this sub-section. The simulation is done again assuming incorrect setting of the magnetising inductance. Magnetising inductance in the controller/ estimator is set to $0.8L_{mn}$, L_{mn} and $1.2L_{mn}$. All the other parameters in the machine and controller/estimator remain the same and equal to rated values. Induction machine model with both iron loss and main flux saturation accounted for, given in section 5.4 with equations (5.53)-(5.56), is utilised here. Stator voltage components, required by the estimator, are reconstructed using (5.52)

$$v_{\alpha s} = R_s i_{\alpha s}^{*} + L_{\sigma s}\frac{di_{\alpha s}^{*}}{dt} + R_{Fe}\left(i_{\alpha s}^{*} + i_{\alpha r} - \frac{\psi_{\alpha m}}{L_m}\right)$$
$$v_{\beta s} = R_s i_{\beta s}^{*} + L_{\sigma s}\frac{di_{\beta s}^{*}}{dt} + R_{Fe}\left(i_{\beta s}^{*} + i_{\beta r} - \frac{\psi_{\beta m}}{L_m}\right) \qquad (7.8)$$

The Simulink model is included in Appendix C.

At first the simulation is done for magnetising inductance set to $L_m^{*}=L_{mn}$. Sequence of transients is as follows. Excitation of the machine is initiated at t = 0 s at zero speed under no-load conditions with rated rotor flux reference. At t = 0.5 s rated speed command is applied in a ramp-wise manner. Rated load torque is applied at t = 1 s and at t = 1.5 s load torque is reduced to one half of the rated. Then, the same simulation is repeated with $L_m^{*}=0.8L_{mn}$. For case of $L_m^{*}=1.2L_{mn}$, sequence of transients is as follows. Excitation of the machine is initiated at t = 0 s at zero speed under no-load conditions

with rated rotor flux reference. At $t = 0.5$ s rated speed command is applied. Rated load torque is applied at $t = 1.5$ s and is not changed any more. Figures 7.27-7.29 illustrate the simulation results for these three cases, respectively.

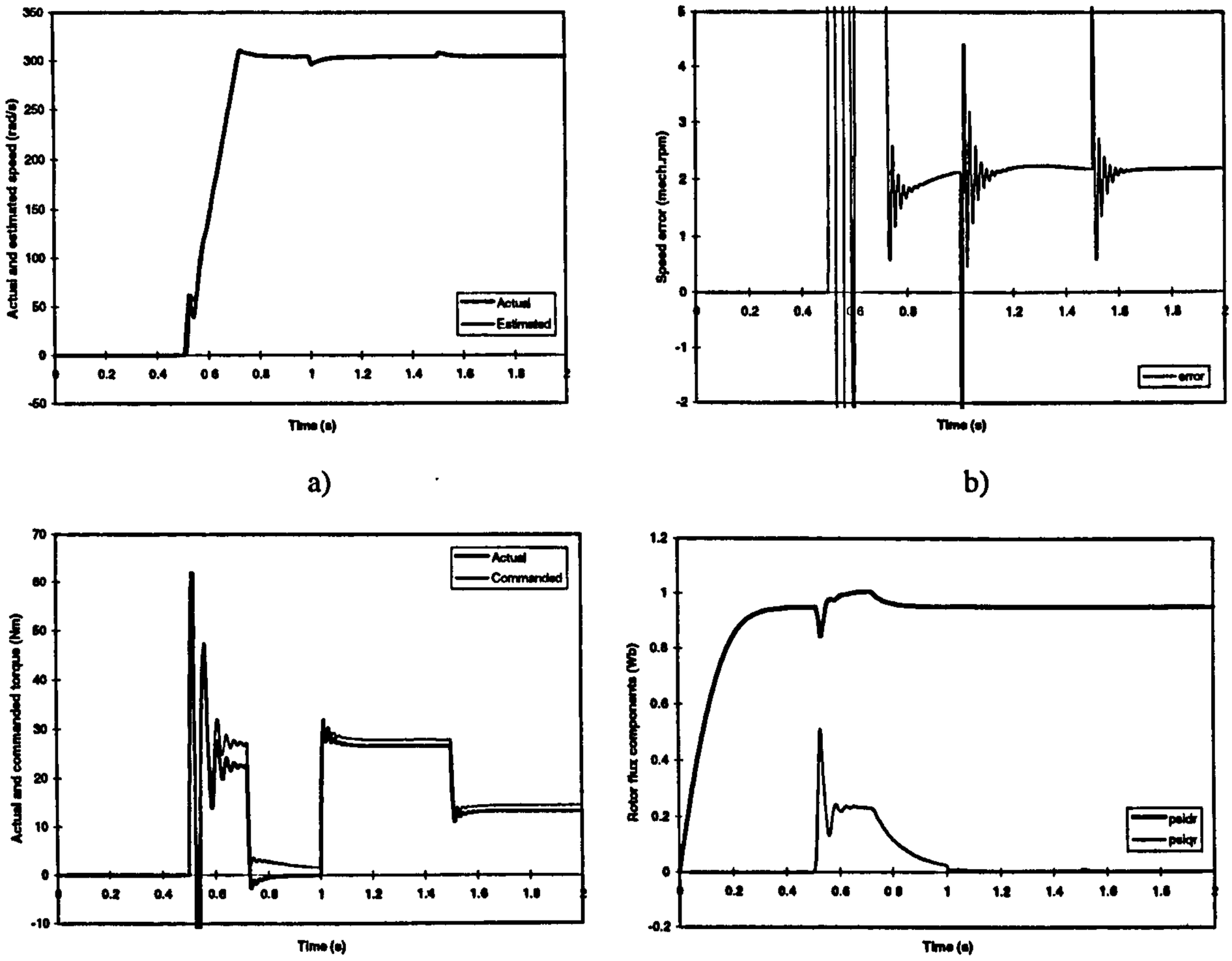

a) b)

c) d)

Figure 7.27: Detuning in transient operation due to iron loss and incorrect setting of the magnetising inductance ($L_m^* = L_{mn}$): a) actual and estimated speed, b) speed error, c) actual and commanded torque, d) rotor flux components.

For case of $L_m^* = L_{mn}$, it can be seen that estimated speed tracks actual one very well, except during acceleration, Figure 7.27a. As iron loss does exist, speed estimation error is around 2 rpm for all load torque conditions in final steady-state operation, Figure 7.27b. Actual torque is smaller than commanded torque, Figure 7.27c. Orientation angle error is very small, as rotor flux q-axis component is essentially zero. All the steady-state values shown here fully correspond to the results of steady-state analysis presented in section 6.7.

For $L_m^* = 0.8L_{mn}$, it can be seen that the simulation results shown in Figure 7.28 are similar to those shown in Figure 7.27, except for the speed estimation error. Speed estimation error in final steady-state operation is dependent on load torque. It is about 2

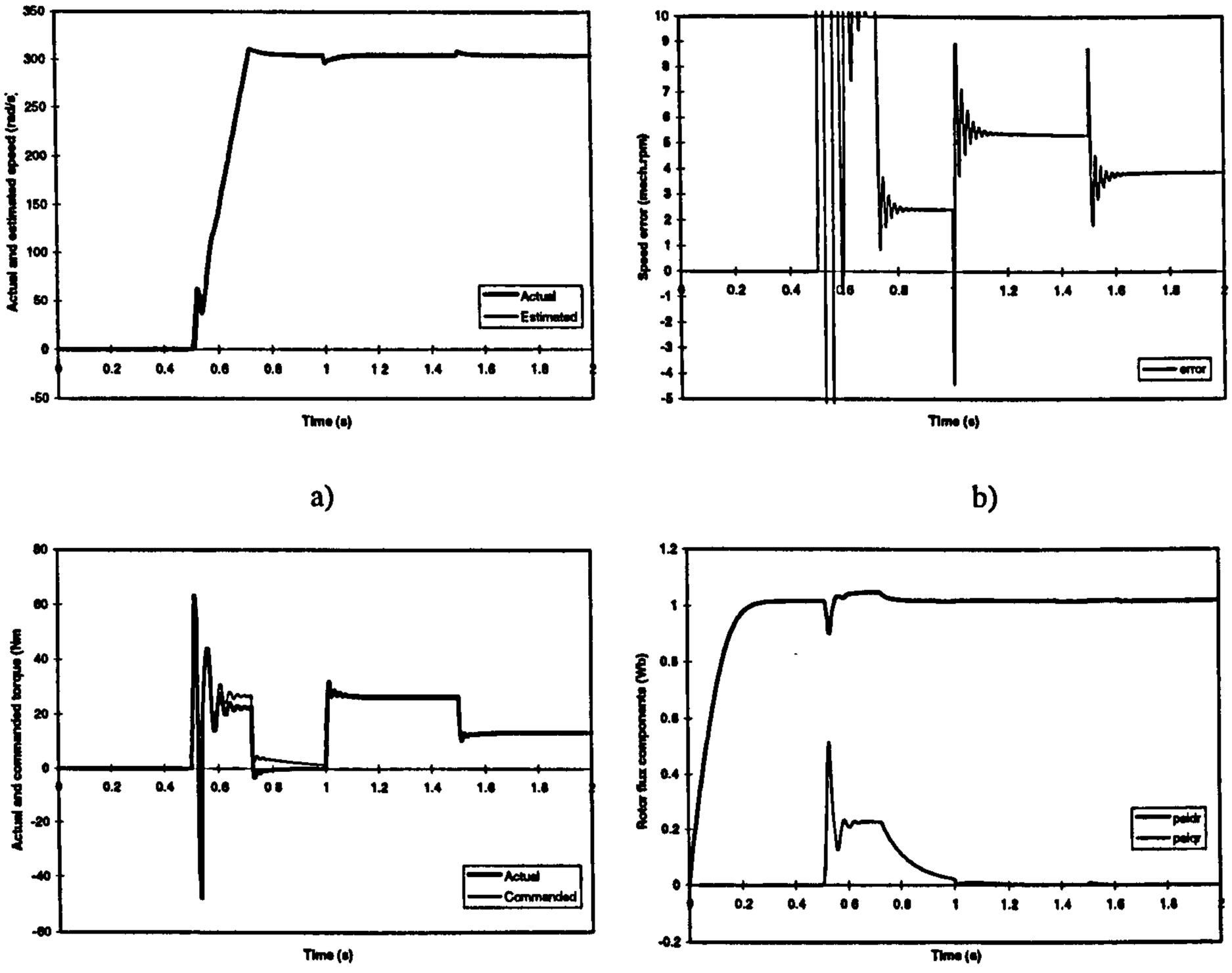

a) b)

c) d)

Figure 7.28: Detuning in transient operation due to iron loss and incorrect setting of the magnetising inductance ($L_m^*=0.8L_{mn}$): a) actual and estimated speed, b) speed error, c) actual and commanded torque, d) rotor flux components.

rpm for no-load condition. It is 5.3 rpm for rated load torque and 3.8 rpm for one half of the rated load torque, Figure 7.28b.

For $L_m^*=1.2L_{mn}$, speed estimation error in final steady-state operation is about 2 rpm for no-load condition and is 1.7 rpm for rated load torque condition, Figure 7.29b. Torque error is slightly larger than in the previous two cases, Figure 7.29c. Orientation angle error is again very small, Figure 7.29d. The simulation results are again in good agreement with results of steady-state analysis presented in section 6.7.

7.9 Summary

A detailed study of transient behaviour of a sensorless indirect rotor flux oriented current-fed induction machine, with rotor flux based MRAC speed estimator, in the presence of parameter uncertainties, iron loss, and main flux saturation is presented.

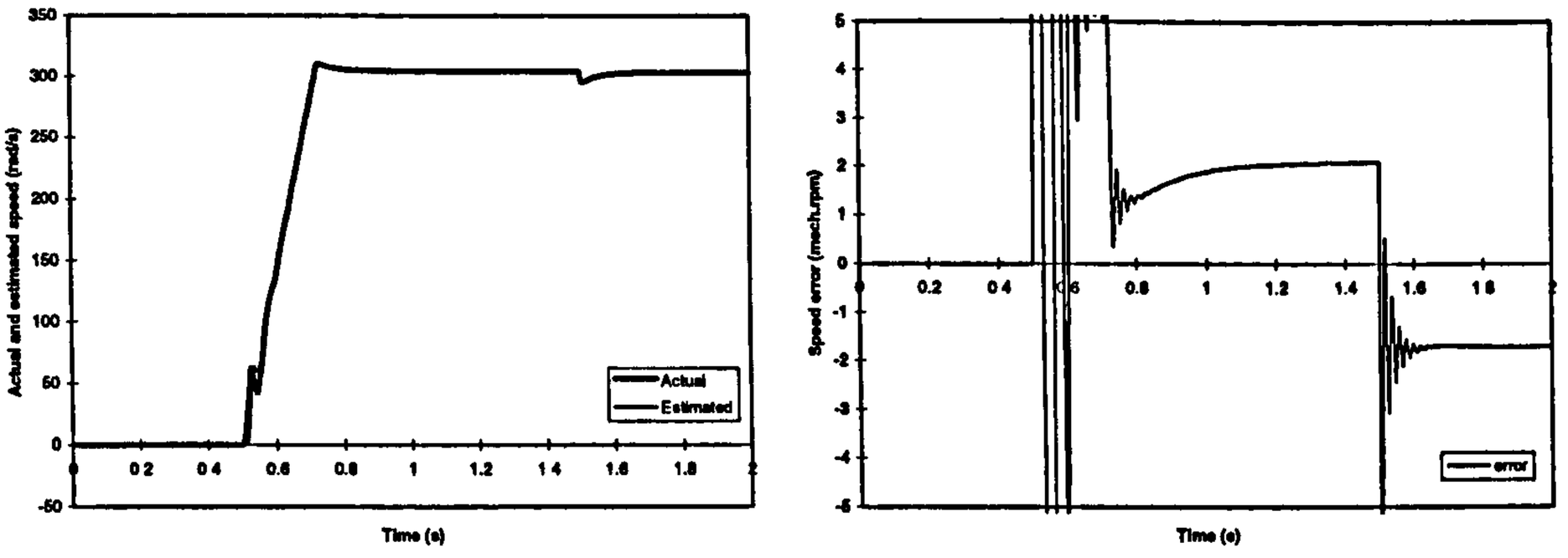

Figure 7.29: Detuning in transient operation due to iron loss and incorrect setting of the magnetising inductance ($L_m^*=1.2L_{mn}$): a) actual and estimated speed, b) speed error, c) actual and commanded torque, d) rotor flux components.

The major results of this chapter were reported in [Wang and Levi, 1998; Wang and Levi, 1999]. The results obtained in this chapter are in good agreement with results of steady-state analysis given in chapter 6. It is shown that the major consequence of parameter detuning is a speed estimation error, that is of the highest value when rotor resistance varies. Speed estimation error caused by stator resistance variation is speed dependent, with weak load dependence. It is the highest at low speed. Combined detuning effects due to iron loss and main flux saturation are studied. It is shown that speed estimation error is dominated by iron loss in base speed region and is of the same order as the one caused by other parameter variations. In field-weakening region, speed estimation error is up to 20 rpm and is dominated by main flux saturation. In order to obtain high performance of a sensorless induction machine drive, one can conclude that iron loss and main flux saturation should be compensated.

8 COMPENSATION OF PARAMETER VARIATION EFFECTS BY MODIFIED INDUCTION MACHINE MODELS

8.1 Introduction

Compensation of parameter variation effects in sensorless vector controlled induction motor drives with model based speed estimation has been a subject of considerable interest in recent past. In majority of cases attempts are made to provide on-line identification of either stator resistance [Umanand and Bhat,1995; Blasco-Gimenez et al, 1995; Yang and Chin, 1993], or rotor resistance [Kubota and Matsuse, 1994; Pana, 1997; Jiang and Holtz, 1997]. Simultaneous identification of both the stator and the rotor resistance is proposed in [Zhen and Xu, 1995; Lee et al, 1996], while the possibility of simultaneous on-line estimation of rotor resistance and magnetising inductance is discussed in [Attaianese et al, 1997]. However, very little effort has been put so far into compensation of iron loss and main flux saturation by means of the model based approach in sensorless vector controlled induction machine drives, the exception being [Blasco-Gimenez et al, 1996b]. Detuning due to iron loss and main flux saturation was discussed in detail in the previous two chapters. These two effects can be compensated by means of modified vector controller and speed estimator, whose structure is derived from modified induction machine models. Compensation schemes for iron loss only, main flux saturation only and both iron loss and main flux saturation are developed in this chapter. Modified indirect vector controllers, already available in literature, are used in conjunction with modified speed estimators that are developed. Modified estimators are used in conjunction with suitable modified indirect vector controllers and their effectiveness in compensating the given phenomenon is confirmed by simulation.

Section 8.2 discusses compensation of iron loss, while compensation of main flux saturation is elaborated in section 8.3. Simultaneous compensation of both the iron loss and main flux saturation is the subject of section 8.4, while section 8.5 summaries the chapter. Major results of this chapter are available in [Levi et al, 1999; Wang et al, 1999; Levi and Wang, 1999].

8.2 Compensation of iron loss in sensorless indirect rotor flux oriented induction machine

Iron loss inevitably leads to a speed estimation error, since it always exists in an induction machine. Although the speed estimation errors are not excessive, they are not negligible either, as discussed in section 6.2 and section 7.7. A modified indirect vector controller, that enables full compensation of iron loss induced detuning in a drive with speed sensor is proposed in [Levi, 1995]. It requires knowledge of the functional dependence of the equivalent iron loss resistance on the supply frequency, which can be determined for a particular induction machine on the basis of the experimental method described in [Levi et al, 1996]. This modified indirect vector controller is to be used here, in conjunction with newly developed modified speed estimator, to compensate the detuning due to iron loss.

8.2.1 Description of the system

The modified indirect feed-forward rotor flux oriented controller with iron loss compensation is shown in Figure 8.1 [Levi, 1995]. It is derived from the general model of an induction machine that accounts for iron loss (5.1) - (5.5) under the assumption of ideal current feeding and by application of the rotor flux orientation constraints. The model is given with [Levi, 1995]:

$$
\begin{aligned}
&\psi_r + T_{\sigma rn}\, d\psi_r/dt = L_{mn} i_{dm} \\
&\omega_{sl} = L_{mn} i_{qm} / \left(T_{\sigma rn} \psi_r\right) \\
&\left(L_{rn}/L_{\sigma rn}\right) i_{dm} + T_{Fe}\, di_{dm}/dt = i_{ds} + \psi_r / L_{\sigma rn} + \omega_r T_{Fe} i_{qm} \\
&\left(L_{rn}/L_{\sigma rn}\right) i_{qm} + T_{Fe}\, di_{qm}/dt = i_{qs} - \omega_r T_{Fe} i_{dm} \\
&T_e = \frac{3}{2} P \frac{L_{mn}}{L_{\sigma rn}} \psi_r i_{qm}
\end{aligned}
\qquad (8.1)
$$

where once more $T_{Fe}=L_{mn}/R_{Fe}$, $T_{\sigma rn}=L_{\sigma rn}/R_{rn}$ and $R_{Fe}=f(f_e)$.

Assuming that rate of change of the rotor flux reference is slow, the term $T_{\sigma rn} d\psi_r/dt$ in the first equation of (8.1) can be neglected. The modified indirect vector controller is then described with

$$\psi_r^* = \psi_{rn} \qquad |\omega| \le \omega_n$$
$$\psi_r^* = \psi_{rn}\frac{\omega_n}{\omega^*} \qquad |\omega| > \omega_n \tag{6.6}$$

$$i_{dm}^* = \psi_r^* / L_{mn}$$
$$i_{qm}^* = \frac{2}{3P}\left(L_{\sigma rn}/L_{mn}\right)T_e^*/\psi_r^*$$
$$\omega_{sl}^* = \frac{L_{mn}}{T_{\sigma rn}}\frac{i_{qm}^*}{\psi_r^*} \tag{8.2}$$
$$\phi_r = \int\left(\omega_{sl}^* + \omega\right)dt$$
$$i_{ds}^* = i_{dm}^* - \left(\omega_{sl}^* + \omega\right)T_{Fe}i_{qm}^*$$
$$i_{qs}^* = \left(\omega_{sl}^* + \omega\right)T_{Fe}i_{dm}^* + \left[\left(L_{rn}/L_{\sigma rn}\right) + pT_{Fe}\right]i_{qm}^*$$

Taking into account that for a sensorless drive actual speed ω needs to be substituted with estimated speed ω^{est}, that $\omega_r^* = \omega_{sl}^* + \omega^{est}$ and that the last, derivative, term in equation for stator q-axis current command can be neglected as time constant T_{Fe} is very small [Levi, 1995], the structure of the modified controller of Figure 8.1 is obtained. Note that the term di_{dm}/dt in the third equation of (8.1) automatically disappears when rate of change of rotor flux is neglected. (It is worth mentioning that main flux saturation is here neglected, although field-weakening region is encompassed. The reason is the same as in chapters 6 and 7.) Constants TG and SG in Figure 8.1 stand for $TG = \frac{2}{3P}L_{\sigma rn}/L_{mn}$ and $SG = L_{mn}/T_{\sigma rn}$.

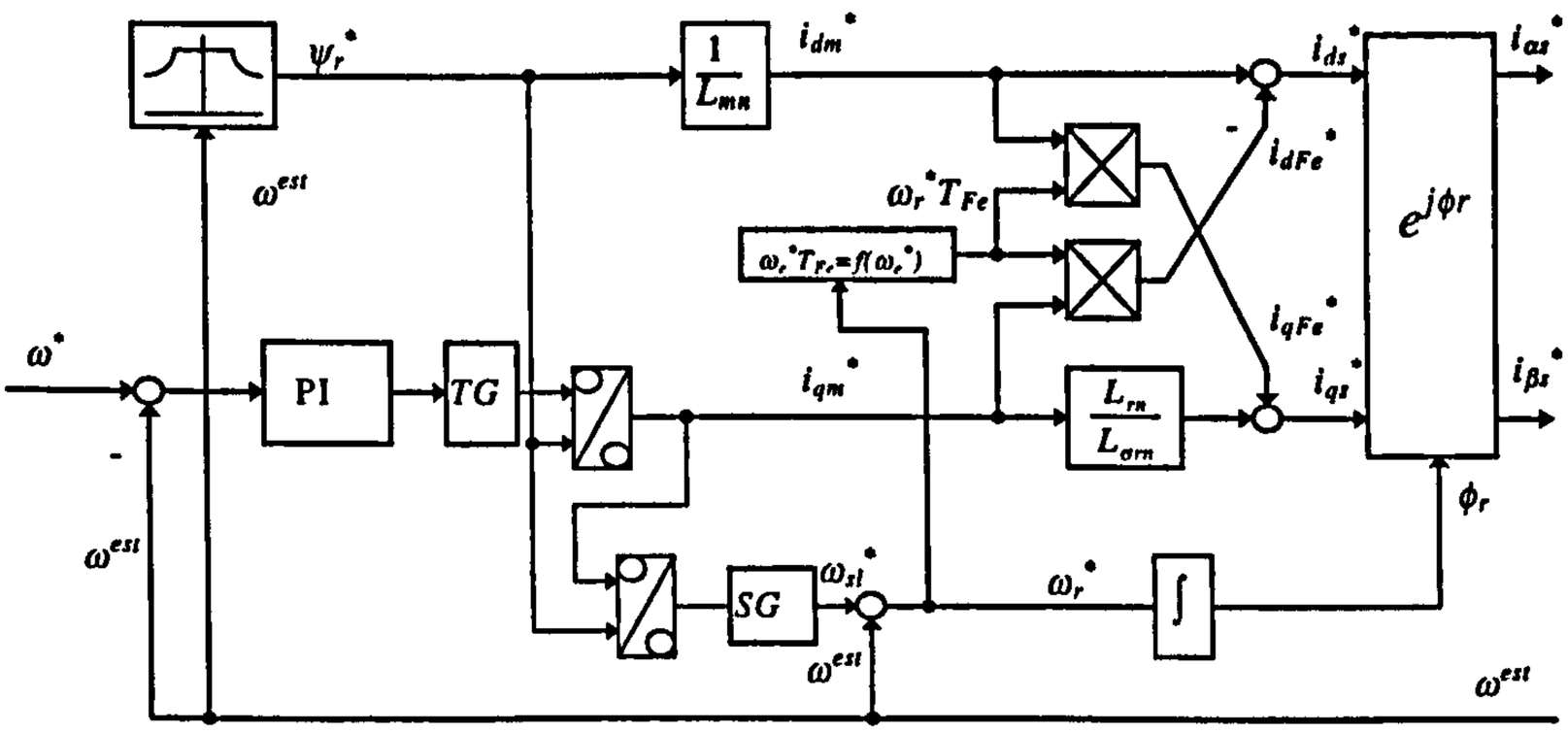

Figure 8.1: Modified indirect vector controller with compensation of iron loss.

In order to retain the simple structure of the speed estimator of Figure 7.3, it is desirable to avoid modification of the estimator structure by means of modified induction machine's equivalent circuit. An alternative and indeed very simple way consists of modification of the input into the estimator rather than of change of its structure. Stator current references in Figure 8.1 are obtained by adding iron loss compensation currents to the controller outputs. Estimator input is therefore modified in such a way that input currents are obtained by deducting iron loss compensation currents from the measured stator current components. As iron loss compensation currents are available in the rotating reference frame, while speed estimator operates in the stationary reference frame, this method requires co-ordinate transformation of iron loss currents from *d-q* reference frame to stationary α,β reference frame. Modified speed estimator is illustrated in Figure 8.2 [Levi et al, 1999].

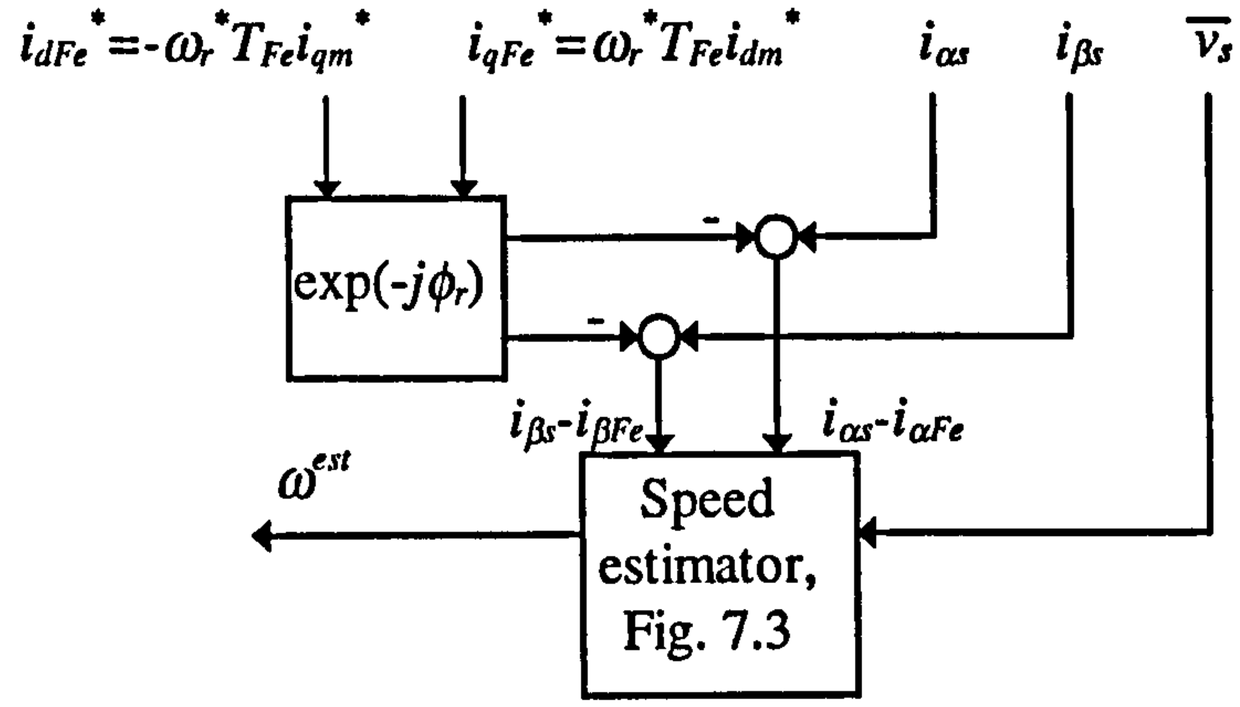

Figure 8.2: Approximate method of iron loss compensation in the speed estimator.

The behaviour of the proposed compensation method is examined by steady-state analysis and dynamic simulation in what follows.

8.2.2 Results of the study

In steady-state analysis, commanded speed is taken as independent variable (normalised with respect to the rated speed) and the commanded torque is set to a constant value in the base speed region. For operation in the field-weakening region, torque command is reduced inversely proportionally to the speed so that constant power operation is obtained. Induction machine model that includes iron loss, given in section 5.2, is

utilised here. Structure of the control system is a combination of Figures 8.1 and 8.2. From Figure 8.1 and (8.2), the following relations can be obtained ($\omega_r^* = \omega_e^*$):

$$\begin{aligned} i_{ds}^* &= i_{dm}^* - i_{dFe}^* = i_{dm}^* - \omega_e^* T_{Fe} i_{qm}^* \\ i_{ds}^* &= \psi_r^* \Big/ L_{mn} - \omega_e^* T_{Fe} \left(\frac{2}{3P} \frac{L_{\sigma rn}}{L_{mn}} \frac{1}{\psi_r^*} \right) T_e^* \end{aligned} \tag{8.3}$$

$$i_{qs}^* = i_{qm}^* L_{rn} / L_{\sigma rn} + i_{qFe}^* = i_{qm}^* L_{rn} / L_{\sigma rn} + \omega_e^* T_{Fe} i_{dm}^*$$

$$i_{qs}^* = \left(\frac{2}{3P} \frac{L_{rn}}{L_{mn}} \frac{1}{\psi_r^*} \right) T_e^* + \omega_e^* T_{Fe} \psi_r^* / L_{mn} \tag{8.4}$$

All the parameters in both the controller/estimator and the induction machine model are equal to rated values. The approach to analysis of steady-state operation is the same as the one described in section 6.2 and involves iterative calculation that forces equality of the two values of the q-axis magnetising current component. Figure 8.3 displays the results of steady-state calculations as function of the speed command.

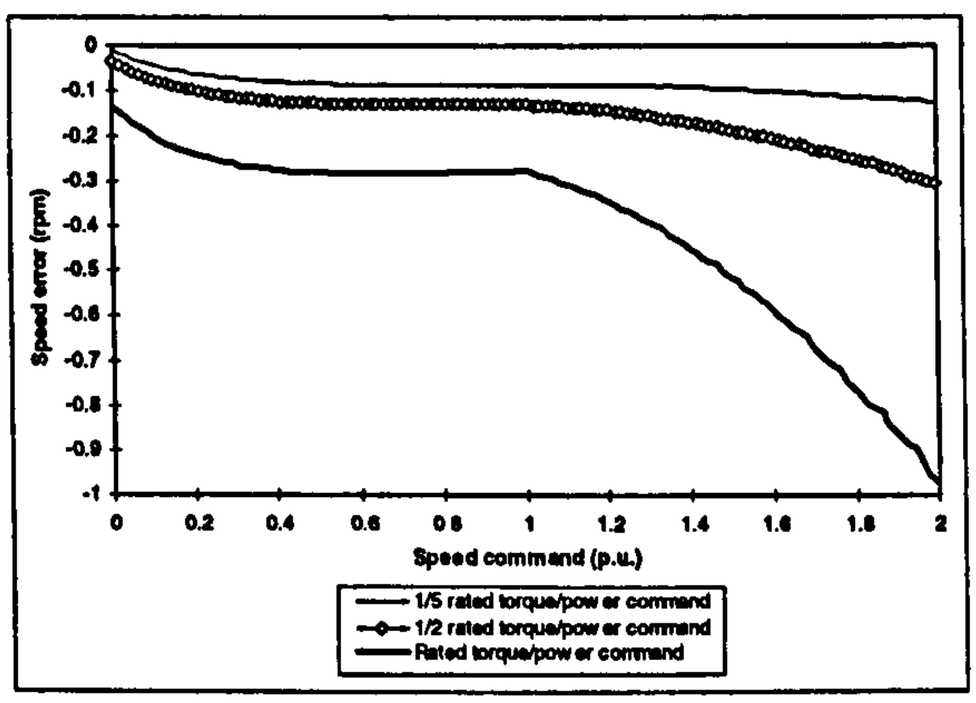

a. speed error

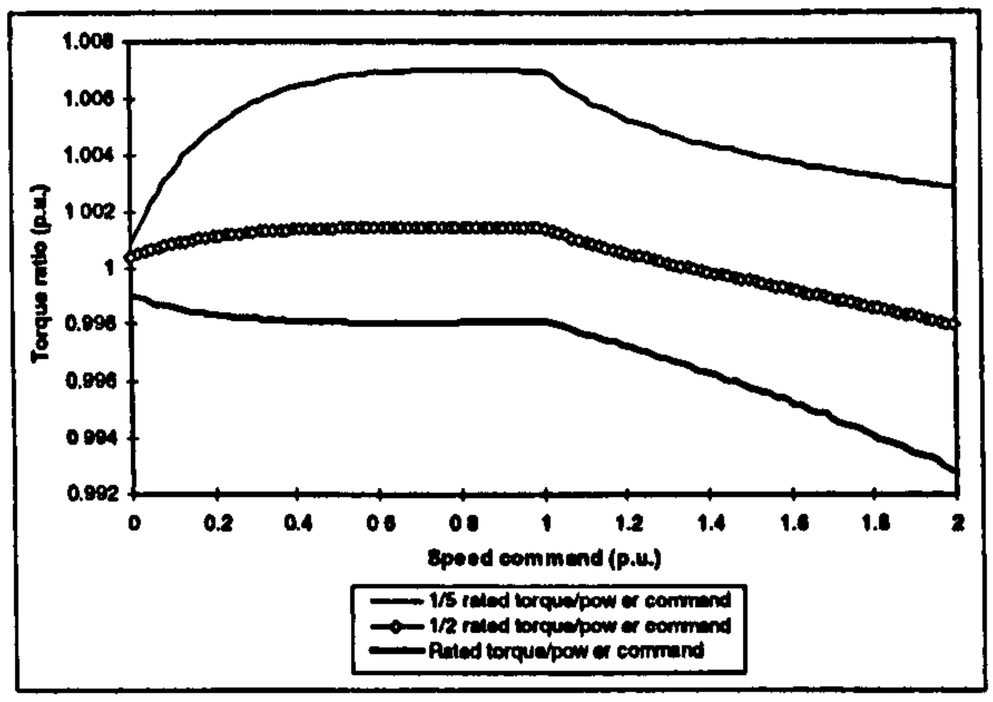

b. torque ratio

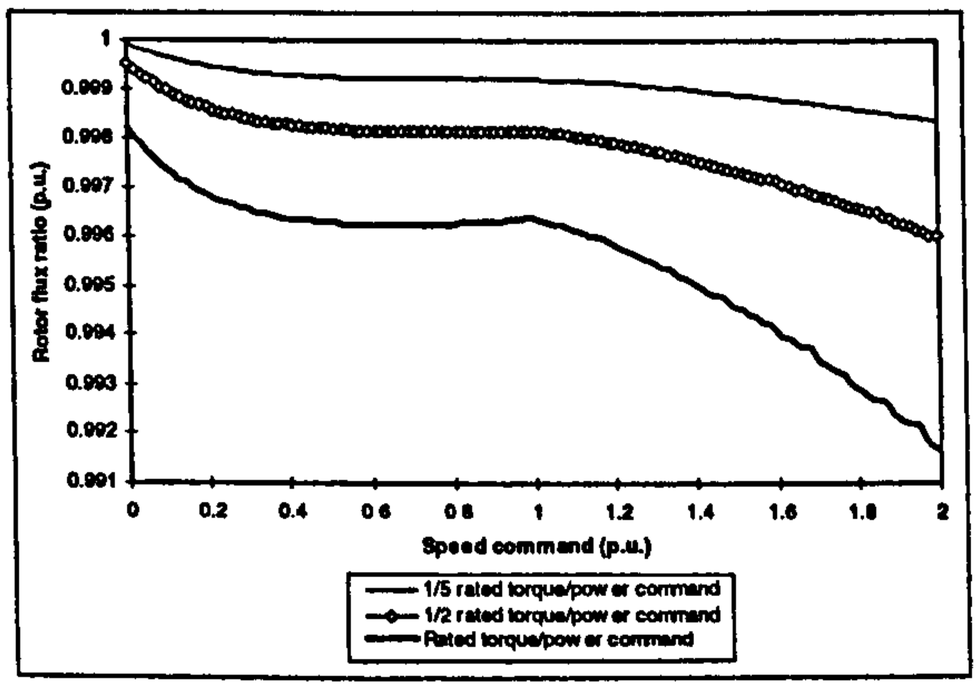

c. rotor flux ratio

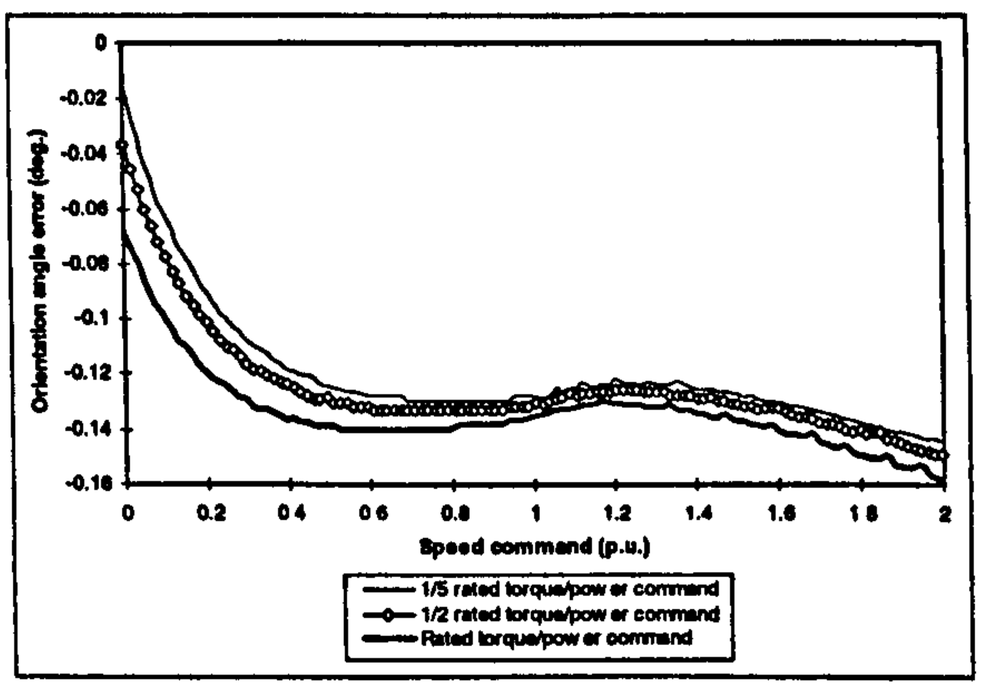

d. orientation angle error

Figure 8.3: Steady-state behaviour of the sensorless drive with iron loss compensation.

One can observe that speed estimation error is significantly reduced, Figure 8.3a, when compared to Figure 6.4a. Speed estimation error is less than -0.3 rpm in the base speed region with rated torque command. In field-weakening region, maximum speed estimation error is up to 1 rpm with rated power command, while it is up to 4.5 rpm in Figure 6.4. Maximum torque error is only 0.8% in Figure 8.3b for machine speeds up to twice the rated speed, while it is up to 20% without iron loss compensation. Rotor flux error and orientation angle error are negligibly small. These results illustrate the effectiveness of the iron loss compensation scheme, developed in the preceding section.

The explanation why the speed estimation error, although small, is still present after the compensation is as follows. Modified indirect vector controller of Figure 8.1 is obtained from the model in which equivalent iron loss resistance is placed in parallel with the magnetising branch. On the other hand, method of iron loss compensation in the speed estimator of Figure 8.2 corresponds to the placement of the equivalent iron loss resistance immediately before the stator resistance. As equivalent iron loss current and resistance slightly differ for these two representations of the iron loss [Sokola, 1998], compensation of the iron loss induced detuning is not perfect.

Compensating effects are further studied by dynamic simulation using Simulink. Dynamic induction machine model with iron loss accounted for, given in section 5.2, is again utilised here for induction machine representation. Main flux saturation is neglected in the controller, speed estimator and the machine. The structure of the modified vector control system is shown in Figure 8.1, while modified speed estimator is depicted in Figure 8.2. The Simulink simulation model is included in Appendix C.

In order to examine dynamic properties of the system, simulations for four speed commands, namely 0.5, 1, 1.5 and 2 p.u. speed, are done. Sequence of transients is as follows. Excitation of the machine, with rated rotor flux command, is initiated at $t = 0$ s at zero speed under no-load conditions. At $t = 0.5$ s speed command equal to one half of the rated is applied. Rated load torque is applied at $t = 1$ s and at $t = 2$ s load torque is reduced to one half of the rated. The same simulations are repeated for rated value of the speed command. Simulation results for these two speed commands are displayed in Figure 8.4. For speed commands above rated, load torque such that power is rated at

final speed is applied at t = 1.5 s and at t = 2.5 s load torque is reduced to such a value that power is one half of the rated. Simulation results are displayed in Figure 8.5.

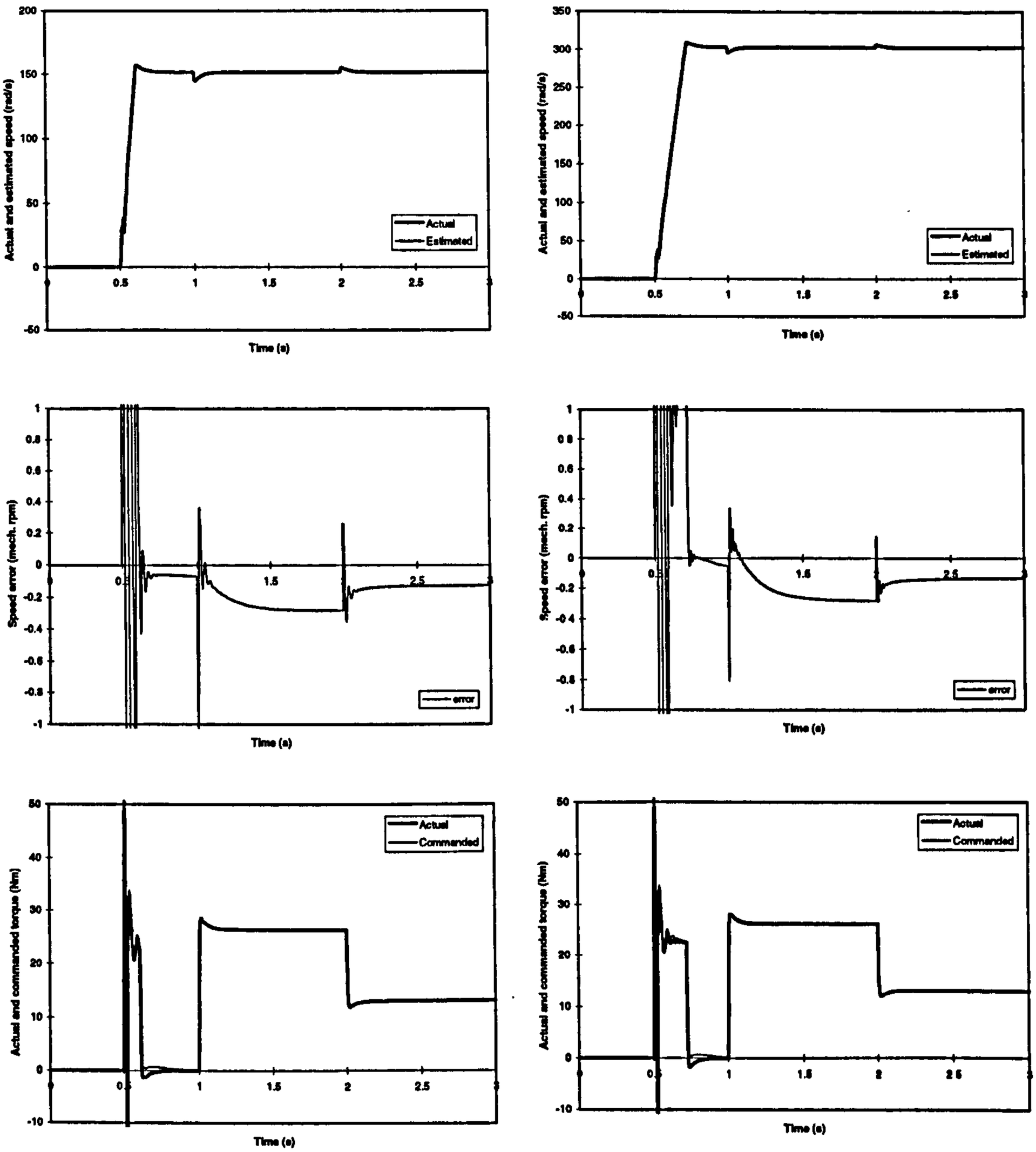

a) b)

Figure 8.4: Dynamic response for drive operation with modified controller/estimator at: a) speed command of 0.5 p.u. b) rated speed command.

It can be seen that actual and commanded torque now essentially coincide for both base speed region and field-weakening region. Speed estimation error is significantly reduced and is below 0.4 rpm for rated speed operation with rated load torque (worst case in the base speed region), Figures 8.4 a, b. In the field-weakening region, at 1.5

p.u. speed, speed estimation error is about 0.5 for rated power operation, Figure 8.5 a. At twice the rated speed, speed estimation error is up to 1 rpm for rated power operation, Figure 8.5 b. For load torque such that power is one half of the rated, speed estimation error is below 0.5 rpm. Once more, these values fully correspond to those predicted by steady-state analysis, discussed previously in this section.

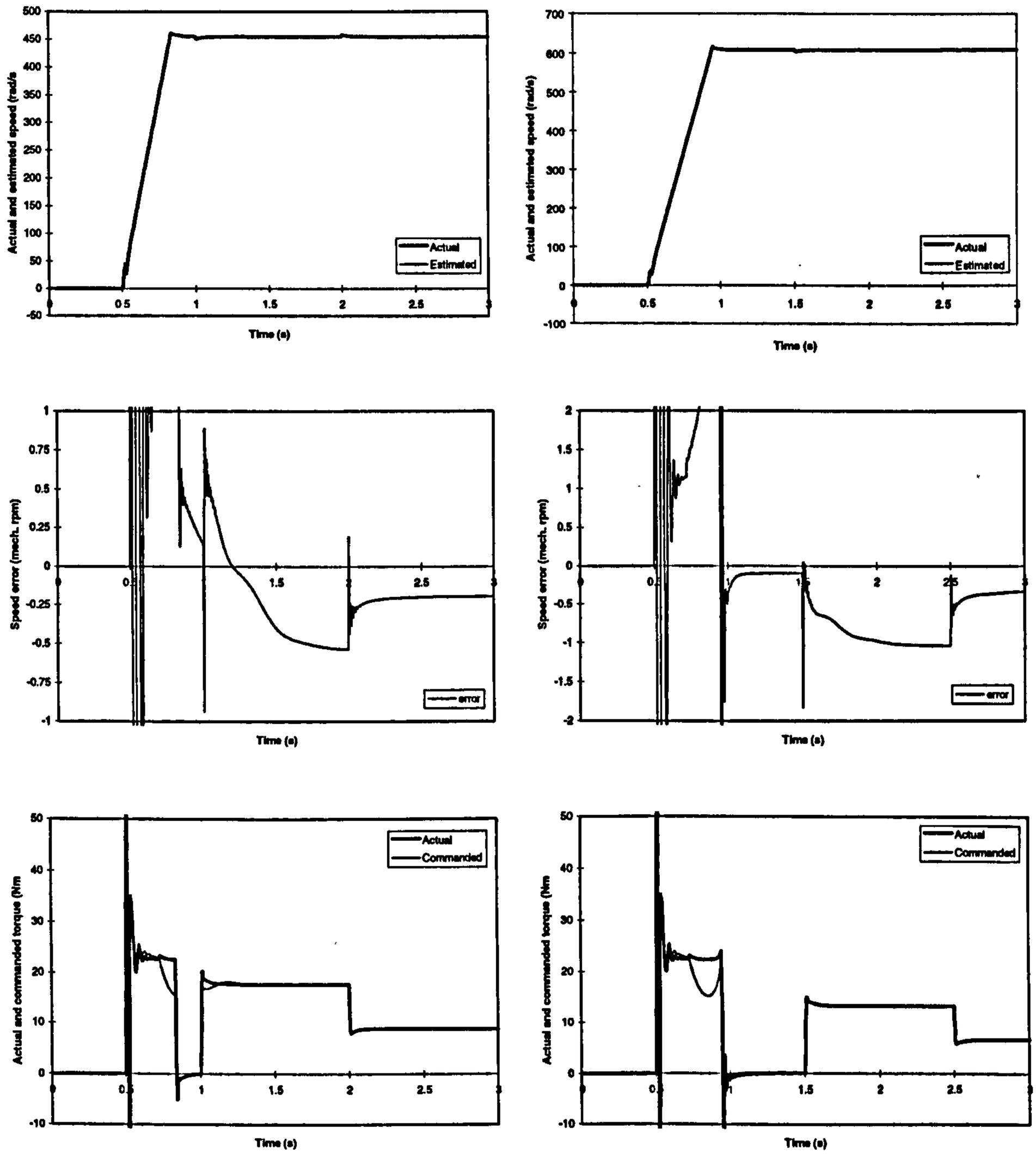

a) b)

Figure 8.5: Dynamic response for drive operation with modified controller/estimator at: a) speed command of 1.5 p.u. b) speed command of 2 p.u..

Figures 8.4 and 8.5 confirm again that the approximate method of compensation of iron loss, used in the design of the modified controller of Figure 8.1 and speed estimator of Figure 8.2, significantly reduces the speed estimation error and confines it to the negligible values of up to 0.4 rpm in the base speed region and up to 1 rpm in the field-weakening region.

8.3 Compensation of main flux saturation by means of modified rotor flux based MRAC speed estimator

If a sensorless vector controlled induction machine drive is designed to operate in both base speed region and field-weakening region, it becomes an imperative that main flux saturation is compensated for. In field-weakening region impact of stator resistance variation is negligible, while level of main flux saturation significantly varies with operating speed. In this section, modified rotor flux based speed estimator is developed and is used in conjunction with an existing suitably modified indirect vector controller. The effectiveness of the scheme in compensating main flux saturation is confirmed by simulation [Levi and Wang, 1999; Wang et al, 1999].

8.3.1 Description of the system

As already discussed, extension of the operating region of the system above base speed region requires modification of the indirect vector controller, by accounting for main flux saturation. Such a modified indirect vector controller was introduced in section 7.4 (equations (7.4) to (7.6)) and its outlook is depicted in Figure 7.17. The indirect vector controller of Figure 7.17 is applied in simulations in this section.

In order to compensate for the main flux saturation in the speed estimator, both the reference and the adaptive part of the estimator have to be modified. In order to modify the speed estimator, the use is now made of the two alternative models of a saturated induction machine, that were given in section 5.3 and were not used until now. Mixed magnetising flux-stator current model, described with (5.41) - (5.45), is used for development of the modified reference part of the speed estimator, while mixed stator

current-rotor flux model, described with (5.33) - (5.40), is utilised in development of the modified adjustable part of the speed estimator.

Magnetising flux-stator current model of a saturated induction machine is characterised with the absence of any saturation dependent terms in the stator voltage equations. As stator voltages and currents are known, then not only that the rotor flux estimation is possible, but an information regarding the actual saturation level in the machine can be obtained as well [Levi and Vuckovic, 1993]. In particular, actual magnetising inductance in the machine can be estimated as well. The equations of the reference model therefore become:

$$
\begin{aligned}
&\psi_{\alpha s} = \int \left(v_{\alpha s} - R_{sn} i_{\alpha s} \right) dt && \psi_{\beta s} = \int \left(v_{\beta s} - R_{sn} i_{\beta s} \right) dt \\
&\psi_{\alpha m} = \psi_{\alpha s} - L_{\sigma sn} i_{\alpha s} && \psi_{\beta m} = \psi_{\beta s} - L_{\sigma sn} i_{\beta s} \\
&\psi_m = \sqrt{\psi_{\alpha m}^2 + \psi_{\beta m}^2} && i_m = f(\psi_m) \\
&i_{\alpha m} = \left(\psi_{\alpha m} / \psi_m \right) i_m && i_{\beta m} = \left(\psi_{\beta m} / \psi_m \right) i_m \\
&\psi_{\alpha r}^{(1)} = \psi_{\alpha m} + L_{\sigma rn} \left(i_{\alpha m} - i_{\alpha s} \right) \\
&\psi_{\beta r}^{(1)} = \psi_{\beta m} + L_{\sigma rn} \left(i_{\beta m} - i_{\beta s} \right) \\
&L_m^{est} = \psi_m / i_m
\end{aligned}
\tag{8.5}
$$

Reference model, described with (8.5), is illustrated in Figure 8.6. Not only that main flux saturation is fully accounted for in the calculation of the rotor flux components, but the estimate of the magnetising inductance is provided as well. Estimate of the magnetising inductance, obtained from the reference model, will be used in the adaptive model. It should be noted that the complexity of the scheme given in Figure 8.6 can be reduced for real-time application by suitably re-arranging equations (8.5).

Modified adaptive model is obtained from the stator current-rotor flux model of a saturated induction machine. Inspection of (5.33) - (5.40) shows that in this case the only saturation dependent coefficient that appears in the rotor voltage equations is the steady-state magnetising inductance, L_m. As shown in [Levi and Sokola, 1997], main flux saturation is fully accounted for provided that the appropriate value of the saturated steady-state magnetising inductance is used instead of the constant one. Such a value is delivered by the reference model. In other words, structure of the adaptive model needs

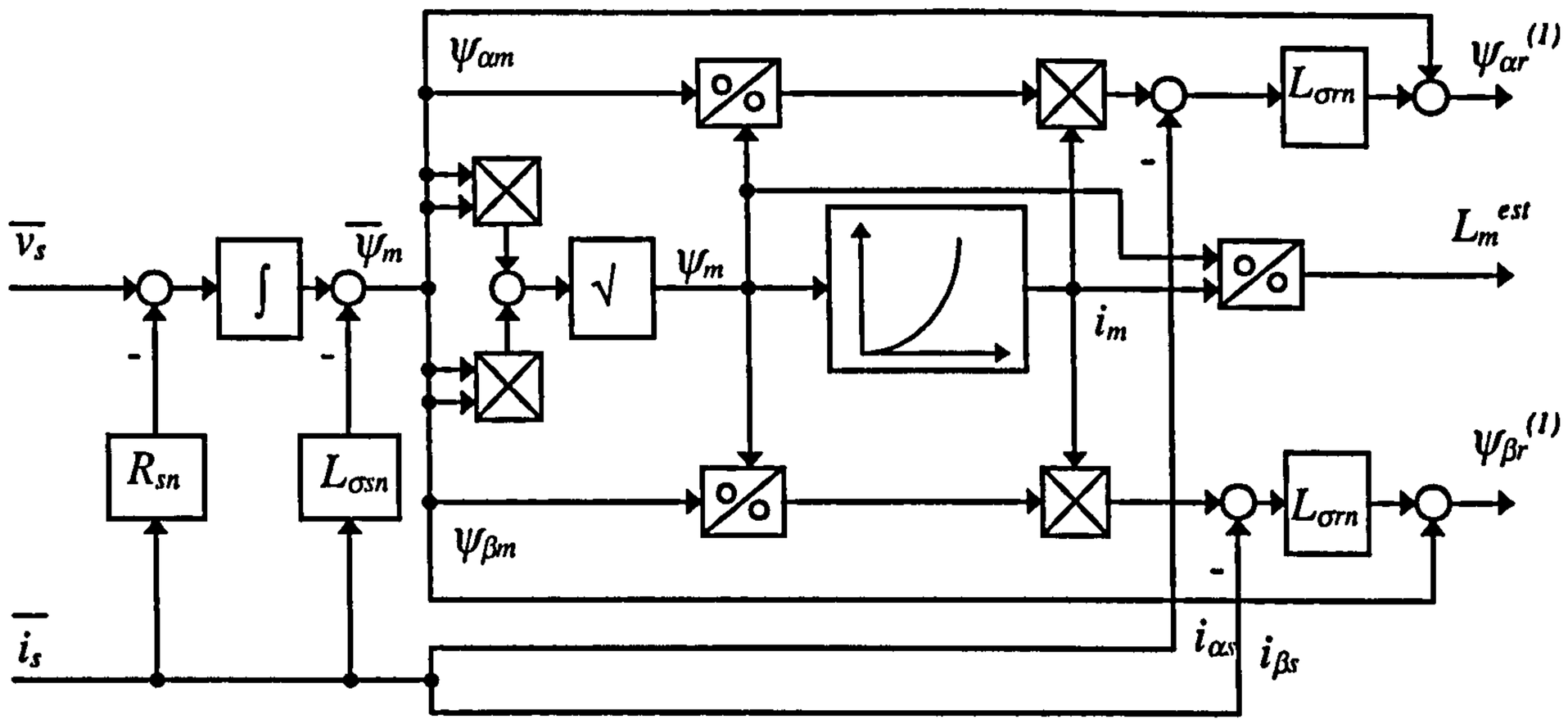

Figure 8.6: Structure of the modified reference model with compensation of main flux saturation.

not be changed at all, as dynamic inductance terms do not appear in this equation when stator current and rotor flux components are selected as state space variables. An appropriate value of the saturated steady-state magnetising inductance is obtained from the reference model. The adaptive model then takes the following form:

$$\frac{d\overline{\psi}_r^{(2)}}{dt} = \left(j\omega^{est} - \frac{R_{rn}}{L_{\sigma rn} + L_m^{est}} \right) \overline{\psi}_r^{(2)} + \frac{L_m^{est}}{L_{\sigma rn} + L_m^{est}} R_{rn} \bar{i}_s \qquad (8.6)$$

Error calculation remains the same:

$$\varepsilon = \psi_{\alpha r}^{(2)} \psi_{\beta r}^{(1)} - \psi_{\beta r}^{(2)} \psi_{\alpha r}^{(1)} \qquad (8.7)$$

Resultant structure of the proposed modified speed estimator is shown in Figure 8.7.

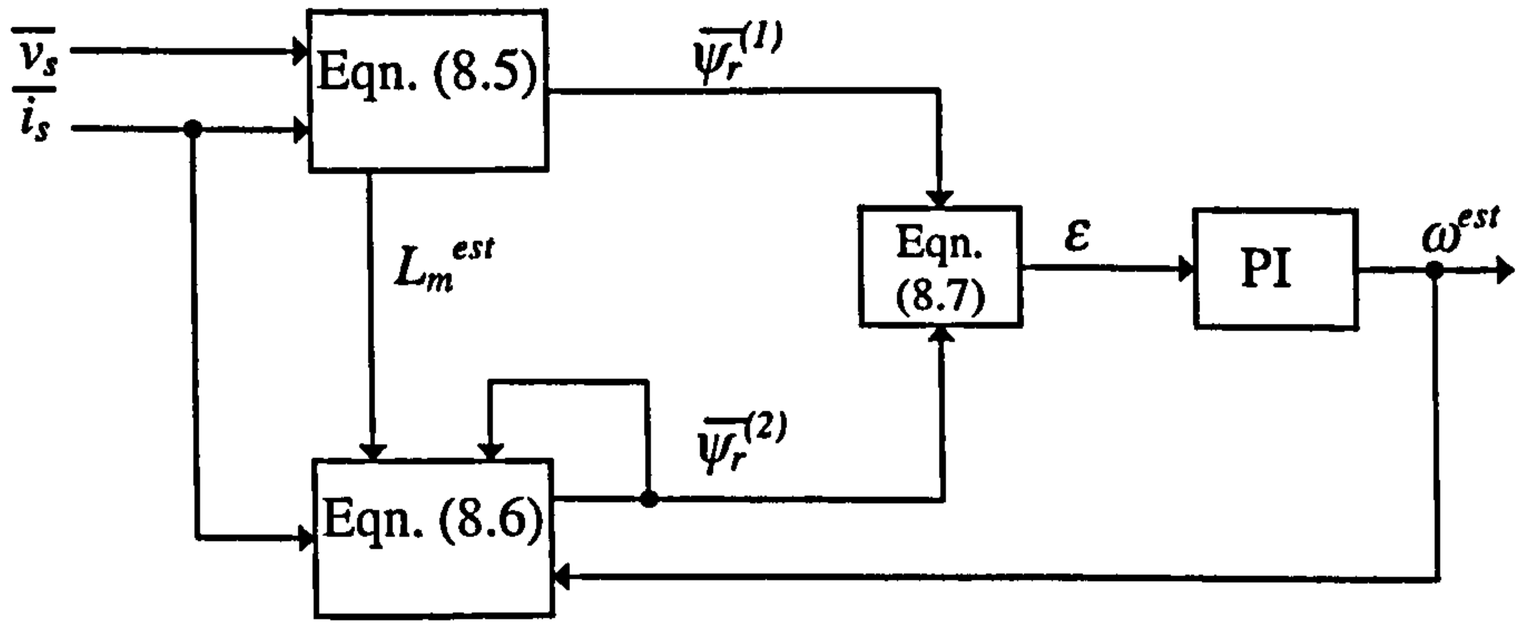

Figure 8.7: Modified speed estimator with compensation of main flux saturation.

The estimator provides full compensation of main flux saturation in both transient and steady-state operation.

8.3.2 Results of the study

A number of simulations are done using the indirect vector controller of Figure 7.17 and the modified speed estimator of Figure 8.7. Induction machine model with main flux saturation accounted for and with stator and rotor currents selected as state-space variables, given in section 5.3, is utilised here once more for induction machine representation. Simulation model is given in Appendix C. The following sequence of transients is simulated. The machine is initially excited at zero speed with rated rotor flux command under no load conditions. Speed command is then applied, so that rated speed operation (1 p.u.) under no load conditions is achieved. During operation at rated speed, a load torque of 1 p.u. is applied in a step-wise manner at $t = 0.5$ s. At $t = 1$ s, load torque is stepped down to 0.5 p.u. and this value is not changed any more. Finally, at $t = 1.5$ s speed command is further increased in a ramp-wise manner, so that field-weakening region is entered. Final operating steady-state is therefore with 0.5 p.u. load torque. Transients for four different final speeds are studied, namely 1.25 p.u., 1.5 p.u., 1.75 p.u. and 2 p.u. speed. Figures 8.8 to 8.11 summarise results obtained with modified speed estimator. Graphs of actual and commanded speed, speed error, actual and commanded torque, actual and commanded rotor flux and actual rotor flux *d-q* axis components are given.

From Figures 8.8 to 8.11, it can be observed that operation in the base speed region is insignificantly changed with the application of the saturation adaptive speed estimator. Pattern of discrepancy between actual and commanded torque and between actual and commanded rotor flux is during acceleration into field weakening region very similar to those in Figure 7.18. These differences occur due to the absence of the stator *d*-axis current command boost during the transient (rate of change of the rotor flux reference is neglected in the design of the controller) and can not be compensated by the modified speed estimator. However, speed estimation error during this transient is reduced significantly. Once when reference speed in the field-weakening region has become

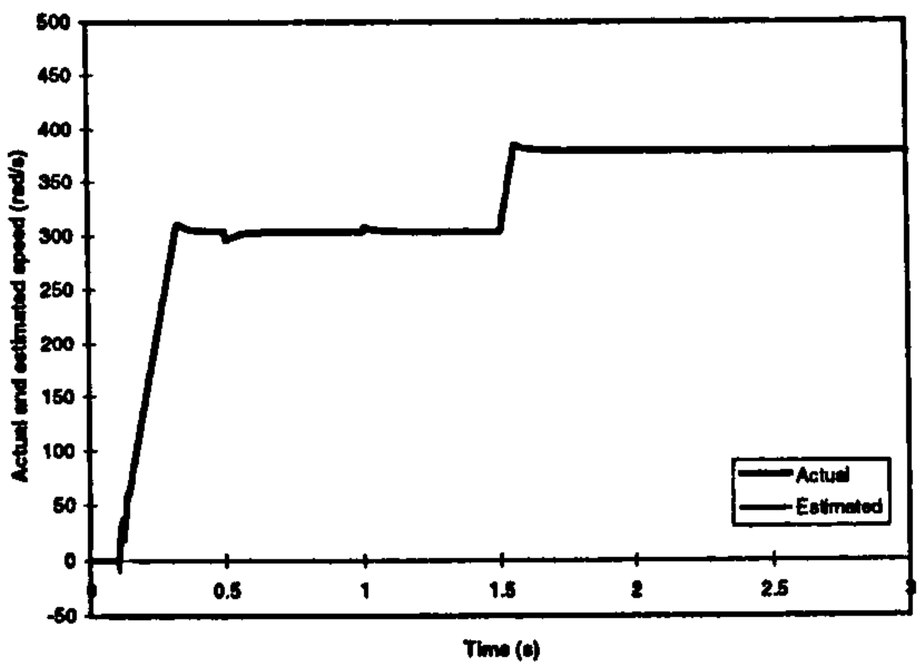

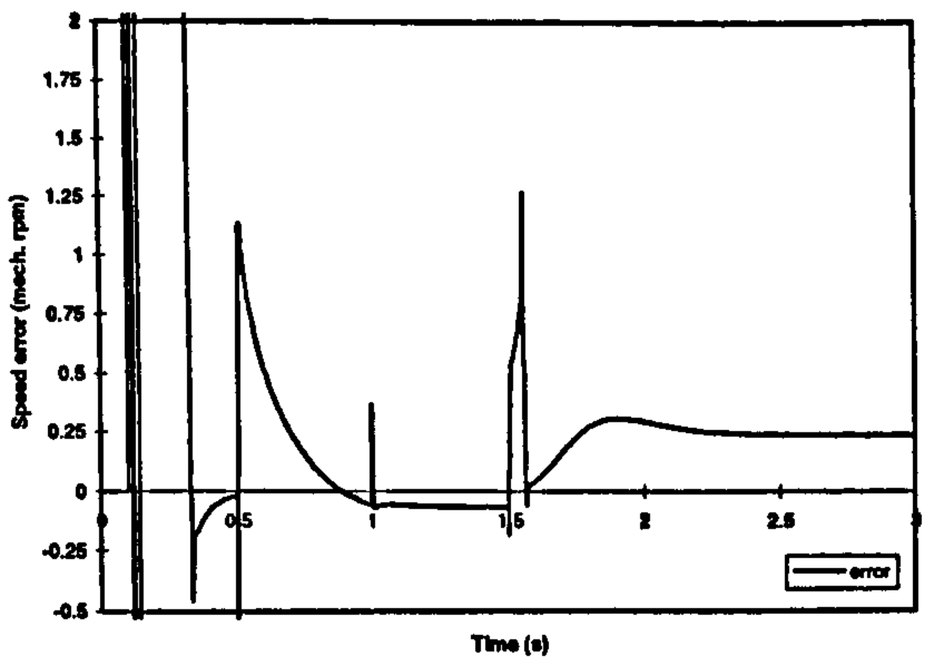

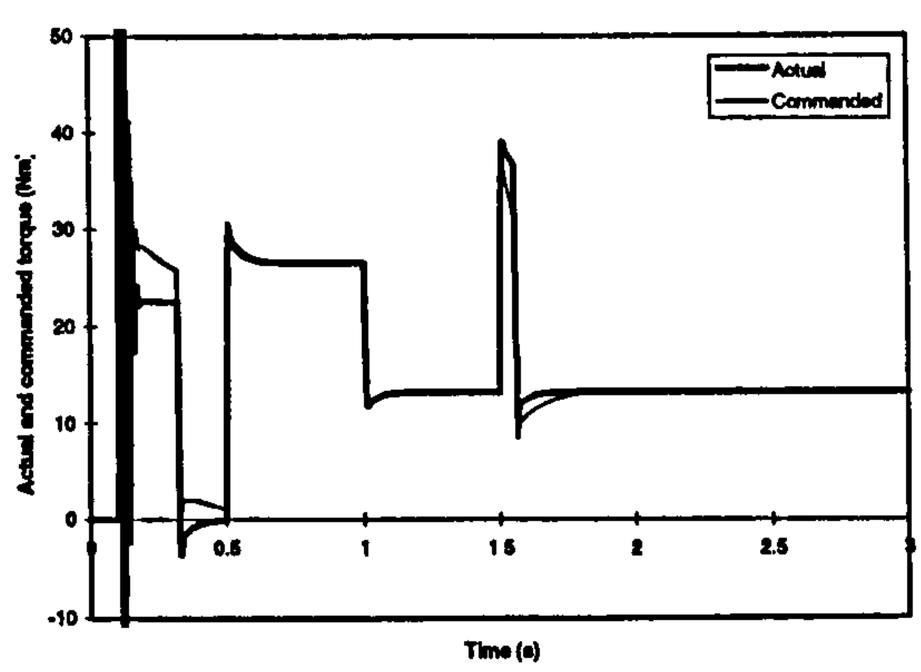

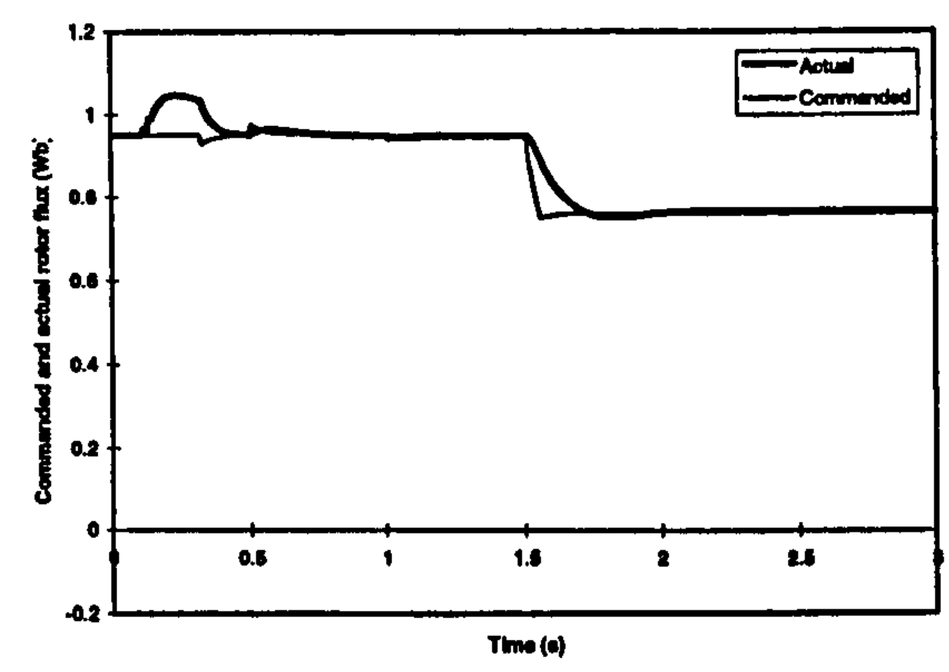

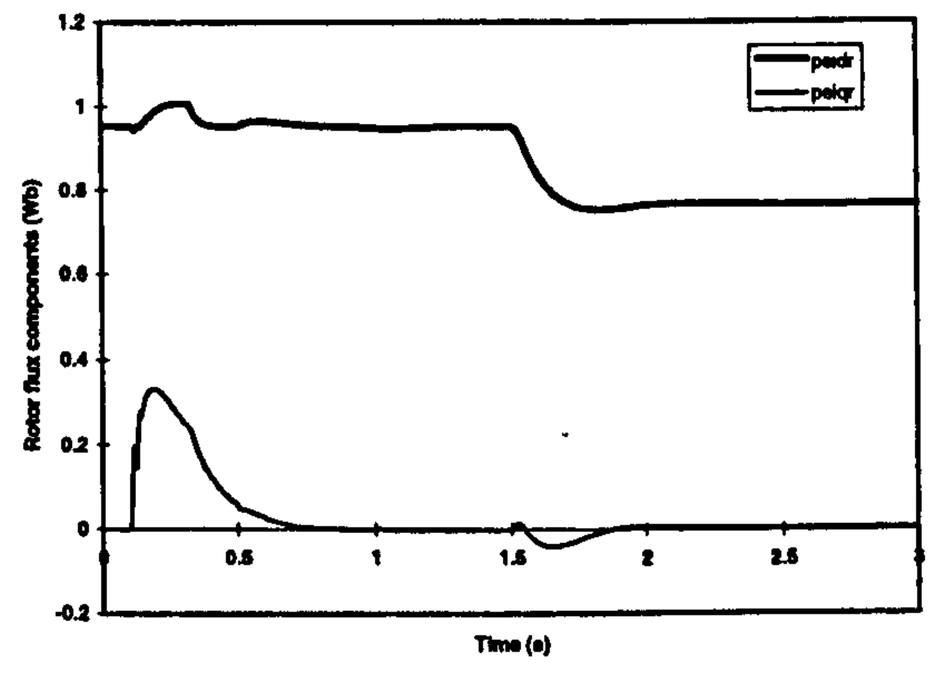

Figure 8.8: Dynamic response of the drive with main flux saturation compensation (final speed command 1.25 p.u.).

constant, the compensating effects become even more remarkable. Final steady-state shown in Figures 8.8-8.11 is characterised with perfect field orientation as *q*-axis component of the rotor flux equals zero. Actual rotor flux in the machine exactly matches the reference value. Consequently, actual and reference torque are equal as well. Speed estimation error is essentially zero for operation at 2 p.u., while for operation at 1.25 p.u., 1.5 p.u. and 1.75 speed it is less than 1 rpm. The reason for this small residual speed estimation error is explained as follows. Machine model requires use of the magnetising curve approximation, while the controller and the estimator ask for approximation of the inverse magnetising curve. The two approximations, obtained

using curve fitting, are characterised with identical values for rated operating point and for the initial linear portions of the curve, while some minor discrepancies exist in between. Speed estimation error is therefore zero for operation in the base speed region (rated operating point) and for operation at 2 p.u. speed (linear portion of the curve).

For operation between these two areas of the magnetising curve, where matching is not perfect, small residual speed estimation error may result. These considerations indicate that accurate knowledge of the magnetising curve is important for successful implementation of the developed speed estimator and existing modified vector controller.

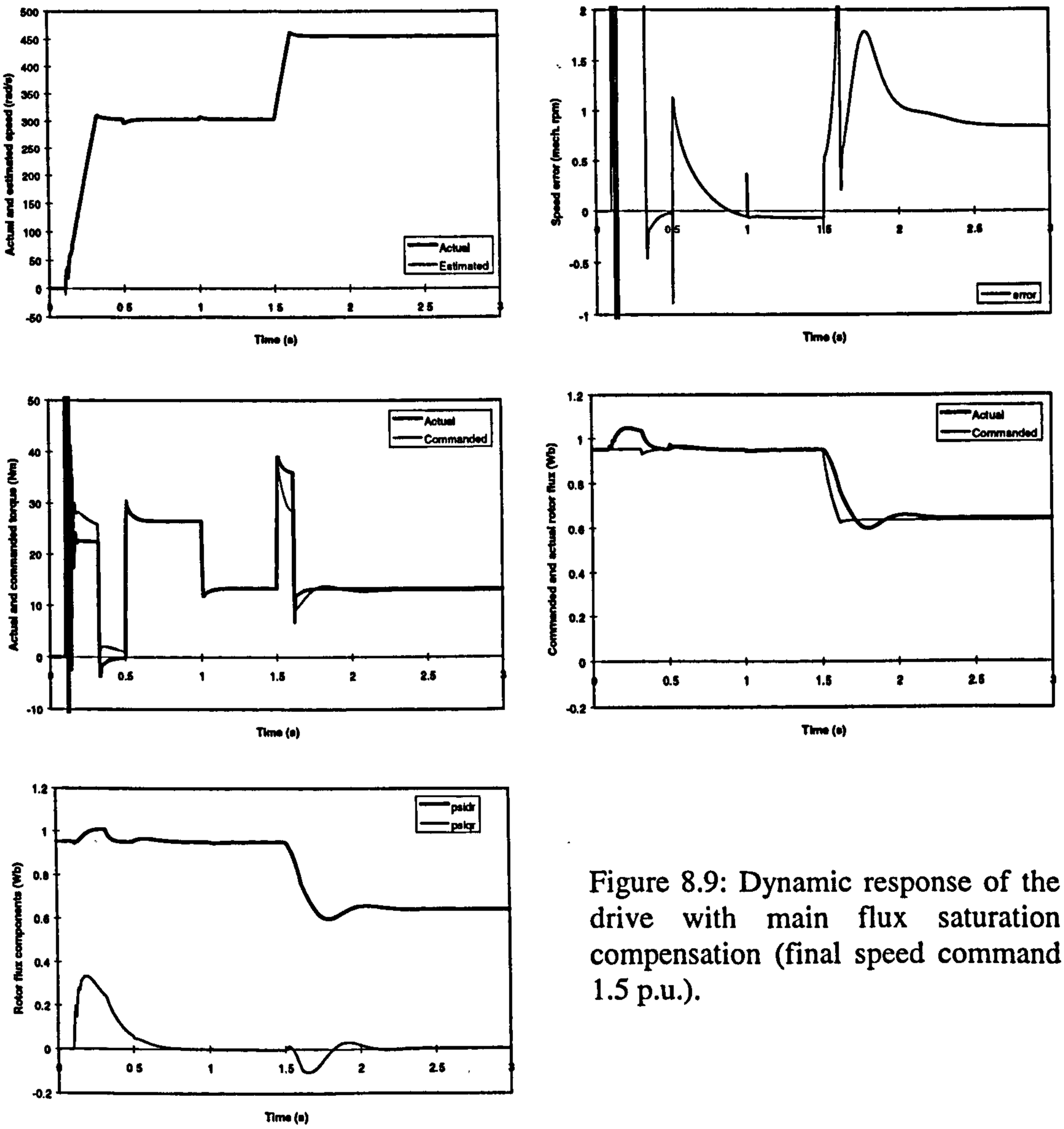

Figure 8.9: Dynamic response of the drive with main flux saturation compensation (final speed command 1.5 p.u.).

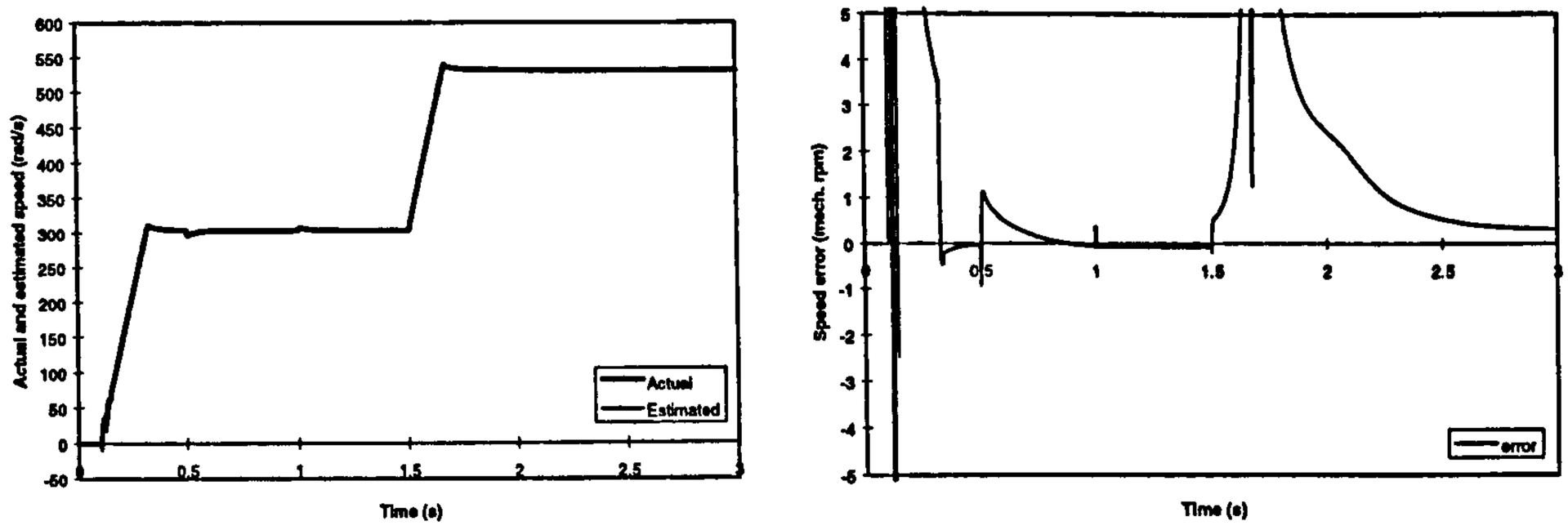

Figure 8.10: Dynamic response of the drive with main flux saturation compensation (final speed command 1.75 p.u.).

8.4 Compensation of both main flux saturation and iron loss by means of modified indirect vector controller and modified MRAC speed estimator

Simultaneous compensation of both the main flux saturation and iron loss is discussed here. It can be realised by suitably modifying both the indirect vector controller and the MRAC speed estimator, on the basis of indirect vector controller structures and modified MRAC speed estimator structures elaborated in sections 8.2 and 8.3.

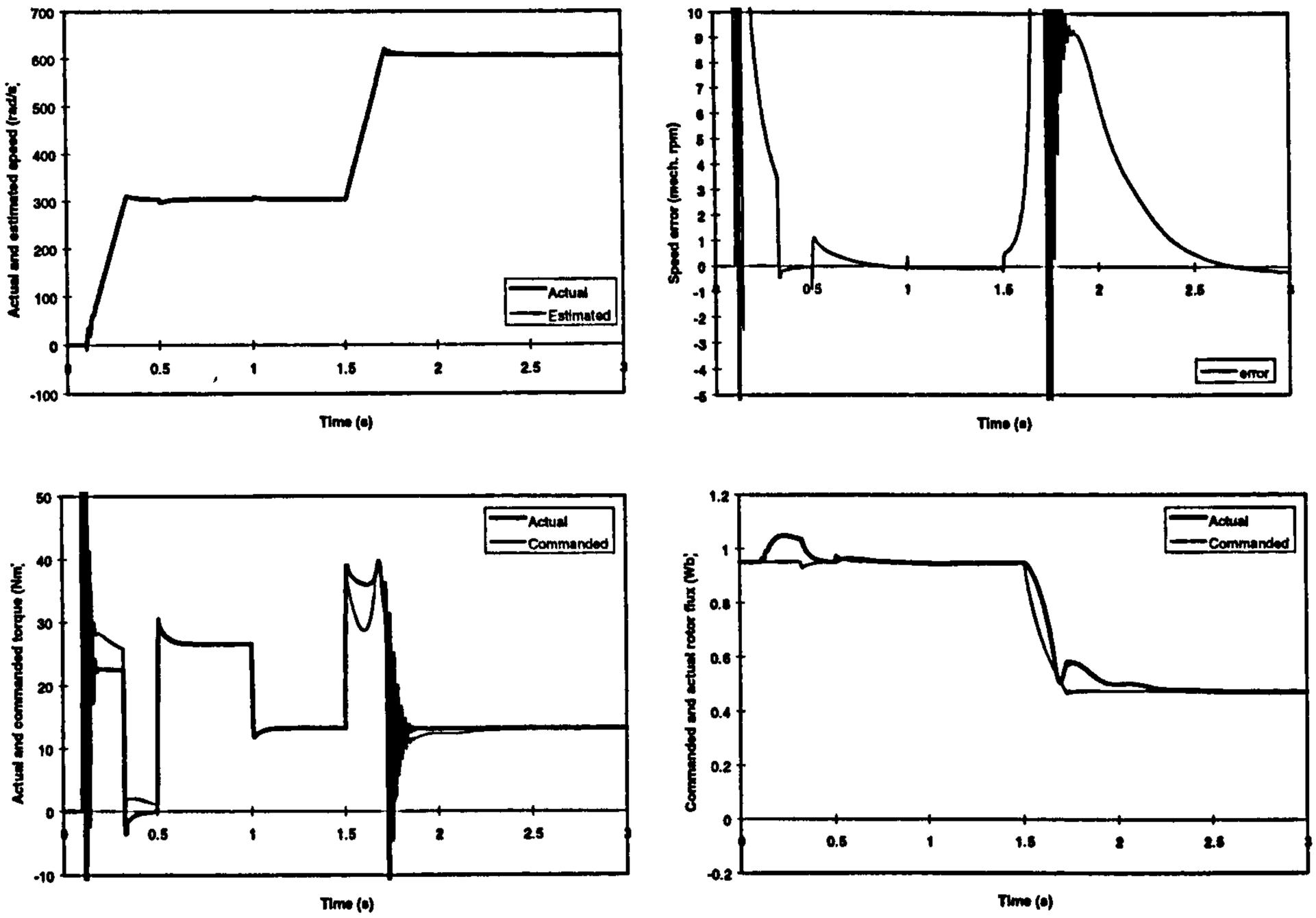

Figure 8.11: Dynamic response of the drive with main flux saturation compensation (final speed command 2 p.u.).

8.4.1 Description of the system

The structure of an indirect vector controller that will provide compensation of both main flux saturation and iron loss and therefore enable operation in both base speed region and field-weakening region is obtained by combining the two controllers, shown in Figures 8.1 and 7.17. The resulting controller is illustrated in Figure 8.12 [Sokola, 1998]. Constants TG and SG are defined as $TG=[2/(3P)]L_{\sigma rn}/L_{mn}$ and $SG=L_{mn}/T_{\sigma rn}$. Time constant T_{Fe} is defined as ratio of magnetising inductance to equivalent iron loss resistance, $L_m(i_m)/R_{Fe}(\omega_e)$. Note that product of TG and SG in calculation of the

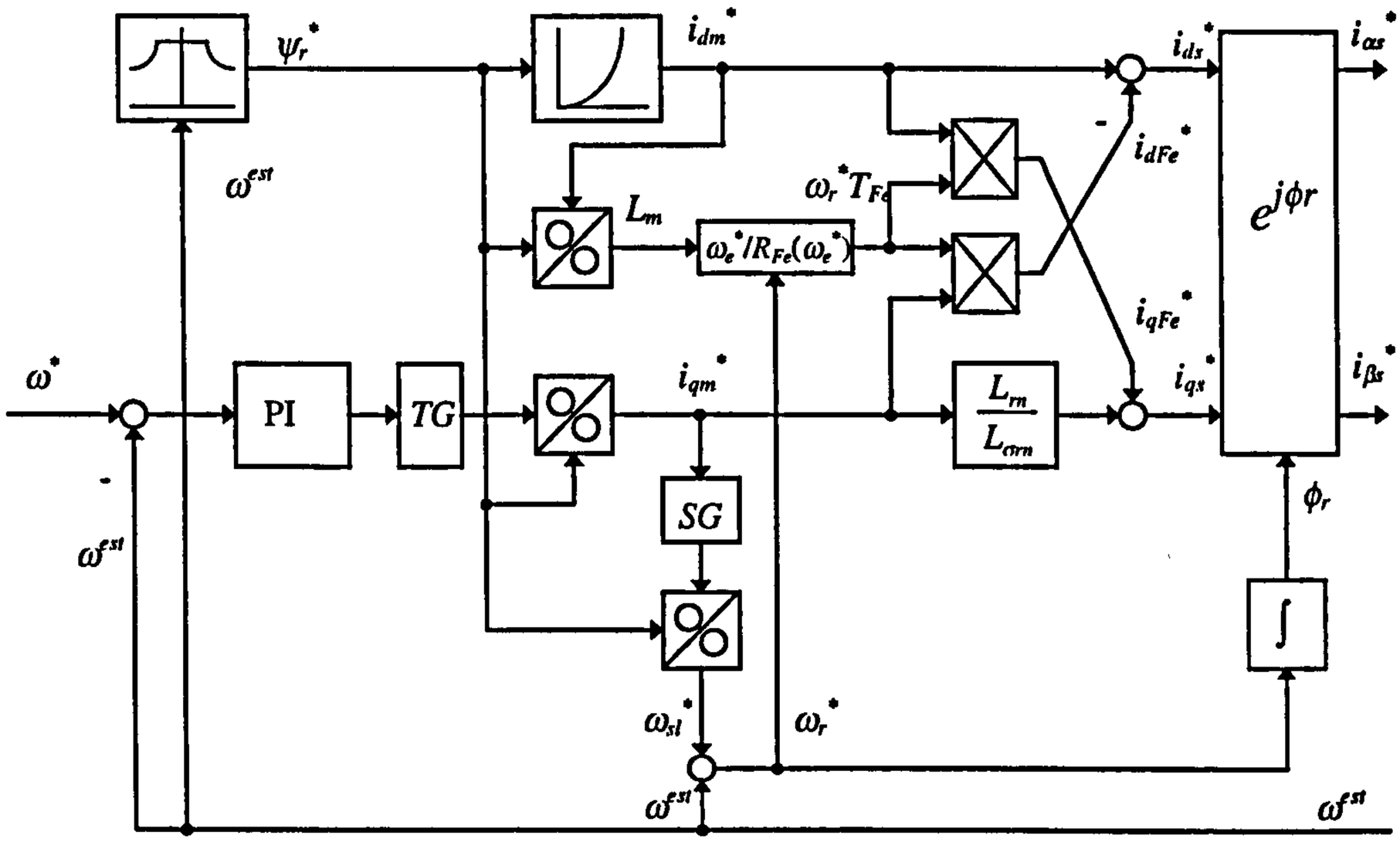

Figure 8.12: Indirect vector controller with simultaneous compensation of main flux saturation and iron loss.

reference angular slip frequency cancels dependence on the magnetising inductance, while in the calculation of the reference stator q-axis current this dependence is approximately cancelled by the product of TG and ratio of rated rotor self-inductance to rotor leakage inductance. Function ω_e^*/R_{Fe} takes into account dependence of iron loss resistance on frequency, while magnetising inductance is calculated from rotor flux reference and output of the inverse magnetising curve.

Speed estimator with compensation of the both phenomena is constructed in very much the same way as the indirect controller. The two schemes, proposed for individual compensation of iron loss and main flux saturation, are combined to yield simultaneous compensation of both effects. The resulting structure of the speed estimator is shown in Figure 8.13 and it combines structures depicted in Figures 8.2 and 8.7.

8.4.2 Results of the study

Simulations regarding simultaneous compensation of both the main flux saturation and the iron loss are conducted using the indirect vector controller of Figure 8.12 and the

novel speed estimator of Figure 8.13, with induction machine model accounting for both main flux saturation and iron loss, section 5.4 [Wang et al, 1999]. Sequence of transients is as follows. Excitation of the machine is initiated at $t = 0$ s at zero speed under no-load conditions. At $t = 0.5$ s speed command equal to rated is applied, under no-load conditions. Rated torque is applied at $t = 1$ s and at $t = 1.5$ s load torque is reduced to one half of the rated. This value is not changed any more. Finally, at $t = 2$ s speed command is further increased in a ramp-wise manner, so that field-weakening region is entered. Final operating steady-state is therefore with 0.5 p.u. load torque and transients for four different final speeds are analysed, namely 1.25 p.u., 1.5 p.u., 1.75 p.u. and 2 p.u. speed.

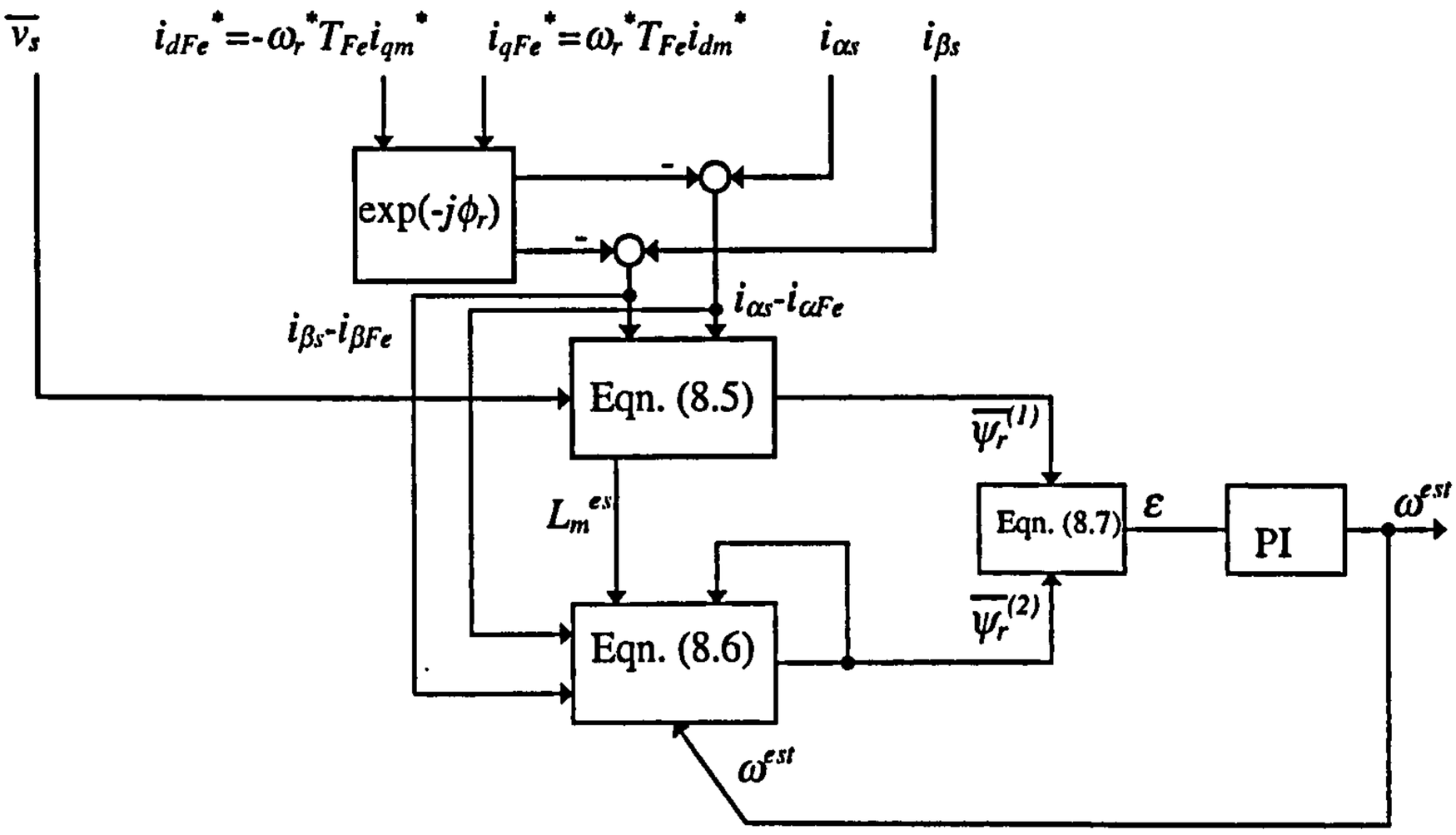

Figure 8.13: Modified MRAC speed estimator with compensation of both iron loss and main flux saturation.

Figures 8.14-8.17 summarise simulation results obtained with modified controller and modified speed estimator. Graphs of actual and estimated speed, speed estimation error, commanded and actual torque, reference and actual rotor flux, and rotor flux *d-q* axis components are given.

It can be seen that estimated speed tracks the actual speed very well in the base speed region. Steady-state speed estimation error equals zero for no-load conditions at rated speed. It is equal to 0.5 rpm for rated load torque (the worst case in the base speed region) and 0.25 rpm for one half of the rated torque at rated speed. In field-weakening

region, speed estimation errors are confined to values less than 1 rpm and perfect field orientation is achieved in all the steady-state operating regimes. Complete annulment of speed estimation error is not achieved due to approximate nature of the iron loss compensation and due to non-ideal mapping of the magnetising curve and the inverse magnetising curve, as explained previously. Actual and reference rotor flux coincide in all the steady-state operating conditions. Rotor flux q-component equals zero for all the cases in steady-state operation. It can also be observed that commanded torque and actual torque are in good agreement.

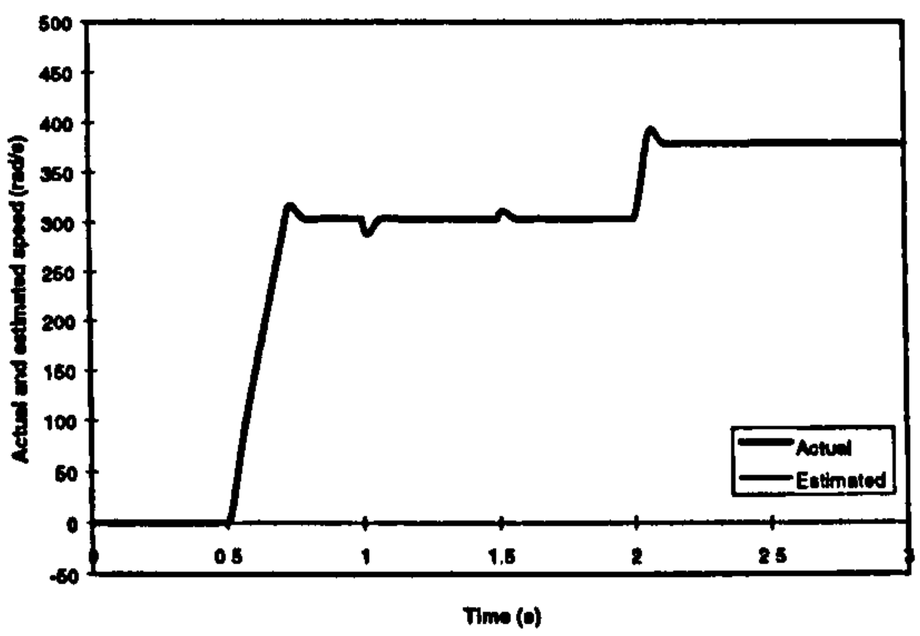

Figure 8.14: Operation with modified controller of Figure 8.12 and modified estimator of Figure 8.13 (final speed 1.25 p.u.).

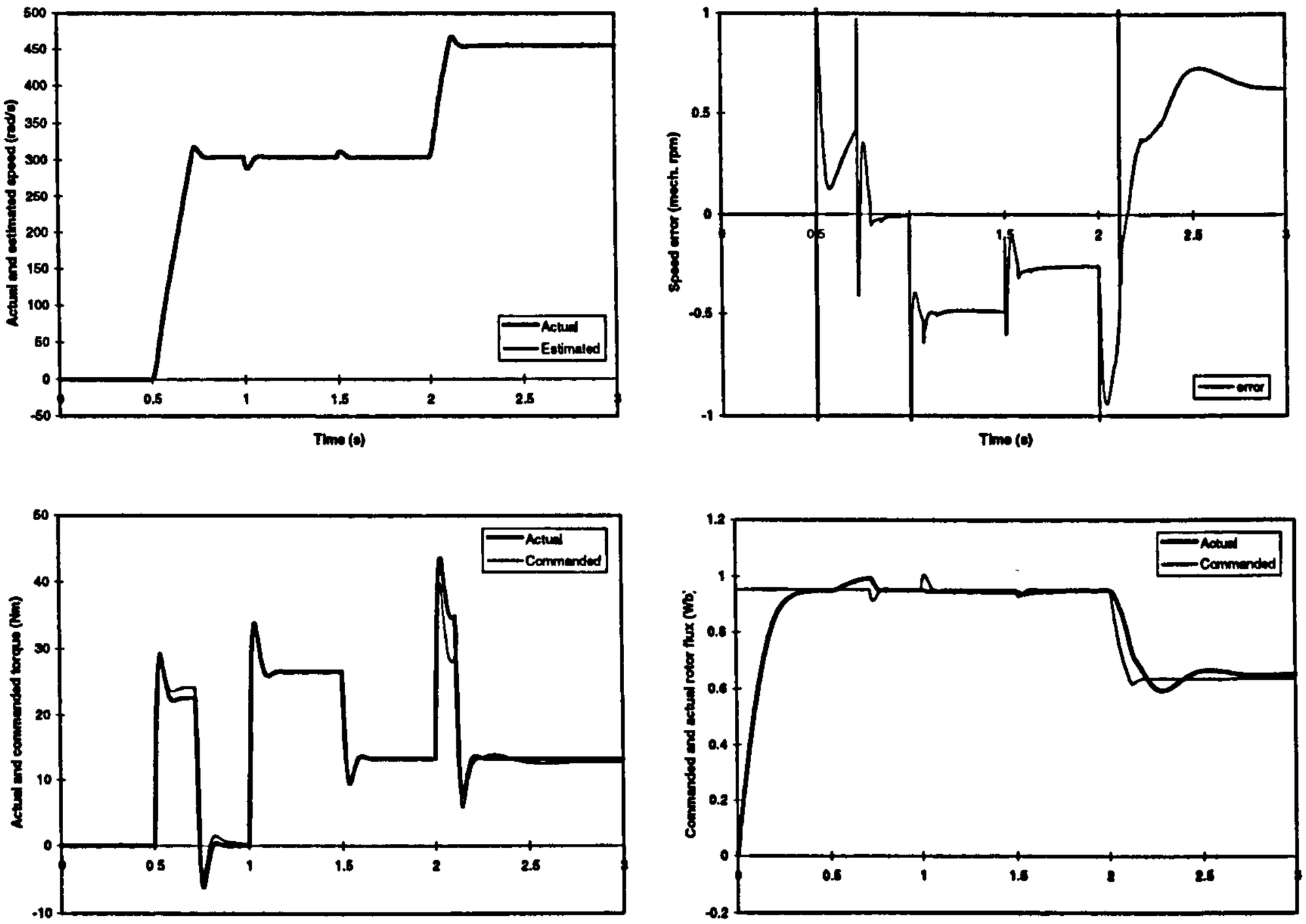

Figure 8.15: Operation with modified controller of Figure 8.12 and modified estimator of Figure 8.13 (final speed 1.5 p.u.).

8.5 Summary

Compensation of detuning due to iron loss, main flux saturation and both the iron loss and main flux saturation was discussed in this chapter. In order to compensate the given phenomenon, existing improved vector controllers were used and novel improved speed estimators were developed. The improved schemes are sufficiently simple for real time application. Their effectiveness was confirmed by dynamic simulations.

Compensation of iron loss is elaborated first. It was shown that the detuning due to iron loss significantly reduces when modified controller and speed estimator are used. The

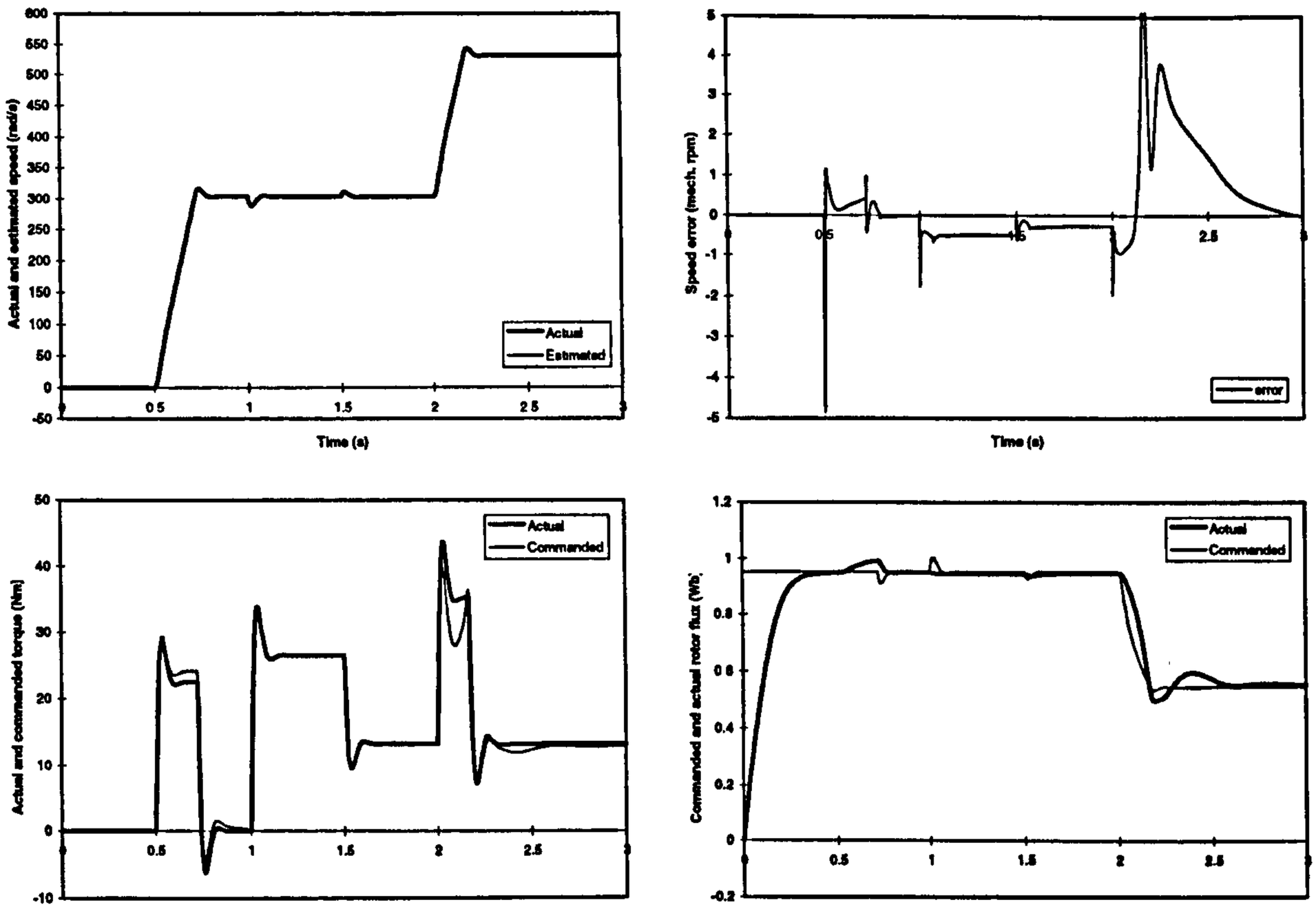

Figure 8.16: Operation with modified controller of Figure 8.12 and modified estimator of Figure 8.13 (final speed 1.75 p.u.).

speed estimation error is less than 0.4 rpm in base speed region and less than 1 rpm in field-weakening region. The existence of the residual speed estimation error is explained.

Detuning in the field-weakening region is mainly due to main flux saturation. It therefore needs to be compensated by suitably incorporating main flux saturation within the controller and speed estimator. Such an existing improved controller is used and novel improved speed estimator, with main flux saturation compensation, is developed.

The scheme successfully compensates main flux saturation in field-weakening region, as confirmed by simulation. Speed estimation error is confined to less than 1 rpm for all

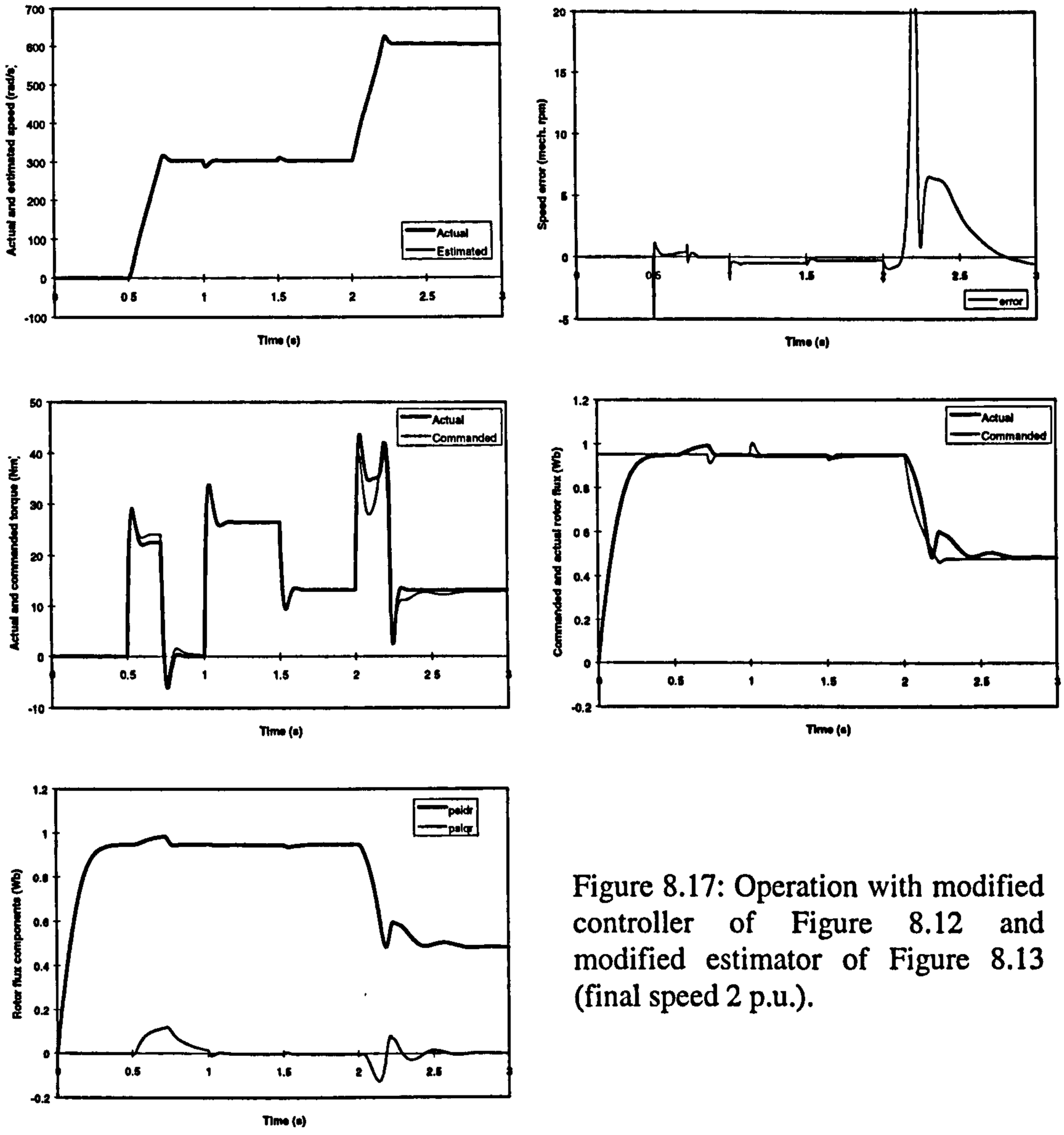

Figure 8.17: Operation with modified controller of Figure 8.12 and modified estimator of Figure 8.13 (final speed 2 p.u.).

speeds up to 2 p.u. and is a consequence of non-ideal mapping of the machine's magnetising curve into the inverse magnetising curve.

Finally, simultaneous compensation of both the iron loss and main flux saturation was studied. Simulation results show that detuning due to both iron loss and main flux saturation can be significantly reduced by means of the developed modified indirect vector controller and modified speed estimator. Although detuning was not completely compensated, speed error was confined to negligible values. The reason for residual errors is analysed and explained.

9 EXPERIMENTAL INVESTIGATION

9.1 Introduction

Theoretical studies of detuning due to parameter variations in sensorless MRAC based indirect vector controlled induction machines and means for compensation of iron loss and main flux saturation have been elaborated and results have been presented in previous chapters. The purpose of this chapter is to describe the experimental work undertaken in order to confirm the theoretical findings. An indirect rotor flux oriented induction motor drive is used and operation of the MRAC based rotor speed estimator of rotor flux type is analysed. Standard constant parameter speed estimator is at first used and detuning due to incorrect rotor resistance setting and magnetising inductance setting is investigated experimentally. Next, implementation of the novel saturation adaptive speed estimator, developed in section 8.3, is discussed and its capability of compensating for the saturation effects in the field-weakening region is confirmed by experiments. The chapter is organised as follows. The experimental rig is described in section 9.2, while section 9.3 deals with tuning of the speed estimator. Sections 9.4 and 9.5 present the experimental results for the speed estimator operation in the base speed region under tuned conditions and detuned conditions, respectively. Results regarding operation of the constant parameter and saturation-adaptive speed estimators in field-weakening region are given in sections 9.6 and 9.7, respectively. Section 9.8 summaries the chapter.

9.2 Description of the experimental rig

9.2.1 The approach to experimental investigation

An indirect rotor flux oriented induction motor drive, with speed sensor, was available for the experimental study. As this is a commercially available servo drive, it does not offer the flexibility of substituting the actual speed feedback with the estimated speed feedback. It was therefore decided to retain operation of the drive with speed sensor feedback, and to design and operate the speed estimator in parallel to the drive. Estimated speed is therefore not used for either closed-loop speed control or for the calculation of the rotor flux position. A schematic diagram, showing the major components of the experimental rig, is given in Figure 9.1. The part of the rig,

contained within the dashed-line box, was constructed during the course of this project and was used for the experimental evaluation of the speed estimators presented in subsequent sections. All the major components of the set-up of Figure 9.1 are described in the following subsections of this section.

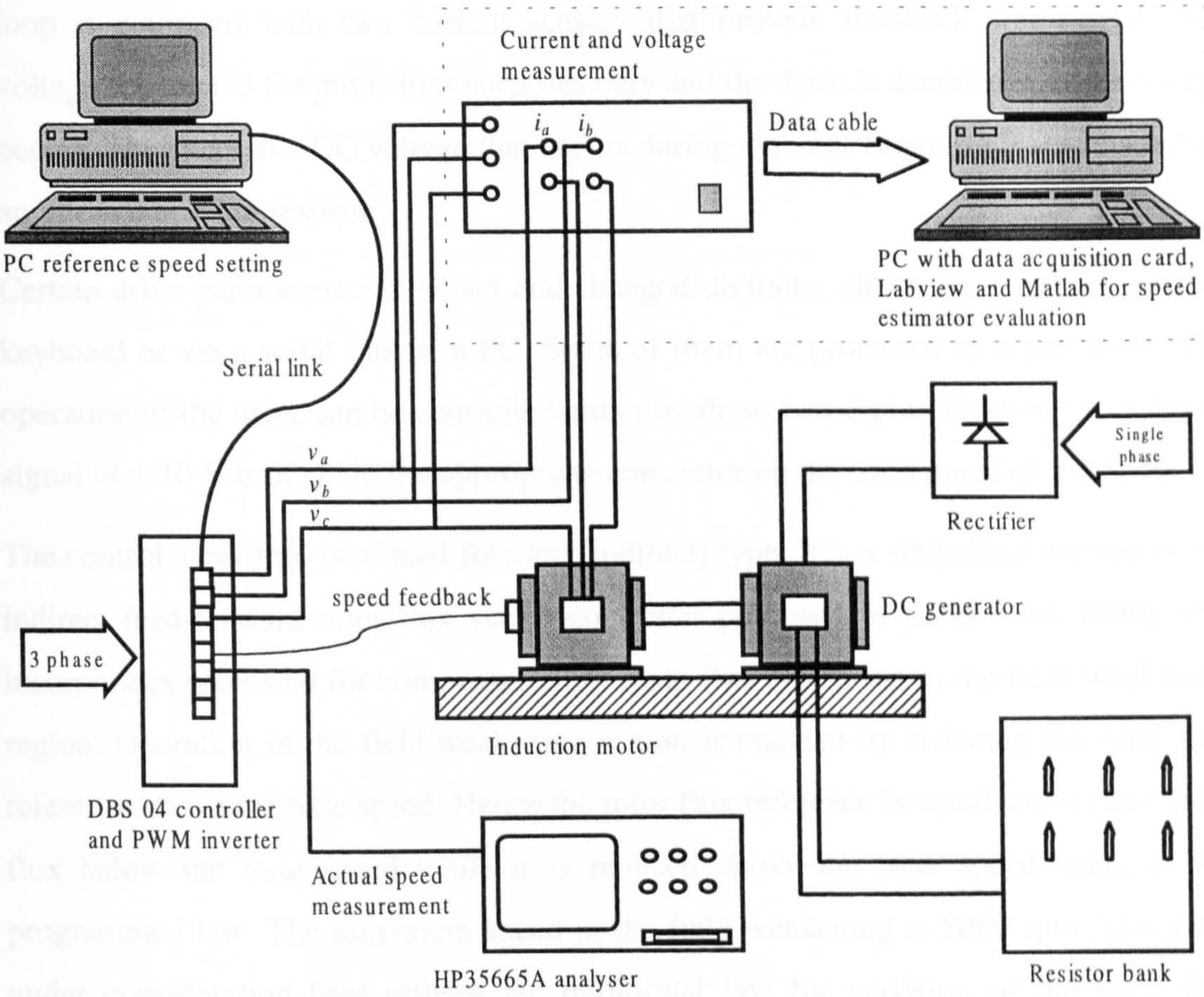

Figure 9.1: Experimental rig.

9.2.2 **Vector controlled induction motor drive with speed sensor**

The vector controlled induction motor drive used in this experimental study is the drive produced by the Vickers company. The induction motor is a 2.3 kW three-phase 50 Hz four-pole induction motor (its data and parameters are given in Appendix A), which is supplied by the DBS 04 type vector controller from 8/22 inverter (8 A rms is the nominal current, while 22 A is the peak short-term current of the inverter). The control system is based on 8051 micro-controller and TMS30C14 digital signal processor and it encompasses cascaded closed-loop speed and current control. The speed control and

field orientation are digital, while the current control loop is analogue, resulting in the hybrid realisation.

The induction motor incorporates a resolver as a speed sensor. The current-controlled voltage source inverter operates at 10 kHz switching frequency. The current control loop is equipped with two current sensors that provide feedback signals. DC bus voltage is detected for protection purposes only and the drive is disabled if undervoltage occurs. The excessive DC voltage that occurs during dynamic breaking is suppressed by an internal braking resistor.

Certain drive parameters can be set and changed digitally, either via a special Vickers keyboard or via a serial link of a PC. Some of them are protected by a password. The operation of the drive can be controlled either by these two digital links or by analogue signal of $\pm$ 10 V brought to the appropriate connector on the front panel of the drive.

The control algorithm is of feed-forward (indirect) type. It is a simplified version of the indirect feed-forward rotor flux vector controller proposed in [Levi et al, 1990], that incorporates provision for compensation of main flux saturation in the field-weakening region. Operation in the field-weakening region is enabled by reducing the rotor flux reference above the base speed. Hence the rotor flux reference is equal to the rated rotor flux below the base speed while it is reduced above the base speed using a pre-programmed law. The maximum speed in the field weakening is 8000 rpm. The drive under consideration here utilises the traditional law for variation of the rotor flux reference in the field-weakening region, [Joetten et al, 1983], $\psi_r^* = \psi_{rn}\omega_B/\omega$.

The indirect vector controller with compensation of main flux saturation, implemented in the Vickers drive, is essentially the one elaborated in section 7.4 and illustrated in Figure 7.17. As discussed in section 7.4, rate of change of the rotor flux reference can be neglected due to relatively high inertia of the system and this simplification is adopted in the Vickers drive. Some minor modifications are however present and these are described next.

If rated magnetising current is taken as an independent input into the system, it is possible to introduce the normalised rotor flux value and the normalised inverse magnetising curve. The indirect feed-forward rotor flux oriented controller then takes the form shown in Figure 9.2. The constant K_2 and the variable rotor flux reference

value, required for generation of the stator q-axis current reference in (7.5), are taken care of by the PI speed controller. PI speed controller therefore operates with variable gains in the field-weakening region. The stator d-axis current reference is generated as the product of the rated value and a per unit value. The per unit value is obtained at the output of the inverse magnetising curve as a function of the per unit rotor flux reference (which is a function of speed). All the per unit values in Figure 9.2 are identified with the index *pu*. Slip gain of the drive (denoted in Figure 9.2 as *SG*) is a constant parameter, given from (7.4) with $SG=L_{mn}^{*}/(T_{rn}^{*}\psi_{rn})$. The output of the speed controller is stator q-axis current reference, so that the constant *TG* of the Figure 7.17 is incorporated into the PI controller gains.

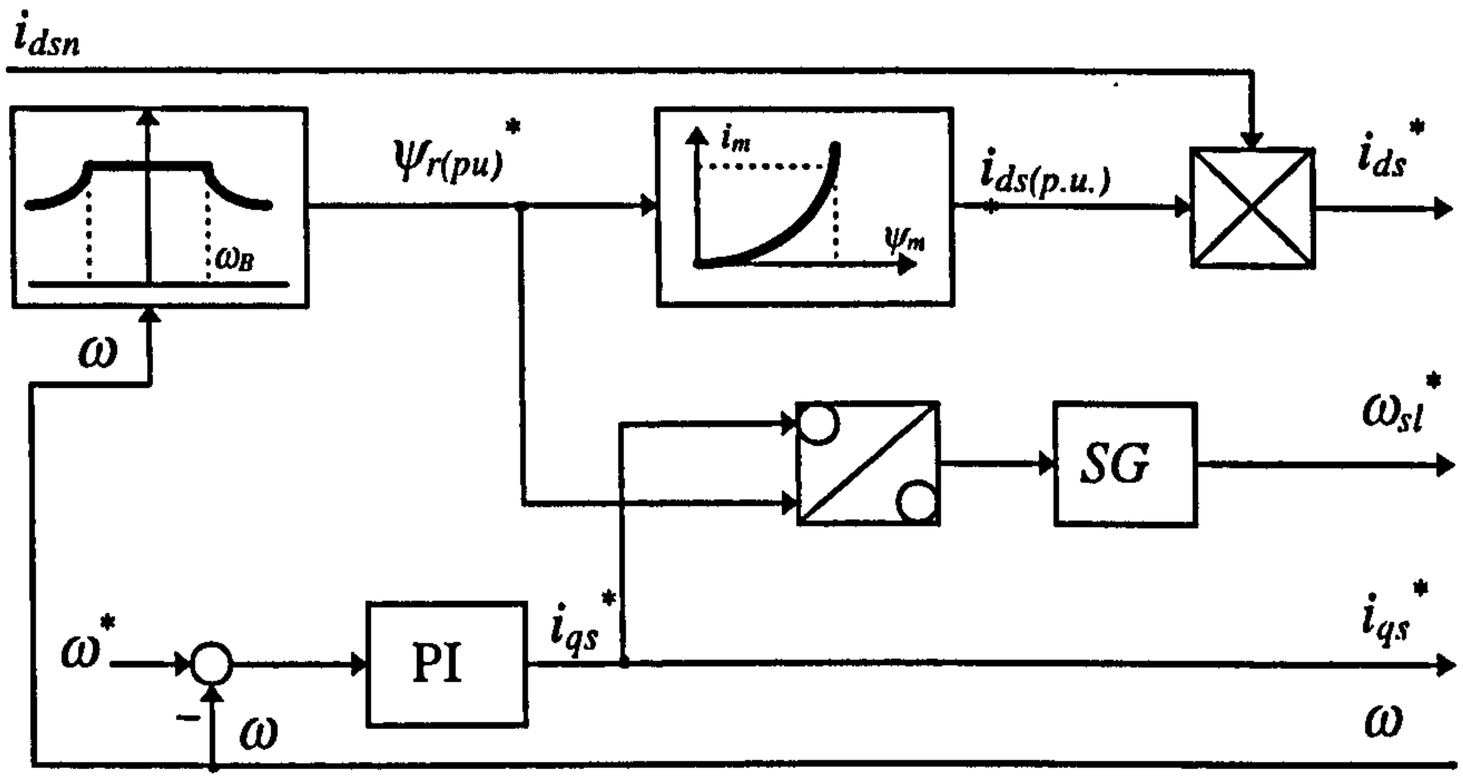

Figure 9.2: Indirect feed-forward vector controller of the Vickers drive with compensation of main flux saturation.

Parameters that can be changed by the user are the gains of the PI speed controller (KP and KI), rated stator d-axis current (ID), base speed at which field-weakening starts (MN), two parameters of the magnetising curve (FB and FS) and the slip gain (SG). Such a variety of user-adjustable parameters enables paring of an inverter to any motor that has rated power up to the inverter capability. Additionally, this enables great versatility of the drive and results in a very good performance in various applications, pending appropriate setting of these parameters.

Inverse magnetising curve of the machine, embedded in the controller of Figure 9.2 in per-unit form, is described with a simple approximation of the form

$$i_{m(pu)} = a\psi_{m(pu)} + (1-a)\psi_{m(pu)}^{b} \tag{9.1}$$

where $i_{m(pu)} = i^*_{ds(pu)}$ and $\psi_{m(pu)} = \psi^*_{r(pu)}$. The relevant parameters of this function (a and b) were identified for the motor under consideration by Sokola [1998]. Similarly, the correct slip gain was determined in [Sokola, 1998] as well. Thus a=0.9, b=7 and SG=47 (in DSP units) and these values are used in all experiments. The vector controlled drive with speed sensor therefore always operates under tuned conditions.

Parameters of the induction motor steady-state equivalent circuit were determined by Sokola [1998], using standard tests (no-load and locked rotor tests with sinusoidal supply) and are therefore known quantities (all the values are listed in Appendix A).

Loading of the vector controlled induction machine is provided by a DC machine. It is operated as a generator, feeding a resistor bank. The load torque therefore linearly rises with speed for a given resistor bank switch position, while the power rises with the square of speed. The switch in the 10 A position of the resistor bank corresponds to the rated torque of the induction machine at 1500 rpm [Sokola, 1998].

9.2.3 Design and implementation of the speed estimator

The two speed estimators used in the experimental investigation are the constant parameter MRAC speed estimator, discussed in section 4.2, and the novel modified MRAC speed estimator, that compensates the main flux saturation, described in section 8.3. As the binary control signals of the inverter switches could not be accessed within the controller, it was not possible to use reconstructed stator voltages. The inputs of the speed estimators are therefore measured stator voltages and stator currents. As the speed estimator is constructed based on the induction machine model in the stationary reference frame, three-phase voltages and currents need to be transformed into two phase (α-β reference frame) voltages and currents. The transformation, given with equation (2.15a), can be written as:

$$\begin{aligned} v_{\alpha s} &= \frac{2}{3}\left(v_a - \frac{1}{2}v_b - \frac{1}{2}v_c\right) = v_a \\ v_{\beta s} &= \frac{2}{3}\left(\frac{\sqrt{3}}{2}v_b - \frac{\sqrt{3}}{2}v_c\right) = \frac{\sqrt{3}}{3}\left(v_b - v_c\right) \end{aligned} \tag{9.2}$$

$$i_{\alpha s} = \frac{2}{3}\left(i_a - \frac{1}{2}i_b - \frac{1}{2}i_c\right) = i_a$$
$$i_{\beta s} = \frac{2}{3}\left(\frac{\sqrt{3}}{2}i_b - \frac{\sqrt{3}}{2}i_c\right) = \frac{\sqrt{3}}{3}\left(i_b - i_c\right) = \frac{\sqrt{3}}{3}\left(i_a + 2i_b\right) \tag{9.3}$$

Equation (9.2) applies to phase-to-neutral voltages of the motor. However, as the neutral point of the star connected stator winding cannot be approached, line-to-line voltages have to be used instead. Phase voltage α-β components can be given in terms of line-to-line voltages with the following expression:

$$v_{\alpha s} = \frac{1}{3}\left(v_{ab} - v_{ca}\right)$$
$$v_{\beta s} = -\frac{\sqrt{3}}{3}\left(v_{ab} + v_{ca}\right) \tag{9.4}$$

As indicated by (9.3), α-β components of the stator current ask for measurement of only two currents, since the sum of the three-phase currents always equals zero in a star connected winding with isolated neutral. Currents of phases a and b are therefore measured.

Circuits for voltage and current measurement have been designed and built. The inputs of the voltage circuit card are three voltages of phases a, b, and c with respect to ground and the outputs of the card are attenuated and filtered line-to-line voltage signals v_{ab} and v_{ca}. For current measurement, Hall effect current sensors were used. The inputs of the current circuit card are phase currents, i_a and i_b, and outputs of the card are attenuated current signals of i_a and i_b. Both the outputs of the voltage card and current card are then sent to an A/D card (PCI-DAS1200) installed in the computer. The sampling frequency of the A/D card is 20 kHz for each signal. A PC with LabVIEW software is used for data acquisition and it collects all the signals. The detailed circuit schematic is given in Appendix D. The data obtained in this way are stored in a file and used further on to investigate the operation of the speed estimator.

The operation of the voltage and current measurement circuits and the data acquisition system was at first tested using sinusoidal supply and was found to be satisfactory. However, operation with the inverter proved to be of much poorer quality. The sampled input data of a voltage and a current are illustrated in Figure 9.3.

It can be seen from Figure 9.3 that the voltage and current waveforms contain certain high frequency harmonics, although analogue filtering of the input voltages and currents was performed at the measurement stage. No attempt was made to find out the source of this distortion. Instead, the waveforms are filtered before being used as inputs

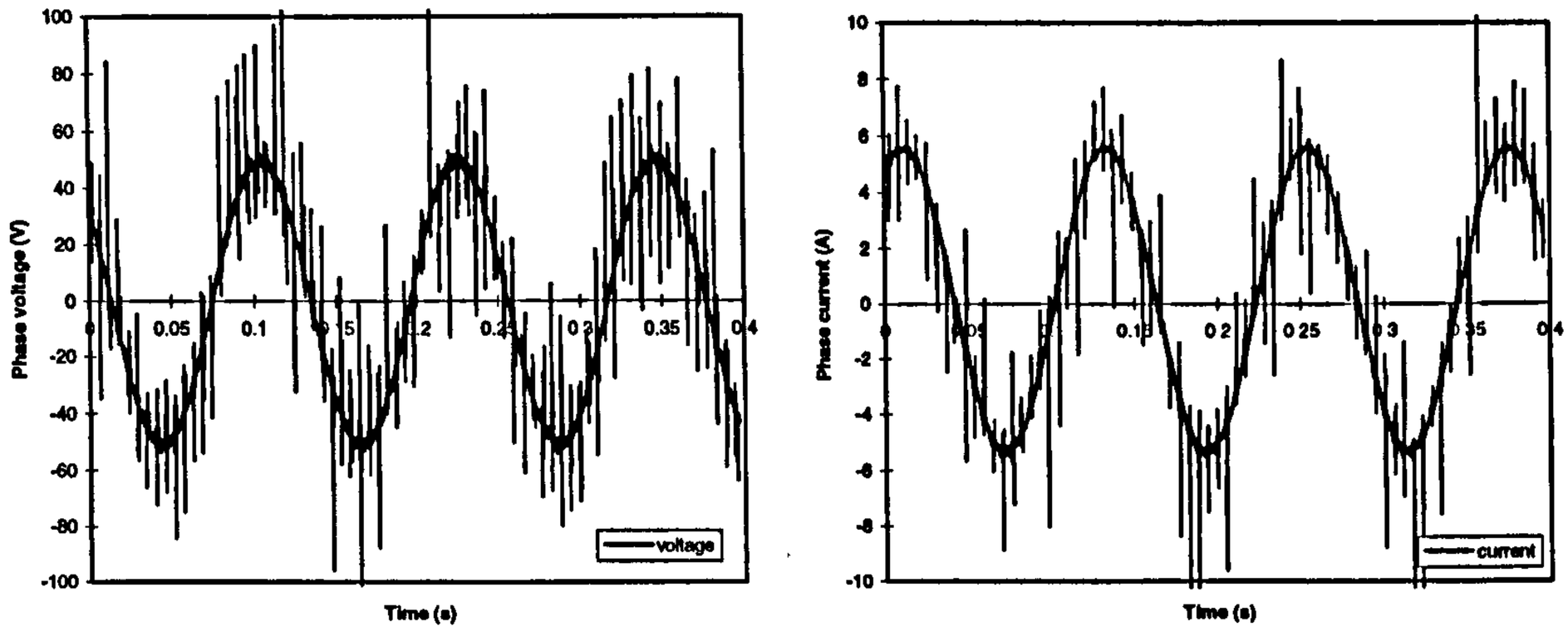

Figure 9.3: Sampled phase voltage and phase current.

to the speed estimator. For this purpose, Butterworth low-pass filters in Matlab are used for each input signal. The filtered voltage and current are shown in Figure 9.4. The selected parameters of the filter are: cut-off frequency = 500π rad/s, order = 2.

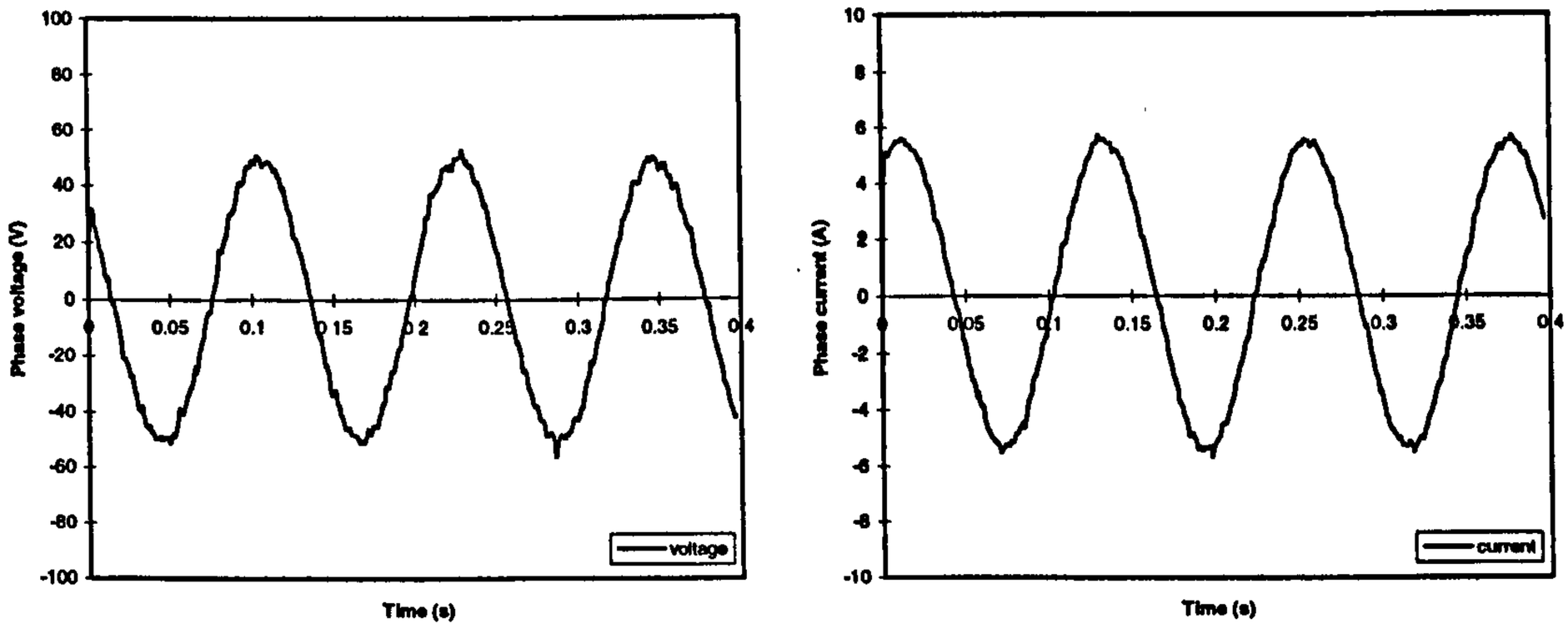

Figure 9.4: Filtered phase voltage and phase current.

It can bee seen that high frequency harmonics have been greatly attenuated. The signals can now be used as the inputs of the speed estimators.

It should be noted that use of Butterworth filters does introduce a phase shift in the filtered voltage and current waveforms. However, as the same phase shift in introduced in both α and β components of both voltages and currents, and due to the structure of

the speed estimator (that yields the speed estimate by forcing the position of the two rotor flux space vectors to the same value), accuracy of speed estimation is not affected in any way by this additional filtering.

9.2.4 Monitoring of the actual speed

The vector controlled induction machine system comes with resolver as the speed sensor. The speed information can be obtained from the panel of the vector controller, which is a blank ± 10 V voltage signal with resolution of 800 rpm/V. The actual speed signal is recorded by the HP35665A dynamic signal analyser and saved as text file. As the probe of the analyser detects the signal with 1/10 attenuation, the actual speed should be equal to the voltage signal timed with the scaling factor of 8000. However, for an unknown reason, this scaling factor was found not to be correct.

In order to find the correct scaling factor, the following procedure is used. In no-load operation, rotor speed is close to the synchronous speed. Even more so, if the reference speed is set to a low value, where mechanical and iron loss become very small.

The synchronous speed can be obtained by analysing the current signal in no load conditions through FFT analysis.

Figure 9.5 illustrates stator phase current spectra for no-load operation at 500 rpm.

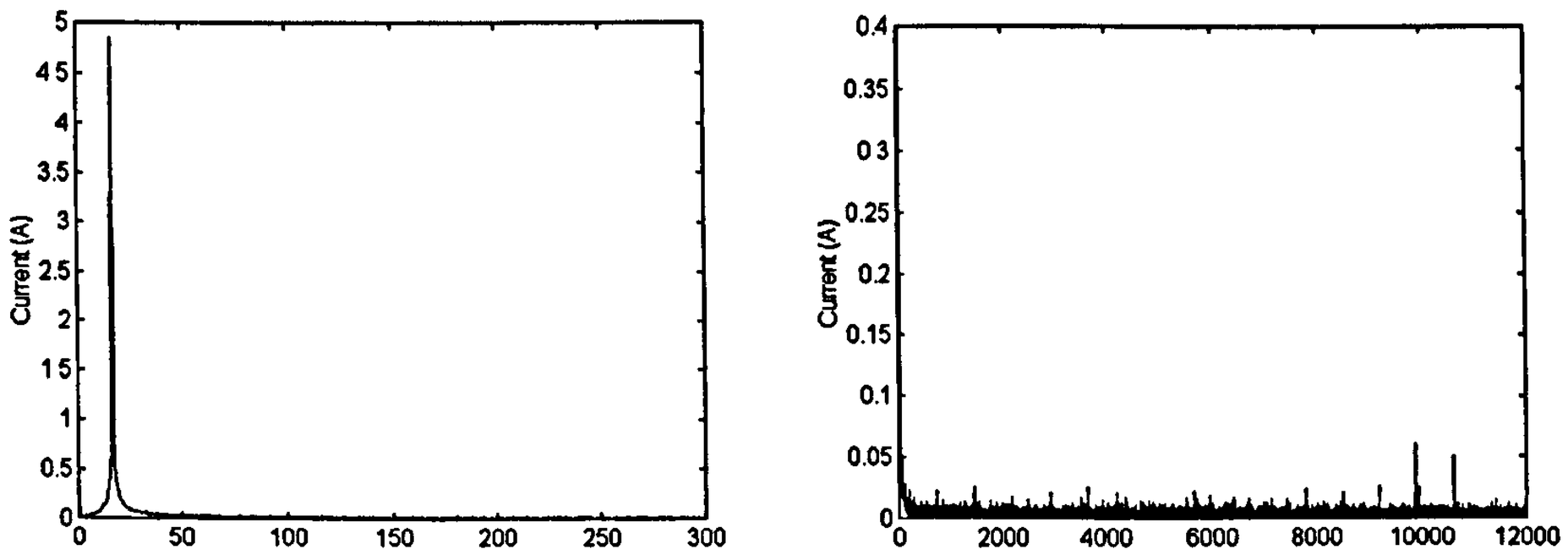

Figure 9.5: Current spectra during PWM no-load operation at 500 rpm: a) spectrum up to 300 Hz; b) spectrum up to 12 kHz.

The frequency of the fundamental component for this operation is 16.63 Hz, Figure 9.5a. It corresponds to the synchronous speed of 500 rpm. By measuring the actual speed, and knowing that it has to be 500 rpm, the value of the scaling factor was

determined. Therefore, the actual scaling factor used in subsequent studies is set to 8600, which will convert the voltage signal to the correct actual speed value.

9.3 Tuning of the speed estimator

9.3.1 Tuning of induction motor parameters

An experiment is at first conducted under no load conditions in the base speed region. The commanded speed is 500 rpm and the data are recorded over 4 seconds interval. All the data are saved and are further used as inputs into Simulink model of the speed estimator. As already noted, the actual speed was recorded using HP35665A analyser, while the voltage and current signals were recorded through A/D card in the PC. It is obvious that the time instant in which data recording starts is not the same for the actual speed and the data acquisition system. In order to compare the actual speed and the estimated speed, zero time instant has to be shifted for one of the two speeds. Consequently, the time scales in the figures displaying speed are shifted, while time scales for all the figures giving currents and voltages are the original time scale of the data acquisition procedure.

The purpose of the experiments at 500 rpm reference speed under no-load conditions is to investigate whether the parameters of the motor used in the speed estimator exactly correspond to those of the machine. Since the operation is without load, at a low speed of rotation, the relevant parameters of the motor in steady-state operation are the magnetising inductance and the stator leakage inductance (essentially, the stator self-inductance). Stator resistance has negligible impact on accuracy of speed estimation in this case since the operation is under no-load conditions. Figure 9.6 shows estimated and actual speed during no-load acceleration from zero to 500 rpm and the corresponding stator phase current. Zoomed portion of the Figure 9.6a for steady-state operation, shown in Figure 9.6c, reveals that speed estimation error is of the order of 1-2 rpm, that is, negligibly small. It can therefore be concluded that values of the rated magnetising inductance and the stator leakage inductance, used in the speed estimator, are well tuned.

The same experiment was repeated for loaded operation. The switch was put in the 10 A position on the resistor bank. This means that the applied load torque at 500 rpm

speed is approximately 1/3 of the rated. The estimated and actual speed are compared in Figure 9.7a. The purpose of this test is to establish whether the setting of the remaining parameters in the speed estimator (most of all, rotor resistance) is correct.

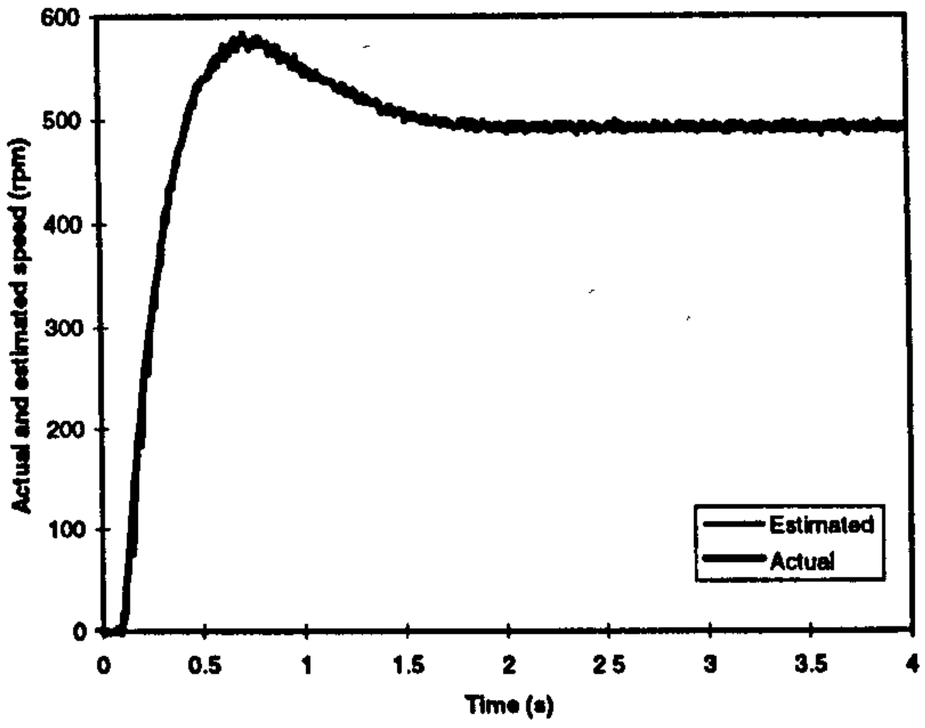

a)

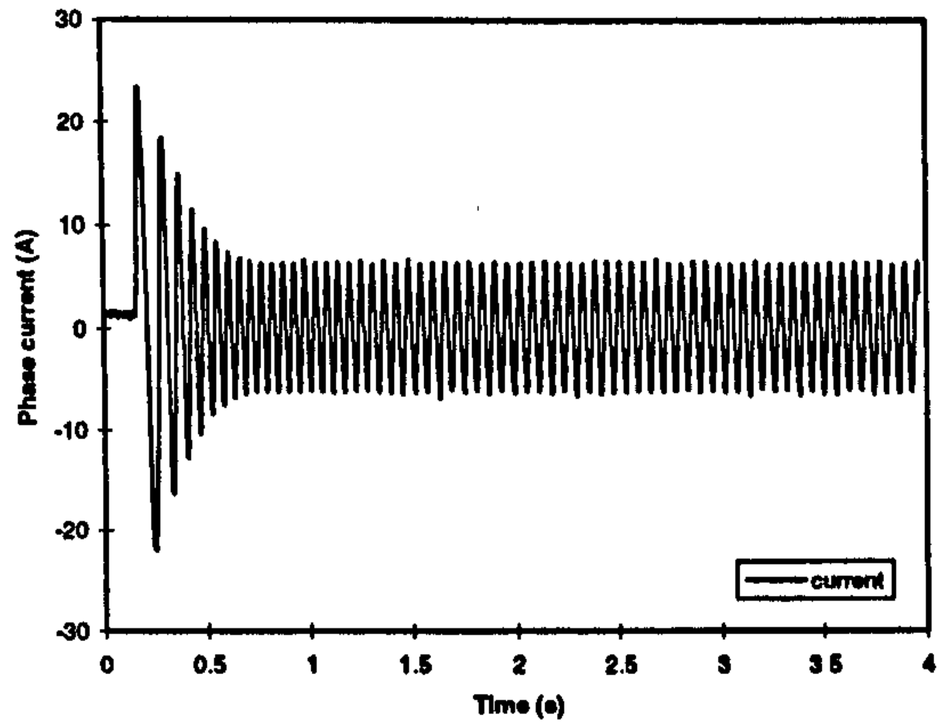

b)

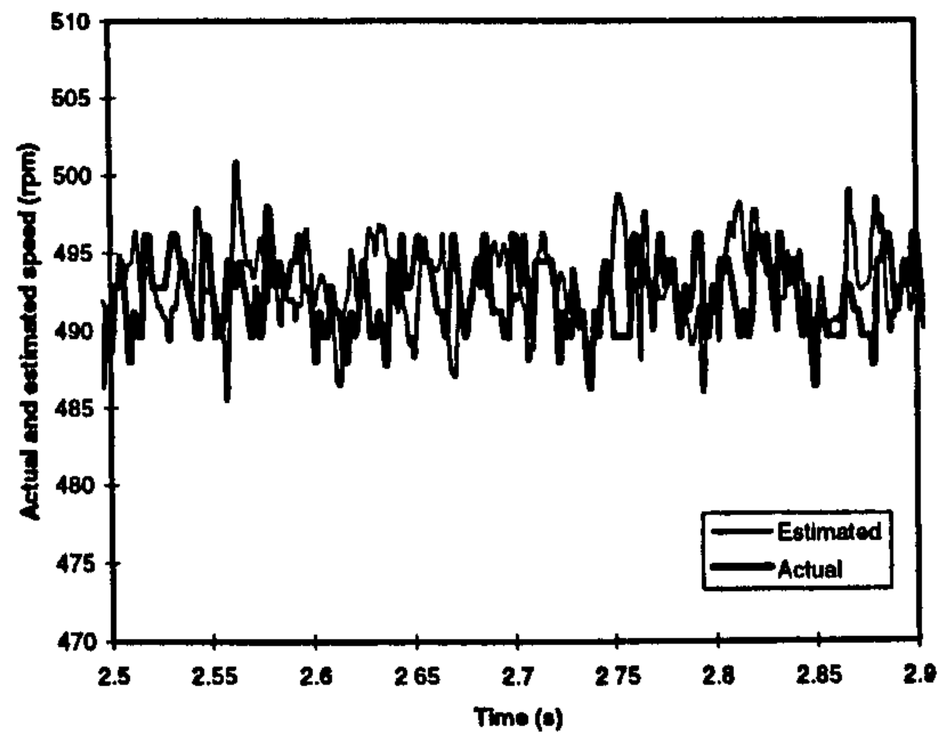

c)

Figure 9.6: a) Actual speed and estimated speed under no-load conditions at 500 rpm set speed. b) Stator phase current. c) Extract from a).

It can be seen from Figure 9.7a that the estimated speed and the actual speed differ considerably in steady-state. The estimated speed is lower that the actual speed. The estimation error is about 20 rpm.

On the basis of the analysis of chapter 6, one can assign this error in speed estimation to the detuned value of the rotor resistance in the speed estimator. The value of the motor rotor resistance, R_{rn} of Appendix A, was determined in [Sokola, 1988] using locked rotor test under nominal thermal conditions. Hence the value of R_{rn} applies to 50 Hz rotor frequency and to rated operating temperature. However, in a vector controlled drive, rotor frequency does not exceed the value of approximately 5 Hz in the base speed region. Moreover, all the experiments described here apply to operation of the machine in more or less cold state. Thus it follows that a different, smaller value of

rotor resistance needs to be used in the speed estimator instead of the R_{rn} value. Traces of Figure 9.7a are used to find the most appropriate rotor resistance value, that will yield near-zero speed estimation error. It was established in this way that the proper rotor resistance value is $R_{rn}^{*}=0.5R_{rn}$. Speed traces for this rotor resistance value are compared in Figure 9.7b and 9.7c.

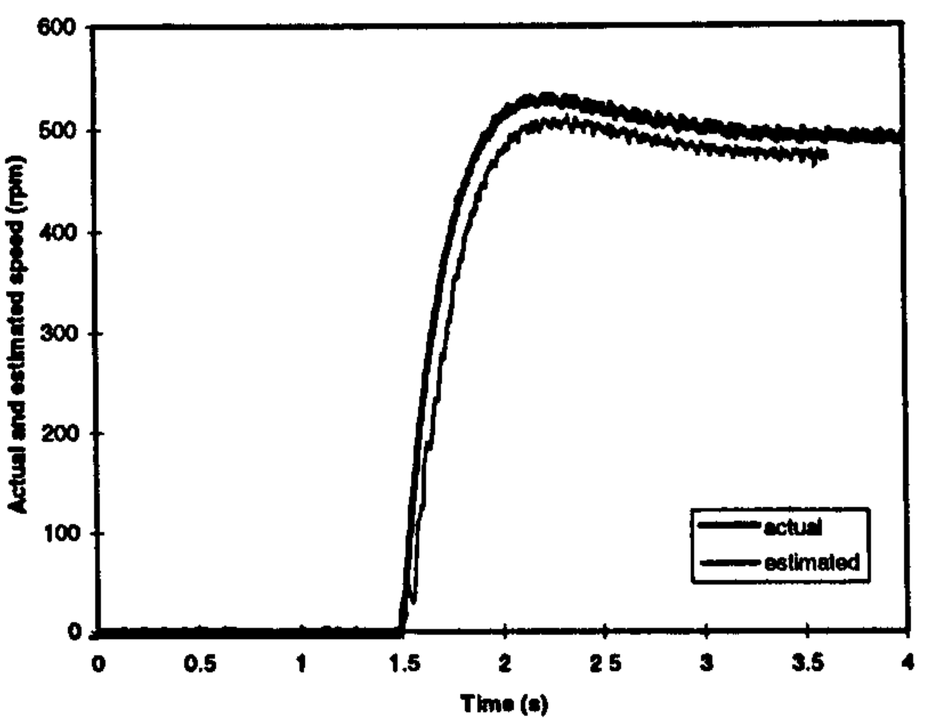

a)

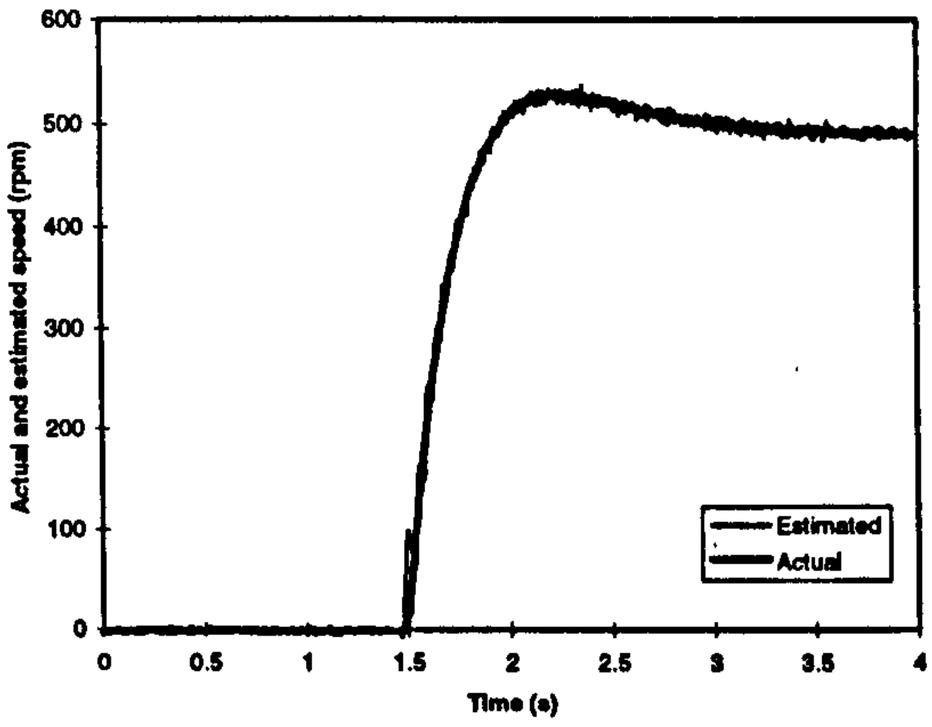

b)

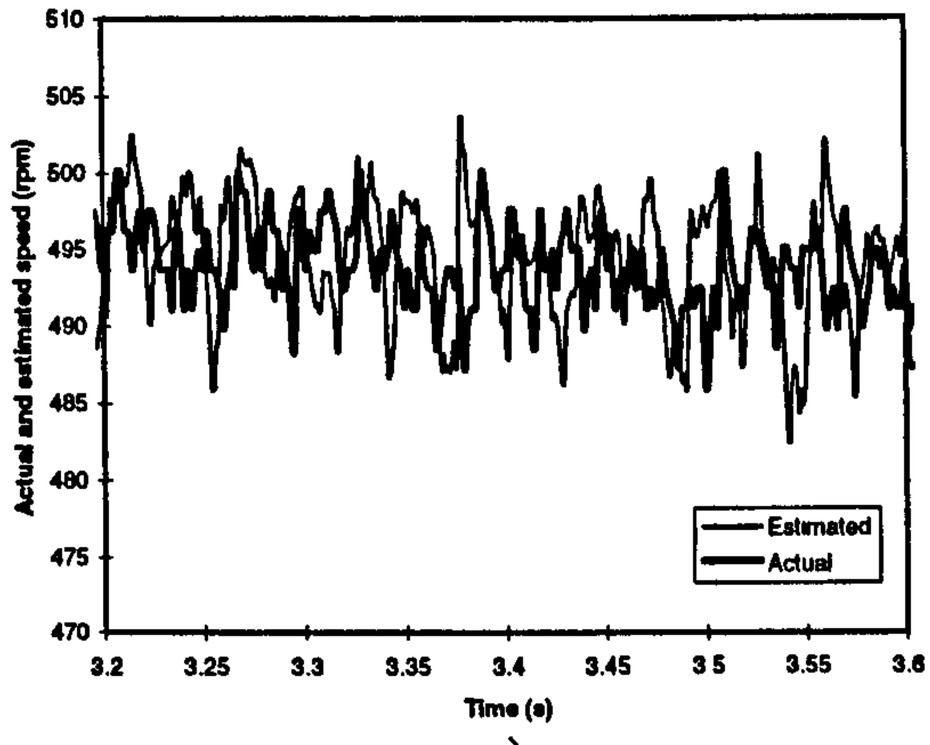

c)

Figure 9.7: Actual and estimated speed in loaded operation: a) rotor resistance equal to the rated; b) rotor resistance equal to one half of the rated; c) extract from b).

Results of Figure 9.7b show that the estimated speed is now in good agreement with the actual speed. The speed estimation error in steady-state is the same as under no-load conditions. The rotor resistance in the speed estimator is set to $0.5R_{rn}$ for all subsequent investigations.

9.3.2 Filtering of the speed estimate

One specific problem encountered in the operation of the speed estimator is that the speed estimate is characterised with a high level of noise. As such, it would be inappropriate for direct use for closed-loop speed control and field orientation. High level of noise is due to the high gains of the PI controller within the speed estimator.

High gains are necessary since the input into the PI controller is essentially the angular difference between the two rotor flux estimates. The output of the speed estimator is therefore subjected to additional filtering using a first order filter with transfer function $1/(1+T_1p)$. Figure 9.8 shows the two estimated speeds for the 500 rpm acceration transient under no-load conditions. The estimated speed shown in Figure 9.8a is not filtered. The estimated speed shown in Figure 9.8b is filtered. The results show that the quality of the estimated speed has been greatly improved. It has to be noted that the speed estimate that is used in the adjustable model is the unfiltered one (i.e. Figure 9.8a). The filtered estimate, Figure 9.8b, is aimed for use as the speed feedback signal and for field orientation. The speed estimate shown in all the previous and the subsequent figures is the filtered one.

It is obvious that inserting a filter in the estimated speed channel will cause time delay and affect the response time. A compromise value of T_1 is selected in such way that smoothed estimated speed is obtained and time delay is reasonably small. Figure 9.9 shows the estimated speeds for different values of T_1.

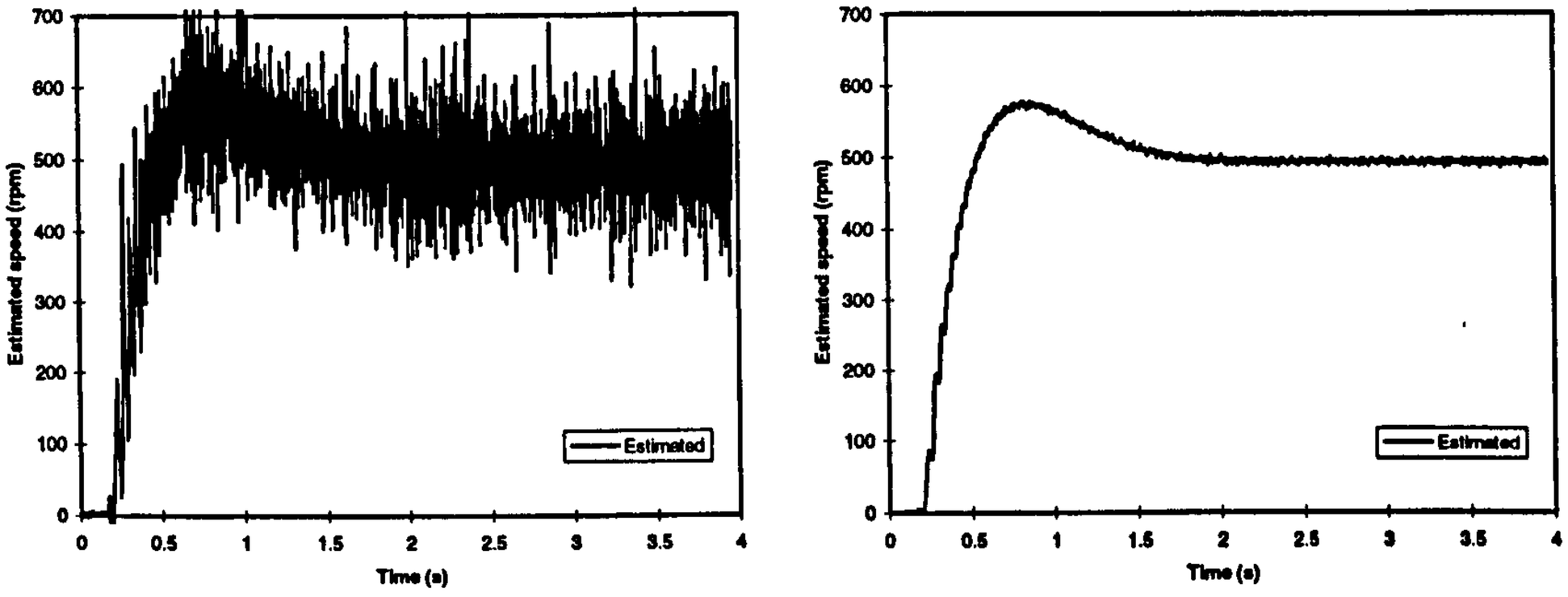

Figure 9.8: Estimated speeds: a) without the first order filter, b) with the first order filter.

It can be seen from Figure 9.9b that the filtered estimated speed is much smoother when time constant T_1 increases. However, the time delay is also larger due to larger time constant. In order to minimise the error caused by the time delay, the time constant T_1 is set to 0.03. This value gives reasonably smoothed estimated speed and small time delay. Figure 9.9c shows the actual speed and estimated speed for T_1=0.03.

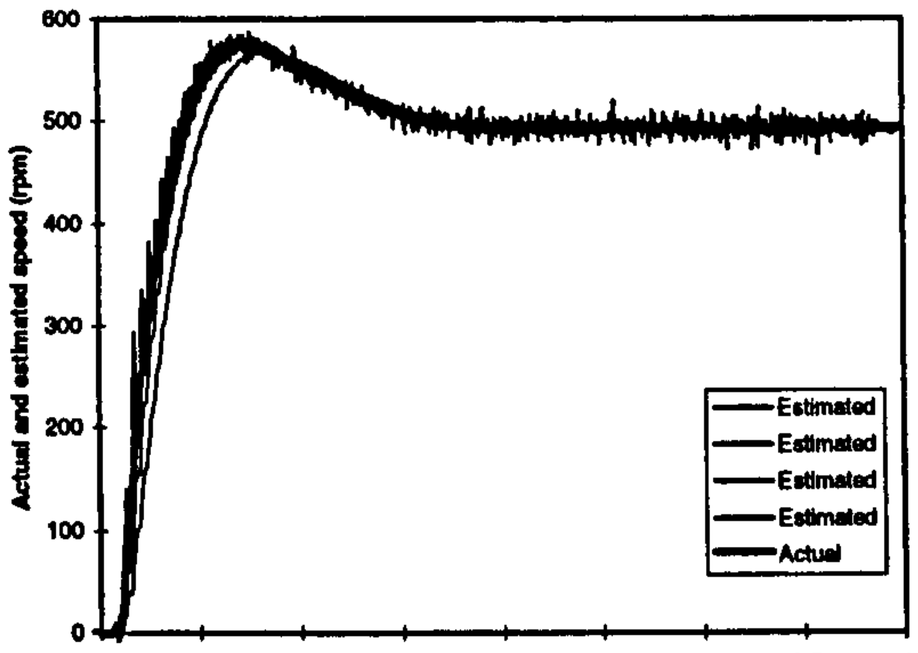

a)

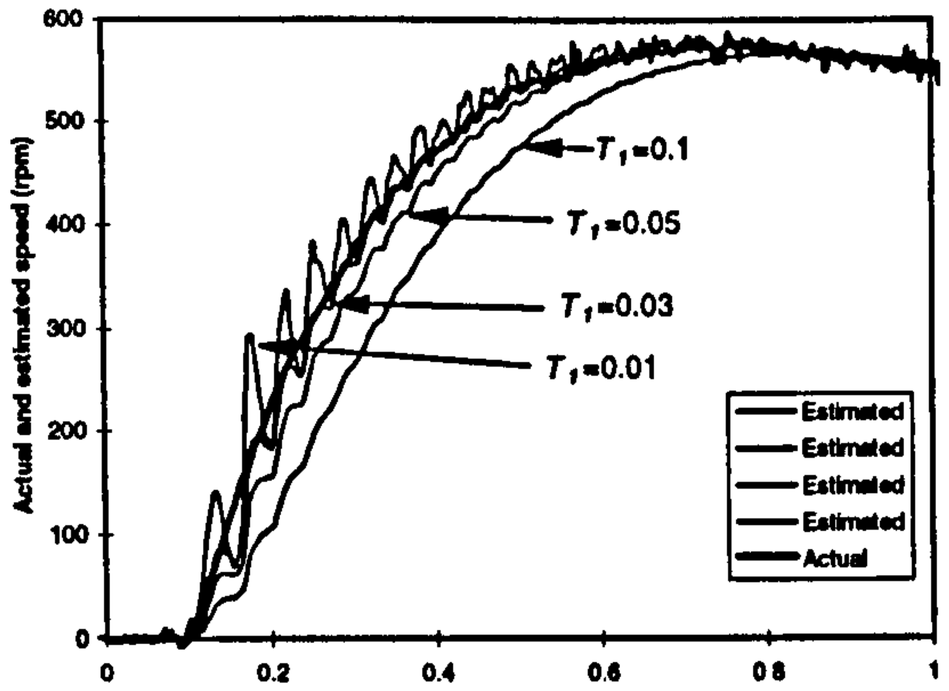

b)

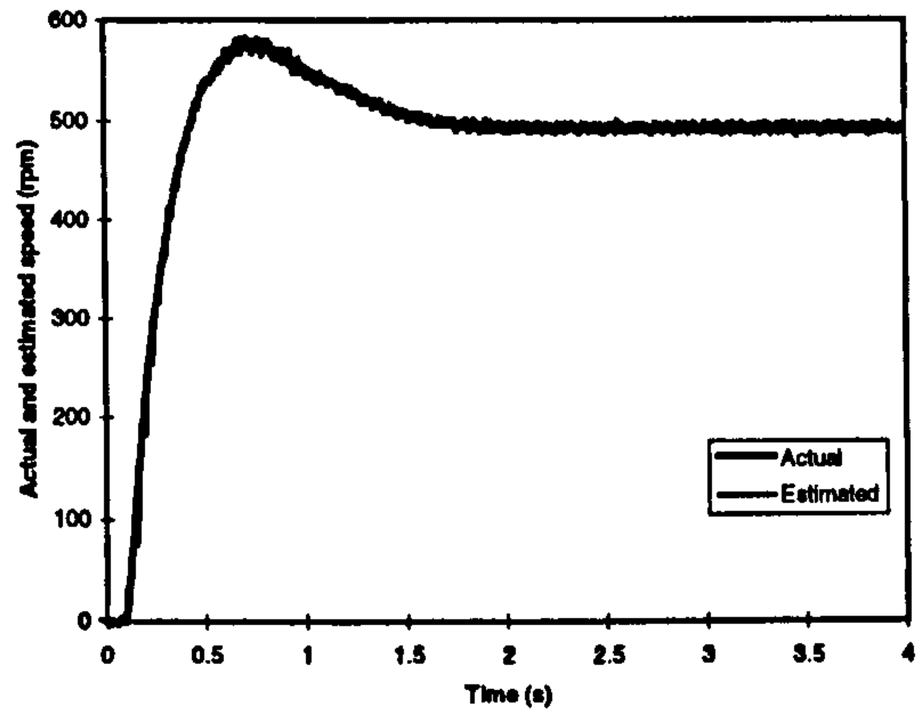

c)

Figure 9.9: Actual and estimated speed: a) estimated speeds with T_1=0.01, 0.03, 0.05 and 0.1, respectively; b) zoomed extracts from a); c) actual and estimated speed with T_1=0.03.

9.3.3 Tuning of the integrator filters

The parameter in transfer function $\frac{p}{p+(1/T)}$ employed in the output of both the reference and adjustable model is selected in such way that the best behaviour of the estimated speed is obtained. Figure 9.10 shows the estimated speed for different values of $1/T$ for the same no-load 500 rpm acceleration transient.

It can be seen from Figure 9.10 that the estimated speed is affected by the value of $1/T$. The largest difference between the estimated speeds is in vicinity of zero speed. When $1/T$= 100 is used, the estimated speed error is quite large. The error is reduced as value of $1/T$ increases. It can be seen that the best estimated speed is obtained with $1/T$=800. Therefore, this value is used in the speed estimator further on.

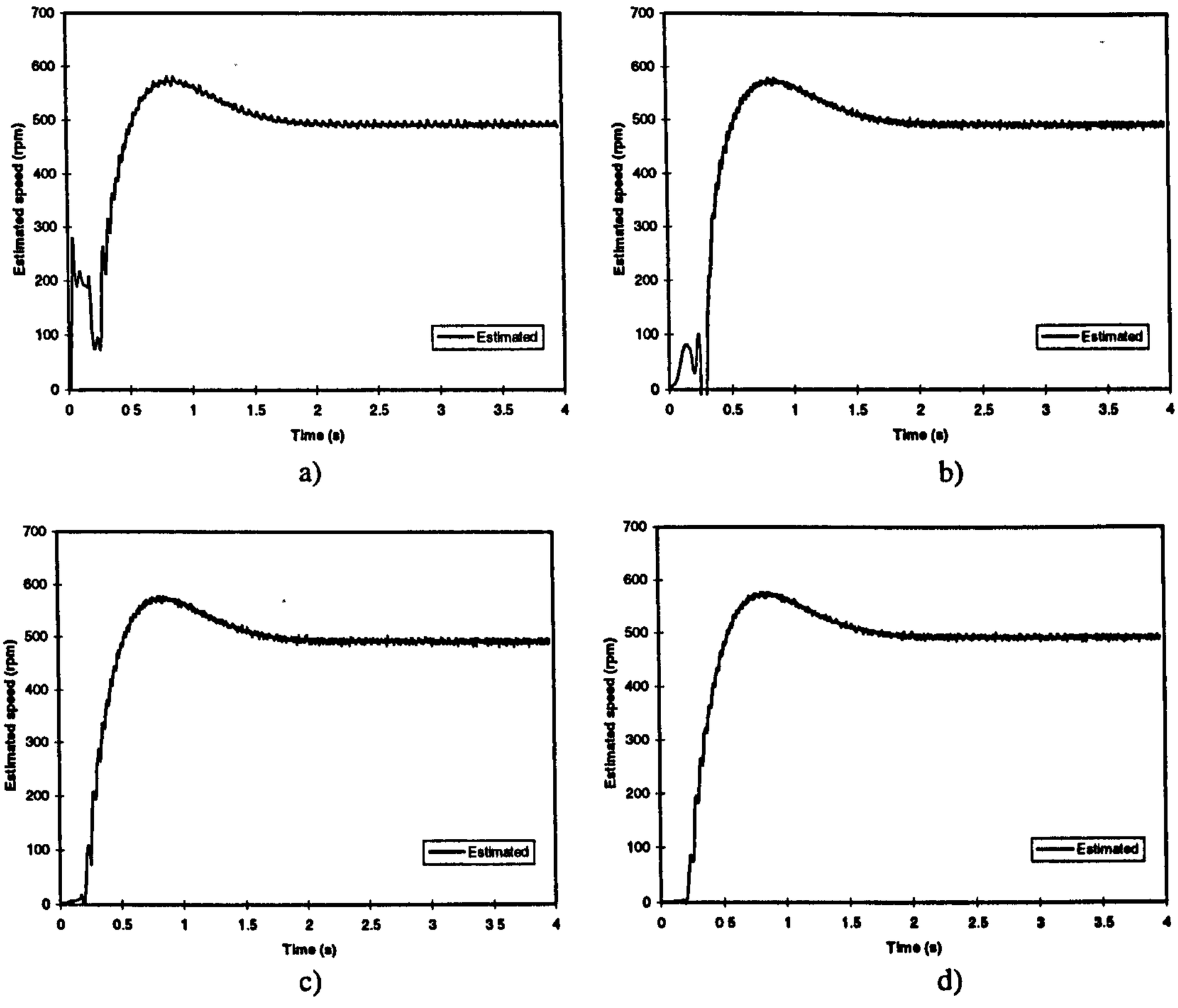

Figure 9.10: Estimated speed for T_l=0.03s and: a) $1/T$=100, b) $1/T$=300, c) $1/T$=500, d) $1/T$=800.

9.3.4 Tuning of the PI controller

As already noted, parameters of the PI controller within the speed estimator have a profound influence on the quality of the speed estimate. Figure 9.11 illustrates the speed estimate for the same 500 rpm no-load acceleration transient, obtained using three distinctly different pairs of PI controller gains. The values K_p = 150 and K_i = 800 are used for subsequent work (and apply to all the previously presented results as well).

Figure 9.12 illustrates the complete structure of the constant parameter speed estimator used in experimental investigation. Parameters of the motor used in the adjustable and reference model are those of subsection 9.3.1. The values of all the other estimator parameters, tuned as described in various subsections of this section, are kept at values shown in Figure 9.12 in subsequent work.

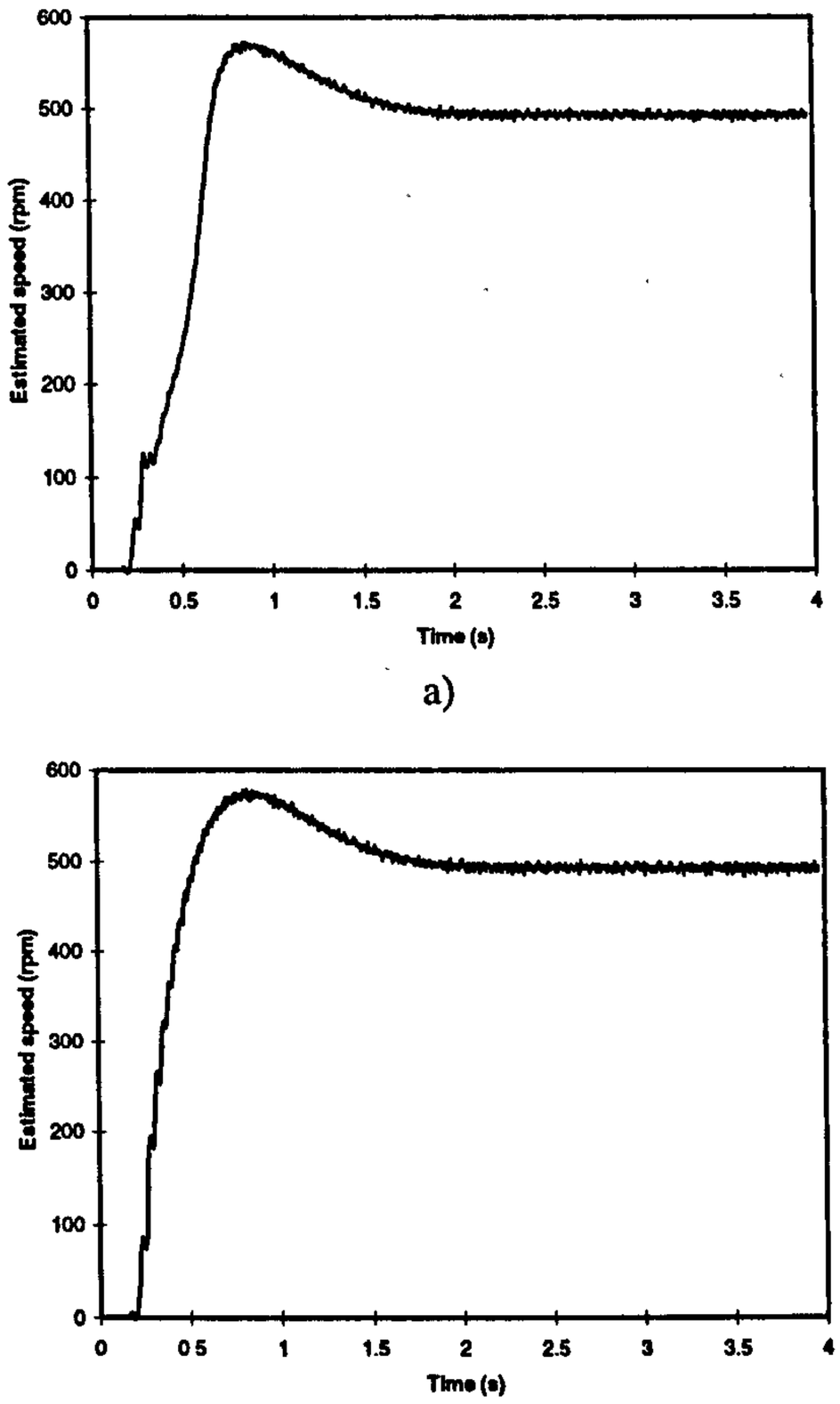

Figure 9.11: Estimated speed for $1/T$=800 s^{-1}, T_1 = 0.03 s and: a) K_p= 50, K_i = 100; b) K_p=300, K_i=1000; c) K_p = 150, K_i=800.

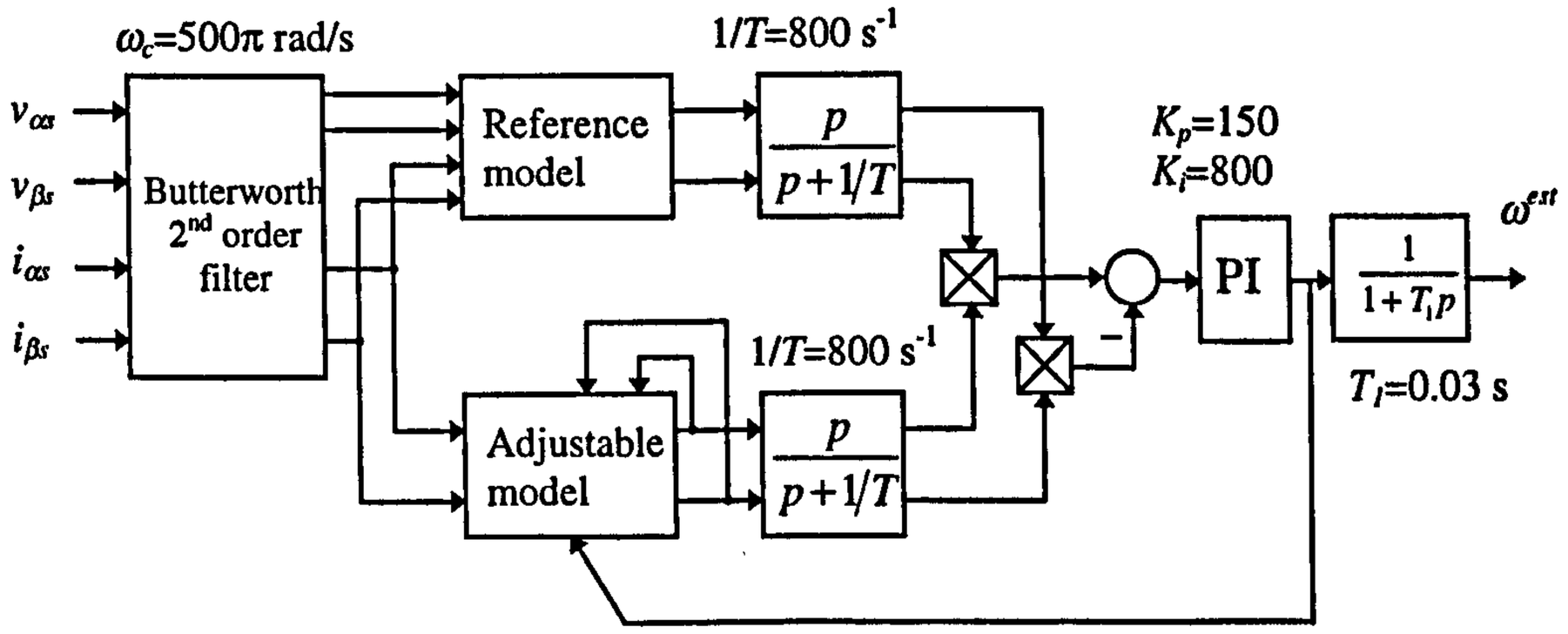

Figure 9.12: Implementation of the constant parameter MRAC speed estimator.

9.4 Operation of the speed estimator in the base speed region - tuned conditions

Two sets of experiments are performed, for operation under no-load conditions and operation with load, respectively. The base speed is set to 1500 rpm. The first set of experiments comprises of acceleration transients under no-load conditions for different speed commands. The experiments for speed command of 900 rpm, 1200 rpm and 1500

rpm were performed. The second set of experiments consists of acceleration transients of the loaded machine. The switch of the resistor bank is on the 10 A position for all the speed commands. Speed commands were the same as those in no-load conditions. The constant parameter speed estimator is used. Comparison of actual and the estimated speed is shown in Figure 9.13 for all the speed commands and both no-load and loaded operation.

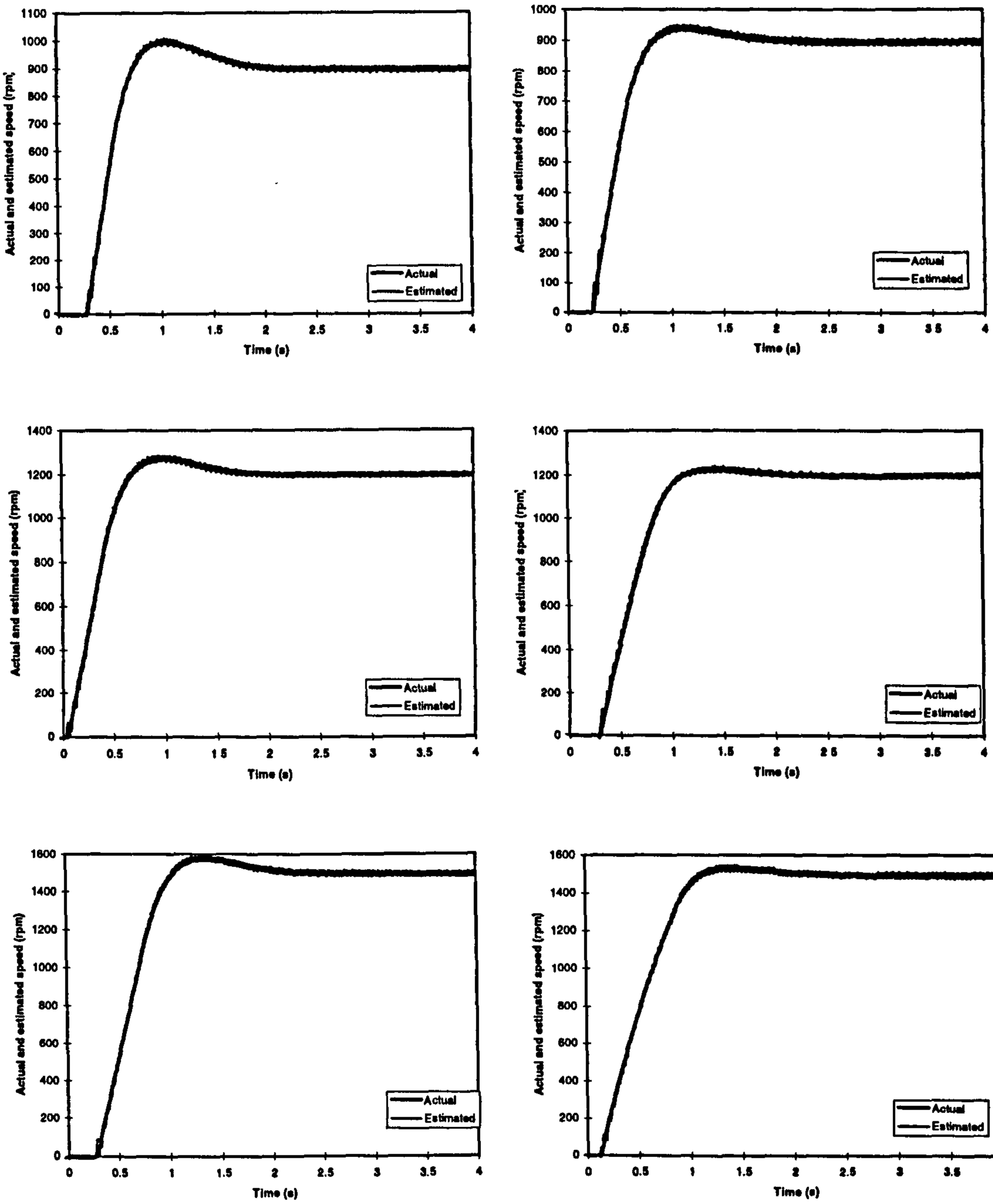

a) b)

Figure 9.13: The estimated speed and actual speed for speed commands of 900 rpm, 1200 rpm and 1500 rpm, respectively: a) no-load operation, b) loaded operation.

One observes from Figure 9.13 that estimated and actual speed are in very good agreement, both during the transient and in subsequent steady-state operation.

The speed estimation errors for no-load cases are about 1-2 rpm. With an increase in the load, the speed estimation error slightly increases and is about 4 rpm for rated torque operation at 1500 rpm. Figure 9.14 presents zoomed extracts from Figure 9.13 that

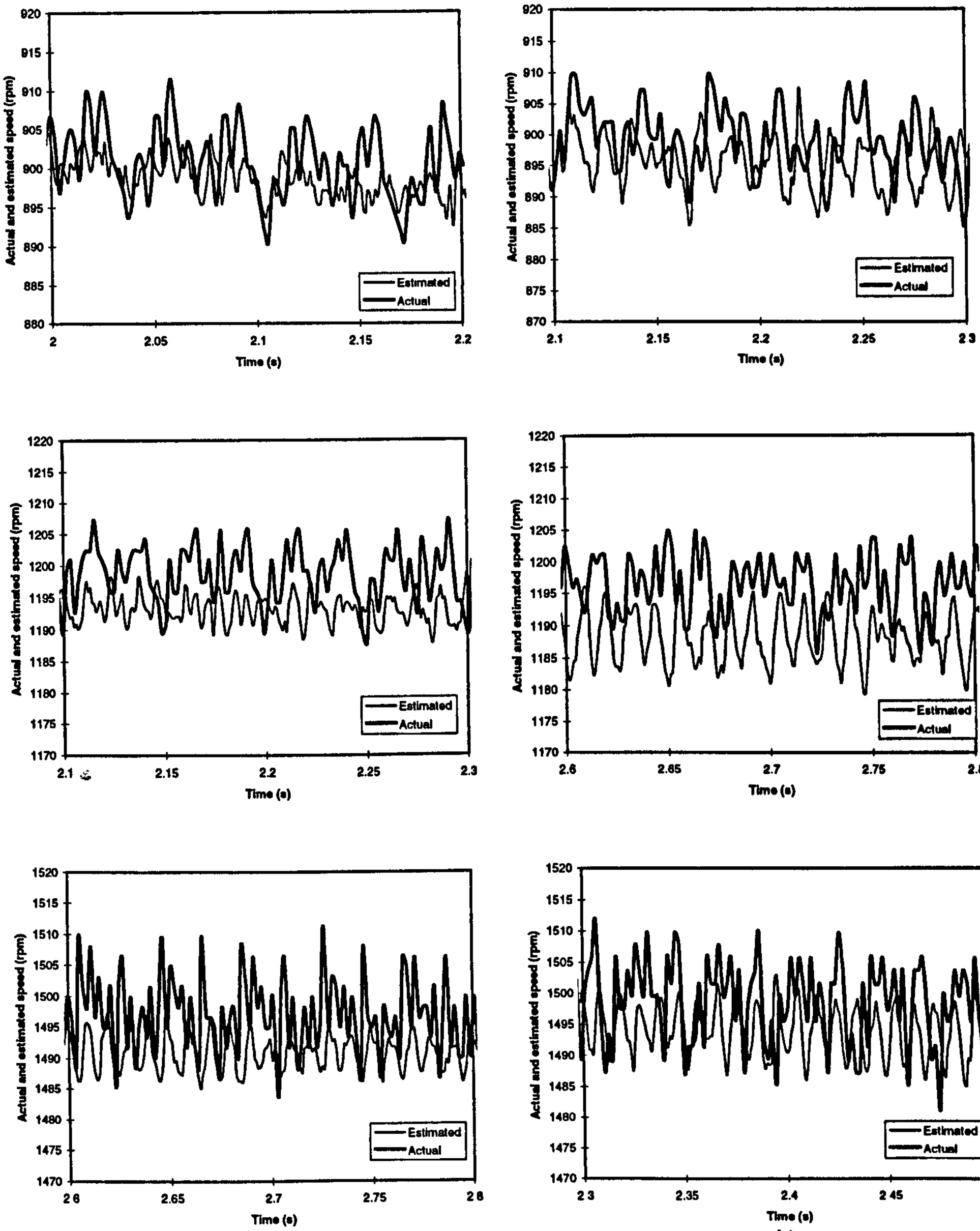

Figure 9.14: Zoomed extracts from Figure 9.13: a) no-load steady-states, b) steady-state with load.

show actual and estimated speed in final steady-states. Cited approximate speed estimation errors serve as a guide-line only, since the noise in Figure 9.14 clearly prevents any accurate reading.

Experiments for deceleration transients were performed as well. When the machine was running in steady-state at 900 rpm, the speed command was reduced from 900 rpm to 500 rpm. The phase current, the phase voltage and the estimated and actual speed are shown in Figure 9.15 for deceleration transient under no-load conditions and with load. The speed estimator once more gives good prediction of the actual speed of rotation.

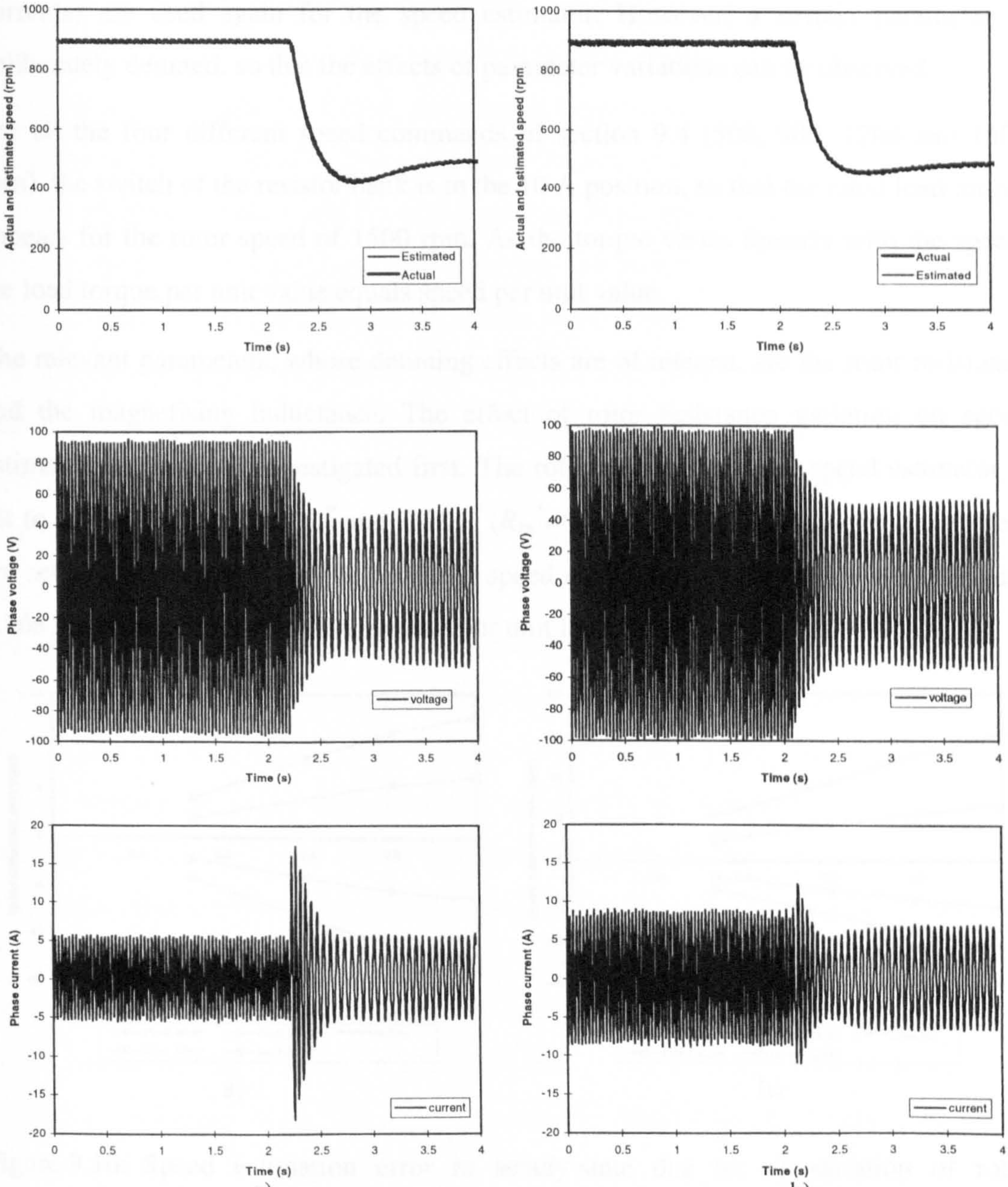

a) b)

Figure 9.15: Speed response for deceleration transient (900 rpm to 500 rpm): a) no-load conditions, b) loaded operation.

9.5 Operation of the speed estimator in the base speed region - detuned conditions

Parameter variations will cause detuned operation of the speed estimator. In this section, parameter variation effects are investigated using experimental data. In order to investigate the detuning caused by incorrect setting and/or parameter variations, the constant parameter speed estimator was used to estimate the rotor speed.

The approach to the assessment of the speed estimation error caused by incorrect parameter values is the following. Actual speed has been measured for a number of transients and was shown in the section 9.4. The corresponding input data (voltages and currents) are used again for the speed estimator. However, a certain parameter is deliberately detuned, so that the effects of parameter variations can be observed.

For all the four different speed commands of section 9.4 (500, 900, 1200 and 1500 rpm), the switch of the resistor bank is in the 10 A position, so that the rated load torque appears for the rotor speed of 1500 rpm. As the torque varies linearly with the speed, the load torque per unit value equals speed per unit value.

The relevant parameters, whose detuning effects are of interest, are the rotor resistance and the magnetising inductance. The effect of rotor resistance variation on speed estimation accuracy is investigated first. The rotor resistance in the speed estimator is set to values between $0.8R_{rn}^*$ and $1.2R_{rn}^*$ ($R_{rn}^*=0.5R_{rn}$), while all the other parameters are set to the rated values. The resulting speed estimation errors are shown in Figure 9.16a for steady-state operation, against per unit load torque.

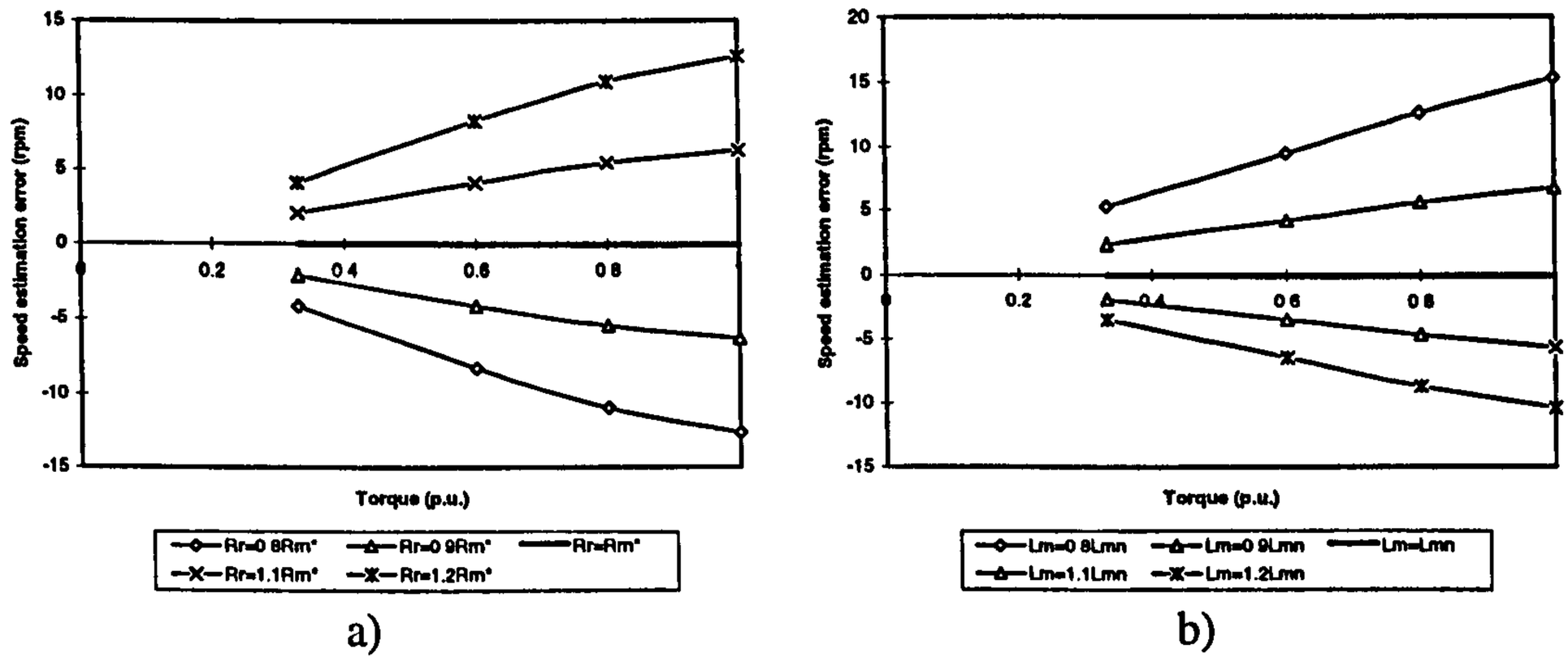

Figure 9.16: Speed estimation error in steady-state due to: a) variation of rotor resistance, b) variation of magnetising inductance.

It can be seen that speed estimation error ($\Delta n=n-n^{est}$) is load dependent. When the rotor resistance is smaller than the rated value, the estimated speed is higher than the actual speed. When the rotor resistance in the speed estimator is larger than the rated value, the estimated speed is lower than the actual speed, Figure 9.16a. When rotor resistance varies by ± 20 %, the maximum speed error is about 13 rpm at 1500 rpm with the rated torque.

Direct comparison of the experimental results in Figure 9.16a with results of the theoretical study, presented in section 6.6 (Figure 6.9a), is not possible because of the difference in the procedures used in theoretical and experimental investigation. While in the theoretical work detuning simultaneously took place in both the indirect vector controller and the speed estimator, detuning in experiments is introduced in the speed estimator only. Additionally, estimated speed was used in chapters 6 and 7 for both closed-loop speed control and the transformation angle calculations, while here actual speed is used for these purposes. Nevertheless, comparison of Figures 9.16a and 6.9a shows striking similarities. Speed estimation error increases almost linearly with the load torque, detuning of the rotor resistance by the same amount in plus/minus direction causes speed estimation errors of the same absolute value and opposite signs, and, finally, even the values of the speed estimation error are very similar although the machines are quite different (maximum error, for rated torque operation, is ± 13 rpm in Figure 9.16a and ± 10 rpm in Figure 6.9a). One important difference is that the speed estimation error is of opposite sign in Figures 6.9a and 9.16a for the same amount of detuning in the rotor resistance. This difference is only apparent however. Figure 6.9 was obtained by keeping the rotor resistance value in the controller/estimator at rated and by varying the rotor resistance in the motor. Hence rotor resistance value of for example 1.2 times the rated means in Figure 6.9 that rotor resistance in the motor is 20% higher than the value in the controller/estimator. In contrast to this, rotor resistance of 1.2 times rated in Figure 9.16a means that resistance in the estimator is 20% higher than the one in the motor. To put it simply, coefficient of 1.2 in Figure 6.9a corresponds to 1/1.2=0.83 in Figure 9.16a, while coefficient of 0.8 in Figure 6.9a corresponds to 1/0.8=1.25 in Figure 9.16a. The sign of the speed estimation error predicted by theory and by experiments is therefore the same.

The information compiled in Figure 9.16a was extracted from the traces illustrated in Figure 9.17. Due to the noise present in the signals, some error is inevitably present in extracted values in Figure 9.16.

The effects of the magnetising inductance incorrect setting on the speed estimation are studied next. The magnetising inductance in the speed estimator varies from 0.8 to 1.2 of the rated value, while all the other parameters are set to the rated values. The results, compiled and extracted in the same way as explained in conjunction with Figure 9.16a are shown in Figure 9.16b.

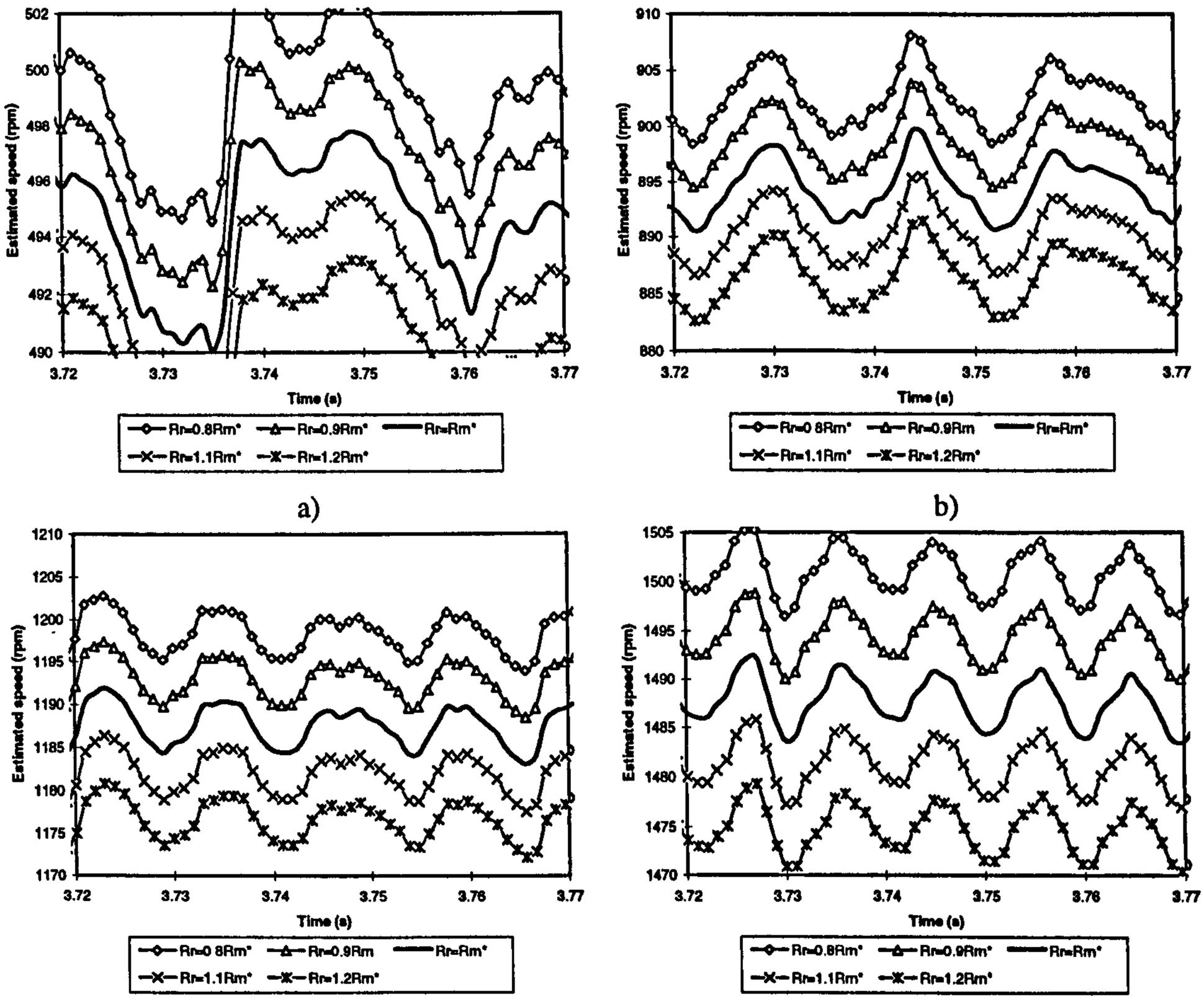

Figure 9.17: Impact of detuned rotor resistance on speed estimation accuracy: a) speed command of 500 rpm, b) speed command of 900 rpm, c) speed command of 1200, d) speed command of 1500 rpm.

It can be seen that the speed estimation errors are load dependent as well, as predicted by steady-state analysis of section 6.4. The maximum error appears to be 15 rpm when the machine runs at 1500 rpm with the rated load torque. When the magnetising inductance is smaller than the rated value, the estimated speed is lower than the actual speed. When the magnetising inductance is larger than the rated value, the estimated

speed is higher than the actual speed, Figure 9.16b. Comparison of Figure 9.16b with the Figure 6.6a shows again a number of similarities. Speed estimation error linearly increases with the load torque. The sign of the speed estimation error is the same for the given detuned value of the magnetising inductance. This is so as the same approach to detuning is used in theoretical and experimental work (that is, a value of kL_{mn} is used in the controller/estimator in chapters 6 and 7 and in the speed estimator in this section). The values of the speed estimation error are of the similar absolute value and opposite sign for the same plus/minus deviation of the magnetising inductance. Some shift upwards, due to iron loss, is evident. The only important difference between Figures 6.6a and 9.16b is in the amount of the speed estimation error, as the experimental values are considerably higher. Figure 9.18 shows a set of traces in steady-state from which data of Figure 9.16b were compiled.

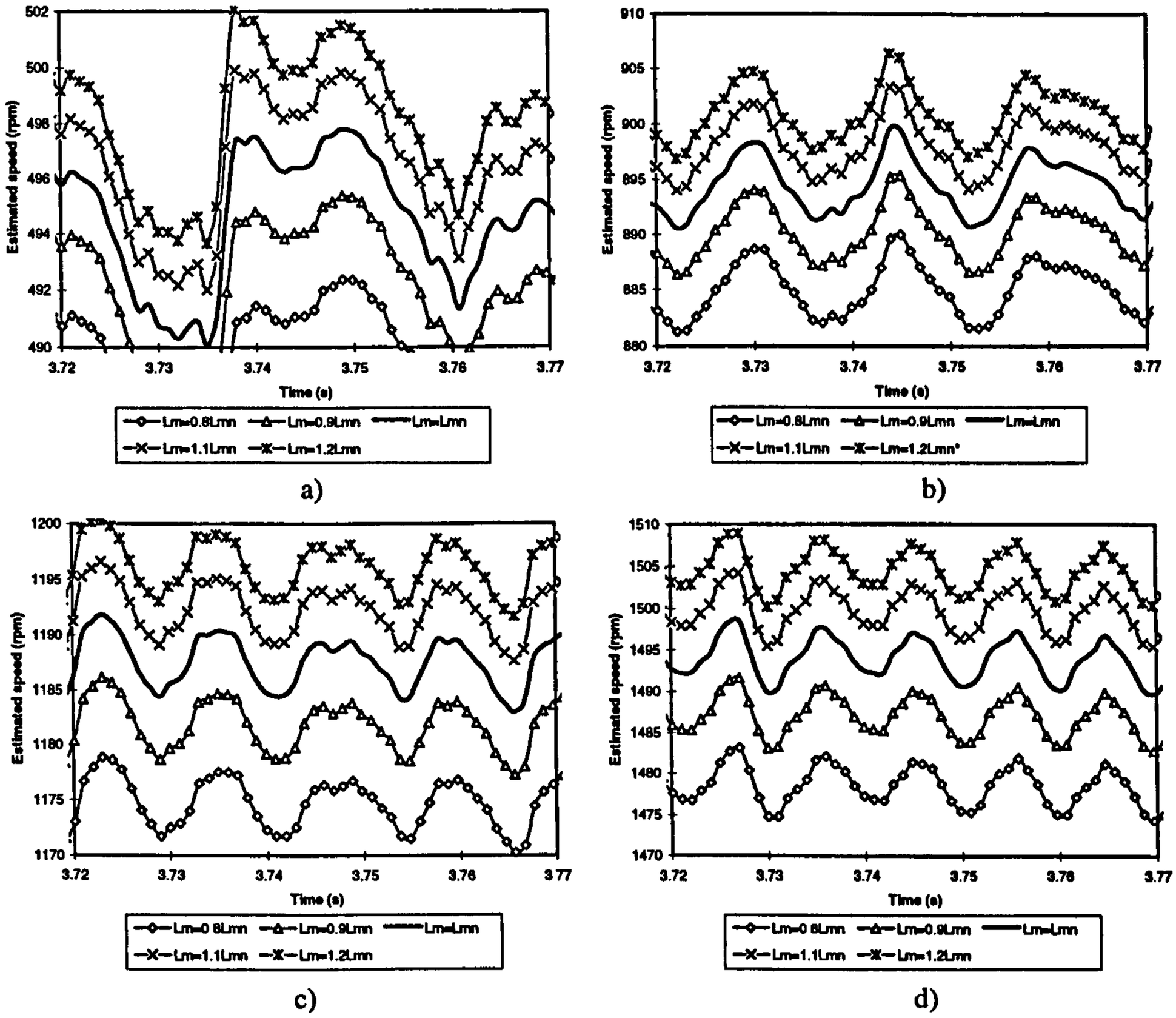

Figure 9.18: Impact of detuned magnetising inductance on speed estimation accuracy: a) speed command of 500 rpm, b) speed command of 900 rpm, c) speed command of 1200, d) speed commanded of 1500.

Speed estimation errors caused by variations of stator resistance were investigated as well and were found to be very small. For all the speeds of 500 to 1500 rpm, errors are within 0.5 -1 rpm.

9.6 Operation of the speed estimator in the field-weakening region

In order to investigate the detuning effect caused by main flux saturation, experiments in the field-weakening region were performed. Due to the limitations imposed by the DC machine, which is the load of the induction motor, the speed cannot exceed 1500 rpm. The base speed was therefore set to 650 rpm, so that the field-weakening operation starts at 650 rpm. Load setting was determined so that the output power at 1500 rpm does not exceed the rated power of the induction machine. Therefore, the load switch was set to 4 A position for all the experiments in the field-weakening region. All the parameters of the indirect vector controller of Figure 9.2 are set to rated values (coefficients of the inverse magnetising curve approximation and slip gain).

Constant parameter speed estimator is used. All the parameters, including the magnetising inductance, are set to constant rated values. Transients related to acceleration from zero to 900 rpm speed, from zero to 1050, from zero to 1200 and from zero to 1350 rpm speed are studied, for both no-load and loaded conditions. The actual and estimated speed are shown in Figures 9.19 and 9.20 for no-load and loaded acceleration, respectively.

When machine is running in the field-weakening region, speed estimation errors increase with increase in speed, if constant parameter speed estimator is used. This is so because the magnetising inductance in the induction machine increases in the field-weakening region. The rated inductance in the speed estimator is thus smaller than the actual inductance. The estimated speeds were found to be about 7 rpm lower than the actual speed for the speed command of 900 rpm and about 8 rpm lower for the speed command of 1350 rpm. Figure 9.21 shows zoomed extracts from Figures 9.19 and 9.20 in vicinity of the steady-state.

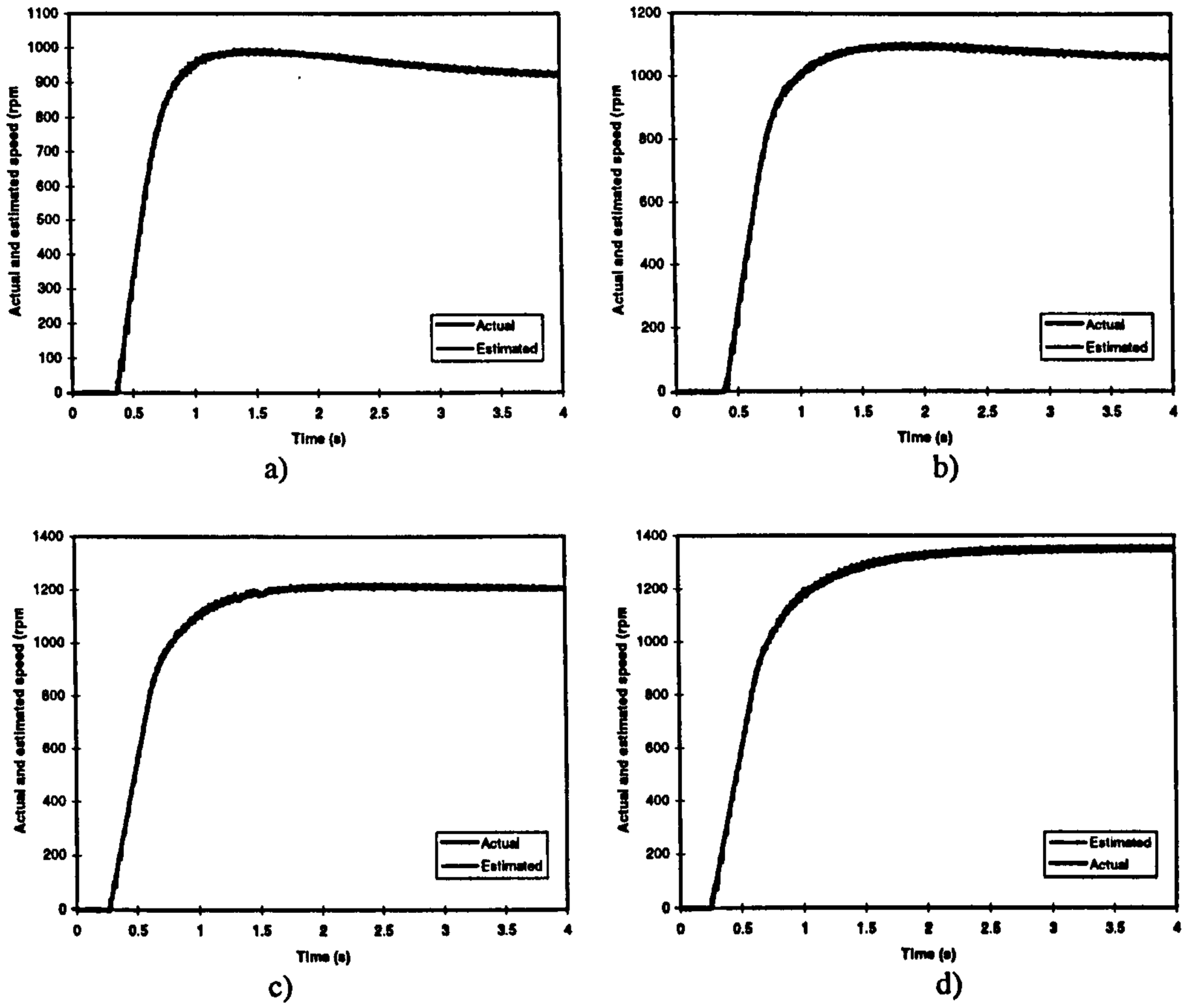

Figure 9.19: Operation in the field-weakening region - the actual speed and the estimated speed using constant parameter speed estimator, no-load conditions: a) speed command = 900 rpm; b) speed command=1050 rpm, c) speed command=1200 rpm, d) speed command=1350 rpm.

It should be noted that the experimentally observed speed estimation errors are much smaller (but of the same sign) than those predicted in section 7.4. Rated operating point on the magnetising curve for the machine used in chapter 7 is in the saturated region. Due to slight incompatibility between the controller and the motor used in experiments, rated operating point on the magnetising curve of the experimental motor is very close to the linear region of the curve. Detuning effects are therefore less pronounced and the speed estimation error is smaller.

9.7 Operation of the modified speed estimator, with main flux saturation compensation, in the field-weakening region

The modified rotor flux based speed estimator used in this section is the one developed in section 8.3. The problem experienced in using the modified speed estimator is the integration of stator flux components in the reference model. As initial values for the

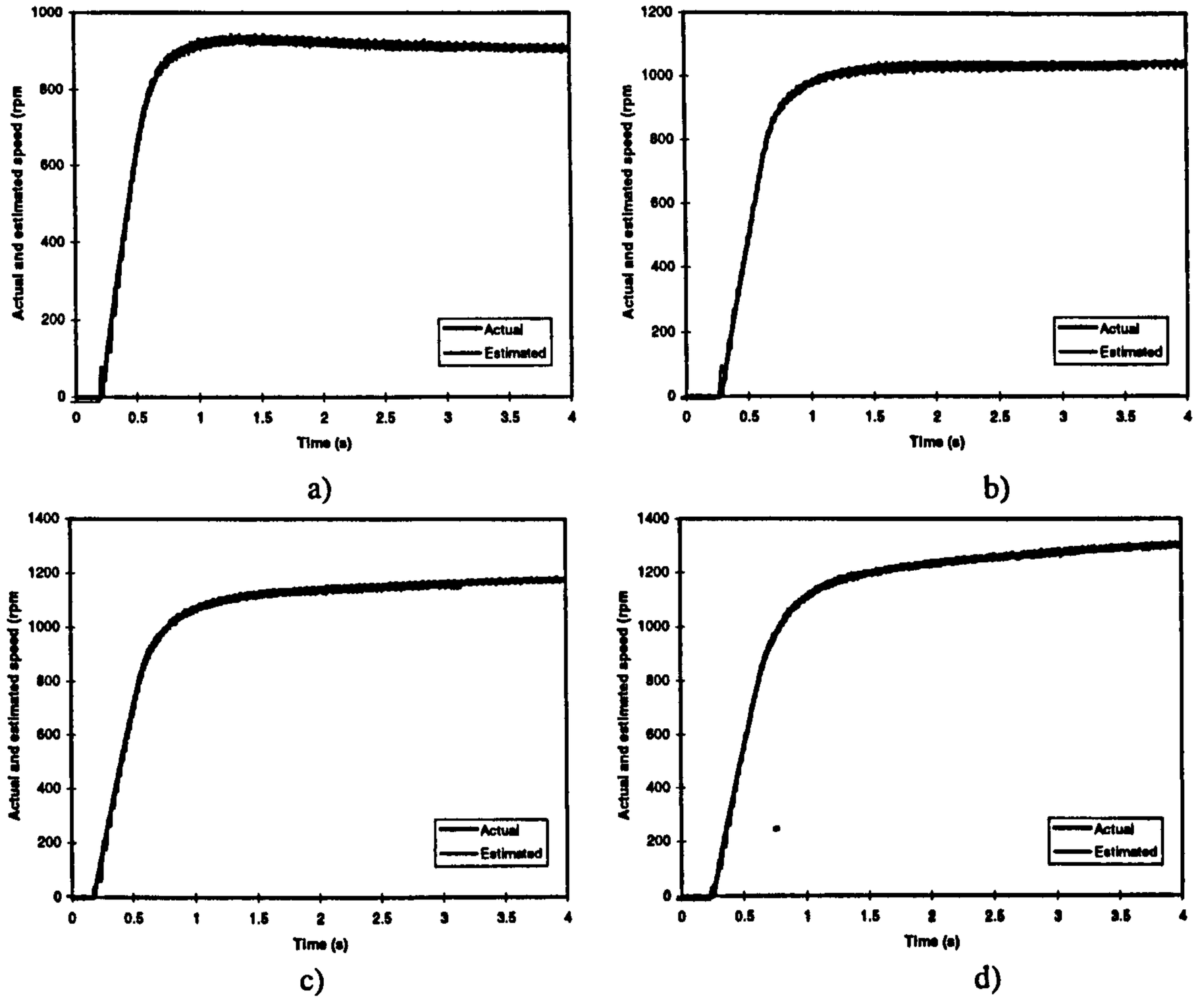

Figure 9.20: Operation in the field-weakening region - the actual speed and the estimated speed using constant parameter speed estimator, loaded conditions: a) speed command=900 rpm, b) speed command=1050 rpm, c) speed command=1200 rpm, d) speed command=1350 rpm.

pure integrator are unknown, an offset at the output of the integrator appears and drives the output of the pure integrator to saturation. Figure 9.22a shows the stator flux components obtained by pure integration in the reference model. It can be seen that the both stator flux components are increasing in negative direction. This results in incorrect operation of the speed estimator. In order to solve this problem, the modified integration algorithm, proposed by Wu and Hu [1997] and discussed in section 7.2 (Figure 7.11), is utilised instead of the pure integrators. Figure 9.22b shows the stator flux components in the reference model obtained by modified integration algorithm. In this algorithm the cut-off frequency ω_c is critical for stable operation of the speed estimator. In this experimental study, the cut-off frequency ω_c is set to 100, which gives the best estimated speed output. Figure 9.23 shows the stator flux components for different cut-off frequencies.

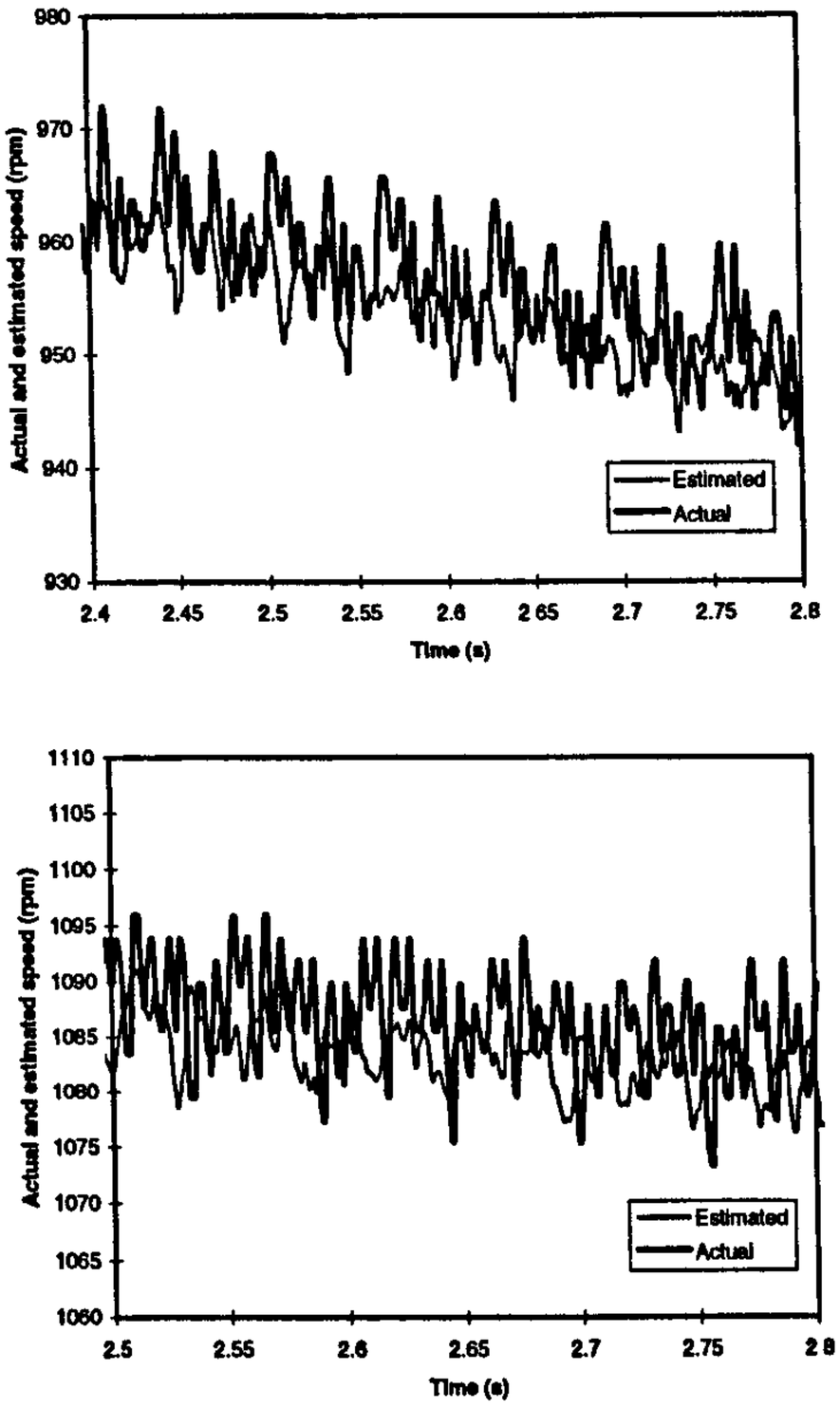

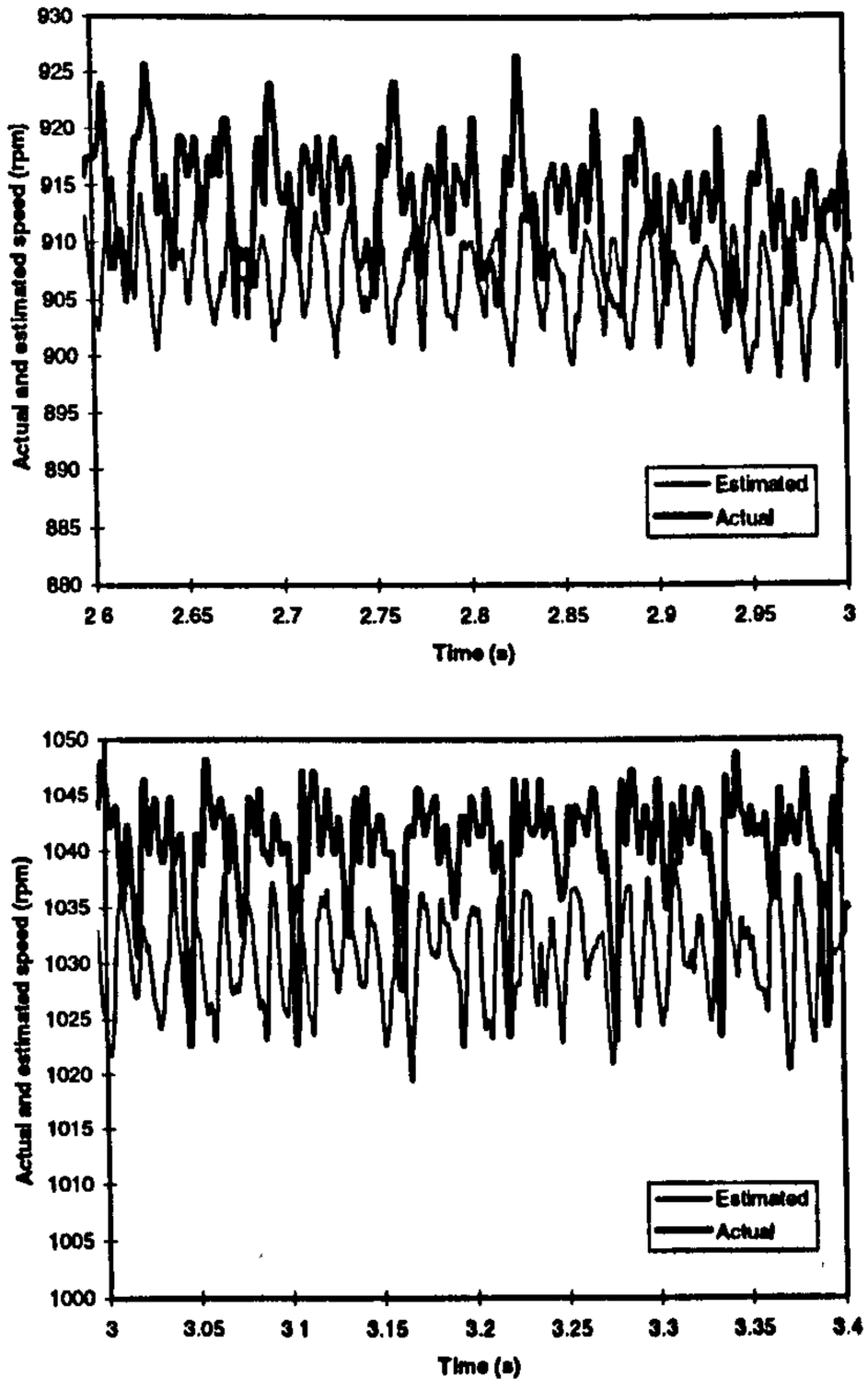

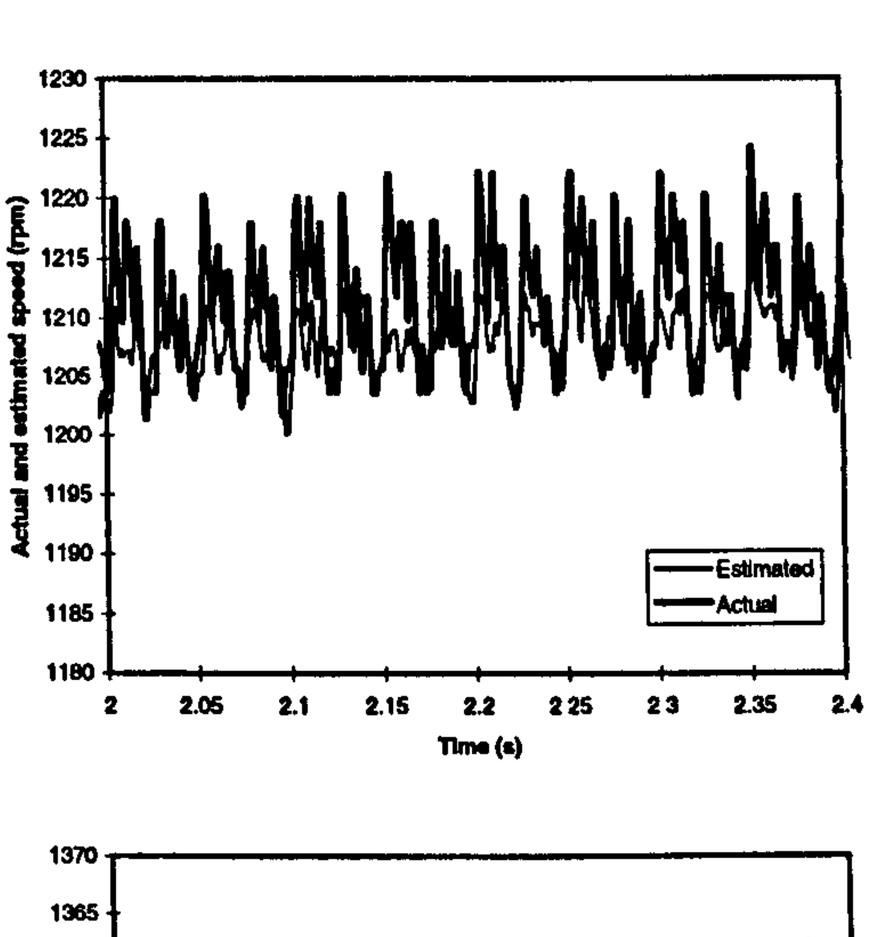

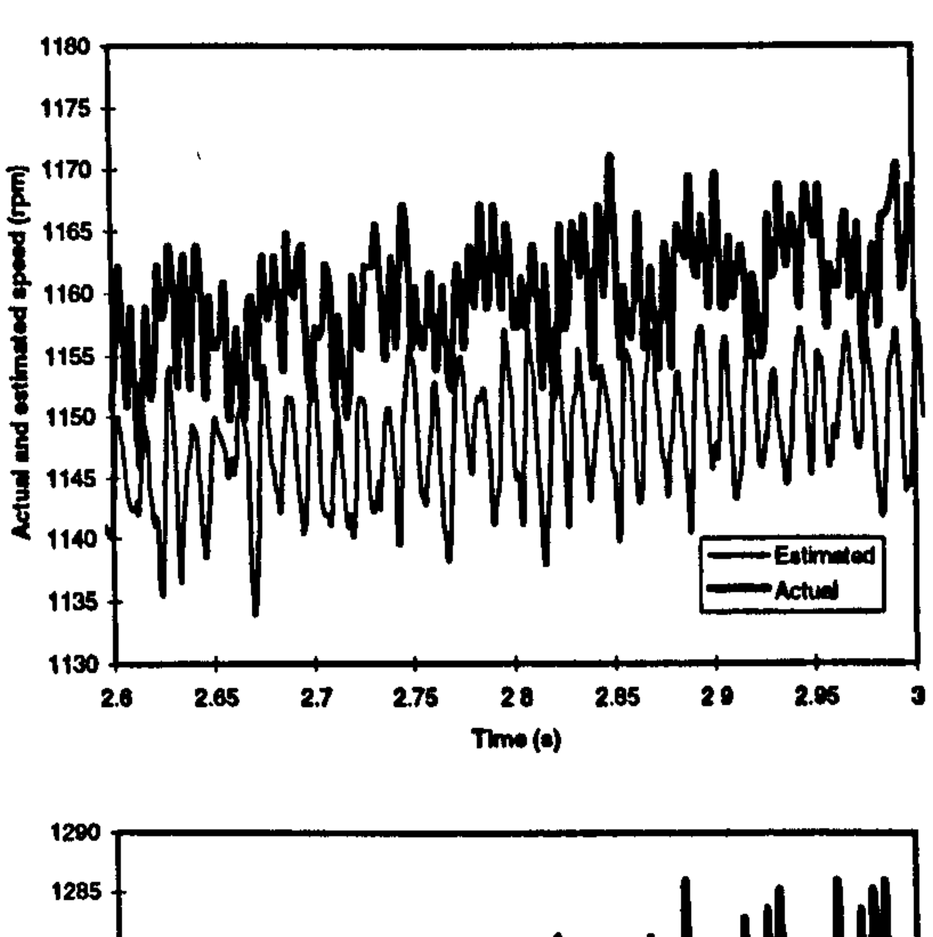

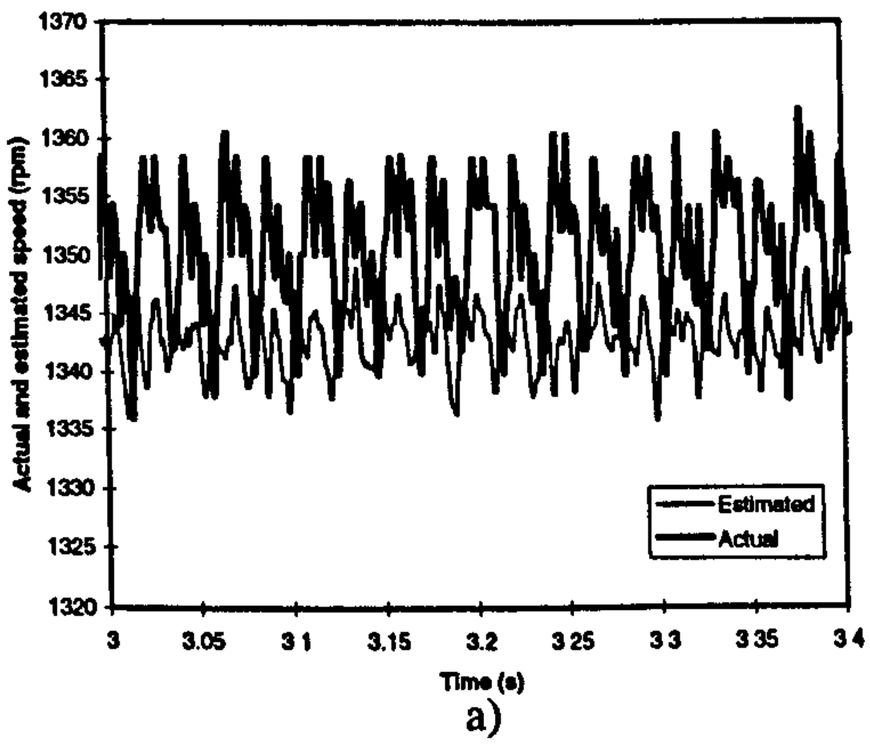

a)

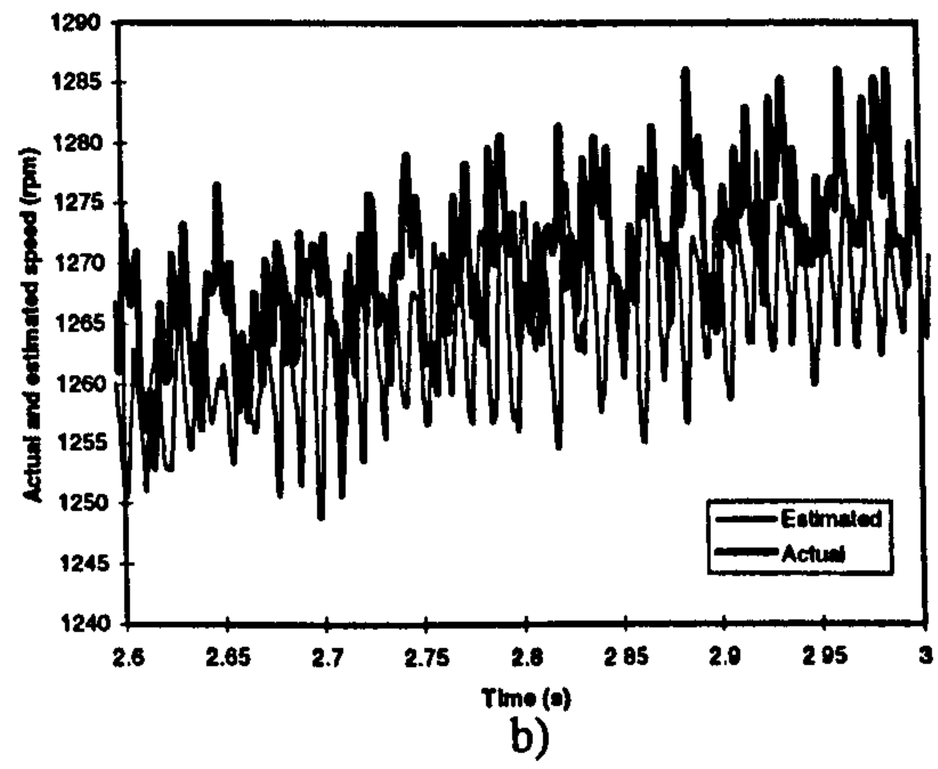

b)

Figure 9.21: Zoomed extracts from Figures 9.19 and 9.20: a) no-load operation, b) loaded operation.

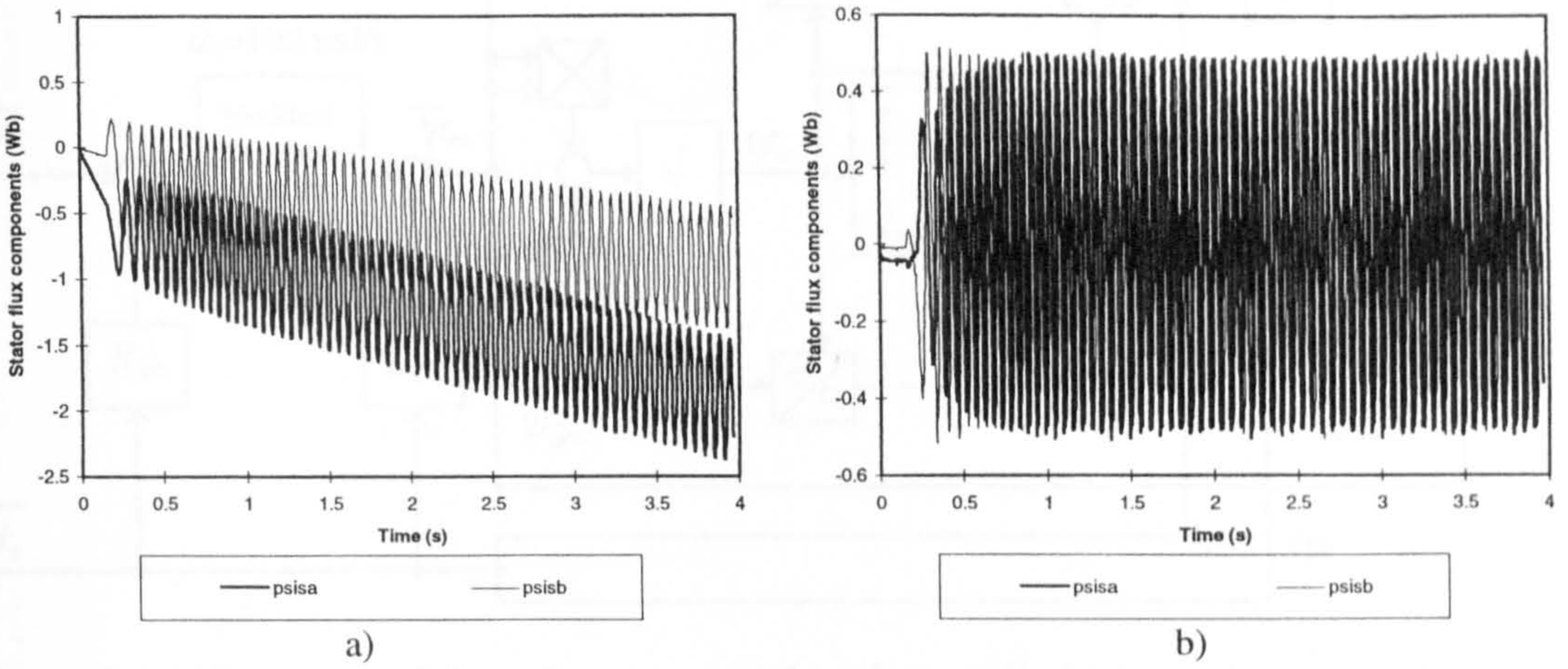

Figure 9.22: Stator flux components in the reference model: a) using pure integrator, b) using modified integration algorithm (psis ≡ ψ_s).

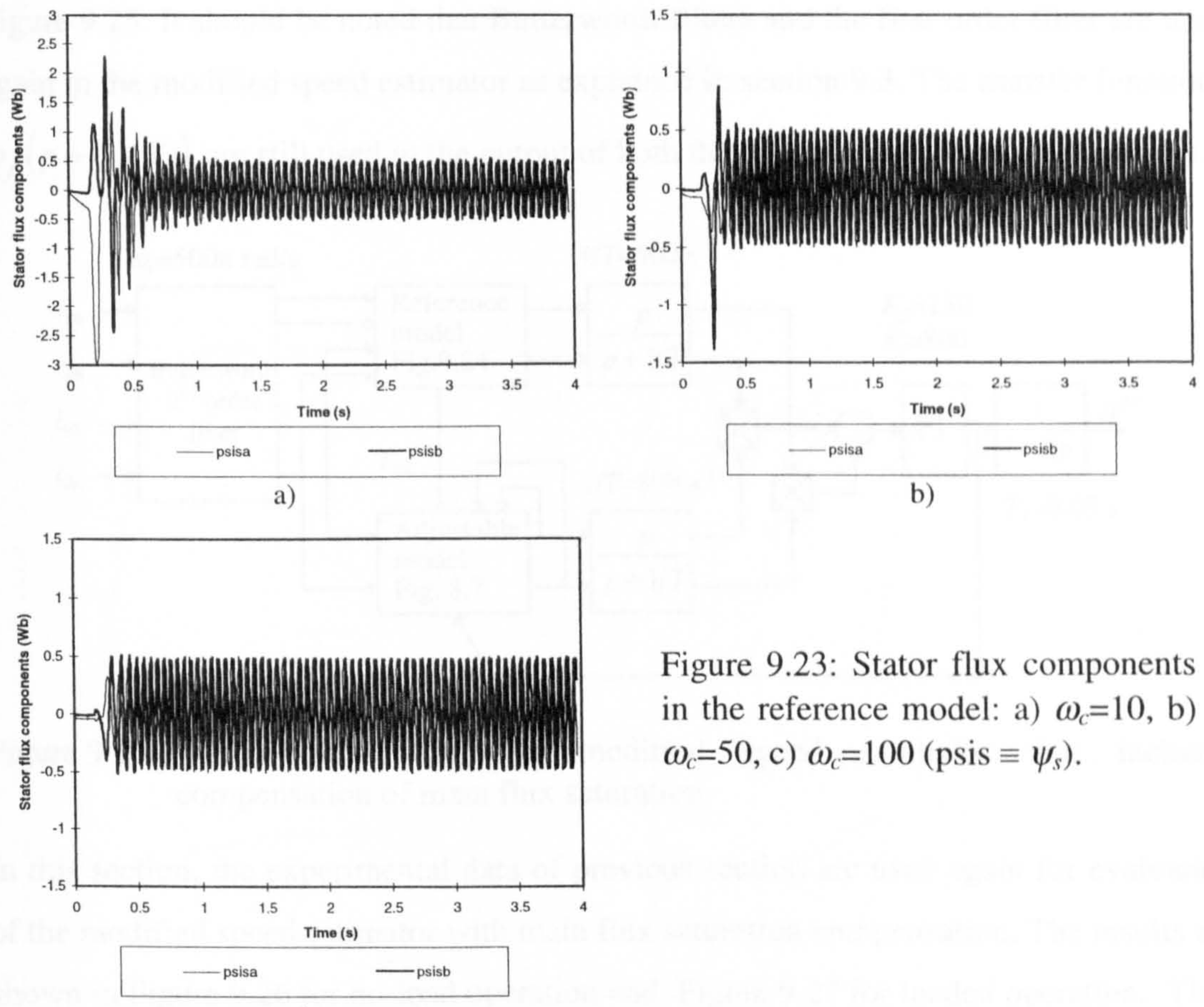

Figure 9.23: Stator flux components in the reference model: a) ω_c=10, b) ω_c=50, c) ω_c=100 (psis ≡ ψ_s).

Therefore, the pure integrators in Figure 8.6 are replaced by the modified integration algorithm. The structure of the reference model with the modified integration algorithm is illustrated in Figure 9.24.

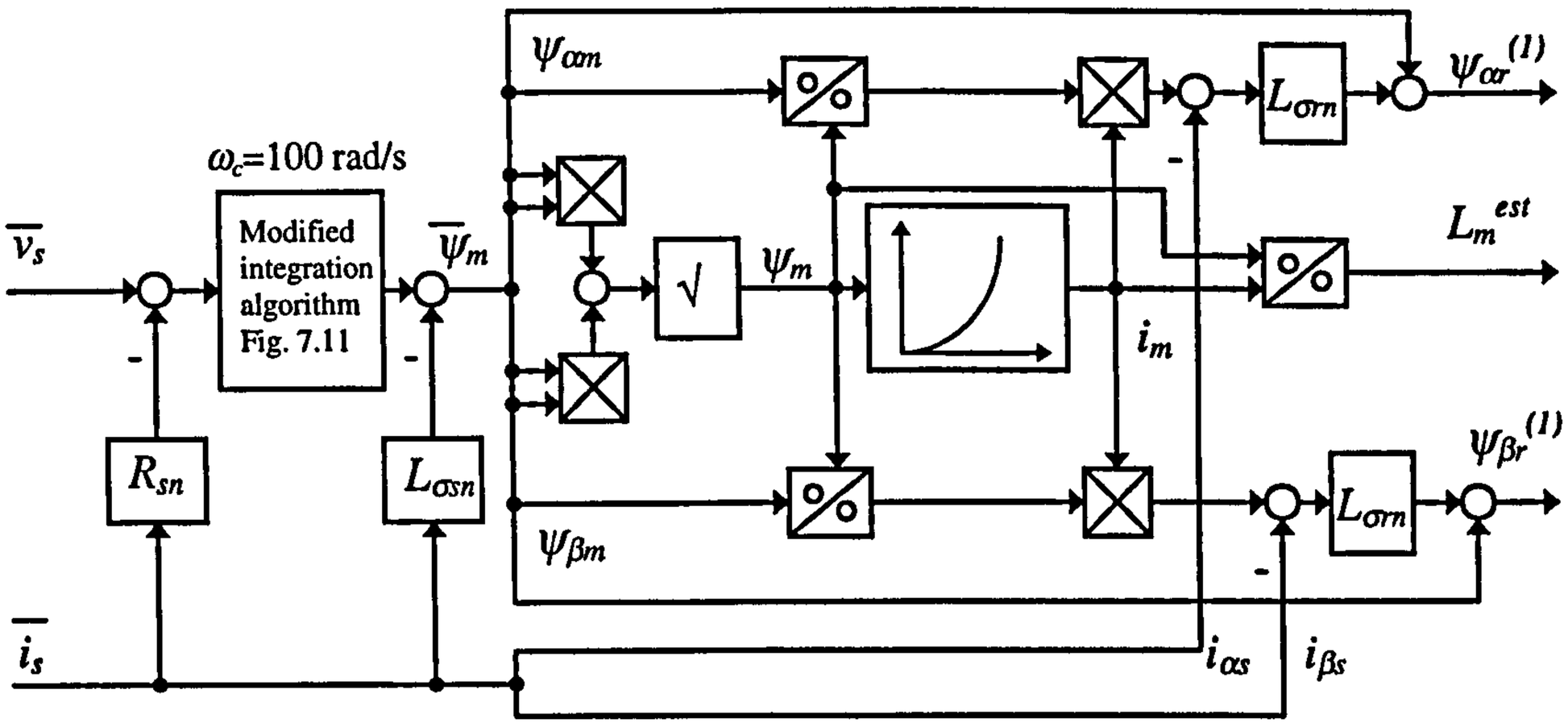

Figure 9.24: Structure of the reference model with modified integration algorithm.

The complete modified speed estimator used in experimental investigations is shown in Figure 9.25. It should be noted that Butterworth filters and the first order filter are used again in the modified speed estimator as explained in section 9.3. The transfer functions $p/(p+(1/T))$ are still used in the output of both the reference and adjustable models.

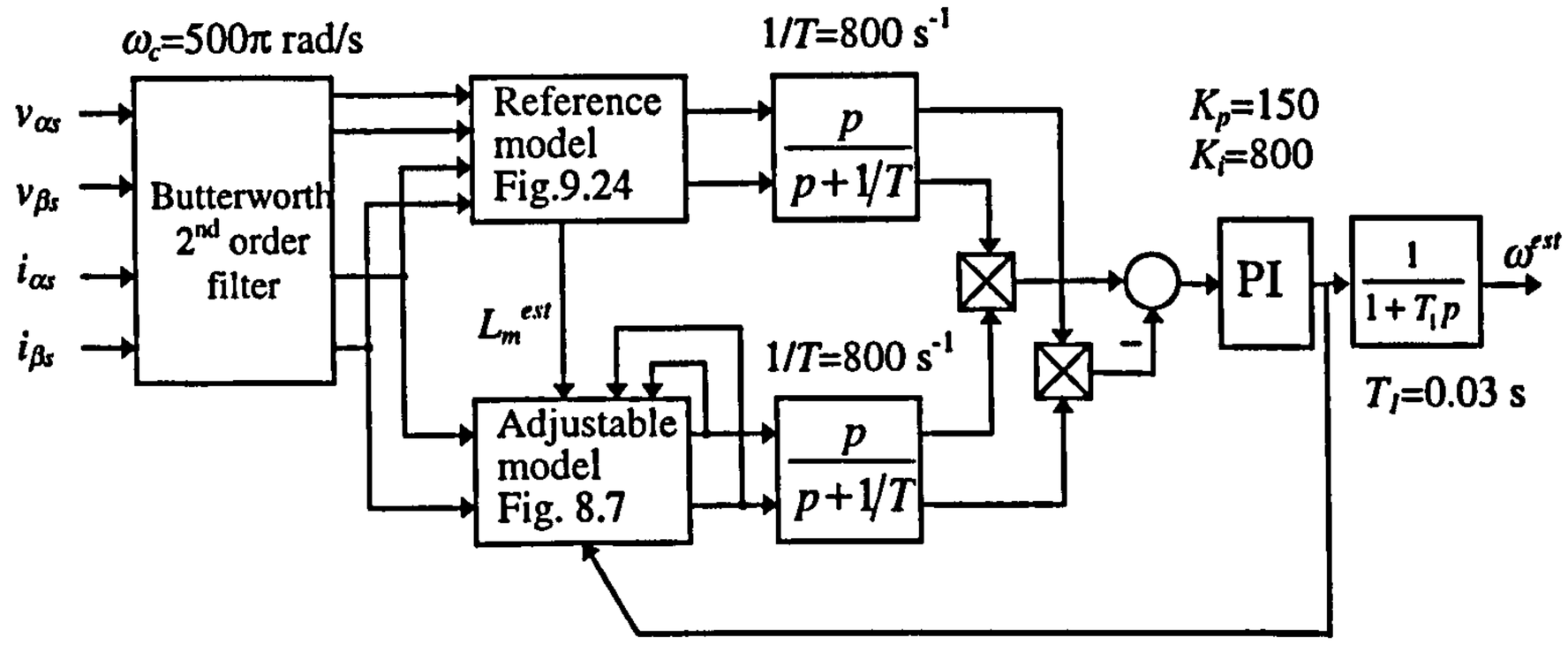

Figure 9.25: Implementation of the modified speed estimator that includes compensation of main flux saturation.

In this section, the experimental data of previous section are used again for evaluation of the modified speed estimator with main flux saturation compensation. The results are shown in Figure 9.26 for no-load operation and Figure 9.27 for loaded operation. They are essentially the same as in Figures 9.19-20. However, the difference can be seen from zoomed extracts shown in Figure 9.28. Speed estimation error in no-load

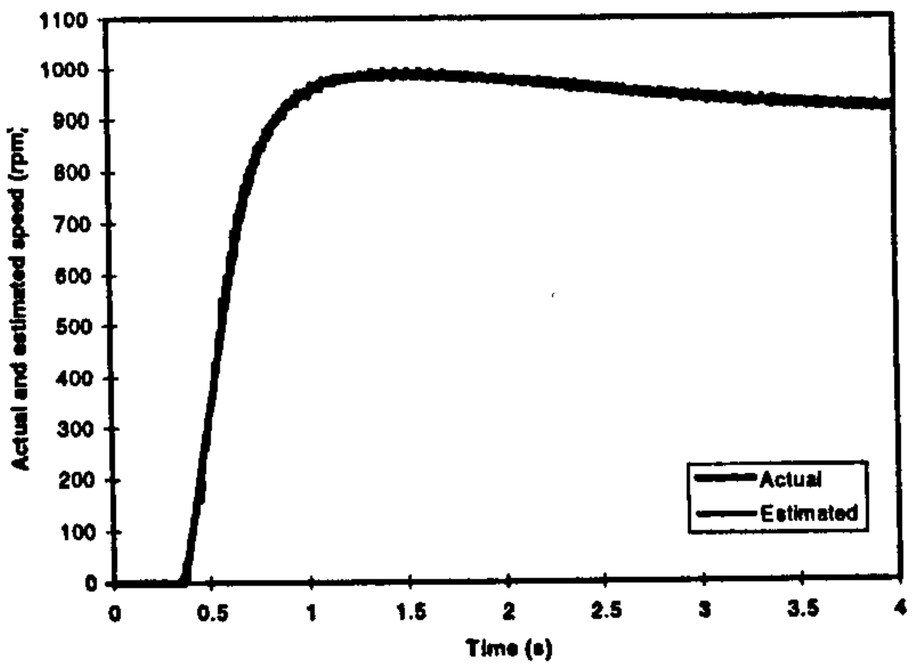

a)

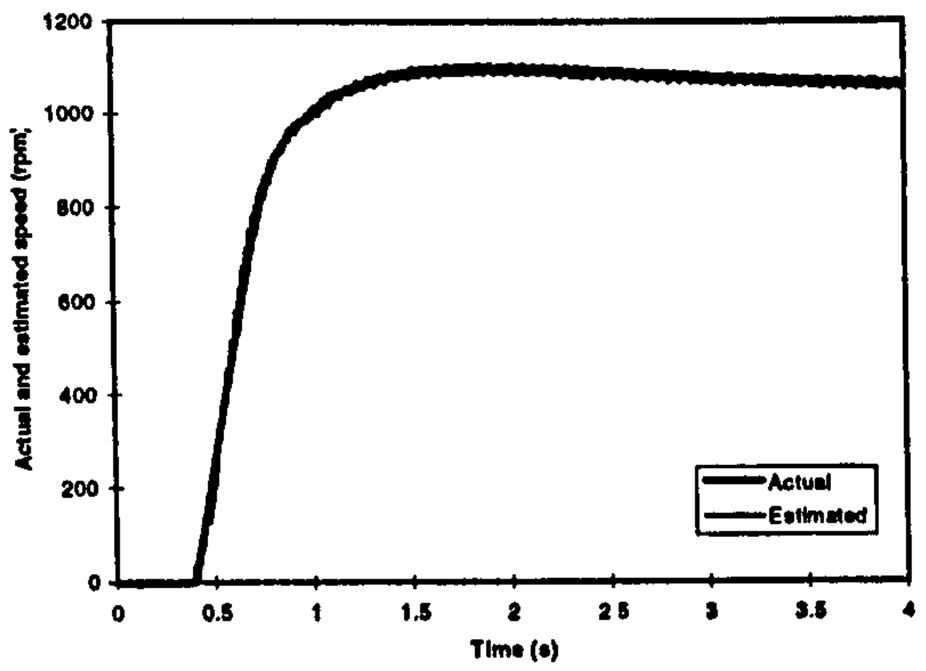

b)

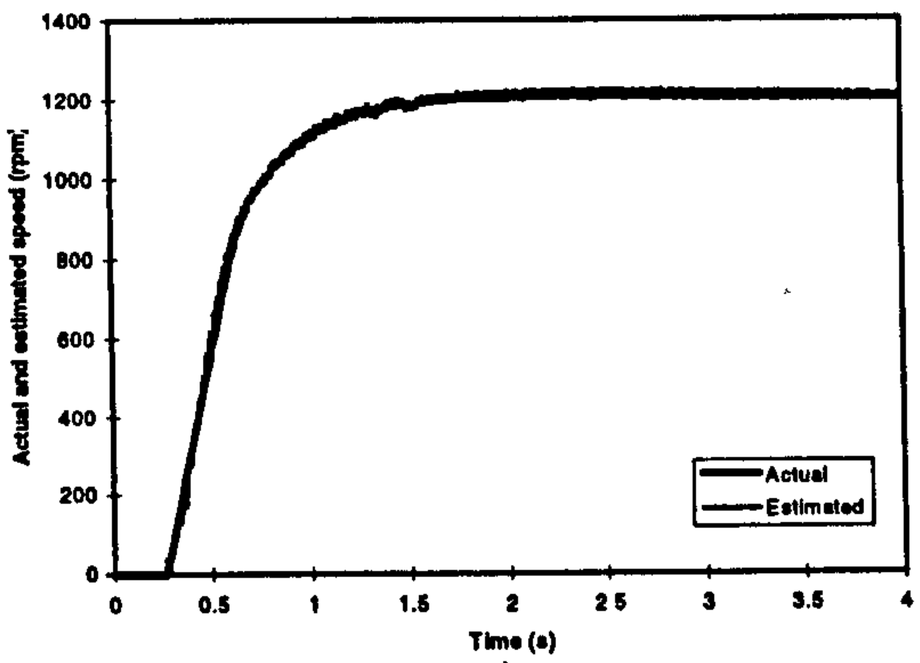

c)

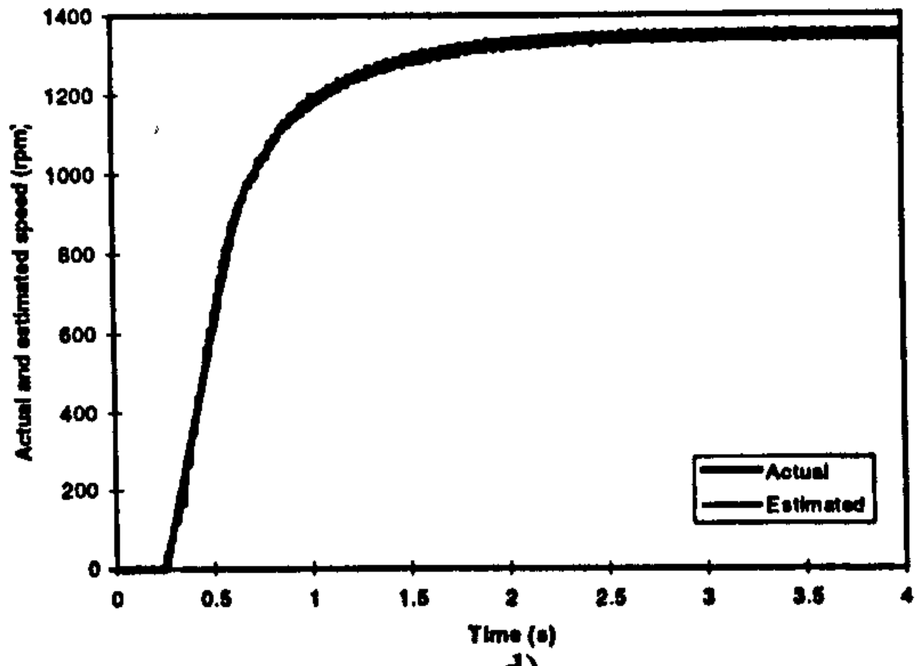

d)

Figure 9.26: Actual and estimated speed using modified speed estimator, no-load operation, speed command of: a) 900 rpm, b) 1050 rpm, c) 1200 rpm, d) 1350 rpm.

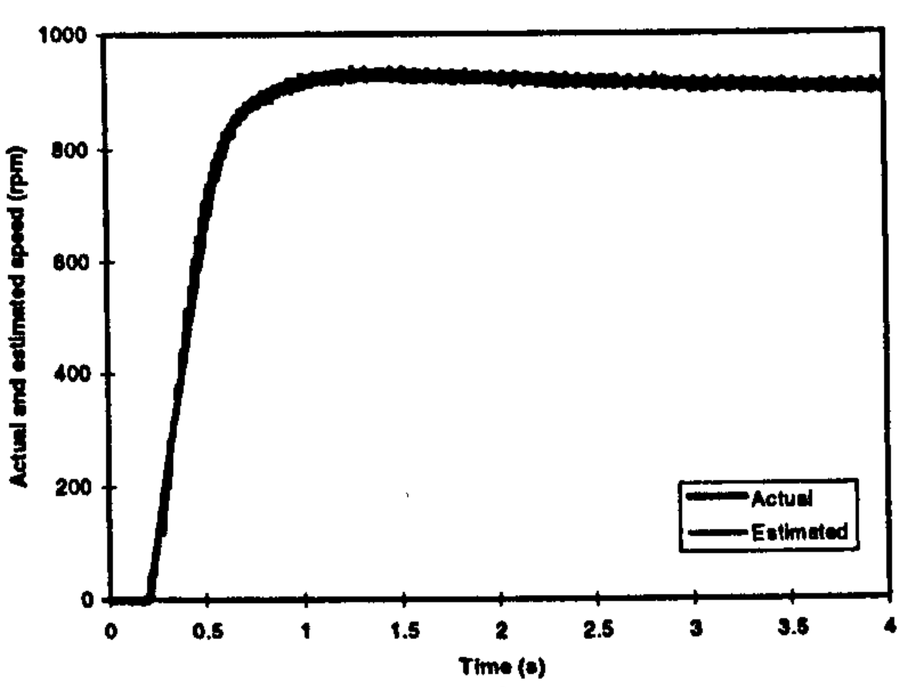

a)

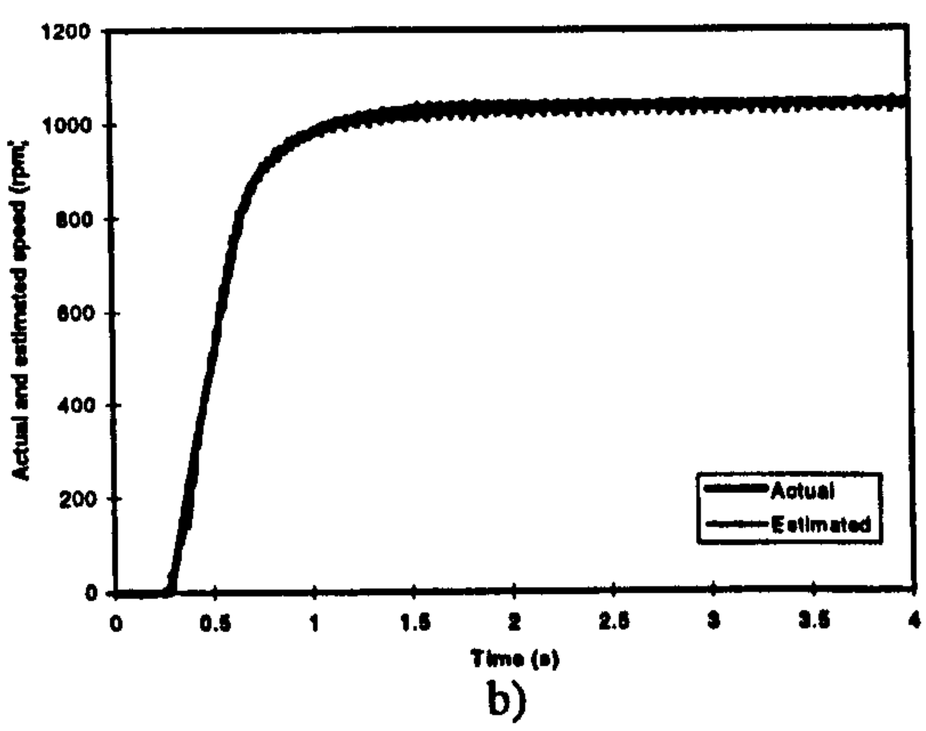

b)

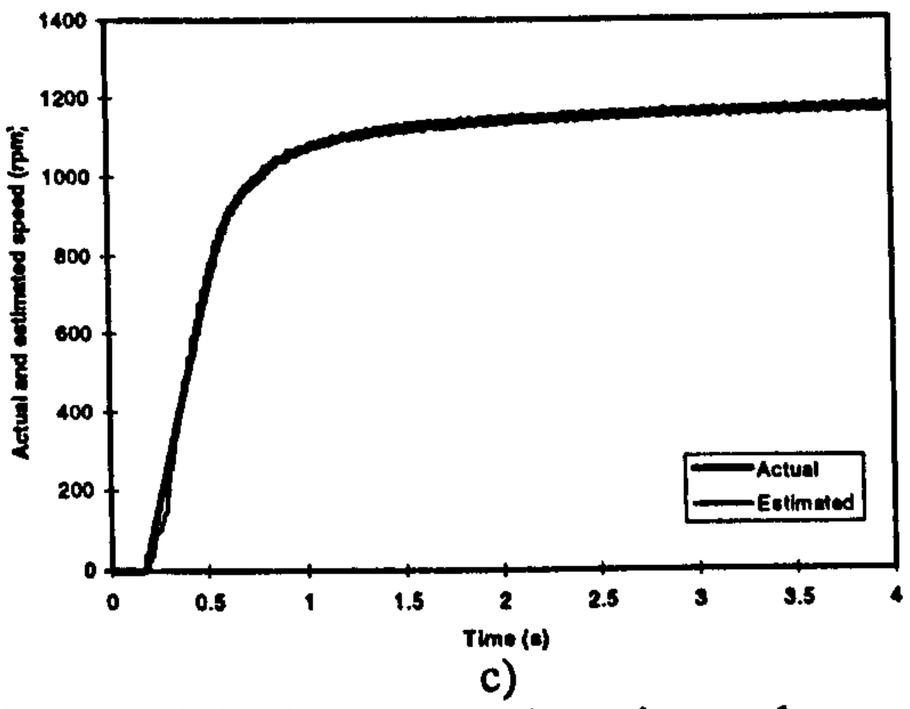

c)

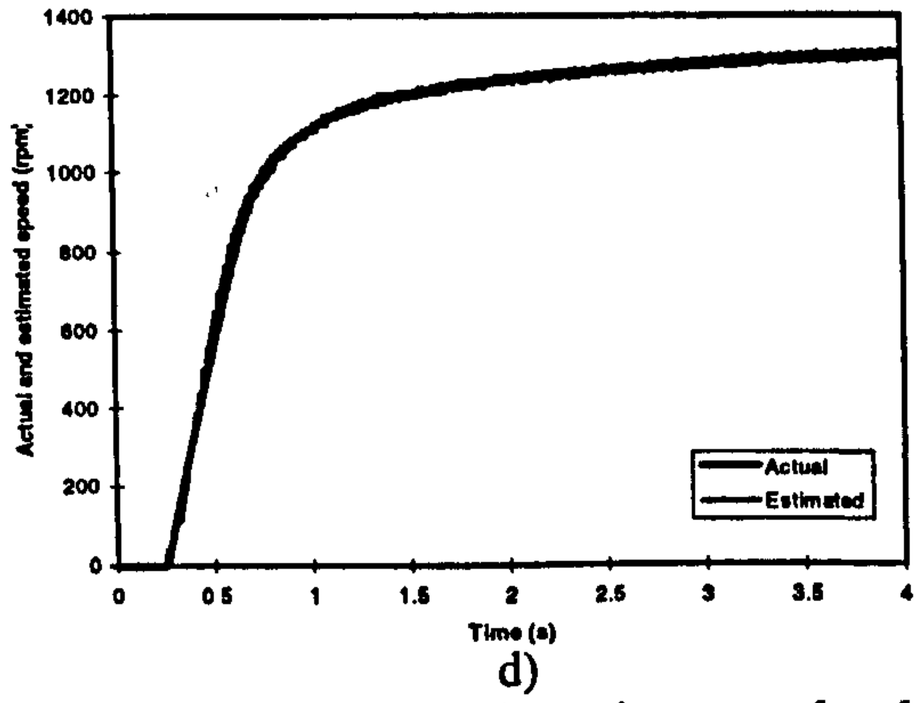

d)

Figure 9.27: Actual and estimated speed using modified speed estimator, loaded operation, speed command of: a) 900 rpm, b) 1050 rpm, c) 1200 rpm, d) 1350 rpm.

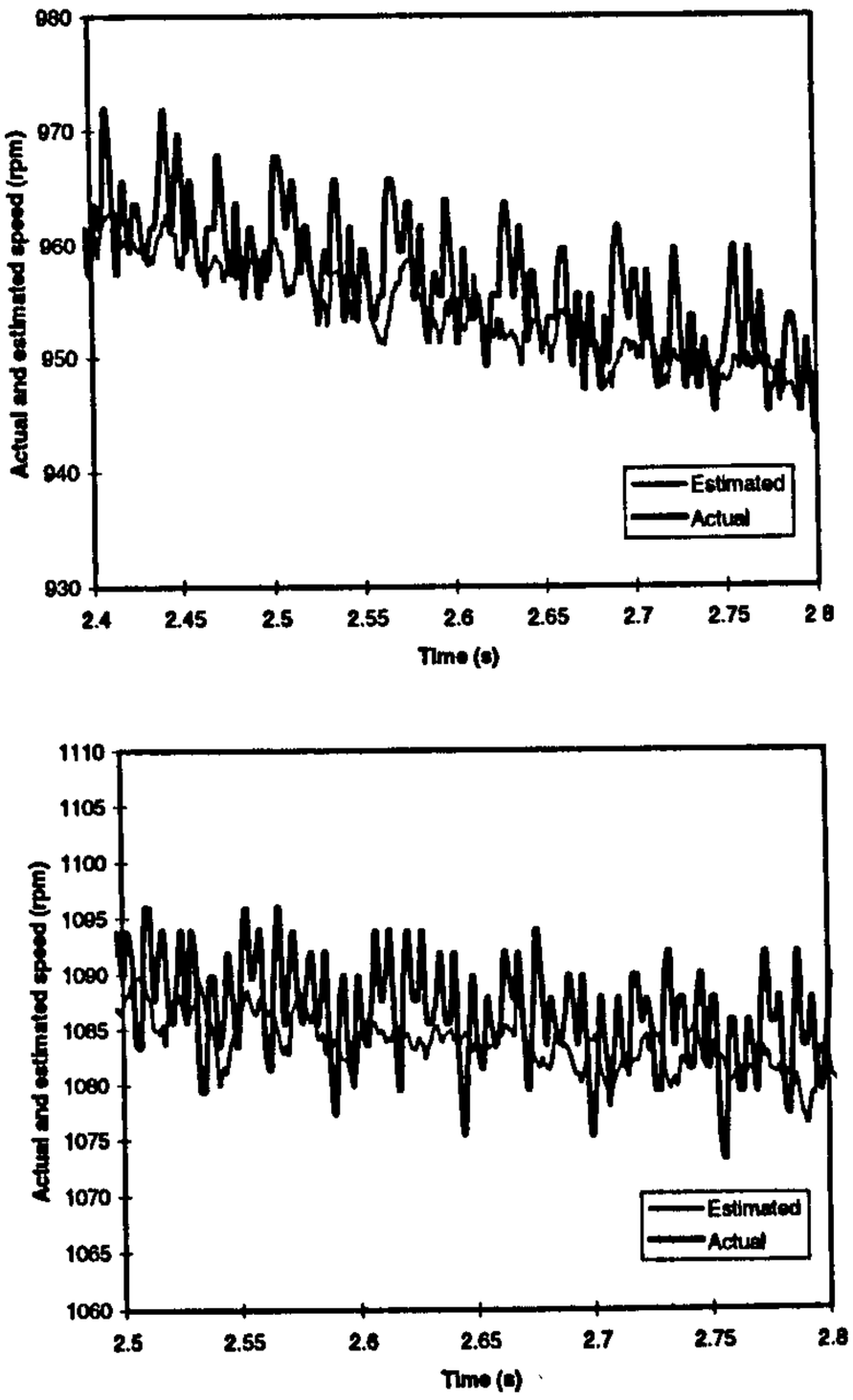

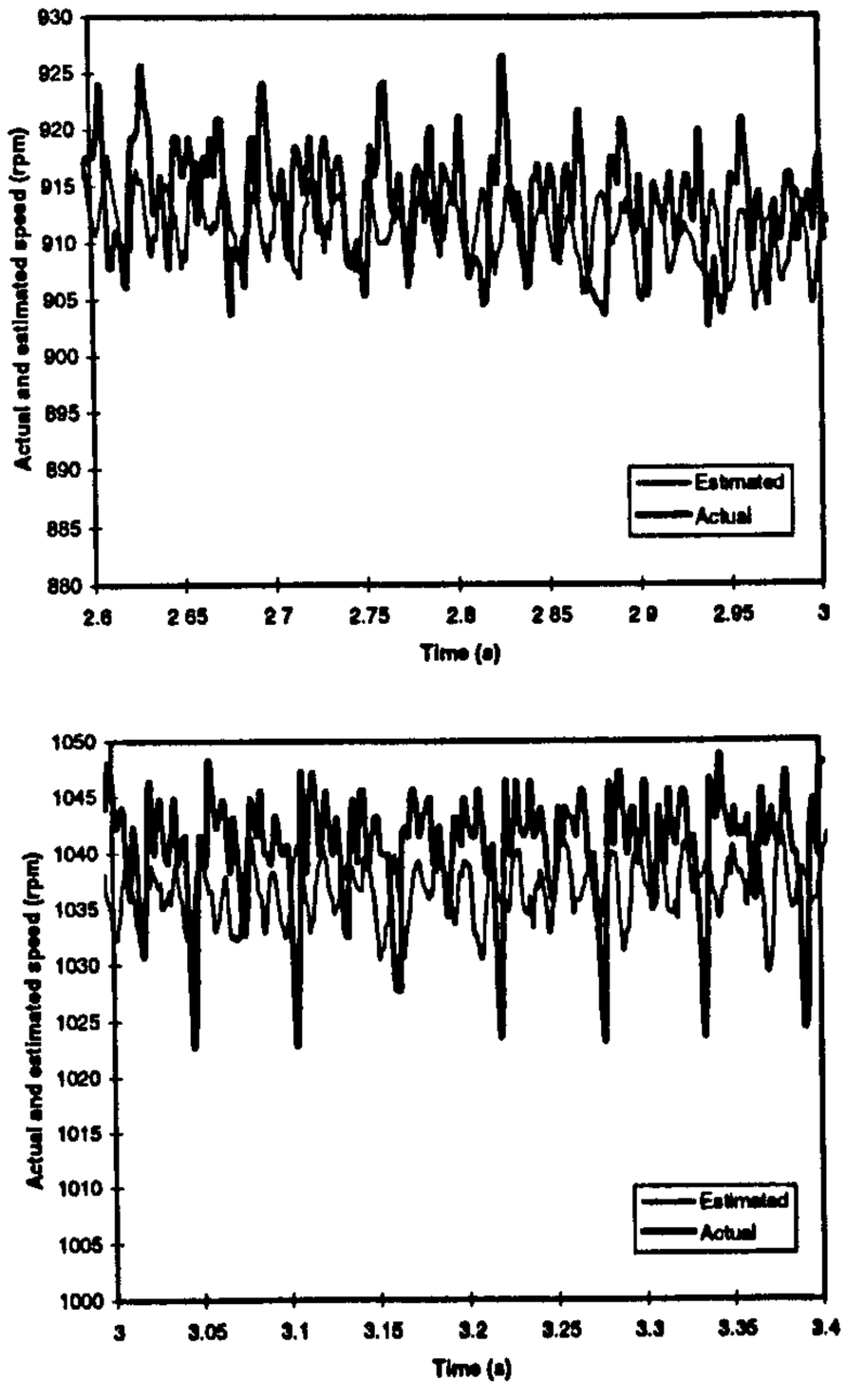

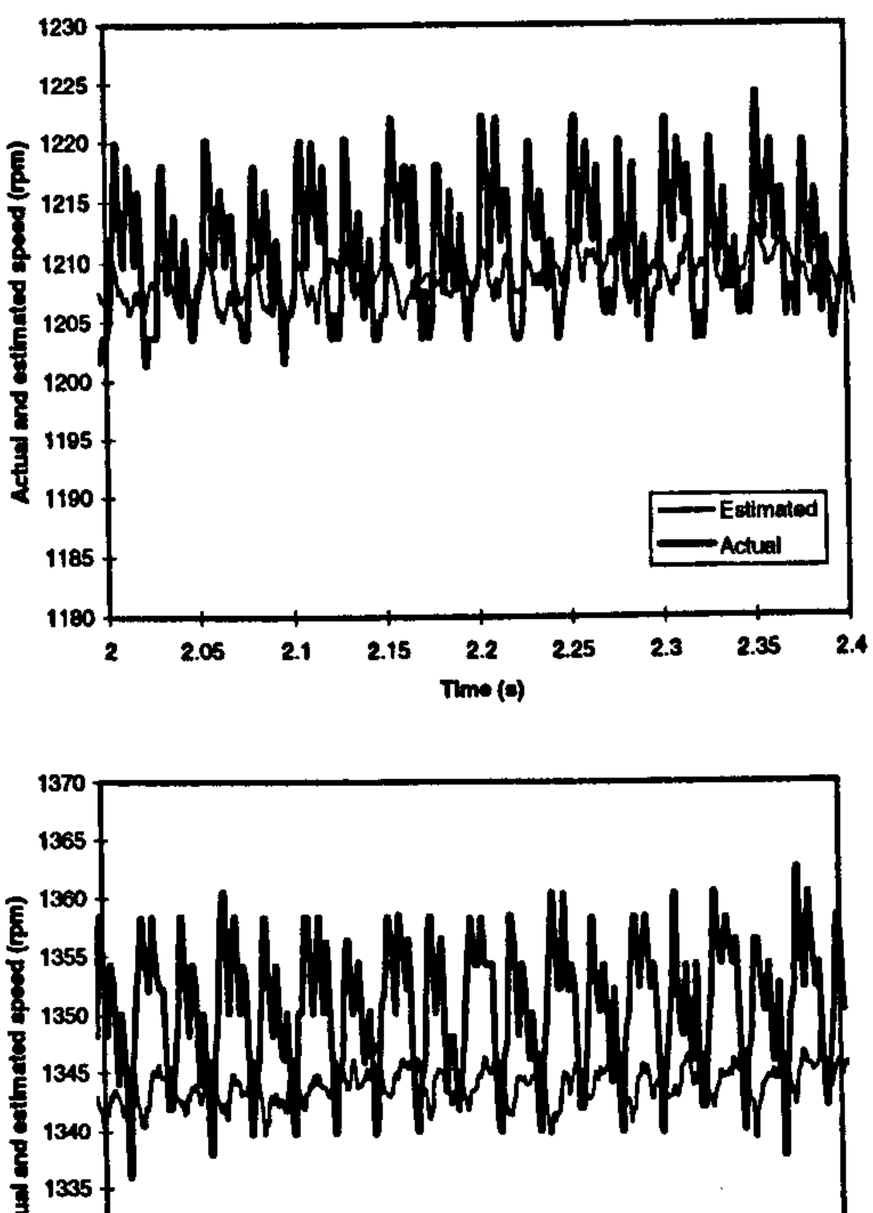

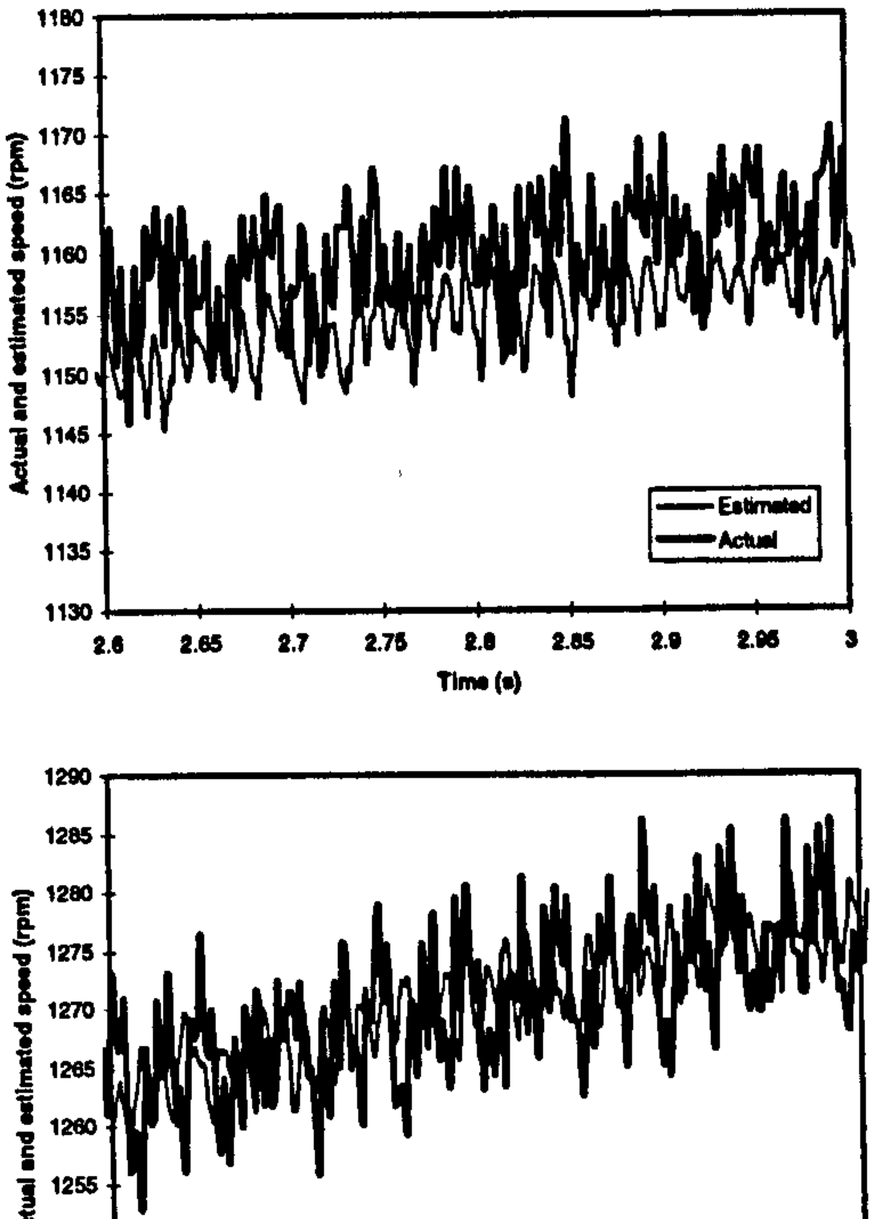

a) b)

Figure 9.28: Zoomed extracts from Figure 9.26 and Figure 9.27: a) no-load operation, b) loaded operation.

operation is still very small. As the speed estimation error is load dependent, there are visible errors in loaded operation. Comparing Figure 9.28 with Figure 9.21, one can see that the speed estimation error with the modified speed estimator is much smaller than the estimation speed error of the constant parameter speed estimator. The speed estimation errors are reduced to 2-3 rpm in loaded operation. This fact confirms the theoretical findings of section 8.3, that the speed estimation error caused by main flux saturation can be compensated by the modified speed estimator.

9.8 Summary

Experimental investigation of MRAC speed estimator is elaborated in this chapter. The experimental rig is at first described. A data acquisition system is designed in order to sample the voltage and current signals.

Constant parameter speed estimator is investigated first. Detailed description of the tuning procedure is given. The speed estimator was found to be working well in the base speed region. The speed estimation error is less than 2 rpm for no-load operation and about 4 rpm for loaded operation.

Detuning due to parameter variations is studied as well. The results are found to be in good agreement with those of the theoretical studies. The speed estimation error due to rotor resistance variation and magnetising inductance variation is load dependent. The maximum speed estimation error caused by rotor resistance variation is about 13 rpm when machine runs at the rated speed with the rated load. The maximum speed estimation error caused by magnetising variation is about15 rpm when machine runs at the rated speed with the rated load. Speed estimation error caused by stator resistance variation is very small, less than 1 rpm.

Detuning in the field-weakening region is mainly due to main flux saturation. Therefore, in order to investigate the detuning caused by main flux saturation when constant parameter speed estimator is used, operation of the induction machine in the field-weakening is analysed. The experimental results show that there are speed estimation errors in the field-weakening region for loaded operation. The speed estimation error is about 1 to 2 rpm for no-load operation and about 7-8 rpm for loaded operation.

In order to eliminate the speed estimation error, the novel modified speed estimator is used. The evaluation of the modified speed estimator shows that the speed estimation error is reduced. The speed estimation error is about 2 to 3 rpm in the field-weakening region in loaded operation. This result shows that the modified speed estimator is able to compensate the detuning due to main flux saturation.

10 CONCLUSION

10.1 Summary

Since the theory of induction machine vector control had been introduced, numerous vector control schemes have been developed. Vector controlled induction machines have now reached the status of a mature technology and are used in a broad range of applications in industries. One specific issue that has recently come into focus of the attention of the research community world-wide is the possibility of elimination of the speed (position) sensor in vector controlled drives. Speed signal information is required for closed-loop speed control and, in majority of commercially available vector controlled induction motor drives, for field orientation as well. However, speed (position) sensor is very expensive, it reduces reliability of the drive, and it requires additional space for mounting. Hence the concept of so-called sensorless vector control has emerged. Instead of being measured, speed of rotation is now estimated from easily measured quantities, such as stator currents and stator voltages. Therefore, high performance sensorless vector controlled induction motor drives have been under extensive development in the recent years.

The origins of vector control of induction machines are briefly reviewed in chapter one. As sensorless vector control of induction machine has many advantages, it has become an important area of research. With rapid advance in hardware development, it is possible nowadays to implement high performance vector control of induction machine without a speed sensor. The existing methods of sensorless vector control are reviewed and problems experienced in sensorless vector control are addressed in chapter one. The main objectives of the study are set on the basis of identified topics that have not been exhaustively investigated so far.

The basic principles of vector control of induction machines are reviewed in chapter two. Constant parameter induction machine model is at first developed and is then used to show the procedure of derivation of vector control principles. Stator flux oriented control and rotor flux oriented control are looked at and various control schemes are explained. As stator flux oriented induction machine requires more complicated control system than rotor flux oriented control of an induction machine, rotor flux oriented

control is selected for further study in this project. Concepts of voltage-fed and current-fed induction machine are introduced and reasons for prevailing application of the current-fed concept are discussed. The basic structures of indirect feed-forward rotor flux oriented control system and direct feedback rotor flux oriented control are illustrated. The scheme selected for all the subsequent studies is the indirect feed-forward rotor flux oriented control of a current-fed induction machine.

Sensorless vector control of induction machines has emerged as the most important research topic in the area of high performance drives in the last decade. Numerous speed estimation methods have been developed in recent years. Existing speed estimation methods are reviewed in chapter three. They are divided into two basic categories. The first one utilises stator current harmonics to extract the rotor speed information. The second one relies on the induction machine model to estimate the rotor speed. Speed estimation methods based on stator current harmonics are independent of machine parameters. However, they are computationally involved and time-consuming. Model based speed estimation methods are relatively easy to implement and they could be regarded as having a wider acceptance at present. Model based approach to speed estimation is the one elaborated in this project.

Speed estimation methods, based on the machine model only, are the simplest and easiest to implement. However, they are very sensitive to parameter variations due to the open-loop nature of calculations. Addition of a closed-loop inside the speed estimation scheme improves the quality of the speed estimation process. Different types of speed estimation based on MRAC are reviewed. They mainly differ with respect to which quantity is selected as the output of the reference model and adjustable model. Four MRAC based speed estimation schemes are discussed. Rotor flux based speed estimation method is based on rotor flux as the output of the reference and adjustable model. Back emf based speed estimation method is designed to eliminate the pure integration from the reference model. Reactive power based MRAC speed estimation method has the advantage of being completely robust with respect to the stator resistance variations as the stator resistance is eliminated from the reference model. Air-gap power based speed estimation method eliminates the transient stator inductance from the reference model. Among these methods, rotor flux based MRAC speed

estimation method is believed to be the most common choice due to its relative design simplicity. Therefore, rotor flux based MRAC speed estimation scheme is used in the study of sensorless vector controlled induction motor drives in this thesis in conjunction with the indirect feed-forward rotor flux oriented control of a current-fed induction machine.

The selected control scheme for further analysis requires precise knowledge of a number of induction motor parameters for its successful operation. This project attempts to provide original contributions by looking at two specific issues. The first one is the impact of parameter variations and unmodelled phenomena on accuracy of the control, while the second one is the possibility of compensation of the unmodelled phenomena by introduction of modified structures of the control system and the speed estimator.

The principles of vector control of induction machines were developed based on the constant parameter mathematical model of an induction machine, that neglects the iron loss and main flux saturation in the machine. The same applies to the speed estimation scheme under consideration. Therefore, detuned operation will inevitably result both due to neglected phenomena and due to variation of the machine parameters. In order to investigate the detuning effects caused by iron loss and main flux saturation in sensorless vector controlled induction machines, machine models that include representation of iron loss and main flux saturation are needed. Three types of modified dynamic and steady-state models of induction machine are introduced for this reason. The first one is the model that includes iron loss representation. The iron loss is represented as an equivalent iron loss resistance, which is placed in parallel with the magnetising branch in the equivalent circuit and is a function of frequency. Next, three existing induction machine models that account for main flux saturation are elaborated. Finally, an induction machine model that includes representation of both iron loss and main flux saturation is given.

Influence of iron loss and main flux saturation on operation of sensorless vector controlled induction machines has not been studied yet. One of the main aims of this thesis is to attempt to investigate the influence of iron loss and main flux saturation on

operation of a sensorless vector controlled induction motor drive with rotor flux based MRAC speed estimator.

Steady-state analyses are performed at first. Detuning due to iron loss in sensorless rotor flux oriented induction machines is evaluated. Influence of parameter variations and/or incorrect parameter setting, such as stator resistance, rotor resistance, stator and rotor leakage inductance, and magnetising inductance, is investigated next. Based on the results conclusions regarding relative importance of various parameter variation effects are given. A series of dynamic simulations is then undertaken in order to evaluate detuning due to iron loss, main flux saturation and parameter variations in transient operation. The results show that speed estimation errors caused by iron loss and main flux saturation are not negligible. It is therefore necessary to compensate the detuning effects for high performance sensorless drives.

In order to compensate the detuning effects, standard vector controller and constant parameter MRAC speed estimator of a sensorless indirect rotor flux oriented induction machine have to be modified. Three improved vector control schemes with improved rotor flux based MARC speed estimators are proposed. Vector control system with compensation of iron loss is introduced at first. Modified speed estimator, that compensates for the negative impact of the iron loss existence on the drive operation, is developed. By subtracting equivalent iron loss currents from the inputs of the constant parameter MRAC speed estimator, the speed estimation errors are almost eliminated. Compensation of main flux saturation is realised by utilising an existing modified indirect vector controller with main flux saturation compensation. Modified MRAC speed estimator that accounts for the main flux saturation, is then developed. Its capability to compensate for the variable degree of main flux saturation in the field-weakening region is verified. Finally, by combining the two schemes that compensate for either iron loss or main flux saturation, the third sensorless vector control scheme with simultaneous iron loss and main flux saturation compensation is designed.

A number of experiments are performed to confirm some of the results of the theoretical studies. Detailed speed estimator design and tuning procedure is at first developed. Next, a study of parameter variation effects on the speed estimator

performance is conducted, with the aim of confirming the results of the theoretical steady-state analyses. Finally, a modified speed estimator capable of main flux saturation compensation, developed during the course of this project, is implemented. Its ability to adapt to the saturation level in the machine is verified experimentally.

10.2 Conclusions

The thesis represents a research into the effects of the various phenomena on the performance of the sensorless rotor flux oriented induction machine and means for their compensation. All the research objectives, set in section 1.4 are satisfactorily met.

Quantitative studies of detuning, caused by parameter variations and unmodelled phenomena, in a sensorless rotor flux oriented induction machine with rotor flux based MRAC speed estimator have been conducted for steady-state operation and transient operation. Steady-state analysis has been conducted by developing an appropriate set of mathematical expressions that describe the drive. Transient operation is investigated by building appropriate drive dynamic models within the Simulink environment. The results of the dynamic simulations are found to be in excellent agreement with results of the steady-state analyses. The novel approach, developed for the study of detuning effects in steady-state operation, is thus fully verified.

The results show that parameter variations will inevitably cause detuned operation of a sensorless RFO induction machine. The major consequence of the parameter variations and the unmodelled phenomena is a speed estimation error. One very interesting conclusion is that dynamics of the drive remain to a large extent unaffected by the parameter variations. This is so because the orientation angle error caused by parameter variations is either negligible or very small. Such situation is in huge contrast to a sensored vector controlled drive where parameter variation effects are predominantly reflected in the orientation angle error, so that dynamics of the drive are significantly affected in detuned operation. As far as the speed estimation error is concerned, variation of rotor resistance leads to the highest values. Stator resistance variation at low speed of operation, iron loss and incorrect setting of the magnetising inductance all

lead to a moderate speed estimation error. Variation of leakage inductances appears to be of the least importance.

The influence of iron loss and main flux saturation on the performance of a sensorless vector controlled induction machine has been investigated in detail. It is concluded that speed estimation errors caused by the iron loss are of the same order as those caused by other parameter variations in the base speed region. Main flux saturation causes substantial speed estimation in the field-weakening region. Based on these findings, it is concluded that it is necessary to compensate the detuning effects. Therefore, three novel MARC speed estimators have been developed. As the idea is to compensate either iron loss, or main flux saturation or both, so-called model based approach is used in development of novel speed estimators. The principle of compensation of iron loss is to extract the iron loss currents from the indirect vector controller and subtract them from the measured stator current components. This is applicable in conjunction with modified indirect vector controller, that introduces separate iron loss current components in the process of the stator current command creation. For compensation of main flux saturation, an existing modified vector controller with compensation of main flux saturation is employed. Constant parameter speed estimator is then modified in such a way that it fully adapts itself to the actual saturation level in the machine. In particular, modification of the reference model enables estimation of the magnetising inductance, that is then used in the adjustable model. Finally, by combining the two developed modified speed estimators with an existing modified vector controller, a novel improved sensorless vector controlled induction machine system is proposed, which can instantaneously and simultaneously compensate both the iron loss and main flux saturation. The improved performance, obtainable with novel speed estimators, is verified by simulations. It is concluded that each of the three developed novel speed estimators enables very satisfactory compensation of the given phenomenon (phenomena).

Finally, experimental investigation is performed in order to investigate the detuning effects in the constant parameter speed estimator due to parameter variations and to examine the performance of the developed modified MRAC speed estimator, that compensates for the main flux saturation. The results show that the speed estimation

errors due to parameter variations are very similar to the results of theoretical studies although the machines used in theoretical studies and in experiments are different. It is therefore concluded that the results of the analytical investigations and simulations can be regarded as proved. The performance of the novel modified speed estimator is examined. The speed estimation error is shown to be greatly reduced in the field-weakening region when saturation-adaptive speed estimator is used. Theoretical considerations are therefore once more confirmed by experimental investigation.

10.3 Future work

Parameter variations effects in a sensorless vector-controlled induction machine with one specific form of MRAC based speed estimator have been studied in detail.

A rather obvious direction for possible future work is to conduct the same type of study for other MRAC based speed estimation schemes. One contribution to this direction has been provided here by the analysis of the impact of iron loss on the reactive power based type of MRAC based speed estimator.

Assuming that the proposed study is completed, the next stage would be to compare all the different types of the MRAC speed estimator in terms of their sensitivity to parameter variation effects. The comparison would additionally have to encompass the implementation related issues, such as those discussed in the section on speed estimator tuning in the chapter related to experimental investigation. The ultimate goal of this study would be to conclude which of the numerous possibilities of the MRAC based speed estimation offers the best prospects for industrial applications.

The other model based closed-loop speed estimators, of observer and EKF type, could be covered by the next stage of the study. Parameter variation effects and the implementation requirements would again constitute the basis for comparison. Ultimately, certain guide-lines could be produced, detailing the best model based approaches to speed estimation for the given hardware platform.

The approach to development of modified speed estimators, that are inherently capable of compensating for one or more of the phenomena, can be extended to other types of MRAC based speed estimators, as well as to observer and EKF based speed estimation.

The issue of speed estimation is relevant not only for sensorless vector control, but for direct torque control (DTC) as well. DTC of induction machines is rapidly evolving as a viable concept for industrial applications. As DTC does not require speed information for the control algorithm itself, speed estimate has to be provided only for closed-loop speed control. Investigation of parameter variation effects in DTC induction motor drives therefore constitutes another possible area for future research.

11 REFERENCES

Abbondanti,A., Brennen,M.B. (1975). Variable speed induction motor drives use electronic slip calculator based on motor voltages and currents, *IEEE Transactions on Industry Applications*, Vol. 11, No. 5, pp. 483-488.

Akin,E., Can,H., Ertan,H.B., Uctug,Y. (1998). Comparison of integration algorithms for vector control, *Proc. Proc. Int. Conf. on Electrical Machines ICEM*, Istanbul, Turkey, pp. 1626-1631.

Arcker-Hissel,A.M., Ammar,F.B., Pietrzak-David,M., Fornel,B. (1998). Speed sensorless variable structure control of high power induction motor drives, *Proc. IEE Power Elec. and Variable Speed Drives Conf. PEVD*, London, UK, IEE Conf. Pub. No. 456, pp. 335-340.

Armstrong,G.J., Atkinson,D.J. (1997). A comparison of model reference adaptive system and extended Kalman filter estimators for sensorless vector drives, *Proc. Eur. Conf. on Power Elec. and Applications EPE*, Trondheim, Norway, pp. 1.424-1.429.

Armstrong,G.J., Atkinson,D.J., Acarnley,P.P. (1997). A comparison of estimation techniques for sensorless vector controlled induction motor drives, *Proc. IEEE Power Elec. and Drive System Conf. PEDS*, Singapore, pp. 110-116.

Attaianese,C., Marongiu,I., Perfetto,A. (1995). A speed sensorless digitally controlled induction motor drive estimating rotor resistance variation, *Proc. Eur. Conf. on Power Elec. and Applications EPE*, Sevilla, Spain, pp. 1.741-1.746.

Attaianese,C., Tomasso,G., Damiano,A. Marongiu,I., Perfetto,A. (1997). On line estimation of speed and parameters in induction motor drives, *Proc. IEEE Int. Symp. on Industrial Electronics ISIE*, Guimaraes, Portugal, pp. 1054-1059.

Baader,U., Depenbrock,M., Gierse,G. (1992). Direct self control (DSC) of inverter-fed induction machine: a basis for speed control without speed measurement, *IEEE Transactions on Industry Applications*, Vol.28, No.3, pp. 581 - 588.

Beguenane,R., Benbouzid,M.E.H. and Capolino,G.A. (1995). Design of slip frequency detector with improvement accuracy for induction motor rotor parameters

updating, *Proc. Eur. Conf. on Power Elec. and Applications EPE*, Sevilla, Spain, pp. 3.417-3.422.

Beguenane,R., Benbouzid,M.E.H., Capolino,G.A. (1996). Rotor parameter updating for induction motor vector control by non-invasive slip frequency measurement, *Proc. Int. Conf. on Electrical Machines ICEM*, Vigo, Spain, Vol.3, pp. 153-157.

Beierke,S., Vas,P., Simor,B. Stronach,A.F. (1997). DSP-controlled sensorless AC vector drives using the extended Kalman filter, *Proc. Power Conversion and Intelligent Motion Conf. PCIM*, Nuremberg, Germany, pp. 31-41.

Ben-Brahim,L. (1995). Motor speed identification via neural networks, *IEEE Industry Applications Magazine*, January/February, pp. 28-32.

Ben-Brahim,L., Kawamura,A. (1992). A fully digitized field-oriented controlled induction motor drive using only current sensors, *IEEE Transactions on Industrial Electronics*, Vol.39, No.3, pp. 241-249.

Ben-Brahim,L., Kurosawa,R. (1993). Identification of induction motor speed using neural networks, *Proc. Power Conversion Conf. PCC*, Yokohama, Japan, pp. 689-694.

Benchaib,A., Tadjine,M., Rachid,A., Tayebi,A. (1997). Adaptive sliding mode observer for state estimation of an induction motor on DSP-based system, *Proc. IEEE Int. Elec. Machines and Drives Conf. IEMDC*, Milwaukee, WI, pp. MC2-3.1-MC2-3.3.

Blaabjerg,F., Pedersen,J.K., Kazmierkowski,M.P. (1996). DSP based current regulated PWM inverter-fed induction motor drive without speed sensor, *Proc. IEEE Int. Symp. on Industrial Electronics ISIE*, Warsaw, Poland, pp. 659 -664.

Blaschke,F. (1971). The principle of field orientation - the basis for the TRANSVEKTOR control of three phase machines, *Siemens - Zeitschrift*, Vol. 45, No.10, pp. 757 - 760.

Blasco-Gimenez,R., Asher,G.M., Sumer,M. (1995). A new method of stator resistance estimation for enhanced dynamic performance of sensorless vector control drives, *Proc. Eur. Conf. on Power Elec. and Applications EPE*, Sevilla, Spain, pp. 1.689-1.694.

Blasco-Gimenez,R., Asher,G.M., Sumner,M., Bradley,K.J. (1996a). Dynamic performance limitations for MRAS based sensorless induction motor drives. Part 1: Stability analysis for the closed loop drive, *IEE Proc.-Electr. Power Applications*, Vol.143, No.2, pp. 113-122.

Blasco-Gimenez,R., Asher,G.M., Sumner,M., Bradley,K.J. (1996b). Dynamic performance limitation for MRAS based sensorless induction motor drives. Part 2: On-line parameter tuning and dynamic performance studies, *IEE Proc.-Electr. Power Applications*, Vol.143, No,2, pp. 123-134.

Boldea,I., Nasar,S.A. (1987). Unified treatment of core losses and saturation in the orthogonal-axis model of electric machines, *IEE Proceedings*, Vol.134, Pt.B, No.6, pp. 355-363.

Boldea,I., Nasar,S.A. (1992). *Vector control of AC drives*, Boca Raton, FL: CRC Press.

Bonanno,C.J., Zhen,L., Xu,L. (1995). A direct field oriented induction machine drive with robust flux estimator for position sensorless control, *Proc. IEEE Ind. Appl. Soc. Annu. Meeting IAS*, Orlando, FL, pp. 166-173.

Bose,B.K. (1988). Technology trends in microcomputer control of electrical machines, *IEEE Transactions on Industrial Electronics*, Vol. 35, No. 1, pp. 160-177.

Bose,B.K. (1997). High performance control and estimation in AC drives, *Proc. IEEE Ind. Electronics Soc. Annu. Meeting IECON*, New Orleans, LA, pp. 377 - 385.

Bose,B.K., Simoes,M.G. (1995). Speed sensorless hybrid vector controlled induction motor drive, *Proc. IEEE Ind. Appl. Soc. Annu. Meeting IAS*, Orlando, FL, pp. 137-143.

Choy,I., Kwon,S.H., Lim,J., Hong,S.W. (1996). Robust speed estimation for tacholess induction motor drives, *Electronics Letters*, Vol. 32, No. 19, pp.1836-1838.

Cilia,J., Asher,G.M., Bradley,K.J., Sumner,M. (1997). Sensorless position detection for vector-controlled induction motor drives using an asymmetric outer-section cage, *IEEE Transactions on Industry Applications*, Vol. 33, No. 5, pp. 1162-1169.

Cilia,J., Asher,G.M., Bradley,K.J., Sumner,M. (1998a). Dynamic studies for MRAS-based speed and flux observers in high-performance sensorless induction motor

drives, *Proc. Power Electronics and Motion Control Conf. PEMC*, Prague, Czech Republic, pp. 4.70-4.75.

Cilia,J., Asher,G.M., Shuli,J., Sumner,M., Bradley,K.J., Ferrah,A. (1998b). The estimation of the fundamental frequency in sensorless vector controlled induction motor drives using a real-time adaptive filter, *Proc. Int. Conf. on Electrical Machines ICEM*, Istanbul, Turkey, pp. 1017-1021.

Conroy,B.P., Sumner,M., Alexander,T. (1995). Application of encoderless vector control techniques in a medium performance induction motor drive, *Proc. Eur. Conf. on Power Elec. and Applications EPE*, Sevilla, Spain, pp. 3.469-3.474.

Degner,.M.W., Lorenz,R.D., (1997). Position estimation in induction machines utilising rotor bar slot harmonics and carrier frequency signal injection, *Proc. Power Conversion Conf. PCC*, Nagaoka, Japan, pp. 69-72.

Degner,M.W., Lorenz,R.D. (1998). Using multiple saliencies for the estimation of flux, position, and velocity in AC machines, *IEEE Transactions on Industry Applications*, Vol. 34, No. 5, pp. 1097-1104.

Dixon,J.W., Rivarola,J.N., (1996). An improved method to measure speed in induction motors, based on induced irregularities, *Proc. IEEE Applied Power Elec. Conf. APEC*, San Jose, CA, pp. 399-404.

Doki,S., Sangwongwanich,S. Okuma,S. (1992). Implementation of speed-sensor-less field-oriented vector control using adaptive sliding observer, *Proc. IEEE Ind. Electronics Soc. Annu. Meeting IECON*, San Diego, CA, pp. 453-458.

Ferrah,A., Bradley,K.G. and Asher,G.M. (1992a). A FFT-based novel approach to noninvasive speed measurement in induction motor drives, *IEEE Transactions on Instrumentation and Measurement*, Vol. 41, No. 6, pp. 797-802.

Ferrah,A., Bradley,K.G. and Asher,G.M. (1992b). Sensorless speed detection of inverter fed induction motors using rotor slot harmonics and fast Fourier transform, *IEEE Power Electronics Specialist Conference PESC*, Toledo, Spain, pp. 279-286.

Ferrah,A., Bradley,K.J., Hogben,P.J. Woolfson,M.S., Asher,G.M. (1996). A transputer-based speed identifier for induction motor drives using real-time adaptive

filtering, *Proc. IEEE Ind. Appl. Soc. Annu. Meeting IAS,* San Diego, CA, pp. 394-400.

Ferrah,A., Bradley,K.J., Hogben-Laing,P.J., Woolfson,M.S., Asher,G.M., Sumner,M., Cilia,J., Shuli,J. (1998). A speed identifier for induction motor drives using real-time adaptive digital filtering, *IEEE Transactions on Industry Applications*, Vol.34, No.1, pp. 156-162.

Garcia,G.O., Santisteban,J.A., Brignone,S.D. (1994). Iron losses influence on a field-oriented controller, *Proc. IEEE Ind. Electronics Soc. Annu. Meeting IECON*, Bologna, Italy, pp. 633-638.

Harnefors,L. (1998). A comparison between directly parameterised observers and extended Kalman filters for sensorless induction motor, *Proc. IEE Power Elec. and Variable Speed Drives Conf. PEVD*, London, UK, IEE Conf. Pub. No. 456, pp. 275-280.

Hasse,K. (1969). Zur dynamic drehzahlgeregelter Antriebe mit Stromrichter-gespeisten Asynchron-Kurzschlusslaufermaschinen, *PhD Dissertation*, Tech. Hochschule Darmstadt, Germany.

Holliday,D., Fletcher,J.E., Williams,B.W. (1995). Non-invasive rotor position and speed sensing of asynchronous motors, *Proc. Eur. Conf. on Power Elec. and Applications EPE*, Sevilla, Spain, pp. 1.333-1.337.

Holtz,J. (1993). Speed estimation and sensorless control of AC drives, *Proc. IEEE Ind. Electronics Soc. Annu. Meeting IECON*, Miaui, Hawaii, pp. 649-654.

Holtz,J. (1995). State of the art of controlled AC drives without speed sensor, *Proc. IEEE Power Elec. And Drive System Conf. PEDS*, Singapore, pp. 1-6.

Holtz,J., Jiang,J., Pan,H. (1997). Identification of rotor position and speed of standard induction motors at low speed including zero stator frequency, *Proc. IEEE Ind. Electronics Soc. Annu. Meeting IECON*, New Orleans, LA, pp. 971-976.

Hu,J., Wu,B. (1997). New integration algorithms for estimating motor flux over a wide speed range, *Proc. IEEE Power Elec. Spec. Conf. PESC*, St. Louis, MI, pp. 1075-1081.

Hur,N., Hong,K., Nam,K. (1996). Real-time parameter identification scheme for the sensorless control of induction motors using a reduced order model, *Proc. IEEE Ind. Electronics Soc. Annu. Meeting IECON*, Taipei, Taiwan, pp. 1161-1166.

Hurst,K.D., Habetler,T.G. (1997). A comparison of spectrum estimation techniques for sensorless speed detection in induction machines, *IEEE Transactions on Industry Applications*, Vol.33, No.4, pp. 898-905.

Hurst,K.D., Habetler,T.G., Griva,G., Profumo,F. (1994). Speed sensorless field-oriented control of induction machines using current harmonic spectral estimation, *Proc. IEEE Ind. Appl. Soc. Annu. Meeting IAS*, Denver, CO, pp. 601-607.

Hurst,K.D., Habetler,T.G., Griva,G. Profumo,F., Jansen,P.L. (1997). A self-tuning closed-loop flux observer for sensorless torque control of standard induction machines, *IEEE Transactions on Power Electronics*, Vol. 12, No. 5, pp. 807-815.

Ilas,C., Bettini,A., Ferraris,L., Griva,G., Profumo,F. (1994). Comparison of different schemes without shaft sensors for field oriented control drives, *Proc. IEEE Ind. Electronics Soc. Annu. Meeting IECON*, Bologna, Italy, pp. 1579-1588.

Ilas,C., and Magureanu,R. (1996). DSP-based sensorless direct field oriented control of induction motor drives, *Proc. Power Electronics and Motion Control Conf. PEMC*, Budapest, Hungary, pp. 2/309-2/313.

Jansen,P.L., Lorenz,R.D. (1993). Accuracy limitations of velocity and flux estimation in direct field oriented induction machines, *Proc. Eur. Conf. on Power Elec. and Applications EPE*, Brighton, UK, pp. 312-318.

Jansen,P.L., Lorenz,R.D. (1995a). Transducerless field orientation concepts employing saturation-induced saliencies in induction machines, *Proc. IEEE Ind. Appl. Soc. Annu. Meeting IAS*, Orlando, FL, pp. 174-181.

Jansen,P.L., Lorenz,R.D. (1995b). Transducerless position and velocity estimation in induction and salient AC machines, *IEEE Transactions on Industry Applications*, Vol. 31, No. 2, pp. 240-247.

Jansen,P.L., Lorenz,R.D. (1996). Transducerless field orientation concepts employing saturation-induced saliencies in induction machines, *IEEE Transactions on Industry Applications*, Vol. 32, No. 6, pp. 1380-1393.

Jemli,M., Boussak,M., Gossa,M., Kamoun,M.B.A. (1998). MRAS identification scheme for sensorless indirect field oriented control of induction motor drives with rotor resistance tuning, *Proc. Int. Conf. on Electrical Machines ICEM*, Istanbul, Turkey, pp. 1572-1577.

Jiang,J., Holtz,J. (1995). Speed sensorless AC drive for high performance and steady state accuracy, *Proc. IEEE Ind. Electronics Soc. Annu. Meeting IECON*, Orlando, FL, pp. 1029-1034.

Jiang,J., Holtz,J. (1997). High dynamic speed sensorless AC drive with on-line model parameter tuning for steady-state accuracy, *IEEE Transactions on Industrial Electronics*, Vol. 44, No. 2, pp. 240-246.

Joetten,R., Schierling,H. (1983). Control of the induction machine in the field weakening range, *Proceedings of IFAC Symposium on Power Electronics and Electric Drives*, pp. 297-304, Lausanne, Switzerland.

Kanmachi,T., Takahashi,I. (1993). Sensor-less speed control of an induction motor with no influence of secondary resistance variation, *Proc. IEEE Ind. Appl. Soc. Annu. Meeting IAS*, Miaui, Hawaii, pp. 408-413.

Kataoka,Y., Kubota,H., Matsuse,K. (1997). Sensorless vector control of induction machines with stator voltage offset compensation, *Proc. Eur. Conf. on Power Elec. and Applications EPE,* Trondheim, Norway, pp. 4.508-4.511.

Kelmen,A., Pana,T., Stugren,F. (1996). Implementation of sensorless vector-controlled induction motor drive system with rotor resistance estimation using floating point DSP, *Proc. Power Electronics and Motion Control Conf. PEMC*, Budapest, Hungary, pp. 2/186-2/191.

Kim,M., Hung,J.C. (1995). Vector control system for induction motor without speed sensor at very low speed, *Proc. IEEE Ind. Electronics Soc. Annu. Meeting IECON*, Orlando, FL, pp. 524-529.

Kim,S., Kim,J., Kim,H., Kim,Y. (1997). Binary observer for speed sensorless vector control of induction motors, *Proc. IEEE Power Elec. Spec. Conf. PESC*, St. Louis, MI, pp. 1061-1067.

Kim,T., Kawamura,A. (1996). Slip frequency estimation for sensorless low speed control of induction motor, *Proceedings of the 1996 4th International Workshop on Advanced Motion Control*, Vol.1, Tsu-City, Japan, pp. 156-161.

Kim,Y., Sul,S., Park,M. (1994). Speed sensorless vector control of induction motor using extended Kalman filter, *IEEE Transactions on Industry Applications*, Vol. 30, No. 5, pp. 1225-1233.

Kubota,H., Matsuse,K. (1992). Compensation for core loss of adaptive flux observer-based field-oriented induction motor drives. *Proc. IEEE Ind. Electronics Soc. Annu. Meeting IECON*, San Diego, CA, pp. 67-71.

Kubota,H., Matsuse,K. (1994a). Speed sensorless field oriented control of induction machines using flux observer, *Proc. IEEE Ind. Electronics Soc. Annu. Meeting IECON*, Bologna, Italy, pp. 1611-1615.

Kubota,H., Matsuse,K. (1994b). Speed sensorless field-oriented control of induction motor with rotor resistance adaptation, *IEEE Transactions on Industry Applications*, Vol.30, No.5, pp. 1219-1224.

Kubota,H., Matsuse,K. (1996). The improvement of performance at low speed by offset compensation of stator voltage in sensorless vector controlled induction machines, *Proc. IEEE Ind. Appl. Soc. Annu. Meeting IAS*, San Diego, CA, pp. 257-261.

Kubota,H., Matsuse,K., Nakano,T. (1993). DSP-based speed adaptive flux observer of induction motor, *IEEE Transactions on Industry Applications*, Vol. 29, No. 2, pp. 344-348.

Kulkarni,A.S., El-Sharkawi,M.A. (1997). Speed estimator for induction motor drives using artificial neural network, *Proc. IEEE Int. Elec. Machines and Drives Conf. IEMDC*, Milwaukee, WI, pp. MD2-2.1 - MD2-2.3.

Lai,Y.S., Liu,C.N., Chang,K.Y., Luo,Y.C., Lee,Y.C., Liu,C.H. (1997). Sensorless vector controllers for induction motor drives, *Proc. IEEE Power Elec. and Drive Systems Conf. PEDS*, Singapore, pp. 663-669.

Lee,S.H., Ha,I.J., Yoo,H.S., Hong,B.Y., Yoon,S.J. (1996). An on-line identification method for both stator and rotor resistances of induction motors without rotational transducers, *Proc. IEEE Int. Symp. on Industrial Electronics ISIE*, Warsaw, Poland, pp. 325-330.

Leonhard,W. (1985). *Control of electrical drives*, Berlin: Springer-Verlag.

Levi,E. (1994). Mathematical models of field-oriented induction machines incorporating the iron loss, *Proc. Int. Conf. on Electrical Machines ICEM*, Paris, France, Vol. 2, pp. 683-687.

Levi,E. (1995). Impact of iron loss on behaviour of vector controlled induction machines, *IEEE Transactions on Industry Applications*, Vol.31, No.6, pp. 1287-1296.

Levi,E, Krzeminski,Z (1996). Main flux saturation modelling in d-q axis models of induction machines using mixed current-flux state-space models, *European Transactions on Electrical Power Engineering ETEP*, Vol. 6, No. 3, pp. 207-215.

Levi,E., Sokola,M. (1997). A novel saturation adaptive rotor flux estimator for rotor flux oriented induction machines, *Proc. European Conf. on Power Electronics and Applications, EPE*, Trondheim, Norway, pp. 1.518-1.523.

Levi,E., Sokola,M., Boglietti,A., Pastorelli,M. (1996). Iron loss in rotor-flux-oriented induction machines: identification, assessment of detuning, and compensation, *IEEE Transactions on Power Electronics*, Vol. 11, No. 5, pp. 698-709.

Levi,E., Vuckovic,V. (1989). Field-oriented control of induction machines in the presence of magnetic saturation, *Electric Machines and Power Systems*, Vol.16, pp. 133-147.

Levi,E., Vuckovic,V. (1993). Rotor flux computation in saturated field-oriented induction machines, *Electric Machines and Power Systems*, Vol. 21, No.6, pp. 741-754.

Levi,E., Vukosavic,S., Vuckovic,V. (1990). Saturation compensation schemes for vector controlled induction motor drives, *Proc. IEEE Power Electronics Specialist Conference PESC*, San Antonio, TX, pp. 591-598.

Levi,E., Wang,M. (1997). Impact of iron loss on speed estimation in sensorless vector controlled induction machines, *Proc. IEEE Ind. Electronics Soc. Annu. Meeting IECON*, New Orleans, LA, pp. 977-982.

Levi,E., Wang,M. (1998). Impact of parameter variations on speed estimation in sensorless rotor flux oriented induction machines, *Proc. IEE Power Elec. and Variable Speed Drives Conf. PEVD*, London, UK, pp. 305-310.

Levi,E., Wang,M. (1999). Main flux saturation compensation in sensorless vector controlled induction machines for operation in the field weakening region, *Proc. Eur. Power Electronics and Application Conf. EPE*, Lausanne, Switzerland.

Levi,E., Wang,M., Williams,D. (1999). Evaluation of iron loss influence on speed estimation in sensorless MRAC-based field-oriented induction machines, *European Transactions on Electrical Power ETEP*, Vol. 9, No. 2, pp. 77-84.

Lin,Y., Chen,C. (1996). Automatic IM parameter measurement under sensorless field-oriented control, *Proc. IEEE Int. Symp. on Industrial Electronics ISIE*, Warsaw, Poland, pp. 894-899.

Marchesoni,M., Segarich,P., Soressi,E. (1997). A simple approach to flux and speed observation in induction motor drives, *IEEE Transactions on Industrial Electronics*, Vol. 44, No. 4, pp. 528-535.

Marwali,M.N., Keyhani,A. (1997). A comparative study of flux based MRAS and back emf based MRAS speed estimators for speed sensorless vector control of induction machines, *Proc. IEEE Ind. Appl. Soc. Annu. Meeting IAS*, New Orleans, LA, pp. 160-166.

Mehrotra,P., Quaicoe,J.E., Venkatesan,R. (1996). Development of an artificial neural network based induction motor speed estimator, *Proc. IEEE Power Elec. Spec. Conf. PESC*, Baveno, Italy, pp. 682-688.

Nardocci,V., Parasoliti,F., Tursini,M. (1997). Speed sensorless field-oriented control of induction motors by sliding mode observer, *Proc. Universities Power Eng. Conf. UPEC*, Manchester, UK, pp. 999-1002.

Nguyen,M.T., Sathiakumar,S., Shrivastava,Y. (1998). Speed estimation for induction machine, *Proc. Power Electronics and Motion Control Conf. PEMC*, Prague, Czech Republic, pp. 3.160-3.165.

Novotny,D.W., Lipo,T.A. (1996) *Vector control and dynamics of ac drives*, Oxford: Clarendon Press.

Ohmori,Y., Takagi,M., Kiriya,T. (1997). Improvement of low side speed control characteristics of an induction motor without a speed sensor, *Proc. Power Conversion Conf. PCC*, Nagaoka, Japan, pp. 531-534.

Ohtani,T., Takada,N., Tanaka,K. (1992). Vector control of induction motor without shaft encoder, *IEEE Transactions on Industry Applications*, Vol.28, No.1, pp. 157-164.

Orlowska-Kowalska,T., Wojsznis,P. (1996). Comparative study of rotor flux estimators sensitivity in the speed sensorless induction motor drive, *Proc. IEEE Int. Symp. on Ind. Elec. ISIE*, Warsaw, Poland, pp. 348-353.

Pana,T. (1996). Model based speed and rotor resistance estimation for sensorless vector controlled induction motor drives using floating point DSP, *Proc. Int. Workshop on Advanced Motion Control*, Tsu-City, Japan, pp. 168-173.

Pana,T. (1997). Sensorless vector-controlled induction motor drive system with rotor resistance estimation using parallel processing with floating point DSP, *Proc. Power Conversion Conf. PCC*, Nagaoka, Japan, pp. 79-84.

Peng,F.Z., Fukao,T. (1994). Robust speed identification for speed-sensorless vector control of induction motors, *IEEE Transactions on Industry Applications*, Vol. 30, No. 5, pp 1234-1240.

Perng,S, Lai,Y. Liu,C. (1997). A novel sensorless controller for induction motor drives, *Proc. Eur. Conf. on Power Elec. and Applications EPE*, Trondheim, Norway, pp. 4.480-4.485.

Rajashekara,K., Kawamura,A., Matsuse,K., editors, (1996). *Sensorless control of AC motor drives*, Piscataway, NJ: IEEE Press.

Salvatore,L., Stasi,S., Cupertino,F. (1998). Speed-sensorless vector controlled induction motors using EKF, *Proc. Int. Conf. on Electrical Machines ICEM*, Istanbul, Turkey, pp. 994-999.

Schauder,C. (1992). Adaptive speed identification for vector control of induction motor without rotational transducers, *IEEE Transactions on Industry Applications*, Vol. 28, No. 5, pp. 1054-1061.

Shirsavar,S.A., McCulloch,M.D. (1996). Speed sensorless vector control of induction motors with parameter estimation, *Proc. IEE Power Elec. and Variable Speed Drives Conf. PEVD*, Nottingham, UK, IEE Conf. Pub. No. 429, pp. 267-272.

Sng,E.K.K., Liew,A., Lipo,T.A. (1998). New observer-based DFO scheme for speed sensorless field-oriented drives for low-zero-speed operation, *IEEE Transactions on Power Electronics*, Vol. 13, No. 5, pp. 959-968.

Sokola,M. (1998). Vector control of induction machines using improved machine models, *PhD Thesis*, Liverpool John Moores University, Liverpool, UK.

Staines,C.S., Asher,G.M., Bradley,K.J. (1998). A new method for sensorless derivation of an induction motor shaft position and other machine characteristics, *Proc. Int. Conf. on Electrical Machines ICEM*, Istanbul, Turkey, pp. 902-907.

Tajima,H., Hori,Y. (1993). Speed sensorless field-orientation control of the induction machine, *IEEE Transactions on Industry Applications*, Vol. 29, No. 1, pp. 175-180.

Trzynadlowski,A.M. (1994). *The field orientation principle in control of induction motors*, Norwell, MA: Kluwer Academic Publishers.

Tsuji,T., Oguro,R., Ide,K., Hazama,K., Yang,Z. (1996). Speed sensorless field oriented control of induction motors with an observer compensating stator voltage errors, *Proc. Int. Conf. on Electrical Machines ICEM*, Vigo, Spain, Vol. 3, pp. 190-195.

Tzou,Y., Lee,W., Lin,S. (1996). Dual-DSP sensorless speed control of an induction motor with adaptive voltage compensation, *Proc. IEEE Power Elec. Spec. Conf. PESC*, Baveno, Italy, pp. 351-357.

Umanand,L., Bhat,S.R., (1995). On-line estimation of stator resistance of an induction motor for speed control applications, *IEE Proc.-Electr. Power Applications*, Vol.142, No.2, pp. 97-103.

Vas,P. (1990) *Vector control of AC machines*, Oxford: Oxford University Press

Vas,P. (1992). *Electrical machines and drives - A space-vector theory approach*, Oxford: Clarendon Press.

Vas,P. (1998). *Sensorless vector and direct torque control*, Oxford: Oxford University Press.

Wang,M., Levi,E. (1998). Impact of parameter variations on dynamics of sensorless indirect rotor flux oriented induction machine, *Proc. Universities Power Eng. Conf. UPEC*, Edinburgh, UK, pp. 855-858.

Wang,M., Levi,E. (1999). Evaluation of steady-state and transient behaviour of a MRAS based sensorless rotor flux oriented induction machine in the presence of parameter detuning, *Electric Machines and Power Systems*, Vol. 27, No. 11.

Wang,M., Levi,E., Jovanovic,M. (1999). Compensation of parameter variation effects in sensorless indirect vector controlled induction machines using model based approach, *Electric Machines and Power Systems*, Vol. 27, No. 9.

Wang,M., Levi,E., Williams,D. (1997). Impact of iron loss on speed estimation accuracy in reactive power MRAC based sensorless rotor flux oriented induction machines, *Proc. Universities Power Eng. Conf. UPEC*, Manchester, UK, pp. 995-998.

Westerholt,E. (1997). A PCMCIA DSP-card to boost inverter performance: sensorless drive control via extended Kalman filter, *Proc. Eur. Conf. on Power Elec. and Applications EPE*, Trondheim, Norway, pp. 4.498-4.503.

Williamson,S., Healey,R.C. (1996). Space vector representation of advanced motor models for vector controlled induction motors, *IEE Proc. - Electr. Power Applications*, Vol.143, No.1, pp. 69-77.

Wong,J.K.J., Lefley,P.W. (1996). Review of the latest sensorless techniques for induction motor control, *Proc. Universities Power Eng. Conf. UPEC*, Heraklion, Crete, Greece, pp. 1039-1042.

Xu,X., Novotny,D.W. (1991). Implementation of direct stator flux orientation control on a versatile DSP based system, *IEEE Transactions on Industry Applications*, Vol. 27, No. 4, pp. 694-700.

Yang,G., Chin,T.H. (1993). Adaptive speed identification scheme for a vector-controlled speed sensorless inverter-induction motor drive, *IEEE Transactions on Industry Applications*, Vol.29, No.4, pp. 820-825.

Yong,S., Choi,J., Sul,S. (1994). Sensorless vector control of induction machine using high frequency current injection, *Proc. IEEE Ind. Appl. Soc. Annu. Meeting IAS*, Denver, CO, pp. 503-508.

Yoo,H.S., Ha,I.J., Lee,S.H, Yoon,S.J, Ko,Y. (1994). A polar coordinate-oriented method of identifying rotor flux and speed of induction motors without rotational transducers, *Proc. IEEE Ind. Electronics Soc. Annu. Meeting IECON*, Bologna, Italy, pp. 2116-2121.

Zeng,Y., Feng,D., Chen,B. (1997). A speed calculation method for induction motor based on voltage decoupling control principle, *Proc. Power Conversion Conf. PCC*, Nagaoka, Japan, pp. 573-578.

Zhang,J. (1996). Speed sensorless AC drive fed by a 3-level inverter with improved low-speed torque and speed control, *Proc. IEEE Ind. Electronics Soc. Annu. Meeting IECON*, Taipei, Taiwan, pp. 1128-1133.

Zhen,L., Xu,L. (1995). A mutual MRAS identification scheme for position sensorless field orientation control of induction machines, *Proc. IEEE Ind. Appl. Soc. Annu. Meeting IAS*, Orlando, FL, pp. 159-165.

Zinger,D.S., Profumo,F., Lipo,T.A., Novotny,D.W. (1990). A direct field-oriented controller for induction motor drive using tapped stator windings. *IEEE Transactions on Power Electronics*, Vol. 5, No. 4, pp. 446-453.

APPENDIX A: DATA OF INDUCTION MACHINES

A1. 4 kW motor used in simulations

4 kW 380 V 8.7 A 1440 rpm

50 Hz stator winding star connected

$T_{en} = 26.5$ Nm $R_s = 1.37\ \Omega$ $R_r = 1.1\ \Omega$

$L_{mn} = 0.1433$ H $L_{\sigma s} = 4.87$ mH $L_{\sigma r} = 7.96$ mH

$$R_{Fe} = \begin{cases} 128.92 + 8.242 f_e + 0.07788 f_e^2 \quad (\Omega) & f_e \le 50 \text{ Hz} \\ 1841 - 55275 / f_e \quad (\Omega) & f_e > 50 \text{ Hz} \end{cases}$$

$$L_m = \begin{cases} 0.1964285 \quad (\text{H}) & \Psi_m \le 0.432 \text{ Wb} \\ 0.8032 - 0.6874\Psi_m - 0.1338 / \Psi_m \quad (\text{H}) & \Psi_m > 0.432 \text{ Wb} \end{cases}$$

A2. 2.3 kW motor used in experiments

2.3 kW 380 V 10 A 1450 rpm

50 Hz stator winding star connected

R_s=0.7 Ω $R_r = 0.926\ \Omega$ $L_{\sigma s}$+$L_{\sigma r}$=7.723 mH

The inverse magnetising curve approximation in per unit:

$$i_{m(p.u.)} = 0.9\psi_{m(p.u.)} + 0.1\psi^7_{m(p.u.)}$$

Rated magnetising current: 4.15 A (rms)

Rated magnetising flux: 0.33 Wb (rms)

$L_{mn} = 78$ mH

APPENDIX B: DETUNING DUE TO IRON LOSS IN THE SENSORLESS SCHEME WITH REACTIVE POWER BASED MRAC SPEED ESTIMATOR

B.1 Analysis of the system

In this investigation, a 4-pole, 50 Hz, 4kW induction machine is used again. All the parameters of the machine are given in Appendix A.

Sensorless indirect rotor flux oriented current-fed induction machine is studied. The speed estimator is the reactive power based MRAC speed estimator discussed in section 4.4. Iron loss is represented in the induction machine model with an equivalent iron loss resistance in parallel with magnetising inductance, as described in section 5.2. Structure of the sensorless rotor flux oriented induction machine remains to be as shown in Figure 6.1.

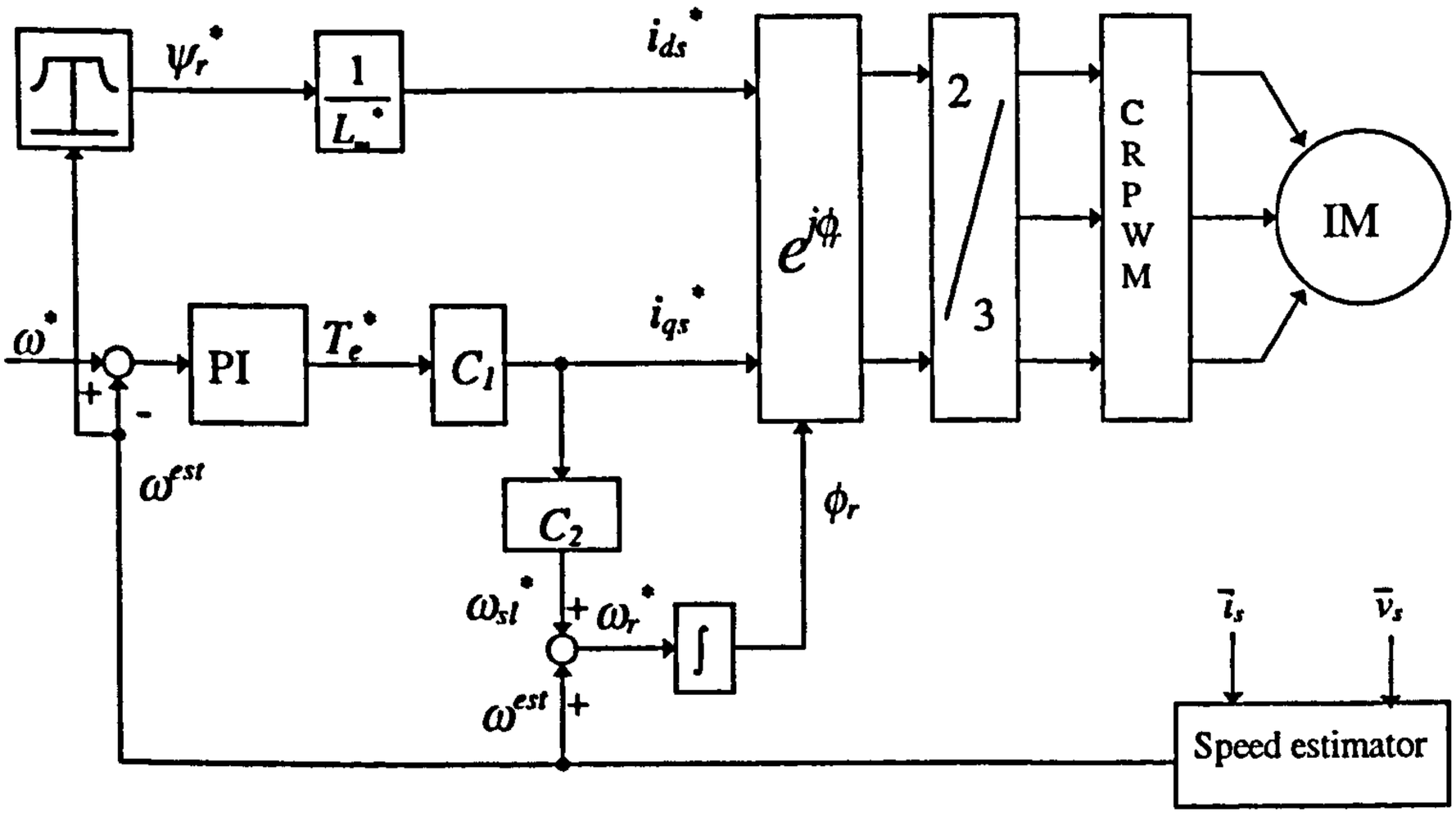

Figure 6.1: Sensorless rotor flux oriented induction machine.

Rotor flux reference is constant and equal to the rated value in the base speed region. In the field-weakening region rotor flux reference is reduced in inverse proportion to the rotor speed. Rate of change of the rotor flux reference in the field-weakening region is neglected. The current controlled PWM inverter is assumed to be ideal and steady-state operation is discussed only. Mathematical modelling is performed in the reference frame firmly attached to the commanded rotor flux space vector. The speed estimator of Figure 6.1 is the one of section 4.4 and is shown in Figure B.1. It relies on measurement

of stator currents and voltages. Existence of iron loss is neglected in both the speed estimator and the control system.

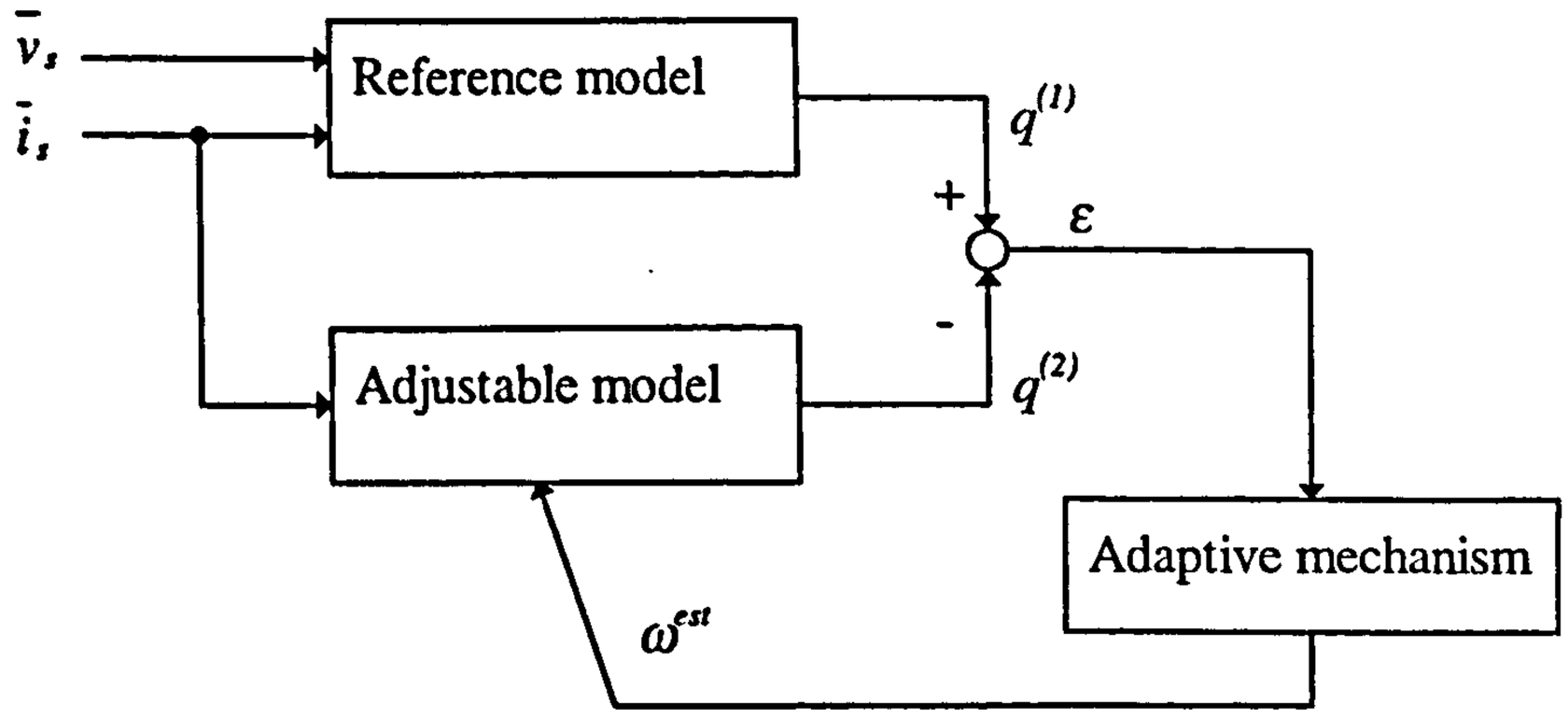

Figure B.1: Basic configuration of the reactive power based MRAC speed estimator.

The output quantity of the reference and adjustable models was defined in section 4.4 with:

$$q = \bar{i}_s \otimes \bar{e}_m \tag{4.12}$$

where $\bar{e}_m$ is the back emf.

By considering equations (4.2) and (4.3), the outputs of the reference model and adjustable model are obtained as:

$$q^{(1)} = \bar{i}_s \otimes \left(\bar{v}_s - \sigma L_s \frac{d\bar{i}_s}{dt} \right) \tag{4.13}$$

$$q^{(2)} = \bar{i}_s \otimes \frac{L_m}{L_r} \left(-\frac{1}{T_r} + j\omega \right) \bar{\psi}_r \tag{4.14}$$

The reactive powers of the reference and adjustable models are expressed from (4.13) and (4.14) in the stationary reference frame, as:

$$q^{(1)} = v_{\beta s} i_{\alpha s} - v_{\alpha s} i_{\beta s} - \sigma L_s \left(i_{\alpha s} \frac{di_{\beta s}}{dt} - i_{\beta s} \frac{di_{\alpha s}}{dt} \right) \tag{4.15}$$

$$q^{(2)} = \frac{L_m}{L_r} \left[\frac{1}{T_r} \left(\psi_{\alpha r} i_{\beta s} - \psi_{\beta r} i_{\alpha s} \right) + \omega \left(\psi_{\alpha r} i_{\alpha s} + \psi_{\beta r} i_{\beta s} \right) \right] \tag{4.16}$$

In steady-state operation, by letting $d/dt = j\omega_e$, ($\omega_e^* = \omega_e$) it follows that:

$$\frac{di_{\alpha s}}{dt} = -\omega_e^* i_{\beta s}$$
$$\frac{di_{\beta s}}{dt} = \omega_e^* i_{\alpha s} \tag{B.1}$$

The output of the reference part of the speed estimator (4.15) in steady-state operation becomes then equal to:

$$q^{(1)} = i_{\alpha s} v_{\beta s} - i_{\beta s} v_{\alpha s} - \sigma^* L_s^* (i_{\alpha s}^2 + i_{\beta s}^2)\omega_e^* \tag{B.2}$$

Similarly, by considering the rotor equations (5.12), the rotor flux α-β components in steady-state can be expressed as:

$$\psi_{\alpha r} = \frac{L_m^* i_{\alpha s} + \omega_{sl}^* T_r^* L_m^* i_{\beta s}}{1 + \left[T_r^* (\omega_e^* - \omega^*)\right]}$$
$$\psi_{\beta r} = \frac{L_m^* i_{\beta s} - \omega_{sl}^* T_r^* L_m^* i_{\alpha s}}{1 + \left[T_r^* (\omega_e^* - \omega^*)\right]} \tag{B.3}$$

where $\omega_{sl}^* = \omega_e^* - \omega^*$. Substitution of equations (B.3) into (4.16) enables the output of the adjustable part of the speed estimator to be expressed as:

$$q^{(2)} = \frac{L_m^{*2}}{L_r^*} \frac{\left(i_{\alpha s}^2 + i_{\beta s}^2\right)\omega_e^*}{1 + \left[T_r^* (\omega_e^* - \omega^*)\right]} \tag{B.4}$$

Equations (B.2) and (B.4) describe reactive power balance when existence of the iron loss is neglected in the motor.

In any steady-state operation, the PI speed controller forces the estimated speed to be equal to the commanded speed ($\omega^* = \omega^{est}$), as the estimated speed is used as feedback signal to form the closed loop system. The independent inputs in the control system of Figure B.1 are reference speed and reference rotor flux. The output of the PI speed controller is the reference torque, whose value is in general unknown. However, for each value of the torque command there is a corresponding value of the actual torque. In any steady-state, actual torque must equal load torque. Therefore, it is possible to regard torque command as an independent input. The relationship between rotor flux and reference stator *d*-axis current is, as shown in section 6.2.1, given with:

$$\psi_r^* = L_m^* i_{ds}^* \tag{6.5}$$

$$\psi_r^* = \begin{cases} \psi_{rn} & \omega \le \omega_n \\ \psi_{rn}\omega_n / \omega & \omega > \omega_n \end{cases} \tag{6.6}$$

$$i_{ds}^* = \psi_r^* / L_m^* \tag{6.7}$$

The commanded torque is equal to:

$$T_e^* = \frac{3}{2} P \frac{L_m^*}{L_r^*} \psi_r^* i_{qs}^* \tag{6.8}$$

The commanded slip angular speed and the commanded electrical angular frequency are:

$$\omega_{sl}^* = \frac{L_m^* i_{qs}^*}{T_r^* \psi_r^*} \tag{6.9}$$

$$\omega_e^* = \omega_{sl}^* + \omega^{est} \tag{6.10}$$

Commanded stator q-axis current can be expressed from equation (6.8) as:

$$i_{qs}^* = \frac{T_e^*}{\frac{3}{2} P \frac{L_m^*}{L_r^*} \psi_r^*} \tag{6.11}$$

The induction machine model, with iron loss accounted for, given in section 5.2, is utilised here. In steady-state operation, all the derivative terms become zero. Therefore, the induction machine model can be written as:

$$\begin{aligned} \bar{v}_s &= R_s^* \bar{i}_s + j\omega_e^* \bar{\psi}_s \\ R_{Fe} \bar{i}_{Fe} &= j\omega_e^* L_m^* \bar{i}_m \\ 0 &= R_r^* \bar{i}_r + j\omega_{sl} \bar{\psi}_r \\ \bar{i}_m + \bar{i}_{Fe} &= \bar{i}_s + \bar{i}_r \\ \bar{\psi}_s &= L_{\sigma s}^* \bar{i}_s + L_m^* \bar{i}_m \\ \bar{\psi}_r &= L_{\sigma r}^* \bar{i}_r + L_m^* \bar{i}_m \\ T_e &= \frac{3}{2} P \frac{L_m^*}{L_{\sigma r}^*} (\psi_{dr} i_{qm} - \psi_{qr} i_{dm}) \end{aligned} \tag{6.12}$$

All the parameters in the machine model, that are the same as those of the controller/estimator, are identified with an asterisk.

Elimination of iron loss current and rotor current space vectors, followed by resolution of (6.12) into d-q axis components, yields:

$$\begin{aligned} v_{ds} &= R_s i_{ds}^{\bullet} - \omega_e^{\bullet} L_{\sigma s}^{\bullet} i_{qs}^{\bullet} - \omega_e^{\bullet} L_m^{\bullet} i_{qm} \\ v_{qs} &= R_s i_{qs}^{\bullet} + \omega_e^{\bullet} L_{\sigma s}^{\bullet} i_{ds}^{\bullet} + \omega_e^{\bullet} L_m^{\bullet} i_{dm} \\ L_m^{\bullet} i_{dm} &= \psi_{dr} - \omega_{sl} T_{\sigma r}^{\bullet} \psi_{qr} \\ L_m^{\bullet} i_{qm} &= \psi_{qr} + \omega_{sl} T_{\sigma r}^{\bullet} \psi_{dr} \end{aligned} \tag{6.13}$$

$$\begin{aligned} -\omega_e^{\bullet} T_{Fe} i_{qm} &= i_{ds}^{\bullet} + \psi_{dr} / L_{\sigma r}^{\bullet} - i_{dm} L_r^{\bullet} / L_{\sigma r}^{\bullet} \\ \omega_e^{\bullet} T_{Fe} i_{dm} &= i_{qs}^{\bullet} + \psi_{qr} / L_{\sigma r}^{\bullet} - i_{qm} L_r^{\bullet} / L_{\sigma r}^{\bullet} \end{aligned} \tag{6.14}$$

The torque equation remains as in (6.12) and electrical angular frequency is determined with (6.10):

$$\omega_e^{\bullet} = \omega_{sl}^{\bullet} + \omega^{est} = \omega + \omega_{sl} \tag{6.10}$$

Time constants in (6.13) and (6.14) are once more defined as $T_{Fe}=L_m^{\bullet}/R_{Fe}$ and $T_{\sigma r}^{\bullet}=L_{\sigma r}^{\bullet}/R_r^{\bullet}$.

The equations can be solved in conjunction with the controller and speed estimator equations. The independent inputs are reference speed and reference rotor flux. The output of the PI speed controller is reference torque, whose value is in general unknown. However, for each value of the torque command there will be a corresponding value of the actual torque. Thus, the torque command may be regarded as an independent input. By solving (6.13) - (6.14) while accounting for the additional constraint imposed by the speed estimator, it is then possible to determine the value of the actual torque that corresponds to the given torque command. Such an approach is utilised here: independent inputs are taken as reference speed, reference torque and reference rotor flux. The constraint imposed by the control is that

$$\omega_e^{\bullet} = \omega^{\bullet} + \omega_{sl}^{\bullet} \equiv \omega_e \tag{6.15}$$

as estimated and reference speeds are equal and commanded and actual supply frequencies are equal as well. The error in speed estimation is defined once more in mechanical rpm as

$$\Delta n = n - n^{\bullet} = n - n^{est} \tag{6.24}$$

The outputs of the reference and adjustable models in speed estimator are defined with equations (B.2) and (B.4). Due to the presence of the PI controller, the error between these two models is zero in any steady-state, i.e.:

$$\varepsilon=0 \tag{6.16}$$

Taking into account that $i_s^2=i_{\alpha s}^2+i_{\beta s}^2$, it follows from (B.2) and (B.4) that:

$$i_{\alpha s}v_{\beta s}-i_{\beta s}v_{\alpha s}=\sigma L_s^*\omega_e^* i_s^2+\frac{L_m^{*2}}{L_r^*}\frac{\omega_e^* i_s^2}{1+(T_r^*\omega_{sl}^*)^2} \tag{B.5}$$

It follows that rotor speed is determined with the condition that input reactive power must equal reactive power spent in the motor in any steady-state.

The reactive power spent in the motor, when iron loss is accounted for, is determined with:

$$Q=\omega_e^* L_{\sigma s}^* i_s^2+\omega_e^* L_{\sigma r}^* i_r^2+\omega_e^* L_m^* i_m^2 \tag{B.6}$$

The values of i_r^2 and i_m^2 can be obtained from the induction machine equations (6.12), that account for the iron loss, in the following form:

$$i_r^2=\frac{\left(T_{\sigma r}^*-T_r^*\right)^2\omega_{sl}^2 i_s^2}{\left(1-\omega_{sl}\omega_e^* T_{\sigma r}^* T_{Fe}\right)^2+\left(T_{Fe}\omega_e^*+T_r^*\omega_{sl}\right)^2} \tag{B.7}$$

$$i_m^2=\frac{\left[1+\left(\omega_{sl}T_{\sigma r}^*\right)^2\right]i_s^2}{\left[\left(1-\omega_{sl}\omega_e^* T_{Fe}\right)^2+\left(T_{Fe}\omega_e^*+T_r^*\omega_{sl}\right)^2\right]^2} \tag{B.8}$$

Substitution of (B.7) and (B.8) into (B.6) enables reactive power to be expressed as:

$$i_{\alpha s}v_{\beta s}-i_{\beta s}v_{\alpha s}=\omega_e^* i_s^2\left[L_{\sigma s}^*+\frac{L_{\sigma r}^*\left(T_{\sigma r}^*-T_r^*\right)^2\omega_{sl}^2+L_m^*\left(1+\left(\omega_{sl}T_{\sigma r}^*\right)^2\right)}{\left(1-\omega_e^*\omega_{sl}T_{\sigma r}^* T_{Fe}\right)^2+\left(\omega_e^* T_{Fe}+\omega_{sl}T_r^*\right)^2}\right] \tag{B.9}$$

As input reactive power in (B.5) and (B.9) is the same, then for any given operating condition it is possible to calculate from (B.9) the unknown angular slip speed ω_{sl} and hence the actual rotor speed ω. Once when the actual speed is calculated, it becomes possible to solve for the remaining unknowns in the induction machine model (6.13) - (6.14).

B.2 Results of the study

Impact of iron loss on behaviour of the drive is studied first for constant speed command operation, with torque command as the independent input. Figure B.2a shows speed estimation error for three values of the reference speed, namely one fifth of the rated speed, rated speed and twice the rated speed.

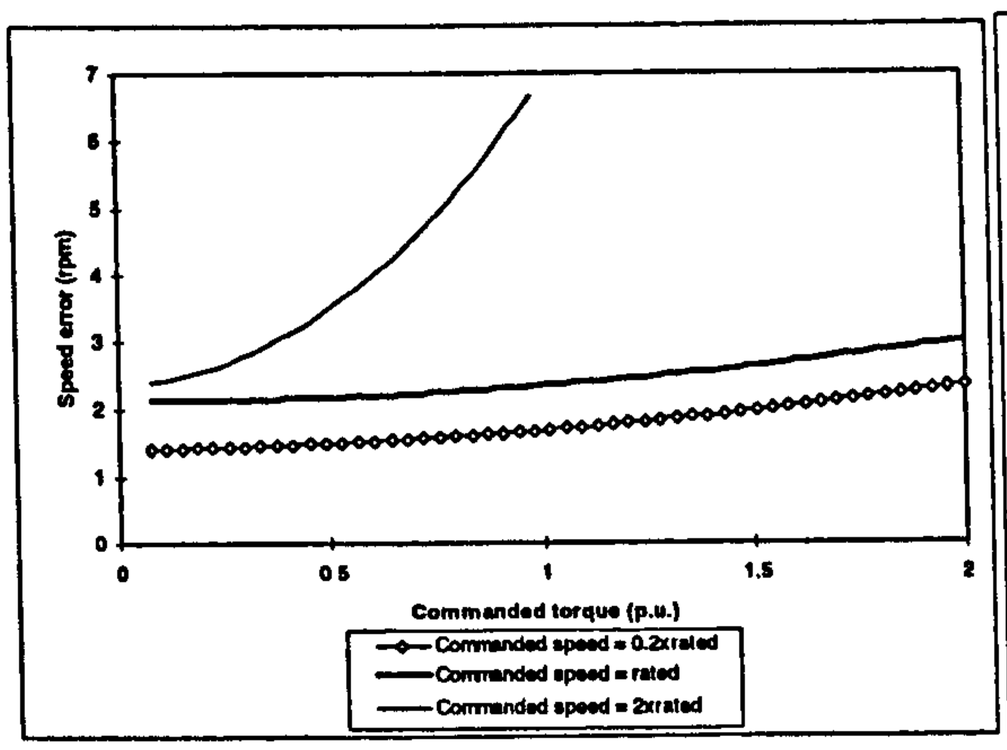

a. speed error

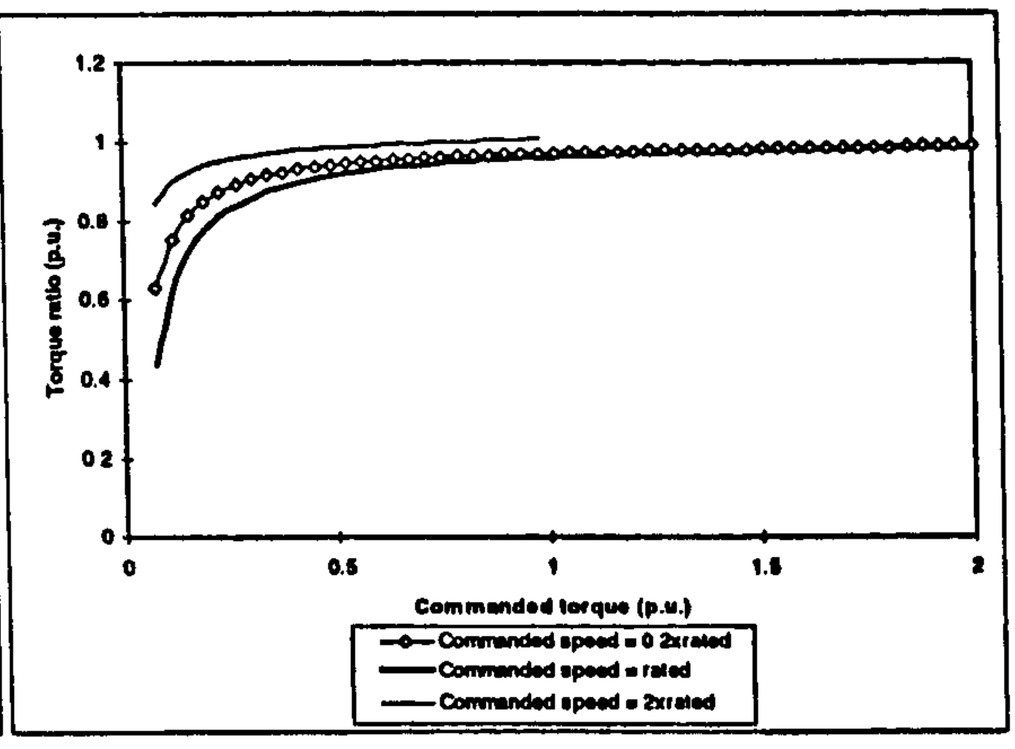

b. torque ratio

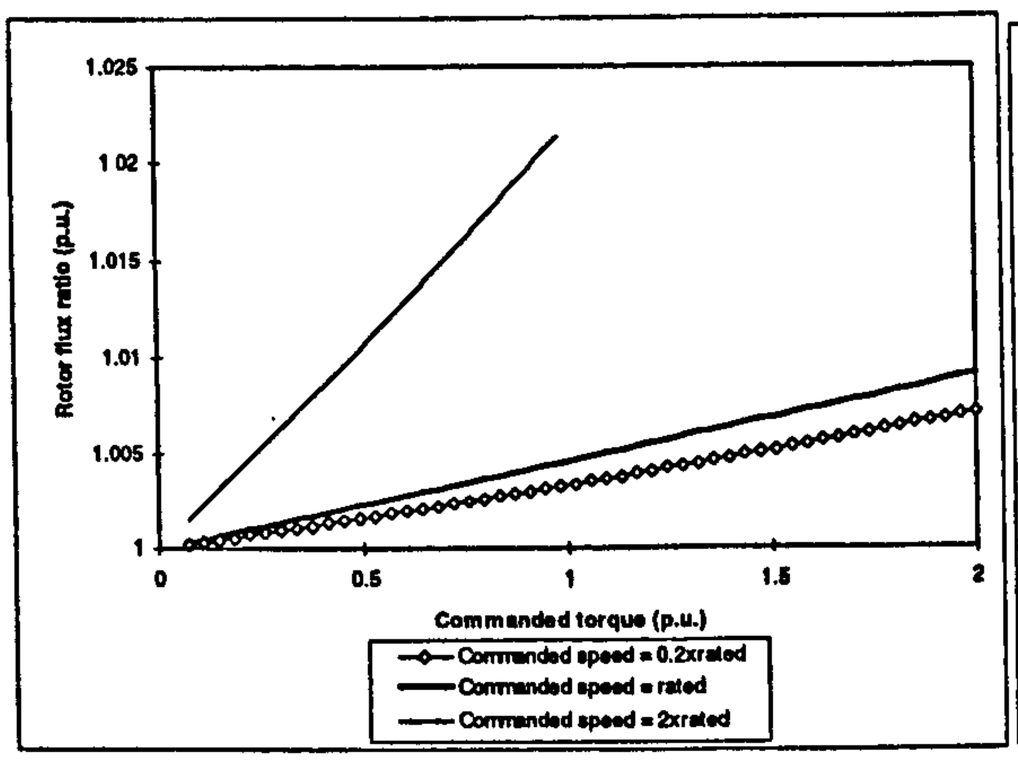

c. rotor flux ratio

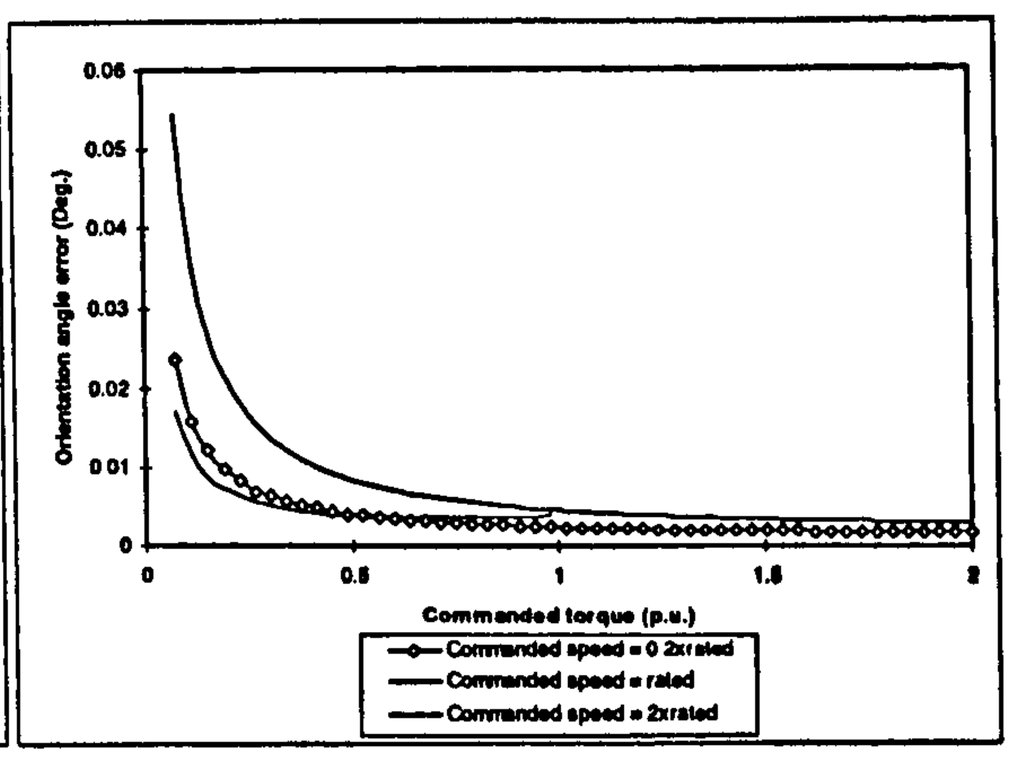

d. orientation angle error

Figure B.2: Detuning effects due to iron loss as function of commanded torque for operation with constant speed command.

Speed estimation error is from Figure B.2a load dependent and it increases as load increases. Speed estimation error appears to be typically two to three rpm for operation at the rated speed, for commanded torque up to the rated. Speed estimation error is smaller at low speeds, typically 1.5 to 2 rpm at one fifth of the rated speed for variation of the torque command from zero to the rated value. If the machine is operated in the field weakening region, speed estimation error may increase significantly, reaching 7 rpm for operation at twice the rated speed with the rated torque command. On the other

hand, torque ratio has maximum error always at low torque commands. As the torque command increases error in the torque ratio decreases, Figure B.2b.

Figure B.2c shows rotor flux ratio for constant speed operation. Error in rotor flux magnitude is extremely small. For operation in the base speed region actual rotor flux in the machine exceeds commanded rotor flux less than 1% for all the operating points. Maximum error appears for operation with the rated speed and rated torque command, when ratio of actual to commanded rotor flux equals 1.005. The error of rotor flux increases in the field-weakening region. When machine runs at twice the rated speed with rated torque, the error in rotor flux is about 2.3%.

Orientation angle error is shown in Figure B.2d and is very small, indeed. The orientation angle error is larger at light load torque. As the torque command increases, the error in orientation angle decreases. For operation at the rated speed with the rated torque, the error is about 0.005 degrees.

The impact of iron loss on sensorless vector controlled induction machine is further examined with reference speed taken as the independent variable. Commanded torque is set to a constant value in the base speed region. For operation in the field-weakening region torque command is reduced inversely proportionally to the speed, so that constant power operation is assumed. Figure B.3a shows the speed estimation error as function of the normalised speed command. In the base speed region, a typical speed estimation error due to iron loss is 2 to 3 rpm (except at low speeds). Speed estimation error slightly increases in the field weakening region and approaches 4 rpm for operation with rated power at twice the rated speed. It is interesting to note that speed estimation error appears to be rather independent from the loading of the machine in the base speed region.

Torque error increases with decreasing load. Actual torque is up to 5% less than the commanded torque with rated torque/power command operation from zero to twice the rated speed command. When machine is operating with light load, say one fifth of the rated torque value, in the base speed region, the error becomes up to 20 % (Figure B.3b).

The impact of iron loss on rotor flux ratio and orientation angle error is extremely small, Figures B.3c and B.3d. For base speed region with rated torque command, the

rotor flux error is about 0.5% and the orientation angle error is only 0.005 degrees. The orientation angle error is load dependent. It increases with load torque decrease. When load torque is one fifth of the rated, the orientation angle error is about 0.02 degrees in base speed region. When the machine runs in the field-weakening region, the maximum rotor flux error is just above 1%, while orientation angle error is reduced.

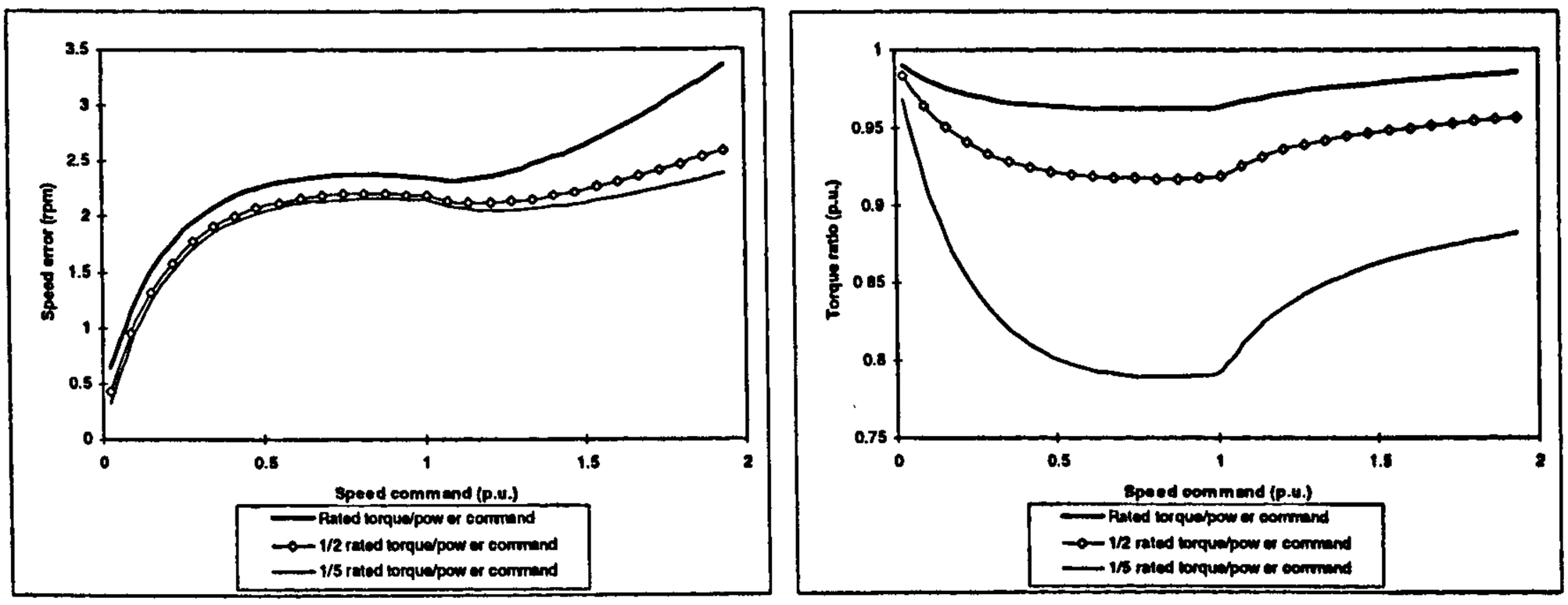

a. speed error

b. torque ratio

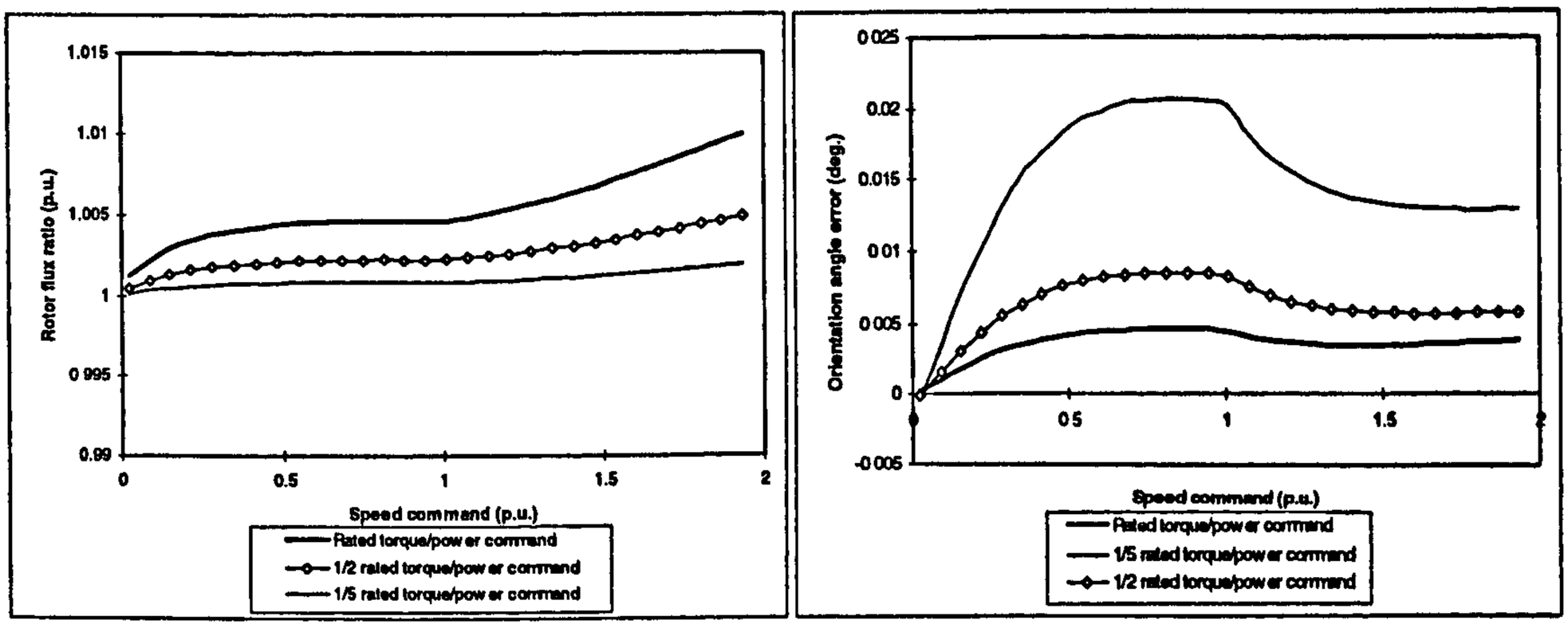

c. rotor flux ratio

d. orientation angle error

Figure B.3: Detuning effects due to iron loss as function of commanded speed for operation with constant torque/power command.

It is interesting to note that the results of this study are very similar to those discussed in section 6.2. It therefore follows that the impact of iron loss on operation of the rotor flux (and back emf) based MRAC speed estimator is essentially the same as for the reactive power based MRAC speed estimator. The results of this section were reported in [Wang et al; 1997].

APPENDIX C: SIMULINK MODELS FOR SIMULATION OF DYNAMICS OF THE DRIVE

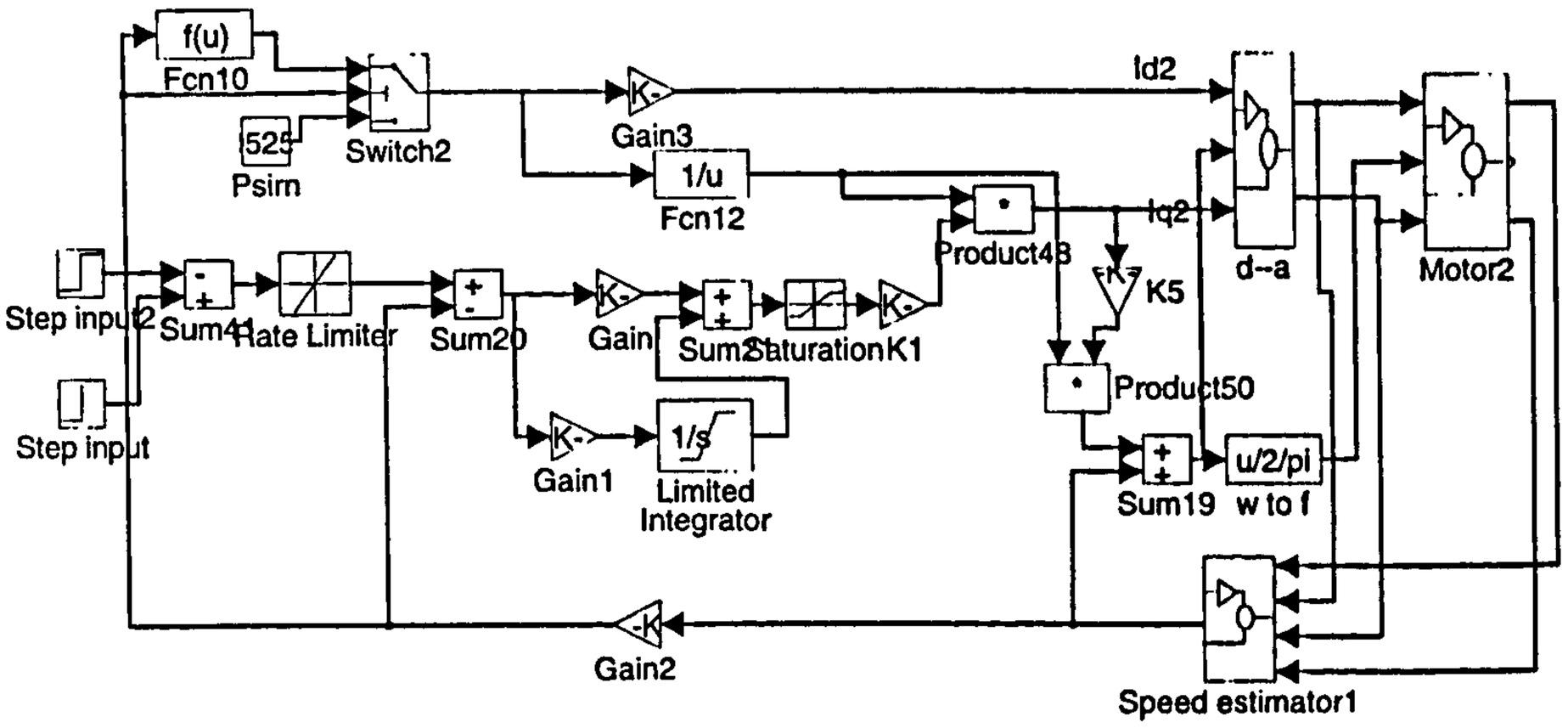

Figure C.1: Model for evaluation of detuning due to iron loss.

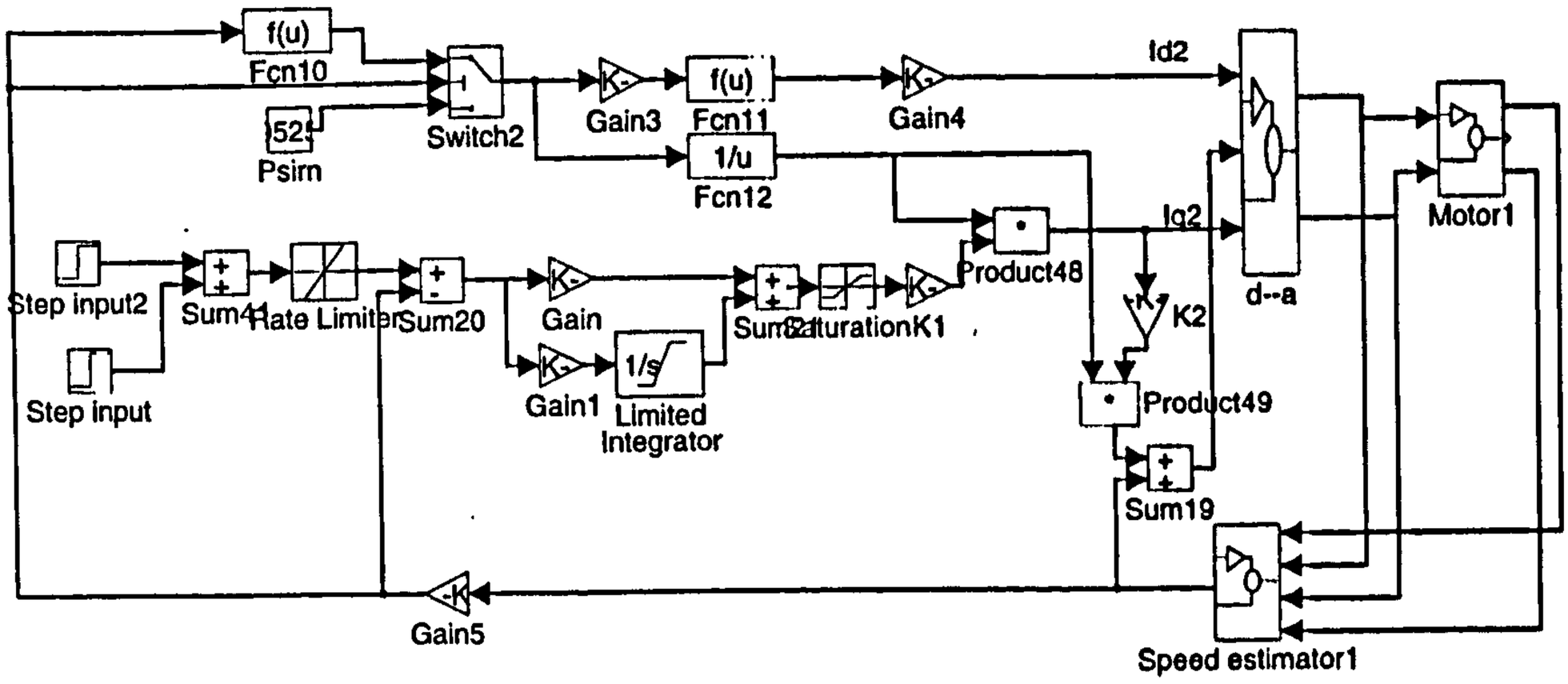

Figure C.2: Model for evaluation of detuning due to main flux saturation.

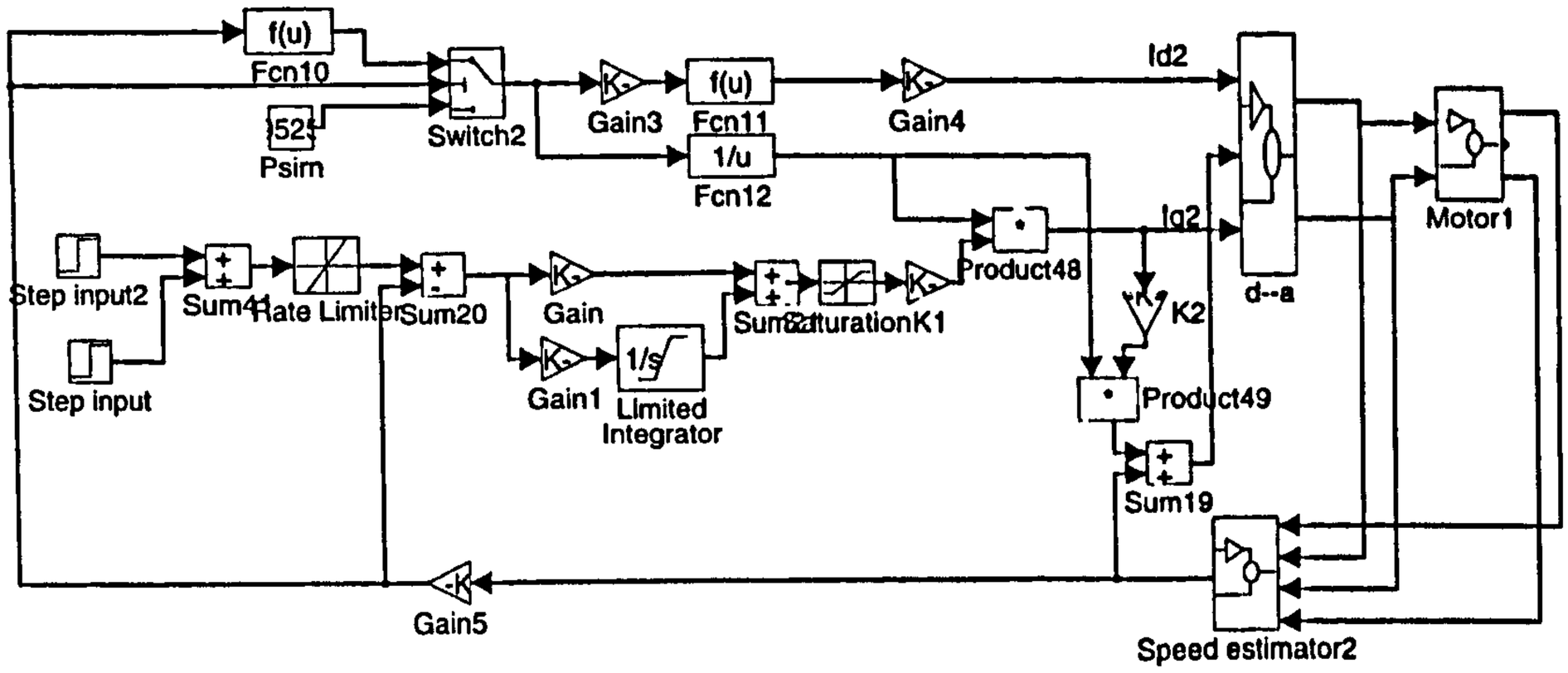

Figure C.3: Model for evaluation of compensation of main flux saturation.

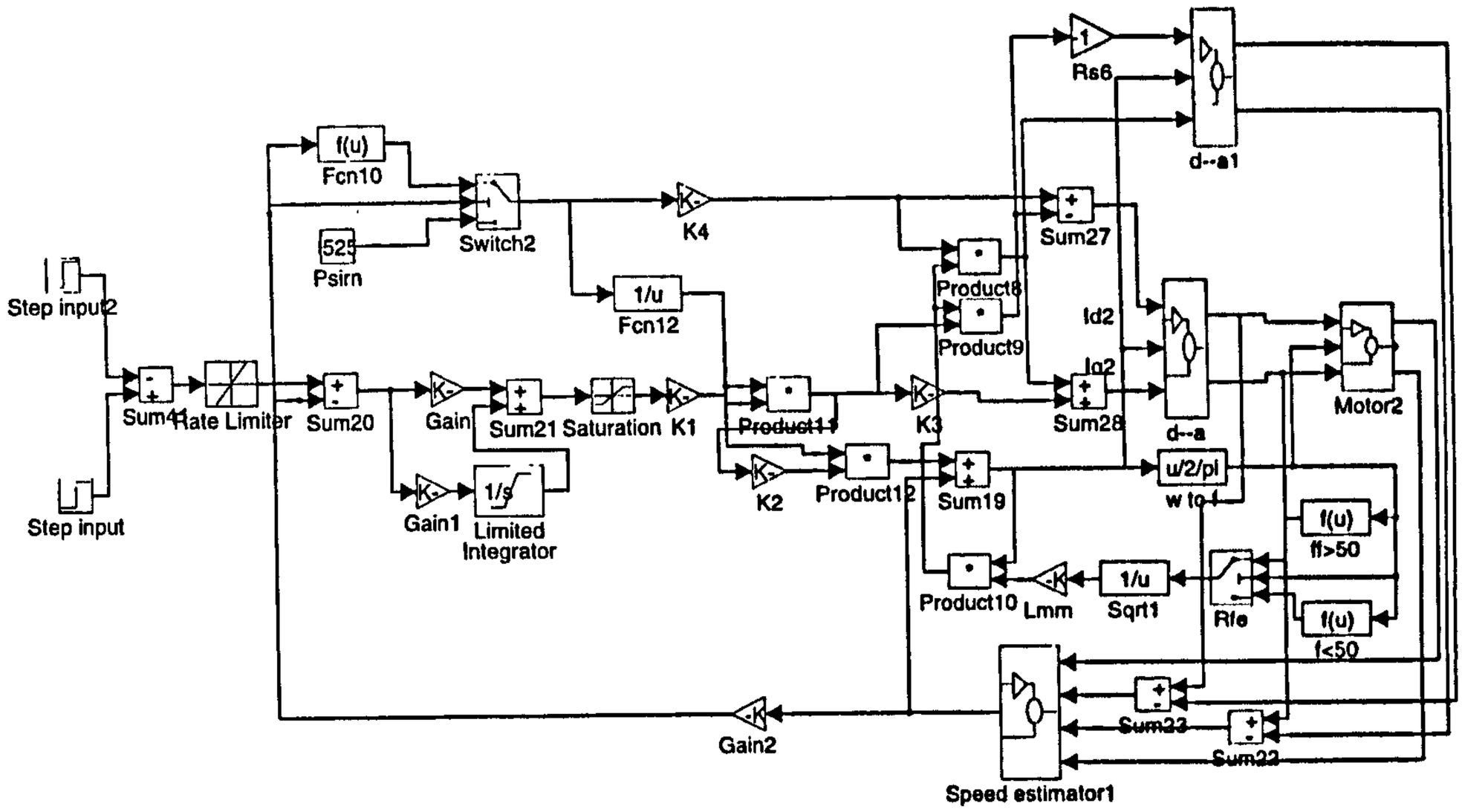

Figure C.4: Model for evaluation of compensation of iron loss.

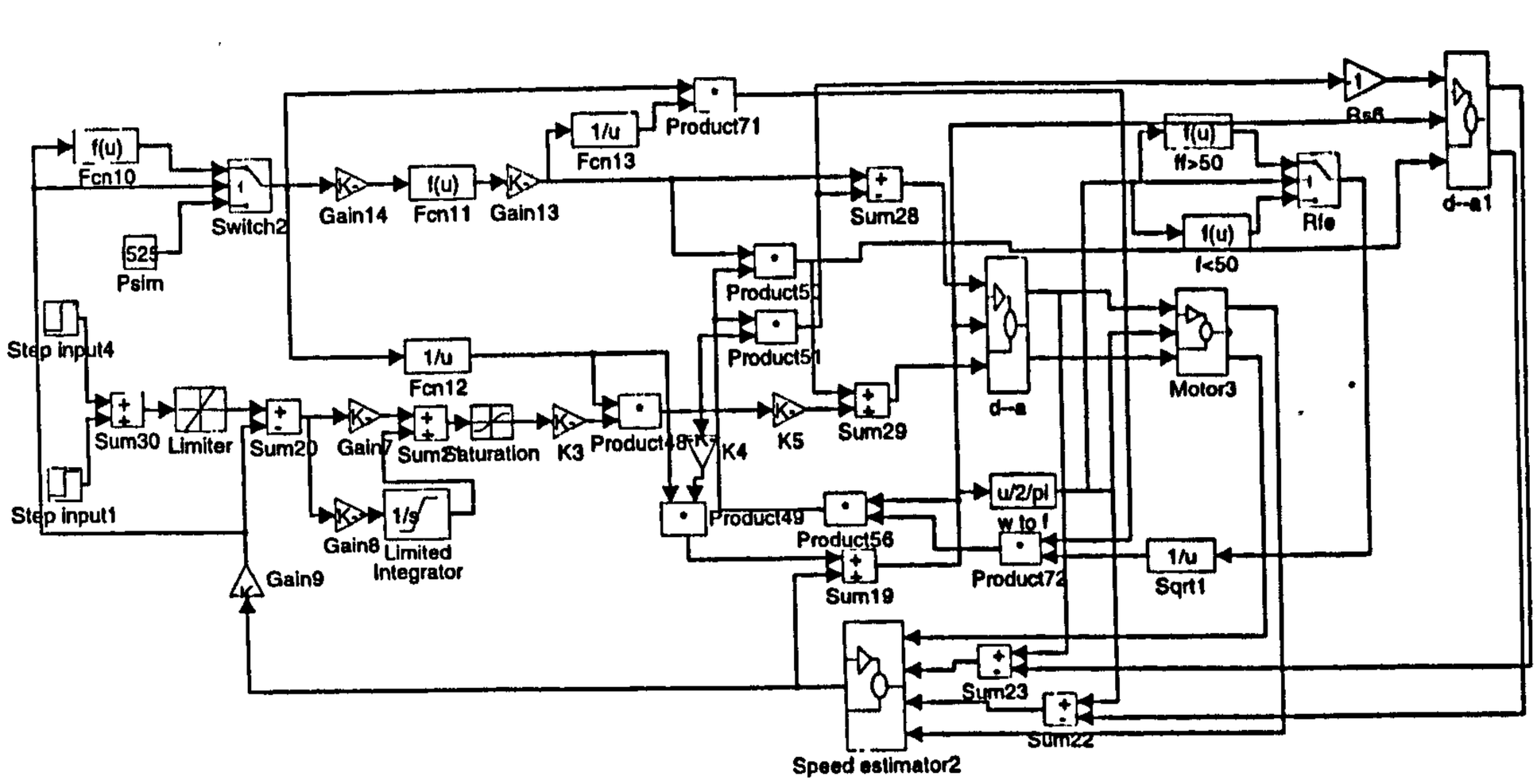

Figure C.5: Model for evaluation of compensation of both iron loss and main flux saturation.

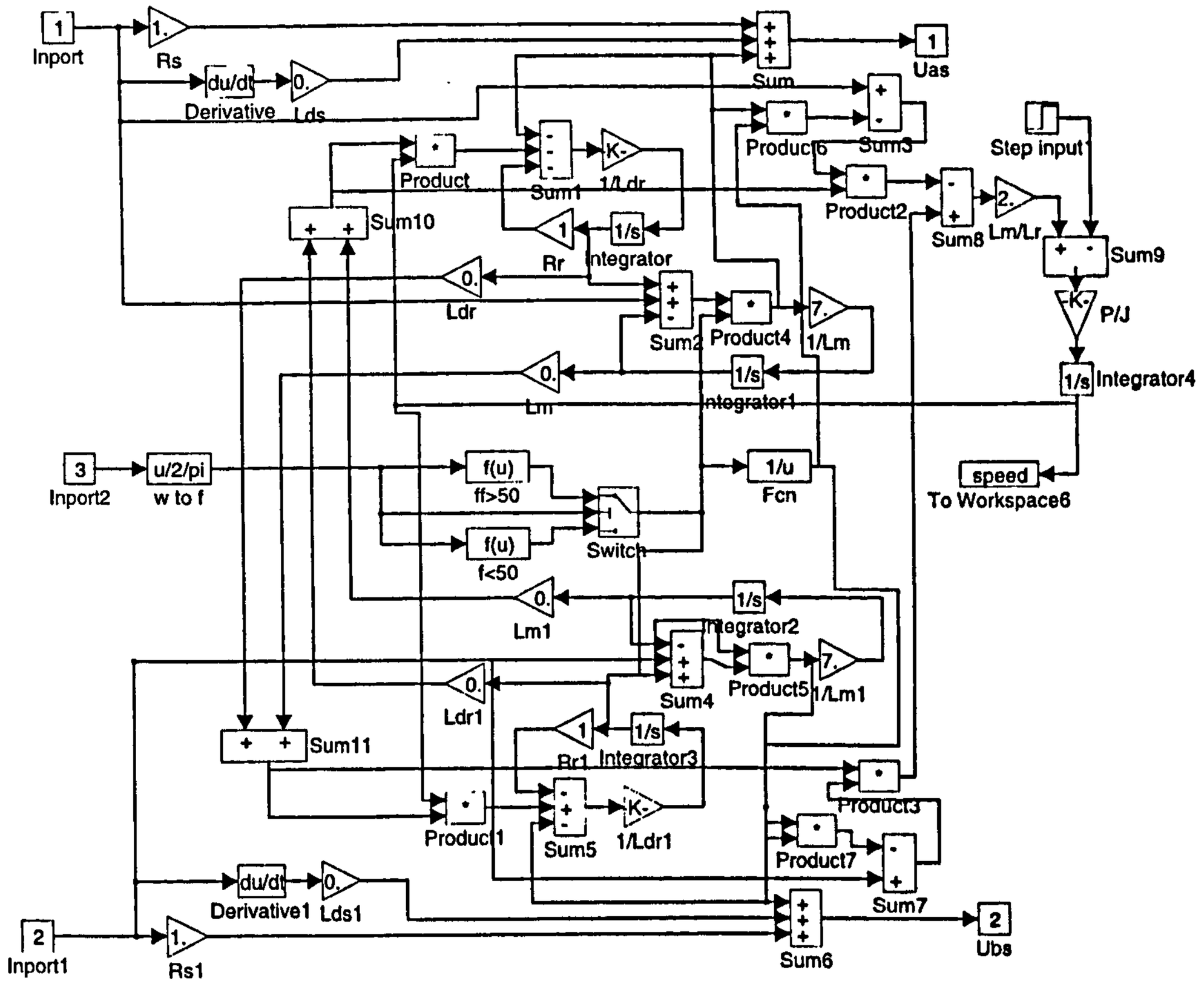

Figure C.6: Model of induction machine that includes iron loss.

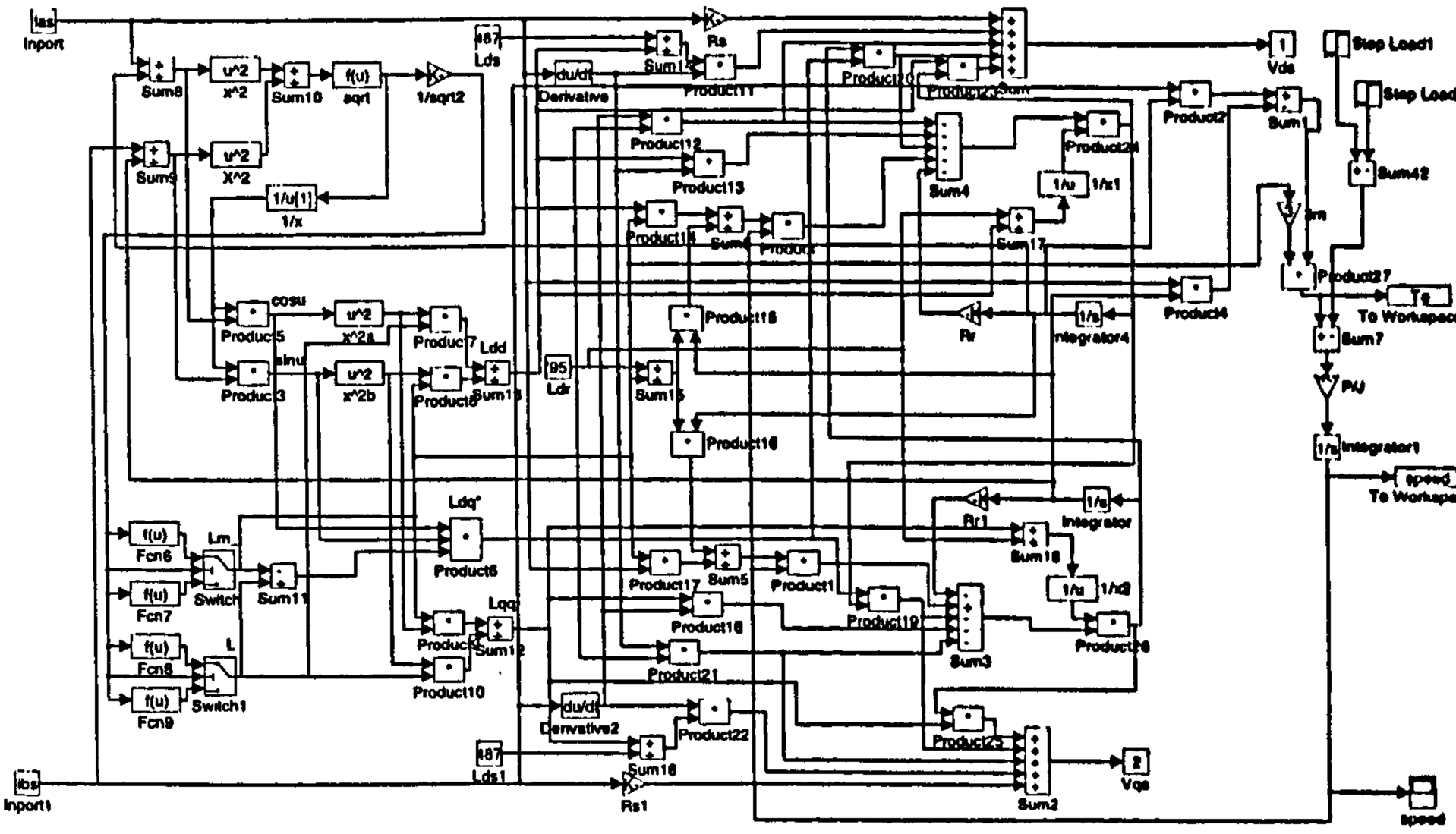

Figure C.7: Model of induction machine that includes main flux saturation.

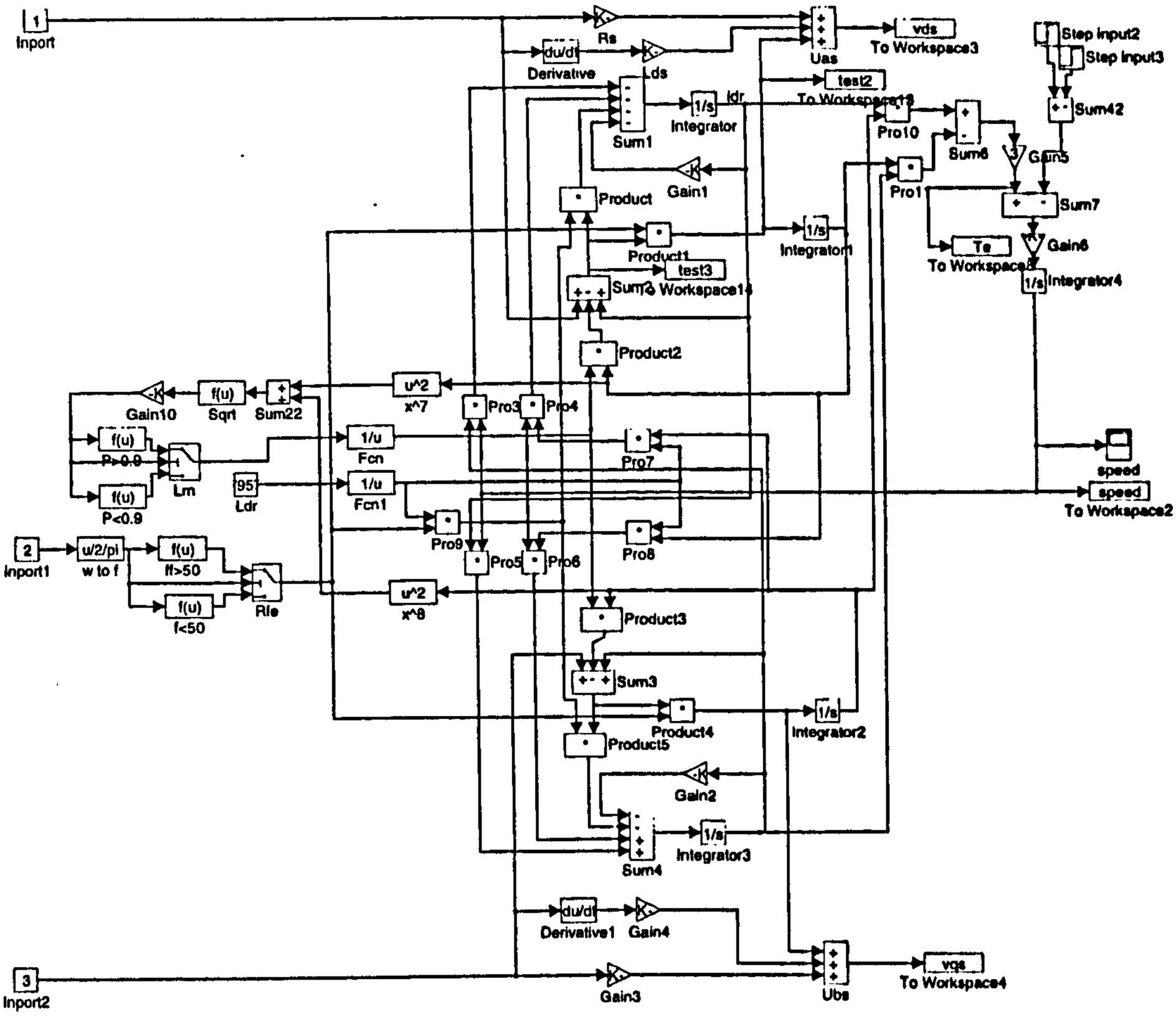

Figure C.8: Model of induction machine that includes both iron loss and main flux saturation.

APPENDIX D: DESCRIPTION OF THE DATA ACQUISITION SYSTEM

The data acquisition system consists of a voltage measurement circuit, a current measurement circuit and an A/D card inside a PC.

As the vector controlled induction motor drive and the PC have the same grounded power supply, there is no need to isolate the signals to be sampled. As mentioned in section 9.2, the inputs of the speed estimator can be obtained by suitable transformation of line-to-line voltages and phase currents. Therefore, the signals to be measured are v_{ab}, v_{ca}, i_a and i_b.

The voltage measurement circuit is design to process the stator voltages of the induction machine. The inputs of the circuit are three voltages of phases *a*, *b* and *c* with respect to ground. The outputs of the card are filtered and attenuated line-to-line voltage signals v_{ab} and v_{ca}. The schematic of the voltage sampling circuit is shown in Figure D.1 .

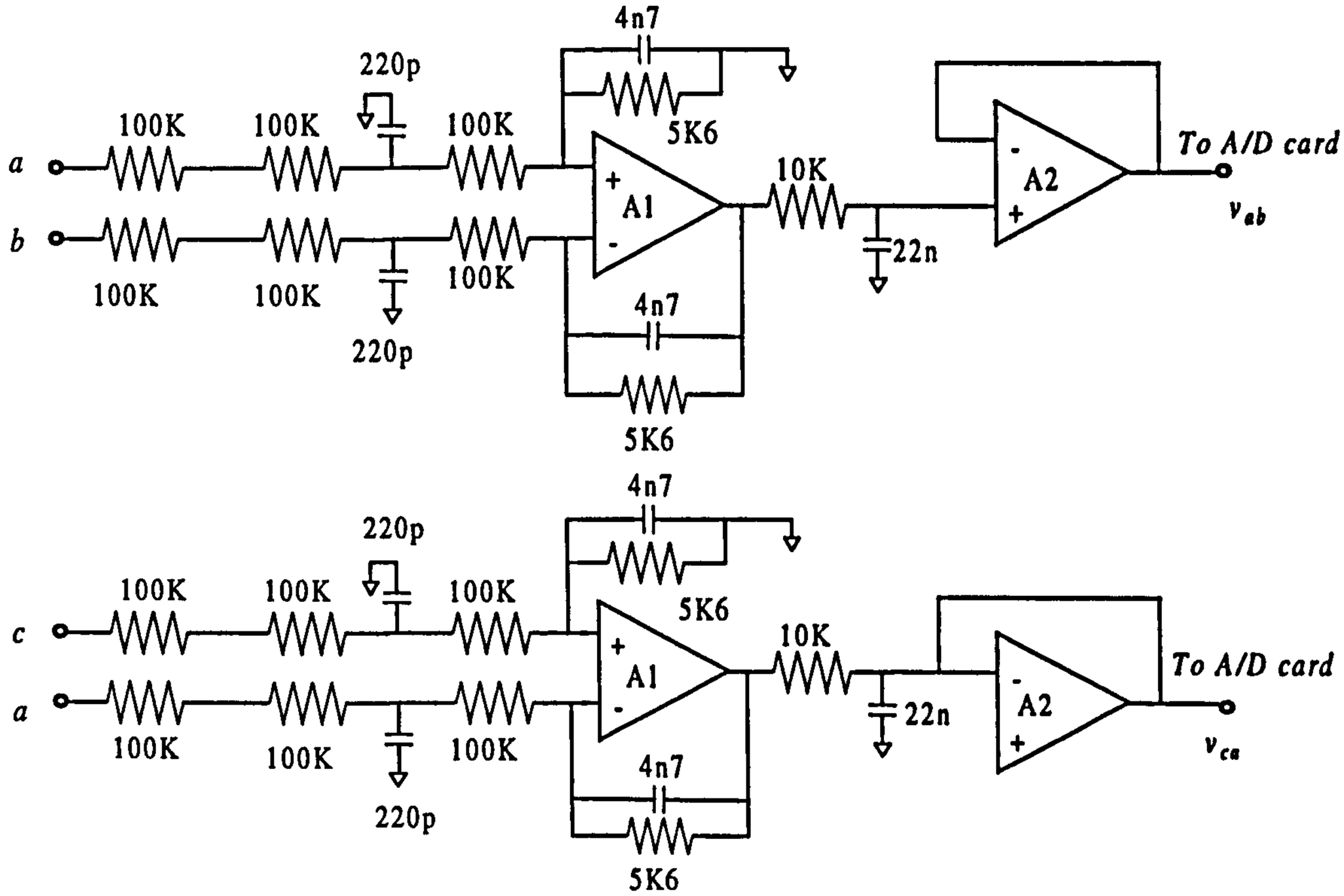

Figure D.1: Schematic of the voltage measurement circuit.

The circuit has two identical signal paths for creation of v_{ab} and v_{ca}. In each signal path, three 100k resistors and one 5k6 resistor paralleled with a 4n7 capacitor and an operational amplifier form a voltage divider and filtering circuit. Operational amplifiers used in the circuit are TL072. On the output side of the operational amplifier A1, a 10k resistor and 22 nF capacitor provide further filtering. Then the signal passes through a follower A2 to the A/D card.

The voltage signals obtained are equal to:

$$v_{ab} = \frac{5.6}{300}(v_a - v_b)$$
$$v_{bc} = \frac{5.6}{300}(v_b - v_c) \qquad \text{(D.1)}$$

For current measurement, two Hall effect current transducers are utilised to measure the phase currents. The current transducer has a voltage output that is proportional to the input current. Two identical current detection circuits are employed. The schematic of the circuit is shown in Figure D.2.

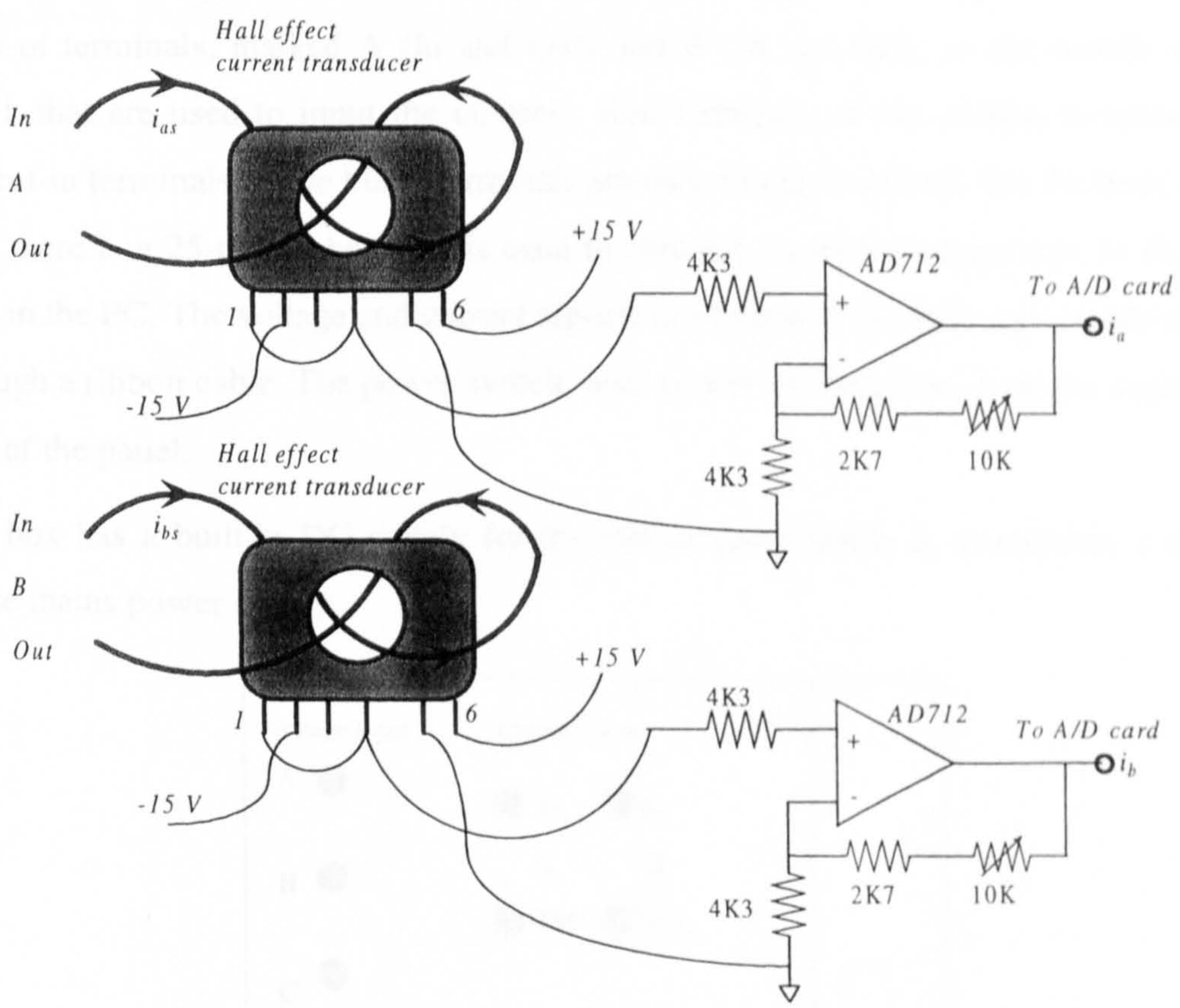

Figure D.2: Schematic of the current measurement circuit.

The rated primary current of the current transducer is 50 A. The rated output of the transducer is 5 V. It should be noted that the primary wire passes through the hole twice in the configuration. It means the gain of the transducer is increased twice. It provides 0.2 V/A. As the rated current of the machine is 10 A, it is necessary to increase the gain for the A/D card input. An operational amplifier AD712 is utilised. The gain of the amplifier is adjusted by a variable resistor. The gain of the amplifier is set to two for the experiments. Hence the relationship between input motor current and output signal has the form of:

$$\begin{aligned} i_a &= 0.4 i_{as} \\ i_b &= 0.4 i_{bs} \end{aligned} \tag{D.2}$$

where i_a and i_b represent the output of the circuit, while i_{as} and i_{bs} represent the input stator currents.

Both of the cards are mounted in a metal box. The panel of the data acquisition box is shown in Figure D.3. There are three input terminals, marked A, B and C, on the left hand side of the panel. They are used to input the three line voltages. There are two pairs of terminals, marked A (In and Out) and B (In and Out), in the middle of the panel, that are used to input the currents. Red terminals of the current terminals are current-in terminals, while black terminals are current-out terminals. On the back of the box, there is a 25-pin socket, that is used to connect the measurement box to the A/D card in the PC. The voltage and current signals are linked to the A/D card inside the PC through a ribbon cable. The power switch, with power-on indicator, is on the right hand side of the panel.

The box has a built-in DC supply for the circuit cards inside it. It requires a single-phase mains power supply.

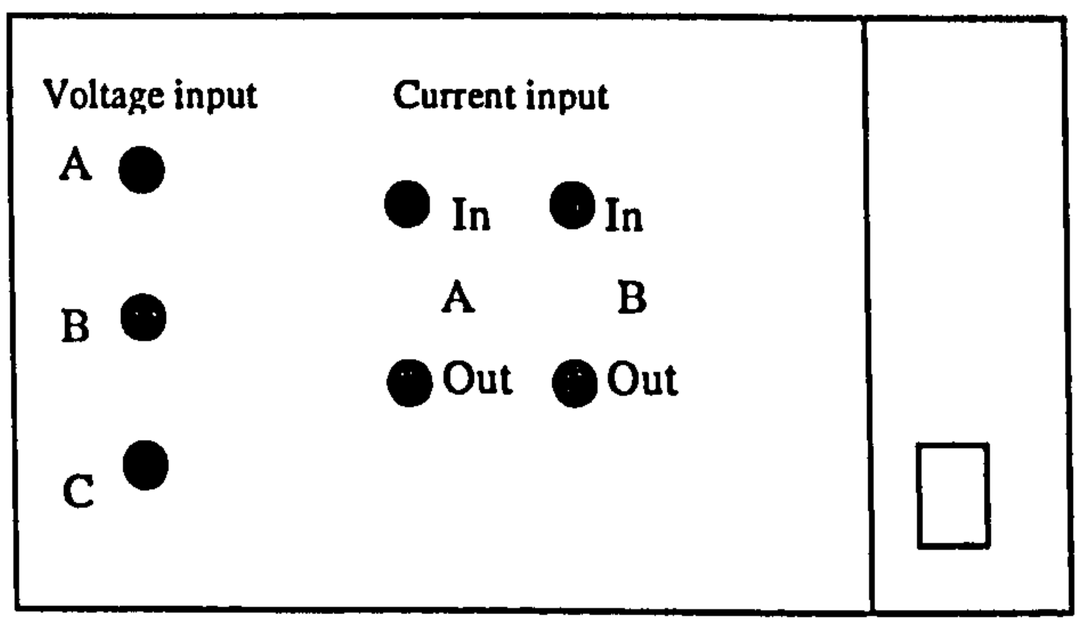

Figure D.3: Panel of the data acquisition box.

The model of the A/D card is PCI-DAS1200, produced by ComputerBoards company. The card is placed in a PCI socket on the motherboard. The A/D card provides 8 differential / 16 single ended 12-bit analogue inputs and supports sample rate of up to 330 kHz (detailed specification is given in the user manual). In this experimental investigation, channels 0 to 3 are used to collect the voltage and current signals. The sampling frequency for each signal is 20 kHz.

The software used for the data acquisition system is LabVIEW. A program was designed to collect all the signals. Some parameters need to be entered first. They are A/D card Board Number (BoardNum = 0), Low channel, first A/D channel of scan (LowChan = 0), High channel, last A/D channel of scan (HighChan = 3), Count, number of A/D samples to collect (count = 80000x4), rate, sample rate in scans per second (rate = 20000) and range, A/D range code (range = ± 10V). After sampling process is finished, all the waveforms of the four channels and the actual sampling rate are displayed on the monitor screen. If all the data of four channels are satisfactory, the data are saved in text file format on the hard drive. The data in the saved files can be processed by Matlab for evaluation of the speed estimator.

APPENDIX E: PUBLISHED AND ACCEPTED PAPERS

Journal papers:

Levi,E., Wang,M., Williams,D. (1999). Evaluation of iron loss influence on speed estimation in sensorless MRAC-based field-oriented induction machines, *European Transactions on Electrical Power ETEP*, Vol. 9, No. 2, pp. 77-84.

Wang,M., Levi,E., Jovanovic,M. (1999). Compensation of parameter variation effects in sensorless indirect vector controlled induction machines using model based approach, *Electric Machines and Power Systems*, Vol. 27, No. 9.

Wang,M., Levi,E. (1999). Evaluation of steady-state and transient behaviour of a MRAS based sensorless rotor flux oriented induction machine in the presence of parameter detuning, *Electric Machines and Power Systems*, Vol. 27, No. 11.

Conference papers:

Levi,E., Wang,M. (1997). Impact of iron loss on speed estimation in sensorless vector controlled induction machines, *Proc. IEEE Ind. Electronics Soc. Annu. Meeting IECON*, New Orleans, LA, pp. 977-982.

Levi,E., Wang,M. (1998). Impact of parameter variations on speed estimation in sensorless rotor flux oriented induction machines, *Proc. IEE Power Elec. and Variable Speed Drives Conf. PEVD*, London, UK, pp. 305-310.

Wang,M., Levi,E., Williams,D. (1997). Impact of iron loss on speed estimation accuracy in reactive power MRAC based sensorless rotor flux oriented induction machines, *Proc. Universities Power Eng. Conf. UPEC*, Manchester, UK, pp. 995-998.

Wang,M., Levi,E. (1998). Impact of parameter variations on dynamics of sensorless indirect rotor flux oriented induction machine, *Proc. Universities Power Eng. Conf. UPEC*, Edinburgh, UK, pp. 855-858.

Levi,E., Wang,M. (1999). Main flux saturation compensation in sensorless vector controlled induction machines for operation in the field weakening region, *Proc. Eur. Power Electronics and Application Conf. EPE*, Lausanne, Switzerland.

Evaluation of Iron Loss Influence on Speed Estimation in Sensorless MRAC-Based Field-Oriented Induction Machines

E. Levi, M. Wang, D. Williams

Abstract

Rotor speed estimation in sensorless field-oriented control of induction machines is usually performed on the basis of a mathematical model of an induction machine. An estimate of speed is obtained utilising one of the control techniques and its accuracy is affected by parameter variations. When the iron loss is neglected in the mathematical model, inaccuracy in speed estimation results due to iron loss existence in the machine. This paper evaluates the impact of iron loss on speed estimation for common model reference adaptive control (MRAC) schemes, based on rotor flux, back e.m.f. and reactive power. It is shown that the existence of iron loss leads to a typical speed estimation error of 2 min^{-1} to 3 min^{-1}, which is comparable with errors caused by other detuning effects. A modified sensorless MRAC-based scheme, that is applicable to both rotor flux and back e.m.f. methods, is then proposed. It is verified that the novel scheme enables good compensation of iron loss, yielding a very small speed estimation error of less than 0.5 min^{-1}.

1 Introduction

Methods of sensorless vector control of induction machines may be classified into two groups [1, 2]. The first one encompasses all the techniques that estimate rotor speed from stator current spectrum, on the basis of rotor slot and eccentricity harmonics or saturation-induced saliency. The common feature of all the methods within this group is that speed estimation is not based on a mathematical model of an induction machine and is therefore not sensitive to parameter variation effects. Hence the existence of iron loss in the machine does not affect the accuracy of speed estimation.

The second group of speed-sensorless vector control methods encompasses all the schemes in which speed estimation relies on utilisation of the mathematical model of an induction machine [1, 2]. The most frequently applied estimation approaches are model reference adaptive control (MRAC), full-order observers and extended Kalman filter. Among the three, the MRAC approach offers the simplest hardware and software realisation.

A number of different MRAC-based schemes have emerged during the last couple of years [3–8]. These mainly differ with respect to the quantities that are calculated in the reference and adaptive parts of the estimator and may be classified as rotor-flux-based [3, 7, 8], modified rotor-flux-based [3, 5, 6, 8], back-e.m.f.-based [4, 8] and reactive-power-based [4, 8]. Calculations and speed estimation are most frequently undertaken in the stationary reference frame [3, 4, 6–8], although solutions based on rotor-flux oriented frame exist as well [5].

The speed control loop in a sensorless drive is effectively decoupled from the actual mechanical sub-system of the machine. As the MRAC methods (as well as all the other methods of the second group) utilise standard *d-q* axis induction machine model, the accuracy of the speed estimation strongly depends on parameter variation effects. The impact of variations in rotor resistance (time constant), stator resistance, magnetising inductance and total leakage inductance have been studied in detail in a number of papers for different MRAC-based speed estimation schemes [2, 6, 7]. Typical steady-state speed estimation errors due to variation of motor parameters are examined in [7] for a 4 kW, 50 Hz, four-pole induction machine. It is shown that 10 % variations in rotor resistance and in total leakage inductance cause a speed-independent speed estimation error of approximately 5 min^{-1} and 2.5 min^{-1}, respectively. Speed estimation errors due to 10 % variations in magnetising inductance and in stator resistance are, however, speed-dependent, attaining at most 4 min^{-1} and 3 min^{-1}, respectively, in the very low speed region and reduce to zero as the speed increases.

Iron loss, as a source of speed estimation error in sensorless vector-controlled induction machines, has not been dealt with in the past. Indeed, iron loss as a source of detuned operation of vector-controlled induction machines was the last of the parameter variation effects to attract attention [9, 10]. However, all the available studies are applicable only to vector-controlled induction machines that have a speed (position) sensor. The presence of the speed sensor forces both the actual and reference rotor speeds, and the actual and reference slip speeds, to be mutually equal in steady-state operation. Thus detuning due to the iron loss manifests itself predominantly in an orientation angle error [9, 10]. The situation in a sensorless drive is, however, quite different. As speed is estimated, rather than measured, actual and estimated rotor and slip speeds are not necessarily mutually equal.

The aim of this paper is to evaluate speed estimation errors that will take place in a MRAC-based sensorless rotor-flux-oriented (RFO) induction machine in steady-state operation purely due to the existence of the iron loss in the machine, the iron loss being neglected in the speed

estimator and in the control system. An indirect rotor-flux-oriented induction machine is studied and the previously mentioned MRAC speed estimation methods are elaborated. Iron loss is represented with an equivalent iron loss resistance, as suggested in [9], and this resistance is identified experimentally using the procedure presented in [10] over the frequency range from zero up to twice the rated frequency. The speed estimation error, due to iron loss, is evaluated in the speed range from zero up to twice the rated speed for a 4-kW, 50-Hz, four-pole machine the data of which are given in the **Appendix**. It is shown that the speed estimation error for rotor flux, modified rotor flux and back e.m.f. methods is the same and is between 2 min^{-1} and 3 min^{-1} in the base speed region, increasing to almost 5 min^{-1} in the field-weakening region at twice the rated speed. The reactive power method yields somewhat smaller speed estimation errors, especially in the field-weakening region. These results indicate that the speed estimation error due to iron loss is of the same order as the errors introduced by other parameter variation effects. Finally, a modified indirect rotor-flux-oriented sensorless scheme is proposed that enables very good compensation of iron loss impact on speed estimation. The scheme is applicable in conjunction with rotor flux, modified rotor flux and back e.m.f. methods and yields speed estimation errors below 0.5 min^{-1}.

2 Description of the Sensorless Drive

2.1 Control Part of the Drive

The structure of the sensorless indirect rotor-flux-oriented induction machine is shown in **Fig. 1**. The current-regulated pulse-width modulated (CRPWM) inverter is assumed to be ideal and only the steady-state operation is discussed. The rotor flux reference is kept constant and equal to the rated value in the base speed region. In the field-weakening region, the rotor flux reference decreases inversely proportionally to the rotor speed. Coefficients C_1 and C_2 are dependent on the rotor flux reference and are defined in Fig. 1. The general form of the MRAC-based speed estimator of Fig. 1 is shown in **Fig. 2** and is discussed in detail in the following subsection. Measured stator currents and voltages are utilised for the estimator inputs. The outputs of the reference

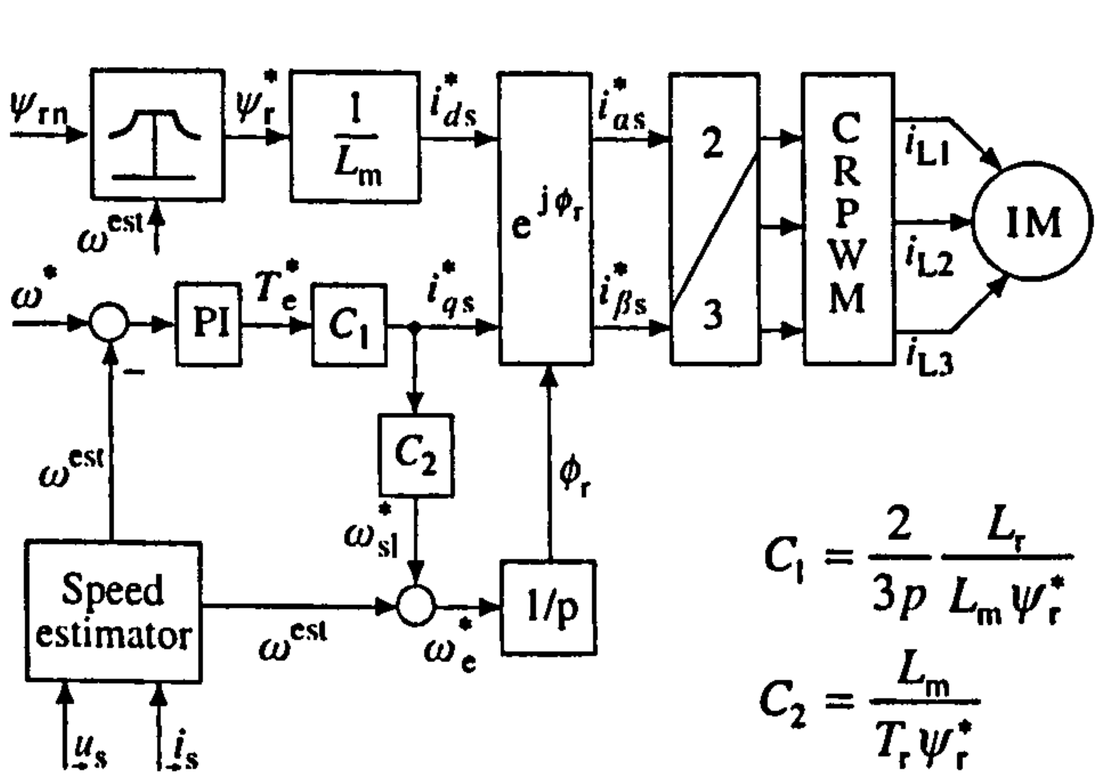

Fig. 1. Structure of the speed-sensorless rotor-flux-oriented induction machine

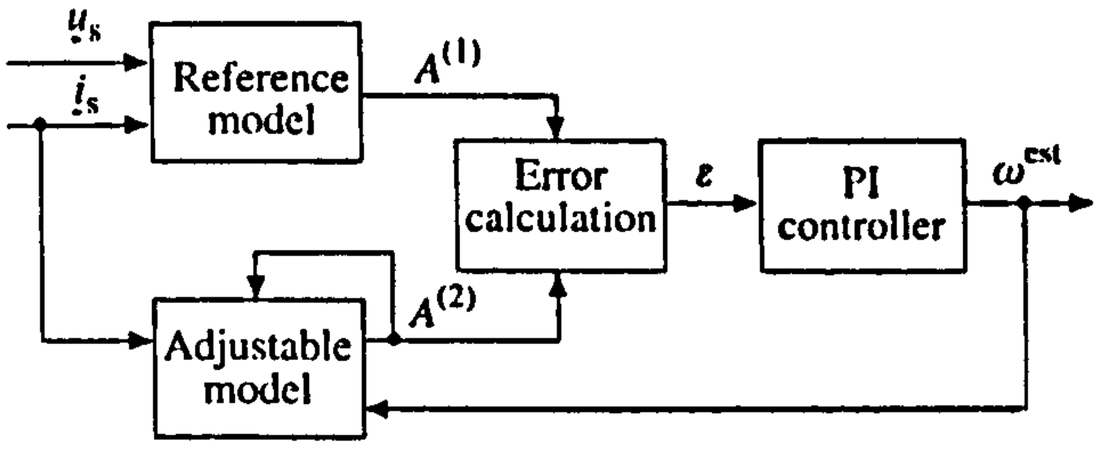

Fig. 2. General form of an MRAC-based rotor speed estimator

and the adjustable model, denoted as A, may take the form of the rotor flux space phasor, back e.m.f. or reactive power.

2.2 Rotor Speed Estimators

As already pointed out, three types of rotor speed estimators are discussed. The first approach is based on the dual estimation of rotor flux, which is evaluated in both the reference and adjustable models in Fig. 2, using the following two equations in the stationary reference frame:

$$\frac{d\underline{\psi}_r^{(1)}}{dt} = \frac{L_r}{L_m}[\underline{u}_s - (R_s + \sigma L_s p)\underline{i}_s], \tag{1}$$

$$\frac{d\underline{\psi}_r^{(2)}}{dt} = \left(j\omega^{est} - \frac{1}{T_r}\right)\underline{\psi}_r^{(2)} + \frac{L_m}{T_r}\underline{i}_s. \tag{2}$$

The error is given in terms of rotor flux components in the stationary reference frame as:

$$\varepsilon = \psi_{\alpha r}^{(2)}\psi_{\beta r}^{(1)} - \psi_{\beta r}^{(2)}\psi_{\alpha r}^{(1)}. \tag{3}$$

Due to the problems with pure integration in eq. (1), the estimator is often modified in such a way that outputs of the reference and adjustable models become modified rotor flux space phasors. These, and the error, are defined as:

$$\underline{\psi}_r^{(1)\prime} = \left(\frac{p}{p + 1/T}\right)\underline{\psi}_r^{(1)}, \quad \underline{\psi}_r^{(2)\prime} = \left(\frac{p}{p + 1/T}\right)\underline{\psi}_r^{(2)}, \tag{4}$$

$$\varepsilon = \psi_{\alpha r}^{(2)\prime}\psi_{\beta r}^{(1)\prime} - \psi_{\alpha r}^{(1)\prime}\psi_{\beta r}^{(2)\prime}.$$

If back e.m.f. is used instead of the rotor flux, an alternative form of the speed estimator, which avoids pure integration, is obtained:

$$\underline{e}^{(1)} = \frac{L_m}{L_r}\frac{d\underline{\psi}_r^{(1)}}{dt} = \underline{u}_s - (R_s + \sigma L_s p)\underline{i}_s,$$

$$\underline{e}^{(2)} = \frac{L_m}{L_r}\frac{d\underline{\psi}_r^{(2)}}{dt} = \frac{L_m}{L_r}\left[\left(j\omega^{est} - \frac{1}{T_r}\right)\underline{\psi}_r^{(2)} + \frac{L_m}{T_r}\underline{i}_s\right], \tag{5}$$

$$\varepsilon = e_\alpha^{(1)}e_\beta^{(2)} - e_\beta^{(1)}e_\alpha^{(2)},$$

where the rotor flux for the adjustable model is evaluated using eq. (2).

The third possibility is to construct a speed estimator on the basis of reactive powers. Outputs of the

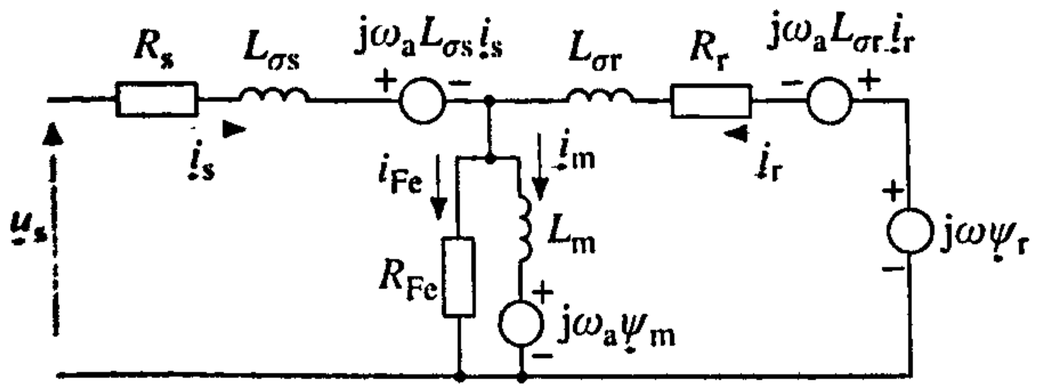

Fig. 3. Space phasor dynamic equivalent circuit of an induction machine that includes iron loss representation

reference and adjustable models and the error in this case equal:

$$q^{(1)} = i_{\alpha s} e_\beta^{(1)} - i_{\beta s} e_\alpha^{(1)}, \quad q^{(2)} = i_{\alpha s} e_\beta^{(2)} - i_{\beta s} e_\alpha^{(2)}, \qquad \varepsilon = q^{(1)} - q^{(2)}. \tag{6}$$

2.3 Induction Machine Representation

The induction machine is represented with the dynamic space phasor equivalent circuit which in an arbitrary reference frame has the form shown in **Fig. 3**, [9]. This induction machine model, in contrast to the model used in the speed estimator and the control system design, accounts for the iron loss by means of an equivalent iron loss resistance.

2.4 Experimental Iron Loss Resistance Identification

Iron loss is determined, in the frequency range from zero up to twice the rated frequency, utilising the procedure described in [10]. An inverter, with a sinusoidal pulse-width modulation and 5 kHz switching frequency, is used as supply for the induction motor during no-load tests at different operating frequencies. The modulation index linearly increases in the base speed region up to 0.95 and is kept at this value in the field-weakening region. The fundamental component of the input power is measured using the power analyser and the fundamental component of the iron loss, which is relevant for the detuning discussed here [9], is extracted by deducting mechanical loss and fundamental component of the stator copper loss. In order to enable as accurate as possible identification of the fundamental component of the iron loss, a complete no-load test is additionally performed at each frequency. The purpose of these tests is an accurate determination of mechanical losses at various frequencies. The results of the experimental identification are summarised in **Fig. 4**, where mechanical loss, fundamental component of the iron loss and the equivalent iron loss resistance are shown, all against frequency. The analytical approximation of the iron loss resistance, used later on in analytical studies, is included in Fig. 4c.

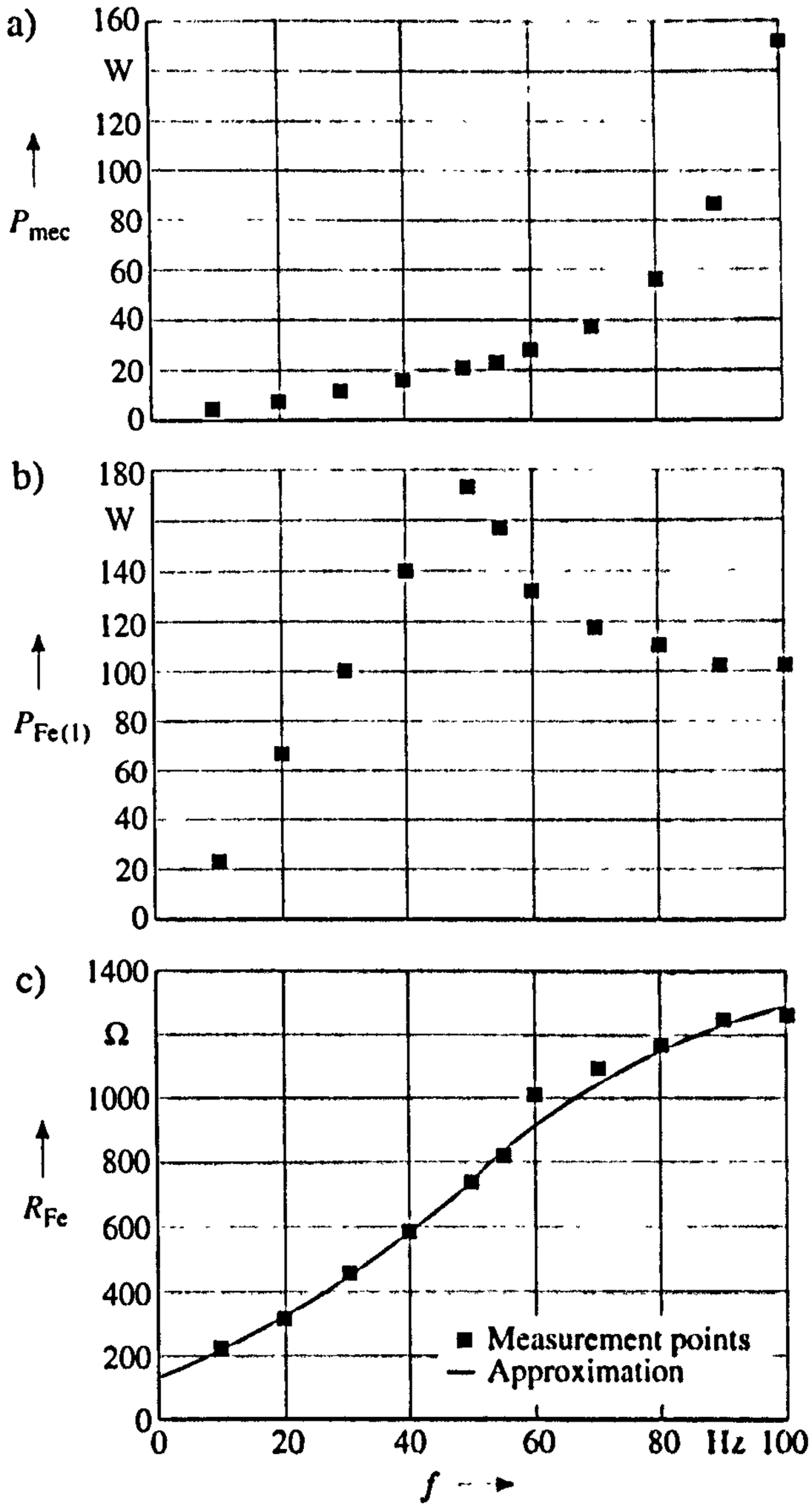

Fig. 4. Results of experimental identification of the equivalent iron loss resistance
a) Mechanical loss versus frequency
b) Fundamental iron loss versus frequency
c) Equivalent iron loss resistance versus frequency

3 Modelling and Analysis of the Drive

3.1 Induction Machine Model

The analysis of the drive is performed in the reference frame which is firmly attached to the reference of the rotor flux space phasor (d-q components). Therefore ω_u in the induction machine model of Fig. 3 equals ω_e^* of Fig. 1. Due to idealised representation of the inverter, stator d-q axis current references are identically equal to the machine d-q axis currents. Induction machine steady-state operation may under these conditions be described with the following set of equations, obtainable from Fig. 3:

$$\begin{aligned} u_{ds} &= R_s i_{ds}^* - \omega_e^* L_{\sigma s} i_{qs}^* - \omega_e^* L_m i_{qm}, \\ u_{qs} &= R_s i_{qs}^* + \omega_e^* L_{\sigma s} i_{ds}^* + \omega_e^* L_m i_{dm}, \end{aligned} \tag{7}$$

$$\begin{aligned} L_m i_{dm} &= \psi_{dr} - \omega_{sl} T_{\sigma r} \psi_{qr}, \\ L_m i_{qm} &= \psi_{qr} + \omega_{sl} T_{\sigma r} \psi_{dr}, \\ -\omega_e^* T_{Fe} i_{qm} &= i_{ds}^* + \psi_{dr}/L_{\sigma r} - i_{dm} L_r/L_{\sigma r}, \\ \omega_e^* T_{Fe} i_{dm} &= i_{qs}^* + \psi_{qr}/L_{\sigma r} - i_{qm} L_r/L_{\sigma r}, \end{aligned} \tag{8}$$

$$T_e = (3P/2)(L_m/L_{\sigma r})(\psi_{dr} i_{qm} - \psi_{qr} i_{dm}), \tag{9}$$

$$\omega_e^* = \omega + \omega_{sl}.$$

Time constants utilised in eqs. (8) are defined as $T_{Fe} = L_m/R_{Fe}$ and $T_{\sigma r} = L_{\sigma r}/R_r$.

Inspection of eqs. (7) to (8) shows that there are six equations that contain seven unknowns (stator voltage, magnetising current and rotor flux d-q axis components, plus angular slip frequency). Thus it is not possible to solve this system of equations without determining which of the seven variables is only apparently unknown. It will be shown that the speed estimator actually pre-determines one of the unknowns so that the system of equations becomes solvable.

3.2 Control System

The independent inputs into the control system are speed reference and rotor flux reference. The output of the proportional-plus-integral (PI) speed controller is the torque reference, the value of which is in general unknown. However, for each value of torque reference there will be a corresponding value of the actual torque, determined with eq. (9). Thus the torque reference may be regarded as an independent input. By solving eqs. (7) to (8), with the additional constraint imposed by the speed estimator accounted for, it is then possible to determine the value of the actual torque that corresponds to the given torque reference. Such an approach is utilised in the simulation procedure the results of which are presented in the next section. Independent inputs are taken to be speed reference, torque reference and rotor flux reference.

The constraint imposed by the control system is:

$$\omega_e^* = \omega^* + \omega_{sl}^* \equiv \omega_e, \tag{10}$$

as estimated and reference speeds are equal and reference and actual supply frequencies are also equal. The error in the speed estimation, that is to be discussed in the next section, is defined in terms of the speed (in mechanical min^{-1}) as

$$\Delta n = n - n^* \equiv n - n^{est} \equiv n_{sl}^* - n_{sl}. \tag{11}$$

3.3 Analysis of Speed Estimators

Rotor-flux- and back-e.m.f.-based speed estimators are initially discussed. In any steady-state operation, with ideal sinusoidal feeding, rotor flux estimates of eqs. (1) and (2) are equal to:

$$\begin{aligned} \underline{\psi}_r^{(1)} &= -j\frac{L_r}{\omega_e^* L_m}[\underline{u}_s - (R_s + j\omega_e^*\sigma L_s)\underline{i}_s^*], \\ \underline{\psi}_r^{(2)} &= \frac{L_m}{T_r}\underline{i}_s^* \frac{1}{1/T_r + j(\omega_e^* - \omega^{est})}. \end{aligned} \tag{12}$$

Due to the presence of the PI controller in the speed control loop (Fig. 1), estimated and reference speeds are equal. Similarly, the PI controller within the speed estimator of Fig. 2 imposes the constraint that $\varepsilon = 0$ in any steady state. This means that instantaneous positions of the two rotor flux estimates with respect to the fixed stator axis are equal, i. e.:

$$\phi_r^{(1)} = \phi_r^{(2)} = \phi_r. \tag{13}$$

However, the rotor speed estimator does not require that magnitudes of the two rotor flux estimates are equal. Hence, in rotor-flux-oriented reference frame determined with the transformation angle of eq. (13), rotor flux estimates are:

$$\begin{aligned} &\underline{\psi}_r^{(2)} = \psi_{dr}^{(2)} + j\psi_{qr}^{(2)}, \quad \psi_{dr}^{(2)} = \psi_r^*, \quad \psi_{qr}^{(2)} = 0; \\ &\underline{\psi}_r^{(1)} = \psi_{dr}^{(1)} + j\psi_{qr}^{(1)}, \quad \psi_{dr}^{(1)} \neq \psi_r^*, \quad \psi_{qr}^{(1)} = 0. \end{aligned} \tag{14}$$

It follows from eq. (14) that the rotor flux q-axis component in the commanded reference frame must equal zero for both flux estimates. However, the d-axis component of the first estimate is not necessarily equal to the rotor flux reference (the magnitude of the second flux estimate is by definition equal to the rotor flux reference). If the q-axis component of the first rotor flux estimate is expressed from eq. (12) and equated to zero (in the commanded rotor flux reference frame), then the d-axis component of the stator voltage is found to be:

$$u_{ds} = R_s i_{ds}^* - \omega_e^* \sigma L_s i_{qs}^*. \tag{15}$$

Eq. (15) is the well-known stator voltage d-axis equation, which is valid under the correct rotor flux orientation conditions (with neglected iron loss). The speed estimator operation makes the stator d-axis voltage equal to that required for perfect rotor flux orientation. However, as the estimator does not require equality of magnitudes of rotor flux estimates, the stator q-axis voltage will deviate from the one required for perfect rotor-flux orientation.

If the modified rotor-flux-based estimator, described with eqs. (1), (2) and (4), is used, it can be easily shown that exactly the same conditions hold true and that the speed estimator operation again leads to the condition given with eq. (15).

In the case of the back-e.m.f.-based speed estimator, outputs of the reference and adjustable model in eqs. (5) are in any steady state equal to:

$$\underline{e}^{(1)} = j\omega_e^*(L_m/L_r)\underline{\psi}_r^{(1)}, \quad \underline{e}^{(2)} = j\omega_e^*(L_m/L_r)\underline{\psi}_r^{(2)}. \tag{16}$$

The error is defined in the same way as it is for the rotor-flux-based estimator. The outputs of the two models in Fig. 2 are now shifted by 90° with respect to the rotor flux positions and scaled with the same factor. Thus, the back-e.m.f.-based estimator again leads to the condition expressed in eq. (15).

The stator d-axis voltage is hence known, for any given set of operating conditions, for both rotor-flux-based and back-e.m.f.-based speed estimators and it is now possible to solve the model of the machine given with eqs. (7) to (9). In particular, the magnetising current q-axis component follows directly from the first equation of eqs. (7) and hence its value is known. An expression for the q-axis magnetising current as a function of the actual angular slip frequency may be derived from eq. (8). The actual angular slip frequency can then be found numerically by forcing the q-axis magnetising current to the value obtained from the first equation in eqs. (7).

Bearing in mind that for sinusoidal steady-state operation $p\,i_{\alpha s} = -\omega_e^* i_{\beta s}$ and $p\,i_{\beta s} = \omega_e^* i_{\alpha s}$, the outputs of the reference and adjustable model in the reactive-power-based estimator can be obtained from eqs. (6) in the form:

$$q^{(1)} = i_{\alpha s} u_{\beta s} - i_{\beta s} u_{\alpha s} - \sigma L_s \omega_e^* i_s^2,$$

$$q^{(2)} = \frac{L_m^2}{L_r} \frac{i_s^2 \omega_e^*}{1 + \left[T_r(\omega_e^* - \omega^{est})\right]^2}, \quad (17)$$

where $i_s^2 = i_{\alpha s}^2 + i_{\beta s}^2$. From eqs. (17) it follows that the rotor speed is determined with the condition that the input reactive power must equal the reactive power required by the motor, as the difference between the two quantities in eqs. (17) equals zero in any steady state. It can be shown that, if the iron loss is accounted for by means of the equivalent circuit of Fig. 3, the corresponding reactive power correlation is found in the form:

$$i_{\alpha s} u_{\beta s} - i_{\beta s} u_{\alpha s} = \omega_e^* i_s^2 \left[L_{\sigma s} + \frac{L_{\sigma r}(T_{\sigma r} - T_r)^2 \omega_{sl}^2 + L_m[1 + (\omega_{sl} T_{\sigma r})^2]}{(1 - \omega_e^* \omega_{sl} T_{\sigma r} T_{Fe})^2 + (\omega_e^* T_{Fe} + \omega_{sl} T_r)^2} \right]. \quad (18)$$

As the input reactive power in eqs. (17) and (18) is the same, then for any given operating condition it is possible to calculate from eqs. (17) and (18) the unknown slip speed and hence the rotor speed. It follows that, in the case of the reactive-power-based speed estimator, the actual speed is obtainable directly from the reactive power equations and it is then once more possible to solve for the remaining unknowns in the induction motor model, eqs. (7) to (9).

4 Results of the Study

Detuning effects are examined with the reference speed taken as the independent variable and normalised with respect to the rated speed. Torque reference is set to a constant value in the base speed region. For operation in the field-weakening region, the torque reference decreases in an inversely proportional manner to the speed, so that constant power operation is assumed. The iron loss resistance is adjusted to an appropriate value for each operating frequency using the approximation of Fig. 4c.

Fig. 5 summarises the main results obtained for the rotor-flux-based speed estimator. As already noted, the same results apply to the modified rotor flux method and to the back e.m.f. method. The speed error (in min^{-1}) and ratio of actual to reference torque are given, for three different torque/power references. It follows from Fig. 5a that a typical speed estimation error of 2 min^{-1} to 3 min^{-1} can be expected in the base speed region (except at low speeds), purely because of the iron losses. The speed estimation error increases in the field-weakening region reaching almost 5 min^{-1} when operating with rated power at twice the rated speed. The error in torque ratio, Fig. 5b, increases for a given speed reference as loading decreases and is over 20 % for the torque/power reference of 0.2 p.u. Such behaviour reflects the fact that iron loss represents a relatively high proportion of the total power reference when loading is light.

The same detuning characteristics are displayed once more in **Fig. 6**, this time for the reactive power method. Comparison of Fig. 5 and Fig. 6 indicates that the reactive power method leads to slightly reduced

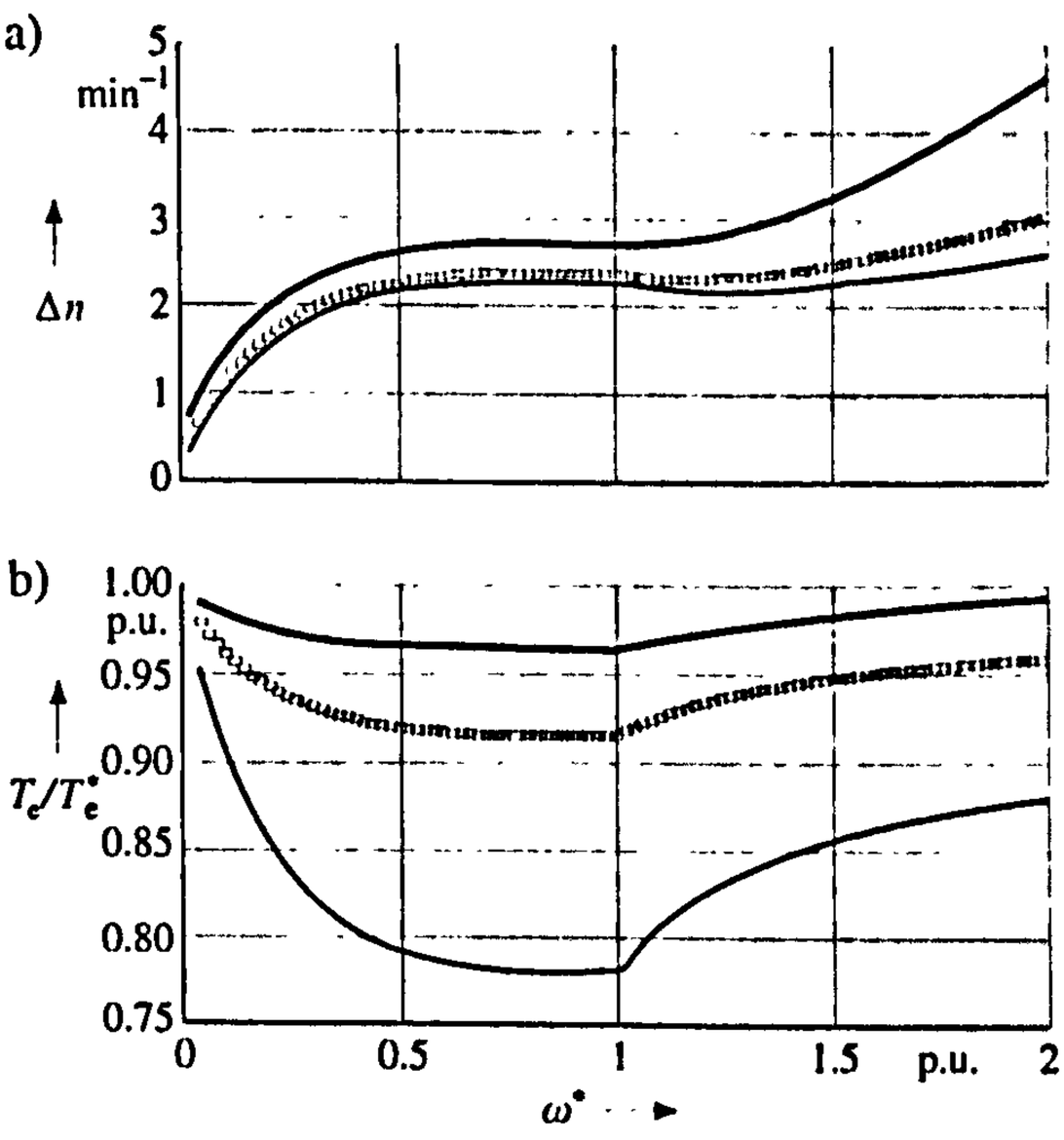

Fig. 5. Impact of iron loss on sensorless rotor-flux-oriented induction machine with rotor-flux- and back-e.m.f.-based MRAC speed estimators
a) Speed estimation error
b) Ratio of actual to reference torque

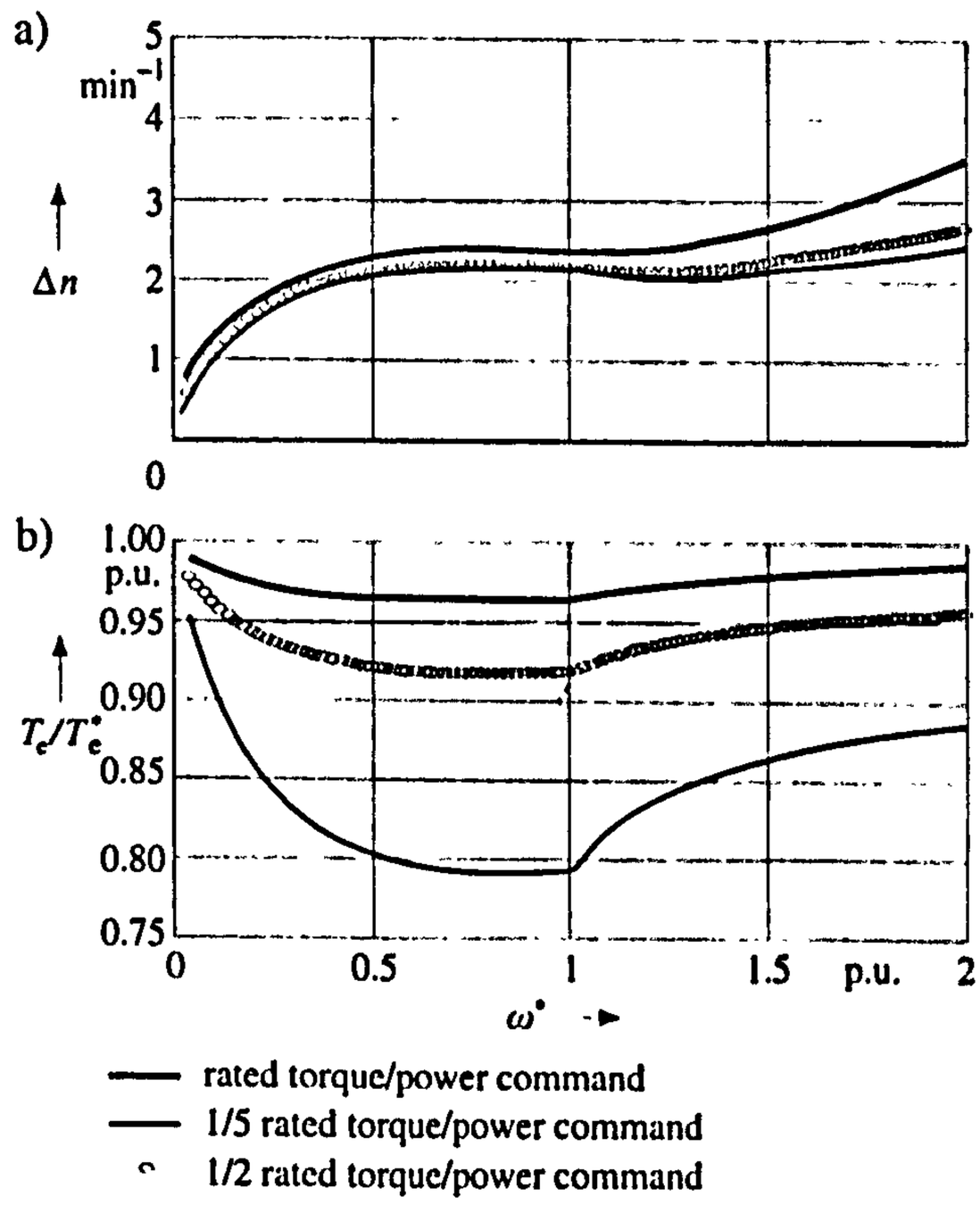

Fig. 6. Impact of iron loss on sensorless rotor-flux-oriented induction machine with reactive power-based MRAC speed estimator
a) Speed estimation error
b) Ratio of actual to reference torque

speed estimation errors in both the base speed region and the field-weakening region. The torque ratio shows slightly more favourable behaviour as well, with smaller errors especially at light load.

It is worth noting that the orientation angle error for both methods is negligibly small and is within the numerical accuracy of the calculations. Similarly, the difference in rotor flux amplitudes, which for rotor flux and back e.m.f. methods must exist according to eq. (14), is below 1 % for all operating conditions.

5 Iron Loss Compensation

Compensation of iron loss could be achieved by developing modified speed estimators from the dynamic equivalent circuit of an induction machine shown in Fig. 3. However, the inclusion of iron loss representation would significantly increase the complexity of the speed estimator and the main advantage of relative simplicity in MRAC-based speed estimation would be lost. An alternative way to compensate for the impact of iron loss on speed estimation is therefore desirable and it consists of modification of the control part of the drive. It has already been shown in [9] that an indirect vector controller may be altered on the basis of the equivalent circuit of Fig. 3, and that such a modified controller will provide complete compensation of iron loss in a drive with a speed (position) sensor. It is suggested here that the same modified indirect vector controller should be applied in a sensorless rotor-flux-oriented induction machine. Assuming operation in the constant flux region only, the control part of the drive shown in Fig. 1 now becomes as shown in Fig. 7a. The controller operation is described with the following equations [9]:

$$i_{dm}^* = \psi_r^*/L_m, \quad i_{qm}^* = [2/(3p)]\, L_{\sigma r} T_e^*/(L_m \psi_r^*),$$
$$\omega_{sl}^* = (L_m/T_{\sigma r}) i_{qm}^*/\psi_r^*, \tag{19}$$
$$i_{ds}^* = i_{dm}^* - \omega_e^* T_{Fe} i_{qm}^*, \quad i_{qs}^* = \omega_e^* T_{Fe} i_{dm}^* + (L_r/L_{\sigma r}) i_{qm}^*.$$

Coefficients K_1 and K_2 of Fig. 7a follow directly from eqs. (19).

Although the speed estimator structure remains the same, it is necessary to modify its inputs when the indirect vector controller of Fig. 7a is applied. Indeed, total stator d-q axis current commands in eqs. (19) contain steady-state iron loss current d-q axis components, $i_{dFe}^* = -\omega_e^* T_{Fe} i_{qm}^*$ and $i_{qFe}^* = \omega_e^* T_{Fe} i_{dm}^*$, while the speed estimator is not aware of the existence of the iron loss. It is therefore suggested to take as input into the speed estimator difference between measured stator $\alpha - \beta$ current components and iron loss $\alpha - \beta$ current components. Iron loss $\alpha - \beta$ current components are calculated in a feed-forward manner, using reference values of d-q axis iron loss current components and inverse co-ordinate transformation, as shown in Fig. 7b.

The control system of Fig. 7 enables substantial improvement in the accuracy of the speed-sensorless control, when the MRAC speed estimator utilises either the rotor flux or back e.m.f. method. Such a conclusion fol-

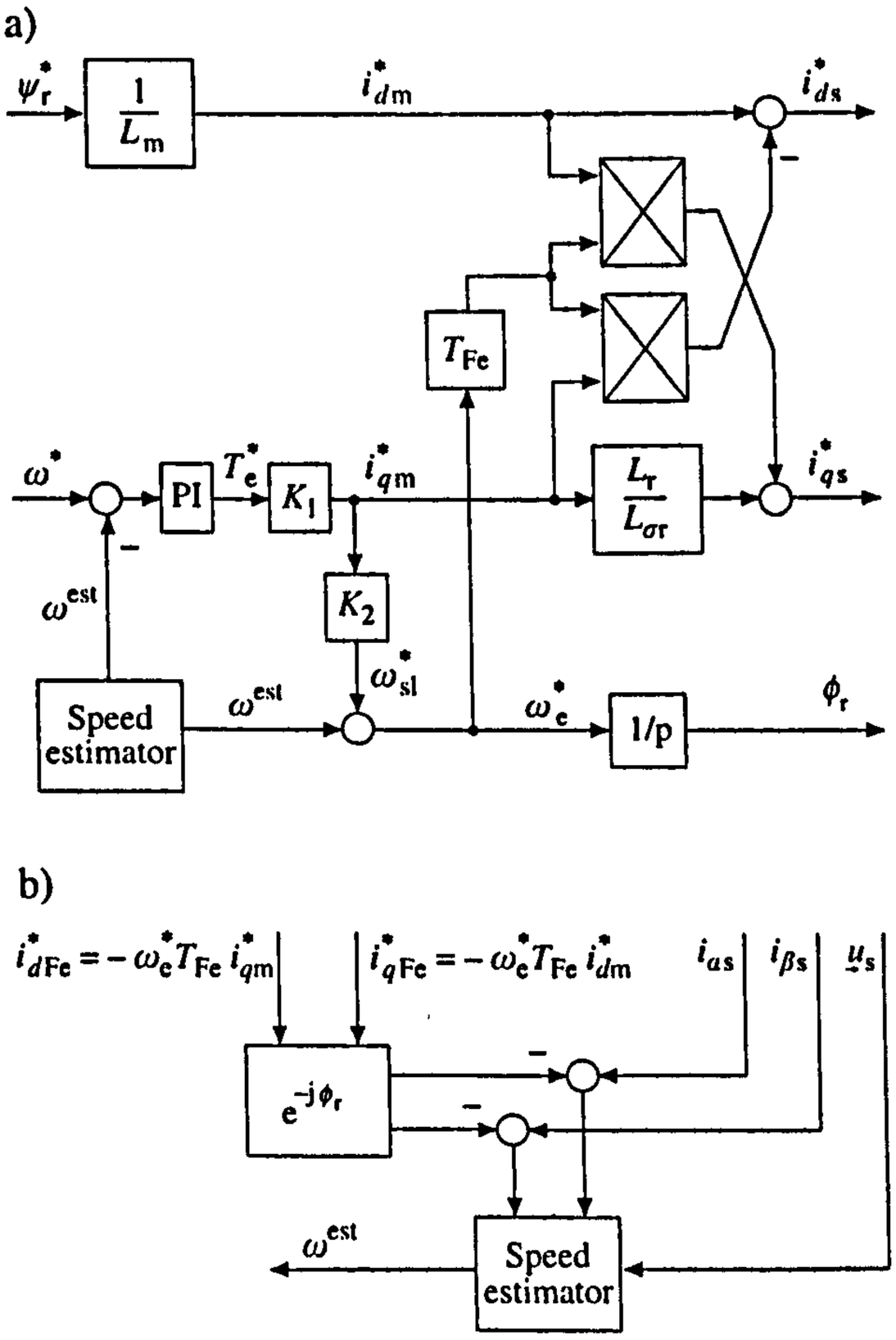

Fig. 7. Modified sensorless rotor-flux-oriented control scheme with rotor-flux- or back-e.m.f.-based MRAC speed estimator
a) Modified indirect rotor-flux-oriented controller
b) Modified current input into the speed estimator

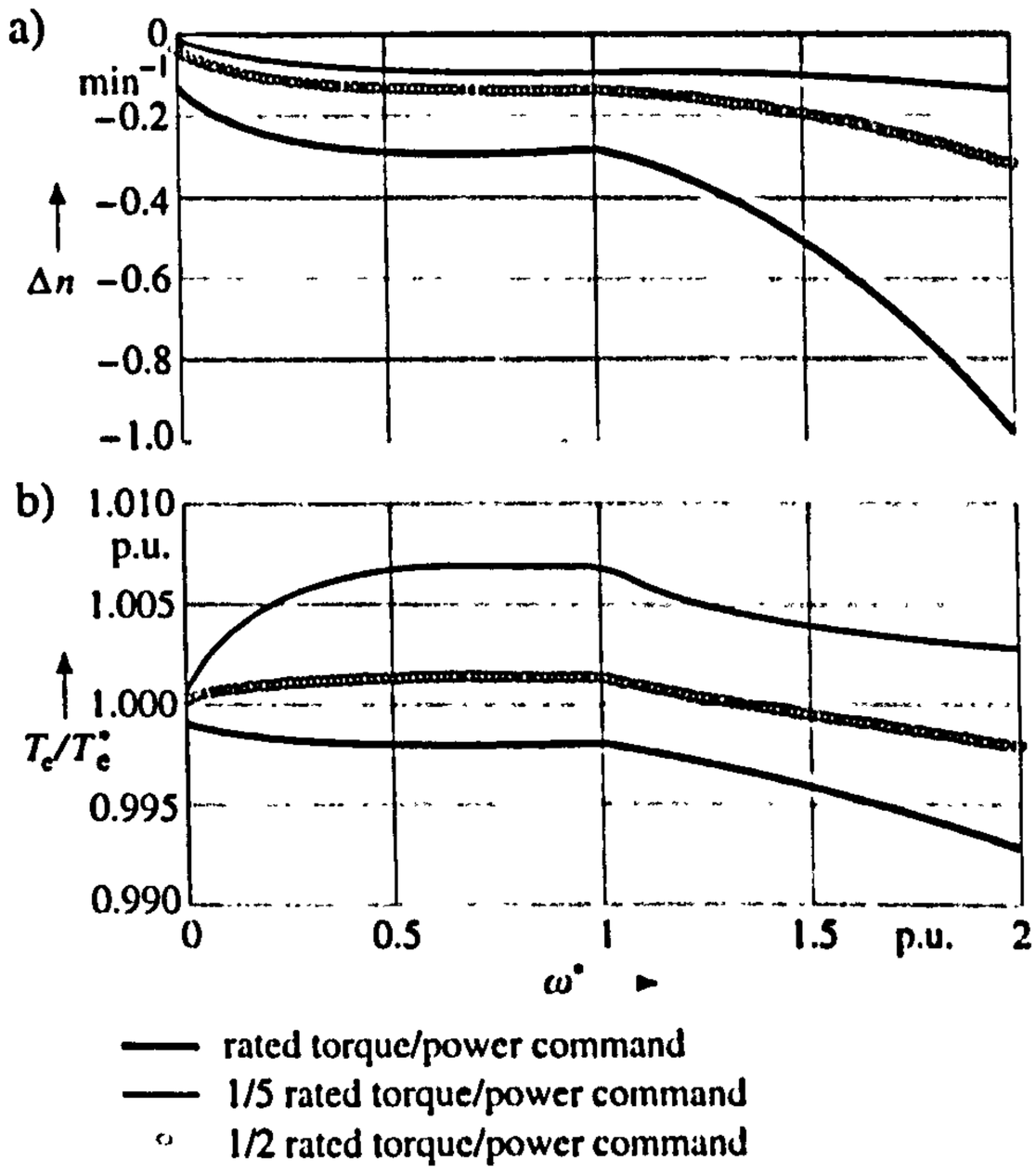

Fig. 8. Impact of iron loss on rotor-flux-oriented induction machine with modified rotor-flux-/back-e.m.f.-based MRAC sensorless control
a) Speed estimation error
b) Ratio of actual to reference torque

lows from the analysis that is now performed using the scheme of Fig. 7 instead of the scheme of Fig. 1. Speed estimation error and torque ratio are shown in Fig. 8, for the same operating conditions that apply to Fig. 5. Application of the scheme of Fig. 7 confines speed estimation error to values smaller than $-0.4\ \text{min}^{-1}$ in the entire base speed region, for all operating conditions. Speed estimation error is at most $-1\ \text{min}^{-1}$ in the field-weakening region. Torque error is also very small and within boundaries of ± 1 %.

6 Conclusions

The paper evaluates the impact of iron loss on speed estimation accuracy in MRAC-based sensorless rotor-flux-oriented induction machines. Speed estimators that utilise rotor flux, back e.m.f. and reactive power as outputs from the reference and the adjustable model are elaborated. It is shown that iron loss leads to the same detuning in rotor-flux- and back-e.m.f.-based estimators. Typical speed estimation error is found to be $2\ \text{min}^{-1}$ to $3\ \text{min}^{-1}$ in the base speed region and the torque ratio error exceeds 20 % at light loads. The reactive power method leads to somewhat smaller speed estimation and torque ratio errors.

Speed estimation error due to iron loss is not negligible and is of the same order as the errors due to other parameter variation effects. It is therefore desirable to compensate for the iron loss and it is suggested to modify the indirect vector controller in such a way that it compensates the iron loss. It is shown that the application of the modified indirect vector controller in conjunction with the rotor-flux-/back-e.m.f.-based speed estimator, whose current inputs are modified, leads to a significant reduction in both speed estimation error and torque ratio error. The speed error is typically below $0.4\ \text{min}^{-1}$ in the base speed region while error in torque ratio does not exceed 1 %.

7 List of Symbols

- e back e.m.f.
- f frequency
- i current
- L inductance
- n mechanical speed of rotation (in min^{-1})
- Δn speed estimation error
- p Laplace operator
- p number of pole pairs
- $P_{\text{Fe(1)}}$ fundamental iron loss component
- P_{mec} mechanical loss
- q reactive power
- R resistance
- R_{Fe} equivalent iron loss resistance
- T filter time constant
- T_r rotor time constant
- $T_{\sigma r}$ rotor leakage time constant
- T_{Fe} equivalent iron loss time constant
- T_e electromagnetic torque
- u voltage
- ε error
- ϕ_r instantaneous spatial position of rotor flux space phasor with respect to stationary axis
- σ total leakage coefficient ($\sigma = 1 - L_m^2/(L_s L_r)$)
- ψ flux linkage
- ω angular speed of rotation, angular slip speed
- ω_a speed of rotation of an arbitrary reference frame
- ω_e angular frequency of the supply

– *Subscripts*

- d, q d-q axis components of space phasors in rotating reference frame
- Fe iron loss related quantities
- m parameters and variables associated with main (magnetising) flux and current
- n rated data
- sl slip
- s, r stator and rotor, respectively
- α, β α-β axis components of space phasors in stationary reference frame
- σ identifies leakage inductances

– *Superscripts*

- * reference values
- est estimates
- (1), (2) outputs of reference and adjustable parts of the speed estimator, respectively

– *Other*

- → underarrowed variables are space phasors
- j imaginary unity

– *Abbreviations*

- CRPWM current-regulated pulse-width modulated
- e.m.f. electromotive force
- MRAC model reference adaptive control
- PI proportional plus integral
- RFO rotor-flux oriented

Appendix: Induction Motor Data

$P_n = 4\,\text{kW}, U_n = 380\,\text{V}, f_n = 50\,\text{Hz}, 2p = 4, I_n = 8.7\,\text{A (star)}$

$T_{en} = 26.526\,\text{Nm}, n_n = 1448\ \text{min}^{-1}, P_{\text{Fe.n}} = 0.047\,P_n$

$R_s = 1.37, R_r = 1.1\ \Omega$

$X_{\sigma s} = 1.53\ \Omega, X_{\sigma r} = 2.5\ \Omega, X_m = 44.3\ \Omega$

$$R_{\text{Fe}} = \begin{cases} 128.92 + 8.242 f + 0.07788 f^2 & f < 50\,\text{Hz} \\ 1841 - 55275/f & f > 50\,\text{Hz} \end{cases}$$

References

[1] *Holtz, J.:* State of the art of controlled AC drives without speed sensors. Int. J. Electron. 80 (1996) no. 2, pp. 249–263

[2] *Ilas, C.; Bettini, A.; Ferraris, L.; Griva, G.; Profumo, F.:* Comparison of different schemes without shaft encoders for field oriented control drives. IEEE 20th Annu. Int. Conf. of the Ind. Electron. Soc. (IECON'94), Bologna /Italy 1994, Conf.-rec. pp. 1579–1588

[3] *Schauder, C.:* Adaptive speed identification for vector control of induction motors without rotational transducers. IEEE Trans. on Ind. Appl. IA-28 (1992) no. 5, pp. 1054–1061

[4] *Peng, F. Z.; Fukao, T.:* Robust speed identification for speed-sensorless vector control of induction motors. IEEE Trans. on Ind. Appl. IA-30 (1994) no. 5, pp. 1234–1240

[5] *Kim, M. H.; Hung, J. C.:* Vector control system for induction motor without speed sensor at very low speed. IEEE 21th Ann. Int. Conf. of the Ind. Electron. Soc. (IECON'95), Orlando/Florida USA 1995, Conf.-rec. pp. 524–529

[6] *Tajima, H.; Hori, Y.:* Speed sensorless field-orientation control of the induction machine. IEEE Trans. on Ind. Appl. IA-29 (1993) no. 1, pp. 175–180

[7] *Blasco-Gimenez, R.; Asher, G. M.; Sumner, M.; Bradley, K. J.:* Dynamic performance limitations for MRAS based sensorless induction motor drives. Part 1: Stability analysis for the closed loop drive. IEE Proc. – Electr. Power Appl. 143 (1996) no. 2, pp. 113–122

[8] *Rajashekara, K.; Kawamura, A.; Matsuse, K.* (Ed.): Sensorless control of AC motor drives. Piscataway/USA: IEEE Press, 1996

[9] *Levi, E.:* Impact of iron loss on behaviour of vector controlled induction machines. IEEE Trans. on Ind. Appl. IA-31 (1995) no. 6, pp. 1287–1296

[10] *Levi, E.; Sokola, M.; Boglietti, A.; Pastorelli, M.:* Iron loss in rotor flux oriented induction machines: identification, assessment of detuning and compensation. IEEE Trans. on Power Electr. PE-11 (1996) no. 5, pp. 698–709

Manuscript received on April 11, 1997

The Authors

Dr. Emil Levi (1958) received the Diploma degree from the University of Novi Sad/Yugoslavia, the MSc and the PhD degree from the University of Belgrade/Yugoslavia in 1982, 1986 and 1990, respectively, all in Electrical Engineering. In 1982 he joined the Department of Electrical Engineering at the University of Novi Sad, where he became Assistant Professor in 1991. He joined Liverpool John Moores University/UK in May 1992 as a Senior Lecturer. Since 1995 he is Reader in Electrical Power Engineering. His main areas of research interest are modelling and simulation of electric machines, control of high performance drives and power electronic converters. (Liverpool John Moores University, School of Engineering, Byrom Street, Liverpool L3 3AF/UK, Phone: +44 151/231-2257, Fax: +44 151/2982624, E-mail: e.levi@livjm.ac.uk)

Mingyu Wang (1960) received the B.Eng. degree in Electrical Engineering from Chongquing University/P.R. China, in 1982. He became a member of academic staff at Chongquing University, Dept. of Automation Engineering in 1982, and was a lecturer there from 1988 until 1993. He was a Visiting Scholar in the Dept. of Electrical Engineering, University of Manchester/UK from 1993 until 1995. Since 1995 he is studying towards the PhD at Liverpool John Moores University/UK. His research interests are in power electronics, adjustable speed drives and vector control of induction machines. (Liverpool John Moores University, School of Engineering, Byrom Street, Liverpool L3 3AF/UK, Phone: +44 151/231-2261, Fax: +44 151/298-2624, e-mail: eeemwang@livjm.ac.uk)

Prof. David Williams (1946) received his B.Eng. in 1967 in Electrical and Electronic Engineering and the PhD in 1970 in Control Engineering. In 1975 he joined Liverpool John Moores University/UK (then Liverpool Polytechnic). He progressed through Principal Lecturer in 1986 and Reader in 1991 to Professor in 1992. His main area of research is the application of intelligent control systems to a range of processes and systems (Liverpool John Moores University, School of Engineering, Byrom Street, Liverpool L3 3AF/UK, Phone: +44 151/231-2048, Fax: +44 151/298-2624, e-mail: d.williams@livjm.ac.uk)

ELECTRIC
MACHINES and
POWER SYSTEMS

EDITOR
S. A. NASAR
Department of Electrical Engineering
University of Kentucky
Lexington, Kentucky 40506

October 8, 1998

Dr. Emil Levi
Liverpool John Moores University
School of Engineerng
Byrom St.
Liverpool L3 3AF
England, UK

Paper No: 5697

Dear Dr. Levi:

I am pleased to write that your paper "Compensation of Parameter Variation Effects in Sensorless Indirect Vector Controlled Induction Machines Using Model Based Approach" has been accepted for publication in our journal subject to the revision suggested by the reviewers. Please prepare the manuscript according to the enclosed instructions, and incorporating the changes suggested by the reviewers. Copies of the reviewer's comments are also enclosed.

Please return the final manuscript and the copyright release form to me.

Sincerely,

S. A. Nasar

S.A. Nasar
Editor

DATE: Jan 5 '99
AUTHOR(S): Levi
MS. #: 5697
TITLE: Compensation —

Dear Author:

A final copy of the above mentioned manuscript has been received in our office. It will be published in Volume 27(1)'99 Number 9. Thank you for your contribution.

S. A. Nasar
Editor

Taylor & Francis
Publishers since 1798

COMPENSATION OF PARAMETER VARIATION EFFECTS IN SENSORLESS INDIRECT VECTOR CONTROLLED INDUCTION MACHINES USING MODEL BASED APPROACH

M.Wang, E.Levi and M.Jovanovic

Liverpool John Moores University
School of Engineering,
Byrom St
Liverpool L3 3AF, UK

ABSTRACT

The majority of speed estimation schemes for sensorless vector control of induction machines utilise a mathematical model of the machine in the estimation process. These schemes are therefore inherently sensitive to parameter variation effects in the machine. The variety of speed estimation methods makes any attempt to develop a universal approach to compensation of parameter variation effects impossible. This paper concentrates on one of the most frequently utilised schemes, in which speed is estimated using model reference adaptive control approach (MRAC) on the basis of two estimated values of the rotor flux space vector. The estimator is analysed in conjunction with indirect feed-forward rotor flux oriented induction machine. An attempt is made to improve the accuracy of the speed estimation by appropriate modification of the speed estimator and the indirect vector controller structures, using modified induction motor models that account for one or more of the phenomena that are neglected in development of the basic constant parameter scheme. In particular, compensation of main flux saturation, compensation of iron loss, and simultaneous compensation of both the iron loss and main flux saturation are elaborated. Novel structures of the speed estimator are developed for each of the three cases and are applied in conjunction with the appropriate modified form of the indirect rotor flux oriented controller. Excellent compensation capability is demonstrated in all the cases by performing extensive simulation studies.

1. INTRODUCTION

Numerous methods of speed-sensorless vector control of induction machines have recently been developed (Rajashekara et al., 1996). In general, two major approaches can be identified. The first one encompasses all the techniques that estimate rotor speed from the stator current spectrum: speed estimation is therefore inherently not sensitive to parameter variation effects in the machine. The second approach relies on utilisation of induction machine model in the process of speed estimation and the accuracy of speed

estimation thus unavoidably depends on accurate knowledge of the machine parameters. Among many different methods that utilise the second approach, speed estimation based on MRAC (Schauder, 1992) has gained substantial popularity due to its relatively simple implementation requirements. This is the technique analysed in this paper, in conjunction with indirect feed-forward current-fed rotor flux oriented induction machine.

MRAC based speed estimation techniques mutually differ with respect to the quantity that is selected as output of the reference and the adjustable model. This quantity can take the form of rotor flux (Schauder, 1992), back e.m.f (Peng and Fukao, 1994), reactive power (Peng and Fukao, 1994), air-gap active power (Zhen and Xu, 1995) etc.. The most frequent choices appear to be rotor flux and back e.m.f. (Marwali and Keyhani, 1997). The method discussed in this paper is the rotor flux based one, that is characterised with simpler design (Marwali and Keyhani, 1997).

As mechanical sub-system of the control part of the drive and of the machine itself are in any sensorless drive effectively decoupled, and as standard d-q axis constant parameter induction machine model is utilised in the design of the controller and the speed estimator, accuracy of speed estimation in all the model based methods, including the MRAC ones, strongly depends on parameter setting and parameter variation effects in the machine. Numerous studies related to parameter variation effects in MRAC based sensorless drives are available. Comprehensive investigations of steady-state speed estimation errors caused by variation of all the motor parameters are reported by Blasco-Gimenez et al. (1996a) and Jansen and Lorenz (1993) for a direct rotor flux oriented induction machine that combines a MRAC based speed estimator with a closed loop flux observer and includes a mechanical system model. The validity of these results is therefore restricted to that specific drive structure. Impact of rotor resistance variation on transient behaviour of the drive is studied by Ilas et al. (1994) and Griva et al. (1996) using simulation. Effects of main flux saturation on dynamics of indirect feed-forward rotor flux oriented induction machine are examined by El-Kholy et al. (1994). An experimental study of impact of rotor resistance, stator resistance and magnetising inductance induced detuning is reported for operation in the low speed region by Armstrong and Atkinson (1997). Steady-state analysis of impact of iron loss on speed estimation in indirect feed-forward rotor flux oriented induction machine with rotor flux based MRAC speed estimator is elaborated by Levi and Wang (1997). The most comprehensive studies of detuning effects in the scheme under consideration (Levi and Wang, 1998; Wang and Levi, 1998) report on detailed analysis of speed estimation error and other detuning effects in steady-state and transient operation, respectively. Detuning is evaluated in these two studies for incorrect setting of the magnetising inductance, stator and rotor resistance variation and leakage inductance variation for operation in the base speed region. A four-pole, 50 Hz induction machine is analysed by Levi and Wang (1997), Levi and Wang (1998) and Wang and Levi (1998) and the relative importance of different sources of detuning can be summarised as follows. Variation of rotor resistance yields a speed independent, load dependent large speed estimation error of up to 10 rpm for a 20% discrepancy between rotor resistance value in the motor and the value used in the control structure. Stator resistance variation leads to a speed dependent, load independent speed estimation error that is of moderate value at low speed (around 4 to 5 rpm at 5% of the rated speed, with stator resistance detuned by 20%). Speed estimation error progressively reduces as the operating speed increases. However, correct value of the stator resistance is crucial for stable operation at low speeds (Armstrong and

Atkinson, 1997). Incorrect setting of leakage inductances gives speed independent, load dependent speed estimation error that is negligibly small (below 1 rpm for deviation of leakage inductances by 50%). Iron loss results in speed dependent, weakly load dependent moderate speed estimation error of around 3 rpm in the base speed region, while detuned magnetising inductance causes speed independent, load dependent moderate speed estimation error in the base speed region (up to 3.5 rpm when the value is detuned by 20%). It follows that iron loss and incorrect magnetising inductance setting cause moderate speed estimation errors, of the same order as stator resistance variation at low speeds, while rotor resistance induced detuning is by far the highest.

Compensation of parameter variation effects in sensorless vector controlled induction motor drives with model based speed estimation has been a subject of considerable interest in recent past. In majority of cases attempts are made to provide on-line identification of either stator resistance (Yang and Chin, 1993; Blasco-Gimenez et al., 1995), or rotor resistance (Kubota and Matsuse, 1994; Jiang and Holtz, 1997; Shirsavar et al., 1996). Simultaneous identification of both the stator and the rotor resistance is proposed by Zhen and Xu (1995) and Blasco-Gimenez et al. (1996b). As changes in stator and rotor resistance are temperature dependent, the only way to compensate for their variation is to employ a method of on-line identification. However, a different, so-called model based approach is advantageous when parameter variations of electro-magnetic nature are under consideration. In this case it is easier to design the control system and the speed estimator using an appropriate, modified induction motor model that accounts for the given phenomenon. Such a situation arises when compensation of detuning due to main flux saturation and/or iron loss is to be achieved. Model based approach has been extensively used in the past to achieve main flux saturation compensation (Levi and Vuckovic, 1989; Levi et al., 1990; Levi and Vuckovic, 1993; Williamson and Healey, 1996; Levi and Sokola, 1997) and iron loss compensation (Levi, 1995; Levi et al., 1996) in vector controlled drives that do posses a speed (position) sensor. However, very little effort has been put so far into compensation of these phenomena by means of the model based approach in sensorless vector controlled induction motor drives, the exceptions being works of Levi et al. (1999) and Blasco-Gimenez et al. (1996c). A modified rotor flux based speed estimator of MRAC type, that provides compensation of iron loss in conjunction with the modified indirect feed-forward vector controller, is introduced by Levi et al. (1999) and its suitability is confirmed by steady-state analysis. Need for compensation of main flux saturation for operation in the field weakening region is recognised by Blasco-Gimenez et al. (1996c) and a modified speed estimator is developed. The sensorless scheme discussed by Blasco-Gimenez et al. (1996c) incorporates closed loop flux control and utilises speed estimation algorithm based on MRAC in conjunction with closed-loop flux observer. It is therefore of the same type as the scheme discussed by Blasco-Gimenez et al. (1996a, 1996b) and its general applicability is limited by the high level of complexity.

If a vector controlled induction motor drive is designed to operate in both base speed region and field weakening region, it becomes an imperative that main flux saturation is compensated. In field weakening region impact of stator resistance variation is negligible, while level of main flux saturation significantly varies with operating speed. On the other hand, iron loss is an unavoidable source of detuning as its existence is neglected in the design of the speed estimator and the vector controller. The aim of the present paper is to propose a couple of relatively simple sensorless rotor flux oriented control schemes, that

provide compensation of main flux saturation, compensation of iron loss and simultaneous compensation of main flux saturation and iron loss. Modified rotor flux based speed estimators of MRAC type are developed for each of the three cases using model based approach. Modified estimators are used in conjunction with suitably modified indirect vector controllers and their effectiveness in compensating the given phenomenon is confirmed by simulation.

2. BASIC STRUCTURE OF THE DRIVE

Basic structure of the sensorless indirect rotor flux oriented induction machine, elaborated in the paper, is shown in Fig. 1. The machine is assumed to be fed from a current source, so that the current controlled PWM inverter is taken as ideal in simulations (i.e., reference and actual phase currents are equal). Structure shown in Fig. 1 is aimed at operation in the base speed region only, so that rotor flux reference is shown as constant and equal to rated (index n denotes rated values). The speed estimator of Fig. 1 is shown in Fig. 2 (Schauder, 1992). It relies on measurement of stator currents and voltages, utilises principles of MRAC, and the two left-hand side blocks perform integration of equations (1) and (2). Speed estimator operates in the stationary α,β reference frame and is described with the following space vector equations ($\sigma_n = 1 - L_{mn}^2 / \left(L_{sn} L_{rn}\right)$):

$$\frac{d\underline{\psi}_r^{(1)}}{dt} = \frac{\tilde{L}_{rn}}{L_{mn}} \left[\underline{v}_s - \left(R_{sn} + \sigma_n L_{sn} p \right) \underline{i}_s \right] \tag{1}$$

$$\frac{d\underline{\psi}_r^{(2)}}{dt} = \left(j\omega^{est} - \frac{1}{T_{rn}} \right) \underline{\psi}_r^{(2)} + \frac{L_{mn}}{T_{rn}} \underline{i}_s \tag{2}$$

$$\varepsilon = \psi_{\alpha r}^{(2)} \psi_{\beta r}^{(1)} - \psi_{\beta r}^{(2)} \psi_{\alpha r}^{(1)} \tag{3}$$

Equation (1) is the reference model, while equation (2) is the adaptive model. All the machine parameters in (1)-(2) and in the controller of Fig. 1 are constant and correspond to the rated operating conditions. The major problem experienced in application of this speed estimator is the pure integration that is involved in (1). As a consequence, the speed estimator is not operational at zero speed and at low frequencies. Operating region of the estimator can be improved by appropriately modifying the estimator equations, so that pure integration is eliminated. For example, low pass filters can be added either at inputs or at outputs of the reference and the adjustable models, (1) and (2) (Schauder, 1992). The problem of pure integration is however beyond the scope of this paper.

3. INDUCTION MACHINE MODELLING FOR SIMULATION PURPOSES

Induction machine is modelled on the basis of the general dynamic space vector equivalent circuit (space vectors are underlined), that is shown in Fig. 3 for a reference frame rotating at arbitrary angular speed ω_a. Notation used further on is defined in Fig. 3. Circuit of Fig. 3 accounts for both iron loss and main flux saturation. Machine equations in space vector form can be written from Fig. 3 as

$$\underline{v}_s = R_s \underline{i}_s + L_{\sigma s} \frac{d\underline{i}_s}{dt} + \frac{d\underline{\psi}_m}{dt} + j\omega_a \left(L_{\sigma s} \underline{i}_s + \underline{\psi}_m \right)$$

$$0 = R_r \underline{i}_r + L_{\sigma r} \frac{d\underline{i}_r}{dt} + \frac{d\underline{\psi}_m}{dt} + j(\omega_a - \omega)\left(L_{\sigma r} \underline{i}_r + \underline{\psi}_m \right)$$

$$R_{Fe} \underline{i}_{Fe} = j\omega_a \underline{\psi}_m + \frac{d\underline{\psi}_m}{dt} \qquad (4)$$

$$\underline{i}_{Fe} + \underline{i}_m = \underline{i}_s + \underline{i}_r$$

$$R_{Fe} = f(\omega_e) \qquad L_m = f(i_m)$$

A convenient selection of the state-space variables is the set comprising $\underline{i}_s, \underline{i}_r, \underline{\psi}_m$ (Sokola, 1998). As ideal current feeding is assumed, stator voltage equation can be omitted from (4). The machine can then be represented with the following system of equations in the stationary α,β reference frame ($\omega_a = 0$):

$$\frac{di_{\alpha r}}{dt} = -\frac{1}{T_{\sigma r}} i_{\alpha r} - \frac{1}{T_{\sigma Fe}} \left(i_{\alpha s}^* + i_{\alpha r} - \frac{\psi_{\alpha m}}{L_m} \right) - \omega i_{\beta r} - \omega \frac{\psi_{\beta m}}{L_{\sigma r}}$$

$$\frac{di_{\beta r}}{dt} = -\frac{1}{T_{\sigma r}} i_{\beta r} - \frac{1}{T_{\sigma Fe}} \left(i_{\beta s}^* + i_{\beta r} - \frac{\psi_{\beta m}}{L_m} \right) + \omega i_{\alpha r} + \omega \frac{\psi_{\alpha m}}{L_{\sigma r}}$$

$$\frac{d\psi_{\alpha m}}{dt} = R_{Fe} \left(i_{\alpha s}^* + i_{\alpha r} - \frac{\psi_{\alpha m}}{L_m} \right) \qquad \frac{d\psi_{\beta m}}{dt} = R_{Fe} \left(i_{\beta s}^* + i_{\beta r} - \frac{\psi_{\beta m}}{L_m} \right) \qquad (5)$$

$$T_e = (3/2) P \left(i_{\alpha r} \psi_{\beta m} - i_{\beta r} \psi_{\alpha m} \right)$$

$$L_m = f(\psi_m) = f\left(\sqrt{\psi_{\alpha m}^2 + \psi_{\beta m}^2} \right) \qquad R_{Fe} = f(\omega_e) = f(\omega_e^*) = f(\omega_{sl}^* + \omega^{est})$$

Asterisk in (5) denotes reference values of the stator current components and the angular slip frequency. The two time constants in (5) are $T_{\sigma r} = L_{\sigma r} / R_r$ and $T_{\sigma Fe} = L_{\sigma r} / R_{Fe}$. The model given with (5) accounts fully for both the iron loss and the main flux saturation. It is therefore used to represent the induction machine in the case when both phenomena are simultaneously considered. The same model is used to represent the induction machine when only iron loss is considered, while main flux saturation is neglected (magnetising inductance is equated to the constant rated value). For studies concerned with main flux saturation only (iron loss neglected), induction machine is represented with the current state-space saturated machine model in stationary reference frame (Levi and Vuckovic, 1989). Equivalent iron loss resistance approximation is given in Appendix, together with the induction machine data. Approximations used to represent magnetising curve and inverse magnetising curve (needed later) are included as well.

4. COMPENSATION OF MAIN FLUX SATURATION

4.1 Modified Indirect Vector Controller

In order to extend the operating region of the system of Fig. 1 above base speed, it is necessary to modify the indirect vector controller by accounting for main flux saturation.

The simplest solution (Levi et al., 1990) is used here and is illustrated in Fig. 4. Rate of change of the rotor flux reference is neglected. Ratio of magnetising to rotor inductance is assumed to remain constant and equal to the one under rated rotor flux conditions, so that $SG = R_m(L_{mn}/L_m)$ and $K = (3/2)P\,L_{mn}/L_m$. Impact of cross-saturation is not compensated either. Control system of Fig. 4 however provides full compensation of saturation in steady-state in the field-weakening region in a drive with speed (position) sensor (Levi et al., 1990). As in a sensorless drive speed sensor does not exist, situation is quite different here. If control system of Fig. 4 is applied in conjunction with constant parameter speed estimator of Fig. 2, operation of the drive will be characterised with large speed estimation errors, as shown in section on simulation results. It is therefore necessary to compensate the main flux saturation in the speed estimator of Fig. 2 as well.

4.2 Compensation of Main Flux Saturation in the Speed Estimator

In order to compensate for the main flux saturation in the speed estimator, both the reference and the adaptive part of the estimator, (1)-(2), have to be modified. Estimation of rotor flux in the reference model (1) is based on stator voltage and current measurements, which contain sufficient information to yield, apart from estimates of rotor flux components, the estimate of the magnetising inductance as well (Levi and Vuckovic, 1993). Instead of (1), the following equations are used (Levi and Vuckovic, 1993):

$$
\begin{aligned}
\psi_{\alpha s} &= \int\left(v_{\alpha s} - R_{sn} i_{\alpha s}\right)dt & \psi_{\beta s} &= \int\left(v_{\beta s} - R_{sn} i_{\beta s}\right)dt \\
\psi_{\alpha m} &= \psi_{\alpha s} - L_{\sigma sn} i_{\alpha s} & \psi_{\beta m} &= \psi_{\beta s} - L_{\sigma sn} i_{\beta s} \\
\psi_m &= \sqrt{\psi_{\alpha m}^2 + \psi_{\beta m}^2} & i_m &= f\left(\psi_m\right) \\
i_{\alpha m} &= \left(\psi_{\alpha m}/\psi_m\right) i_m & i_{\beta m} &= \left(\psi_{\beta m}/\psi_m\right) i_m \\
\psi_{\alpha r}^{(1)} &= \psi_{\alpha m} + L_{\sigma rn}\left(i_{\alpha m} - i_{\alpha s}\right) & \psi_{\beta r}^{(1)} &= \psi_{\beta m} + L_{\sigma rn}\left(i_{\beta m} - i_{\beta s}\right) \\
L_m^{est} &= \psi_m / i_m
\end{aligned}
\qquad (6)
$$

Reference model, described with (6), is illustrated in Fig. 5. Not only that main flux saturation is fully accounted for in the calculation of the rotor flux components, but the estimate of the magnetising inductance is provided as well. Estimate of the magnetising inductance, obtained from the reference model, will be used in the adaptive model, as explained next. It should be noted that the complexity of the scheme given in Fig. 5 can be reduced for real time applications by suitably re-arranging equations (6). Means for accounting for main flux saturation in the adaptive model (2) are elaborated in detail in Levi and Sokola (1997). Main flux saturation is fully accounted for provided that the appropriate value of the saturated steady-state magnetising inductance is used instead of the constant one. Structure of (2) needs not be changed at all, as dynamic inductance terms do not appear in this equation when stator current and rotor flux components are selected as state space variables. An appropriate value of the saturated steady-state magnetising inductance is yielded by the reference model (6) and the adaptive model is

$$
\frac{d\underline{\psi}_r^{(2)}}{dt} = \left(j\omega^{est} - \frac{R_m}{L_{\sigma rn} + L_m^{est}}\right)\underline{\psi}_r^{(2)} + \frac{L_m^{est}}{L_{\sigma rn} + L_m^{est}} R_m \underline{i}_s \qquad (7)
$$

Resultant structure of the modified speed estimator is shown in Fig. 6. The estimator provides full compensation of main flux saturation in transient and steady-state operation.

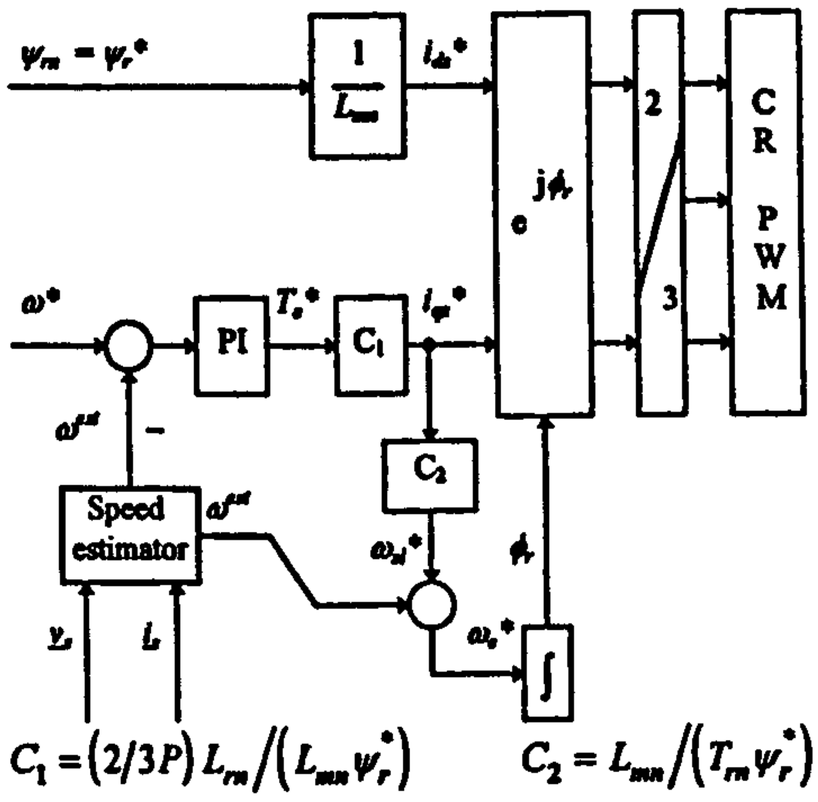

FIGURE 1. Speed sensorless indirect rotor flux oriented induction machine for operation in the base speed region.

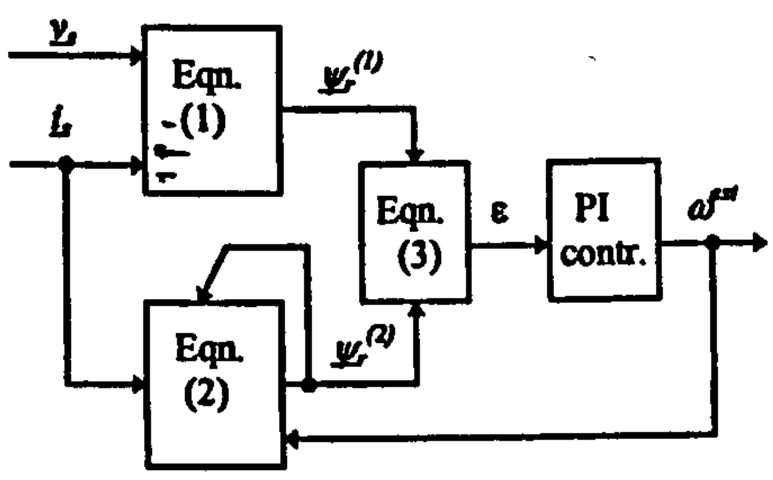

FIGURE 2. Rotor flux based, constant parameter rotor speed estimator.

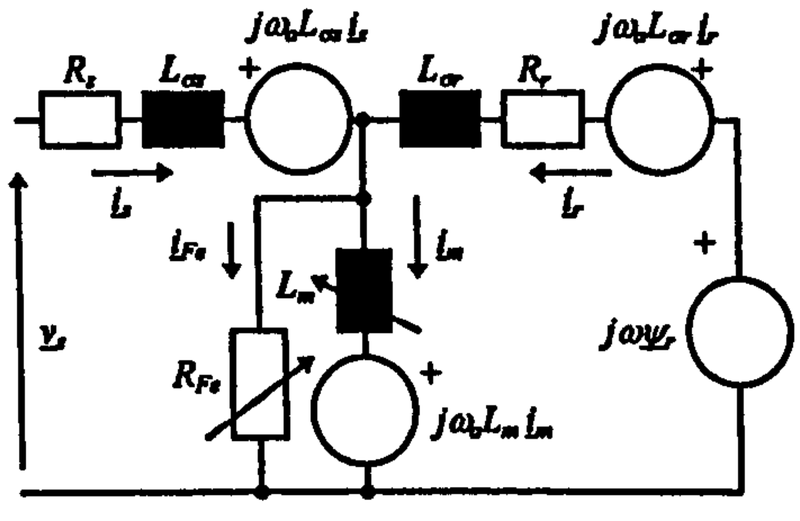

FIGURE 3. Space vector dynamic equivalent circuit of an induction machine in an arbitrary reference frame.

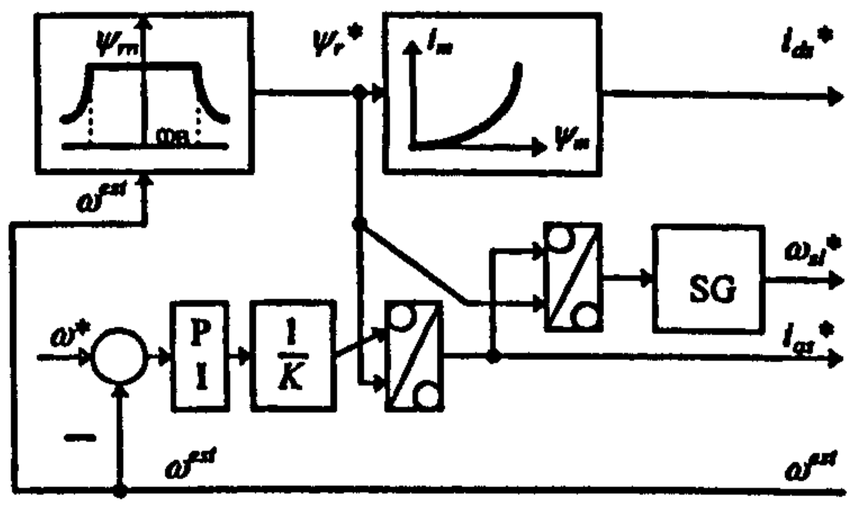

FIGURE 4. Indirect rotor flux oriented controller with compensation of main flux saturation.

5. COMPENSATION OF IRON LOSS

5.1 Modified Indirect Vector Controller

A modified indirect vector controller, that enables full compensation of iron loss in a drive with speed sensor was proposed by Levi (1995). It requires knowledge of the dependence of the equivalent iron loss resistance on the frequency, which can be determined on the basis of the experiments (Levi et al., 1996). The indirect feed-forward rotor flux oriented controller with compensated iron loss is shown in Fig. 7. Time constant T_{Fe} in Fig. 7 is ratio of magnetising inductance to equivalent iron loss resistance. As saturation is neglected, T_{Fe} is function of operating frequency only, through R_{Fe}. Constants K_1 and K_2 are $K_1 = (2/3P)\, L_{\sigma rn} / (L_{mn} \psi_r^*)$ and $K_2 = L_{mn} / (T_{\sigma r} \psi_r^*)$. Operation in the base speed region, with constant rotor flux reference, is assumed.

5.2 Compensation of Iron Loss in the Speed Estimator

In order to retain the simple structure of the speed estimator of Fig. 2, it is desirable to

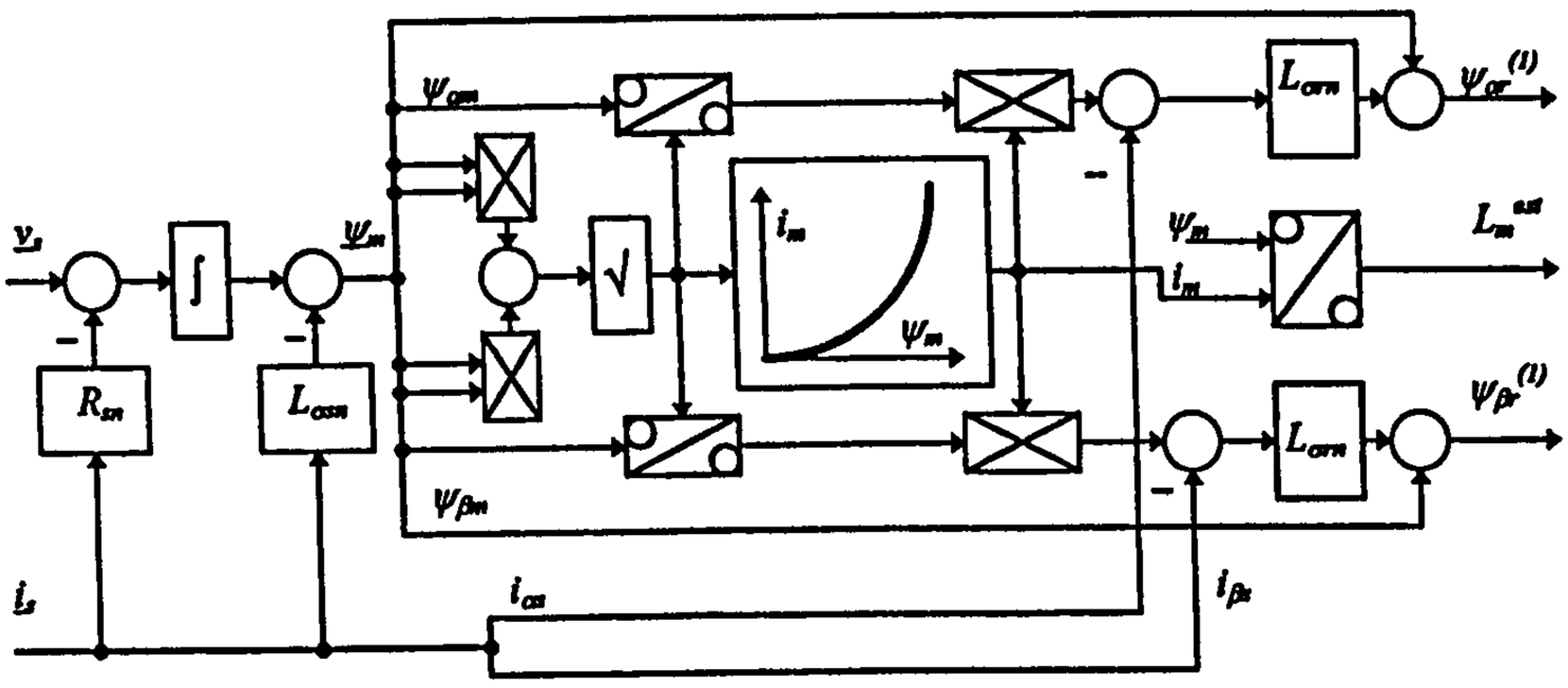

FIGURE 5. Modified reference model with compensation of main flux saturation.

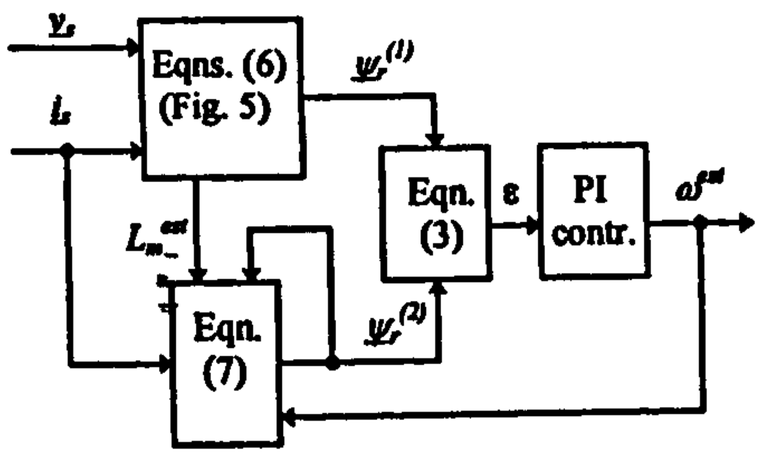

FIGURE 6. Rotor flux based speed estimator with full compensation of main flux saturation.

avoid modification of the estimator structure by means of induction machine's equivalent circuit of Fig. 3. An alternative and indeed very simple way, proposed by Levi et al. (1999), consists of modification of the input into the estimator rather than of change of the structure. Stator current references in Fig. 7 are obtained by adding iron loss compensation currents to the controller outputs. Estimator input is therefore modified in such a way that input currents are obtained by deducting iron

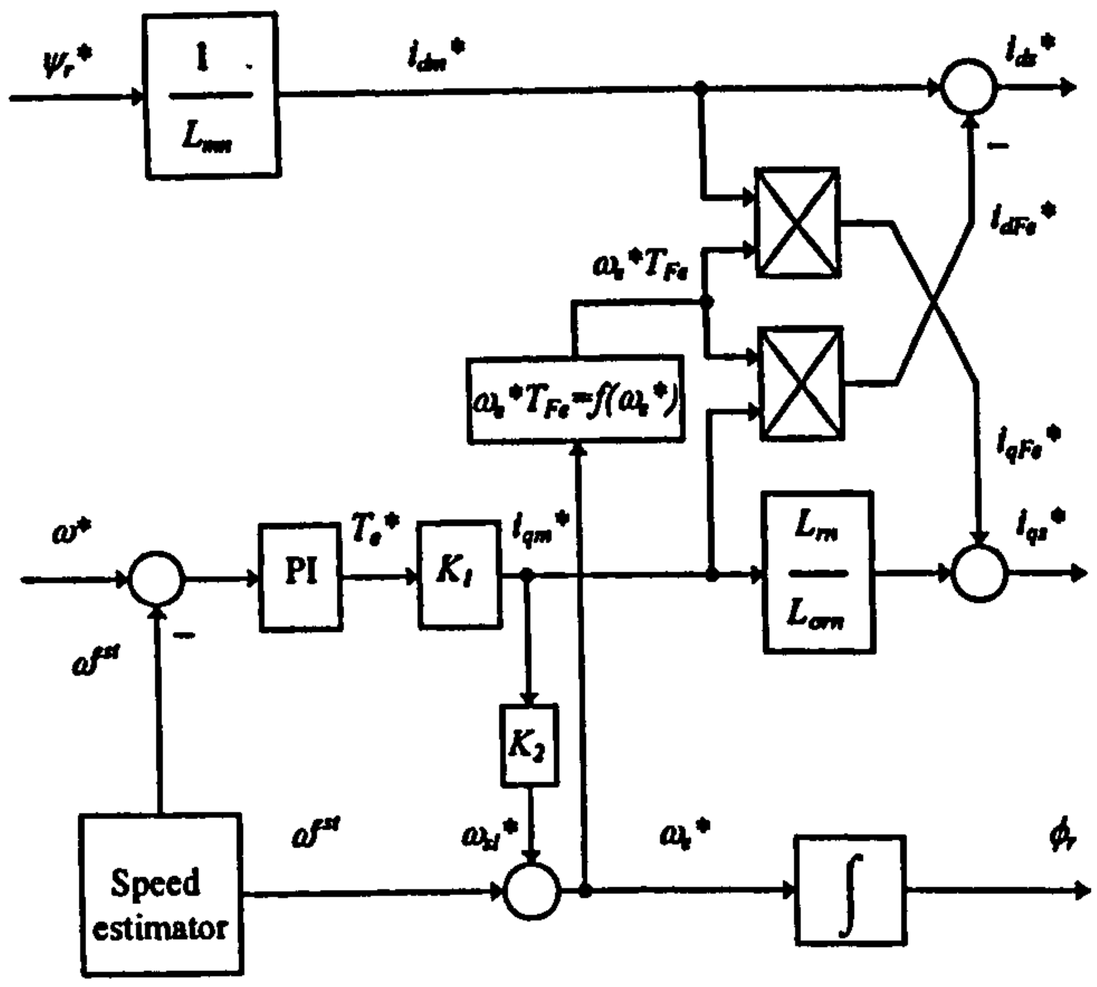

FIGURE 7. Modified indirect vector controller with compensation of iron loss.

loss compensation currents from the measured stator current components. As iron loss compensation currents are available in the rotating reference frame, while speed estimator operates in the stationary reference frame, this method requires co-ordinate transformation of iron loss current components from d-q reference frame to stationary α,β reference frame. Modified speed estimator is illustrated in Fig. 8.

6. COMPENSATION OF IRON LOSS AND MAIN FLUX SATURATION

6.1 Indirect Vector Controller

The structure of an indirect vector controller that will provide compensation of both main flux saturation and iron loss is obtained by combining the two controllers, shown in Figs. 4 and 7. The controller is illustrated in Fig. 9. Constants are defined as $TG = (2/3P)L_{arm}/L_{mn}$, $SG = L_{mn}/T_{ar}$. Note that product of TG and SG in calculation of the reference angular slip frequency cancels dependence on the magnetising inductance, while in the calculation of the reference stator q-axis current this dependence is approximately cancelled by the product of TG and ratio of rotor self-inductance to rotor leakage inductance. Function ω_e^*/R_{Fe} takes into account dependence of iron loss resistance on frequency, while magnetising inductance is calculated from rotor flux reference and output of the inverse magnetising curve.

6.2 Compensation of Main Flux Saturation and Iron Loss in the Speed Estimator

Speed estimator with compensation of the both phenomena is constructed in very much the same way as the indirect controller. The two schemes, proposed for individual compensation of iron loss and main flux saturation, are combined to yield simultaneous compensation of the both effects. The resulting structure of the speed estimator is shown in Fig. 10 and it combines structures depicted in Figs. 6 and 8.

7. SIMULATION RESULTS

7.1 General Considerations

Estimated speed, as obtained from the speed estimator, is used at all times for closed loop speed control and for orientation angle calculation. Actual speed of the machine is used for monitoring purposes only. Induction machine is represented with an appropriate model, as explained in section 3. Simulations are carried out for a number of different combinations of the indirect vector controller and the speed estimator and are classified into three groups.

The first group relates to main flux saturation. Indirect vector controller of Fig. 4 is used. At first, the speed estimator of Fig. 2 is applied, in order to visualise effects of omission of the main flux saturation representation within the speed estimator. Next, the speed estimator proposed in sub-section 4.2 and illustrated in Figs. 5 and 6 is used in order to verify its compensation capability. The second group deals with iron loss only. Main flux saturation is neglected in the control system, speed estimator and the motor. Indirect vector controller of Fig. 1 is used. Rotor flux reference in the field weakening is taken as

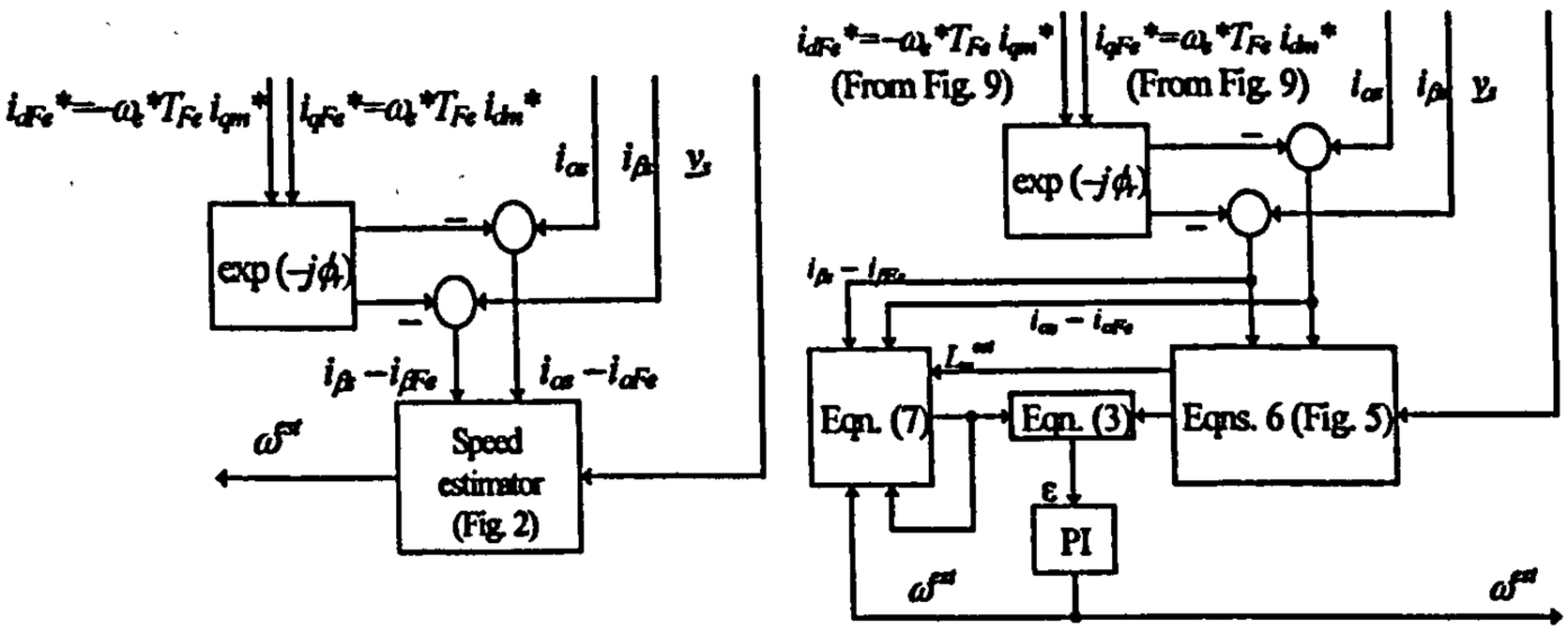

FIGURE 8. Approximate method of iron loss compensation in the speed estimator.

FIGURE 10. Speed estimator with iron loss and main flux saturation compensation.

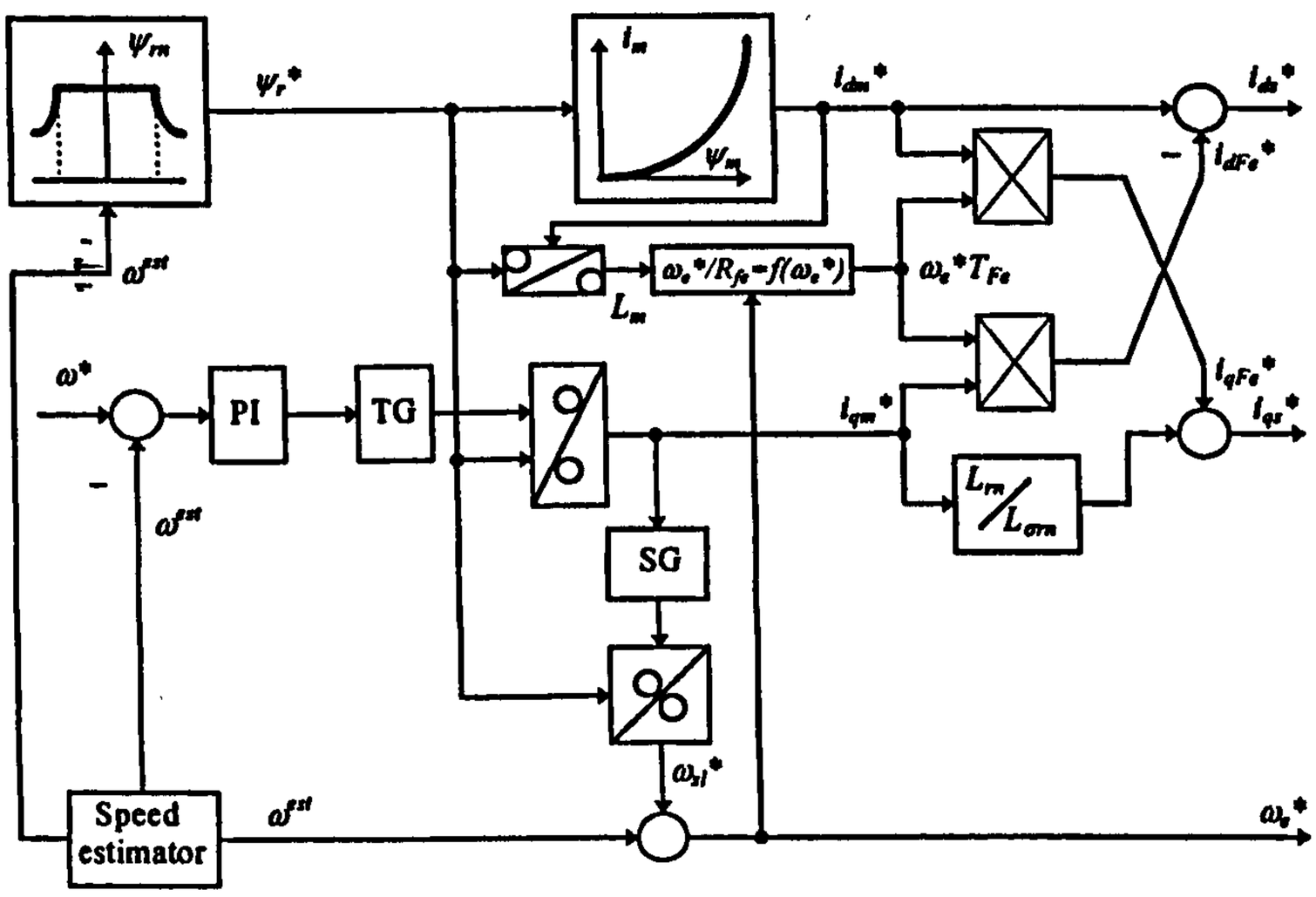

FIGURE 9. Indirect vector controller with compensation of iron loss and saturation.

inversely proportional to the rotor speed and calculation of stator q-axis current reference and angular slip reference involves division with rotor flux reference. Although omission of main flux saturation representation in the field weakening is unrealistic, this approach enables examination of detuning purely due to iron loss. Speed estimator of Fig. 2 is again at first utilised and impact of iron loss on the drive behaviour is examined. Next, simulations are repeated with the indirect vector controller of Fig. 7 (appropriately modified to include operation in the field weakening region) and speed estimator of Fig. 8. The third group of simulations employs indirect vector controller of Fig. 9 and speed estimator of Fig. 10. It verifies that almost complete compensation of both iron loss and main flux saturation is possible by the drive structure proposed in section 6. In all the cases speed response is illustrated in terms of electrical angular speed of rotation, while speed error is the difference between actual and estimated speed in mechanical rpm.

7.2 Main Flux Saturation

The following sequence of transients is simulated. The machine is initially excited at zero speed under no-load conditions (this transient is not shown in graphs). Speed command is then applied, so that rated speed operation (1 p.u.) under no load conditions is achieved. During operation at rated speed a load torque of 1 p.u. is applied in a step-wise manner at $t = 0.5$ s. At $t = 1$ s load torque is stepped down to 0.5 p.u. and this value is not changed any more. Finally, at $t = 1.5$ s speed command is further increased in a ramp-wise manner, so that field-weakening region is entered. Final operating steady-state is therefore with 0.5 p.u. load torque and transients for two different final speeds are shown, namely speed command of 1.5 p.u. and speed command of 2 p.u.. Figures 11 and 12 summarise results obtained with constant parameter speed estimator of Fig. 2. Graphs of actual and commanded speed, speed error, actual and commanded torque, actual and commanded rotor flux, and actual rotor flux q axis component are given, for final speeds of 1.5 p.u. and 2 p.u., respectively.

In the base speed region estimated speed tracks the actual one very well and commanded and actual torque are in good agreement, except during the initial part of the acceleration. Field orientation is initially lost, as witnessed by oscillatory torque behaviour and large value of rotor flux q-axis component. Poor performance of the estimator during the starting transient is the consequence of the high PI speed controller proportional gain. An improvement during initial acceleration is possible if the proportional gain of the speed PI controller is reduced, as shown in results of the sub-section 7.4.

Once when acceleration in the base speed region is completed, the machine operates with correct rotor flux orientation as rotor flux q-axis component is zero and rotor flux equals the reference value. Steady-state speed error equals zero for all the loading conditions in this region. The problems however begin once when the field-weakening operation is initiated at $t = 1.5$ s. Speed estimation error quickly increases and its final values are over 10 rpm and 20 rpm in Figs. 11 and 12, respectively. Difference between actual torque (that equals load torque of 0.5 p.u.) and reference torque appears and is higher at final reference speed of 2 p.u. (Fig. 12) than at final reference speed of 1.5 p.u. (Fig. 11). There is substantial difference between reference rotor flux and actual rotor flux and field oriented control is lost, as final steady-state is characterised with substantial value of rotor flux q-axis component in both cases. Figures 11 and 12 clearly demonstrate the need for incorporation of the main flux saturation in the speed estimator, if satisfactory performance is to be achieved in the filed-weakening region.

The same simulations are repeated once more. This time the proposed speed estimator of Fig. 6 is used instead of the constant parameter one. The same sets of results for the same sequence of transients and the same final operating conditions are given in Figs. 13 and 14. Operation in the base speed region is insignificantly changed with the application of the saturation adaptive speed estimator. Pattern of discrepancy between actual and commanded torque and between actual and commanded rotor flux is during acceleration into field weakening region very similar in Figs. 13 and 14 to those in Figs. 11 and 12, respectively. These differences occur due to the absence of the stator d-axis current command boost during the transient (rate of change of the rotor flux reference is neglected in the design of the controller of Fig. 4) and cannot be compensated by the modified speed estimator. However, speed estimation error during this transient is

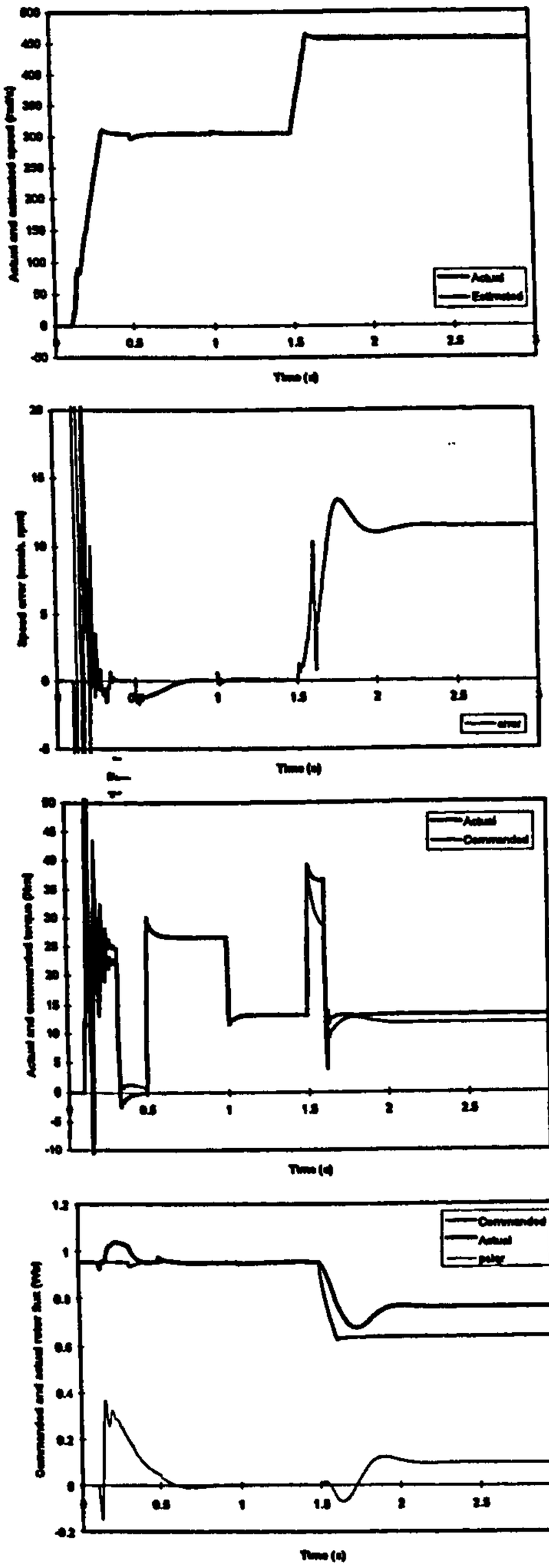

FIGURE 11. Drive operation with constant parameter speed estimator (final speed 1.5 p.u.): estimated and actual speed; speed error; actual and reference torque; actual and reference rotor flux, and rotor flux q-axis component ('psiqr' trace).

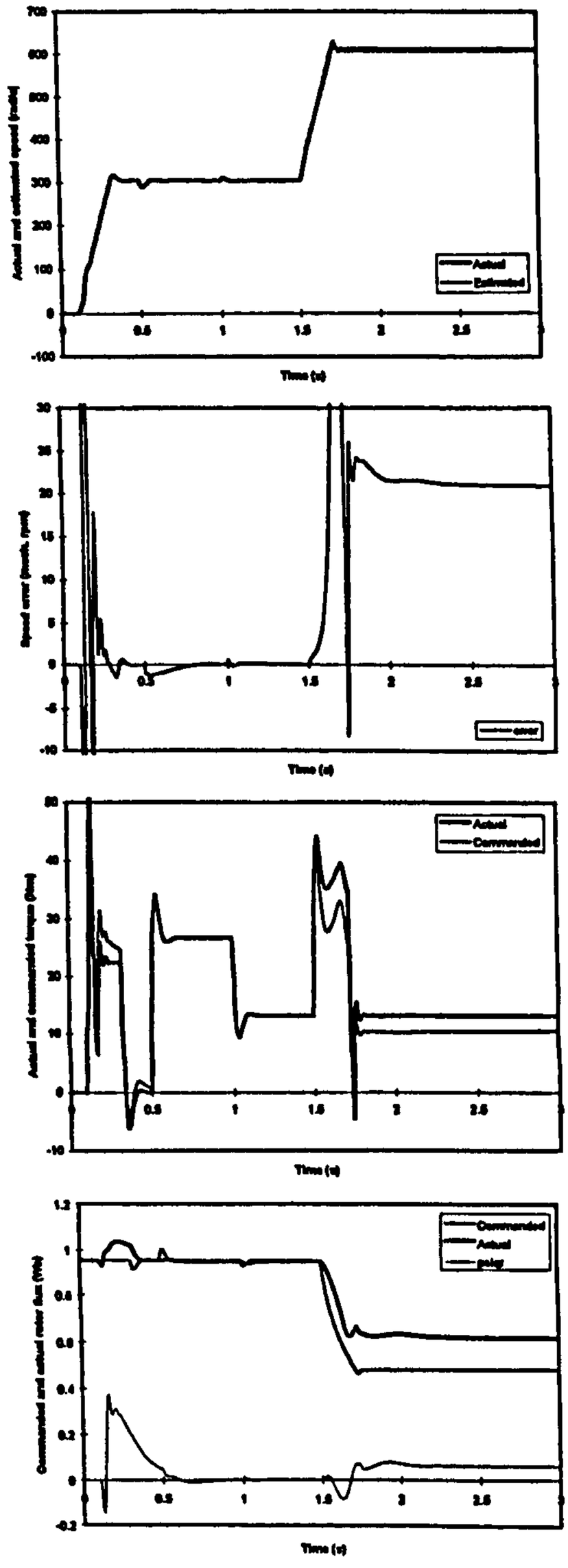

FIGURE 12. Drive operation with constant parameter speed estimator (final speed 2 p.u.): actual and estimated speed; speed error; actual and reference torque; actual and reference rotor flux, and rotor flux q-axis component ('psiqr' trace).

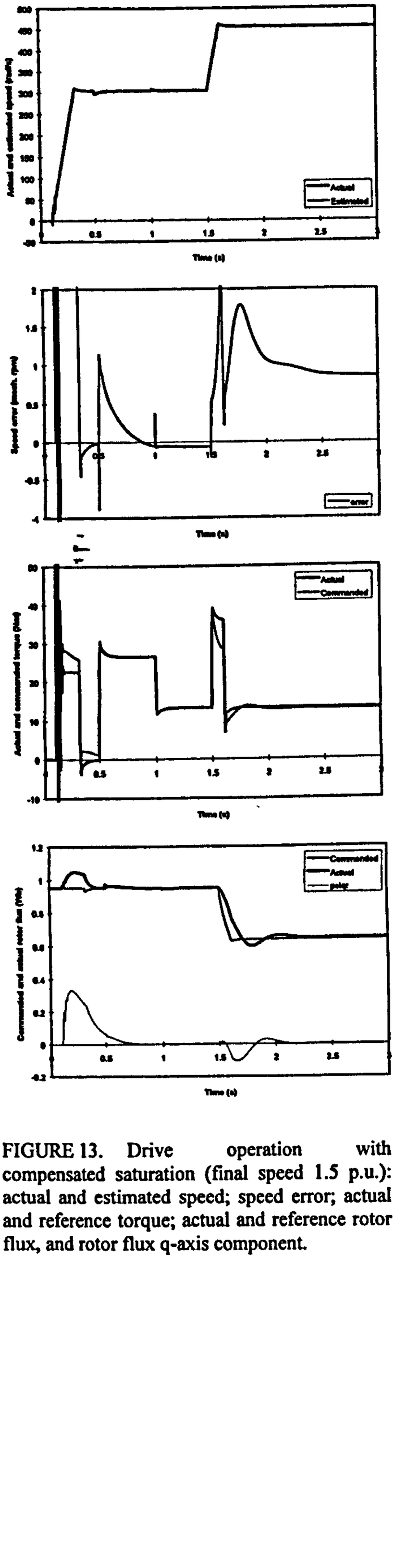

FIGURE 13. Drive operation with compensated saturation (final speed 1.5 p.u.): actual and estimated speed; speed error; actual and reference torque; actual and reference rotor flux, and rotor flux q-axis component.

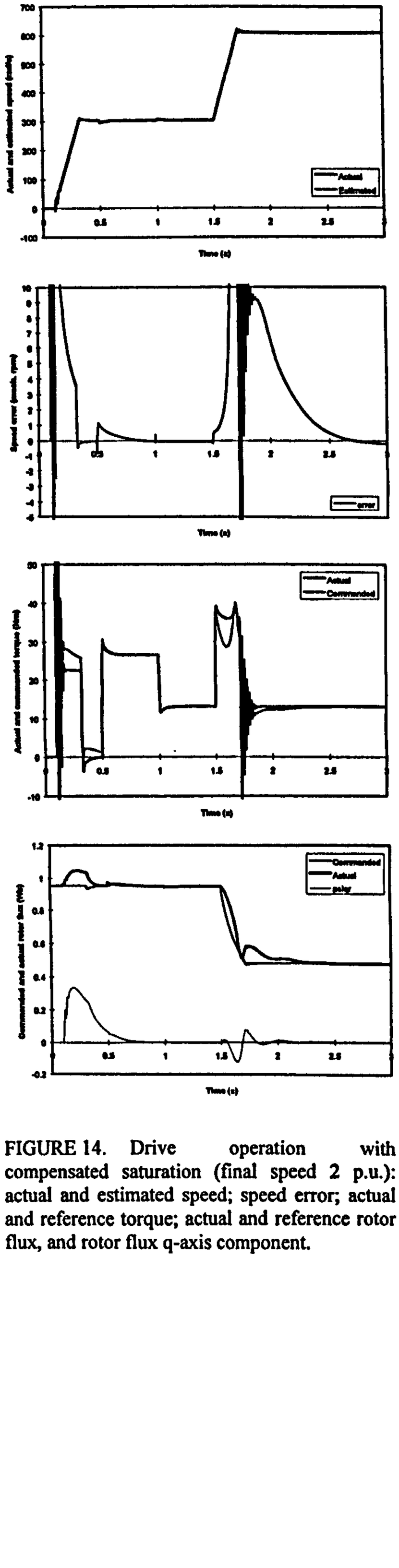

FIGURE 14. Drive operation with compensated saturation (final speed 2 p.u.): actual and estimated speed; speed error; actual and reference torque; actual and reference rotor flux, and rotor flux q-axis component.

reduced significantly (its maximum value does not exceed 3 rpm in Fig. 13 and 40 rpm in Fig. 14, while corresponding values in Figs. 11 and 12 are 13 rpm and 55 rpm). Once when reference speed in the field weakening has become constant, the differences between responses in Figs. 13 and 14 and those of Figs. 11 and 12 become even more remarkable. Final steady-state in Figs. 13 and 14 is characterised with perfect field orientation as q-axis component of the rotor flux equals zero. Actual rotor flux in the machine exactly matches the reference value. Consequently, actual and reference torque are equal as well. Speed estimation error in Fig. 14 is essentially zero, while for operation at 1.5 p.u. speed (Fig. 13) it is less than 1 rpm. The reason for this small residual speed estimation error is explained as follows. Motor model requires use of the magnetising curve approximation, while the controller and estimator ask for approximation of the inverse magnetising curve (Figs. 4 and 5). The two approximations, obtained using curve fitting, are characterised with identical values for rated operating point and for the initial linear portions of the curves, while some minor discrepancies exist in between. Speed estimation error is therefore zero for operation in the base speed region (rated operating point) and for operation at 2 p.u. speed (linear portion of the curve). Operation at 1.5 p.u. speed takes place in between these two areas of the magnetising curve, where matching is not perfect, so that some very small amount of speed estimation error results (speed estimation error at 1.25 p.u. speed is, repeating the same simulation, found to be 0.25 rpm; at 1.75 p.u. speed error is 0.3 rpm). These considerations indicate that accurate knowledge of the magnetising curve is important for successful implementation of the developed speed estimator.

7.3 Iron Loss

Sequence of transients is as follows. Excitation of the machine is initiated at $t = 0$ s at zero speed under no-load conditions. At $t = 0.5$ s speed command equal to rated is applied, under no load conditions. Rated load torque is applied at $t = 1$ s and at $t = 1.5$ s load torque is reduced to one half of the rated. The results are displayed in Fig. 15. The same simulation is repeated once more, with speed command now equal to twice the rated speed. Load torque such that power is rated is now applied at $t = 1.5$ s and at $t = 2.5$ s load torque is reduced to such a value that power is one half of the rated. The results for this case are shown in Fig. 16. Actual and estimated speed, speed error, actual and commanded torque, commanded and actual rotor flux, and rotor flux q axis component are given in both Figs. 15 and 16.

Steady-state analysis (Levi and Wang, 1997; Levi et al. 1999) predicted that orientation angle error and difference between reference and actual rotor flux will be negligible in any steady-state operation. Figs. 15 and 16 fully confirm those results, as q-axis component of the rotor flux is zero and there is not any difference between reference and actual rotor flux in steady-state operation. Discrepancy between commanded and actual torque is noticeable for rated speed operation, while at twice the rated speed it is very small and cannot be observed in Fig. 16. Speed error for rated speed operation is between 2 and 3 rpm depending on the loading, while at twice the rated speed it increases to around 4.5 rpm for rated power operation. These values exactly correspond to the results of steady-state analysis (Levi and Wang, 1997; Levi et al. 1999).

As shown next, satisfactory compensation of iron loss can be achieved by means of the modified indirect vector controller of Fig. 7 (with appropriate modifications for operation

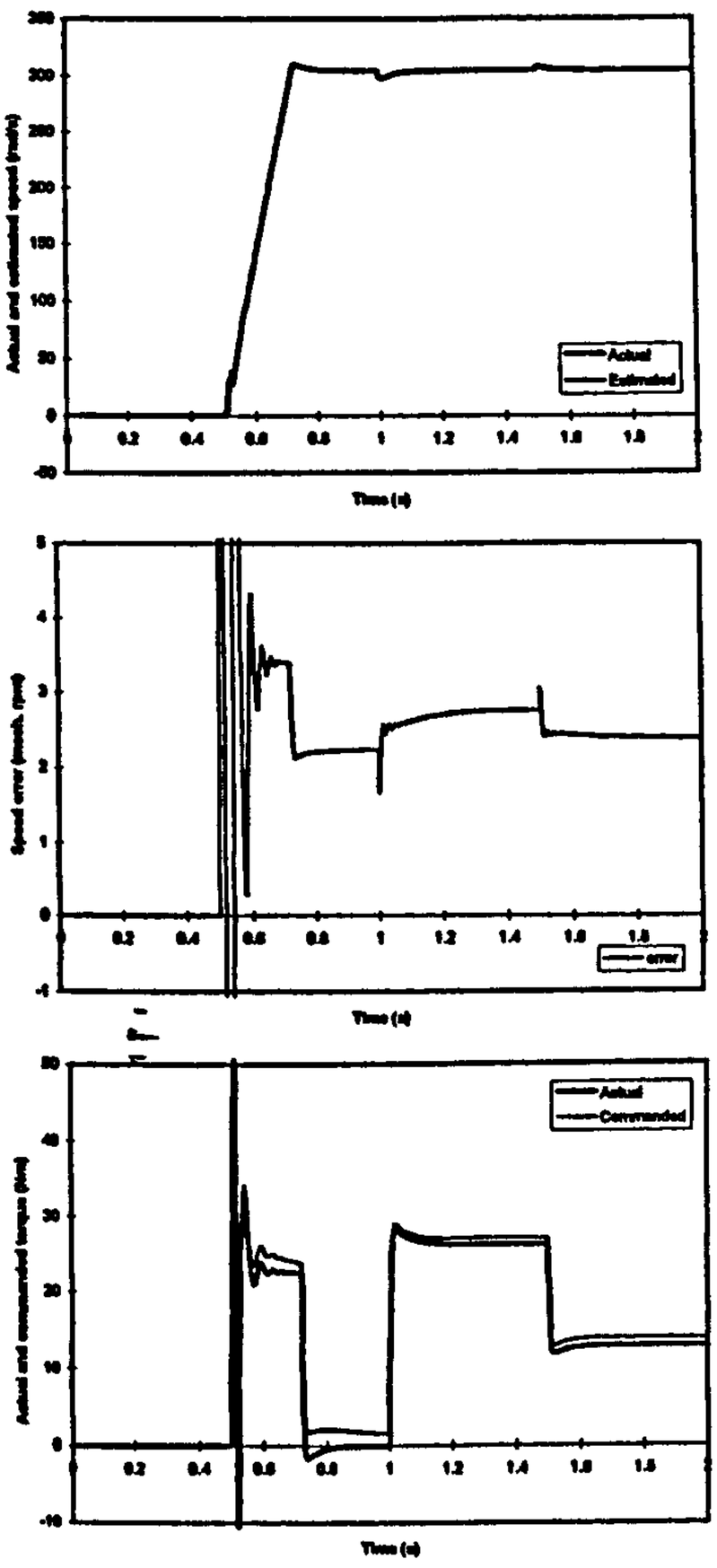

FIGURE 15. Transient detuning due to iron loss (speed command of 1 p.u.): estimated and actual speed; speed error; actual and reference torque; actual and reference rotor flux, and actual rotor flux q-axis component.

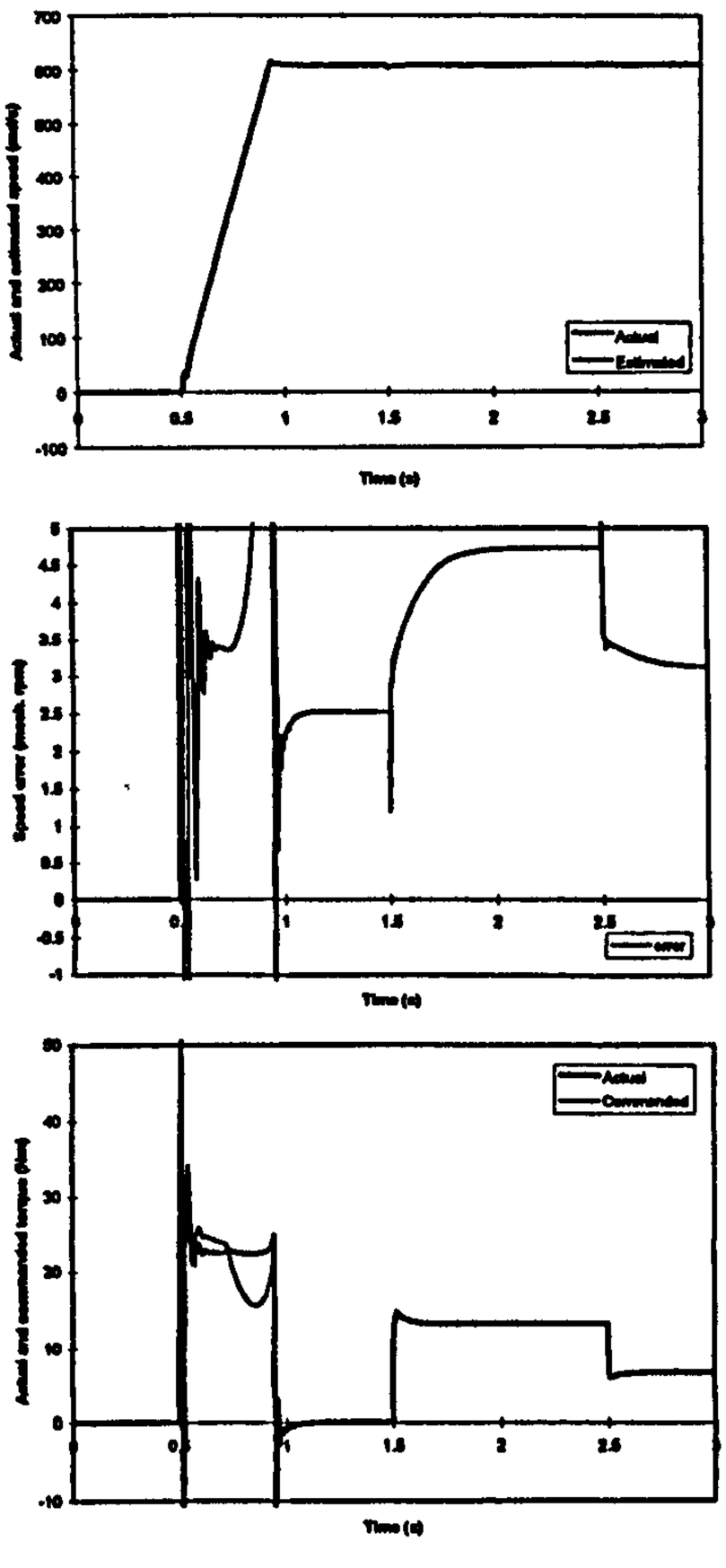

FIGURE 16. Transient detuning due to iron loss (speed command of 2 p.u.): estimated and actual speed; speed error; actual and reference torque; actual and reference rotor flux, and actual rotor flux q-axis component.

in the field weakening region) and the proposed speed estimator of Fig. 8. Identical simulations to those illustrated in Figs. 15 and 16 are now done using the drive model with controller and speed estimator of Figs. 7 and 8 and the results are summarised in Figs. 17 and 18. Only speed error and torque graphs are given, as there is not any observable difference in the remaining traces. Actual and commanded torque now essentially coincide for both rated speed and twice the rated speed operation (steady-state analysis reported by Levi et al. (1999) predicted torque error of approximately 1%). Speed estimation error is significantly reduced and is below 0.4 rpm for rated speed operation (the worst case in the base speed region). In the field weakening region, at twice the rated speed, speed estimation error is up to 1 rpm for rated power operation. For load torque such that power is one half of the rated speed estimation error is below 0.5 rpm. Once more, these values fully correspond to those predicted by steady-state analysis.

Figures 17 and 18 confirm that the approximate method of compensation of iron loss, used in the design of the speed estimator of Fig. 8, significantly reduces the speed estimation error and confines it to the negligibly small values of up to 0.4 rpm in the base speed region and up to 1 rpm in the field weakening region.

7.4 Main Flux Saturation and Iron Loss

No attempt was made in this case to study detuned operation. Obviously, detuning effects visualised in sub-sections 7.2 and 7.3 would now combine to yield resulting detuning.

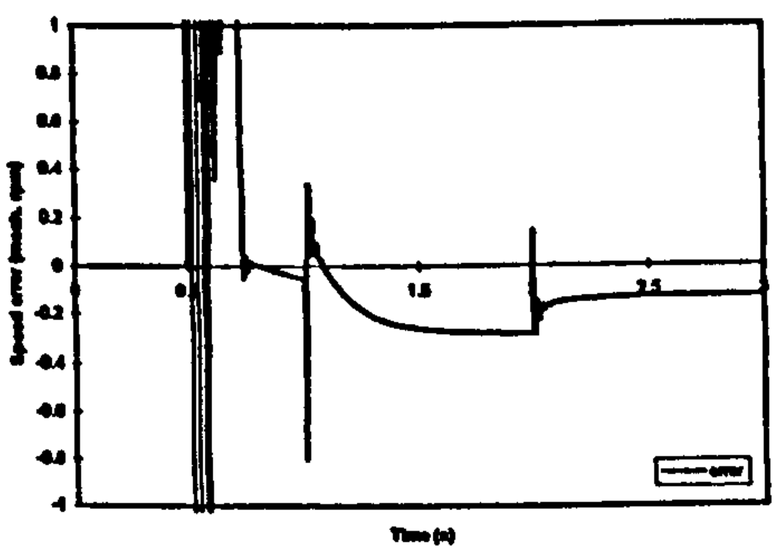

FIGURE 17. Drive operation with compensated iron loss (speed command of 1 p.u.): speed error and actual and reference torque.

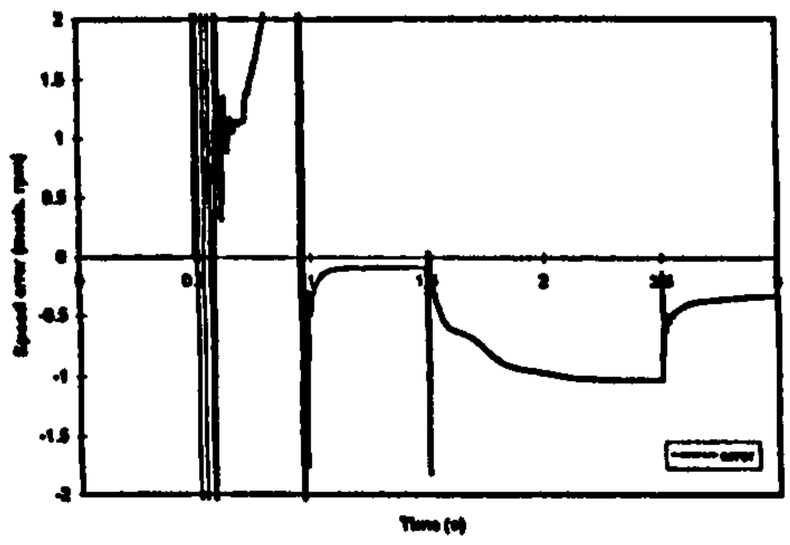

FIGURE 18. Drive operation with compensated iron loss (speed command of 2 p.u.): speed error and actual and reference torque.

Simulations regarding simultaneous compensation of both the main flux saturation and the iron loss are conducted using the proposed indirect vector controller of Fig. 9 and the novel speed estimator of Fig. 10. Sequence of transients and final operating states are the same as when only main flux saturation was considered, sub-section 7.2 (Figs. 13 and 14). The only differences are that the excitation transient, starting at zero time instant, is included, and that instants of speed command changes and load torque application are shifted in time. Additionally, proportional gain of the speed PI controller is reduced, resulting in better quality of response during acceleration. Figures 19 and 20 summarise the results for final operating speeds of 1.5 p.u. and 2 p.u., respectively, and include the same traces as Figs. 13 and 14. Speed estimation error is now confined to values less than 1 rpm and perfect field orientation is achieved in all the steady-state operating regimes (rotor flux q-component equals zero). Complete annulment of speed estimation error is not achieved due to approximate nature of the iron loss compensation and due to non-ideal mapping of the magnetising curve and the inverse magnetising curve, as explained in sub- sections 7.3 and 7.2. Actual and reference rotor flux coincide in all the steady-states as well. The same holds true for commanded and actual torque. Figures 19 and 20 clearly demonstrate that the model based approach adopted in the paper is capable of providing almost complete compensation of both main flux saturation and the iron loss in a sensorless indirect rotor flux oriented induction machine.

8. CONCLUSION

Some of the phenomena responsible for detuning in vector controlled induction machines can be compensated in a relatively simple manner using model-based approach. These include main flux saturation and iron loss. The idea behind this method is to use a modified induction machine model for development of the control system, that accounts for the phenomenon under consideration. The paper applies this approach to an indirect feed-forward rotor flux oriented induction machine operated as a sensorless drive, with speed estimator of MRAC type. It is shown that successful compensation of main flux saturation, iron loss, and both iron loss and main flux saturation, asks for modification of both the indirect vector controller and the speed estimator. Appropriate structures of the controller and the speed estimator are proposed, that are capable of compensation of main flux saturation only, iron loss only, and both the main flux saturation and the iron loss.

Simulation is used to at first visualise the impact of main flux saturation and iron loss on operation of the drive, when standard constant parameter speed estimator is employed. It is shown that performance deteriorates in the field weakening region due to saturation, while impact of iron loss is less serious but far from negligible. Proposed modified speed estimators are verified next. Speed estimation error is in all the cases reduced to below one rpm and correct field orientation is achieved in any steady-state operating point.

Implementation of the scheme with compensation of both the iron loss and main flux saturation asks for knowledge of the two non-linear functions (inverse magnetising curve and frequency dependence of the equivalent iron resistance). The complexity added to the indirect vector controller and the speed estimator by the compensation is considered to be moderate. One additional co-ordinate transformation is required, three look-up tables are needed and there is a certain number of additional algebraic operations. This is believed to be acceptable when compared to on-line identification requirements.

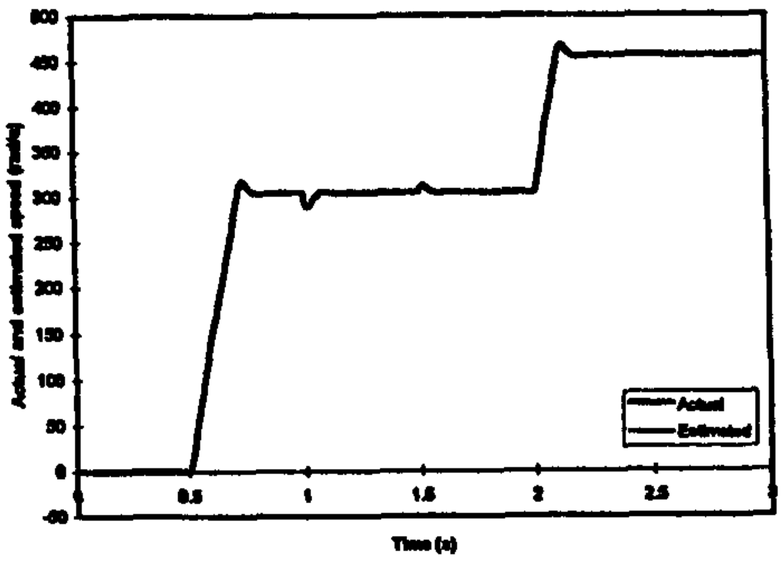

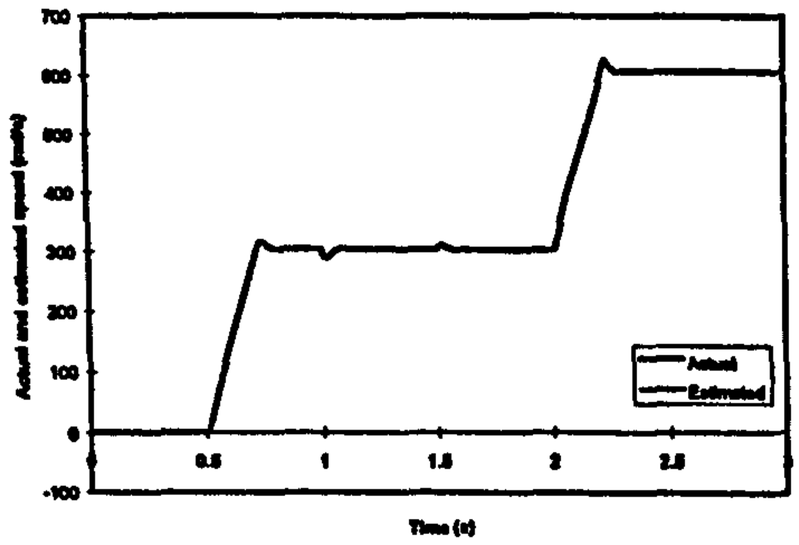

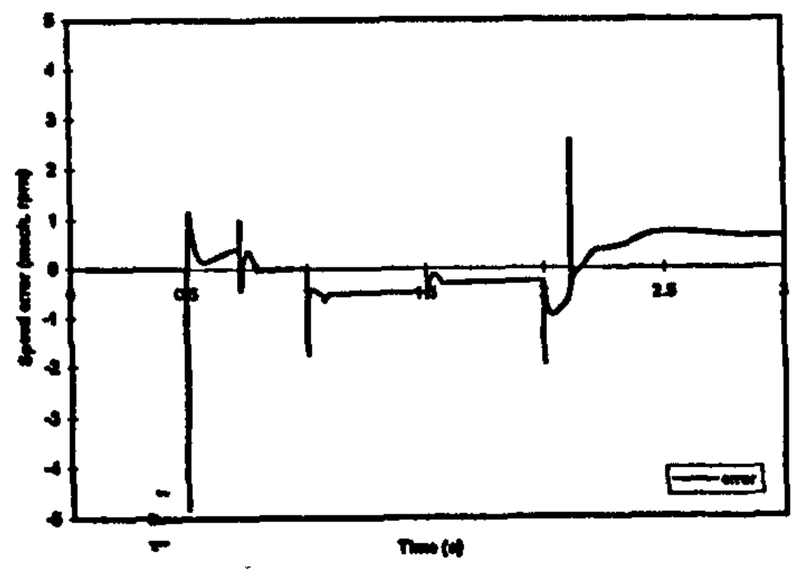

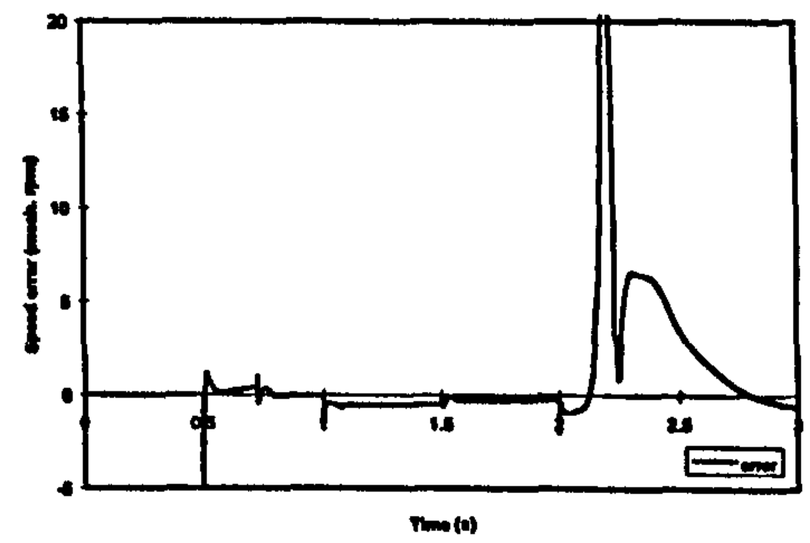

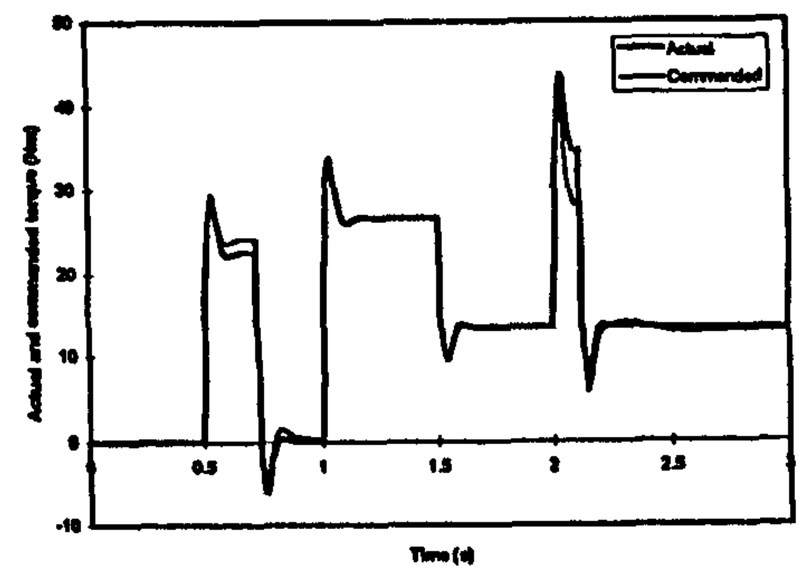

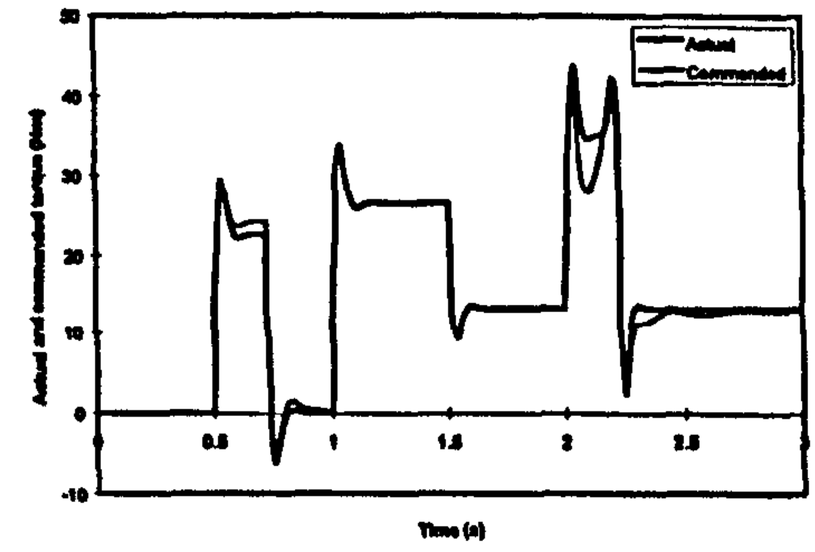

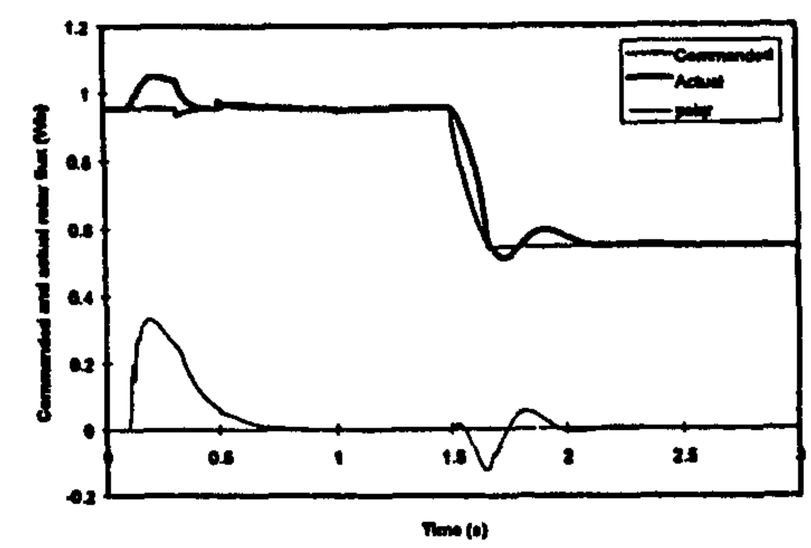

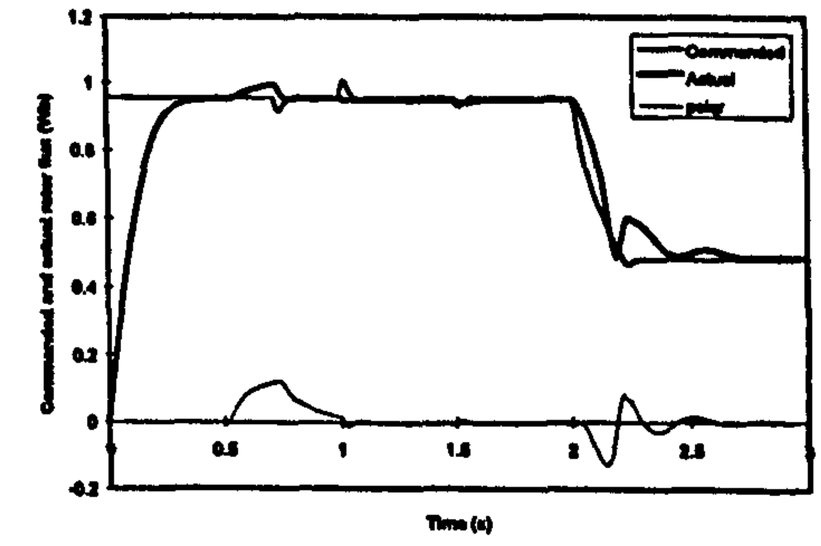

FIGURE 19. Operation with controller of Fig. 9 and estimator of Fig. 10 (final speed 1.5 p.u.): actual and estimated speed; speed error; actual and reference torque; actual and reference rotor flux, and rotor flux q-axis component.

FIGURE 20. Operation with controller of Fig. 9 and estimator of Fig. 10 (final speed 2 p.u.): actual and estimated speed; speed error; actual and reference torque; actual and reference rotor flux, and rotor flux q-axis component.

9. APPENDIX: Induction Motor Data

4 kW 380 V 50 Hz 8.7 A Y 2P = 4 $T_{en} = 26.5\ Nm$

$R_{sn} = 1.37\ \Omega$ $R_{rn} = 1.1\ \Omega$ $L_{\sigma sn} = 4.87$ mH $L_{\sigma rn} = 7.96$ mH $L_{mn} = 0.143$ H

Magnetising curve approximation (motor model; rms values):

$$\Psi_m = \begin{cases} 0.1964285 I_m & I_m < 2.2 \text{ A} \\ 0.8374 + 0.0067 I_m - 0.924/I_m & I_m > 2.2 \text{ A} \end{cases}$$

$$L = d\Psi_m / dI_m = \begin{cases} 0.1964285 & I_m < 2.2 \text{ A} \\ 0.0067 + 0.924/I_m^2 & I_m > 2.2 \text{ A} \end{cases}$$

$$L_m = \Psi_m / I_m$$

Inverse magnetising curve approximation (controller and speed estimator):

$$I_m = -0.04 + 7.19\Psi_m - 23.88\Psi_m^2 + 104.43\Psi_m^3 - 200.62\Psi_m^4 + 145.08\Psi_m^5$$

Iron loss resistance approximation:

$$R_{Fe} = \begin{cases} 128.92 + 8.242 f + 0.7788 f^2 \ (\Omega) & f \le 50 \text{ Hz} \\ 1841 - 55272/f \ (\Omega) & f > 50 \text{ Hz} \end{cases}$$

REFERENCES

Armstrong, G.J. and Atkinson, D.J., 1997,A comparison of model reference adaptive system and extended Kalman filter estimators for sensorless vector drives, *Proc. Eur. Conf. on Power Elec. and Appl. EPE*, Trondheim, Norway, pp. 1.424-1.429.

Blasco-Gimenez, R., Asher, G.M. and Sumner, M., 1995, A new method of stator resistance estimation for enhanced dynamic performance of sensorless vector control drives, *Proc. 6th Eur. Conf. on Power Elec. and Appl. EPE*, Sevilla, Spain, pp. 1.689-1.694.

Blasco-Gimenez, R., Asher, G.M., Sumner, M. and Bradley, K.J., 1996a, Dynamic performance limitation for MRAS based sensorless induction motor drives. Part 1: Stability analysis for the closed loop drive, *IEE Proc. - Electr. Power Appl.*, vol. 143, pp. 113-122.

Blasco-Gimenez, R., Asher, G.M., Sumner, M. and Bradley, K.J., 1996b, Dynamic performance limitations for MRAS based sensorless induction motor drives. Part 2: Online parameter tuning and dynamic performance studies, *IEE Proc. - Electr. Power Appl.*, vol. 143, pp. 123-134.

Blasco-Gimenez, R., Asher, G.M., Cilia, J. and Bradley, K.J., 1996c, Field weakening at high and low speed for sensorless vector controlled induction motor drives, *Proc. IEE Int. Conf. Power Elec. and Var. Speed Drives PEVD*, IEE Conf. Pub. No. 429, Nottingham, UK, pp. 258-261.

El-Kholy, E.E., Abdel-Karim, M., Mahmoud, S.A. and Iung, C., 1994, Effects of main flux saturation on behaviour of indirect field oriented induction motor drives without speed sensor, *Proc. EPE Chapter Symp. 'Elec. drive design and appl.'*, Lausanne, Switzerland, pp. 203-208.

Griva, G., Profumo, F., Ilas, C., Magureanu, R. and Vranka, P., 1996, A unitary approach to speed sensorless induction motor field oriented drives based on various model reference schemes, *Proc. IEEE Ind. Appl. Soc. Annu. Meet. IAS*, San Diego, CA, pp. 1594-1599.

Ilas, C., Bettini, A., Griva, G. and Profumo, F., 1994, Comparison of different schemes without shaft sensors for field oriented control drives", *Proc. IEEE Ind. Elec. Soc. Annu. Meet. IECON*, Bologna, Italy, pp. 1579-1588.

Jansen, P.L. and Lorenz, R.D., 1993, Accuracy limitations on velocity and flux estimation in direct field oriented induction machines, *Proc. Eur. Conf. on Power Elec. and Appl. EPE*, Brighton, UK, pp. 312-318.

ELECTRIC
MACHINES and
POWER SYSTEMS

EDITOR
S. A. NASAR
Department of Electrical Engineering
University of Kentucky
Lexington, Kentucky 40506

January 25, 1999

Dr. Emil Levi
Liverpool John Moores Univeristy
School of Engineeirng
Byrom St.
Liverpool L3 3AF, England UK

Paper No: 5719

Dear Dr. Levi:

I am pleased to write that your paper "Evaluation of Steady-state and Transient...." has been accepted for publication in our journal subject to the revision suggested by the reviewers. Please prepare the manuscript according to the enclosed instructions, and incorporating the changes suggested by the reviewers. Copies of the reviewer's comments are also enclosed.

Please return the final manuscript and the copyright release form to me.

Sincerely,

S. A. Nasar

S.A. Nasar
Editor

DATE: Mar 3, 1999
AUTHOR(S): Levi
MS. #: 5719
TITLE: Evaluation of —

Dear Author:

A final copy of the above mentioned manuscript has been received in our office. It will be published in Volume 27 (19
Number 11. Thank you for your contribution.

S. A. Nasar
Editor

Taylor&Francis
Publishers since 1798

EVALUATION OF STEADY-STATE AND TRANSIENT BEHAVIOUR OF A MRAS BASED SENSORLESS ROTOR FLUX ORIENTED INDUCTION MACHINE IN THE PRESENCE OF PARAMETER DETUNING

M.Wang, E.Levi

Liverpool John Moores University
School of Engineering
Liverpool L3 3AF, UK

ABSTRACT

One of the most frequently applied methods of speed-sensorless rotor flux oriented control of induction machines relies on utilisation of model reference adaptive system (MRAS) based speed estimation. Accuracy of this method heavily depends on correct setting of the machine parameters within the estimator and the controller. The paper discusses sensorless indirect feed-forward current-fed rotor flux oriented induction motor drive in which speed estimation is performed utilising rotor flux based MRAS scheme. A study is conducted in order to evaluate speed estimation error and other detuning effects in both steady-state and transient operation of the drive, caused by incorrect setting and/or variation of parameters. Theoretical principles behind the steady-state analysis are at first developed and steady-state detuning effects are then evaluated. Incorrect setting of magnetising inductance, stator resistance variation, rotor resistance variation and leakage inductance variation are encompassed by steady-state analysis. Next, simulation of the complete drive is performed in order to examine impact of parameter detuning on transient behaviour of the drive. Results obtained by simulation, using dynamic model, for any steady-state operating point are found to be in excellent agreement with results obtained by steady-state analysis, so that developed theoretical concepts are fully verified. It is shown that rotor resistance variation leads to the largest speed estimation error, while stator resistance variation at low speeds significantly affects accuracy of field orientation and hence dynamics of the drive.

1. INTRODUCTION

Numerous methods of speed-sensorless vector control of induction machines have recently been developed (Rajashekara et al, 1996). In general, two major approaches can be identified. The first one encompasses all the techniques that estimate rotor speed from the stator current spectrum: speed estimation is therefore inherently not sensitive to parameter variation effects in the machine. The second approach relies on utilisation of induction machine model in the process of speed estimation and the accuracy of speed estimation thus unavoidably depends on accurate knowledge of the machine parameters. Among many different methods that utilise the second approach, speed estimation based on MRAS (Schauder, 1992) has gained substantial popularity due to its rather simple implementation requirements. This is the technique analysed in this paper, in conjunction with a current-fed induction machine controlled by means of the indirect feed-forward rotor flux orientation method.

MRAS based speed estimation techniques mutually differ with respect to the quantity that is selected as output of the reference and the

adjustable model. This quantity can take the form of rotor flux (Schauder, 1992), back e.m.f. (Peng and Fukao, 1994), reactive power (Peng and Fukao, 1994; El-Kholy et al, 1994a), and air-gap active power (Zhen and Xu, 1995). The most frequent choices appear to be rotor flux and back e.m.f. (Marwali and Keyhani, 1997). The method discussed here is the rotor flux based one. It is characterised with simpler design (Marwali and Keyhani, 1997) and is therefore easier to implement.

Accuracy of speed estimation in all the model based methods strongly depends on parameter variation effects in the machine. Some studies related to parameter variation effects in MRAS based sensorless drives are already available. Investigations of steady-state speed estimation errors caused by variation of all the motor parameters are reported by Blasco-Gimenez et al (1996) and Jansen and Lorenz (1993) for a direct rotor flux oriented induction machine that combines a MRAS based speed estimator with a closed loop flux observer and includes a mechanical system model. The validity of the results is restricted to that specific drive structure. Impact of rotor resistance variation on transient behaviour of the drive is studied by Ilas et al (1994) and Griva et al (1996) by simulation. Effects of main flux saturation on dynamics of indirect feed-forward rotor flux oriented induction machine are examined by El-Kholy et al (1994b) by simulation. An experimental study of impact of rotor resistance, stator resistance and magnetising inductance induced detuning is reported for operation in the low speed region by Armstrong and Atkinson (1997). Finally, steady-state analysis of impact of iron loss on speed estimation in indirect feed-forward rotor flux oriented induction machine with rotor flux based MRAS speed estimator is investigated by Levi and Wang (1997).

The aim of this paper is to provide a detailed analysis of speed estimation error and other detuning effects in a sensorless indirect feed-forward current-fed rotor flux induction machine, in which speed estimation is performed using rotor flux based MRAS speed estimator. Steady-state operation, assuming ideal sinusoidal supply, is elaborated first. Modelling is performed utilising the approach developed by Levi and Wang (1997). Iron loss is neglected at all times, while main flux saturation is accounted for in all the cases under consideration. Detuning is evaluated for incorrect setting of the magnetising inductance, stator and rotor resistance variation and leakage inductance variation for operation in the base speed region. Next, simulation of transient behaviour of the drive is performed. Transient detuning due to stator and rotor resistance variation and incorrect magnetising inductance setting is evaluated. Results of simulations, obtained by means of the dynamic model, coincide with results delivered by the steady-state analysis in all steady-state operating points. The approach used in steady-state analysis of detuning is thus fully verified. Detuning is characterised in all the cases by speed estimation error, orientation angle error and error in torque (i.e., ratio of actual to commanded torque).

The paper is organised as follows. Section 2 describes the drive under consideration. Section 3 introduces theoretical bases of the analysis of detuning in steady-state operation, while Section 4 gives results of steady-state analysis. Section 5 gives description of the simulation procedure for transient operation and presents simulation results for both tuned and detuned operation of the drive. Section 6 presents a discussion of the results of the study. Section 7 summarises the conclusions.

2. DESCRIPTION OF THE DRIVE

Structure of the sensorless indirect rotor flux oriented induction machine, analysed in the paper, is shown in Fig. 1. The current regulated PWM inverter (CRPWM) is assumed to be ideal (i.e., reference and actual phase currents are equal). Mathematical analysis of steady-state operation, presented in the next section, is performed in the reference frame firmly

attached to the reference rotor flux space vector. Rotor flux reference is constant and equal to rated, as only base speed region is dealt with. The speed estimator of Fig. 1 is shown in Fig. 2. It relies on measurement of stator currents and voltages, utilises principles of MRAS, and the two left-hand side blocks perform integration of equations (1) and (2). Speed estimator operates in the stationary reference frame (α, β) and is described with the following space vector equations ($\sigma^* = 1 - L_m^{*2}/\left(L_s^* L_r^*\right)$), (Schauder, 1992):

$$\frac{d\underline{\psi}_r^{(1)}}{dt} = \frac{L_r^*}{L_m^*}\left[\underline{v}_s - \left(R_s^* + \sigma^* L_s^* p\right)\underline{i}_s\right] \qquad (1)$$

$$\frac{d\underline{\psi}_r^{(2)}}{dt} = \left(j\omega^{est} - \frac{1}{T_r^*}\right)\underline{\psi}_r^{(2)} + \frac{L_m^*}{T_r^*}\underline{i}_s \qquad (2)$$

$$\varepsilon = \psi_{\alpha r}^{(2)}\psi_{\beta r}^{(1)} - \psi_{\beta r}^{(2)}\psi_{\alpha r}^{(1)} \quad . \qquad (3)$$

Asterisk denotes in (1)-(2) constant values of machine parameters used in the estimator and in the controller of Fig. 1. Symbol p denotes differentiation, while T_r stands for rotor time constant. Induction machine is represented with the dynamic space vector equivalent circuit, given in Fig. 3 in the reference frame rotating at an arbitrary angular speed ω_k. Speed of the reference frame is selected as equal to the reference angular speed of the rotor flux space vector (ω_e^* of Fig. 1) in steady-state analysis and as equal to zero in simulation of dynamics. Actual motor parameters do not bear an asterisk. Induction machine model, in contrast to the speed estimator and the control system, accounts for main flux saturation in both steady-state and transient analysis. As is well-known, level of main flux saturation is significantly affected by rotor resistance variation in indirect rotor flux oriented induction machine with speed sensor. Additionally, impact of incorrect magnetising inductance setting in the estimator and the controller cannot be properly evaluated if main flux saturation in the machine model is neglected. Main flux saturation is therefore accounted for at all times in this study.

The machine used in the study is a four-pole, 50 Hz, 4 kW induction motor, whose data are given in Appendix. Analytical approximations of the magnetising inductance L_m (required for both steady-state and transient analysis) and of the dynamic inductance L (required for transient analysis only) are included.

3. ANALYSIS OF STEADY-STATE OPERATION UNDER DETUNED CONDITIONS

3.1 Induction machine model

Steady-state induction machine model, assuming ideal sinusoidal supply conditions, follows directly from Fig. 3. It is given in the reference frame firmly attached to the commanded rotor flux space vector with the following equations (due to idealised inverter representation and postulated ideal current feeding, stator d-q axis current commands are equal to the actual machine stator d-q axis currents):

$$\begin{aligned}
&v_{ds} = R_s i_{ds}^* - \omega_e^* L_m i_{qs}^* - \omega_e^* L_m i_{qm} \\
&v_{qs} = R_s i_{qs}^* + \omega_e^* L_m i_{ds}^* + \omega_e^* L_m i_{dm} \\
&R_r\left(i_{dm} - i_{ds}^*\right) = \left(\omega_e^* - \omega\right)\left[L_m\left(i_{qm} - i_{qs}^*\right) + L_m i_{qm}\right] \\
&R_r\left(i_{qs}^* - i_{qm}\right) = \left(\omega_e^* - \omega\right)\left[L_m\left(i_{dm} - i_{ds}^*\right) + L_m i_{dm}\right] \\
&L_m = f(I_m) \qquad\qquad I_m = \sqrt{i_{dm}^2 + i_{qm}^2} \\
&T_e = (3P/2)L_m\left(i_{dm} i_{qs}^* - i_{qm} i_{ds}^*\right) \\
&\omega_{sl} = \omega_e^* - \omega \quad .
\end{aligned} \qquad (4), (5)$$

Inspection of equations (4) shows that there are five equations with six unknowns (stator voltage and magnetising current d-q axis components, magnetising inductance and actual speed of rotation ω). Thus it is not possible to solve this system of equations without determining which of the variables is only apparently unknown. As shown in the next sub-section, speed estimator pre-determines stator d-axis voltage, so that the system becomes solvable.

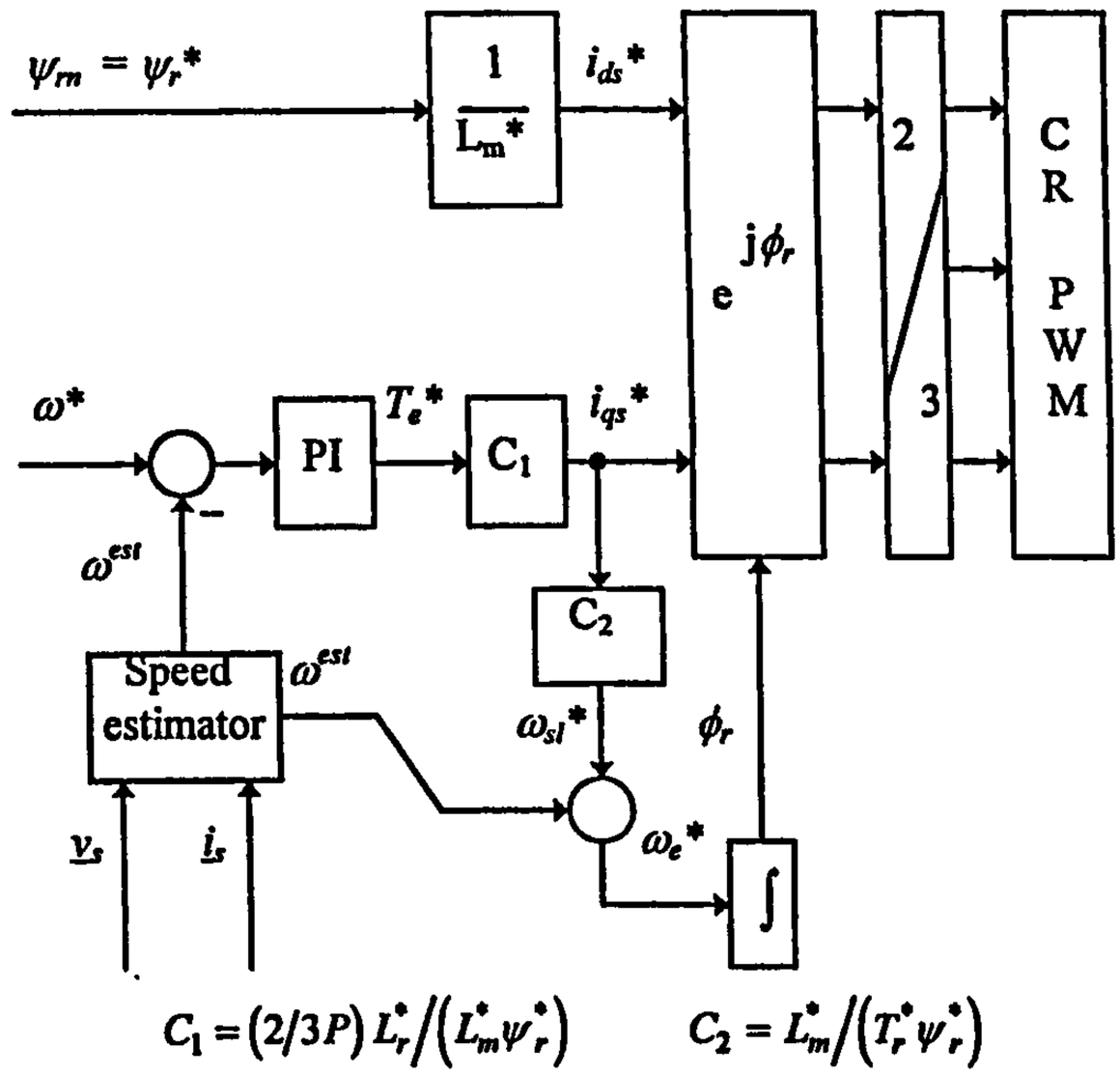

FIGURE 1. Control system of a speed sensorless indirect current-fed rotor flux oriented induction machine.

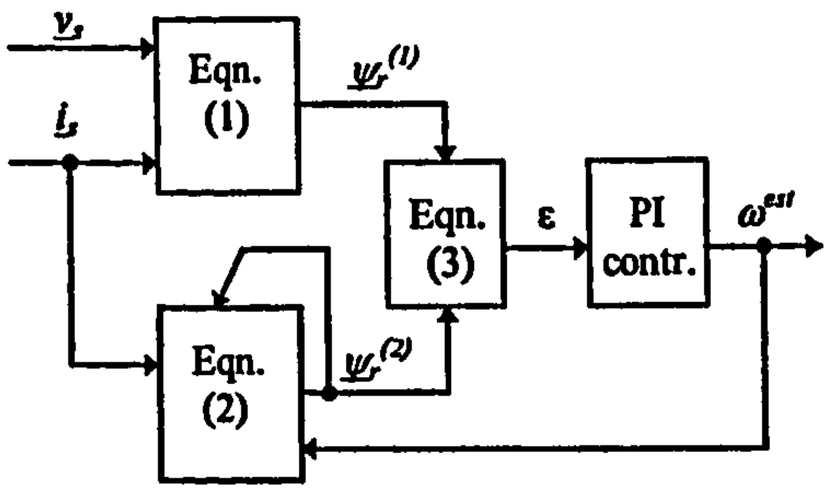

FIGURE 2. Rotor flux based MRAS rotor speed estimator.

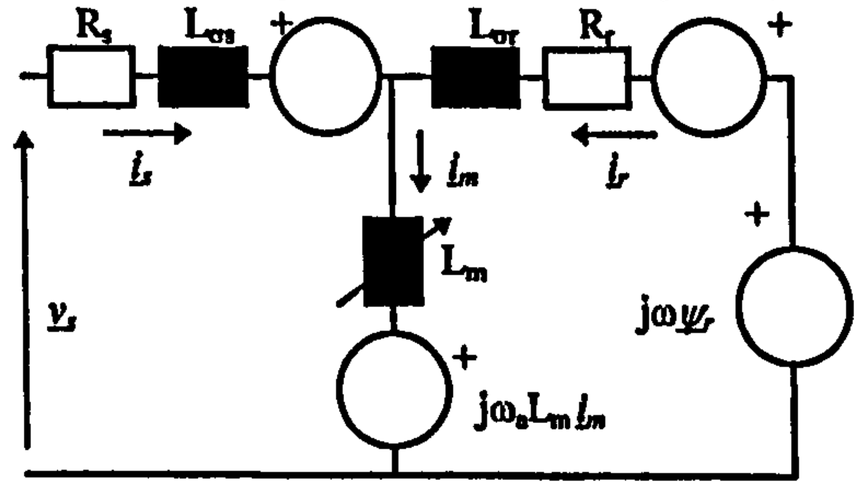

FIGURE 3. Space vector dynamic equivalent circuit of an induction machine in an arbitrary reference frame.

3.2 Analysis of the speed estimator

In any steady-state operation, assuming ideal sinusoidal conditions, ideal integration and neglecting all the delays, rotor flux estimates of (1) and (2) are given in the reference frame attached to the commanded rotor flux space vector (d-q reference frame) with the following expressions:

$$\underline{\psi}_r^{(1)} = -j\frac{L_r^*}{\omega_e^* L_m^*}\left[\underline{v}_s - \left(R_s^* + j\omega_e^*\sigma^* L_s^*\right)\underline{i}_s^*\right]$$
$$\underline{\psi}_r^{(2)} = \frac{L_m^*}{T_r^*}\underline{i}_s^*\frac{1}{1/T_r^* + j\left(\omega_e^* - \omega^{est}\right)} \quad . \tag{6}$$

Due to the presence of the PI controller in the speed control loop estimated speed and reference speed are equal (i.e., $\omega^* = \omega^{est}$). PI

controller in the speed estimator of Fig. 2 imposes the constraint that $\varepsilon = 0$ in steady-state. This means that instantaneous positions of the two rotor flux estimates with respect to the fixed stator axis are equal,

$$\phi_r^{(1)} = \phi_r^{(2)} \quad . \tag{7}$$

However, the rotor speed estimator does not require that magnitudes of the two rotor flux estimates are the same (Levi and Wang, 1997). Hence, in rotor flux oriented reference frame determined with the transformation angle (7), rotor flux estimates are under detuned conditions given with

$$\begin{aligned} \underline{\psi}_r^{(2)} &= \psi_{dr}^{(2)} + j\psi_{qr}^{(2)} \qquad \psi_{dr}^{(2)} = \psi_r^* \qquad \psi_{qr}^{(2)} = 0 \\ \underline{\psi}_r^{(1)} &= \psi_{dr}^{(1)} + j\psi_{qr}^{(1)} \qquad \psi_{dr}^{(1)} \neq \psi_r^* \qquad \psi_{qr}^{(1)} = 0 \ . \end{aligned} \tag{8}$$

It follows from (8) that rotor flux q-axis component in the commanded reference frame must equal zero for both flux estimates. However, d-axis component of the first estimate is not necessarily equal to the commanded rotor flux (the magnitude of the second flux estimate is by default equal to the rotor flux reference). If the q-axis component of the first rotor flux estimate is expressed from (6) and equated to zero (in the commanded rotor flux reference frame), d-axis component of the stator voltage is calculated as equal to

$$v_{ds} = R_s^* i_{ds}^* - \omega_e^* \sigma^* L_s^* i_{qs}^* \quad . \tag{9}$$

Equation (9) is the well known stator voltage d-axis equation, valid under the correct rotor flux orientation conditions. The speed estimator forces stator d-axis voltage to be equal to the one required for perfect rotor flux orientation, for the given set of machine parameters. However, as the estimator does not force equality of magnitudes of rotor flux estimates, stator q-axis voltage is allowed to deviate, under detuned conditions, from the one required for perfect rotor flux orientation. Obviously, if value of any of the parameters in (9) has a value different from the value in the machine, stator d-axis voltage is set to a wrong, but nevertheless known, value.

3.3 Analysis of the control system

The independent inputs in the control system of Fig. 1 are reference speed and reference rotor flux. The output of the PI speed controller is reference torque, whose value is in general unknown. However, for each value of the reference torque T_e^* there is a corresponding value of the actual torque T_e. Actual torque must at all times equal load torque T_L, which is a true independent variable. A more detailed analysis reveals that it is much more convenient to regard reference torque as an independent input, instead of the load torque which is then treated as a dependent variable. By solving the motor equations (4), value of the actual torque that corresponds to the given torque reference can be determined from (5). Such an approach is utilised here: independent inputs are references of speed, torque and rotor flux (rather than references of speed and rotor flux, and load torque). It should be noted that selection of the reference torque as an independent input is merely a choice of convenience, which has no impact whatsoever on the results of the study. Motor model (4) is solved numerically, taking into account (9), for actual speed of rotation. The additional constraint imposed by the control system

$$\omega_e^* = \omega^* + \omega_{sl}^* \quad , \tag{10}$$

(estimated and reference speed are equal) is taken into account and actual torque is calculated from (5). The error in speed estimation, discussed in the following sections, is defined in mechanical rpm as

$$\Delta n = n - n^* \equiv n - n^{est} \equiv n_{sl}^* - n_{sl} \quad . \tag{11}$$

4. DETUNING EFFECTS IN STEADY-STATE OPERATION

4.1 General remarks

As already pointed out, main flux saturation is accounted for in the induction machine model of Fig. 3 in all the studies whose results are presented in this section. Detuning is

characterised with speed estimation error of (11), with the ratio of actual torque (which equals load torque) to the reference torque and with orientation angle error. Additionally, ratio of actual magnetising inductance to rated magnetising inductance is monitored as well. Detuning due to incorrect initial setting or variation of rotor resistance, stator and rotor leakage inductances, and magnetising inductance is speed (frequency) independent. Detuning due to incorrect setting or variation of the stator resistance is however speed dependent. Detuning in the base speed region only is elaborated and all the graphs are given against torque command in per unit.

4.2 Incorrect rotor resistance value

Figure 4 displays speed estimation error, torque ratio, orientation angle error and ratio of actual magnetising inductance to rated magnetising inductance for discrepancies between actual rotor resistance and controller/estimator rotor resistance (which is equal to rated value) of up to ± 20 %. Stator and rotor leakage inductance and stator resistance have the same values in the motor and in the controller/estimator. Magnetising inductance in the controller/estimator is rated. As can be seen from Fig. 4, orientation angle error is negligible. Variation of the saturation level in the machine is very small as well, this being in huge contrast to the situation that arises in a drive with speed sensor. Maximum speed estimation error is around ± 10 rpm for deviation of rotor resistance of ± 20 % at rated torque command. Torque error is very small and is the same regardless of the amount of rotor resistance detuning.

4.3 Incorrect stator and rotor leakage inductance values

Stator and rotor resistance values are the same in the motor and in the controller/estimator. Magnetising inductance in the controller/ estimator is rated. Detuning due to incorrect setting or variation in the stator and rotor leakage inductance is illustrated in Fig. 5. The same amount of detuning is assumed for both leakage inductances. Speed estimation error is below ± 1 rpm and torque error is small as well. Variation in the main flux saturation level in the machine is rather small again (although higher than in the previous case). Orientation angle error is now up to 2 degrees. Due to very small values of the speed estimation error and orientation angle error, variation of stator and rotor leakage inductance is not analysed for transient operation.

4.4 Incorrect magnetising inductance setting

Under the assumption that stator and rotor resistance, as well as stator and rotor leakage inductance, all have the same rated values in the motor and in the estimator/controller, incorrect setting of magnetising inductance produces detuning shown in Fig. 6. Maximum speed estimation error is up to ± 3.5 rpm at rated torque command when magnetising inductance value in the controller/estimator deviates by ± 20 % from the rated value. Torque error is up to ± 8 %. Orientation angle error is once more negligible small. Level of main flux saturation in the motor is, as expected, now considerably affected (ratio of the actual to rated magnetising inductance in Fig. 6 differs from the ratio of controller/ estimator to rated magnetising inductance).

4.5 Incorrect stator resistance value

Impact of incorrect stator resistance value on low speed operation is displayed in Fig. 7, where results are given for speed reference equal to 5 % of the rated. Magnetising inductance in the controller/estimator equals rated and rotor resistance and stator and rotor leakage inductance have the same rated values in the motor and in the controller/estimator. Speed error is up to ± 6 rpm, while error in torque ratio is excessively high at low torque command values. Orientation angle error is significant and reaches up to ± 8 degrees. Main

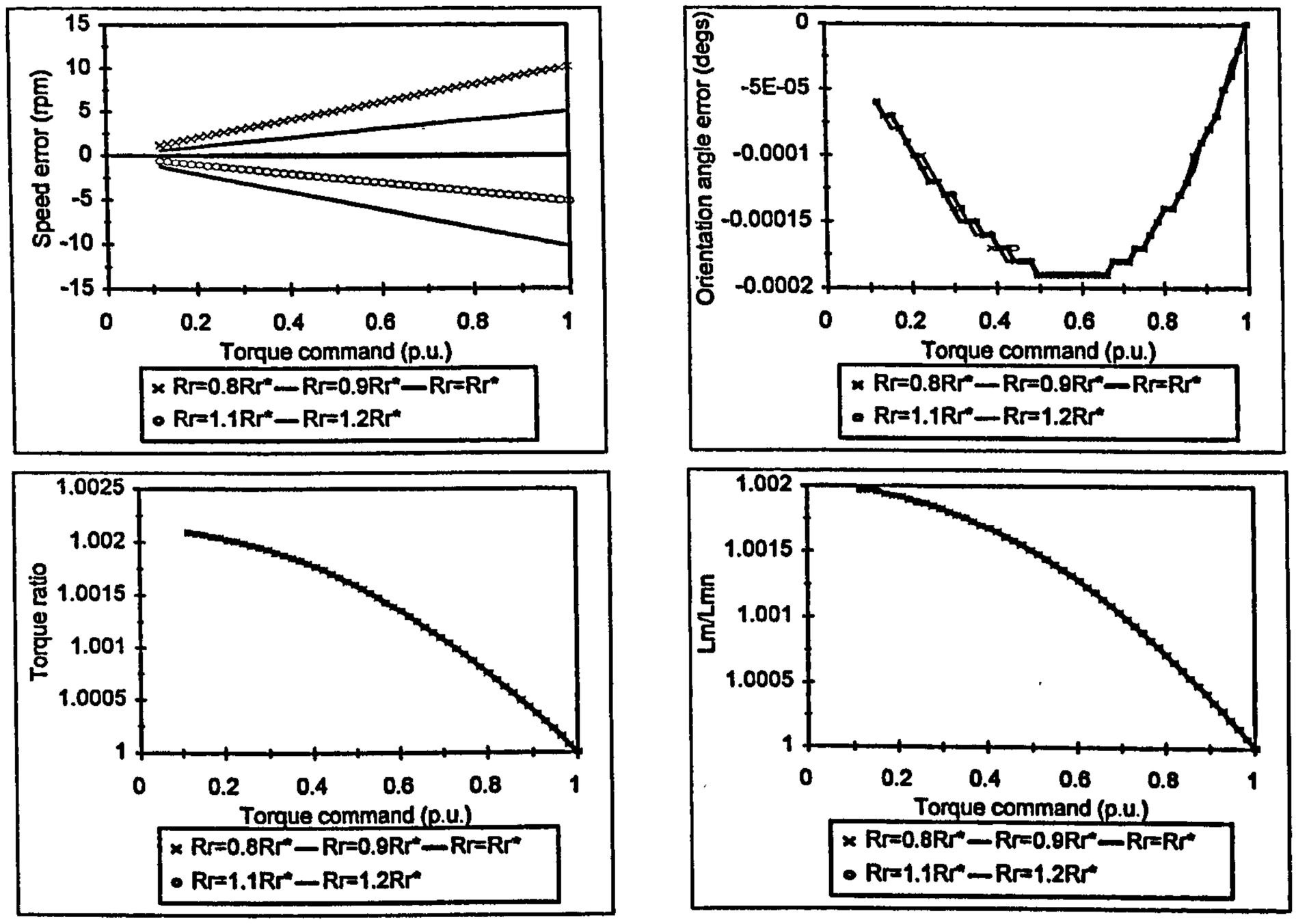

FIGURE 4. Effects of incorrect value of the rotor resistance: speed estimation error, torque ratio, orientation angle error and ratio of actual to rated magnetising inductance.

flux saturation level in the machine is affected as well, as witnessed by the ratio of actual to rated magnetising inductance.

Detuning diminishes as the speed is increased. Detuning for rated speed operation is depicted in Fig. 8. Speed estimation error is up to 0.4 rpm, while orientation angle error and variation in the main flux saturation level are very small indeed.

4.6 Detuning due to iron loss

Detuning due to omission of iron loss representation in the control system and in the speed estimator has been elaborated by Levi and Wang (1997). Speed estimation error depends on the value of the speed command and on the loading of the machine. Its typical values, for the same induction machine, are 2 to 3 rpm in the base speed region. Orientation angle error is negligibly small. Torque ratio depends on the speed command and load torque and can be as low as 0.8 for rated speed operation with one fifth of the rated torque command.

5. DYNAMICS OF THE DRIVE UNDER DETUNED CONDITIONS

5.1 Simulation procedure

Induction machine is represented with the full saturated machine model in stationary reference frame, that accounts for cross-saturation effect, with state-space variables selected as stator current and rotor flux d-q axis components (Levi, 1995). Due to assumed ideal current feeding stator current commands

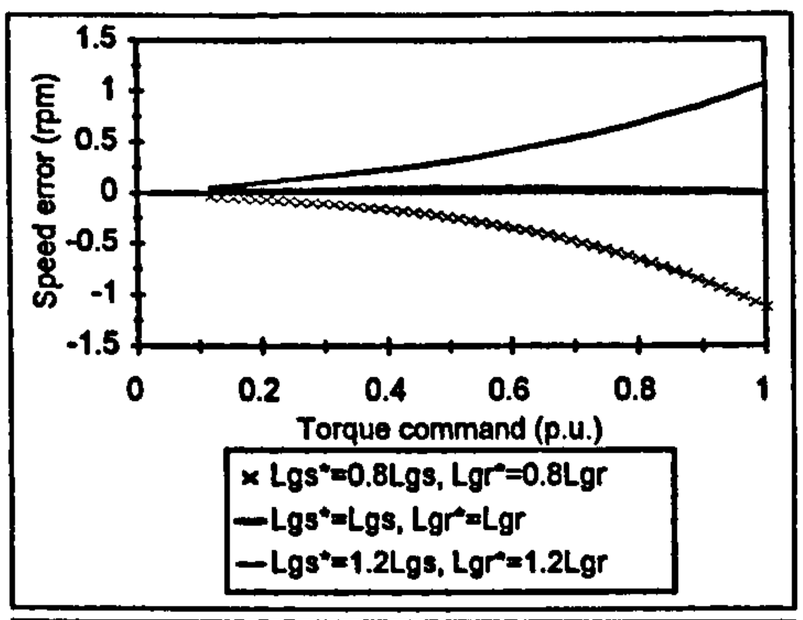

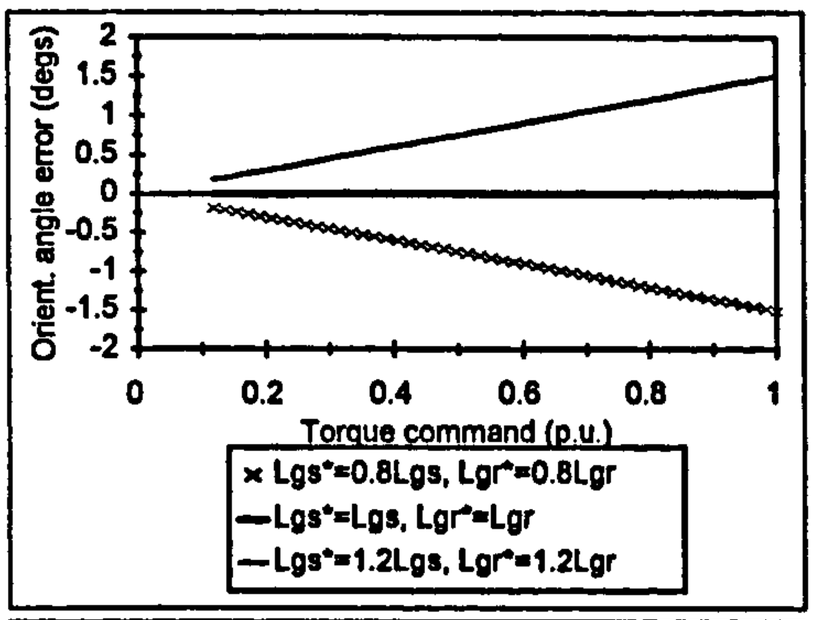

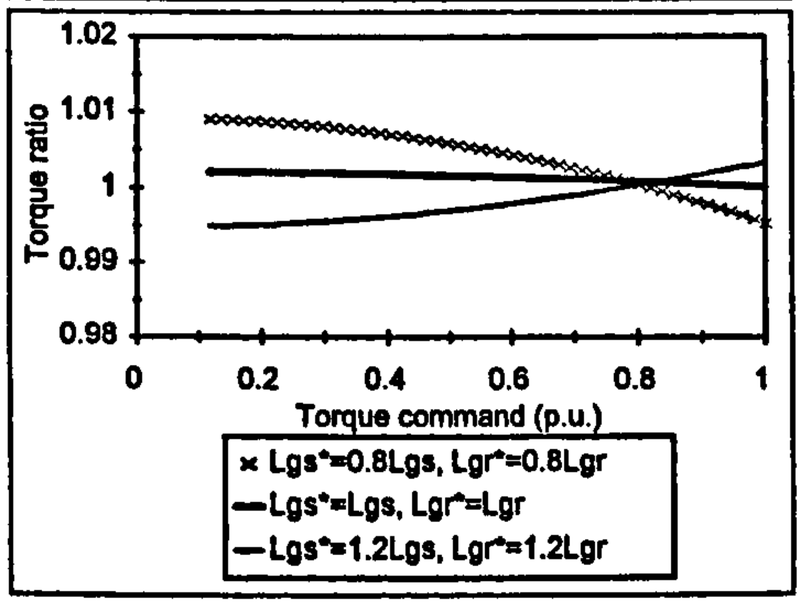

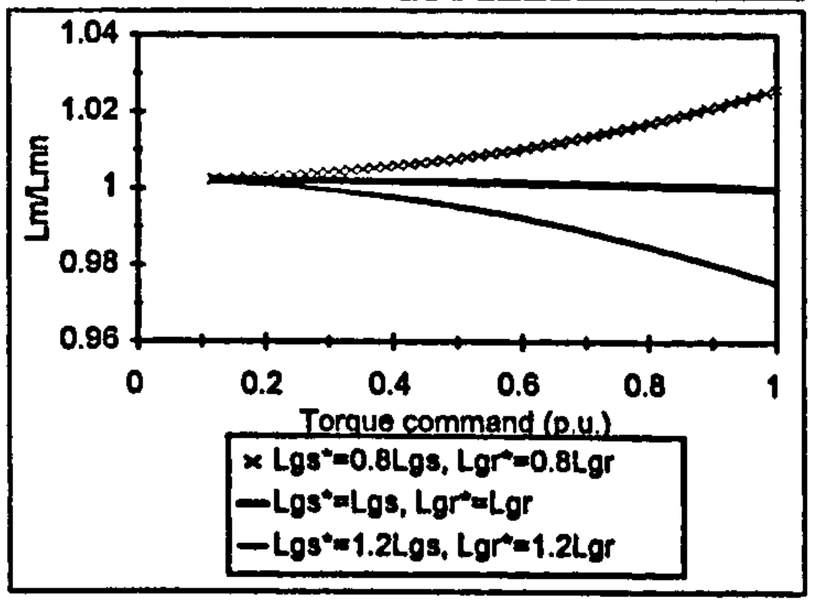

FIGURE 5. Impact of incorrect stator and rotor leakage inductance values ($g \equiv \sigma$).

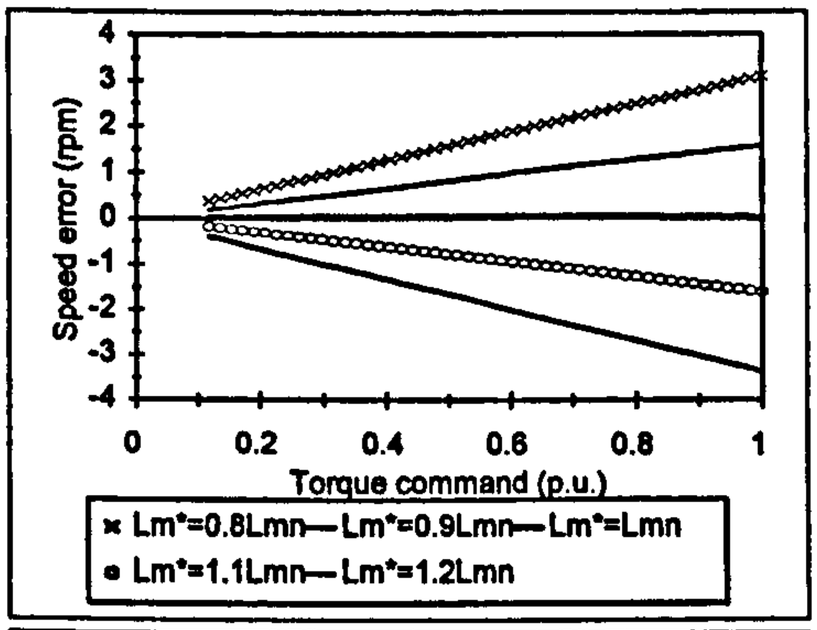

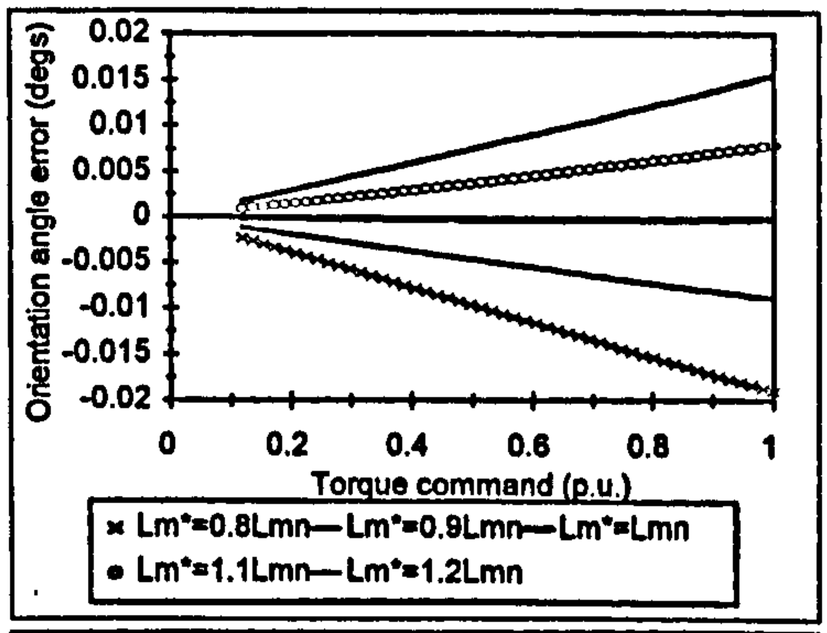

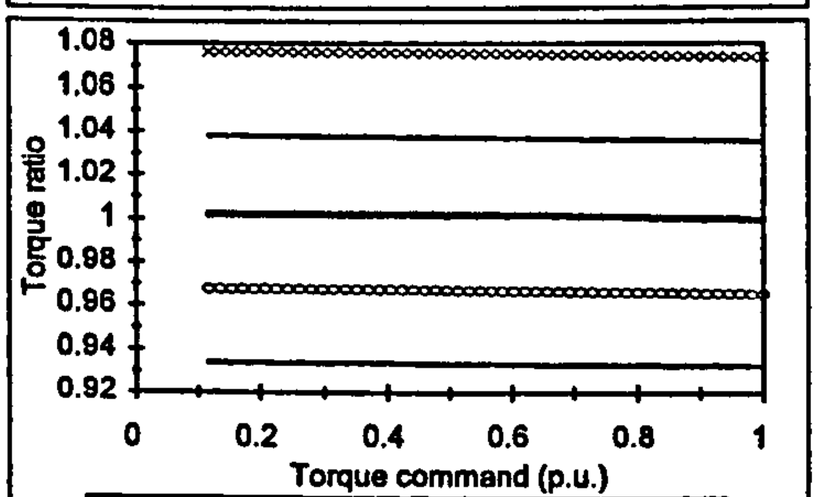

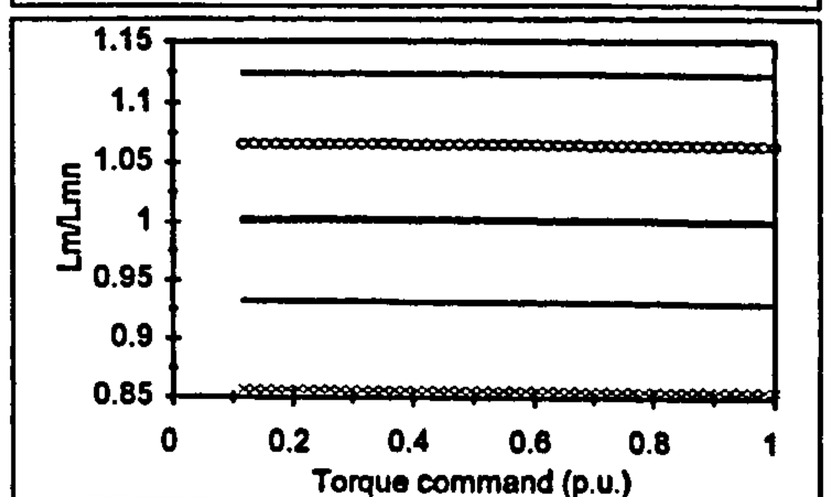

FIGURE 6. Detuning due to incorrect magnetising inductance value.

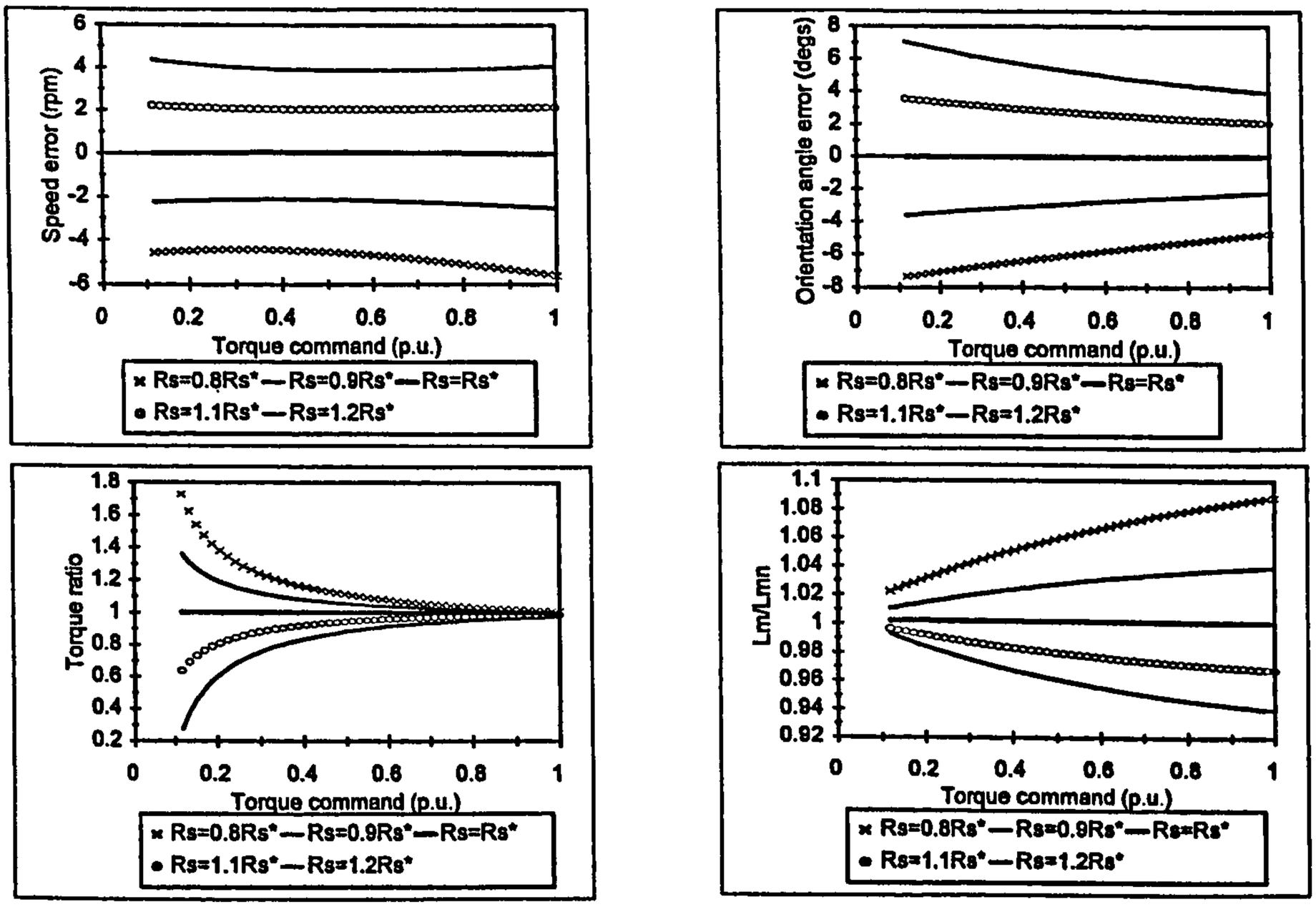

FIGURE 7. Detuning due to incorrect stator resistance - speed reference is 5 % of the rated speed.

in stationary reference frame equal actual stator current components and stator voltage equations are not required in the machine model. As cross-saturation effect for the selected set of state-space variables appears in stator voltage equations only (Levi, 1995), selected set of state-space variables yields overall simulation model of minimum complexity.

Speed estimator of Fig. 2 requires values of stator voltage components in stationary reference frame. These are calculated using stator current commands in stationary reference values frame and their time derivatives, as well as various required saturated inductance and rotor flux components in stationary reference frame obtained from the induction machine model (Levi, 1995). Problem of pure integration in equation (1) is solved by the method proposed by Schauder (1992): a filter, not shown in Fig. 2 and eqns. (1)-(3), is inserted in the output channels of both the reference and the adaptive model. Filter's transfer function is $p/(p+1/T)$, where 1/T = 100.

Model of the control system is identical to the one shown in Fig. 1, with rotor flux reference equal to the rated value at all times, as operation in the base speed region is considered only. Speed estimate is used for both closed loop speed control and for calculation of the orientation angle.

The following transients are simulated. The machine is excited under no-load conditions at zero speed. Speed command, equal to rated, is applied at t = 0.1 s in a ramp-wise manner under no-load conditions. Unless otherwise stated, rated load torque is applied at t = 0.6 s.

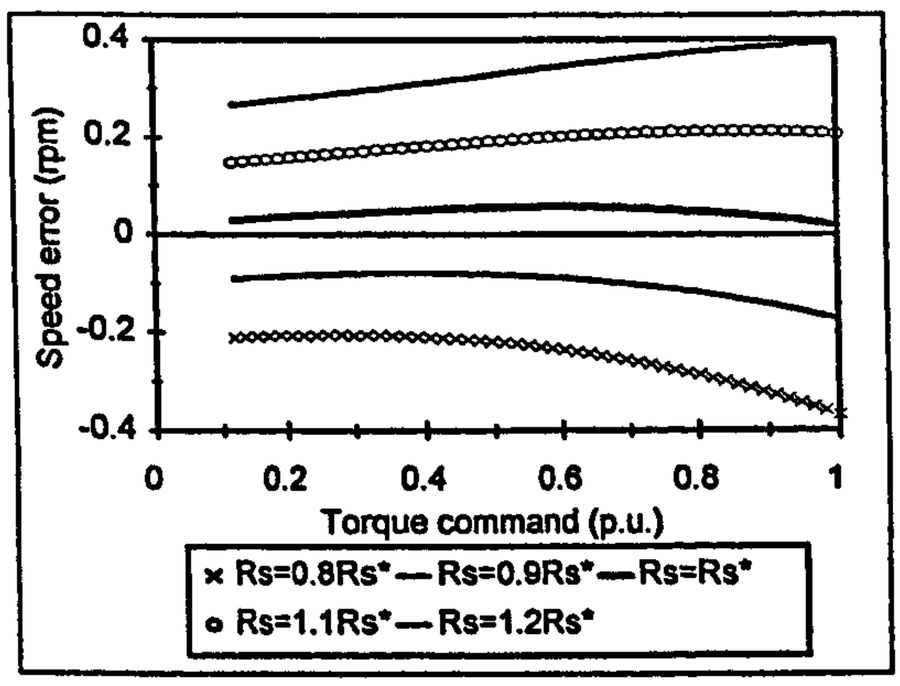

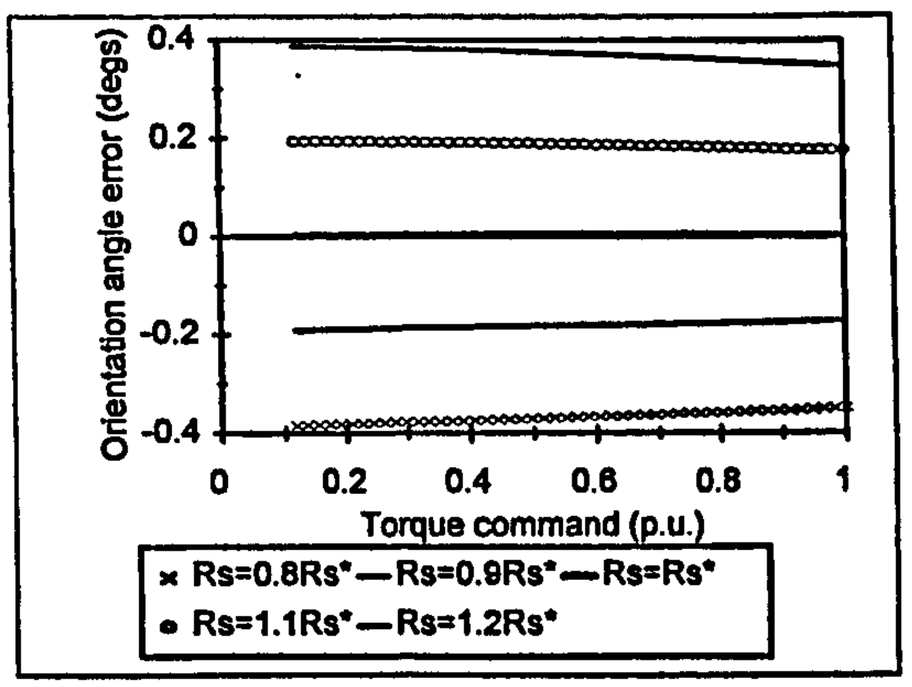

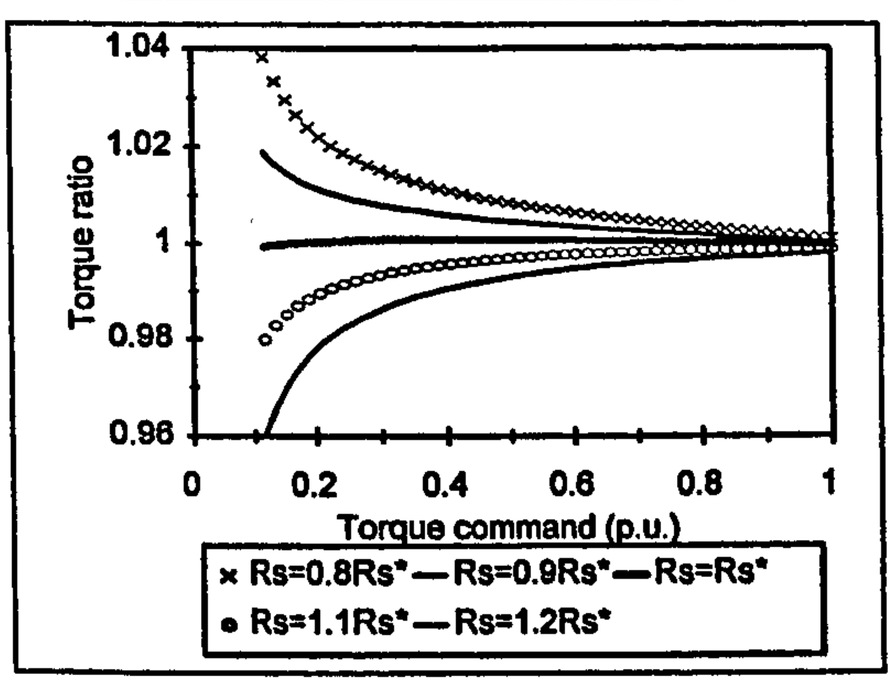

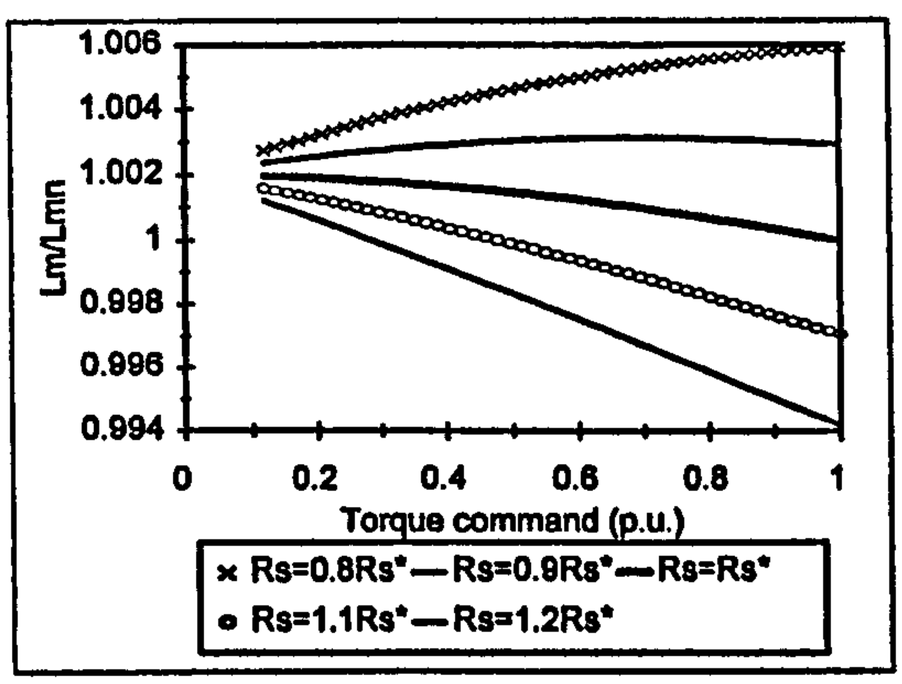

FIGURE 8. Speed estimation error due to incorrect stator resistance value - speed reference equal to rated.

5.2 Operation under tuned conditions

Operation of the drive is at first examined with all the parameters in the controller and in the estimator set to their rated values. Parameters in the machine model are rated as well, except that the machine model accounts for main flux saturation and magnetising inductance in the machine is a variable parameter. Simulation results are summarised in Fig. 9, where actual and estimated speed (in electrical rad/s), actual and commanded torque, actual and commanded rotor flux, and speed error for the complete time interval (in mechanical rpm, defined in equation (11)) are shown. Estimated speed tracks the actual one very well, except during the initial part of the acceleration. Commanded and actual torque are in good agreement, except during initial acceleration. Similar conclusion applies to the actual rotor flux. Field orientation is initially lost, as witnessed by oscillatory torque behaviour. Relatively sluggish response during initial acceleration period is a consequence of the too high gain of the speed controller. Speed estimation error, initially large, is zero for both full load and no-load operation at rated speed and has negligibly small values during transient caused by rated load torque application. Field orientation is fully maintained during step load application, as can be seen from the instantaneous torque response and transient-free trace of rotor flux.

5.3 Variation of rotor resistance

The same simulation is now repeated with $R_r = 0.8R_m = 0.8R_r{}^*$ and $R_r = 1.2R_m = 1.2R_r{}^*$. All the other parameters in the motor and in the controller/estimator are the same (magnetising

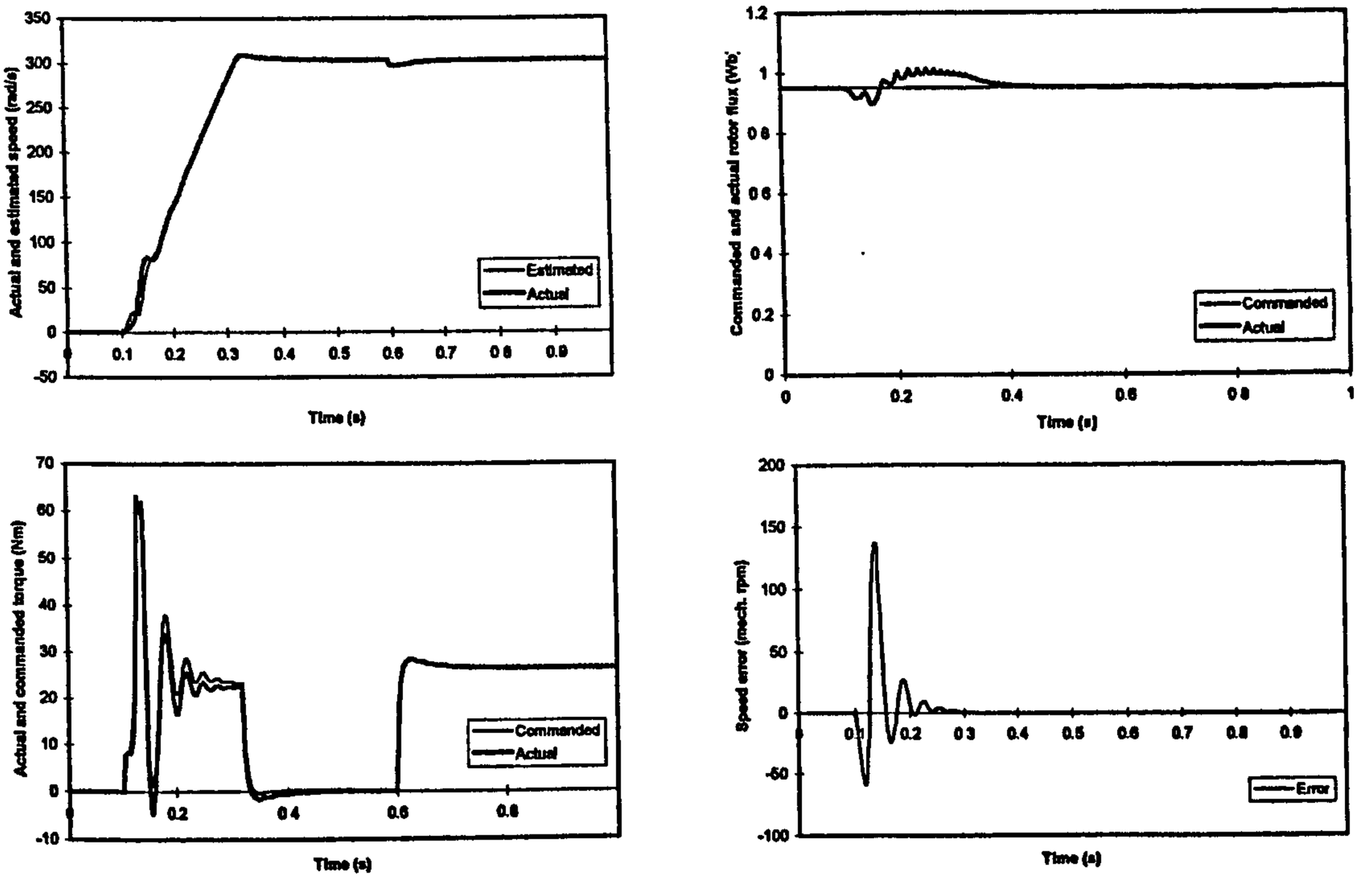

FIGURE 9. Dynamics of the drive under tuned conditions.

inductance is set to rated value). Transient behaviour during acceleration remains essentially the same as in Fig. 9 and Fig. 10 therefore shows speed errors for the two cases for time interval $t \in$ (0.5 s; 1s). Torque response is included as well. It is interesting to note that the orientation angle error is negligibly small when rotor resistance varies, so that transient-free torque response is maintained irrespective of the speed estimation error. This is in close agreement with results of steady-state analysis given in Section 4. Furthermore, speed estimation errors in final steady-state operation with rated speed and rated load torque are ± 10 rpm, which equals the values predicted by steady-state analysis in Section 4. Torque error in final steady-state is negligibly small, this again being in full agreement with results of the steady-state analysis of Section 4.

Consequences of incorrect setting of the magnetising inductance in the controller/ estimator are investigated next.

5.4 Incorrect magnetising inductance setting

The same study is performed two more times, but now with the magnetising inductance set in the controller and the speed estimator to $L_m^* = 0.8L_{mn}$ and $L_m^* = 1.2L_{mn}$, respectively. All the other parameters in the motor and in the controller/estimator are the same and equal to rated values. Speed error during acceleration remains essentially the same as in Fig. 9; therefore the results, given in Fig. 11, contain speed errors for time interval $t \in$ (0.5s ;1s). Torque response is again included in Fig. 11. One observes that speed estimation error in steady-state operation with rated speed and rated load torque is around + 3 rpm and almost – 4 rpm, which again closely agrees with results of steady-state analysis. Response to load torque application is again instantaneous, indicating absence of orientation angle error. However, actual torque differs from torque command in final steady-state operation, as predicted by results of steady- state analysis.

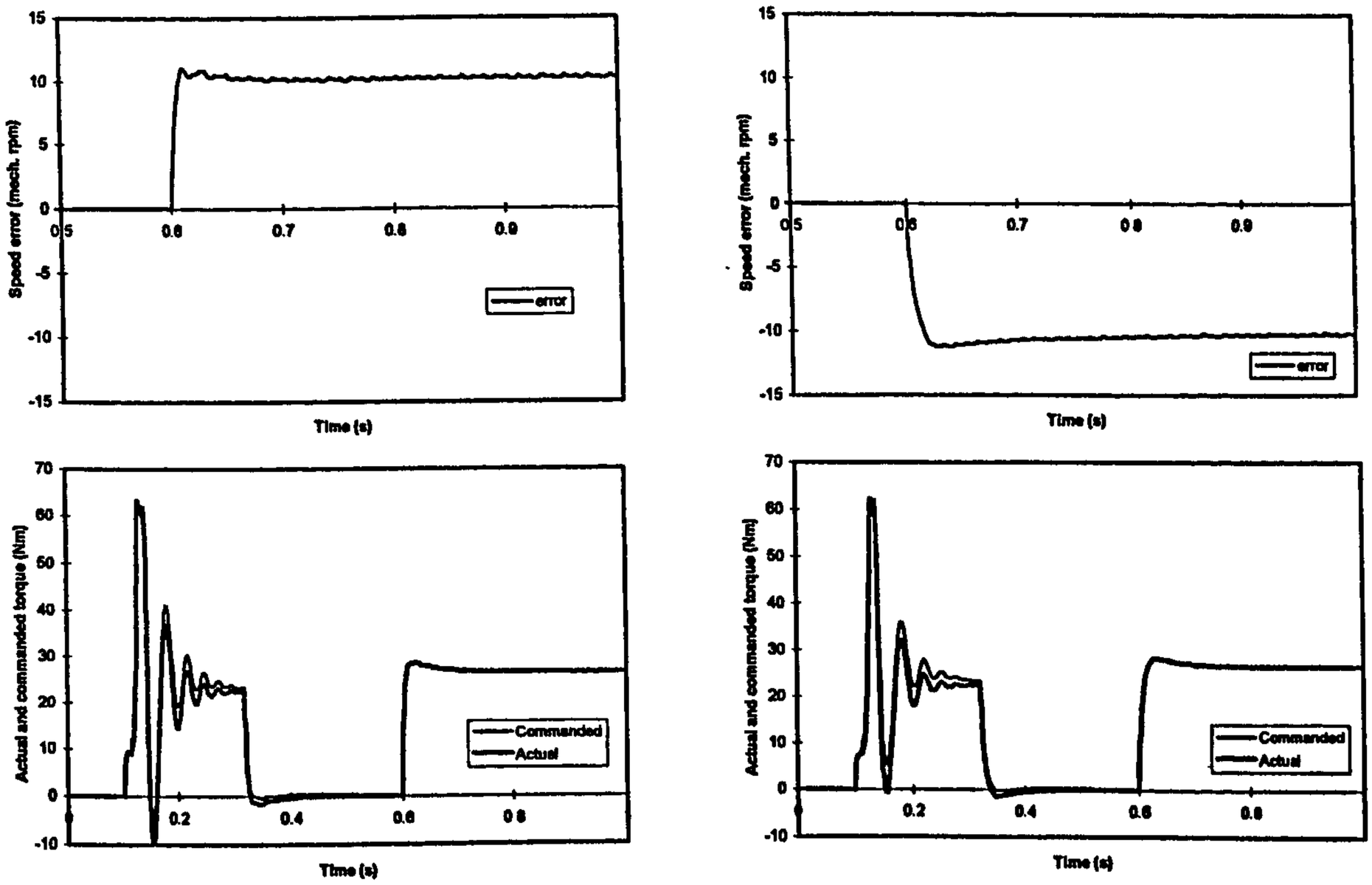

FIGURE 10. Speed error and torque response for operation with incorrect rotor resistance: a) $R_r = 0.8R_m$, $R_r^* = R_m$ and b) $R_r = 1.2R_m$, $R_r^* = R_m$.

5.5 Variation of stator resistance

Detuning due to stator resistance variation is speed (frequency) dependent and is most pronounced at low speeds. On the other hand, steady-state analysis suggests that impact of loading is smaller than in the previous two cases. The simulation is now done by applying speed command of 0.05 p.u. in a ramp-wise manner at $t = 0.1$ s. This is followed by 0.2 p.u. load torque application at $t = 0.6$ s and subsequent rated load torque application at $t = 0.8$ s. Stator resistance in the motor is taken as $R_s = 0.8R_{sn}$ and $R_s = 1.2R_{sn}$, respectively, while the one in the estimator equals rated value. Results for the value of 1.2 p.u. of the stator resistance in the motor are given in Fig. 12. However, it was not possible to get the results for the same speed command for stator resistance of 0.8 p.u, due to complete failure of the speed estimator. It is worth noting that a similar problem at low speeds was observed in experimental study of detuning reported by Armstrong and Atkinson (1997) for a MRAS based speed estimation system, although failure of estimation occurred due to rotor resistance variation rather than stator resistance variation. Speed command for this stator resistance is therefore increased to 0.1 p.u.. Speed response, speed estimation error and torque response are shown in Fig. 13.

Figure 12 shows that speed estimation error at 0.05 p.u. speed hardly depends on the loading and is close to 5 rpm in steady-state operation with both load torque values. There is steady-state torque error for both load torques and this error is higher for lighter loading, as predicted by steady-state analysis. Moreover, torque response to application of the load torque is oscillatory, indicating that field orientation is lost. All these findings fully correspond to what

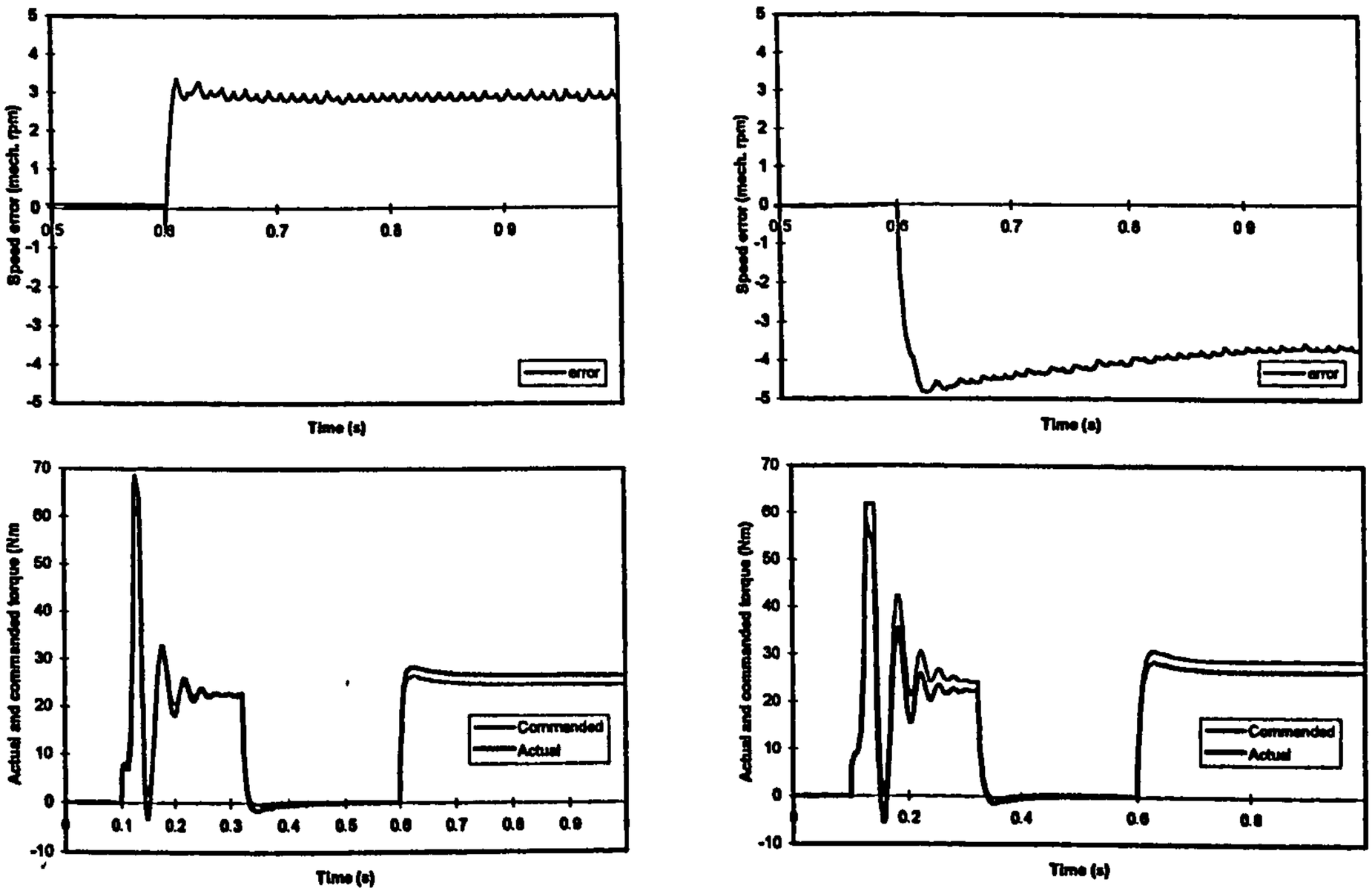

a. b.

FIGURE 11. Speed error and torque response for operation with incorrect setting of the magnetising inductance: a) $L_m^* = 0.8L_{mn}$ and b) $L_m^* = 1.2L_{mn}$.

the steady-state analysis of Section 4 has predicted.

Operation at 0.1 p.u. of the rated speed, shown in Fig. 13, is not covered by steady-state analysis. One notes that speed estimation error and torque error are reduced with respect to Fig. 12 and that torque response is greatly improved as well, indicating that the error in orientation angle is significantly smaller.

As speed of operation is further increased, consequences of detuning will further diminish. Figure 14 shows speed estimation error for operation at rated speed, with 0.2 p.u. load torque application at $t = 0.6$ s and subsequent rated load torque application at $t = 0.8$ s. Stator resistance in the motor is taken again as $R_s = 0.8R_{sn}$ and $R_s = 1.2R_{sn}$, respectively. Speed estimation error is now below 0.5 rpm in all the steady-states, for both values of stator resistance. Orientation angle error and torque error are very small.

6. DISCUSSION

On the basis of the results of steady-state and transient analysis, presented in Sections 4 and 5, it is possible to draw a number of important conclusions regarding relative importance of various sources of detuning. These are summarised in Table I.

It follows from Table I that the critical parameter from the point of view of orientation and associated dynamics of the drive is stator resistance at very low speeds of operation. As far as speed estimation error is concerned, variation of rotor resistance leads to the highest values. It can therefore be concluded that on-line parameter identification is required for

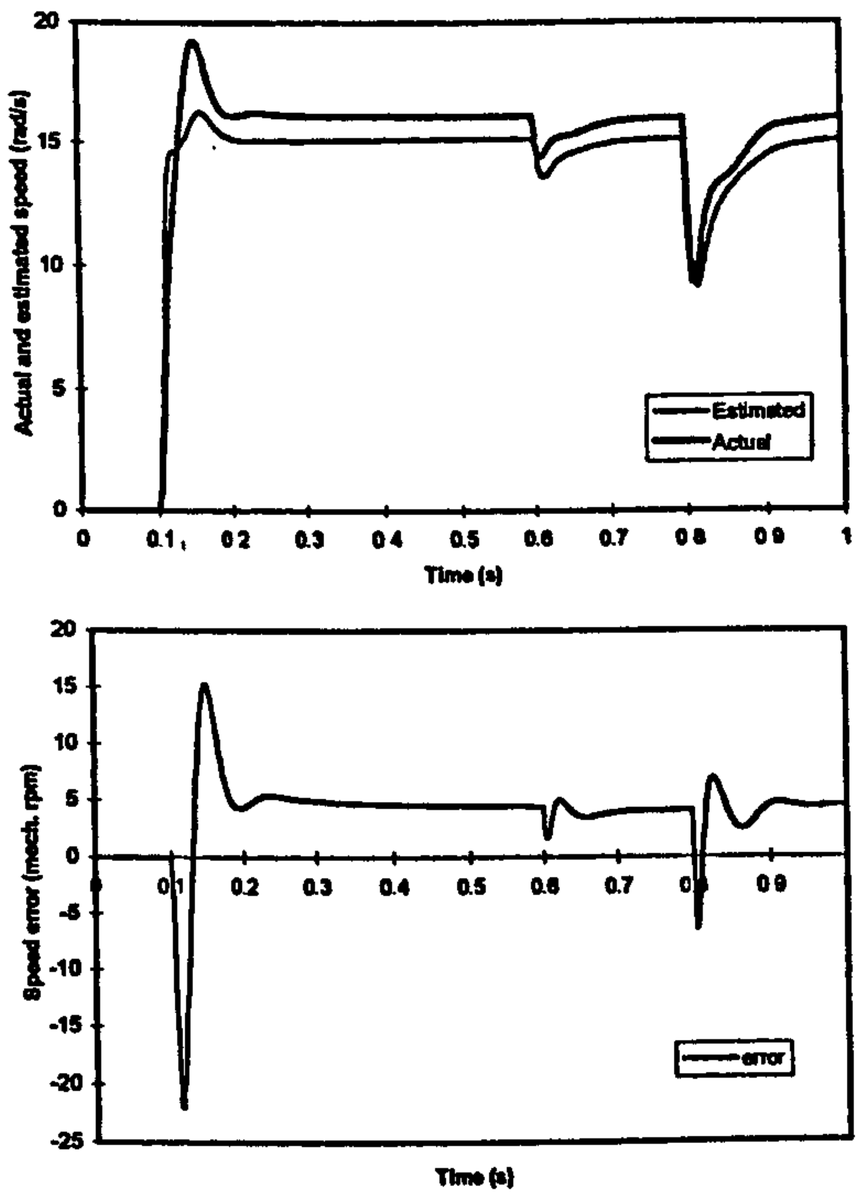

FIGURE 12. Speed response, speed estimation error and torque response at 0.05 p.u. speed command for $R_s = 1.2R_{sn}$, $R_s^* = R_{sn}$.

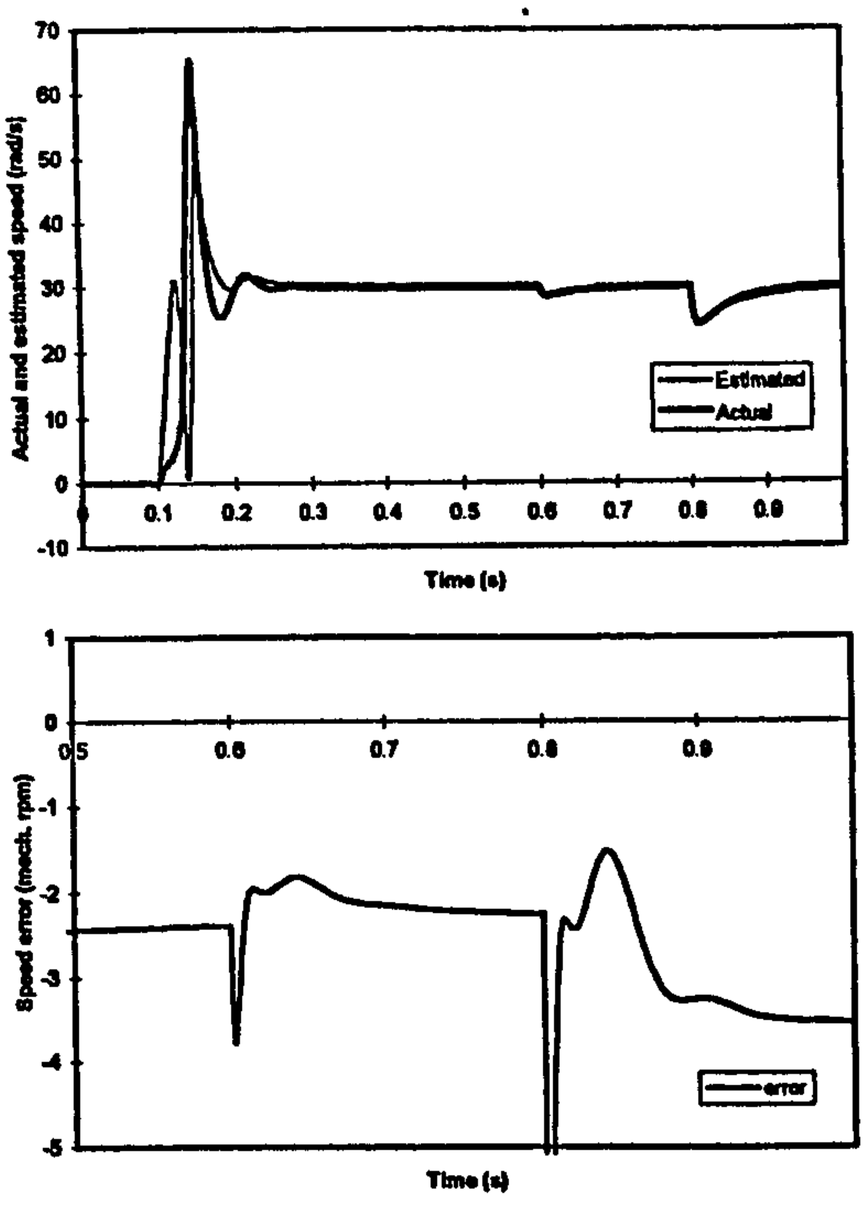

FIGURE 13. Speed response, speed estimation error and torque response at 0.1 p.u. speed command for $R_s = 0.8R_{sn}$, $R_s^* = R_{sn}$.

these two parameters in order to enable accurate speed estimation and correct orientation under all operating conditions.

7. CONCLUSION

A detailed study of behaviour of a sensorless indirect feed-forward current-fed induction machine, with rotor flux based MRAS speed estimator, in the presence of parameter uncertainties is presented in the paper. Both steady-state operation and dynamics are encompassed by the study. Stator and rotor resistance variation, incorrect setting and/or variation of leakage inductances and incorrect setting of the magnetising inductance are all covered in detail and detuning that is introduced by iron loss is reviewed. It is shown that the major consequence of parameter

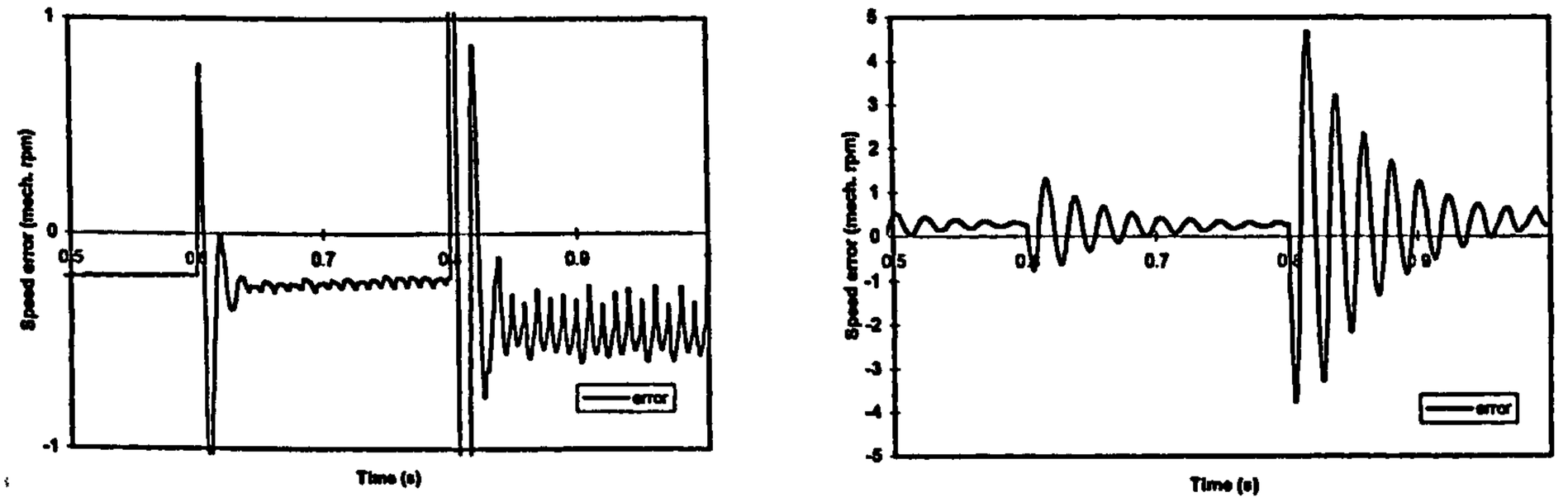

a. b.

FIGURE 14. Speed estimation error at rated speed command for a) $R_s = 0.8R_{sn}$ and b) $R_s = 1.2R_{sn}$,.

TABLE I. Summary of relative importance of various parameter variation effects.

	Speed estimation error	*Torque ratio error*	*Orientation angle error*	*Main flux saturation level*
Rotor resistance variation	speed independent, load dependent, large (10 rpm)	negligible	negligible	not affected
Incorrect magnetising inductance setting	speed independent, load dependent, moderate	moderate	negligible	affected
Incorrect value of leakage inductances	speed independent, load dependent, very small (below 1 rpm)	small	small (up to 2°)	slightly affected
Stator resistance variation	speed dependent, almost load independent; moderate at low speed, very small at high speed	large at low speeds and light load, moderate to small as speed increases	large at low speeds (up to 8°), small at high speeds	affected at low speed only
Iron loss (Levi and Wang, 1997)	speed dependent, lightly load dependent, moderate	moderate to large as load decreases	negligible	not affected

detuning is a speed estimation error, that is of the highest value when rotor resistance varies. Field orientation and hence dynamics of the drive are significantly affected only by stator resistance variation in the low speed region.

Due to the analogy that exists between rotor flux based MRAS speed estimator and the back e.m.f. based MRAS speed estimator, it is believed that the results of the steady-state analysis are fully applicable to the back e.m.f. based scheme as well.

8. REFERENCES

Armstrong, G.J., and Atkinson, D.J., 1997, A comparison of model reference adaptive

system and extended Kalman filter estimators for sensorless vector drives, *Proc. Eur. Conf. on Power Elec. and Appl. EPE*, Trondheim, Norway, pp. 1.424-1.429.

Blasco-Gimenez, R., Asher, G.M., Sumner, M., and Bradley; K.J., 1996, Dynamic performance limitation for MRAS based sensorless induction motor drives. Part 1: Stability analysis for the closed loop drive, *IEE Proc. - Electr. Power Appl.*, vol. 143, pp. 113-122.

El-Kholy, E.E., Abdel-Karim, M., Mahmoud, S.A., and Iung, C., 1994a, Speed sensorless indirect foeld oriented control of an induction motor without using stator and rotor resistance, *Proc. EPE Chapter Symp. 'Electric drive design and applications'*, Lausanne, Switzerland, pp. 615-620.

El-Kholy, E.E., Abdel-Karim, M., Mahmoud, S.A., and Iung, C., 1994b, Effects of main flux saturation on behaviour of indirect field oriented induction motor drives without speed sensor, *Proc. EPE Chapter Symposium 'Electric drive design and applications'*, Lausanne, Switzerland, pp. 203-208.

Griva, G., Profumo, F., Ilas, C., Magureanu, R., and Vranka, P., 1996, A unitary approach to speed sensorless induction motor field oriented drives based on various model reference schemes, *Proc. IEEE Ind. Appl. Soc. Annu. Meet. IAS*, San Diego, CA, pp. 1594-1599.

Ilas, C., Bettini, A., Griva, G., and Profumo, F., 1994, Comparison of different schemes without shaft sensors for field oriented control drives, *Proc. IEEE Ind. Elec. Soc. Annu. Meet. IECON*, Bologna, Italy, pp. 1579-1588.

Jansen, P.L., and Lorenz, R.D., 1993, Accuracy limitations on velocity and flux estimation in direct field oriented induction machines, *Proc. Eur. Conf. on Power Electronics and Appl. EPE*, Brighton, UK, pp. 312-318.

Levi, E., 1995, A unified approach to main flux saturation modelling in d-q axis models of induction machines, *IEEE Trans. on Energy Conversion*, vol. 10, pp. 455-461.

Levi, E., and Wang, M., 1997, Impact of iron loss on speed estimation in sensorless vector controlled induction machines, *Proc. IEEE Ind. Elec. Soc. Annu. Meet. IECON*, New Orleans, LA, pp. 977-982.

Marwali, M.N., and Keyhani, A., 1997, A comparative study of rotor flux based MRAS and back emf based MRAS speed estimators for speed sensorless vector control of induction machines, *Proc. IEEE Ind. Appl. Soc. Annu. Meet. IAS*, New Orleans, LA, pp. 160-166.

Peng, F.Z., and Fukao, T., 1994, Robust speed identification for speed-sensorless vector control of induction motors, *IEEE Trans. on Industry Applications*, vol. 30, no. 5, pp. 1234-1240.

Rajashekara, K., Kawamura, A., and Matsuse, K., (editors), 1996, *Sensorless control of AC motor drives*, Piscataway, NJ: IEEE Press.

Schauder, C., 1992, Adaptive speed identification for vector control of induction motors without rotational transducers, *IEEE Trans. on Industry Applications*, vol. 28, pp. 1054-1061.

Zhen, L., and Xu, L., 1995, A mutual MRAS identification scheme for position sensorless field orientation control of induction machines, *Proc. IEEE Ind. Appl. Soc. Annu. Meet. IAS*, Lake Buena Vista, FL, pp. 159-165.

9. APPENDIX: Induction Motor Data

4 kW 380 V 50 Hz 8.7 A

Y 2P = 4

$T_{en} = 26.5\ Nm$ $R_{sn} = 1.37\ \Omega$

$R_{rn} = 1.1\ \Omega$ $L_{\sigma sn} = 4.87$ mH

$L_{\sigma rn} = 7.96$ mH $L_{mn} = 0.143$ H

$$L_m = \begin{cases} 0.196 & I_m < 2.2 \text{ A} \\ 0.837/I_m + 0.007 - 0.92/I_m^2 & I_m > 2.2 \text{ A} \end{cases}$$

$$L = d\Psi_m/dI_m = \begin{cases} 0.196 & I_m < 2.2 \text{ A} \\ 0.007 + 0.92/I_m^2 & I_m > 2.2 \text{ A} \end{cases}$$

(index n denotes rated values)

Proceedings of the

IECON '97

23rd International Conference on Industrial Electronics, Control, and Instrumentation

Volume 2 of 4

Power Electronics

IEEE

Sponsored by:
IEEE Industrial Electronics Society

Technical Co-Sponsor:
Society of Instrument and Control Engineers of Japan (SICE)

97CH36066

Impact of Iron Loss on Speed Estimation in Sensorless Vector Controlled Induction Machines

E. Levi, M. Wang
School of Electrical Engineering, Electronics & Physics
Liverpool John Moores University
Liverpool L3 3AF, UK

Abstract **— Methods of sensorless vector control of induction machines rely on rotor speed estimation using either stator current spectral estimation techniques, or mathematical model of an induction machine in conjunction with one of the modern control methods. The first approach enables speed estimation which is independent of parameter variations in the machine. The accuracy of all the schemes that belong to the second group is however strongly affected by parameter variations. The impact of iron loss on operation of vector controlled induction machines has been recently examined in detail for the drives that do posses a speed sensor. The aim of this paper is to examine the impact of iron loss on accuracy of speed estimation in sensorless rotor flux oriented induction machines. The scheme elaborated in the paper is the well-known MRAC based method that relies on the mathematical model of an induction machine. Error in speed estimation is evaluated on the basis of experimentally identified iron loss for a particular machine in the speed range from zero up to twice the rated speed, in steady-state operation. It is shown that the omission of iron loss representation in the speed estimator leads to a typical speed estimation error of two to three rpm in the base speed region (for a four pole 50 Hz machine) and that the speed estimation error increases in the field-weakening region, reaching eleven rpm at twice the rated speed with rated torque command. The results of the paper show that the speed estimation error due to iron loss is comparable with speed estimation errors due to other parameter variation effects.**

I. INTRODUCTION

Numerous methods of sensorless vector control of induction machines have been developed recently and excellent reviews are available in [1-5]. In general, all the existing methods can be classified into two groups. The first one encompasses all the techniques that estimate rotor speed from stator current spectrum [6-11], most frequently on the basis of rotor slot and eccentricity harmonics or saturation induced saliencies, using either FFT spectrum estimation techniques or non-FFT parametric algorithms. The common feature of all the methods that belong to this group is that speed estimation is insensitive with respect to parameter variation effects, as speed estimation is in general not based on mathematical model of an induction machine. Consequently, existence of iron loss in the machine (which is neglected in the design of the control system) does not affect accuracy of speed estimation.

The second group of speed sensorless vector control methods encompasses all the schemes in which speed estimation relies on utilisation of induction machine's mathematical model [12-25]. The most frequently utilised control approaches appear to be model reference adaptive control (MRAC) [1-4,12-18], full-order non-linear observers with current error minimisation [1-5,19-21] and extended Kalman filter [1,3,5,22]. As mechanical sub-systems of the control part of the drive and of the machine itself are in any sensorless drive effectively decoupled, and as the methods of this group utilise standard d-q axis constant parameter induction machine model, accuracy of speed estimation strongly depends on parameter variation effects in the machine. Impact of rotor resistance (time constant) variation, stator resistance variation, magnetising inductance variation and total leakage inductance variation have been studied in detail in a number of papers for different speed estimation schemes [3,5,14,16-18,21,23,24]. Furthermore, a number of sensorless schemes employ an on-line identification of stator resistance [19], rotor resistance (time constant) [4,20], or of both stator resistance and rotor time constant [14,18]. Typical steady-state speed estimation errors due to variation of motor parameters are examined in detail in [17] for a 4 kW, 50 Hz, 4-pole induction machine with MRAC based speed estimator. It is shown that 10% variation in rotor resistance and 10% variation in total leakage inductance cause a speed independent speed estimation error of approximately 5 rpm and 2.5 rpm, respectively. Speed estimation errors due to 10% variation in magnetising inductance and 10% variation in stator resistance are speed dependent, have a maximum of approximately 4 rpm and 3 rpm, respectively, in the very low speed region and approach in both cases zero as speed increases. A similar study in [5,21] concludes that 20% variation of rotor resistance causes a 10 rpm speed estimation error at all speeds, while a 20% variation in stator resistance causes a speed estimation error of 10 rpm in very low speed region that gradually decreases towards zero as speed increases.

Iron loss as a source of speed estimation error in sensorless vector controlled induction machines has not been dealt with in the past. Indeed, iron loss as a source of detuned operation of vector controlled induction machines was the last of the parameter variation effects to attract

0-7803-3932-0

attention [26,27]. All the available studies are applicable only to vector controlled induction machines that have a speed (position) sensor. Presence of the speed sensor forces actual and commanded rotor speeds, as well as actual and commanded slip speeds to be mutually equal in steady-state operation, so that detuning due to iron loss manifests itself predominantly in an orientation angle error [26,27]. The situation in a sensorless drive is however quite different. As speed is estimated rather than measured, actual and estimated rotor speeds and actual and estimated slip speeds are not necessarily mutually equal. The aim of this paper is to evaluate speed estimation error that will take place in a sensorless rotor flux oriented (RFO) induction machine in steady-state operation purely due to the existence of the iron loss in the machine, the iron loss being neglected in the speed estimator and in the control system.

Indirect rotor flux oriented current-fed induction machine is studied in the paper and speed estimator is taken in the form proposed in [12]. Iron loss is represented with an equivalent iron loss resistance, as suggested in [26], and this resistance is identified experimentally using the procedure of [27] over the frequency range from zero up to twice the rated frequency. Speed estimation error due to iron loss is studied in the speed region from zero up to twice the rated speed for a 4 kW, 50 Hz, 4-pole machine whose data are given in Appendix. Finally, applicability of the results of the study to other schemes of sensorless rotor flux oriented control is briefly discussed.

II. Sensorless RFO Induction Machine

Structure of the sensorless RFO induction machine, analysed in the paper, is shown in Fig. 1. The current controlled PWM inverter is assumed to be ideal (i.e., reference and actual phase currents are equal) and steady-state operation is discussed only. Mathematical modelling, presented in Section III, is performed in the reference frame firmly attached to the commanded rotor flux space vector. Rotor flux reference is constant and equal to rated in the base speed region. In field weakening rotor flux reference is assumed to decrease inversely proportionally to the commanded rotor speed. Coefficients C_1 and C_2 are constant in the base speed region and they change in the field weakening inversely proportionally to the rotor flux command. The speed estimator of Fig. 1 is shown in Fig. 2, [12]. It relies on measurement of stator currents and voltages, utilises principles of MRAC, and the two left-hand side blocks perform integration of equations (1) and (2). Speed estimator most frequently operates in the stationary reference frame. The speed estimator is described in stationary reference frame with the following equations:

$$\frac{d\underline{\psi}_r^{(1)}}{dt} = \frac{L_r}{L_m}\left[\underline{v}_s - (R_s + \sigma L_s p)\underline{i}_s\right] \tag{1}$$

$$\frac{d\underline{\psi}_r^{(2)}}{dt} = \left(j\omega - \frac{1}{T_r}\right)\underline{\psi}_r^{(2)} + \frac{L_m}{T_r}\underline{i}_s \tag{2}$$

$$\varepsilon = \psi_{\alpha r}^{(2)}\psi_{\beta r}^{(1)} - \psi_{\beta r}^{(2)}\psi_{\alpha r}^{(1)} \tag{3}$$

Induction machine is represented with the dynamic space vector equivalent circuit which in arbitrary reference frame has the form shown in Fig. 3, [26]. Induction machine

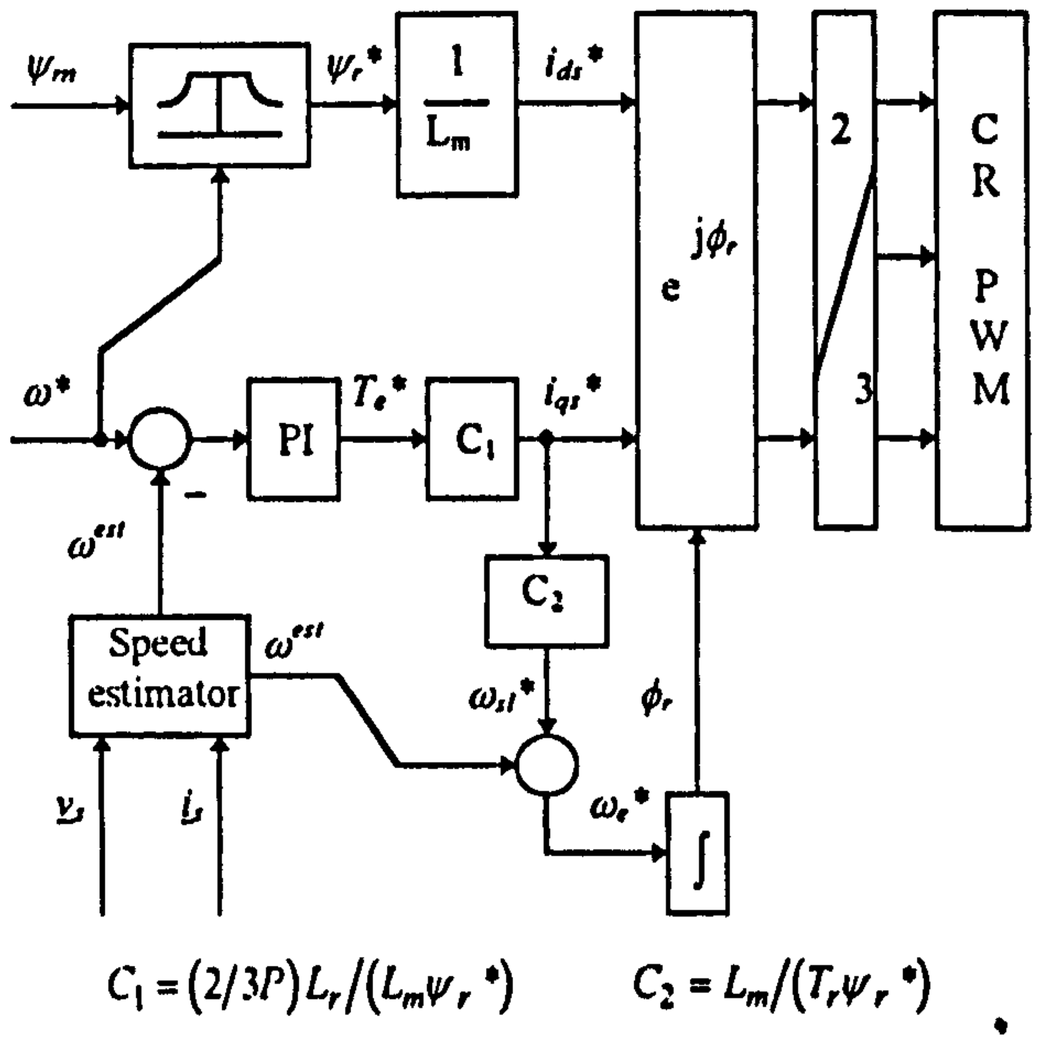

Fig. 1. Structure of the speed sensorless rotor flux oriented induction machine.

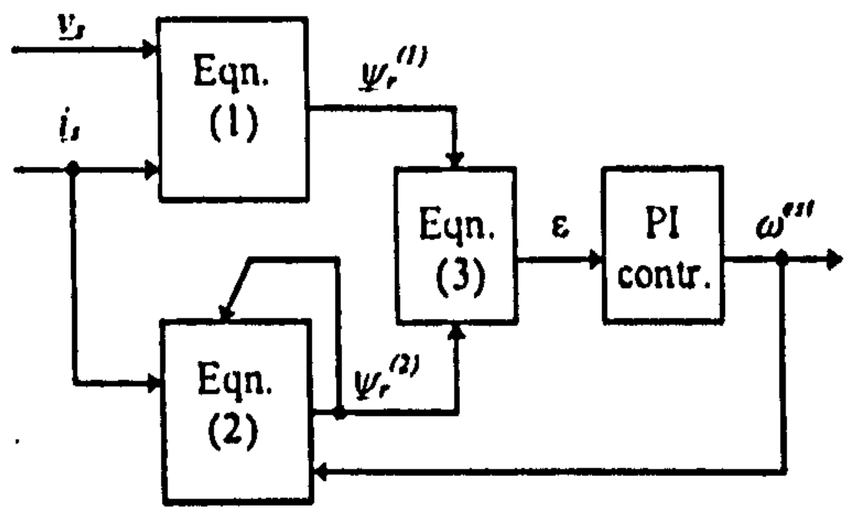

Fig. 2: MRAC based rotor speed estimator.

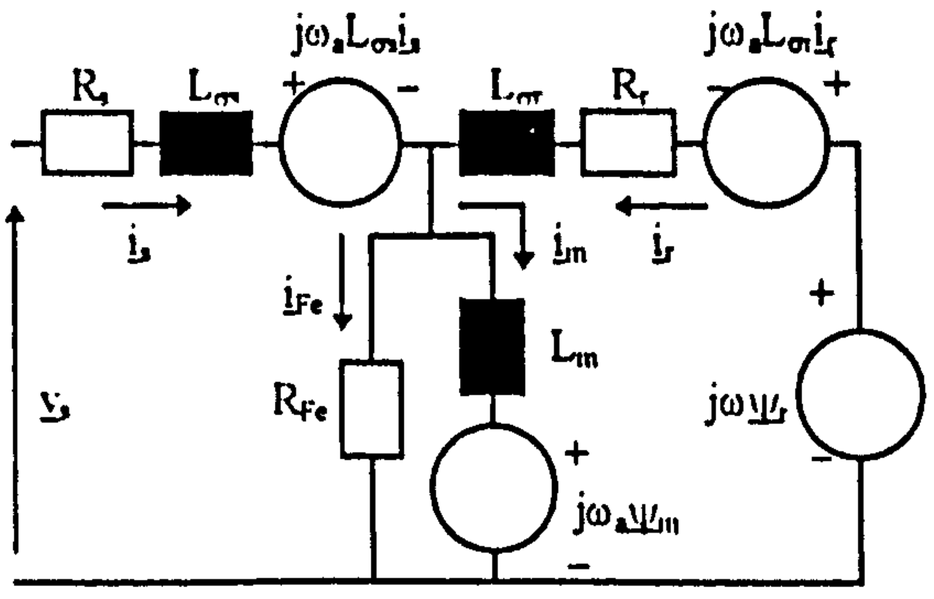

Fig. 3. Space vector dynamic equivalent circuit of an induction machine with included iron loss representation.

model, in contrast to the speed estimator and control system, accounts for the iron loss. Equivalent iron loss resistance in Fig. 3 is a frequency dependent parameter, identified using the experimental procedure described in [27] in the frequency range from zero up to twice the rated frequency. Its variation with frequency is shown in Fig. 4.

III. Modelling and Analysis of the Drive

A. Induction Machine Model

The complete analysis of the drive is performed in the reference frame firmly attached to the commanded rotor flux space vector. Therefore ω_a in induction machine model, Fig. 3, equals ω_e^* of Fig. 1. Moreover, due to idealised inverter representation, stator d-q axis current commands are equal to the machine d-q axis currents. Steady-state operation of the machine may under these conditions be described with the following set of equations, obtainable from Fig. 3:

$$\begin{aligned} v_{ds} &= R_s i_{ds}^* - \omega_e^* L_{\sigma s} i_{qs}^* - \omega_e^* L_m i_{qm} \\ v_{qs} &= R_s i_{qs}^* + \omega_e^* L_{\sigma s} i_{ds}^* + \omega_e^* L_m i_{dm} \end{aligned} \tag{4}$$

$$\begin{aligned} L_m i_{dm} &= \psi_{dr} - \omega_{sl} T_{\sigma r} \psi_{qr} \\ L_m i_{qm} &= \psi_{qr} + \omega_{sl} T_{\sigma r} \psi_{dr} \end{aligned} \tag{5}$$

$$\begin{aligned} -\omega_e^* T_{Fe} i_{qm} &= i_{ds}^* + \psi_{dr}/L_{\sigma r} - i_{dm} L_r/L_{\sigma r} \\ \omega_e^* T_{Fe} i_{dm} &= i_{qs}^* + \psi_{qr}/L_{\sigma r} - i_{qm} L_r/L_{\sigma r} \end{aligned}$$

$$\begin{aligned} T_e &= (3P/2)(L_m/L_{\sigma r})(\psi_{dr} i_{qm} - \psi_{qr} i_{dm}) \\ \omega_e^* &= \omega + \omega_{sl} \; . \end{aligned} \tag{6}$$

Time constants utilised in (5) are defined as $T_{Fe} = L_m / R_{Fe}$ and $T_{\sigma r} = L_{\sigma r} / R_r$.

Inspection of equations (4)-(5) shows that there are six equations that contain seven unknowns (stator voltage, magnetising current and rotor flux d-q axis components, plus angular slip frequency). Thus it is not possible to solve this system of equations without determining which of the seven variables is only apparently unknown. As shown in the next sub-section, speed estimator pre-determines stator d-axis voltage so that system of equations becomes solvable.

B. Analysis of the Speed Estimator

In any steady-state operation, assuming ideal sinusoidal conditions, rotor flux estimates of (1) and (2) are given in commanded reference frame with

$$\begin{aligned} \underline{\psi}_r^{(1)} &= -j \frac{L_r}{\omega_e^* L_m} \left[\underline{v}_s - \left(R_s + j\omega_e^* \sigma L_s \right) \underline{i}_s^* \right] \\ \underline{\psi}_r^{(2)} &= \frac{L_m}{T_r} \underline{i}_s^* \frac{1}{1/T_r + j\left(\omega_e^* - \omega^{est} \right)} \; . \end{aligned} \tag{7}$$

Due to the presence of the PI controller in the speed control loop estimated and commanded (reference) speed are equal. Similarly, PI controller in the speed estimator of Fig. 2 imposes the constraint that $\varepsilon = 0$ in steady-state. This means that instantaneous positions of the two rotor flux estimates with respect to the fixed stator axis are equal, i.e.

$$\phi_r^{(1)} = \phi_r^{(2)} = \phi_r \; . \tag{8}$$

However, the rotor speed estimator does not require that magnitudes of the two rotor flux estimates are the same. Hence, in rotor flux oriented reference frame determined with the transformation angle (8), rotor flux estimates are

$$\begin{aligned} \underline{\psi}_r^{(2)} &= \psi_{dr}^{(2)} + j\psi_{qr}^{(2)} \qquad \psi_{dr}^{(2)} = \psi_r^* \qquad \psi_{qr}^{(2)} = 0 \\ \underline{\psi}_r^{(1)} &= \psi_{dr}^{(1)} + j\psi_{qr}^{(1)} \qquad \psi_{dr}^{(1)} \neq \psi_r^* \qquad \psi_{qr}^{(1)} = 0 \; . \end{aligned} \tag{9}$$

It follows from (9) that rotor flux q-axis component in the commanded reference frame must equal zero for both flux estimates. However, d-axis component of the first estimate is not necessarily equal to the commanded rotor flux (the magnitude of the second flux estimate is by default equal to the rotor flux reference). If the q-axis component of the first rotor flux estimate is expressed from (7) and equated to zero (in the commanded rotor flux reference frame), d-axis component of the stator voltage is calculated as equal to

$$v_{ds} = R_s i_{ds}^* - \omega_e^* \sigma L_s i_{qs}^* \; . \tag{10}$$

Equation (10) is the well known stator voltage d-axis equation, valid under the correct rotor flux orientation conditions (with neglected iron loss). The speed estimator forces stator d-axis voltage to be equal to the one required for perfect rotor flux orientation. However, as the estimator does not force equality of magnitudes of rotor flux estimates, stator q-axis voltage will deviate from the one required for perfect rotor flux orientation.

As stator d-axis voltage is known, it is now possible to solve the model of the machine described with (4)-(5). Magnetising current q-axis component follows directly from the first equation of (4) and hence its value is known for

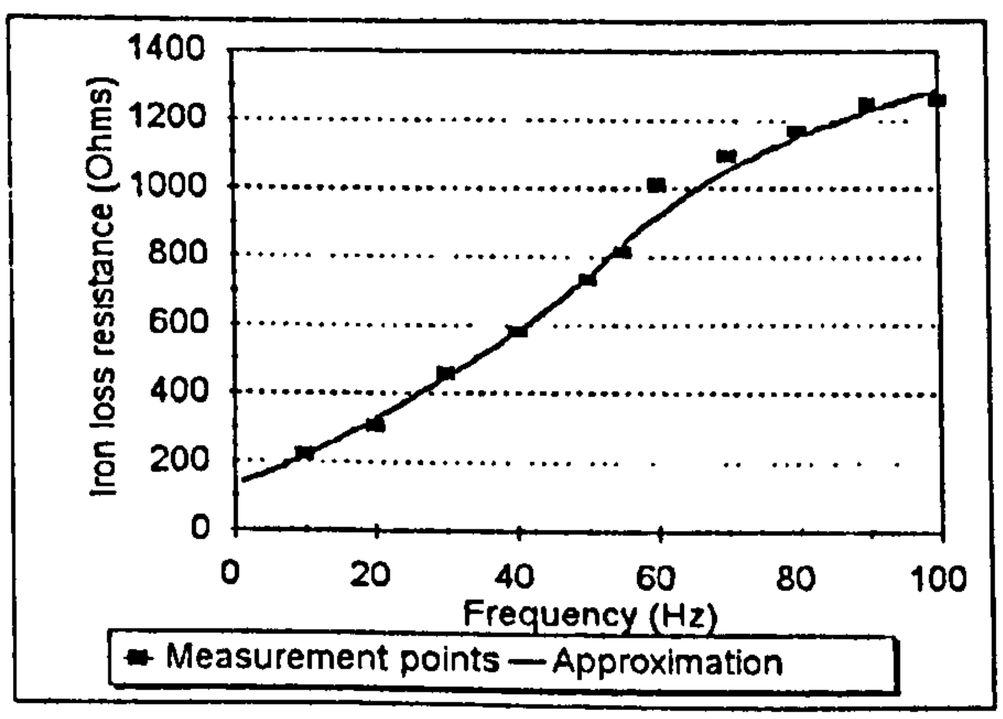

Fig. 4. Equivalent iron loss resistance identified experimentally.

specified operating conditions. An expression for q-axis magnetising current as function of actual angular slip frequency may be derived from (5). The actual angular slip frequency can then be found numerically by forcing q-axis magnetising current to the value obtained from the first equation of (4).

C. Analysis of the Control System

The independent inputs into the control system are commanded (reference) speed and reference rotor flux. The output of the PI speed controller is reference torque, whose value is in general unknown. However, for each value of the torque command there is a corresponding value of the actual torque, determined with (6). Hence it is possible to regard torque command as an independent input. By solving the equations (4)-(6), value of the actual torque that corresponds to the given torque command can be determined. Such an approach is utilised in simulation procedure whose results are presented in the next section: independent inputs are speed, torque and rotor flux commands (references).

The additional constraint imposed by the control system is

$$\omega_e^* = \omega^* + \omega_{sl}^* \quad . \tag{11}$$

as estimated and reference speed are equal. The error in speed estimation, that is to be discussed in the next section, is defined in mechanical rpm as

$$\Delta n = n - n^* \equiv n - n^{est} \equiv n_{sl}^* - n_{sl} \quad . \tag{12}$$

IV. Speed Estimation Error and Other Detuning Effects

Impact of iron loss on behaviour of the drive is at first studied for constant speed operation, as function of the commanded torque (which is given in p.u., normalised with respect to the rated torque of 26.5 Nm). Figure 5 shows speed estimation error for three values of the reference speed, namely one fifth of the rated, rated and twice the rated. Figure 6 depicts ratio of actual to commanded torque under the same conditions. Speed estimation error is from Fig. 5 load-dependent and it increases as loading is increased. Speed estimation error appears to be typically two to three rpm for operation at rated speed, for commanded torques up to the rated. Speed estimation error is smaller at lower speeds, typically 1.5 to 2 rpm at one fifth of the rated speed for variation of the torque command from zero up to the rated torque value. If the machine is operated in the field-weakening, speed estimation error may significantly increase, reaching 11 rpm for operation at twice the rated speed with rated torque command. Maximum of torque ratio error is always at low torque commands and, as the torque command increases, error in the torque ratio decreases.

Speed estimation error and torque ratio are further examined with commanded speed taken as independent

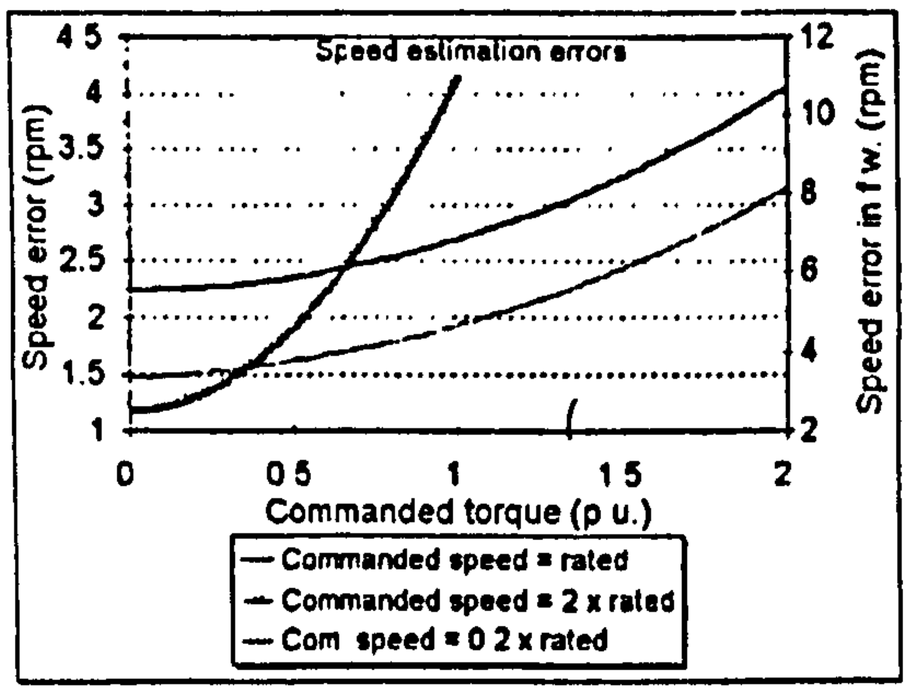

Fig. 5. Speed estimation error as function of commanded torque for operation with constant speed command.

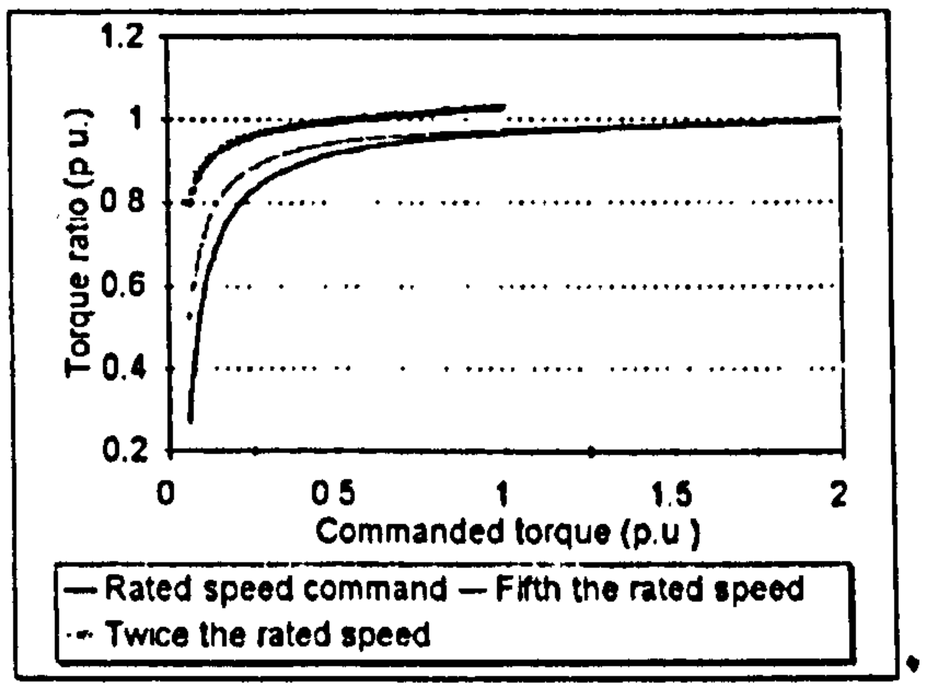

Fig. 6. Actual to commanded torque ratio against commanded torque for constant speed command operation.

variable (normalised with respect to the rated speed of 1448 rpm) and with commanded torque set to a constant value in the base speed region. For operation in the field-weakening region torque command is reduced inversely proportionally to the speed so that constant power operation is obtained. Results are summarised in Fig. 7: speed estimation error and torque ratio are shown as functions of the p.u. commanded speed, with commanded torque (power) as the parameter.

Typical error that may be expected in speed estimation in the base speed region appears to be from Fig. 7 two to three rpm, except at very low speeds. Speed estimation error increases in the field-weakening region, approaching five rpm at twice the rated speed with rated power command. Error in torque ratio strongly depends on the torque command and is in general higher when the load is lighter.

As already pointed out, impact of iron loss on operation of a vector controlled induction machine with speed (position) sensor is manifested in an error in orientation angle, which is typically of the order of a few degrees [26,27]. It is interesting to note that in a sensorless drive error in orientation angle is negligibly small. Thus the major consequence of the iron loss is the error in speed estimation. This consideration is confirmed in Fig. 8 where orientation

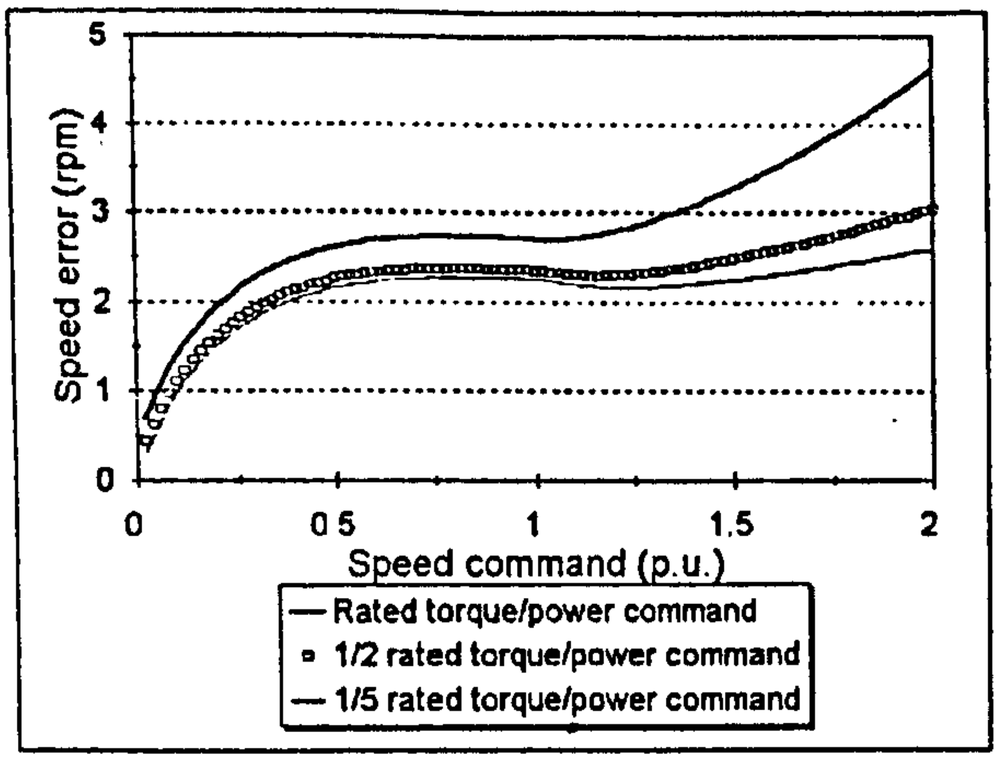

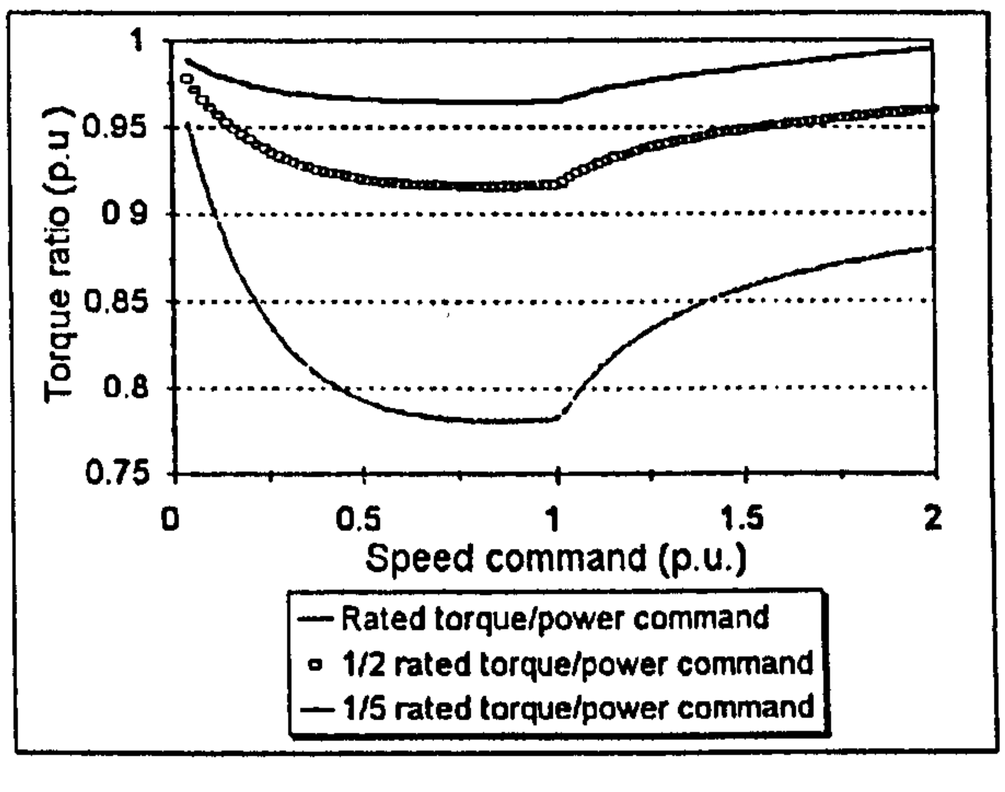

Fig. 7. Speed estimation error and torque ratio against commanded (estimated) p.u. speed.

angle error is shown for the same conditions that apply to Fig. 7. Orientation angle error appears to be under all operating conditions less than 0.2 degrees.

Error in rotor flux magnitude is extremely small. For operation in the base speed region actual rotor flux in the machine exceeds commanded rotor flux by less than 1% for all the operating points shown in Fig. 7. Maximum error appears for operation with rated speed and rated torque command, when ratio of actual to commanded rotor flux equals 1.0092. The error in rotor flux increases in the field-weakening region and is up to 2% for operating regimes studied in Fig. 7. For example, for operation with rated power at twice the rated speed flux ratio equals 1.02, while in operation at twice the rated speed with one half of the rated power command flux ratio is 1.01.

Magnitude of the rotor flux in the machine exactly equals magnitude of the first rotor flux estimate, described with (7), (9). This consideration confirms that the inequality given in (9) holds true, i.e. that the speed estimator operation is such that magnitude of the second rotor flux estimate (adaptive model) exactly equals rotor flux command, while magnitude of the first rotor flux estimate (reference model) differs from the rotor flux command.

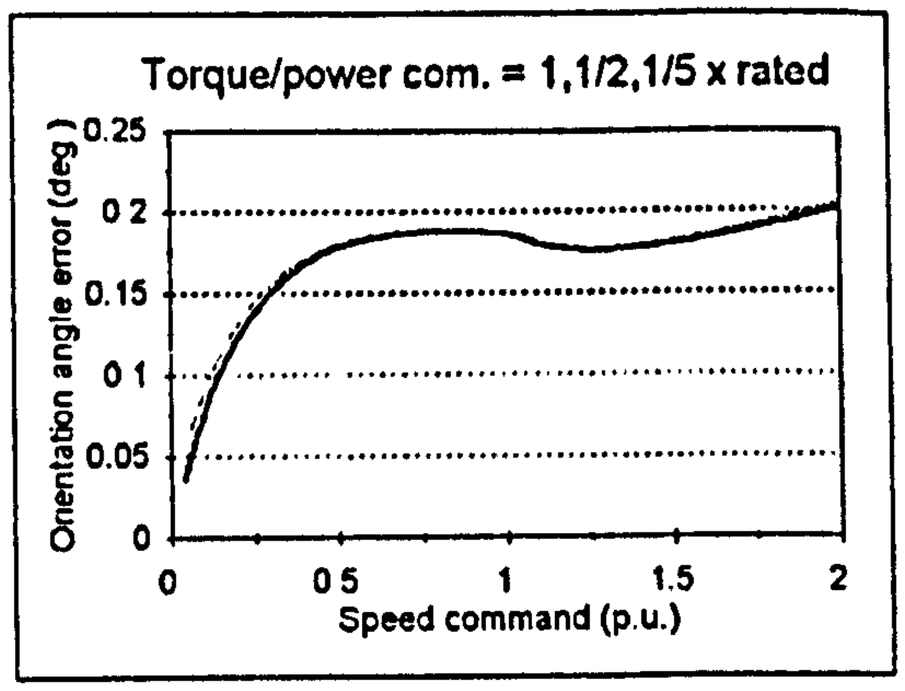

Fig. 8. Orientation angle error due to iron loss in the sensorless rotor flux oriented induction machine.

V. Discussion

The impact of iron loss on speed estimation is analysed for a specific configuration of the drive, that consist of current-fed indirect rotor flux oriented induction machine and MRAC based speed estimator. However, the applicability of results is broader and more or less the same detuning effects can be expected in majority of sensorless vector controlled induction machines. The following clarifies this claim.

Although feed-forward indirect rotor flux oriented control is analysed, the same results are obtained if angular slip frequency and rotor flux magnitude are calculated on the basis of measured stator currents and estimated rotor speed and the control system includes a flux controller.

Speed estimator imposes a constraint on the value of the stator d-axis voltage. The estimator elaborated here is MRAC based, and it forces instantaneous angular position of the two flux estimates to be equal. A number of other speed estimators, based on MRAC, operate utilising the same principle [13-17] although various other quantities are employed instead of the rotor flux. As long as the speed estimator is based on MRAC, and the angles of the two quantities (be it rotor flux or something else) obtained from reference and adaptive model are forced to be equal, the results of this paper remain valid.

As the speed estimator structure has decisive impact on behaviour of the drive, it is not possible to generalise results of this paper to other sensorless schemes, based for example on observers or on extended Kalman filter. However, it is to expect that the iron loss induced speed estimation error will be similar. Indeed, it is interesting to note that experimental results presented in [22,23] for two non-MRAC based systems in steady-state operation show that the actual speed under tuned conditions is slightly higher than the commanded and that the difference tends to increase as load torque increases. It is impossible to state that this error is due to neglected iron loss without detailed consideration of the drive; however, the amounts of and trends in speed error are the same as those observed here due to iron loss.

VI. Conclusion

The paper discusses impact of iron loss on operation of a sensorless rotor flux oriented induction machine. Experimentally identified equivalent iron loss resistance is used to evaluate speed estimation error and other detuning effects caused by omission of iron loss representation in the speed estimator and in the control system. Although a feed-forward indirect current-fed rotor flux oriented induction machine is analysed, the results are applicable for much broader class of sensorless vector control schemes.

Iron loss causes an error in speed estimation. The actual speed is always higher than commanded. Speed error is load dependent and increases with increase in the loading. The error is typically two to three rpm for a 4 kW, 4-pole, 50 Hz machine in the base speed region and it increases in the field-weakening region up to eleven rpm for operation at twice the rated speed with twice the rated power command. Torque ratio deviates from unity and the error is high at light loads. Orientation angle error is negligibly small.

Speed estimation error due to iron loss is relatively substantial. It is of the same order as are the errors due to other parameter variatiion effects. It may be therefore concluded that iron loss should be compensated in a sensorless rotor flux oriented induction machine.

VII. Appendix: Induction Motor Data

4 kW 380 V 50 Hz 2P = 4 star 8.7 A

$T_{en} = 26.526$ Nm $n_n = 1448$ rpm

$R_s = 1.37\ \Omega$ $R_r = 1.1\ \Omega$

$X_{\sigma s} = 1.53\ \Omega$ $X_{\sigma r} = 2.5\ \Omega$ $X_m = 44.3\ \Omega$

$P_{Fen} = 4.7\% P_n$

$$R_{Fe} = \begin{cases} 128.92 + 8.242f + 0.07788f^2 & f < 50 \text{ Hz} \\ 1841 - 55275/f & f > 50 \text{ Hz} \end{cases}$$

VIII. References

[1] J.Holtz "State of the art of controlled AC drives without speed sensors," *Int. J. Electronics*, vol. 80, no. 2. 1996, pp. 249-263.

[2] A.M. Trzynadlowski, *The field orientation principle in control of induction motors*, Norwell, MA: Kluwer Academic Publishers, 1994.

[3] C.Ilas, A.Bettini, L.Ferraris, G.Griva and F.Profumo, "Comparison of different schemes without shaft encoders for field oriented control drives," in *Conf. Rec. IEEE IECON'94*, Bologna, Italy, 1994, pp. 1579-1588.

[4] Tung-Hai Chin, "Approaches for vector control of induction motor without speed sensor," in *Conf. Rec. IEEE IECON'94*, Bologna, Italy, 1994, pp. 1616-1620.

[5] H.Kubota and K.Matsuse, "Speed sensorless field oriented control of induction machines using flux observers," in *Conf. Rec. IEEE IECON'94*, Bologna, Italy, 1994, pp. 1611-1615.

[6] A.Ferrah, K.J.Bradley and G.M.Asher, "An FFT-based novel approach to noninvasive speed measurement in induction motor drives," *IEEE Trans. on Instrumentation and Measurement*, vol. 41, no. 6, 1992, pp. 797-802.

[7] R.Blasco-Gimenez, G.M.Asher, M.Sumner and K.J. Bradley, "Performance of FFT-rotor slot harmonic speed detector for sensorless induction motor drives," *IEE Proc., Pt. B*, vol. 143, no. 3, 1996, pp. 258-268.

[8] K.D Hurst and T.G.Habetler, "Sensorless speed measurement using current harmonic spectral estimation in induction machine drives," *IEEE Trans. on Power Electronics*, vol. 11, no. 1, 1996, pp. 66-73.

[9] P.L.Jansen and R.D Lorenz, "Transducerless position and velocity estimation in induction and salient AC machines," *IEEE Trans. on Industry Applications*, vol. 31, no. 2, 1995, pp. 240-247.

[10] K.D.Hurst and T.G.Habetler, "A comparison of spectrum estimation techniques for sensorless speed detection in induction machines," in *Proc. IEEE Ind. App. Soc. Ann. Meet.*, Orlando, 1995, pp. 553-559.

[11] P.L.Jansen and R.D.Lorenz, "Transducerless field orientation concepts employing saturation-induced saliencies in induction machines," in *Conf. Rec. IEEE Ind. App. Soc. Annual Meeting*, Orlando, FL, 1995, pp. 174-181.

[12] C.Schauder, "Adaptive speed identification for vector control of induction motors without rotational transducers," *IEEE Trans. on Industry Applications*, vol. 28, no. 5, 1992, pp. 1054-1061.

[13] F.Z.Peng and T.Fukao, "Robust speed identification for speed-sensorless vector control of induction motors," *IEEE Trans. on Industry Applications*, vol. 30, no. 5, 1994, pp. 1234-1240.

[14] L.Zhen and L.Xu, "A mutual MRAS identification scheme for position transducerless field orientation control of induction machines," in *Conf. Rec. IEEE Ind. App. Soc. Annual Meeting*, Orlando, FL, 1995, pp. 159-165.

[15] M.H.Kim and J.C.Hung, "Vector control system for induction motor without speed sensor at very low speed," in *Conf. Rec. IEEE IECON'95*, Orlando, FL, 1995, pp. 524-529.

[16] H.Tajima and Y.Hori, "Speed sensorless field-orientation control of the induction machine," *IEEE Trans. on Industry Applications*, vol. 29, no. 1, 1993, pp. 175-180.

[17] R.Blasco-Gimenez, G.M.Asher, M.Sumner and K.J.Bradley, "Dynamic performance limitations for MRAS based sensorless induction motor drives. Part 1: Stability analysis for the closed loop drive," *IEE Proc. - Electr. Power Appl.*, vol. 143, no. 2, 1996, pp. 113-122.

[18] R.Blasco-Gimenez, G.M.Asher, M.Sumner and K.J.Bradley, "Dynamic performance limitations for MRAS based sensorless induction motor drives. Part 2: On-line parameter tuning and dynamic performance studies," *IEE Proc. - Electr. Power Appl.*, vol. 143, no. 2, 1996, pp. 123-134.

[19] G.Yang and T.H Chin, "Adaptive-speed identification scheme for a vector-controlled speed sensorless inverter-induction motor drive," *IEEE Trans. on Industry Applic.*, vol. 29, no. 4, 1993, pp. 820-825.

[20] H.Kubota and K.Matsuse, "Speed sensorless field-oriented control of induction motor with rotor resistance adaptation," *IEEE Trans. on Industry Applications*, vol. 30, no. 5, 1994, pp. 1219-1224.

[21] H.Kubota, K.Matsuse and T.Nakano, "DSP-based speed adaptive flux observer of induction motor," *IEEE Trans. on Industry Applications*, vol. 29, no. 2, 1993, pp. 344-348.

[22] Y.R.Kim, S.K.Sul and M.H.Park, "Speed sensorless vector control of induction motor using extended Kalman filter," *IEEE Trans. on Industry Applications*, vol. 30, no. 5, 1994, pp. 1225-1233.

[23] T.Ohtani, N.Takada and K.Tanaka, "Vector control of induction motor without shaft encoder," *IEEE Trans. on Industry Applications*, vol. 28, no. 1, 1992, pp. 157-164.

[24] C.J.Bonano, L.Xu and X.Xu, "Robust, parameter insensitive position sensorless field orientation control of the induction machine," in *Conf. Rec. IEEE PESC'94*, Taipei, Taiwan, 1994, pp. 752-757.

[25] C.J.Bonnano, L.Zhen and L.Xu, "A direct field oriented induction machine drive with robust flux estimator for position sensorless control," in *Conf. Rec. IEEE Ind. App. Soc. Ann. Meeting*, Orlando, FL, 1995, pp. 166-173.

[26] E.Levi, "Impact of iron loss on behaviour of vector controlled induction machines," *IEEE Trans. on Industry Applications*, vol. 31, no. 6, 1995, pp. 1287-1296.

[27] E Levi, M.Sokola, A.Boglietti and M Pastorelli, "Iron loss in rotor flux oriented induction machines: identification, assessment of detuning and compensation," *IEEE Trans. on Power Electronics*, vol. 11, no. 5, 1996, pp. 698-709.

Power Electronics & VARIABLE SPEED DRIVES

Seventh International Conference on

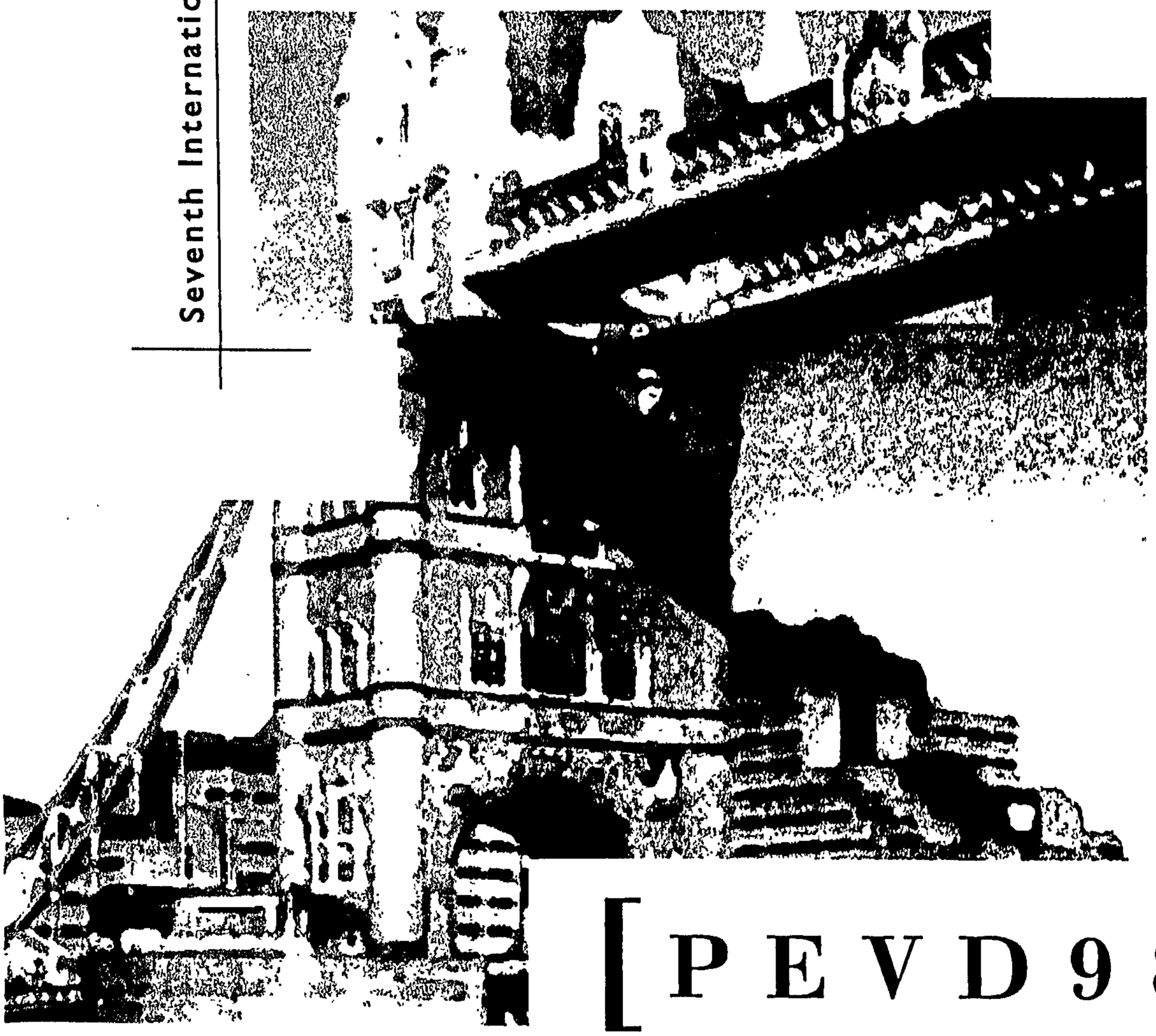

[PEVD 98]

IEE

Conference Publication No. 456

IMPACT OF PARAMETER VARIATIONS ON SPEED ESTIMATION IN SENSORLESS ROTOR FLUX ORIENTED INDUCTION MACHINES

E.Levi, M.Wang

Liverpool John Moores University, UK

INTRODUCTION

Numerous methods of sensorless vector control of induction machines are nowadays available, Rajashekara et al. [1]. Vast majority of the methods rely in the process of speed estimation on utilisation of the induction machine model. As mechanical sub-systems of the control part of the drive and of the machine itself are in any sensorless drive effectively decoupled, and as standard d-q axis constant parameter induction machine model is utilised, accuracy of speed estimation strongly depends on parameter variation effects in the machine. One of the most frequently applied control approaches appears to be model reference adaptive control (MRAC), originally introduced by Tamai et al [2] and further developed by Schauder [3], which is characterised by relatively simple implementation requirements. This is the technique analysed in this paper, in conjunction with indirect feed-forward rotor flux oriented control.

MRAC based speed estimation techniques mutually differ with respect to the quantity that is selected as output of the reference and the adjustable model. The most frequent choices appear to be rotor flux, modified rotor flux and back e.m.f.. It can be shown that, assuming ideal sinusoidal supply conditions and ideal integration, all these three methods exhibit identical behaviour in steady-state operation. Thus detuning caused by parameter mismatch will be the same in steady-state operation for all these methods.

Some studies related to parameter variation effects in MRAC based sensorless drives are already available. For example, impact of rotor resistance variation on transient behaviour of the drive was studied by Ilas et al [4] and by Griva et al [5] by simulation. Effects of main flux saturation on transient behaviour were examined by El-Kholy et al [6] using simulation. Armstrong and Atkinson [7] have studied impact of rotor resistance, stator resistance and mutual inductance variation in low speed region experimentally. The only available comprehensive investigations of steady-state speed estimation errors caused by parameter variation effects appear to be works by Blasco-Gimenez et al [8] and Jansen and Lorenz [9]. However, in both cases structure of the drive dealt with is direct rotor flux oriented control that combines a MRAC based speed estimator with a closed loop flux observer and includes a mechanical system model. The validity of results in [8,9] is thus restricted to that specific drive structure.

The aim of this paper is to investigate speed estimation error and other detuning effects that will take place due to parameter variations in an indirect rotor flux oriented (RFO) induction machine. Speed estimation is performed using rotor flux based MRAC scheme and only steady-state behaviour, under ideal conditions, is dealt with. Variation of all the parameters that influence operation of the drive is considered, in order to enable a comparative insight into the relative importance of various parameter variation effects. The approach used in the study closely parallels the one developed by Levi and Wang [10] for the same drive. However, while [10] investigated only steady-state detuning caused by omission of iron loss representation in the control system and in the estimator, this paper studies all the possible sources of detuning (stator and rotor resistance variation, main flux saturation, leakage inductance variation). All the results are valid for modified rotor flux and back e.m.f. methods as well.

SENSORLESS RFO INDUCTION MACHINE

Structure of the sensorless RFO induction machine, analysed in the paper, is shown in Fig. 1. The current controlled PWM inverter is assumed to be ideal (i.e., reference and actual phase currents are equal) and steady-state operation is discussed only. Mathematical modelling, presented in the next section, is performed in the reference frame firmly attached to the reference rotor flux space vector. Rotor flux reference is constant and equal to rated in the base speed region. The speed estimator of Fig. 1 is shown in Fig. 2. It relies on measurement of stator currents and voltages, utilises principles of MRAC, and the two left-hand side blocks perform integration of equations (1) and (2). Speed estimator most frequently operates in the stationary reference frame and is described with the following space vector equations ($\sigma^* = 1 - L_m^{*2} / \left(L_s^* L_r^* \right)$):

$$\frac{d\underline{\psi}_r^{(1)}}{dt} = \frac{L_r^*}{L_m^*} \left[\underline{v}_s - \left(R_s^* + \sigma^* L_s^* p \right) \underline{i}_s \right] \qquad (1)$$

$$\frac{d\underline{\psi}_r^{(2)}}{dt} = \left(j\omega - \frac{1}{T_r^*} \right) \underline{\psi}_r^{(2)} + \frac{L_m^*}{T_r^*} \underline{i}_s \qquad (2)$$

Power Electronics and Variable Speed Drives, 21-23 September 1998, Conference Publication No. 456 © IEE 1998

$$\varepsilon = \psi_{\alpha r}^{(2)}\psi_{\beta r}^{(1)} - \psi_{\beta r}^{(2)}\psi_{\alpha r}^{(1)} \quad . \qquad (3)$$

Asterisk denotes in (1)-(2) constant values of machine parameters used in the estimator and in the controller of Fig. 1. Induction machine is represented with the dynamic space vector equivalent circuit in an arbitrary reference frame, given in Fig. 3, Sokola and Levi [11].

Actual motor parameters do not bear an asterisk. Induction machine model, in contrast to the speed

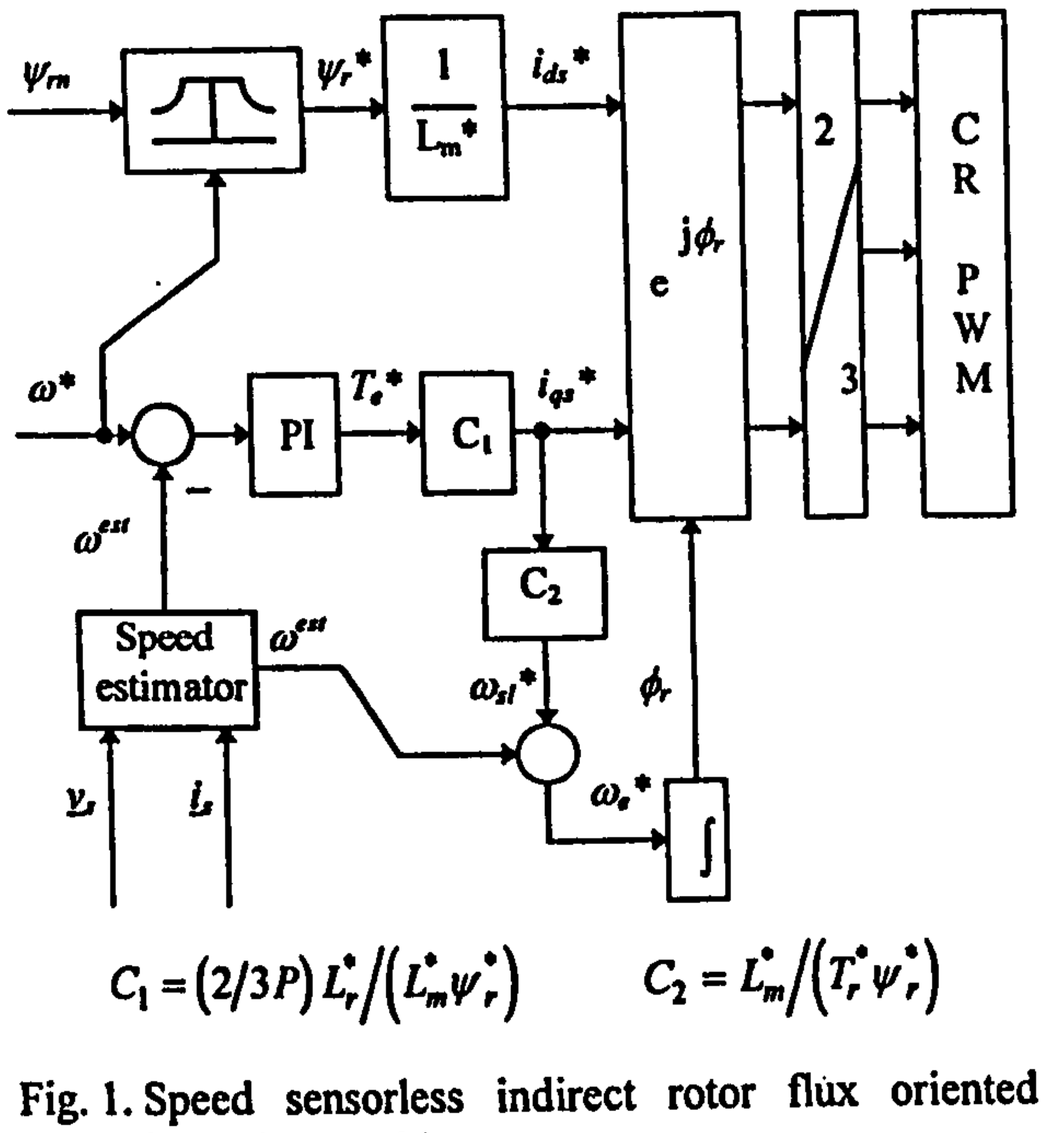

Fig. 1. Speed sensorless indirect rotor flux oriented induction machine.

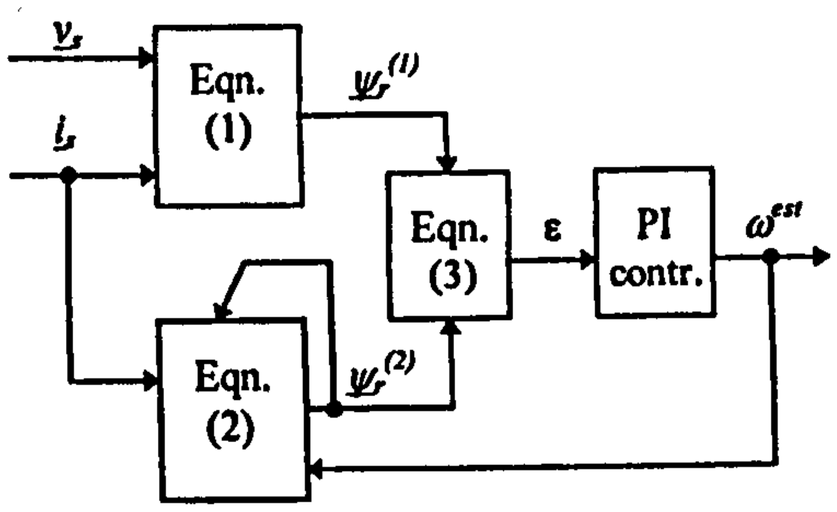

Fig. 2: MRAC based rotor speed estimator.

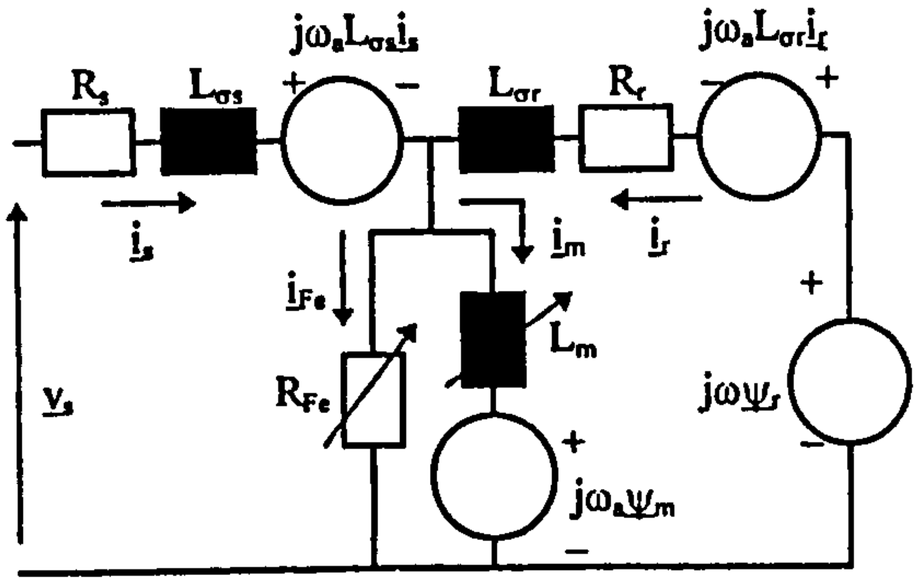

Fig. 3. Space vector dynamic equivalent circuit of an induction machine.

estimator and control system, accounts in general for both main flux saturation (magnetising inductance is a variable parameter) and the iron loss. The machine used in this study is a four-pole, 50 Hz, 4 kW induction motor. Equivalent iron loss resistance in Fig. 3 is a frequency dependent parameter and its variation with frequency is given in [11], together with the machine's magnetising curve and all the other parameters.

STEADY-STATE ANALYSIS

In any steady-state operation, assuming ideal sinusoidal conditions, ideal integration and neglecting all the delays, rotor flux estimates of (1) and (2) are given in commanded reference frame with

$$\underline{\psi}_r^{(1)} = -j\frac{L_r^*}{\omega_e^* L_m^*}\left[\underline{v}_s - \left(R_s^* + j\omega_e^*\sigma^* L_s^*\right)\underline{i}_s^*\right]$$
$$\underline{\psi}_r^{(2)} = \frac{L_m^*}{T_r^*}\underline{i}_s^*\frac{1}{1/T_r^* + j\left(\omega_e^* - \omega^{est}\right)} \quad . \qquad (4)$$

Due to the presence of the PI controller in the speed control loop estimated speed and reference speed are equal. PI controller in the speed estimator of Fig. 2 imposes the constraint that $\varepsilon = 0$ in steady-state. This means that instantaneous positions of the two rotor flux estimates with respect to the fixed stator axis are equal,

$$\phi_r^{(1)} = \phi_r^{(2)} \quad . \qquad (5)$$

However, the rotor speed estimator does not require that magnitudes of the two rotor flux estimates are the same. Hence, in rotor flux oriented reference frame determined with the transformation angle (5), rotor flux estimates are under detuned conditions given with

$$\underline{\psi}_r^{(2)} = \psi_{dr}^{(2)} + j\psi_{qr}^{(2)} \qquad \psi_{dr}^{(2)} = \psi_r^* \qquad \psi_{qr}^{(2)} = 0$$
$$\underline{\psi}_r^{(1)} = \psi_{dr}^{(1)} + j\psi_{qr}^{(1)} \qquad \psi_{dr}^{(1)} \neq \psi_r^* \qquad \psi_{qr}^{(1)} = 0 \quad . \qquad (6)$$

It follows from (6) that rotor flux q-axis component in the commanded reference frame must equal zero for both flux estimates. However, d-axis component of the first estimate is not necessarily equal to the commanded rotor flux (the magnitude of the second flux estimate is by default equal to the rotor flux reference). If the q-axis component of the first rotor flux estimate is expressed from (4) and equated to zero (in the commanded rotor flux reference frame), d-axis component of the stator voltage is calculated as equal to

$$v_{ds} = R_s^* i_{ds}^* - \omega_e^*\sigma^* L_s^* i_{qs}^* \quad . \qquad (7)$$

Equation (7) is the well known stator voltage d-axis equation, valid under the correct rotor flux orientation conditions. The speed estimator forces stator d-axis voltage to be equal to the one required for perfect rotor flux orientation. However, as the estimator does not force equality of magnitudes of rotor flux estimates,

stator q-axis voltage deviates under detuned conditions from the one required for perfect rotor flux orientation.

Induction machine steady-state model follows directly from Fig. 3, with $\omega_a = \omega_e^*$ of Fig. 1. The model is given in [10]. As stator d-axis voltage is known, it is possible to solve the model of the machine numerically for any given operating conditions and for any given sets of motor and controller/estimator parameters [10].

The independent inputs in the control system of Fig. 1 are reference speed and reference rotor flux. The output of the PI speed controller is reference torque, whose value is in general unknown. However, for each value of the torque command there is a corresponding value of the actual torque. Hence it is possible to regard torque command as an independent input. By solving the motor equations, value of the actual torque that corresponds to the given torque reference can be determined. Such an approach is utilised in simulation procedure whose results are presented in the next section: independent inputs are speed, torque and rotor flux references.

The additional constraint imposed by the control system is

$$\omega_e^* = \omega^* + \omega_{sl}^* \quad . \tag{8}$$

as estimated and reference speed are equal. The error in speed estimation, that is to be discussed in the next section, is defined in mechanical rpm as

$$\Delta n = n - n^* \equiv n - n^{est} \equiv n_{sl}^* - n_{sl} \quad . \tag{9}$$

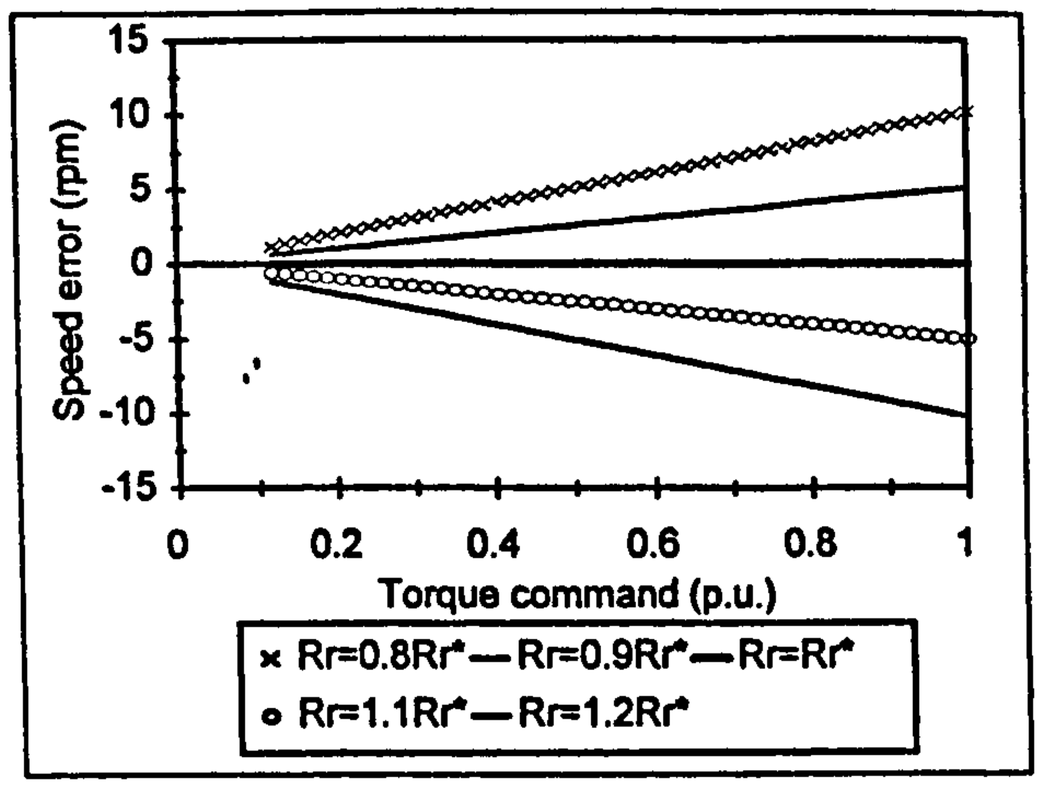

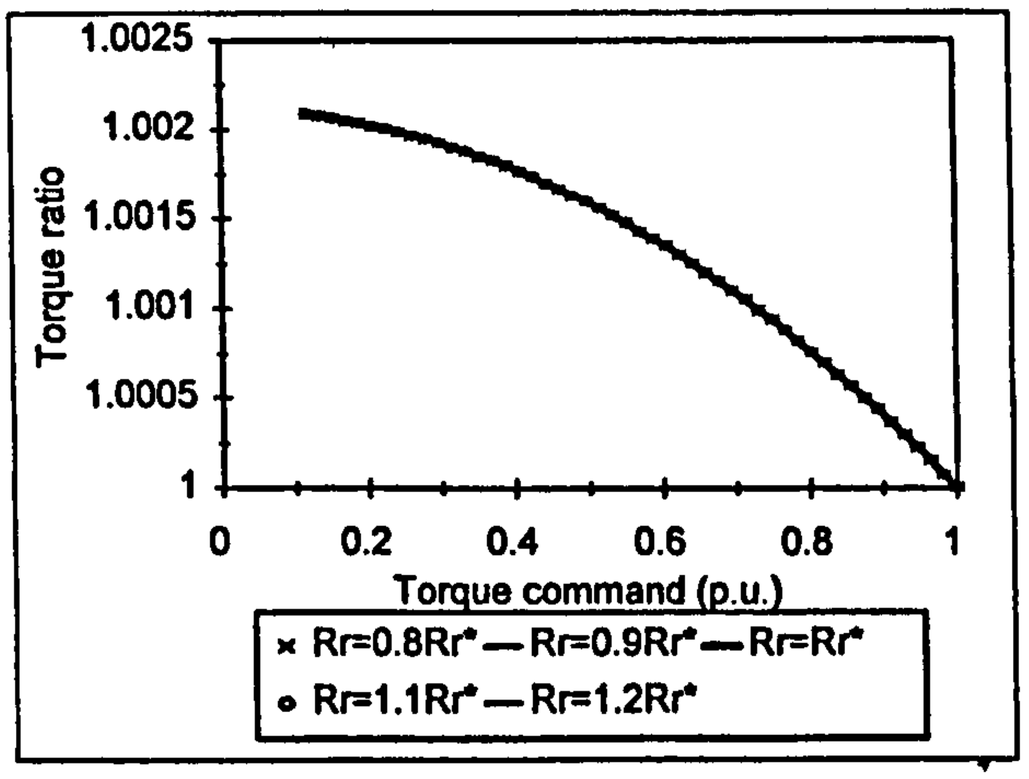

Fig. 4. Effects of incorrect value of the rotor resistance.

SPEED ESTIMATION ERROR AND OTHER DETUNING EFFECTS

Main flux saturation is accounted for in the induction machine model of Fig. 3 in all the studies whose results are presented in what follows. Iron loss is neglected unless stated otherwise. Detuning is characterised with speed estimation error of (9) and with ratio of actual torque (which equals load torque) to the reference torque. Detuning due to incorrect initial setting or variation of rotor resistance, stator and rotor leakage inductances, and main flux saturation is speed independent (with iron loss neglected). Detuning due to incorrect setting or variation of the stator resistance and detuning due to iron loss is speed dependent. Detuning in base speed region is elaborated.

Incorrect rotor resistance value

Figure 4 displays speed estimation error and torque ratio as function of the torque command for discrepancies between actual rotor resistance and controller/estimator rotor resistance of up to ± 20 %. Stator and rotor leakage inductances and stator resistance have the same values in the motor and in the controller/estimator. Magnetising inductance in the controller/estimator is rated. Orientation angle error and variation in the saturation level in the machine are negligible. Maximum speed estimation error is around $\pm$ 10 rpm for deviation of rotor resistance of $\pm$ 20 % at rated torque command. Torque error is very small and is the same regardless of the amount of rotor resistance detuning.

Incorrect stator and rotor leakage inductance values

Stator and rotor resistance values are the same in the motor and in the controller/estimator. Magnetising inductance in the controller/estimator is rated. Detuning due to incorrect setting or variation in the stator and rotor leakage inductances is illustrated in Fig. 5. Plots are again given against torque command. The same amount of detuning is assumed for both leakage inductances. Speed estimation error is below $\pm$ 1 rpm and torque error is small as well. Variation in the main flux saturation level in the machine is rather small again (although higher than in the previous case). Orientation angle error is now up to 2 degrees.

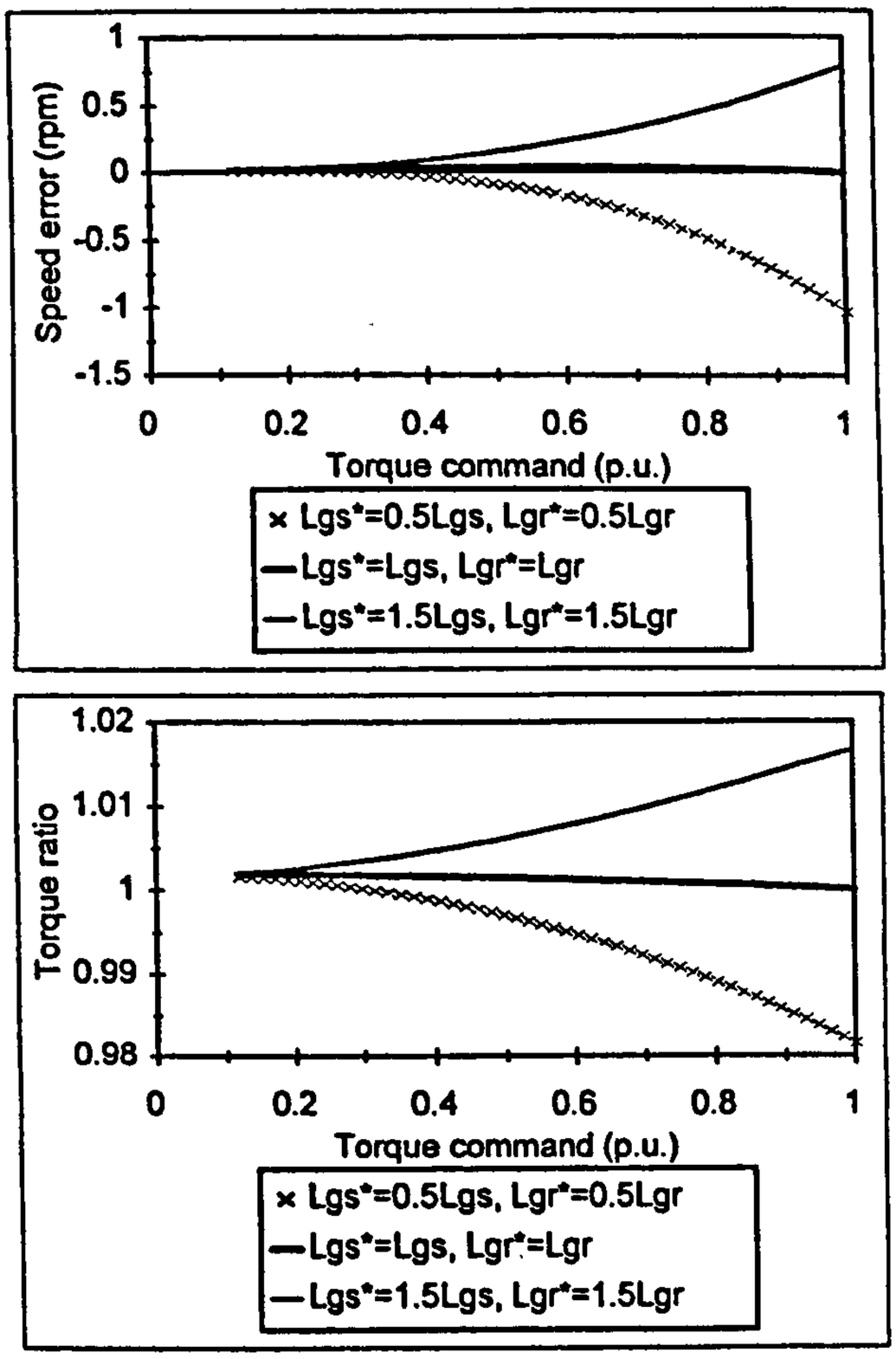

Fig. 5. Impact of incorrect stator and rotor leakage inductance values.

Incorrect magnetising inductance setting

Under the assumption that stator and rotor resistance, as well as stator and rotor leakage inductance, all have the same values in the motor and in the estimator/ controller, incorrect setting of magnetising inductance produces detuning shown in Fig. 6. Maximum speed estimation error is up to ± 3 rpm at rated torque command when magnetising inductance value in the controller/estimator deviates by ± 20 % from the rated value. Torque error is up to ± 8 %. Orientation angle error is once more negligible small. Level of main flux saturation in the motor is, as expected, now considerably affected and Fig. 6 includes ratio of the actual to rated magnetising inductance (which is quite close to the ratio of controller/estimator to rated magnetising inductance).

Incorrect stator resistance value

Impact of incorrect stator resistance value on low speed operation is displayed in Fig. 7, where results are given for speed reference equal to 5 % of the rated. Magnetising inductance in the controller/estimator equals rated and rotor resistance and stator and rotor leakage inductances have the same values in the motor and in the controller/estimator. Speed error is up to ± 6 rpm, while error in torque ratio is excessively high at low torque command values. Orientation angle error is significant and is included in Fig. 7. Main flux saturation level in the machine is affected as well, as witnessed by ratio of actual to rated magnetising inductance, which is included in Fig. 7. Detuning diminishes as the speed is increased. Speed estimation error for rated speed reference is shown in Fig. 8. Torque error and orientation angle error are very small and are therefore not included in Fig. 8.

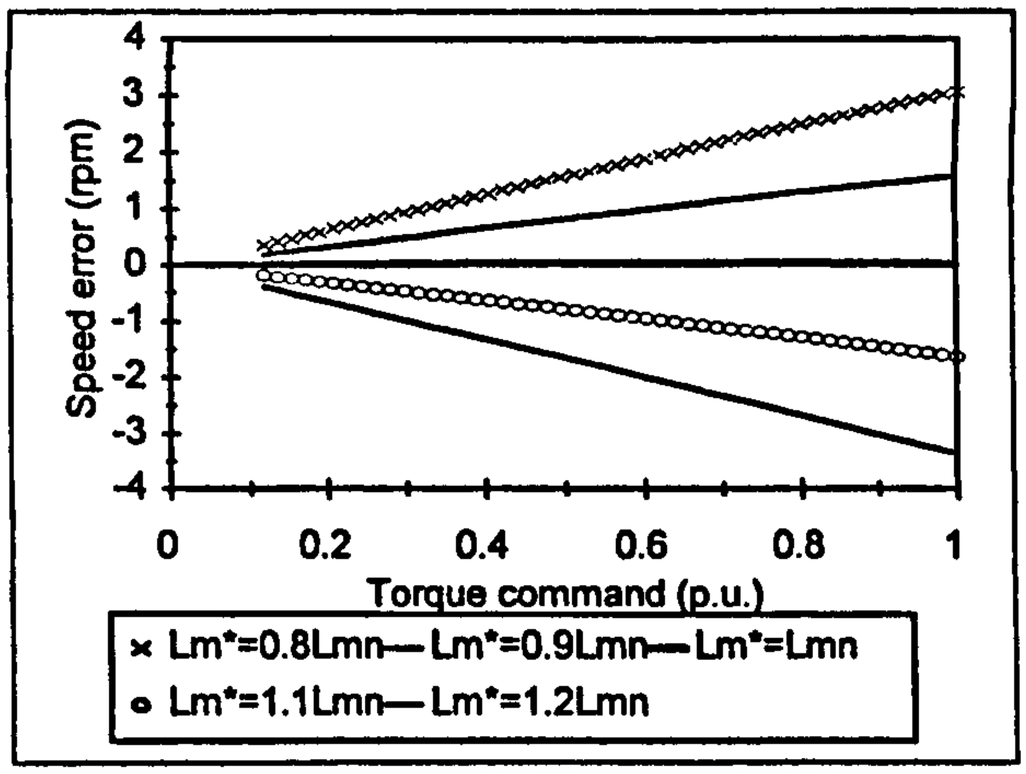

Fig. 6. Detuning due to incorrect magnetising inductance value.

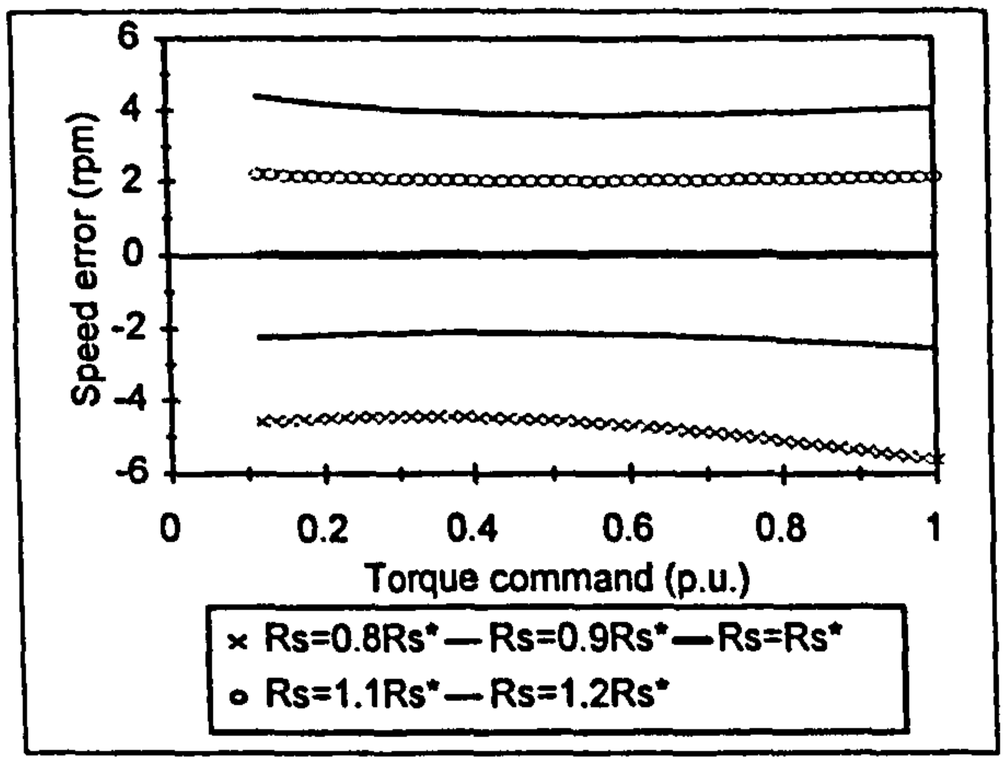

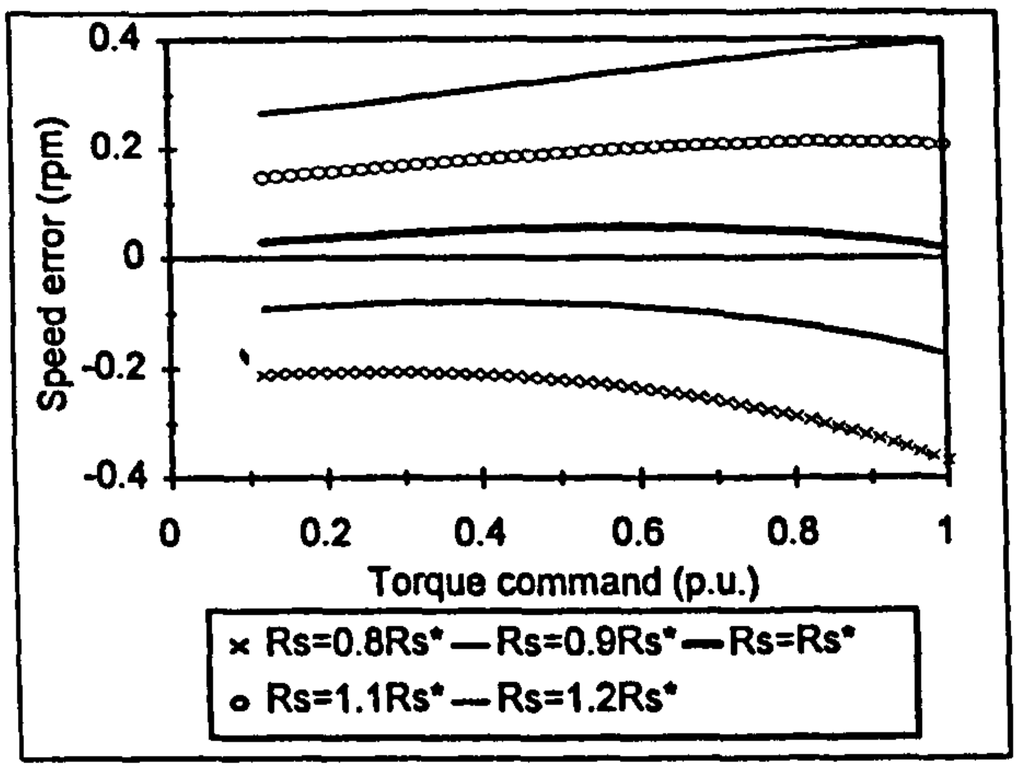

Fig. 8. Speed estimation error due to incorrect stator resistance value - speed reference equal to rated.

Combined impact of iron loss and incorrect magnetising inductance setting

Iron loss, as a sole contributor to the detuned operation of the sensorless drive, has been considered in detail in [10] where it was shown that typical speed estimation error in the most of the base speed region is 2 to 3 rpm, while torque error is high at light loads and speeds close to 1 p.u. As iron loss is frequency dependent, then detuning effects are speed dependent and the highest detuning takes place around rated speed. In this subsection combined impact of iron loss and incorrect magnetising inductance setting is analysed. The results are illustrated in Fig. 9 for operation of the drive at speed reference equal to rated speed. Curves with magnetising inductance setting in the controller/ estimator equal to the rated magnetising inductance essentially illustrate detuning produced solely by iron loss. Ratio of actual to magnetising inductance is very similar to the one shown in Fig. 6 and is therefore not included. Speed error is around 2.5 rpm solely due to iron loss and increases if magnetising inductance in the controller is set to a lower value than rated. However, if magnetising inductance in the controller/estimator is higher than rated, impacts of iron loss and incorrect magnetising inductance setting counteract and speed estimation error is relatively small. Torque error is high at light loads, while orientation angle error does not exceed a few tens of a degree.

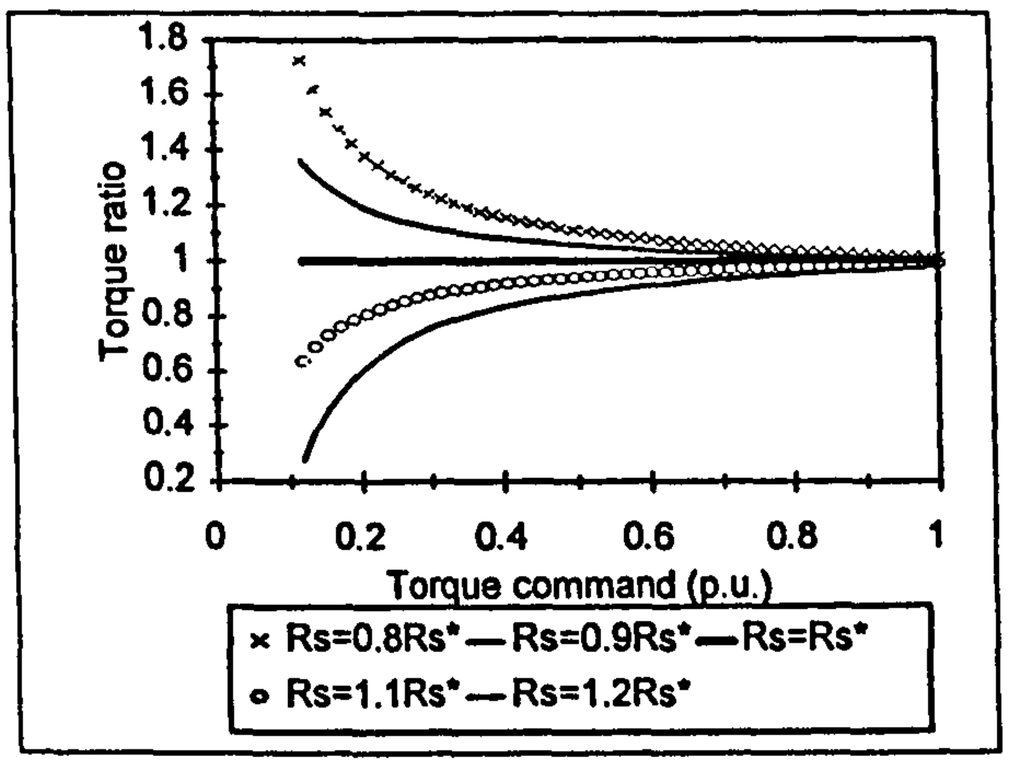

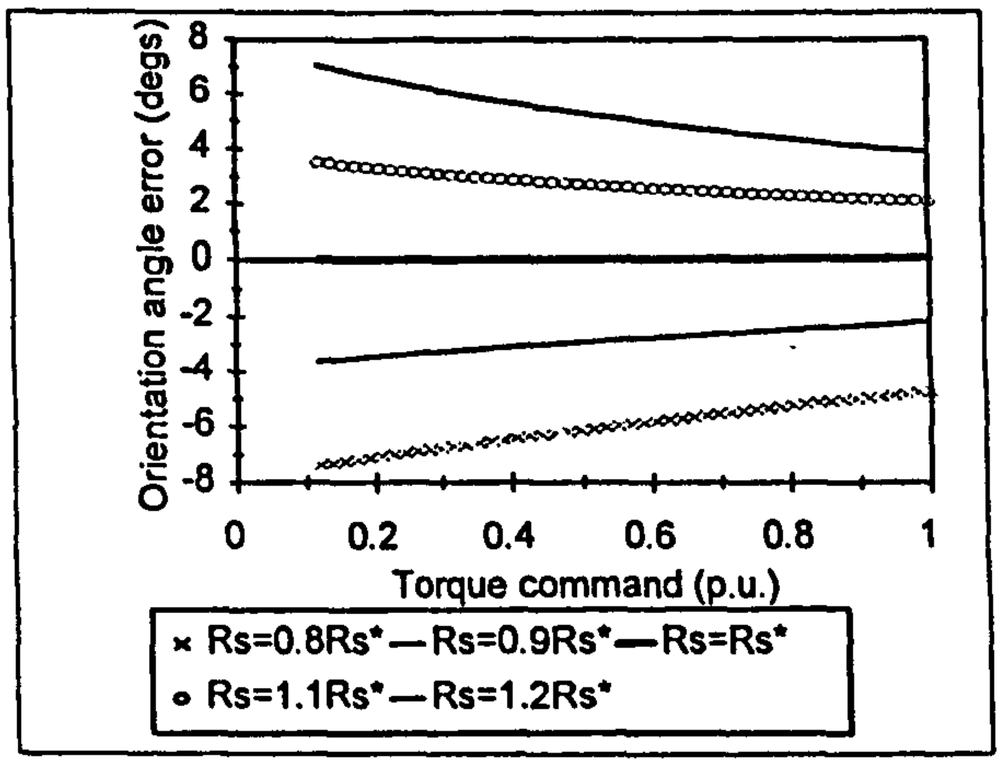

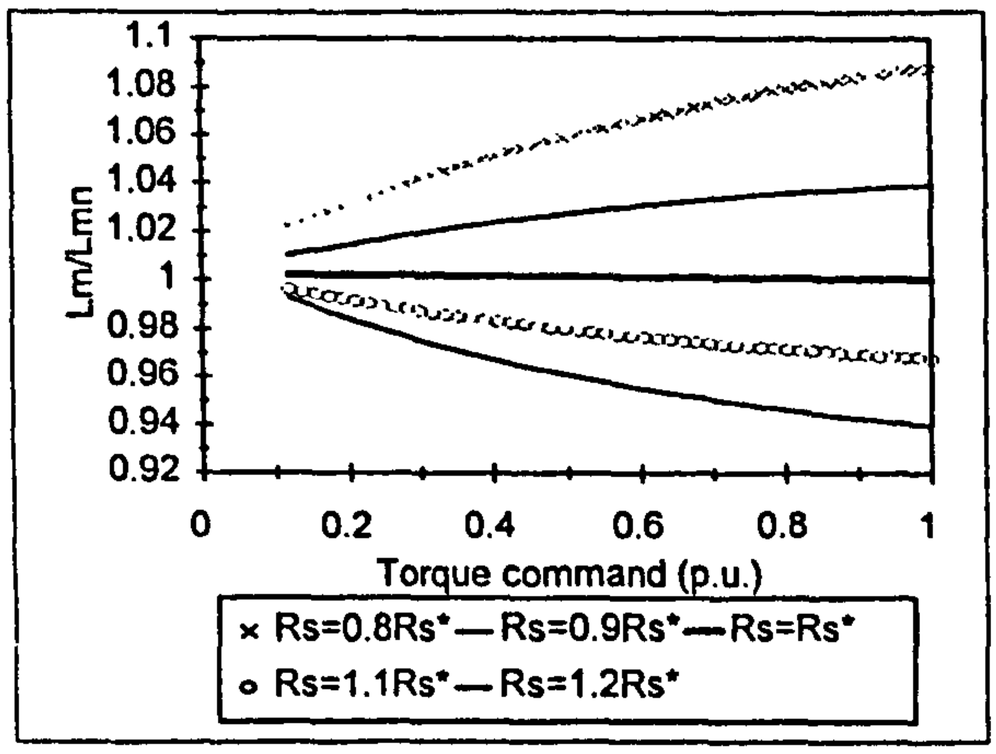

Fig. 7. Detuning due to incorrect stator resistance value - speed reference equal to 5 % of the rated speed.

CONCLUSION

The paper deals with detuning effects in steady-state operation of a sensorless indirect rotor flux oriented induction machine. Speed estimation error and other detuning effects are evaluated assuming ideal sinusoidal supply conditions and ideal integration for the rotor flux based MRAC speed estimation technique. All the results

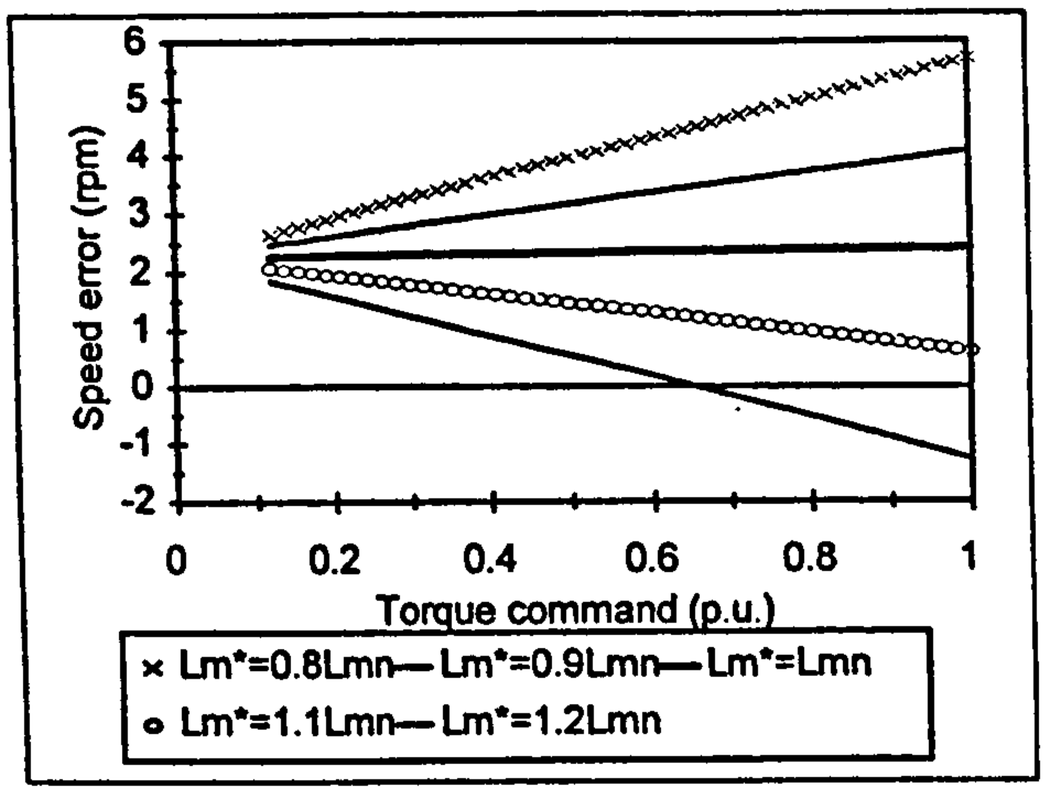

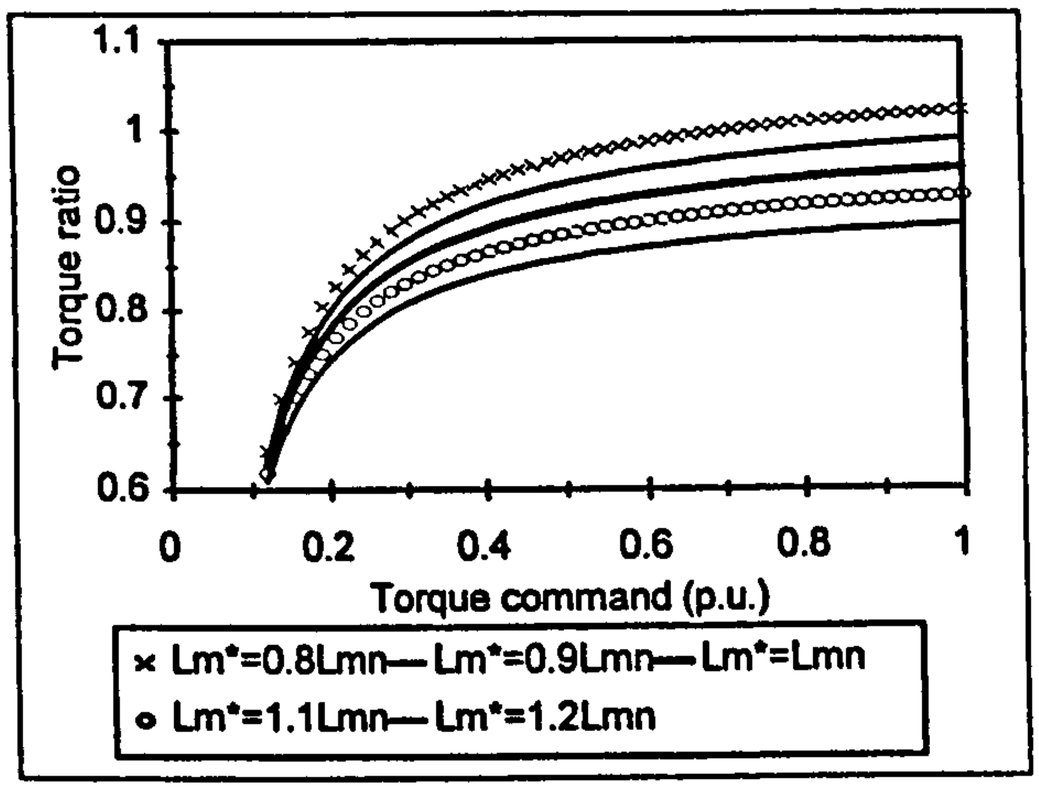

Fig. 9. Combined impact of iron loss and incorrect magnetising inductance setting on operation of the sensorless drive.

are fully applicable to modified rotor flux and back e.m.f. based MRAC speed estimation schemes as well, due to correlation that exists between these quantities under ideal conditions.

It is shown in the paper that incorrect rotor resistance value leads to the highest value of the speed estimation error of up to 10 rpm. Speed estimation error due to incorrect values of the stator and rotor leakage inductance is relatively small, up to 1 rpm. Incorrect setting of the magnetising inductance can cause speed estimation error of up to 3 rpm; however, if iron loss is accounted for, speed estimation error can reach up to 6 rpm when controller/estimator magnetising inductance is 0.8 of the rated. Stator resistance plays an important role in the low speed region. Incorrect value leads to a speed estimation error of up to 6 rpm at 5 % of the rated speed.

Torque error is considerable for incorrect value of the magnetising inductance (both with and without the iron loss) and incorrect stator resistance value at low speed. Orientation angle error appears to be of importance only when stator resistance is detuned and the drive operates in low speed region.

REFERENCES

[1] Rajashekara K, Kawamura A, Matsuse K, (editors), 1996, "Sensorless control of AC motor drives", IEEE Press, Piscataway, NJ.

[2] Tamai S, Sugimoto H, Yano M, 1987, "Speed sensor-less vector control of induction motor with model reference adaptive system", IEEE Ind. Appl. Soc. Anu. Meet. IAS, pp. 189-195.

[3] Schauder C, 1992, "Adaptive speed identification for vector control of induction motors without rotational transducers", IEEE Trans. on Industry Applications, 28, pp. 1054-1061.

[4] Ilas C, Bettini A, Griva G, Profumo F, 1994, "Comparison of different schemes without shaft sensors for filed oriented control drives", IEEE Ind. Elec. Soc. Annu. Meet. IECON, pp. 1579-1588.

[5] Griva G, Profumo F, Ilas C, Magueranu R, Vranka P, 1996, "A unitary approach to speed sensorless induction motor field oriented drives based on various model reference schemes", IEEE Ind. Appl. Soc. Annu. Meet. IAS, pp. 1594-1599.

[6] El-Kholy EE, Abdel-Karim M, Mahmoud SA, Iung C, 1994, "Effects of main flux saturation on behaviour of indirect field oriented induction motor drives without speed sensor", EPE Chapter Symp. 'Elec. drive design & appl.', pp. 203-208.

[7] Armstrong GJ, Atkinson DJ, 1997, "A comparison of model reference adaptive system and extended Kalman filter estimators for sensorless vector drives", EPE 7th Eur. Conf. on Power Elec. and Appl., pp. 1.424-1.429.

[8] Blasco-Gimenez R, Asher GM, Sumner M, Bradley KJ, 1996, "Dynamic performance limitation for MRAS based sensorless induction motor drives. Part 1: Stability analysis for the closed loop drive", IEE Proc. - Electrical Power Appl., 113-122.

[9] Jansen PL, Lorenz RD, 1993, "Accuracy limitations on velocity and flux estimation in direct field oriented induction machines", EPE 5th Eur. Conf. on Power Elec. and Appl., pp. 312-318.

[10] Levi E, Wang M, 1997, "Impact of iron loss on speed estimation in sensorless vector controlled induction machines", IEEE Ind. Elec. Soc. Annu. Meet. IECON, pp. 977-982.

[11] Sokola M, Levi E, 1996, "Combined impact of iron loss and main flux saturation on operation of vector controlled induction machines", IEE 6th Int. Conf. Power Elec. & Variable Speed Drives, Nottingham, UK, IEE Conf. Pub. 429, 1996, pp. 36-41.

UMIST

32nd UNIVERSITIES POWER ENGINEERING CONFERENCE

UPEC '97

MANCHESTER CENTRE FOR ELECTRICAL ENERGY

UMIST
Manchester, UK

10th - 12th September 1997

Proceedings
Volume 2

MCEE

IMPACT OF IRON LOSS ON SPEED ESTIMATION ACCURACY IN REACTIVE POWER MRAC BASED SENSORLESS ROTOR FLUX ORIENTED INDUCTION MACHINES

M.Wang, E.Levi, D.Williams

Liverpool John Moores University, UK

ABSTRACT

Estimation of rotor speed in sensorless vector control of induction machines frequently relies on model reference adaptive control (MRAC) approach, which requires utilisation of an induction machine mathematical model. Iron loss is neglected in the model and therefore its existence in the machine inevitably causes an error in the speed estimate. The aim of this paper is to evaluate detuning in steady-state operation, caused by iron loss, in the MRAC based sensorless rotor flux oriented induction machine. The scheme which calculates reactive powers as outputs of the reference and adjustable models is considered. It is shown that typical speed estimation error in the base speed region, purely due to iron loss, is 2 to 3 rpm for a 4 kW, four-pole, 50 Hz machine.

INTRODUCTION

Numerous methods of sensorless vector control for induction machines have recently emerged [1,2] and they may be classified into two groups. The first one encompasses all the techniques that estimate rotor speed from stator current (voltage) spectrum, on the basis of rotor slot and eccentricity harmonics or saturation induced saliency. Speed estimation does not rely on mathematical model of an induction machine and is therefore insensitive to parameter variation effects. Hence existence of iron loss does not affect speed estimation. The second group of speed sensorless vector control methods encompasses all the schemes in which speed estimation relies on utilisation of induction machine's mathematical model [1,2]. The most frequently applied control approach in conjunction with this group of methods is model reference adaptive control (MRAC). Its popularity is due to relatively simple implementation requirements, when compared with other possible approaches (full-order observers, extended Kalman filter). The quantity that is calculated within the reference and the adjustable parts of the MRAC based estimator may take different forms. Frequent choices include rotor flux, modified rotor flux, back emf and reactive power [1]. The advantages of using reactive power method stem from its insensitivity to stator resistance variations and from the fact that pure integration is not required [3].

Mechanical sub-systems in the control part and in the machine are decoupled in any sensorless drive. As the MRAC methods utilise standard d-q axis induction machine model, accuracy of speed estimation strongly depends on parameter variation effects. Impact of variations of rotor resistance (time constant), stator resistance, magnetising inductance and total leakage inductance have been studied in detail recently for rotor flux based MRAC speed estimation scheme [4]. Typical steady-state speed estimation errors due to variation of motor parameters were examined for a 4 kW, 50 Hz, 4-pole induction machine. Variations in rotor resistance and in total leakage inductance of 10 % cause a speed independent speed estimation error of approximately 5 rpm and 2.5 rpm, respectively. Speed estimation errors due to 10 % variations in magnetising inductance and in stator resistance are speed dependent and are at most 4 rpm and 3 rpm, respectively, in the low speed region and approach in both cases zero as speed increases.

Iron loss as a source of speed estimation error in sensorless vector controlled induction machines has not been dealt with in the past. Indeed, iron loss as a source of detuned operation of vector controlled induction machines with speed sensor has attracted attention only recently [5,6]. Presence of the speed sensor forces actual and commanded rotor and slip speeds to be equal in steady-state operation, so that detuning due to iron loss results in an orientation angle error [5,6]. The situation in a sensorless drive is different. As speed is estimated rather than measured, actual and estimated rotor and slip speeds are not necessarily equal.

The aim of this paper is to evaluate speed estimation errors and other detuning effects that will take place in a MRAC based sensorless rotor flux oriented (RFO) induction machine in steady-state operation purely due to the existence of the iron loss in the machine, the iron loss being neglected in the speed estimator and in the control system. MRAC scheme under consideration utilises reactive powers as outputs of the reference and the adjustable models. Indirect rotor flux oriented

current fed induction machine is studied. As the fundamental iron loss is responsible for detuning [5], current controlled PWM inverter is treated as an ideal current source, so that steady-state is described with sinusoidal stator currents. Iron loss is represented with an equivalent iron loss resistance, as suggested in [5], and this resistance is identified experimentally using the procedure of [6]. Speed estimation error is evaluated in the speed region from zero up to twice the rated speed for a 4 kW, 50 Hz, 4-pole machine whose data are given [6]. It is shown that speed estimation error is typically between two and three rpm and is therefore of the same order as are the errors introduced by other parameter variation effects.

DESCRIPTION OF THE DRIVE

Sensorless indirect rotor flux oriented induction machine is shown in Fig. 1. As already noted, ideal current feeding is assumed and steady-state operation is analysed. Rotor flux reference is constant and equal to rated in the base speed region. In field weakening rotor flux reference decreases inversely proportionally to the rotor speed. Coefficients C_1 and C_2 are dependent on the rotor flux command and are defined in Fig. 1. General form of the MRAC based speed estimator of Fig. 1 is shown in Fig. 2. Measured stator currents and voltages are the estimator inputs. The outputs of the reference and the adjustable model, denoted as A, take here the form of reactive power.

Induction machine is represented with the dynamic space vector equivalent circuit which in arbitrary reference frame has the form shown in Fig. 3, [5], and which accounts for the iron loss. Iron loss is experi-

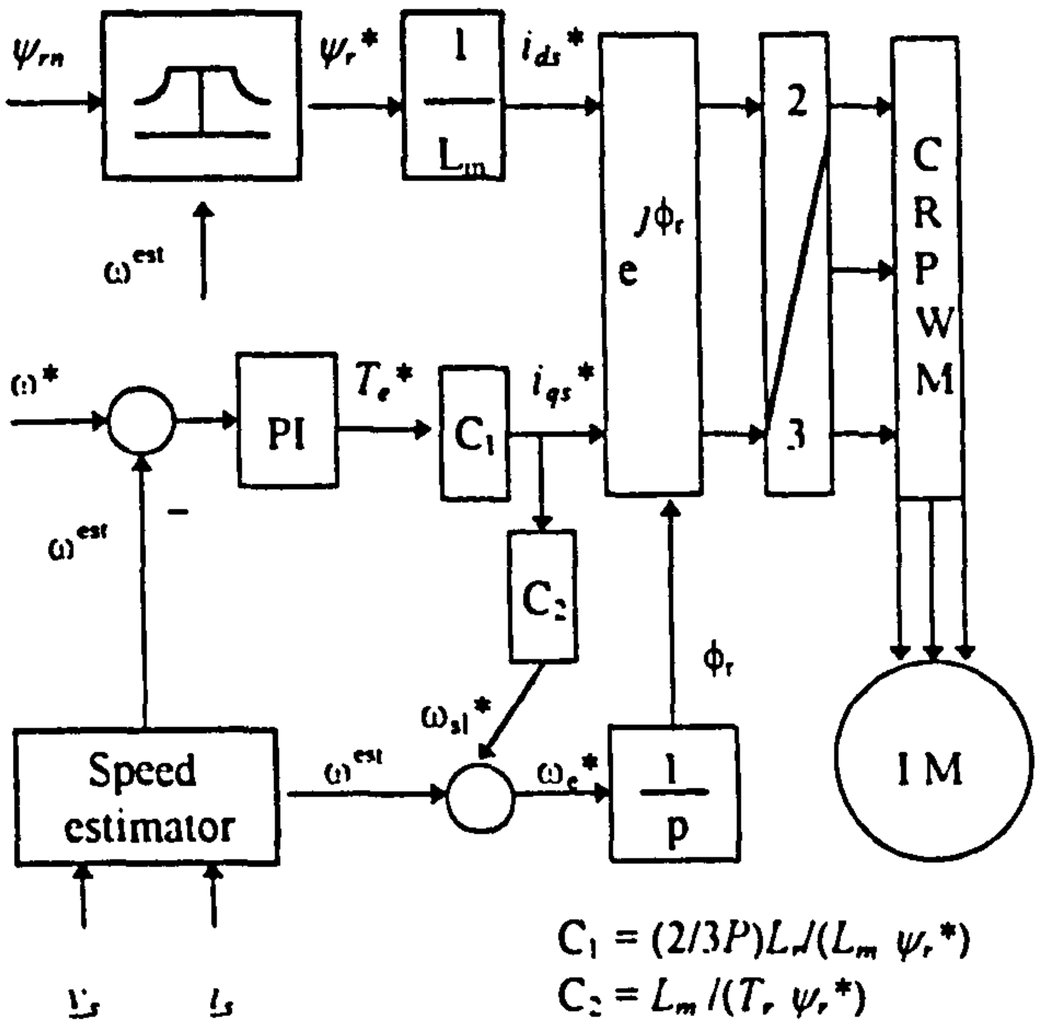

Figure 1 Structure of the Speed Sensorless Indirect Rotor Flux Oriented Induction Machine

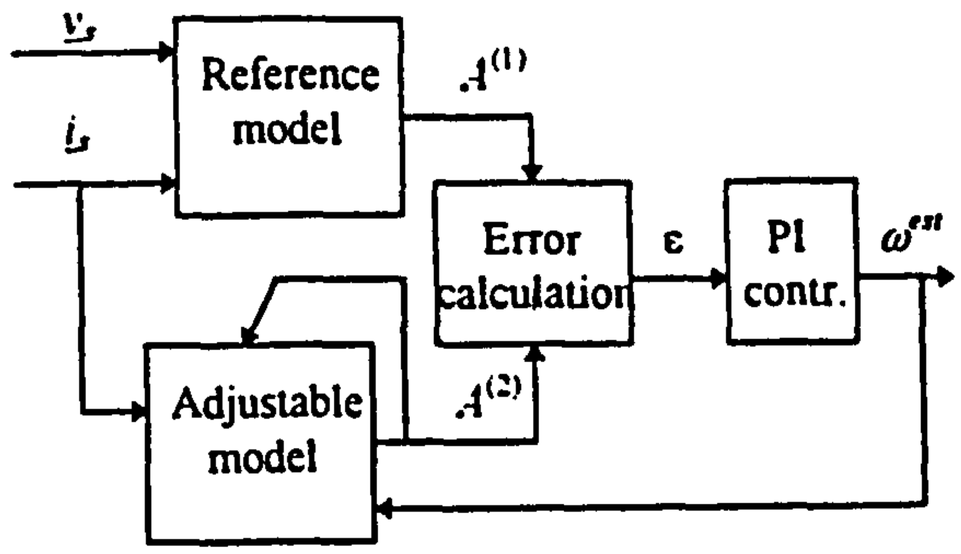

Figure 2 General Form of a MRAC Based Rotor Speed Estimator

mentally identified in the frequency range from zero up to twice the rated frequency and the results are summarised in Fig. 4, where equivalent iron loss resistance is shown against frequency. Analytical approximation, used later on in the study, is included.

ANALYSIS OF THE DRIVE

The study is performed in the reference frame fixed to the commanded rotor flux space vector (d,q reference frame). Therefore ω_a in induction machine model of Fig. 3 equals ω_e^* of Fig. 1. Due to idealised representation of the inverter, stator d-q axis current commands are equal to the machine d-q axis currents. Induction machine steady-state operation may under these conditions be described with the following set of equations, obtainable from Fig. 3:

$$\begin{aligned} v_{ds} &= R_s i_{ds}^{\bullet} - \omega_e^{\bullet} L_{\sigma s} i_{qs}^{\bullet} - \omega_e^{\bullet} L_m i_{qm} \\ v_{qs} &= R_s i_{qs}^{\bullet} + \omega_e^{\bullet} L_{\sigma s} i_{ds}^{\bullet} + \omega_e^{\bullet} L_m i_{dm} \end{aligned} \tag{1}$$

$$\begin{aligned} L_m i_{dm} &= \psi_{dr} - \omega_{sl} T_{\sigma r} \psi_{qr} \\ L_m i_{qm} &= \psi_{qr} + \omega_{sl} T_{\sigma r} \psi_{dr} \\ -\omega_e^{\bullet} T_{Fe} i_{qm} &= i_{ds}^{\bullet} + \psi_{dr}/L_{\sigma r} - i_{dm} L_r/L_{\sigma r} \\ \omega_e^{\bullet} T_{Fe} i_{dm} &= i_{qs}^{\bullet} + \psi_{qr}/L_{\sigma r} - i_{qm} L_r/L_{\sigma r} \end{aligned} \tag{2}$$

$$\begin{aligned} T_e &= (3P/2)(L_m/L_{\sigma r})(\psi_{dr} i_{qm} - \psi_{qr} i_{dm}) \\ \omega_e^{\bullet} &= \omega + \omega_{sl} \end{aligned} \tag{3}$$

Time constants in (2) are defined as $T_{Fe} = L_m / R_{Fe}$ and $T_{\sigma r} = L_{\sigma r} / R_r$. Inspection of (1)-(2) shows that there are six equations that contain seven unknowns (stator voltage, magnetising current and rotor flux d-q axis components, plus angular slip frequency). Thus it is not possible to solve this system of equations without determining which of the seven variables is only apparently unknown. As shown shortly, speed estimator actually pre-determines one of the unknowns so that the system of equations becomes solvable.

As far as the control system is concerned, the independent inputs are reference speed and reference

rotor flux. The output of the PI speed controller is reference torque, whose value is in general unknown. However, for each value of the torque command there will be a corresponding value of the actual torque, determined with (3). Thus the torque command may be regarded as an independent input. By solving (1)-(2), while accounting for the additional constraint imposed by the speed estimator, it is then possible to determine the value of the actual torque that corresponds to the given torque command. Such an approach is utilised here: independent inputs are taken as reference speed, reference torque and reference rotor flux. The constraint imposed by the control is that

$$\omega_e^* = \omega^* + \omega_{sl}^* \equiv \omega_e \tag{4}$$

as estimated and reference speeds are equal and commanded and actual supply frequencies are equal as well. The error in speed estimation is defined in mechanical rpm as

$$\Delta n = n - n^* \equiv n - n^{est} \equiv n_{sl}^* - n_{sl} \tag{5}$$

The speed estimator, whose general form is given in Fig. 2, operates in the stationary (α,β) reference frame and relies on measured stator voltages and currents. The output of the reference model is independent of the rotor speed, while output of the adjustable model depends on the rotor speed. Back emf space vectors are at first calculated by means of (underlined variables are space vectors and σ is total leakage coefficient)

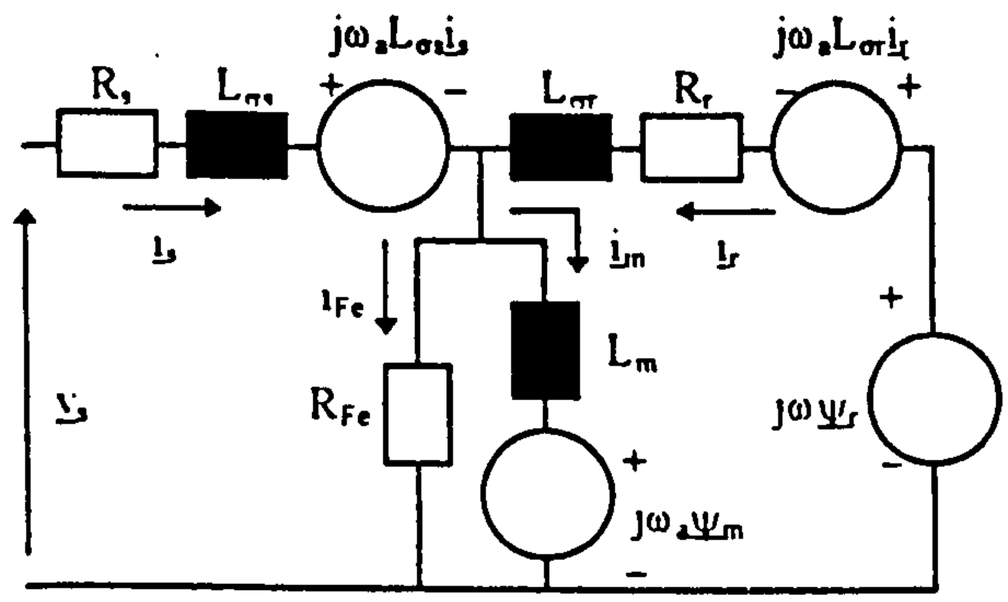

Figure 3 Space Vector Dynamic Equivalent Circuit with Included Iron Loss Representation

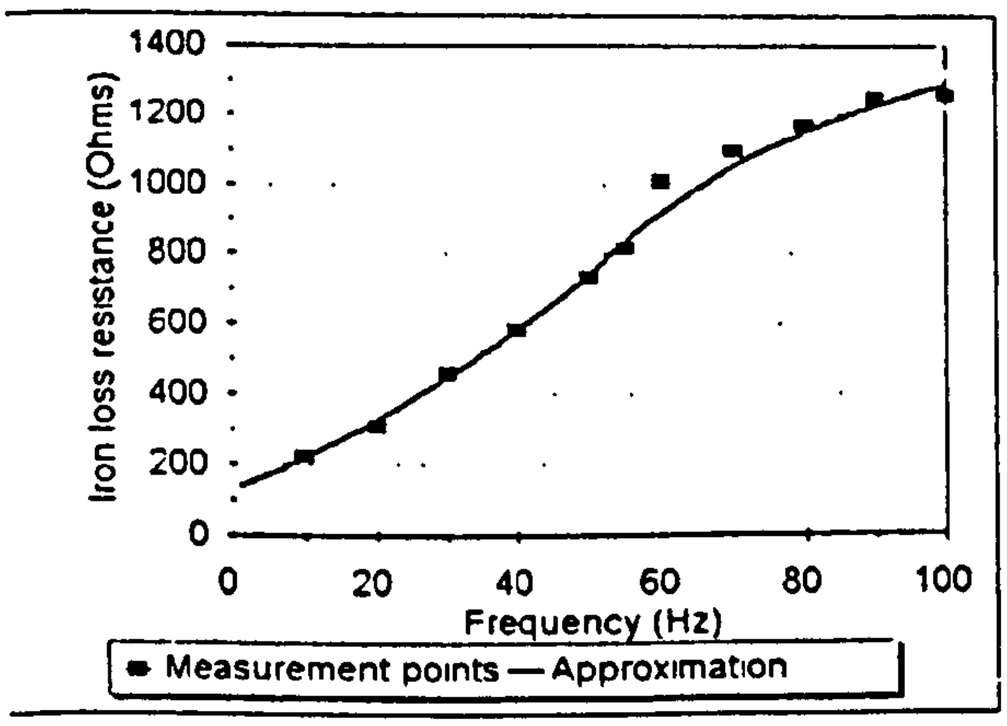

Figure 4 Experimentally Identified Variation of Equivalent Iron Loss Resistance with Frequency

$$\underline{e}^{(1)} = \frac{L_m}{L_r}\frac{d\underline{\psi}_r^{(1)}}{dt} = \underline{v}_s - (R_s + \sigma L_s p)\underline{i}_s$$

$$\underline{e}^{(2)} = \frac{L_m}{L_r}\frac{d\underline{\psi}_r^{(2)}}{dt} = \frac{L_m}{L_r}\left[\left(j\omega^{est} - \frac{1}{T_r}\right)\underline{\psi}_r^{(2)} + \frac{L_m}{T_r}\underline{i}_s\right] \tag{6}$$

where rotor flux for adjustable model is evaluated using the following expression:

$$\frac{d\underline{\psi}_r^{(2)}}{dt} = \left(j\omega^{est} - \frac{1}{T_r}\right)\underline{\psi}_r^{(2)} + \frac{L_m}{T_r}\underline{i}_s \tag{7}$$

Symbol T_r stands for rotor time constant. The outputs of the reference and the adjustable model and the error quantity are defined as reactive powers and reactive power difference, respectively:

$$q^{(1)} = i_{\alpha s}e_\beta^{(1)} - i_{\beta s}e_\alpha^{(1)} \qquad q^{(2)} = i_{\alpha s}e_\beta^{(2)} - i_{\beta s}e_\alpha^{(2)}$$
$$\varepsilon = q^{(1)} - q^{(2)} \tag{8}$$

Sinusoidal steady-state operation is discussed and therefore $pi_{\alpha s} = -\omega_e^* i_{\beta s}$ and $pi_{\beta s} = \omega_e^* i_{\alpha s}$. It can be shown that under these conditions reactive power outputs of the reference and the adjustable model are:

$$q^{(1)} = i_{\alpha s}v_{\beta s} - i_{\beta s}v_{\alpha s} - \sigma L_s \omega_e^* i_s^2$$

$$q^{(2)} = \frac{L_m^2}{L_r}\frac{i_s^2\omega_e^*}{1 + \left[T_r\left(\omega_e^* - \omega^{est}\right)\right]^2} \tag{9}$$

where $i_s^2 = i_{\alpha s}^2 + i_{\beta s}^2$. From (9) it follows that rotor speed is determined with the condition that input reactive power must equal reactive power spent in the motor, as difference between the two quantities in (9) equals zero in any steady-state. It can be shown that, if iron loss is accounted for by means of equivalent circuit of Fig. 3, the corresponding reactive power correlation is

$$i_{\alpha s}v_{\beta s} - i_{\beta s}v_{\alpha s} =$$

$$= \omega_e^* i_s^2\left[L_{\sigma s} + \frac{L_{\sigma r}\left(T_{\sigma r} - T_r\right)^2\omega_{sl}^2 + L_m\left(1 + \left(\omega_{sl}T_{\sigma r}\right)^2\right)}{\left(1 - \omega_e^*\omega_{sl}T_{\sigma r}T_{Fe}\right)^2 + \left(\omega_e^*T_{Fe} + \omega_{sl}T_r\right)^2}\right] \tag{10}$$

As input reactive power in (9) and (10) is the same, then for any given operating condition it is possible to calculate from (9) and (10) the unknown slip speed and hence rotor speed. Once when the actual speed is calculated, it becomes possible to solve for the remaining unknowns in induction motor model (1)-(3).

RESULTS OF THE ANALYSIS

Detuning effects are examined with reference speed taken as independent variable and normalised with respect to the rated speed. Reference torque is set to a constant value in the base speed region. For operation in the field weakening region torque command is

decreased inversely proportionally to the speed, so that constant power operation is assumed. Iron loss resistance is adjusted to an appropriate value for each operating frequency using the approximation of Fig. 4. The major results are summarised in Fig. 5. Speed error, defined with (5), and torque ratio, defined as ratio of the actual to reference torque, are shown, for three values of the commanded torque/power (rated, half of the rated and 0.2 of the rated) in the speed range from zero up to twice the rated speed.

It follows from Fig. 5 that a typical speed estimation error due to iron loss is 2 to 3 rpm in the base speed region (except at low speeds). Speed estimation error slightly increases in the field weakening region and approaches 4 rpm for operation with rated power at twice the rated speed. It is interesting to note that speed estimation error appears to be rather independent from the loading of the machine in the base speed region. To the contrary, error in torque ratio increases for given speed command as loading decreases and is over 20% for torque/power command of 0.2 p.u. between half of the rated and rated speed command. Such a behaviour reflects the fact that iron loss is relatively high compared to total commanded power when load is light. Figure 6 illustrates difference between commanded output power (product of the reference speed and torque) and actual output power (product of the actual speed and torque). Operating conditions are the same as in Fig. 5. Output power difference is load dependent and is higher for light loads.

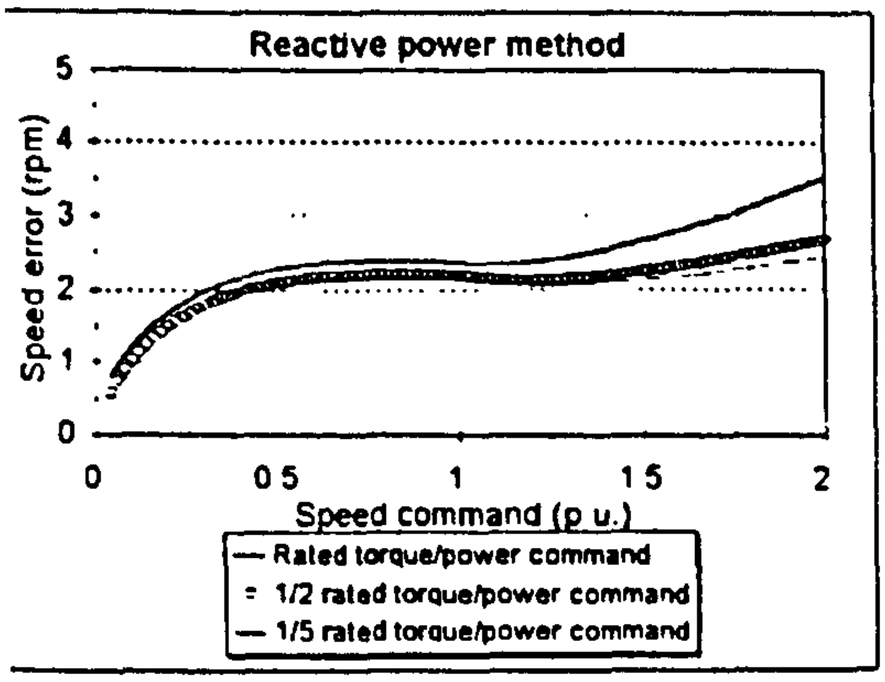

Figure 5 Speed Estimation Error and Torque Ratio for Reactive Power Based MRAC Speed Estimator

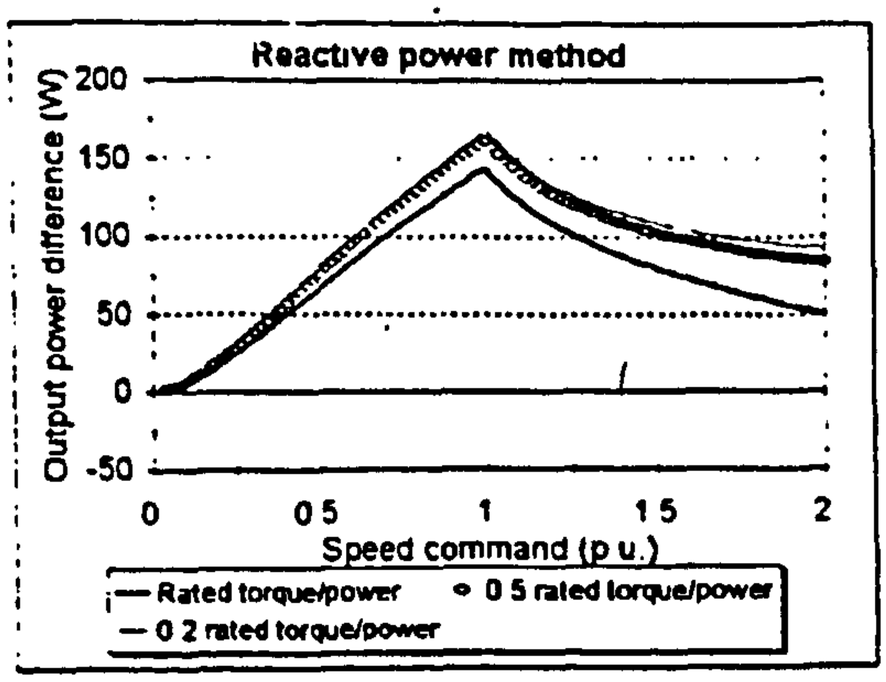

Figure 6 Output Power Difference for Reactive Power Based MRAC Speed Estimator

V. CONCLUSION

The paper evaluates impact of iron loss on speed estimation accuracy in MRAC based sensorless rotor flux oriented induction machines. Speed estimator that utilises reactive powers as outputs from the reference and the adjustable model is analysed for steady-state operation. It is shown that iron loss inevitably leads to a speed estimation error of 2 to 3 rpm in the base speed region. Slight increase is observed in the field-weakening region. Torque ratio error is heavily dependent on the loading of the machine and exceeds 20 % at light loads. Speed estimation error due to iron loss is thus rather significant and is comparable to the errors due to other parameter variation effects.

REFERENCES

[1] Rajashekara, K, Kawamura, A, Matsuse, K, (editors), Sensorless control of AC motor drives, New York: IEEE Press, 1996.

[2] Ilas, C, Bettini, A, Ferraris, L, Griva, G, Profumo, F, Comparison of different schemes without shaft encoders for field oriented control drives, Proc. IEEE IECON'94, Bologna, Italy, pp. 1579-1588, 1994

[3] Peng, FZ, Fukao, T, Robust speed identification for speed-sensorless vector control of induction motors, IEEE Trans. on Ind. Appl., vol. 30, no. 5, pp 1234-1240, 1994.

[4] Blasco-Gimenez, R, Asher, GM, Sumner, M, Bradley, KJ, Dynamic performance limitations for MRAS based sensorless induction motor drives. Part 1: Stability analysis for the closed loop drive, IEE Proc. - Electr. Power Appl., vol. 143, no. 2, pp. 113-122, 1996.

[5] Levi, E, Impact of iron loss on behaviour of vector controlled induction machines, IEEE Trans. on Ind. Appl., vol. 31, no. 6, pp. 1287-1296, 1995.

[6] Levi, E, Sokola, M, Boglietti, A, Pastorelli, M, Iron loss in rotor flux oriented induction machines: identification, assessment of detuning and compensation, IEEE Trans. on Power Electronics, vol. 11, no. 5, pp. 698-709, 1996.

AUTHOR'S ADDRESS

The first author can be contacted at

School of Elec Eng., Electronics and Physics
Liverpool John Moores University
Byrom St
Liverpool L3 3AF, UK

33RD UNIVERSITIES
POWER ENGINEERING CONFERENCE

UPEC '98

CONFERENCE PROCEEDINGS

NAPIER UNIVERSITY, EDINBURGH, UK

8 – 10 SEPTEMBER 1998

Volume 2

NAPIER UNIVERSITY
EDINBURGH

IMPACT OF PARAMETER VARIATIONS ON DYNAMICS OF SENSORLESS INDIRECT ROTOR FLUX ORIENTED INDUCTION MACHINE

M Wang and E Levi

Liverpool John Moores University, UK

ABSTRACT

One of the most frequently applied methods of sensorless rotor flux oriented control of induction machines relies on utilisation of model reference adaptive control (MRAC) based speed estimation. Accuracy of this speed estimation scheme heavily depends on correct setting of the parameters within the estimator and the controller. The paper deals with indirect feed-forward rotor flux oriented induction machine drive in which speed estimation is performed utilising rotor flux based MRAC scheme. A study is conducted in order to evaluate speed estimation error during transient operation of the drive, caused by incorrect setting and/or variation of parameters. Incorrect setting of the magnetising inductance, stator resistance variation and rotor resistance variation are analysed by simulation. Simulation procedure is described and comparative analysis of transient behaviour under different detuning conditions is performed.

INTRODUCTION

Numerous methods of sensorless vector control of induction machines are available nowadays [1]. Vast majority of the methods rely in the process of speed estimation on utilisation of the induction machine model. As mechanical sub-systems of the control part of the drive and of the machine itself are in any sensorless drive effectively decoupled, and as standard d-q axis constant parameter induction machine model is utilised, accuracy of speed estimation strongly depends on parameter setting and parameter variation effects in the machine. One of the most frequently applied control approaches appears to be model reference adaptive control [2], which is characterised by relatively simple implementation requirements. This is the technique analysed in this paper, in conjunction with indirect feed-forward rotor flux oriented control. MRAC based speed estimation techniques mutually differ with respect to the quantity that is selected as output of the reference and the adjustable model. The most frequent choices are rotor flux and back e.m.f. [3]. The method discussed here is the rotor flux based one, that is characterised with simpler design [3].

Some studies related to parameter variation effects in MRAC based sensorless drives are already available. For example, impact of rotor resistance variation on transient behaviour of the drive was studied in [4,5] by simulation. An experimental study of impact of rotor resistance, stator resistance and mutual inductance variation in low speed region is reported in [6]. The only available comprehensive investigations of speed estimation errors caused by parameter variation effects appear to be works reported in [7,8]. However, in both cases structure of the drive dealt with is direct rotor flux oriented control that combines a MRAC based speed estimator with a closed loop flux observer and includes a mechanical sub-system model. Additionally, only steady-states are elaborated. The validity of results in [7,8] is thus restricted to steady-state operation for that specific drive structure.

The aim of this paper is to investigate speed estimation error that will take place due to parameter variations in an indirect feed-forward rotor flux oriented induction machine in transient operation. Speed estimation is performed using rotor flux based MRAC scheme. Corresponding analysis of steady-state operation for the same scheme and the same machine can be found in [9]. Variation of stator and rotor resistance and incorrect setting of the magnetising inductance are considered, in order to enable a comparative insight into the relative importance of various parameter variation effects. Variation of leakage inductances is not elaborated as steady-state analysis of [9] shows that impact of this detuning is the least important (typical steady-state speed estimation error appears to be below 1 rpm for all the operating regimes of a four-pole 50 Hz machine).

DESCRIPTION OF THE DRIVE AND SIMULATION PROCEDURE

Structure of the sensorless indirect feed-forward rotor flux oriented induction machine, analysed in the paper, is shown in Fig. 1. Machine is assumed to be fed from a current source, so that the current controlled PWM inverter is taken as ideal (i.e., reference and actual phase currents are equal). Transient operation is analysed. The induction machine is for all the considered cases represented with the full saturated machine model in stationary reference frame, in which stator current and rotor flux components are taken as state-space variables [10]. Operation in the base speed region is dealt with, so that rotor flux reference is constant and equal to rated at all times. The speed estimator of Fig. 1 is shown in Fig. 2. It relies on

measurement of stator currents and voltages, utilises principles of MRAC, and the two left-hand side blocks perform integration of equations (1) and (2). Speed estimator operates in the stationary reference frame and is described with the following space vector equations ($\sigma^* = 1 - L_m^{*2}/(L_s^* L_r^*)$):

$$\frac{d\underline{\psi}_r^{(1)}}{dt} = \frac{L_r^*}{L_m^*}\left[\underline{v}_s - \left(R_s^* + \sigma^* L_s^* p\right)\underline{i}_s\right] \qquad (1)$$

$$\frac{d\underline{\psi}_r^{(2)}}{dt} = \left(j\omega - \frac{1}{T_r^*}\right)\underline{\psi}_r^{(2)} + \frac{L_m^*}{T_r^*}\underline{i}_s \qquad (2)$$

$$\varepsilon = \psi_{\alpha r}^{(2)}\psi_{\beta r}^{(1)} - \psi_{\beta r}^{(2)}\psi_{\alpha r}^{(1)} \qquad (3)$$

Asterisk denotes in (1)-(2) constant values of machine parameters used in the estimator and in the controller of Fig. 1. Actual motor parameters do not bear an asterisk. Problem of pure integration in (1) is solved by a method proposed in [2]: a filter, not shown in Fig. 2 and eqns. (1)-(3), is inserted in the output channels of both the reference and the adaptive model. Filter's transfer function is $p/(p+1/T)$, where 1/T = 100. Parameters of the induction machine, including magnetising inductance and dynamic inductance approximations, are given in the Appendix.

SIMULATION RESULTS

Operation Under Tuned Conditions

Operation of the drive is at first examined with all the parameters in the controller and in the estimator set to their nominal values (index *n* in the Appendix). The machine is excited under no-load conditions at zero speed. Speed command, equal to rated, is applied at t = 0.1 s in a ramp-wise manner. Rated load torque is applied at t = 0.6 s. Simulation results are summarised

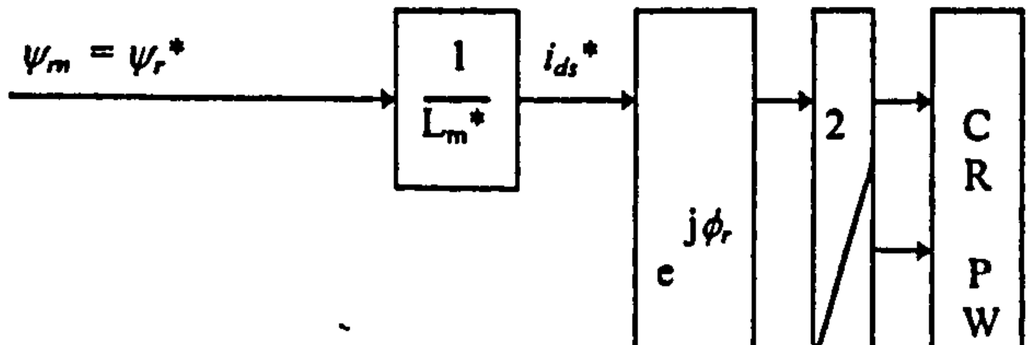

Figure 1 Speed sensorless indirect rotor flux oriented induction machine

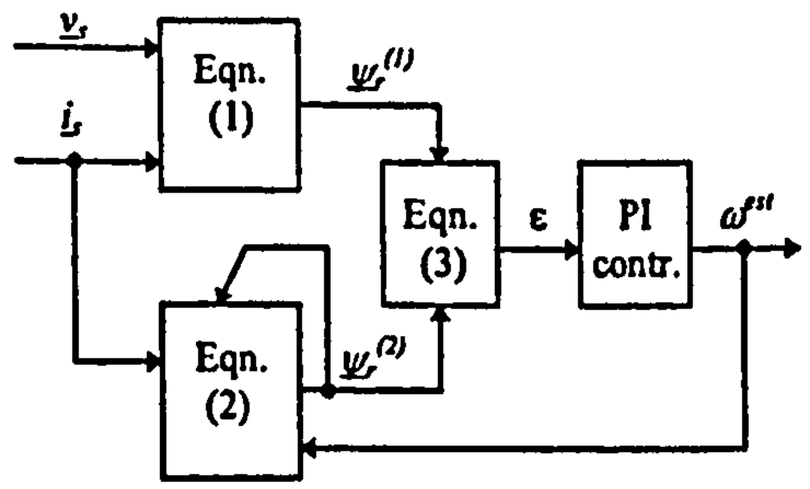

Figure 2 Rotor flux based rotor speed estimator

in Fig. 3, where actual and estimated speed (in electrical rad/s), actual and commanded torque and speed error for the complete time interval (in mechanical rpm, defined as $\Delta n = n - n^{est}$) are shown. Estimated speed tracks the actual one very well, except

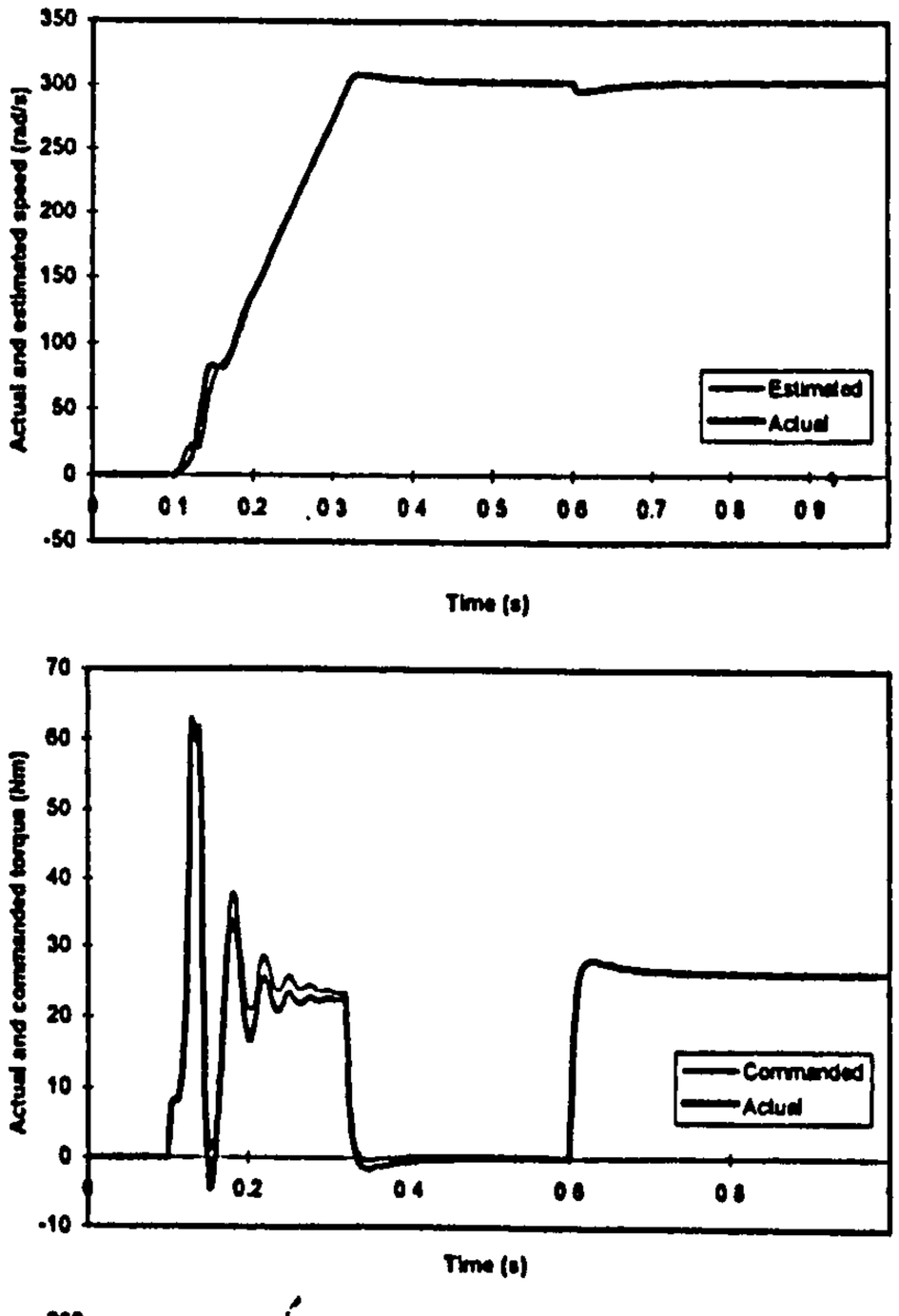

Figure 3 Response of the drive under tuned conditions: actual and estimated speed, actual and estimated torque and speed error (mech. rpm)

in the initial part of the acceleration. Commanded and actual torque are in good agreement, except during acceleration where cross-saturation causes reduction in the actual torque. Field orientation is initially lost, as witnessed by oscillatory torque behaviour. Speed estimation error, initially large, is zero for both full load and no-load operation at rated speed and has negligibly small values during transient caused by rated load torque application.

Incorrect magnetising inductance setting

Detuning due to incorrect setting of the magnetising inductance is independent of speed but load dependent. It is at maximum when load torque is rated [9]. The same simulation study is performed two more times, but now with the magnetising inductance set to values $L_m^* = 0.8L_{mn}$ and $L_m^* = 1.2L_{mn}$, respectively. All the other parameters in the motor and in the controller/estimator are the same. Speed error during acceleration remains essentially the same as in Fig. 3; therefore the results, given in Fig. 4, contain speed errors for time interval $t \in (0.5s; 1s)$.

3.3 Variation of rotor resistance

Variation in rotor resistance will cause once more speed independent but load dependent detuning, being at maximum when load torque is rated [9]. The same simulation is repeated for the following two cases: $R_r = 0.8R_m = 0.8R_r^*$ and $R_r = 1.2R_m = 1.2R_r^*$. All the other parameters in the motor and in the controller/ estimator are the same (magnetising inductance is set to rated value). Fig. 5 shows speed errors for the two cases for time interval $t \in (0.5\ s; 1s)$. It is interesting to note that the orientation angle error is negligibly small when either magnetising inductance is incorrectly set or when rotor resistance varies, so that transient-free torque response is maintained irrespective of the speed estimation error.

Variation of stator resistance

Detuning due to stator resistance variation is speed (frequency) dependent and is most pronounced at low speeds. On the other hand, impact of loading is smaller than in the previous two cases [9]. The simulation is done at speed of 0.05 p.u. with 0.2 p.u. load torque application at $t = 0.6$ s and subsequent rated load torque application at $t = 0.8$ s. Stator resistance in the motor is taken as $R_s = 0.8R_{sn}$ and $R_s = 1.2R_{sn}$, respectively, while the one in the estimator equals rated value. Results for the value of 1.2 p.u. of the stator resistance in the motor are given in Fig. 6. However, it was not possible to get the results for the same speed command for stator resistance of 0.8 p.u. It is worth noting that a similar problem at low speeds was observed in experimental study of detuning reported in [6]. Speed command for this stator resistance is therefore increased to 0.1 p.u. and speed error is shown in Fig. 7.

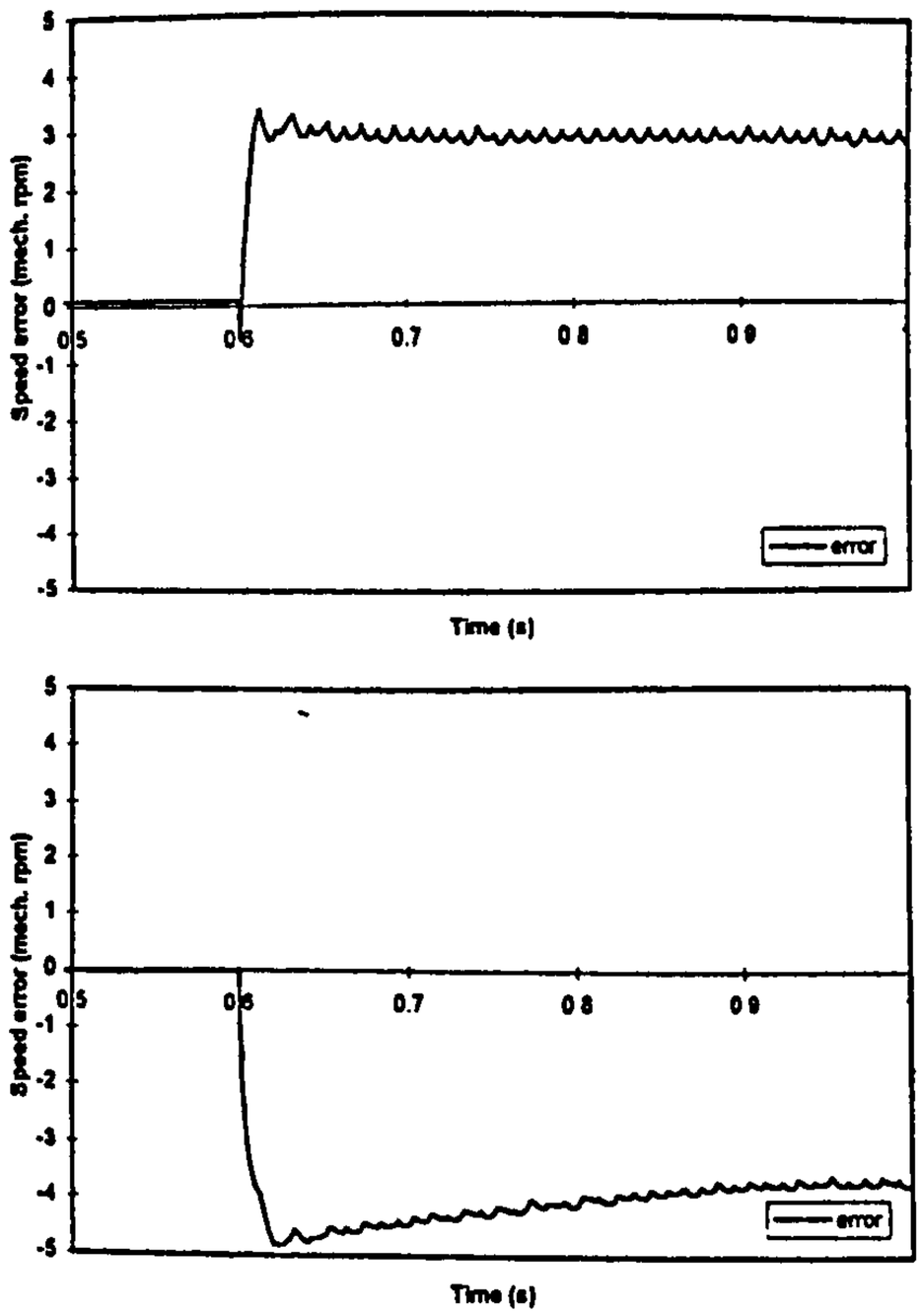

Figure 4 Speed error for operation with incorrect setting of the magnetising inductance: $L_m^* = 0.8L_{mn}$ and $L_m^* = 1.2L_{mn}$, respectively

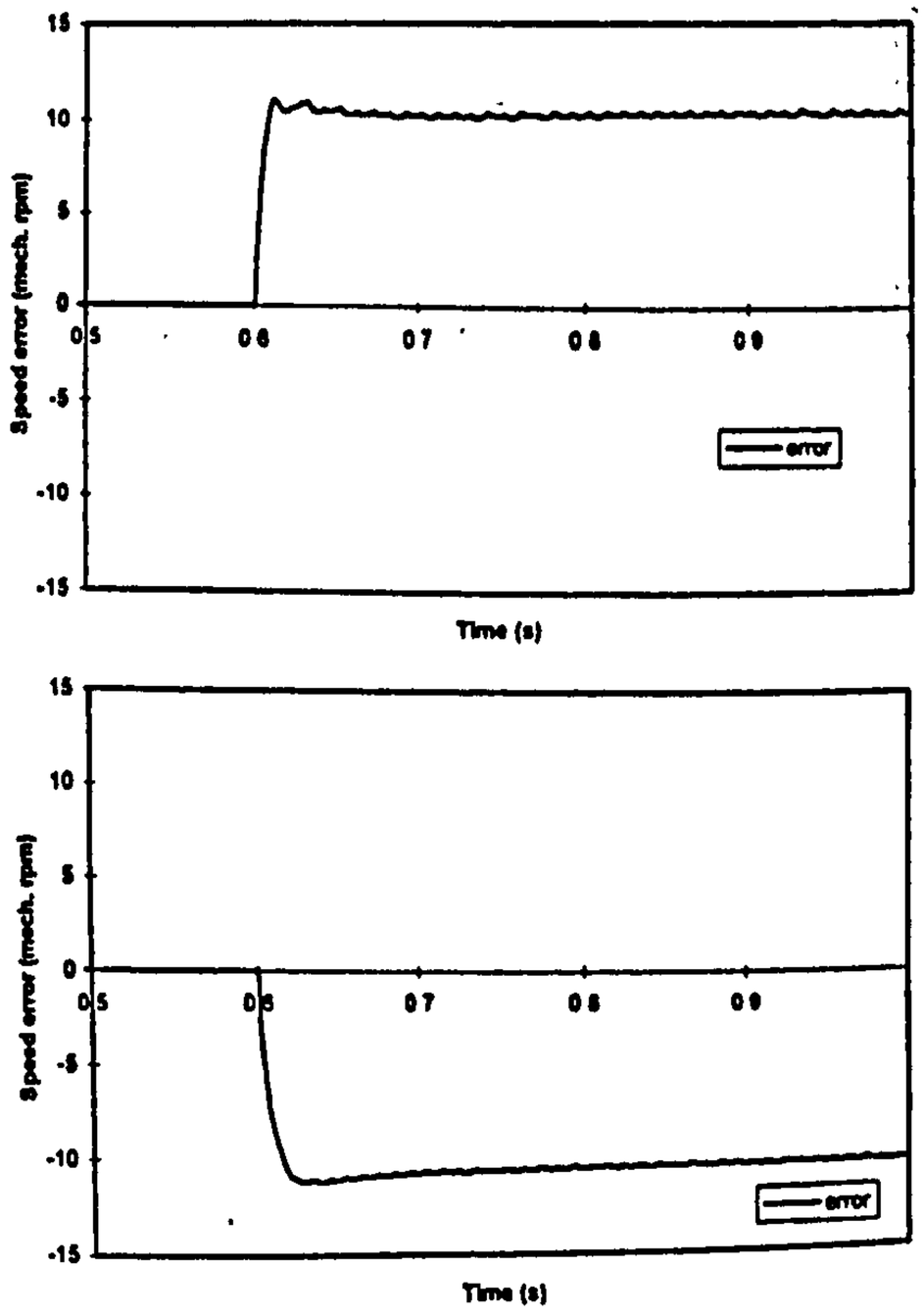

Figure 5 Speed error for operation with incorrect rotor resistance: $R_r = 0.8R_m$, $R_r^* = R_m$ and $R_r = 1.2R_m$, $R_r^* = R_m$, respectively

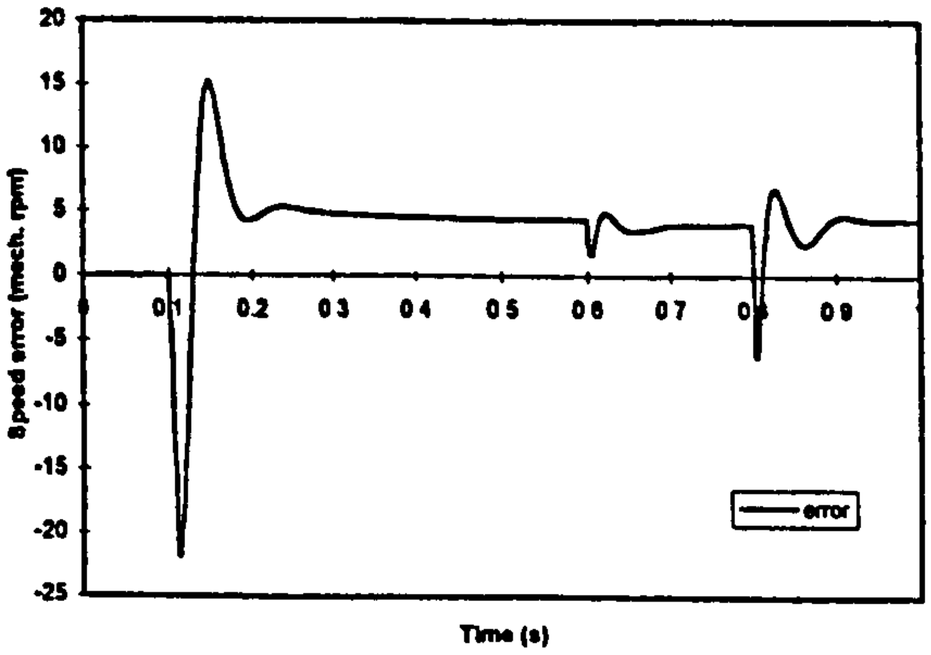

Figure 6 Speed estimation error at 0.05 p.u. speed command for $R_s = 1.2R_{sn}$, $R_s^* = R_{sn}$

Discussion

Speed estimation error due to incorrect setting of the magnetising inductance is speed independent but load dependent. Maximum steady-state values of around 3 rpm and almost -4 rpm, obtained in Fig. 4 for rated torque operation, closely agree with results of [9]. Very much the same holds true for rotor resistance variation, where maximum errors are again obtained for rated torque operation and are ± 10 rpm. Incorrect setting of magnetising inductance and rotor resistance variation cause small discrepancy between actual and commanded torque. Orientation angle error is negligibly small, so that field orientation is maintained.

Situation is however quite different with regard to speed estimation error caused by stator resistance variation. This error is speed dependent, with weak load dependence, and is the highest at low speeds. In the case illustrated in Fig. 6 it is around 4 rpm, while in Fig. 7 the value is close to -4 rpm. Stator resistance variation causes significant discrepancy between actual and commanded torque at low speeds. Moreover, orientation angle error is of rather significant value at low speeds as well [9]. Complete failure of the speed estimator can result, as already discussed. Accurate adjustment of stator resistance thus appears to be of crucial importance.

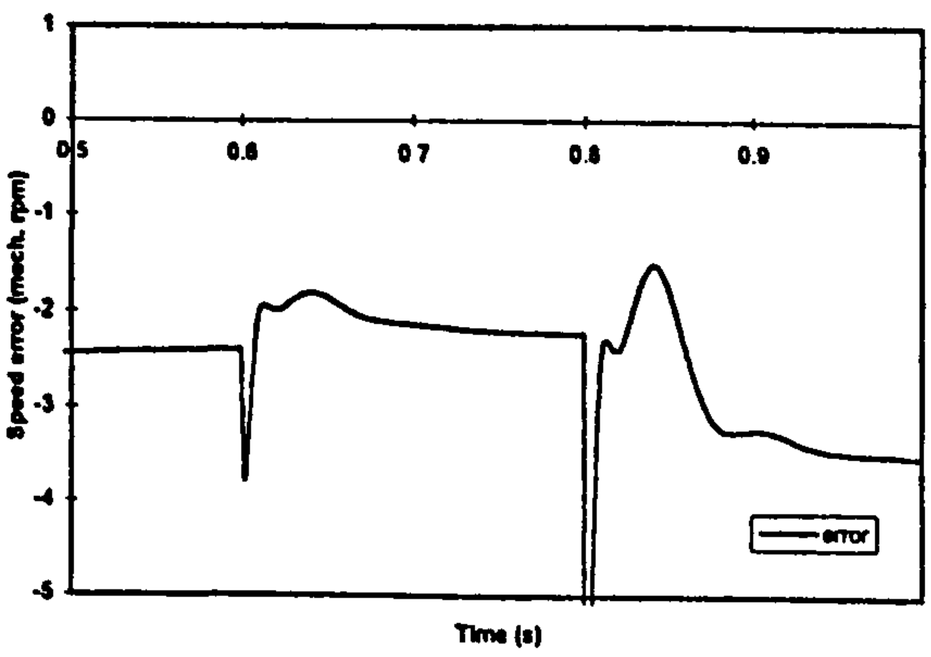

Figure 7 Speed estimation error at 0.1 p.u. speed command for $R_s = 0.8R_{sn}$, $R_s^* = R_{sn}$

CONCLUSION

Speed estimation error in indirect feed-forward rotor flux oriented induction machine with rotor flux based MRAC speed estimator is analysed, by simulating dynamics of the drive. Incorrect setting of the magnetising inductance, and stator and rotor resistance variations are elaborated. All the three sources of detuning cause speed estimation error of the same order. The highest one is due to rotor resistance variation.

REFERENCES

[1] K.Rajashekara, A.Kawamura, K.Matsuse (editors); "*Sensorless control of AC motor drives*", Piscataway, NJ: IEEE Press, 1996.

[2] C.Schauder; "Adaptive speed identification for vector control of induction motors without rotational transducers", *IEEE Trans. Ind. Appl.*, vol. 28, pp. 1054-1061, 1992.

[3] M.N.Marwali, A.Keyhani; "A comparative study of rotor flux based MRAS and back emf based MRAS speed estimators for speed sensorless vector control of induction machines", *Proc. IEEE IAS*, New Orleans, LA, pp. 160-166, 1997.

[4] C.Ilas et al.; "Comparison of different schemes without shaft sensors for filed oriented control drives", *Proc. IEEE IECON*, Bologna, Italy, pp. 1579-1588, 1994.

[5] G.Griva et al.; "A unitary approach to speed sensorless induction motor field oriented drives based on various model reference schemes", *Proc. IEEE IAS*, San Diego, CA, pp. 1594-1599, 1996.

[6] G.J.Armstrong, D.J.Atkinson; "A comparison of model reference adaptive system and extended Kalman filter estimators for sensorless vector drives", *Proc. EPE*, Trodheim, Norway, pp. 1.424-1.429, 1997.

[7] R.Blasco-Gimenez et al.; "Dynamic performance limitation for MRAS based sensorless induction motor drives. Part 1: Stability analysis for the closed loop drive", *IEE Proc. - Electr. Power Appl.*, vol. 143, pp. 113-122, 1996.

[8] P.L.Jansen, R.D.Lorenz; "Accuracy limitations on velocity and flux estimation in direct field oriented induction machines", *Proc. EPE*, Brighton, UK, pp. 312-318, 1993.

[9] E.Levi, M.Wang; "Impact of parameter variations on speed estimation in sensorless rotor flux oriented induction machines", *IEE Int. Conf. Power Elec. and Variable Speed Drives*, London, UK, Sept. 1998.

[10] E.Levi; "A unified approach to main flux saturation modelling in d-q axis models of induction machines", *IEEE Trans. Energy Conv.*, vol. 10, pp. 455-461, 1995.

APPENDIX: Induction Motor Data

4 kW 380 V 50 Hz 8.7 A Y 2P = 4

$T_{en} = 26.5\ Nm$ $R_{sn} = 1.37\ \Omega$ $R_{rn} = 1.1\ \Omega$

$L_{\sigma sn} = 4.87$ mH $L_{\sigma rn} = 7.96$ mH $L_{mn} = 0.143$ H

$$L_m = \begin{cases} 0.1964285 & I_m < 2.2\ \text{A} \\ 0.8374/I_m + 0.0067 - 0.924/I_m^2 & I_m > 2.2\ \text{A} \end{cases}$$

$$L = d\Psi_m/dI_m = \begin{cases} 0.1964285 & I_m < 2.2\ \text{A} \\ 0.0067 + 0.924/I_m^2 & I_m > 2.2\ \text{A} \end{cases}$$

Main Flux Saturation Compensation in Sensorless Vector Controlled Induction Machines for Operation in the Field Weakening Region

E.Levi, M.Wang
LIVERPOOL JOHN MOORES UNIVERSITY
School of Engineering, Byrom St
Liverpool L3 3AF, UK
Tel: +(44-151) 231 2257, Fax: +(44-151) 298 2624
e-mail: e.levi@livjm.ac.uk

Keywords

Sensorless drives, vector control, induction motors, flux model, estimation techniques.

Abstract

Operation of a sensorless indirect rotor flux oriented machine in the field weakening region requires that the variable degree of main flux saturation is recognised and compensated in both the controller and the estimator. The paper proposes a modified version of the rotor flux based MRAC type of speed estimator, that fully compensates for the variable degree of main flux saturation. The estimator is used in conjunction with an appropriate modified indirect vector controller, that accounts for saturation as well. Effectiveness and accuracy of the developed sensorless vector control scheme for operation in the field weakening region are verified by extensive simulation.

Introduction

Numerous methods of sensorless vector control of induction machines are nowadays available: [1]. The majority of methods rely in the process of speed estimation on utilisation of the induction machine model. As mechanical sub-systems of the control part of the drive and of the machine itself are in any sensorless drive effectively decoupled, and as standard d-q axis constant parameter induction machine model is utilised, accuracy of speed estimation strongly depends on parameter variation effects in the machine.

One of the most frequently applied control approaches appears to be model reference adaptive control (MRAC), originally introduced in: [2] and further developed in: [3], which is characterised by relatively simple implementation requirements. MRAC based speed estimation techniques mutually differ with respect to the quantity that is selected as output of the reference and the adjustable model. The most frequent choices appear to be rotor flux, modified rotor flux, back e.m.f. and reactive power: [1]. The technique analysed in this paper is the rotor flux based speed estimation of MRAC type, in conjunction with indirect feed-forward rotor flux oriented control.

Compensation of parameter variation effects in sensorless vector controlled induction motor drives with model based speed estimation has been a subject of considerable interest in recent past. In majority of cases attempts are made to provide on-line identification of either stator resistance: [4-6], or rotor resistance: [7-10]. Simultaneous identification of both the stator and the rotor resistance is discussed in: [11-13], while simultaneous estimation of rotor resistance and magnetising inductance is proposed in: [14]. As changes in stator and rotor resistance are temperature dependent, the only way to compensate for their variation is to employ a method of on-line identification. However, a different approach is advantageous when parameter variations of electro-magnetic nature are under consideration. In this case it is easier to build the control system and the speed estimator using an appropriate, modified induction motor model that accounts for the given phenomenon. Such a

situation arises for example when compensation of detuning due to iron loss is to be achieved. A modified rotor flux based speed estimator of MRAC type, that provides compensation of iron loss in conjunction with the modified indirect feed-forward vector controller, is proposed in: [15]. Similarly, variations in magnetising inductance, caused by variable degree of main flux saturation in the machine during operation with variable rotor flux reference, are most easily compensated for if a saturated induction motor model is used for development of a modified speed estimator and vector controller structure. Numerous schemes that account for main flux saturation have been developed in the past for rotor flux oriented control of an induction machine equipped with speed sensor: [16]. There is however little evidence of similar attempts for sensorless drives.

If a vector controlled induction motor drive is designed to operate in both base speed region and field weakening region, it becomes an imperative that main flux saturation is compensated. In this region impact of stator resistance variation is negligible, while level of main flux saturation significantly varies with operating speed. Studies related to operation of sensorless induction motor drives in the field weakening region appear to be rather rare. A notable exception is the work: [17], where need for compensation of main flux saturation is properly recognised. The sensorless scheme discussed in: [17], although characterised with excellent performance, is rather complicated. It incorporates closed loop flux control and utilises speed estimation algorithm based on MRAC in conjunction with closed-loop flux observer. The aim of the present paper is to propose a simpler sensorless rotor flux oriented control scheme that provides good performance in the field weakening region by compensating for the variable degree of main flux saturation. A modified rotor flux based speed estimator of MRAC type, that provides full compensation of main flux saturation and therefore enables extension of the drive operation into the field weakening region, is developed. The modified speed estimator is used in indirect feed-forward type of rotor flux oriented control, with indirect vector controller accounting for main flux saturation. Effectiveness of the developed control algorithm is confirmed by simulation.

Basic Structure of the Drive

Basic structure of the sensorless indirect rotor flux oriented induction machine, elaborated in the paper, is shown in Fig. 1. The machine is assumed to be fed from a current source, so that the current controlled PWM inverter is taken as ideal in simulations (i.e., reference and actual phase currents are equal). Structure shown in Fig. 1 is aimed at operation in the base speed region only, so that rotor flux reference is shown as constant and equal to rated (index n denotes rated values).

The speed estimator of Fig. 1 is shown in Fig. 2. It relies on measurement of stator currents and voltages, utilises principles of MRAC, and the two left-hand side blocks perform integration of equations (1) and (2). Speed estimator operates in the stationary α,β reference frame and is described with the following space vector equations ($\sigma_n = 1 - L_{mn}^2 / (L_{sn} L_{rn})$):

$$\frac{d\underline{\psi}_r^{(1)}}{dt} = \frac{L_{rn}}{L_{mn}} \left[\underline{v}_s - \left(R_{sn} + \sigma_n L_{sn} p \right) \underline{i}_s \right] \tag{1}$$

$$\frac{d\underline{\psi}_r^{(2)}}{dt} = \left(j\omega^{est} - \frac{1}{T_{rn}} \right) \underline{\psi}_r^{(2)} + \frac{L_{mn}}{T_{rn}} \underline{i}_s \tag{2}$$

$$\varepsilon = \psi_{\alpha r}^{(2)} \psi_{\beta r}^{(1)} - \psi_{\beta r}^{(2)} \psi_{\alpha r}^{(1)} \tag{3}$$

Equation (1) is the reference model, while equation (2) is the adaptive model. All the machine parameters in (1)-(2) and in the controller of Fig. 1 are constant and correspond to the rated operating conditions.

Modified Indirect Vector Controller

In order to extend the operating region of the system of Fig. 1 above base speed, it is necessary to modify the indirect vector controller by accounting for main flux saturation. The simplest solution,

proposed in [16] and used here, is to apply the controller of the structure illustrated in Fig. 3. Rate of change of the rotor flux reference is neglected. Ratio of magnetising to rotor inductance is assumed to remain constant and equal to the one under rated rotor flux conditions, so that $SG = R_{rn}(L_{mn}/L_{rn})$ and $K = (3/2)P\,L_{mn}/L_{rn}$. Impact of cross-saturation is not compensated either. Control system of Fig. 3 however provides full compensation of saturation in steady-state in the field-weakening region in a drive with speed (position) sensor, [16]. As in a sensorless drive speed sensor does not exist, situation is quite different here. If control system of Fig. 3 is applied in conjunction with constant parameter speed estimator of Fig. 2, operation of the drive will be characterised with large speed estimation errors, as shown in section on simulation results. It is therefore necessary to compensate the main flux saturation in the speed estimator of Fig. 2 as well, by modifying its structure.

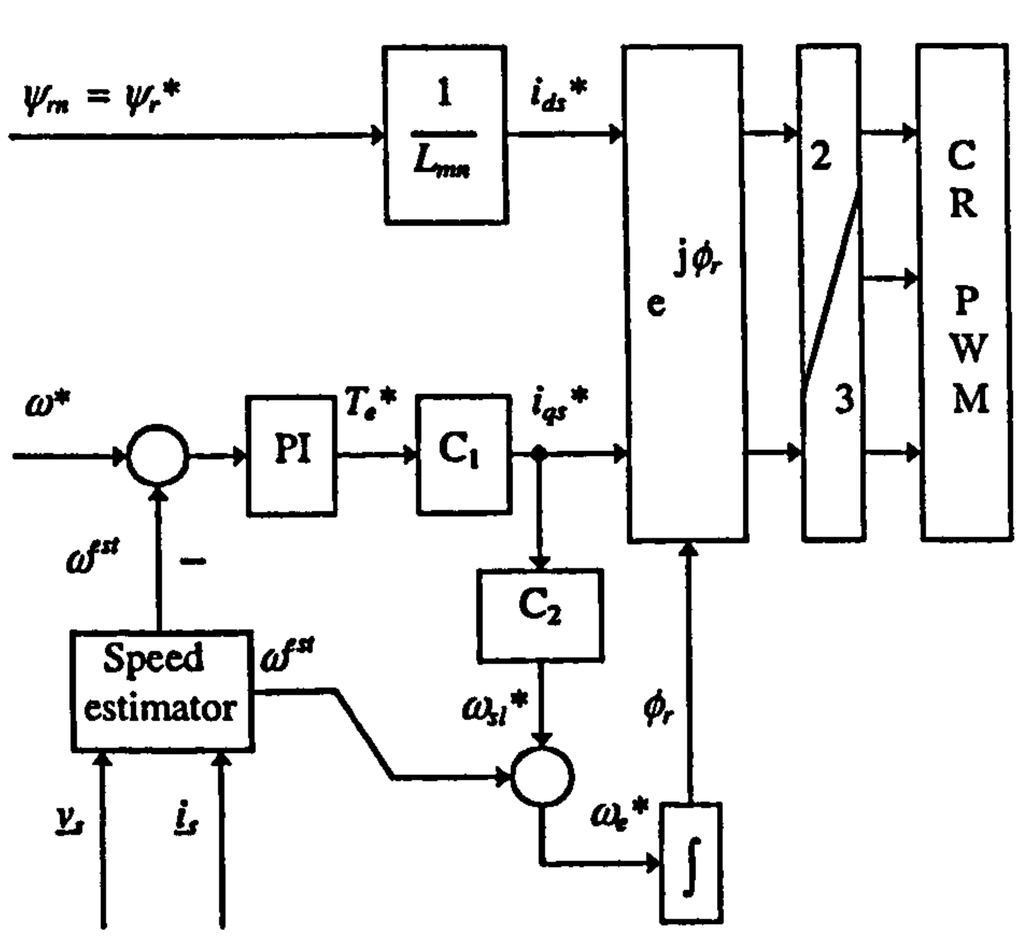

$$C_1 = (2/3P)\,L_{rn}/(L_{mn}\psi_r^*) \qquad C_2 = L_{mn}/(T_{rn}\psi_r^*)$$

Fig. 1: Speed sensorless indirect rotor flux oriented induction machine for operation in the base speed region.

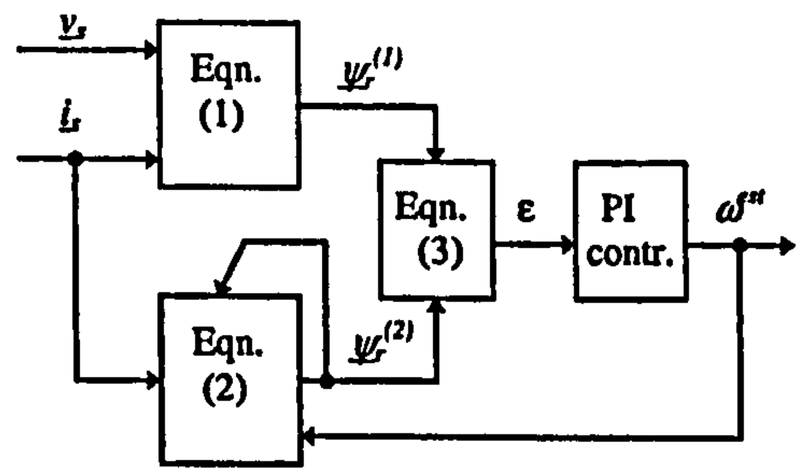

Fig. 2: Rotor flux based, constant parameter rotor speed estimator.

Compensation of Main Flux Saturation in the Speed Estimator

In order to compensate for the main flux saturation in the speed estimator, both the reference and the adaptive part of the estimator, (1)-(2), have to be modified. Estimation of rotor flux in the reference model (1) is based on stator voltage and current measurements, which contain sufficient information to yield, apart from estimates of rotor flux components, the estimate of the magnetising inductance as well: [18]. Instead of (1), the following equations are used: [18]:

$$\psi_{\alpha s} = \int (v_{\alpha s} - R_{sn} i_{\alpha s})\,dt \qquad \psi_{\beta s} = \int (v_{\beta s} - R_{sn} i_{\beta s})\,dt$$

$$\psi_{\alpha m} = \psi_{\alpha s} - L_{\sigma sn} i_{\alpha s} \qquad \psi_{\beta m} = \psi_{\beta s} - L_{\sigma sn} i_{\beta s}$$

$$\psi_m = \sqrt{\psi_{\alpha m}^2 + \psi_{\beta m}^2} \qquad i_m = f(\psi_m)$$

$$i_{\alpha m} = (\psi_{\alpha m}/\psi_m) i_m \qquad i_{\beta m} = (\psi_{\beta m}/\psi_m) i_m \qquad (4)$$

$$\psi_{\alpha r}^{(1)} = \psi_{\alpha m} + L_{\sigma rn}(i_{\alpha m} - i_{\alpha s})$$

$$\psi_{\beta r}^{(1)} = \psi_{\beta m} + L_{\sigma rn}(i_{\beta m} - i_{\beta s})$$

$$L_m^{est} = \psi_m / i_m$$

Reference model, described with (4), is illustrated in Fig. 4. Not only that main flux saturation is fully accounted for in the calculation of the rotor flux components, but the estimate of the magnetising inductance is provided as well. Estimate of the magnetising inductance, obtained from the reference model, will be used in the adaptive model, as explained next. It should be noted that the complexity of the scheme given in Fig. 4 can be reduced for real time applications by suitably re-arranging eqs. (4).

Means for accounting for main flux saturation in the adaptive model (2) are elaborated in detail in: [19]. As shown in: [19], main flux saturation in (2) is fully accounted for provided that the appropriate value of the saturated steady-state magnetising inductance is used instead of the constant one. In other words, structure of the equation (2) needs not be changed at all, as dynamic inductance terms do not appear in this equation when stator current and rotor flux components are selected as state space variables. An appropriate value of the saturated steady-state magnetising inductance is obtained from the reference model (4) and the adaptive model then takes the following form:

$$\frac{d\underline{\psi}_r^{(2)}}{dt} = \left(j\omega^{est} - \frac{R_{rn}}{L_{\sigma rn} + L_m^{est}} \right) \underline{\psi}_r^{(2)} + \frac{L_m^{est}}{L_{\sigma rn} + L_m^{est}} R_{rn} \underline{i}_s \qquad (5)$$

Resultant structure of the proposed modified speed estimator is shown in Fig. 5. The estimator provides full compensation of main flux saturation in both transient and steady-state operation.

Simulation Results

Transient operation of the drive is simulated using SIMULINK. The induction machine is for all the considered cases represented with the full saturated machine model in the stationary reference frame,

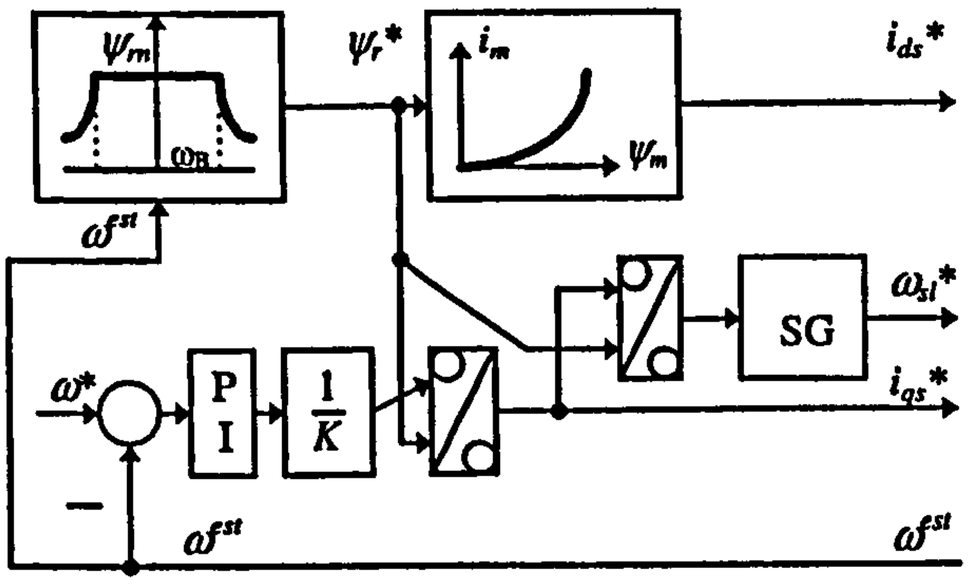

Fig. 3: Indirect rotor flux oriented controller with compensation of main flux saturation.

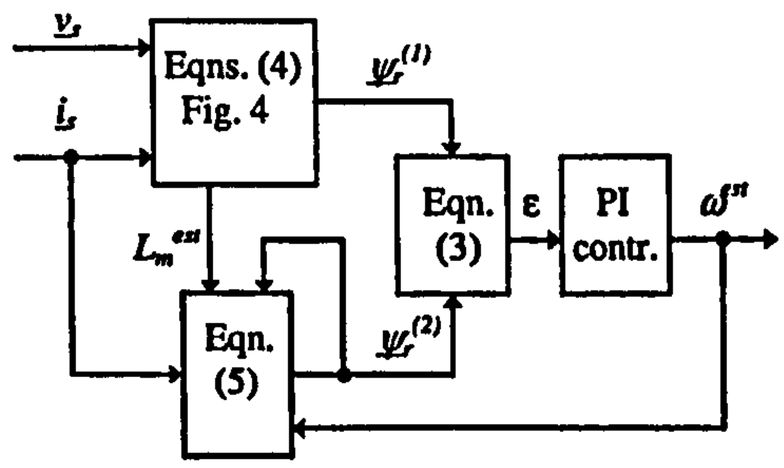

Fig. 5: Rotor flux based speed estimator with full compensation of main flux saturation.

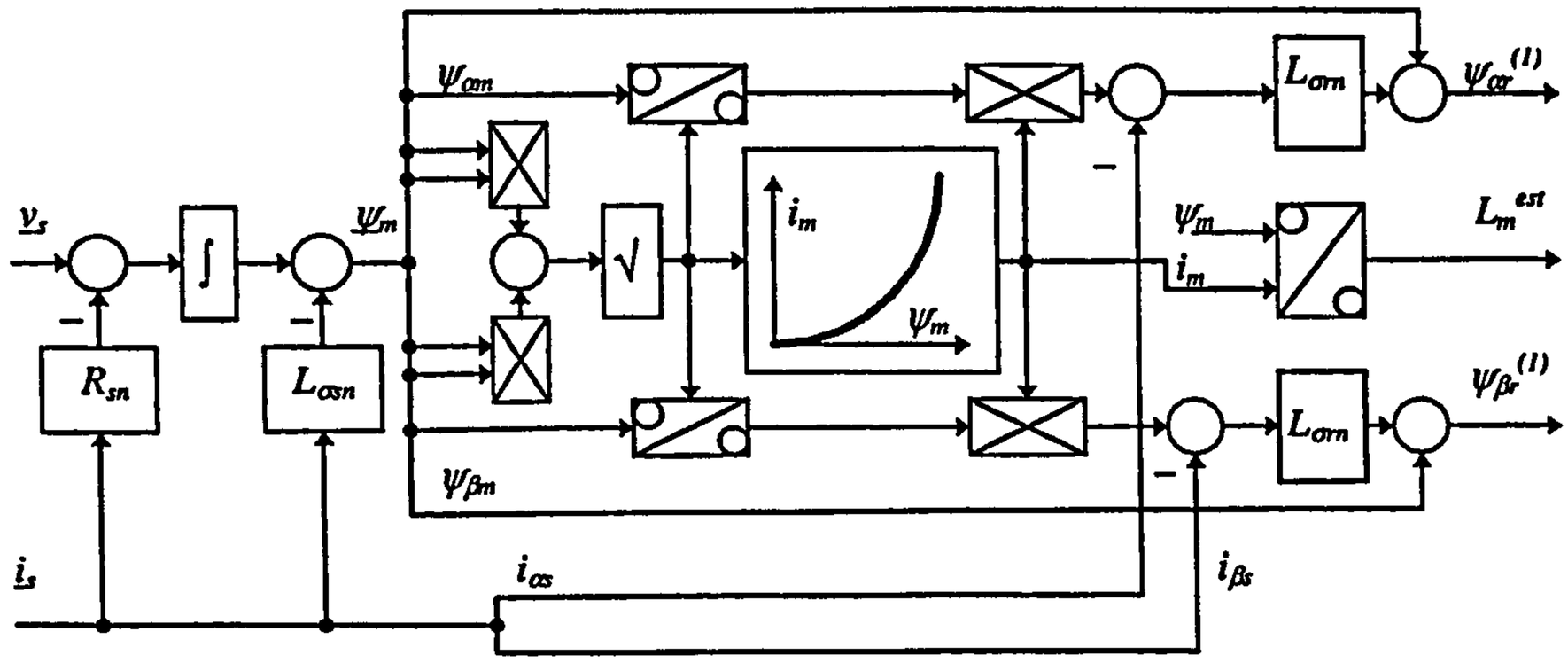

Fig. 4: Structure of the modified reference model with compensation of main flux saturation.

in which stator and rotor current components are taken as state-space variables. Closed loop speed control and calculation of orientation angle utilise in all the cases estimated speed. Actual speed is used only to monitor error in speed estimation. In all the cases speed response is illustrated in terms of electrical angular velocity of rotation, while speed error is given in mechanical rpm and is defined as difference between actual and estimated speed. All the necessary data of the induction machine used in the study are given in Appendix.

Two series of simulation tests are performed. The first one utilises modified indirect vector controller of Fig. 3 and the constant parameter speed estimator of Fig. 2, that is based on (1)-(3). The purpose of these simulations is to show how the operation of the drive is affected by the lack of compensation of main flux saturation in the speed estimator, although the indirect feed-forward controller does compensate for main flux saturation. The second set of simulations applies to the same operating conditions as the first set. The only difference is that the speed estimator of Fig. 5 (which incorporates Fig. 4) is used instead of the constant parameter one. The purpose of these simulations is to verify the proposed modified speed estimator with compensation of main flux saturation.

The following sequence of transients is simulated. The machine is initially excited at zero speed under no-load conditions. Speed command is then applied, so that rated speed operation (1 p.u.) under no load conditions is achieved. During operation at rated speed load torque of 1 p.u. is applied in a step-wise manner at t = 0.5 s. At t = 1 s load torque is stepped down to 0.5 p.u. and this value is not changed any more. Finally, at t = 1.5 s speed command is further increased in a ramp-wise manner, so that field-weakening region is entered. Final operating steady-state is therefore with 0.5 p.u. load torque and transients for two different final speeds are shown, namely speed command of 1.5 p.u. and speed command of 2 p.u..

Figures 6 and 7 summarise results obtained with constant parameter speed estimator of Fig. 2. Graphs of actual and commanded speed, speed error, actual and commanded torque, actual and commanded rotor flux, and actual rotor flux d-q axis components are given, for final speeds of 1.5 p.u. and 2 p.u., respectively.

In the base speed region estimated speed tracks the actual one very well, except during the initial part of the acceleration. Steady-state speed error equals zero for all the loading conditions in this region. Commanded and actual torque are in good agreement, except during initial part of the acceleration. Field orientation is initially lost, as witnessed by oscillatory torque behaviour and large value of rotor flux q-axis component. Unsatisfactory performance during initial acceleration is a consequence of the too high gain of the speed controller. Once when acceleration is completed the machine operates with correct rotor flux orientation as rotor flux q-axis component is zero and rotor flux equals the reference value. Undoubtedly, constant parameter speed estimator enables satisfactory quality of rotor flux oriented control in the base speed region. The problems however begin once when the field-weakening operation is initiated at t = 1.5 s. Speed estimation error quickly increases and its final values are over 10 rpm and 20 rpm in Figs. 6 and 7, respectively. Difference between actual torque (that equals load torque of 0.5 p.u.) and reference torque appears and is higher at final reference speed of 2 p.u. (Fig. 7) than at final reference speed of 1.5 p.u. (Fig. 6). There is substantial difference between reference rotor flux and actual rotor flux and field oriented control is essentially lost. Final steady-state is characterised with substantial value of rotor flux q-axis component in both cases. Figures 6 and 7 clearly demonstrate the need for incorporation of the main flux saturation in the speed estimator, if satisfactory performance is to be achieved in the filed-weakening region.

The same simulations are repeated once more. This time the proposed speed estimator of Fig. 5 is used instead of the constant parameter one. The same sets of results for the same sequence of transients and the same final operating conditions are given in Figs. 8 and 9. Operation in the base speed region is insignificantly changed with the application of the saturation adaptive speed estimator. Pattern of discrepancy between actual and commanded torque and between actual and commanded rotor flux is during acceleration into field weakening region very similar in Figs. 8 and 9 to those

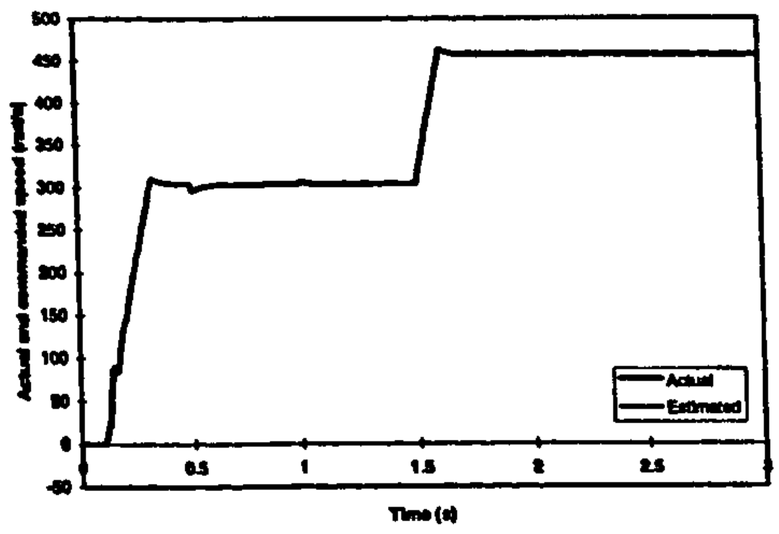

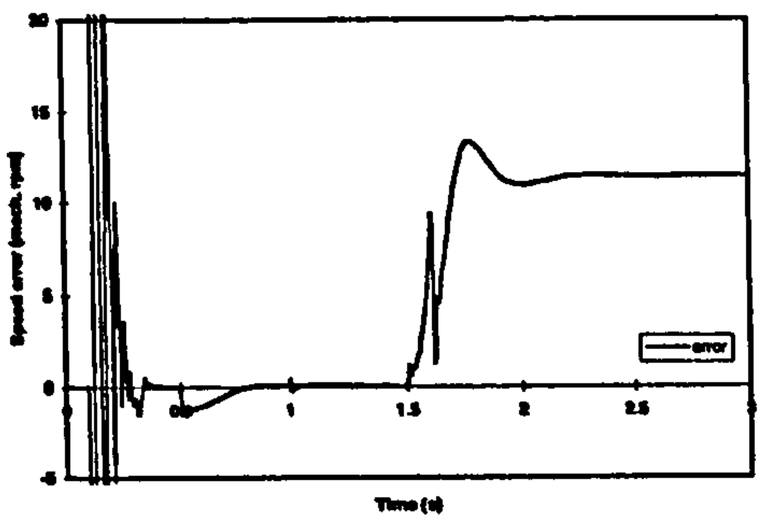

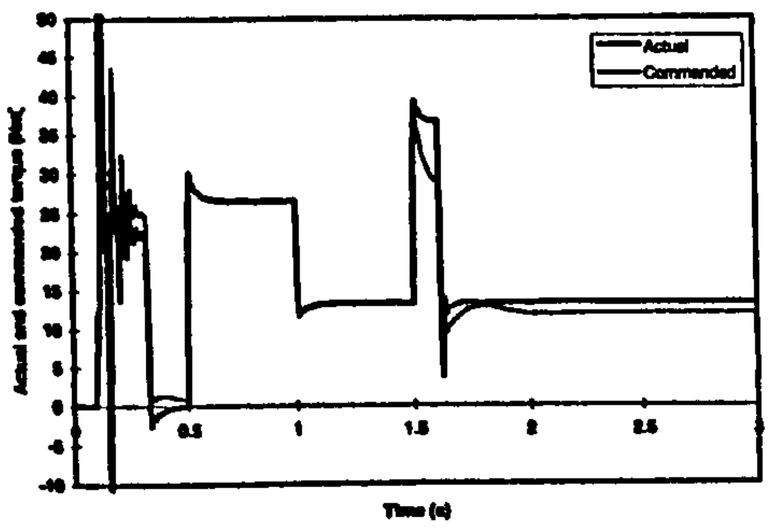

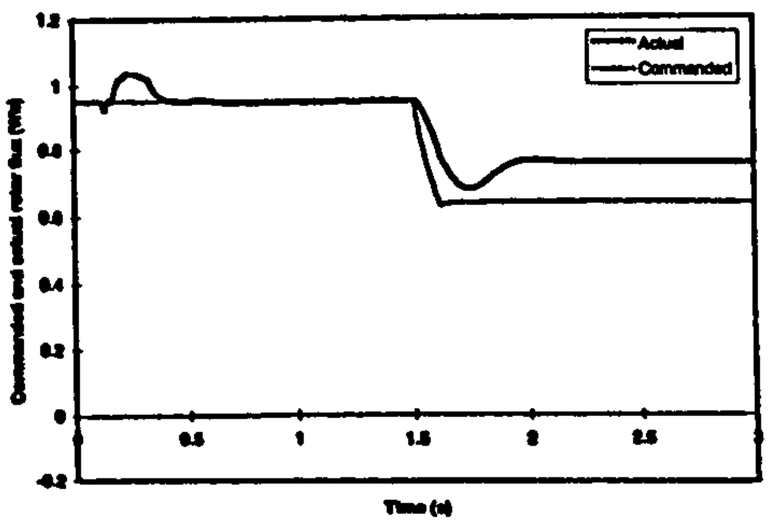

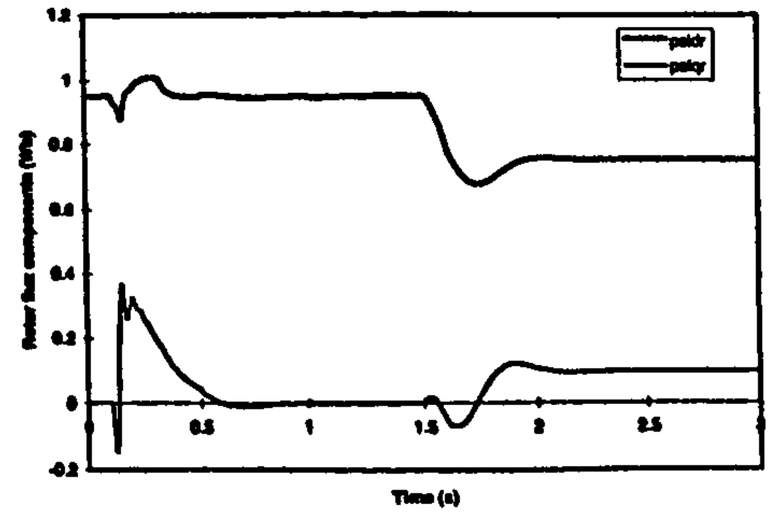

Fig. 6: Drive operation with constant parameter speed estimator (final speed in field weakening 1.5 p.u.): actual and estimated speed, speed error, actual and reference torque, actual and reference rotor flux, and actual rotor flux d-q axis components.

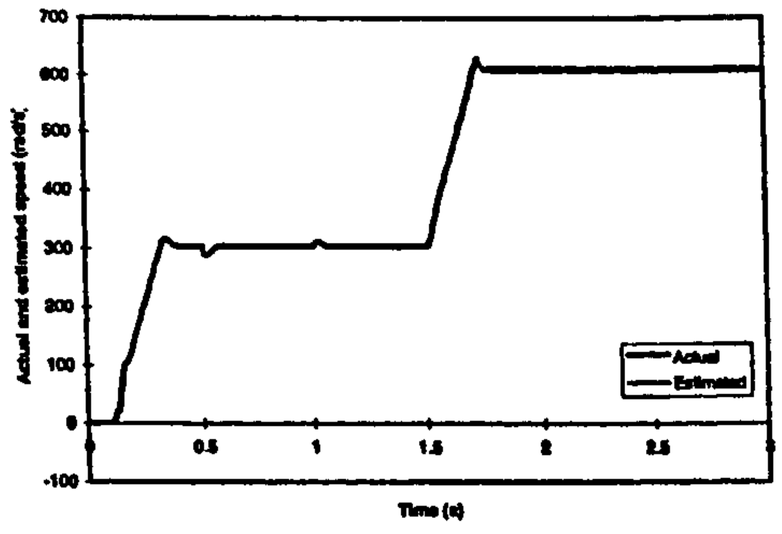

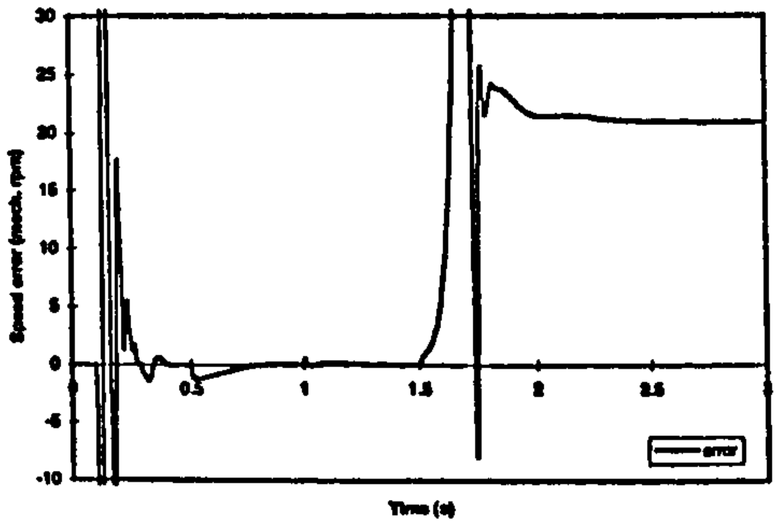

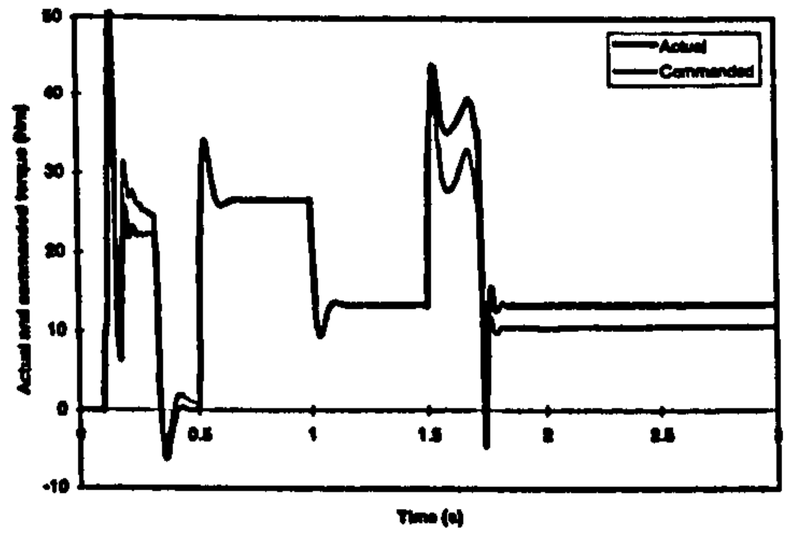

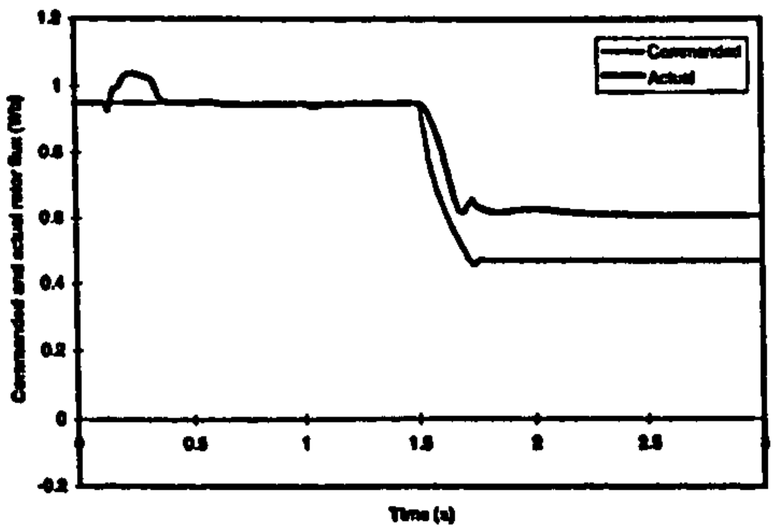

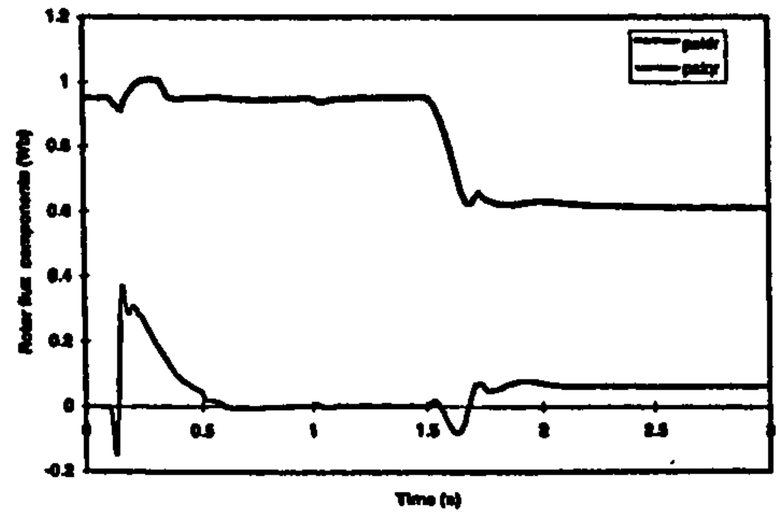

Fig. 7: Drive operation with constant parameter speed estimator (final speed in field weakening 2 p.u.): actual and estimated speed, speed error, actual and reference torque, actual and reference rotor flux, and actual rotor flux d-q axis components.

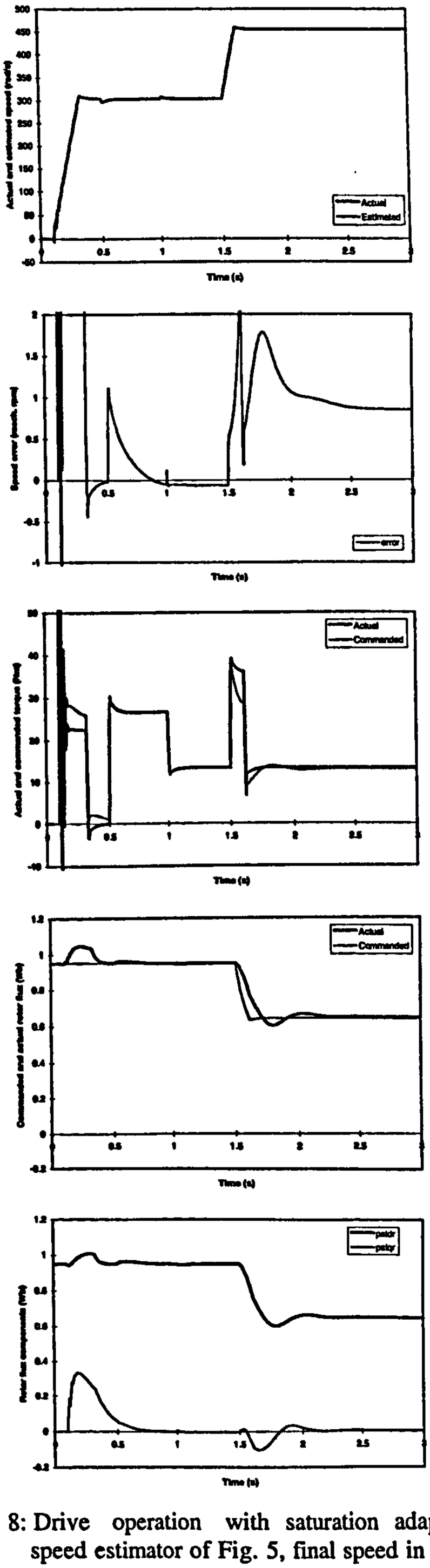

Fig. 8: Drive operation with saturation adaptive speed estimator of Fig. 5, final speed in field weakening is 1.5 p.u.: actual and estimated speed, speed error, actual and reference torque, actual and reference rotor flux, and actual rotor flux d-q axis components.

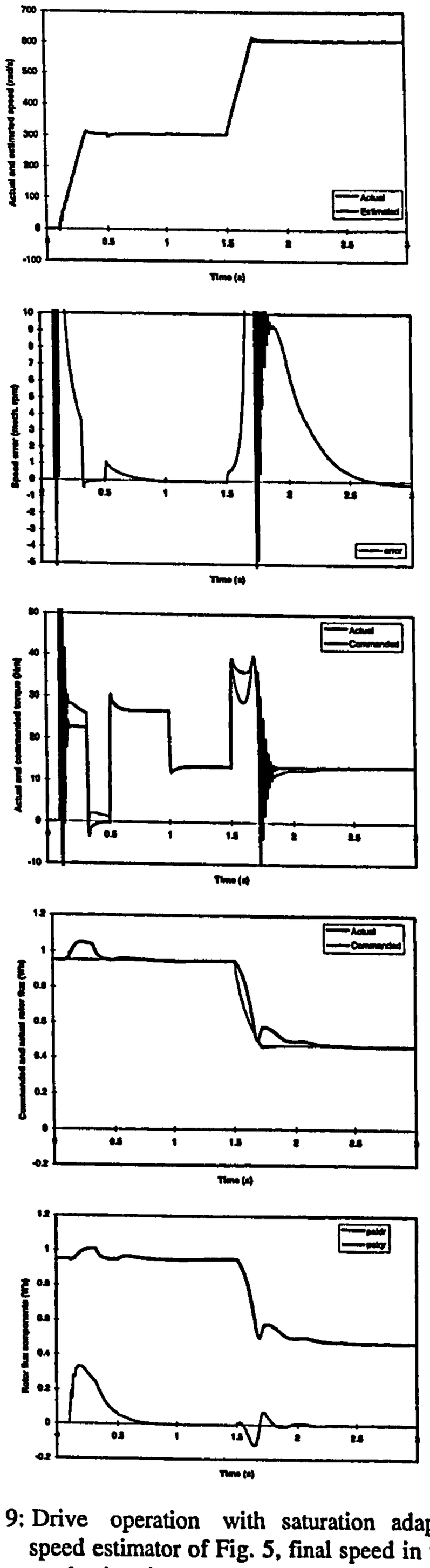

Fig. 9: Drive operation with saturation adaptive speed estimator of Fig. 5, final speed in field weakening is 2 p.u.: actual and estimated speed, speed error, actual and reference torque, actual and reference rotor flux, and actual rotor flux d-q axis components.

in Figs. 6 and 7, respectively. These differences occur due to the absence of the stator d-axis current command boost during the transient (rate of change of the rotor flux reference is neglected in the design of the controller of Fig. 3) and cannot be compensated by the modified speed estimator. However, speed estimation error during this transient is reduced significantly (its maximum value does not exceed 3 rpm in Fig. 8 and 40 rpm in Fig. 9, while corresponding values in Figs. 6 and 7 are 13 rpm and 55 rpm). Once when reference speed in the field weakening has become constant, the differences between responses in Figs. 8 and 9 and those of Figs. 6 and 7 become even more remarkable. Final steady-state in Figs. 8 and 9 is characterised with perfect field orientation as q-axis component of the rotor flux equals zero. Actual rotor flux in the machine exactly matches the reference value. Consequently, actual and reference torque are equal as well. Speed estimation error in Fig. 9 is essentially zero, while for operation at 1.5 p.u. speed (Fig. 8) it is less than 1 rpm. The reason for existence for this small residual speed estimation error is explained as follows. Motor model requires use of the magnetising curve approximation, while the controller and estimator ask for approximation of the inverse magnetising curve (Figs. 3 and 4). The two approximations, obtained using curve fitting, are characterised with identical values for rated operating point and for the initial linear portions of the curves, while some minor discrepancies exist in between. Speed estimation error is therefore zero for operation in the base speed region (rated operating point) and for operation at 2 p.u. speed (linear portion of the curve). Operation at 1.5 p.u. speed takes place in between these two areas of the magnetising curve, where matching is not perfect, so that some very small amount of speed estimation error results (speed estimation error at 1.25 p.u. speed is, repeating the same simulation, found to be 0.25 rpm; at 1.75 p.u. speed error is 0.3 rpm). These considerations clearly indicate that accurate knowledge of the machine's magnetising curve is of utmost importance for successful implementation of the developed speed estimator.

Conclusion

The paper describes development of a modified rotor flux based speed estimator of MRAC type, that enables successful operation of a sensorless vector controlled induction machine in the field weakening region. As the rotor flux reference in the field weakening region varies, it is necessary to compensate for the variable degree of main flux saturation in both the speed estimator and in the indirect feed-forward rotor flux oriented controller. An existing modified indirect feed-forward controller is utilised at first in conjunction with constant parameter speed estimator and the need for main flux saturation compensation within the speed estimator is established by extensive simulation. It is shown that large speed estimation errors take place in the field weakening region and that rotor flux oriented control is effectively lost.

Next, a saturation adaptive rotor speed estimator is developed. Reference part of the speed estimator is modified in such a way that estimated rotor flux components, obtained from it, fully account for main flux saturation. Additionally, estimate of the saturated magnetising inductance is obtained from the reference model. This magnetising inductance estimate is fed into the adaptive part of the model, so that the main flux saturation is completely compensated in the speed estimator during both transient and steady-state operation. It is verified by simulation that application of the saturation adaptive speed estimator preserves correct field orientation in the field weakening region and that the speed estimation error becomes negligibly small.

References

1. K.RAJASHEKARA, A.KAWAMURA, K.MATSUSE, (Editors). *Sensorless control of AC motor drives.* IEEE Press, Piscataway, NJ, 1996.
2. S.TAMAI, H.SUGIMOTO, M.YANO. Speed sensorless vector control of induction motor with model reference adaptive system, *IEEE Ind. Appl. Soc. Anu. Meet. IAS*, 1987, pp. 189-195.
3. C.SHAUDER. Adaptive speed identification for vector control of induction motors without rotational transducers, *IEEE Trans. on Industry Applications*, vol. 28, 1992, pp. 1054-1061.

4. L.UMANAND, S.R.BHAT. Online estimation of stator resistance of an induction motor for speed control applications, *IEE Proc. - Electr. Power Appl.*, vol. 142, 1995, pp. 97-103.

5. G.YANG, T.H.CHIN. Adaptive speed identification scheme for a vector-controlled speed sensorless inverter-induction motor drive, *IEEE Trans. on Industry Applications*, vol. 29, 1993, pp. 820-825.

6. R.BLASCO-GIMENEZ, G.M.ASHER, M.SUMNER. A new method of stator resistance estimation for enhanced dynamic performance of sensorless vector control drives, *Proc. 6th Eur. Conf. Power Elec. & Appl. EPE*, 1995, pp. 1.689-1.694.

7. H.KUBOTA, K.MATSUSE. Speed sensorless field-oriented control of induction motor with rotor resistance adaptation, *IEEE Trans. on Industry Applications*, vol. 30, 1994, pp. 1219-1224.

8. J.JIANG, J.HOLTZ. High dynamic speed sensorless ac drive with on-line model parameter tuning for steady-state accuracy, *IEEE Trans. on Industrial Electronics*, vol. 44, 1997, pp. 240-246.

9. S.A.SHIRSAVAR, M.D.McCULLOCH, C.G.GUY. Speed sensorless vector control of induction motors with parameter estimation, *Proc. IEEE IAS Annual Meeting*, 1996, pp. 262-269.

10. T.PANA. Sensorless vector-controlled induction motor drive system with rotor resistance estimation using parallel processing with floating point DSP, *Proc. Power Conversion Conf. PCC*, 1997, pp. 79-84.

11. L.ZHEN, L.XU. A mutual MRAS identification scheme for position sensorless field orientation control of induction machines, *Proc. IEEE IAS Annual Meeting*, 1995, pp. 159-165.

12. R.BLASCO-GIMENEZ, G.M.ASHER, M.SUMNER, K.J.BRADLEY. Dynamic performance limitations for MRAS based sensorless induction motor drives. Part 2: Online parameter tuning and dynamic performance studies, *IEE Proc. - Electr. Power Appl.*, vol. 143, 1996, pp. 123-134.

13. S.H.LEE, I.J.HA, H.S.YOO, B.Y.HONG, S.J.YOON. An on-line identification method for both stator and rotor resistances of induction motors without rotational transducers, *Proc. IEEE ISIE*, 1996, pp. 325-330.

14. C.ATTAIANESE, G.TOMASSO, A.DAMIANO, I.MARONGIU, A.PERFETTO. On line estimation of speed and parameters in induction motor drives, *Proc. IEEE ISIE*, 1997, pp. 1054-1059.

15. E.LEVI, M.WANG, D.WILLIAMS. Evaluation of iron loss influence on speed estimation in sensorless MRAC-based field-oriented induction machines, *Eur. Trans. on Elec. Power ETEP*, vol. 9, 1999.

16. E.LEVI, S.VUKOSAVIC, V.VUCKOVIC. Saturation compensation schemes for vector controlled induction motor drives, *Proc. IEEE Power Elec. Spec. Conf. PESC*, 1990, pp. 591-598.

17. R.BLASCO-GIMENEZ, G.M.ASHER, J.CILIA, K.J.BRADLEY. Field weakening at high and low speed for sensorless vector controlled induction motor drives, *Proc. IEE Int. Conf. PEVD*, IEE Conf. Pub. 429, 1996, pp. 258-261.

18. E.LEVI, V.VUCKOVIC. A method of rotor flux estimation in saturated induction machines, *Proc. Int. Conf. Elec. Mach. ICEM*, 1990, pp. 344-349.

19. E.LEVI, M.SOKOLA. A novel saturation adaptive rotor flux estimator for rotor flux oriented induction machines, *Proc. 7th Eur. Conf. Power Elec. & Appl. EPE*, 1997, pp. 1.518-1.523.

Appendix: Induction Motor Data

4 kW 380 V 50 Hz 8.7 A Y $2P = 4$ $T_{en} = 26.5\ Nm$ $R_{sn} = 1.37\ \Omega$ $R_{rn} = 1.1\ \Omega$

$L_{\sigma sn} = 4.87$ mH $L_{\sigma rn} = 7.96$ mH $L_{mn} = 0.143$ H

Magnetising curve approximation (motor model; rms values):

$$\Psi_m = \begin{cases} 0.1964285 I_m & I_m < 2.2\ \text{A} \\ 0.8374 + 0.0067 I_m - 0.924/I_m & I_m > 2.2\ \text{A} \end{cases}$$

$$L = d\Psi_m/dI_m = \begin{cases} 0.1964285 & I_m < 2.2\ \text{A} \\ 0.0067 + 0.924/I_m^2 & I_m > 2.2\ \text{A} \end{cases} \qquad L_m = \Psi_m/I_m$$

Inverse magnetising curve approximation (rms values; indirect vector controller and speed estimator):

$$I_m = -0.04 + 7.19\Psi_m - 23.88\Psi_m^2 + 104.43\Psi_m^3 - 200.62\Psi_m^4 + 145.08\Psi_m^5$$